

Northumbria Research Link

Citation: Yik, Francis (1993) Methodologies for simulating heat and moisture transfer in air-conditioned buildings in sub-tropical climates. Doctoral thesis, University of Northumbria.

This version was downloaded from Northumbria Research Link:
<https://nrl.northumbria.ac.uk/id/eprint/15720/>

Northumbria University has developed Northumbria Research Link (NRL) to enable users to access the University's research output. Copyright © and moral rights for items on NRL are retained by the individual author(s) and/or other copyright owners. Single copies of full items can be reproduced, displayed or performed, and given to third parties in any format or medium for personal research or study, educational, or not-for-profit purposes without prior permission or charge, provided the authors, title and full bibliographic details are given, as well as a hyperlink and/or URL to the original metadata page. The content must not be changed in any way. Full items must not be sold commercially in any format or medium without formal permission of the copyright holder. The full policy is available online: <http://nrl.northumbria.ac.uk/policies.html>

Some theses deposited to NRL up to and including 2006 were digitised by the British Library and made available online through the [EThOS e-thesis online service](#). These records were added to NRL to maintain a central record of the University's research theses, as well as still appearing through the British Library's service. For more information about Northumbria University research theses, please visit [University Library Online](#).



**Northumbria
University**
NEWCASTLE



UniversityLibrary

Northumbria Research Link

Citation: Yik, Francis (1993) Methodologies for simulating heat and moisture transfer in air-conditioned buildings in sub-tropical climates. Doctoral thesis, University of Northumbria.

This version was downloaded from Northumbria Research Link:
<http://nrl.northumbria.ac.uk/id/eprint/15720/>

Northumbria University has developed Northumbria Research Link (NRL) to enable users to access the University's research output. Copyright © and moral rights for items on NRL are retained by the individual author(s) and/or other copyright owners. Single copies of full items can be reproduced, displayed or performed, and given to third parties in any format or medium for personal research or study, educational, or not-for-profit purposes without prior permission or charge, provided the authors, title and full bibliographic details are given, as well as a hyperlink and/or URL to the original metadata page. The content must not be changed in any way. Full items must not be sold commercially in any format or medium without formal permission of the copyright holder. The full policy is available online: <http://nrl.northumbria.ac.uk/policies.html>

Some theses deposited to NRL up to and including 2006 were digitised by the British Library and made available online through the [EThOS e-thesis online service](#). These records were added to NRL to maintain a central record of the University's research theses, as well as still appearing through the British Library's service. For more information about Northumbria University research theses, please visit [University Library Online](#).



**Northumbria
University**
NEWCASTLE



UniversityLibrary

**METHODOLOGIES FOR SIMULATING HEAT AND MOISTURE TRANSFER IN AIR-
CONDITIONED BUILDINGS IN SUB-TROPICAL CLIMATES**

Francis Wai Hung YIK

**A thesis submitted in partial fulfilment of the requirements of the University of
Northumbria for the degree of Doctor of Philosophy**

**in collaboration with the Department of Building Services Engineering, Hong Kong
Polytechnic**

August, 1993

Acknowledgements

The author must express his grateful thanks to his supervisors, Dr. C. P. Underwood and Dr. A. J. Newall at the University of Northumbria at Newcastle and Dr. W. K. Chow at the Hong Kong Polytechnic for their valuable suggestions, critical comments, guidance and encouragement given during the course of the work.

This work was supported by the Hong Kong Polytechnic as a staff development programme for the author and thanks for this support is gratefully acknowledged.

The author must thank Miss Rita Yuen and Mr. T. K. Leung for their kind assistance in preparing some of the diagrams and Miss May Chan for her great help in typing majority of the equations in this thesis. The support and encouragement given by the author's colleague at the department of Building Services Engineering at the Hong Kong Polytechnic, especially Dr. J. Burnett, the head of the department, are very much appreciated.

Thanks are also due to Jean and Dominic for being supportive and understanding.

Declaration

The research described in this thesis is the original work of the author except where otherwise specified or where acknowledgements are made by reference. Being a part-time, remote mode research degree study programme, the work was carried out at both the University of Northumbria at Newcastle (the then Newcastle Upon Tyne Polytechnic) and the Hong Kong Polytechnic, under the supervision of Dr. C. P. Underwood, Dr. A. J. Newall and Dr. W. K. Chow.

The work has not been submitted for another degree or award of other academic or professional institution.

Francis Wai Hung YIK

Table of Contents

	Page
Abstract	i
Acknowledgements	ii
Declaration	iii
Table of Contents	iv
List of Tables	xii
List of Figures	xiii
List of Symbols	xix
Chapter 1 Introduction	1
1.1 Background	1
1.2 An Overview of Weather Conditions, Buildings and Air-conditioning Systems in Hong Kong	3
1.2.1 Weather Conditions and Buildings in Hong Kong	3
1.2.2 Use of Air-conditioning in Buildings in Hong Kong	4
1.2.3 Configuration and Operation of Central Air-conditioning Systems	5
1.2.4 Air-conditioning Plant Size	6
1.3 Indoor Humidity and Its Control	6
1.4 Effects of Moisture Adsorption and Desorption of the Building Fabric	8
1.5 Detailed Simulation of Building Thermal Response and Air-conditioning System Performance	9
1.5.1 Detailed Building Thermal Response Modelling Methods	10
1.5.2 System Performance Modelling	12
1.5.3 Deficiencies in Existing Building and System Simulation Programs	13
1.6 Research Objectives & Work Undertaken	15
1.7 Organization and Outline of the Thesis	18

Chapter 2	Modelling Heat and Moisture Transfer in Building Fabrics	22
2.1	Fundamentals of Heat and Moisture Transfer in Porous Media	23
2.1.1	Equilibrium Moisture Content and Sorption Isotherm	23
2.1.2	Sorption Hysteresis	24
2.1.3	Local Thermodynamic Equilibrium	25
2.1.4	A Simplified Picture of Moisture Sorption in Porous Media	26
2.1.5	Heat of Sorption	30
2.1.6	Basic Form of Equations Governing Coupled Heat and Moisture Transfer	30
2.2	Theories of Heat and Moisture Transfer in Porous Media	32
2.3	Investigations into Heat and Moisture Transport in Buildings	39
2.4	Moisture Transfer in Concrete and Cement Paste	47
2.5	The Methods Chosen for Modelling The Coupled Heat and Moisture Transfer in Concrete Buildings in Hong Kong	50
Chapter 3	The Building Heat and Moisture Transfer Model Based on Hunag's Equations	53
3.1	Huang's Equations for Coupled Heat and Moisture Transfer	54
3.1.1	Assumptions	54
3.1.2	The Governing Equations	54
3.2	The Finite Difference Model Based on Huang's Equations	56
3.2.1	Interior Nodes	56
3.2.2	Boundary Nodes	58
3.2.3	Interface Nodes	60
3.2.4	Summary of Finite Difference Equations for a Composite Wall or Slab	60
3.3	Convective Heat and Moisture Fluxes at Boundary Surfaces	61
3.4	Comparative Studies on Significance of Driving Forces for Moisture Transfer	63
3.4.1	Results Obtained by Using the Numerical Model	63
3.4.2	Moisture Flux Components	63

	3.4.3 Correlations Among Various Driving Potentials	64
	3.4.4 Conclusions From The Comparative Studies	65
Chapter 4	A Differential Permeability Model for Simulating Building Heat and Moisture Transfer	66
4.1	An Overview of the Differential Permeability Model	67
4.2	Permeability and Differential Permeability	68
4.3	Calculation of Differential Permeability	70
4.3.1	Approximate Formula for Differential Permeability	70
4.3.2	Comparison with Equation in Huang's Model	71
4.4	Governing Equations of the Differential Permeability Model	72
4.5	Derivatives of the Sorption Isotherm Equation	75
4.6	The Numerical Heat and Moisture Transfer Model	76
4.6.1	The Self-implicit Discretization Scheme and the Runge-Kutta-Merson Method	76
4.6.2	The Merits of The Numerical Scheme	78
4.6.3	Finite Difference Equations for Interior Nodes	79
4.6.4	Finite Difference Equations for Boundary Nodes	80
4.6.5	Finite Difference Equations for Interface Nodes	81
4.6.6	Summary of Equations	84
4.7	Heat and Mass Fluxes at Boundary Surfaces	85
4.7.1	Convective Heat and Mass Fluxes	85
4.7.2	Radiation Heat Flux	87
4.8	Window Model	89
4.9	Air Node Model	91
4.9.1	Sensible Heat Balance Equation	91
4.9.2	Moisture Mass Balance Equation	92
4.9.3	The Air-node Model	92
4.10	Air-conditioning System Operating Conditions	94
4.10.1	"Perfect" Air-conditioning System	94
4.10.2	"Shut-down" Mode	94

4.10.3	"Realistic" Air-conditioning System	94
4.11	Verification of the Differential Permeability Model	95
4.11.1	Drying of a Concrete Slab	95
4.11.2	Drying of a Piece of Gypsum Board	96
Chapter 5	Modelling Air-conditioning Systems	97
5.1	General Approach of System Modelling	97
5.1.1	Component and System Modelling	97
5.1.2	Sequential and Simultaneous Modelling	99
5.2	Air-conditioning System Component Models Developed	100
5.3	Cooling and Dehumidifying Coil Models	101
5.3.1	Coil Configuration	101
5.3.2	Functions of the Coil Model	102
5.3.3	The LMHD and the Finite Difference Coil Models	104
5.3.4	On-coil Air Condition	105
5.4	The Temperature Control System	106
5.4.1	On/Off Control	106
5.4.2	P, PI and PID Controls	107
5.5	Control Valve Model	109
5.5.1	On/Off Valve	109
5.5.2	Linear Control Valve	110
5.5.3	Equal Percentage Valve	110
5.6	Hydronic Flow and Pressure Drop Models	113
5.7	Other System Component Characteristics	115
Chapter 6	A Finite Difference Dynamic Model for a Cooling and Dehumidifying Coil	117
6.1	The Approach for Modelling the Dynamic Performance of a Cooling and Dehumidifying Coil	117
6.2	Idealization of the Coil Construction	119
6.2.1	Geometric Parameters	120
6.2.2	Flow Parameters	122

6.3	Derivation of Governing Equations of the Coil Model	122
6.3.1	Mass Balance on Vapour Moisture in Air-flow	123
6.3.2	Heat Balance on Air-flow	123
6.3.3	Heat Balance on Water Flow	125
6.3.4	Heat Balance on the Tube-core	125
6.3.5	Heat Balance on the Fin-core	126
6.4	Change of Variables	127
6.5	Solution by Finite Difference Method	129
6.5.1	Discretization Scheme	129
6.5.2	Partial Discretization of the Governing PDEs for the Coil	130
6.5.3	Summary of Partially Discretized Equations	134
6.5.4	Fin-core and Tube-core Equations	137
6.5.5	Solving the Governing Equations for Different Variables in Sequence	138
6.5.6	Coil Surface Conditions	140
6.6	Steady-state Version of the Finite Difference Coil Model	141
Chapter 7	Results of Test-runs with the Log Mean Enthalpy Difference (LMHD) and the Finite Difference (FD) Coil Models	143
7.1	Verification of Steady-state Performance Predictions by the Coil Models	143
7.1.1	Effect of Contact Resistance	145
7.1.2	Flat-fins	146
7.1.3	Corrugated Fins with Beecher & Fagan's Correlations Applied to Both Sensible and Total Heat (and Mass) Transfer Coefficients	147
7.1.4	Corrugated Fins with Beecher & Fagan's Correlations Applied to Correct the Sensible Heat Transfer Coefficients Only	147
7.1.5	Discussions on Comparison of Steady-state Model Predictions	148
7.2	Part-load Performance of a Cooling and Dehumidifying Coil	150
7.3	Dynamic Performance of a Cooling and Dehumidifying Coil	153

7.4	Verification of the FD Dynamic Coil Model	154
7.4.1	Comparison with Stoecker et al's Experimental Results	154
7.4.2	Comparison with Tamm & Green's Experimental Results	155
7.4.3	Comparison with Maxwell et al's Experimental Results	157
Chapter 8	The integrated Building and Air-conditioning System Models	159
8.1	The Integrated Models	159
8.1.1	Construction of the Room	161
8.1.2	Configuration of the Air-conditioning System	162
8.1.3	The Inter-relationships Amongst Component Models	163
8.2	The Numerical Solution Methods Adopted	164
8.3	Time Progress Control in the Integrated Model and Staggering of Time Progress in the DERMAC Model	167
8.3.1	Time-step Size Control	167
8.3.2	Staggered Time Progress in the DERMAC Model	168
8.4	Outdoor Weather Input Data	171
8.5	Heat and Moisture Transport Properties Data	172
Chapter 9	Results and Discussion of Simulaiton Studies	174
9.1	Simulation Studies Performed	174
9.1.1	Objectives of the Simulation Studies	174
9.1.2	Model Room Construction and Characteristics of the Air-conditioning System	175
9.1.3	Verification of the Predictive Accuracy of the Integrated Model	176
9.1.4	Cases Studied by Computer Simulation Using the Integrated Model	177
9.2	The First Set of Simulation Studies (Pilot Studies)	181
9.2.1	Initialization Runs with "Perfect" and Continuous Air-conditioning (Cases 1.1 & 1.2)	181
9.2.2	Simulation of Indoor Air Conditionings Under Intermittent Air-conditioning	183

9.2.2.1	Results Obtained by Using Model RKMACC (Case 1.3)	184
9.2.2.2	Results Obtained by Using Model DERMAC (Cases 1.4a & b)	187
9.2.3	The Case With Moisture Adsorption and Desorption at the Building Fabric Ignored (Case 1.5)	191
9.2.4	Cases with Proportional Control and Equal Percentage Valve (Case 1.6)	192
9.2.5	The Cases with No Infiltration (Case 1.7) and Doubled Infiltration Rates (Cases 1.8a & b)	194
9.3	The Second Set of Simulation Studies	195
9.3.1	The Initialization Run (Case 2.1)	196
9.3.2	Intermittent Air-conditioning with On/Off Control (Cases 2.2 & 2.3)	197
9.3.3	The Cases with Pretreated Fresh Air (Cases 2.5 & 2.6)	198
9.3.4	The Case of Air-conditioning Following a Prolonged Shut Down Period (Case 2.7)	199
9.4	Observations from Results of the Simulation Studies	201
9.5	Verification of Model Predictions	202
9.5.1	Conditions of the Measurement	203
9.5.2	Comparison of Model Predictions with Measured Results	204
Chapter 10	Conclusions and Recommended Further Work	207
10.1	Modelling Coupled Heat and Moisture Transfer in Porous Building Materials	208
10.2	Modelling Performance of Air-conditioning Systems	210
10.3	The Numerical Method	213
10.4	The Integrated Building and System Models and Simulation Results	214
10.5	Applications of the Models	217
10.6	Recommended Further Work	218

Tables	221-244
Figures	245-346
References	347-357

Appendix A	The Numerical Scheme Adopted to Solve Differential Equations of the Building and System Models	A1 - A17
Appendix B	A Steady-State Cooling and Dehumidifying Coil Model	B1 - B39
Appendix C	Miscellaneous Methods Used in the Building Model	C1 - C11
Appendix D	Publications Originated from this Work	D1 - D18

List of Tables

	Page
<u>Chapter 3</u>	
Table 3.1	Expressions for evaluation of coefficients in Huang's equations 221
Table 3.2	The finite differencing scheme applied to Huang's equations 222
Table 3.3	Expressions for coefficients in finite difference equations
a)	For interior nodes 223
b)	For boundary nodes 224
c)	For interface nodes 225
Table 3.4	Reference conditions of the simulation studies on drying of a slab of concrete and cement paste 226
<u>Chapter 4</u>	
Table 4.1	Coefficients of the differential permeability wall/slab heat and moisture transfer model - 1 228
Table 4.2	Coefficients of the differential permeability wall/slab heat and moisture transfer model - 2 229
Table 4.3	Reference conditions of Thomas and Burch's experiment on drying of a slab of gypsum board 231
<u>Chapter 6</u>	
Table 6.1	Coefficients in governing equations for a dry coil 232
Table 6.2	Coefficients in governing equations for a wet coil 234
Table 6.3	Coefficients in the fin and tube core equations for a dry coil 237
Table 6.4	Coefficients in the fin and tube core equations for a wet coil 238
<u>Chapter 7</u>	
Table 7.1	Summary of characteristics of coils tested 240
<u>Chapter 9</u>	
Table 9.1	Material property data of the composite walls, slabs and the window of the model room 243
Table 9.2	Indoor air and usage conditions of the model room 243
Table 9.3	Design cooling load of the model room 244
Table 9.4	Characteristics of the fan-coil unit serving the model room 244

List of Figures

	Page
<u>Chapter 1</u>	
Figure 1.1	Schematic diagram of an air-cooled air-conditioning system 245
Figure 1.2	Variations of coil sensible, latent and total cooling capacities with chilled water flow rate 246
Figure 1.3	Psychrometric cycles of an all-air system at full and part load 247
<u>Chapter 2</u>	
Figure 2.1	a) Typical sorption isotherm of building materials b) Sorption isotherm of cement paste 248
Figure 2.2	A picture of moisture transfer in porous medium 249
<u>Chapter 3</u>	
Figure 3.1	Simulation results on drying of a slab of concrete 250
Figure 3.2	Simulation results on drying of a slab of cement paste 251
Figure 3.3	Comparison of filtration flow and diffusion 252
Figure 3.4	Ratio of filtration flow to total moisture transfer (percent) 252
Figure 3.5	Correlations between vapour flux and gradients of various driving potentials 253
	a) Moisture content gradient
	b) Total pressure gradient
	c) Mole-fraction gradient
	d) Vapour pressure gradient
	e) Temperature gradient
<u>Chapter 4</u>	
Figure 4.1	Comparison of permeability values based on Huang's equation and the simplified equation 254
Figure 4.2	Discretization scheme for a wall or slab 255
Figure 4.3	Boundary control volume of a wall or slab 255
Figure 4.4	Control volume at the interface plane 255
Figure 4.5	Simulation results from differential permeability model on drying of a slab of concrete 256
Figure 4.6	Comparison of simulation results between Huang's model and differential permeability model 257
Figure 4.7	Comparison of moisture desorption rates from experiment (by Thomas & Burch 1990) and differential permeability model 258
<u>Chapter 5</u>	
Figure 5.1	Input/output relationship of a component model 259
Figure 5.2	A unidirectional sequence of component models 259

Figure 5.3	Looped relationship of component models	259
Figure 5.4	Schematic diagram of an air-handling system	260
Figure 5.5	Enlarged view of tubes and fins in an air-conditioning coil	260
Figure 5.6	Fin corrugation patterns	260
Figure 5.7	Rectangular and triangular tube arrays	261
Figure 5.8	Indoor temperature variation pattern with on/off control	262
Figure 5.9	Typical inherent characteristics of an equal percentage valve	263
Figure 5.10	Schematic diagram of a branch chilled water circuit	264
<u>Chapter 6</u>		
Figure 6.1	Configuration of the single tube, counterflow heat exchanger model for a cooling and dehumidifying coil	265
Figure 6.2	Elemental section in the idealized coil	265
Figure 6.3	Cross-section of the idealized coil	265
Figure 6.4	Discretization of the idealized coil	266
<u>Chapter 7</u>		
Figure 7.1	Comparison of simulated results with catalogue data (flat fins) a) Coil sensible cooling capacity b) Coil latent cooling capacity c) Coil total cooling capacity	267
Figure 7.2	Comparison of simulated results with catalogue data (corrugated fins; B & F's corrections applied to both sensible and latent heat transfer) a) Coil sensible cooling capacity b) Coil latent cooling capacity c) Coil total cooling capacity	268
Figure 7.3	Comparison of simulated results with catalogue data (corrugated fins; B & F's corrections applied to sensible heat transfer only) a) Coil sensible cooling capacity b) Coil latent cooling capacity c) Coil total cooling capacity	269
Figure 7.4	Variations of coil performance with chilled water flow rate a) Cooling capacity b) Leaving air and water temperatures c) Leaving air humidity ratio	270
Figure 7.5	Dynamic performance of a cooling and dehumidifying coil a) Variation of indoor temperature b) Leaving coil air temperature c) Leaving coil air humidity ratio d) Leaving coil water temperature	271
Figure 7.6	Comparison of dynamic coil model predictions with experimental data from Stoecker et al (1978)	272

Figure 7.7	Comparison of dynamic coil model predictions with experimental data from Tamm & Green (1973)	273
Figure 7.8	Comparison of dynamic coil model predictions with experimental data from Maxwell et al (1989)	274
<u>Chapter 8</u>		
Figure 8.1	Configuration of the room modelled	275
Figure 8.2	Inter-relationships between component models in the integrated model	276
Figure 8.3	Staggered time progress in building and air-conditioning system component models	277
<u>Chapter 9</u>		
Figure 9.1	Construction of the composite walls and slabs of the model room	277
<u>First Set of Simulation Results (Figures 9.2 - 9.12)</u>		
Figure 9.2	Initialization run (first round), continuously air-conditioned by a perfect air-conditioning system from 0:00 1/7/80 to 8:30 4/7/80	
a)	Wall internal surfaces conditions	278
b)	Heat & moisture gains and room cooling load	279
c)	Indoor and outdoor conditions	280
Figure 9.3	Initialization run (second round), continuously air-conditioned by a perfect air-conditioning system from 8:30 1/7/80 to 8:30 4/7/80	
a)	Wall internal surfaces conditions	281
b)	Heat & moisture gains and room cooling load	282
Figure 9.4	Intermittent air-conditioning by LMHD coil model with on/off control from 8:30 4/7/80 to 17:00 5/7/80	
a)	Wall internal surfaces conditions	283
b)	Heat & moisture gains and room cooling load	284
c)	Indoor and outdoor conditions	285
Figure 9.5	Intermittent air-conditioning by FD coil model with on/off control from 8:30 4/7/80 to 17:00 5/7/80	
a)	Wall internal surfaces conditions	286
b)	Heat & moisture gains and room cooling load	287
c)	Indoor and outdoor conditions	288
d)	Variations in indoor and supply air conditions and cooling output of the coil within a short interval	289
Figure 9.6	Intermittent air-conditioning by FD coil model with on/off control from 17:00 5/7/80 to 17:00 7/7/80	
a)	Wall internal surfaces conditions	291
b)	Heat & moisture gains and room cooling load	292
c)	Indoor and outdoor conditions	293
Figure 9.7	Intermittent air-conditioning by FD coil model with on/off control from 8:30 4/7/80 to 17:00 7/7/80	294
a)	Moisture content at interior nodes of Wall 1	
b)	Moisture content distribution in Wall 1	
c)	Moisture content at interior nodes of Wall 2	
d)	Moisture content distribution in Wall 2	

Figure 9.8	Intermittent air-conditioning by LMHD coil model with on/off control from 8:30 4/7/80 to 17:00 7/7/80 and with wall moisture adsorption and desorption ignored	
a)	Wall internal surfaces conditions	295
b)	Heat & moisture gains and room cooling load	296
c)	Indoor and outdoor conditions	297
Figure 9.9	Intermittent air-conditioning by LMHD coil model with proportional control from 8:30 4/7/80 to 17:00 5/7/80	
a)	Wall internal surfaces conditions	298
b)	Heat & moisture gains and room cooling load	299
c)	Indoor and outdoor conditions	300
Figure 9.10	Intermittent air-conditioning by LMHD coil model with proportional control, pretreated fresh air and zero infiltration from 8:30 4/7/80 to 17:00 5/7/80	
a)	Wall internal surfaces conditions	301
b)	Heat & moisture gains and room cooling load	302
c)	Indoor and outdoor conditions	303
Figure 9.11	Intermittent air-conditioning by LMHD coil model with proportional control, pretreated fresh air and infiltration of 1 air-change per hour from 8:30 4/7/80 to 17:00 5/7/80	
a)	Wall internal surfaces conditions	304
b)	Heat & moisture gains and room cooling load	305
c)	Indoor and outdoor conditions	306
Figure 9.12	Intermittent air-conditioning by LMHD coil model with proportional control, pretreated fresh air and infiltration of 1 air-change per hour from 17:00 5/7/80 to 17:00 7/7/80	
a)	Wall internal surfaces conditions	307
b)	Heat & moisture gains and room cooling load	308
c)	Indoor and outdoor conditions	309
	<u>Second Set of Simulation Results (Figures 9.13 - 9.25)</u>	
Figure 9.13	Initialization run, intermittent air-conditioning by a perfect air-conditioning system from 0:00 1/7/80 to 8:30 4/7/80	
a)	Wall internal surfaces conditions	310
b)	Heat & moisture gains and room cooling load	311
c)	Indoor and outdoor conditions	312
Figure 9.14	Initialization run, intermittent air-conditioning by a perfect air-conditioning system from 0:00 1/7/80 to 8:30 4/7/80	313
a)	Moisture content at interior nodes of Wall 1	
b)	Temperature at interior nodes of Wall 1	
c)	Vapour pressure at interior nodes of Wall 1	
Figure 9.15	Initialization run, intermittent air-conditioning by a perfect air-conditioning system from 0:00 1/7/80 to 8:30 4/7/80	314
a)	Moisture content at interior nodes of Wall 2	
b)	Temperature at interior nodes of Wall 2	
c)	Vapour pressure at interior nodes of Wall 2	
Figure 9.16	Intermittent air-conditioning by LMHD coil model with on/off control from 8:30 4/7/80 to 8:30 6/7/80	
a)	Wall internal surfaces conditions	315
b)	Heat & moisture gains and room cooling load	316
c)	Indoor and outdoor conditions	317

Figure 9.17	Intermittent air-conditioning by LMHD coil model with on/off control from 8:30 6/7/80 to 17:00 7/7/80	
a)	Wall internal surfaces conditions	318
b)	Heat & moisture gains and room cooling load	319
c)	Indoor and outdoor conditions	320
Figure 9.18	Intermittent air-conditioning by LMHD coil model with on/off control from 8:30 4/7/80 to 17:00 7/7/80	321
a)	Moisture content at interior nodes of Wall 1	
b)	Moisture content at interior nodes of Wall 2	
Figure 9.19	Intermittent air-conditioning by FD coil model with on/off control from 8:30 4/7/80 to 8:30 6/7/80	
a)	Wall internal surfaces conditions	322
b)	Heat & moisture gains and room cooling load	323
c)	Indoor and outdoor conditions	324
Figure 9.20	Intermittent air-conditioning by FD coil model with on/off control from 8:30 6/7/80 to 17:00 7/7/80	
a)	Wall internal surfaces conditions	325
b)	Heat & moisture gains and room cooling load	326
c)	Indoor and outdoor conditions	327
Figure 9.21	Intermittent air-conditioning by FD coil model with on/off control from 8:30 4/7/80 to 17:00 7/7/80	328
a)	Moisture content at interior nodes of Wall 1	
b)	Moisture content at interior nodes of Wall 2	
Figure 9.22	Comparison of indoor conditions and room cooling loads with and without moisture adsorption and desorption (MAD) at the building fabric	329
a)	Indoor temperature	
b)	Indoor air humidity ratio	
c)	Room sensible cooling load	
d)	Room latent cooling load	
Figure 9.23	Intermittent air-conditioning by LMHD coil model with on/off control & pretreated fresh air from 8:30 4/7/80 to 17:00 5/7/80	
a)	Wall internal surfaces conditions	330
b)	Heat & moisture gains and room cooling load	331
c)	Indoor and outdoor conditions	332
Figure 9.24	Intermittent air-conditioning by LMHD coil model with proportional control and pretreated fresh air from 8:30 4/7/80 to 17:00 5/7/80	
a)	Wall internal surfaces conditions	333
b)	Heat & moisture gains and room cooling load	334
c)	Indoor and outdoor conditions	335
Figure 9.25	Intermittent air-conditioning by FD coil model with no air-conditioning from 8:30 5/7/80 to 8:30 6/7/80 followed by air-conditioning with on/off control from 8:30 6/7/80 to 17:00 6/7/80	
a)	Wall internal surfaces conditions	336
b)	Heat & moisture gains and room cooling load	337
c)	Indoor and outdoor conditions	338

Verification Test Results (Figures 9.26 - 9.28)

Figure 9.26	Intermittent air-conditioning by LMHD coil model with on/off control from 0:00 8/8/91 to 7:30 10/8/91	
a)	Wall internal surfaces conditions	339
b)	Heat & moisture gains and room cooling load	340
c)	Indoor and outdoor conditions	341
Figure 9.27	Intermittent air-conditioning by LMHD coil model with on/off control from 7:30 10/8/91 to 24:00 12/8/91	
a)	Wall internal surfaces conditions	342
b)	Heat & moisture gains and room cooling load	343
c)	Indoor and outdoor conditions	344
Figure 9.28	a) Comparison of indoor conditions on 8 - 9/8/91 measured and predicted (by RKMACC)	345
	b) Comparison of indoor conditions on 10 - 12/8/91 measured and predicted (by RKMACC)	346

Appendix A

Figure A.1	Comparison of solutions by explicit and self-implicit schemes with analytical solution	A15
Figure A.2	Comparison of errors of solutions by explicit and self-implicit schemes	A16
Figure A.3	Comparison of integration step sizes by explicit and self-implicit schemes	A16
Figure A.4	Comparison of mid-plane temperatures predicted by numerical model with analytical solution	A17

Appendix B

Figure B.1	Air and water temperature profiles in a cooling and dehumidifying coil	B38
Figure B.2	Water circuit arrangement in a coil	B39

Appendix C

Figure C.1	Two identical rectangular planes parallel to each other	C9
Figure C.2	Two rectangular planes perpendicular to each other and with a common edge	C9
Figure C.3	Two arbitrary planes	C10
Figure C.4	Two parallel planes with parallel edges	C10
Figure C.5	Two perpendicular planes	C11
Figure C.6	Wind direction relative to a wall	C11

List of Symbols

A	area
a	a general coefficient; or the constant of integration in equation (2.6)
A_a	face (frontal) area of a coil (m ²)
A_{ijk}	coefficients in building or coil model equations
A'_{ijk}	coefficients in dry coil model equations
A_i to L_i	coefficients in Huang's equation (for i = 1, 2 and 3)
a_{ij}	matrix elements
A_{mc}	area of fin collar based on mean diameter (m ²)
A_{mt}	area of coil tube based on mean diameter (m ²)
B_{ij} to H_{ij}	coefficients in building or coil models
b_{ij}	matrix elements
C	mass concentration (kg/m ³ of bulk volume); or heat capacity (J/kgK)(in equation 2.15); or capacity rate in coil models (W/K); or the correlation coefficient as defined in equation (B.66) (1/K); or a general coefficient
c_{ij}	matrix elements
C_n	circuit number of a coil
C_p	specific heat (J/kg K)
C_v	flow coefficient of control valve (m ³ /s Pa ^{1/2})
D	diffusivity of water vapour in air (m ² /s); or control differential in controls
d or D	diameter or depth (m)
D_h	hydraulic mean depth (m)
D_i	inner diameter of the tube (m)
d_i	column vector elements
D_o	outer diameter of the fin collar (m)
f	friction factor; or a general function
F_s	coil surface factor
G	gain in controls
h & h_o	convective heat transfer coefficient (W/m ² K)
h	specific enthalph (J/kg K)
h_{fg}	heat of evaporation or condensation (J/kg)
h_m & h_d	mass transfer coefficient (m/s) & (kg/m ² s)

h_{fg}^0	heat of evaporation or condensation at free liquid surface (J/kg)
I	solar intensity (W/m^2)
J	mass flux ($kg/m^2/s$)
j	Chilton-Colburn j factor
J_v	vapour flux (kg/m^2s)
K	Coefficients in equations (2.16 and 2.17); or flow conductance of pipe fittings (m^6/s^2Pa)
k	thermal conductivity (W/mK)
k_i	incremental terms in Rung-Kutta-Merson scheme
L	thickness or length (m)
L_{eq}	equivalent length of pipe fittings (m)
M	molecular weight of the gas or component (kg/mol); or mass transfer potential (0M) in Luikov's model
m	volumetric moisture content (m^3/m^3) or mass (kg)
m_v''	moisture flux at boundary surface (kg/m^2s)
n	number of moles per unit volume (mol/m^3); or a number
N_r	number of rows of a coil
N_{tu}	number of transfer unit
P	pressure (N/m^2 or Pa); or perimeter length (m)
P_d	fin pattern depth (m)
P_g	total gas pressure (Pa)
Pr	Prandtl number
P_v	water vapour pressure (Pa)
P_{vs}	saturated water vapour pressure (Pa)
P_v^0	free surface water vapour pressure (Pa)
Q	heat gain (W)
q	heat flux (W/m^2K)
q_c	convective heat flux (W/m^2)
q_r	radiant heat flux (W/m^2)
q''	heat flux at boundary surface (W/m^2)
$Q_{ac,s}$	the rate of sensible heat removal from room air by the air-conditioning system (W)
$Q_{inf,s}$	the sensible heat gain rate due to infiltration of outdoor air into the room (W)
$Q_{int,s}$	the total sensible heat release rate from internal sources (e.g. occupants and lighting) (W)

$q_{c,i}''$	convective heat flux from wall i (W/m^2)
R	thermal resistance ($\text{m}^2\text{K}/\text{W}$)
R	universal gas constant ($\text{J}/\text{kmol K}$)
r	radius of curvature of liquid surface (m); or surface radiation reflectance
Re	Reynolds number
RH	relative humidity
S	source or sink term in equation (2.10) or valve position (m)
s	fractional valve position; or fin spacing in a coil (m)
T	temperature (K)
t	time (temporal dimension) (s)
TR	throttling range in controls
U	moisture content by mass (kg/kg dry mass of medium)
u	flow velocity (m/s)
W	width (m)
w	humidity ratio of air (kg/kg dry air)
X	vector of variables
x	length measurement (spatial dimension) (m)
x_a	transverse tube spacing in a coil (m)
x_b	longitudinal tube spacing in a coil (m)
x_f	half of the length of one fin pattern (m)
y	controller output; or fin thickness (m) or a general function
\dot{m}	mass flow rate (kg/s)
\dot{V}	volume flow rate (m^3/s)
\dot{e}	evaporation rate ($\text{kg}/\text{m}^3\text{s}$)
\dot{W}_{ac}	moisture removal rate by air-conditioning system (kg/s)
\dot{W}_{inf}	moisture gain from infiltration (kg/s)
\dot{W}_{int}	moisture release rate from internal sources (kg/s)

Greek symbols

α	radiation adsorptance or thermal diffusivity
δ	permeability ($\text{kg}/\text{Pa ms}$ or s)

ε	heat exchanger effectiveness; or surface radiation emissivity; or truncation error of numerical scheme
ε_g	volume fraction of gases in a porous medium (m^3/m^3)
ε_l	volume fraction of liquid water in a porous medium (m^3/m^3)
ε_o	void fraction of a porous medium at dry state (m^3/m^3)
ϕ	mole fraction of water vapour in a dry-air/water vapour mixture (kmol/kmol); or a general variable or function
η_f	fin efficiency
η_s	surface effectiveness
φ	a general function
κ_g^o	permeability of gas by filtration flow through a dry porous material (m^2)
λ	coefficient in Crank-Nicolson scheme
μ	differential permeability (kg/Pa ms or s); or viscosity of fluid (kg/ms)
μ_g	viscosity of gas (kg/ms)
ν	kinematic viscosity (m^2/s)
\in	deviation signal in controls
θ	fin pattern angle (rad)
ρ	density (kg/m^3)
σ	surface tension of liquid water surface; or or Stefan-Boltzmann's constant ($\text{W}/\text{m}^2\text{K}^4$); or contraction ratio in a coil
τ	transmittance
v_w	fractional water flow rate
ζ	pressure loss coefficient of pipe fitting
ξ	dimensionless coil length (in the air-flow direction)
ζ_g	relative permeability when there is liquid moisture in the porous system

Subscripts

+	the node to the right adjacent to the current node
1	air on-coil plane in a coil
2	air leaving-coil plane in a coil
a	air; or adjacent node
atm	atmospheric
B	bulk (mass averaged) quantity

b	black body; or dry/wet boundary in a coil or fin base condition
c	fin-core; cold fluid
ct	contact
cw	chilled water
d	dry air condition
f	flow; or fouling (in equation B.7 & 9)
fa	fresh air condition
G	window glass
g	gas mixture (dry-air and water vapour)
i	internal
inf	infiltration
l	liquid or leaving coil condition
m	mass
max	maximum
min	minimum
o	outdoor condition; or external condition; or external surface of fin-core in coil model
oc	on-coil conditions
r	radiant component; or room condition
rm	room condition
s	solid or saturated state or surface
sa	supply air
so	fin surface condition in coil models
sr	surrounding
T	temperature
t	total
tb	tube
v	water vapour
w	water
–	the node to the left adjacent to the current node

Superscript

n	the n th (the last solved) time step; or exponent in Kingery's formula (equation 4.14); or exponent associated with Prandtl number in correlations for Nusselt Number
n+1	the n+1 th time step
n-1	the n-1 th time step

Chapter One

Introduction

1.1 Background

Being made of porous materials, the fabric of a building (and the hygroscopic materials inside) can adsorb and release moisture from and to the indoor air. The moisture capacity of these materials, coupled with the hot and humid weather conditions and intermittent air-conditioning, can significantly affect the indoor air humidity inside a building. Besides, the reduced dehumidification capacity of an air-conditioning system while operating under "part-load" conditions should also be a major cause of high indoor air humidity. Moisture adsorption and desorption at building materials was shown to have a significant effect on building cooling load by the measurements carried out by Wong & Wang ^(1,2) in an office building and in a library building in Hong Kong. Their results show that the latent cooling loads of these buildings during the starting phase of the air-conditioned period were both several times greater than those predicted based on conventional load estimation methods (e.g. 3-5) in which no account was taken of the latent loads due to moisture desorption from the building fabric.

The measurements taken inside an office room in the Hong Kong Polytechnic (see Chapter 9) provided further evidence of the moisture sorption effects of building materials. The measured results show that the indoor humidity level did not reach the outdoor level during the period when the air-conditioning system was shut-down. This

was contradictory to what should have happened if a "site" did not exist for storing part of the moisture transported into the building due to continuous infiltration of humid outdoor air into the building during that period. Moreover, when the air-conditioning system resumed operation after a prolonged shut-down period, it took a much longer time for the air-conditioning system to bring the indoor humidity level down to a steady level, as compared with that for the indoor temperature. This should be due to the moisture desorption from the building fabric and the hygroscopic materials inside the building which imposed an extra dehumidifying load onto the system and that the dehumidifying capacity of the system during the starting phase was insufficient to cater for the dehumidification load. Theoretical and experimental investigations done elsewhere (e.g. 6-10) also confirmed the significance of the moisture adsorption and desorption effects of the building fabric materials and the hygroscopic materials inside buildings.

The effects of the moisture capacity of building materials however are not well understood and most design engineers are unaware of the consequential problems and therefore would not take them into account in system designs. One possible reason for this was that relative humidity of indoor air has only a moderate effect on the thermal comfort of occupants ⁽¹¹⁾. When the indoor humidity is high, thermal comfort may be retained by slightly lowering the indoor temperature. As air-conditioning systems are often over-sized, the equipment could cope with the extra cooling load incurred by the lowered indoor temperature and the dehumidification performance of the equipment would also improve with an increased sensible load. However, to maintain such a low indoor temperature would incur more energy be consumed in buildings for air-conditioning and therefore is undesirable. It has been estimated that by lowering the indoor set-point temperature in an office building by 1 °C, the year round energy consumption for air-conditioning will be increased by about 4% ⁽¹²⁾. Nevertheless, as the occupants were satisfied with the indoor environmental conditions, no complaints would arise and hence neither the operational and maintenance personnel nor the designers were aware of the humidity problem.

At present, the established methodologies for estimating heat and mass transfer across building envelopes (e.g. 3-5) cannot predict the effects of moisture adsorption and desorption at the building fabric materials. Those for predicting the part-load and the dynamic performance of the components of air-conditioning systems, particularly the cooling and dehumidifying coils, require improvement before they can be applied to realistically model the performance of an air-conditioning system. This research therefore was aimed at developing such methodologies through which the combined effects of infiltration of hot and humid outdoor air into buildings, the moisture capacity of the building fabric materials and the varying dehumidification performance of the air-conditioning system can be more clearly seen and quantified. When this is possible, the significance of such effects can be assessed and properly taken into account in designs of buildings and air-conditioning systems.

The methodologies developed and the findings of this research are detailed in this thesis. In this chapter, the weather conditions, the buildings and the use of air-conditioning in buildings in Hong Kong are introduced, a qualitative analysis of the problem is described, the limitations of existing building and plant performance simulation programs are reviewed, the objectives of this research are elaborated and the work done are summarized. Finally, the organization of the thesis is outlined.

1.2 An Overview of Weather Conditions, Buildings and Air-conditioning Systems in Hong Kong

1.2.1 Weather Conditions and Buildings in Hong Kong

Hong Kong is a small, densely populated city situated at the southern coast of China. The prevailing weather condition in Hong Kong is hot and humid. In summer, afternoon temperatures often exceed 32°C whereas at night, temperatures generally remain around 26°C. High humidity persists throughout the year; in 1990, the year-round average relative humidity was 79% with monthly average values deviating from it by at most 10% (13).

The total land area of Hong Kong is about one thousand square kilometers only but the total population of Hong Kong is currently around six million. Nevertheless, over 80% of the land in the territory is hilly and hence built-up areas in Hong Kong are concentrated on less than 20% of its total land area ⁽¹⁴⁾. Therefore, the land price in Hong Kong is very high and there are many high rise buildings in Hong Kong to provide the residential, commercial and industrial premises for dwelling and for the support of various kinds of commercial and industrial activities.

Concrete is extensively used in Hong Kong for construction of various kinds of buildings because it has good all-round properties as a building material and raw materials for its production are readily available (cement can be conveniently imported from China whereas good quality aggregate materials, including sand and gravel, can be dredged from offshore areas of Hong Kong ⁽¹⁴⁾). Nonetheless, concrete is a porous material having a substantial capacity for moisture (see Section 2.4).

1.2.2 Use of Air-conditioning in Buildings in Hong Kong

Air-conditioning systems in commercial and residential buildings serve to maintain comfortable indoor environmental conditions. In industrial buildings, besides providing a comfortable condition for the workers, air-conditioning is provided to maintain the required environmental conditions for special manufacturing processes (e.g. in textile mills and in integrated circuits production plants) or for proper storage of special equipments (e.g. computers, electronic products). Due to the hot and humid climate and along with the rise in living standard, air-conditioning is gradually becoming a necessity in Hong Kong.

The widespread use of air-conditioning in buildings in Hong Kong can be seen from the statistics of electricity consumption in that about half of the total amount of electricity generated by power plants in Hong Kong is consumed in commercial buildings ⁽¹⁵⁾. In such buildings, more than half of the total electricity consumption is consumed by air-conditioning systems. For domestic buildings, the difference in

electricity consumption between the second and the third quarter in 1990 was about four thousand Terajoule (TJ, i.e. 10^{12} J) which was primarily due to the more frequent use of air-conditioners in the third quarter, the hottest months in Hong Kong. This amount of electricity is sufficient for 680,000 units of one horse power air-conditioner to run continuously over the three months and costs about seven hundred million Hong Kong dollars.

1.2.3 Configuration and Operation of Central Air-conditioning Systems

Most medium to large size commercial and office buildings and a large number of modern industrial buildings in Hong Kong are centrally air-conditioned. Centralizing the major air-conditioning equipment (the chillers and the water pumpers) in one single plant room reduces the impact on the facet design of a building and allows more energy efficient equipment (e.g. large centrifugal chillers as opposed to packaged type air-conditioners) be used such that the running cost for providing air-conditioning can be reduced. Window units or packaged type air-conditioners are more common in residential buildings but can also be found in some small commercial buildings. In a central air-conditioning system, control over indoor environmental conditions is performed by the air-handling equipment which comprises basically a fan and a coil and is normally called a fan-coil unit (FCU) if its size is small ($0.19 - 0.57 \text{ m}^3/\text{s}$) or an air-handling unit (AHU) if its size is large ($> 0.57 \text{ m}^3/\text{s}$). Figure 1.1 shows a simplified schematic diagram of an air-cooled central air-conditioning system commonly found in Hong Kong.

For economy in energy expenditure, air-conditioning systems in commercial and office buildings in Hong Kong are generally intermittently operated. That is, during normal working days, the air-conditioning system will be started in the morning half to one hour before the building is occupied and will be shut-down in the evening. It will not be operated on Sundays and public holidays. Continuous air-conditioning is provided only when there are special activities or processes being carried-out in the building or in parts of the building.

1.2.4 Air-conditioning Plant Size

Various methods have been developed for determining the required plant size for providing heating or air-conditioning to buildings. Although the actual heat and mass transfer processes taking place in a building are highly complicated, plant-size determination methods often involve simple calculation procedures which resemble steady-state heat transfer calculation methods (3-5). Cooling load of a building is calculated with reference to the anticipated "peak load" conditions, called design conditions or criteria, which include outdoor design weather conditions and design internal loads.

Sizes of equipment based on the design building cooling load will be larger than required to cope with the actual load that will arise in majority of the operating time and hence, the equipment will often be operating under "part-load". The part-load performance of the equipment therefore is an important aspect to be considered in system design as it will affect the energy consumption for air-conditioning and the control over the indoor thermal environment. Besides, for reasons such as to provide a safety margin in cooling capacity of the plant to cover any inaccuracy or omissions in the load calculation or to reserve a spare capacity for future expansion etc., designers may tend to oversize the equipment but this may lead to low system energy efficiency and poor performance in control of indoor environmental conditions.

1.3 Indoor Humidity and Its Control

Although indoor air humidity has only a moderate affect on thermal comfort of occupants (11), prolonged high indoor humidity (>70%) promotes growth of moulds and mildews at wall and furniture surfaces (16,17) which would affect health of occupants and cause deterioration of building materials (18). However, to provide control over both indoor temperature and humidity requires extra equipment and incurs a higher energy consumption (19). This is not considered essential nor economically viable for many commercial and office buildings where control of the main comfort

indoor condition, temperature, is required. Nevertheless, the system will provide simultaneously a certain amount of dehumidification to the air-conditioned space but this varies with the operating conditions from time to time. Hence, the indoor humidity is actually allowed to "float", depending on the balance between the total rate of moisture gain from various sources and the rate that moisture is extracted by the air-conditioning system. This indirect control of indoor humidity is referred to as "passive humidity control" (20).

Under part-load conditions, indoor relative humidity rising above 70% may occur inside air-conditioned buildings. This is because the reduction in building cooling load is normally dominated by the reduction in the sensible load components (due to a lower solar radiation intensity and a lower outdoor air temperature). During the occupied period, the latent load components vary by a much smaller extent (except at the lunch hour) because the number of occupants in a building, the major source of latent load, is normally rather steady. In response to a reduced room sensible cooling load, the indoor temperature control system will reduce the chilled water flow rate at the cooling coil of the air-handling equipment leading to reductions in both the sensible and latent cooling capacities of the coil (Figure 1.2). Reduction in the latter is due to the increased coil surface temperature given rise by the larger chilled water temperature rise across the coil (Figure 1.2). With a relatively steady room latent load but a reduced dehumidification effect from the cooling coil, the indoor air humidity (or moisture content) will rise. This effect may also be seen by comparing the full-load and part-load psychrometric processes for a conventional all-air system as shown in Figure 1.3.

Although modern high rise buildings with central air-conditioning should have well sealed building envelopes, there will still be infiltration of hot and humid outdoor air, driven into the buildings through various door gaps, unintentionally opened doors and windows or other openings by stack effect and wind pressure (5). In building cooling load estimation, an infiltration rate of not less than half air-change per hour is allowed to cater for the extra cooling and dehumidification load incurred (5). When the

air-conditioning system is shut-down, infiltration of hot and humid outdoor air into the building continues and consequently, the indoor humidity level will rise. This is a major factor that gives rise to moisture problems in buildings in humid climate regions.

1.4 Effects of Moisture Adsorption and Desorption of the Building Fabric

With intermittent air-conditioning, the moisture adsorption and desorption effect of building materials significantly affects the indoor humidity level (e.g. 1, 2, 6-10). This arises because most building materials like concrete, cement plastering, wood, wall finishes, etc. are porous materials having large amount of minute void spaces within them (21). The porous building materials will exchange moisture with the indoor air (and with the outdoor air for the external walls) and a substantial amount of moisture can be detained within the voids inside the porous building materials. This provides a storage capacity for indoor moisture, similar to the thermal storage effect for sensible heat load.

Exchange of moisture between the room air and the surface of the porous building material is affected by a difference in vapour pressure between the two. When the air-conditioning system is shut-down, both temperature and vapour pressure of the room air will increase. When the room air vapour pressure becomes higher than the surface vapour pressure of the walls, moisture will start to be adsorbed into the pores within the wall. Similar events happen to furniture and other hygroscopic materials inside the air-conditioned space. This moisture adsorption phenomenon helps maintaining the indoor humidity at a level that is substantially lower than the outdoor humidity. Otherwise, the room air humidity will quickly approach the outdoor level. When air-conditioning is resumed in the following day, the room air temperature and vapour pressure will quickly drop and consequently, the adsorbed moisture will be released back to the room air. This imposes an extra latent load on the air-conditioning system and lengthens the time required for the air-conditioning system to bring the

indoor air humidity back to the controllable range (see simulation study results in Chapter 9).

1.5 Detailed Simulation of Building Thermal Response and Air-conditioning System Performance

Although understanding of the phenomena of building fabric moisture adsorption and desorption and the ability to quantify their effects are important to the proper design and operation of buildings and air-conditioning systems in places with hot and humid weather, insufficient attention has been paid to this subject area and the effects are not fully understood. To quantify and to rigorously evaluate their effects in conjunction with the effects of intermittent air-conditioning require simultaneous modelling of the coupled heat and moisture transfer at the building fabric and the performance of the air-conditioning system. The dehumidification performance of an air-conditioning system is dependent on the characteristics of the air-handling equipment and the type of controls employed. With passive humidity control, performance of the air-handling equipment has to be modelled in detail in order to accurately predict the indoor humidity.

1.5.1 Detailed Building Thermal Response Modelling Methods

There are well established methods for detailed modelling of heat transfer in buildings. Those that are widely used include the Admittance Method (22,23), the Response Factor Method (24) and the Transfer Function Method (25,26). These methods have a common feature in that all of them are based on the analytical solutions of the one-dimensional dynamic heat conduction equation but each adopts a different approach in solving the governing equation. In these methods, the assumption is made that the thermal properties of the materials are constants and hence the governing equation becomes a linear equation. This allows the solutions be obtained when the boundary conditions are arbitrary functions of time (e.g. the outdoor weather conditions) by representing the time varying functions as series of harmonic functions (as in the

Admittance Method) or series of pulses (as in the Response Factor Method and the Transfer Function Method), and by applying the superposition principle. Instead of these special techniques, solving directly the governing equation using numerical methods (e.g. Finite-Difference Method) is also a common approach in building thermal response modelling. However, equally well established and widely adopted methods for modelling the coupled heat and moisture transfer in buildings are not yet available (see review in Chapter Two).

1.5.2 System Performance Modelling

Since air-conditioning and refrigeration processes are basically heat, mass and work transfer processes, fundamental principles of these processes have long been established (e.g. 5,27,28) and applied extensively in determining the rates of heat, mass and work transfers in air-conditioning equipment. Although the basic working principles of equipment and components in an air-conditioning system may be simple, complicated geometric configurations and complex fluid flow situations may be found. Therefore, rigorous modelling of the heat, mass and work transfer processes involved can be complicated and simplifications are often made to overcome this.

As there are wide-ranging degrees of complexity of equipment in an air-conditioning system, different approaches and simplifications are taken to model the performance of various components. For complex equipment such as the centrifugal refrigerant compressor of a chiller, water pumps and fans, the modelling of dynamics of fluid flow in these machines can be extremely complicated. One simple but widely adopted way to model performance of such equipment is to resort to manufacturers' data. Based on the "catalogue" performance data, mathematical models can be derived by applying curve-fitting techniques (27,29). However, a curve-fit model is restricted in applications to the specific design and size of equipment upon which the model was developed and can, in general, only model the steady-state performance of the equipment. Broadening the applicability of the model is possible by grouping the parameters into dimensionless form and by applying the principle of dynamic

similarities ⁽³⁰⁾ but even so, the resultant model may only be applicable to equipment of similar design and over limited ranges of sizes and operating conditions:

For other less complex equipment, such as certain types of heat exchangers and the ducting and piping systems, one can set-up a model from fundamental principles provided details of construction and accurate data of heat and mass transfer coefficients are available ⁽³¹⁾. However, complex fluid flow situations may be encountered due to enhancements to basic designs of the equipment so as to improve efficiency. Multiple tube passes, baffles and finned surfaces in heat exchangers are examples of design enhancements adopted in compact heat exchangers ⁽³²⁾. When a complex fluid flow situation is encountered, it is impossible to determine the transport coefficients by analytical methods nor can empirically determined values based on simple standard situations be applicable to a realistic plant component (e.g. the convective heat and mass transfer coefficients at surfaces of corrugated fins of a cooling and dehumidifying coil). The required heat and mass transfer coefficients for modelling performance of such equipment have to be determined from purposely designed experiments (e.g. those by McQuiston ^(33,34) for finned coils).

Due to the long history of development, many mathematical models have been developed for modelling various kinds of air-conditioning system equipment and components (e.g. 27-29,31). Also, many of these models have been developed into standard modules in computer simulation programs (e.g. ESP ⁽³⁵⁾, HVACSIM+ ⁽³⁶⁾, TRNSYS ⁽³⁷⁾) from which models of components may be constructed and used to predict the system performance.

Based on the argument that the systems will respond to changes in environmental or operating conditions much more quickly than a building, it was suggested that in building energy calculations, steady-state system models would be adequate ⁽²⁹⁾. This was widely accepted but has become less and less acceptable ⁽³¹⁾. Since the mid-seventies, it has become evident that the success of implementing efficient energy control and management in buildings is coupled with the understanding

of the dynamic performance of the mechanical and control systems ⁽³⁸⁾. Augmented by the advancements and lowering in price of computers, dynamic performance of air-conditioning systems in buildings have been actively studied by computer simulation methods ⁽³⁹⁾. Considerable effort has been paid world-wide to the development of dynamic plant components models for detailed building and plant performance studies and several programs with dynamic system models such as ESP ⁽³⁵⁾ and HVACSIM+ ⁽³⁶⁾ have emerged.

In assessing the dehumidification performance of an air-conditioning system, detailed modelling of the dynamic performance of the cooling coil can be important. This is because the coil surface temperature, the major factor that affects the dehumidification capacity of a cooling coil, will change when there are fluctuations in the on-coil air conditions and in the flow rate and temperature of the chilled water. Its rate of change is dependent on the heat capacities of the coil materials and the chilled water in the tubes of the coil. The use of quasi-steady coil models may provide acceptable results when proportional or proportional plus integral control is adopted because operating conditions in such systems only change gradually. However, when on/off control is used, the dynamic performance of the coil should be adequately modelled as there will be cyclic changes in the chilled water flow rate when the control valve is cycling between the open and closed positions from time to time (see Chapters 7 and 9).

1.5.3 Deficiencies in Existing Building and System Simulation Programs

At present, many building energy calculation and air-conditioning system simulation programs have been developed, e.g. ESP ⁽³⁵⁾, HVACSIM+ ⁽³⁶⁾, TRNSYS ⁽³⁷⁾, DoE2 ⁽⁴⁰⁾, BLAST ⁽⁴¹⁾, to name a few. Unfortunately, none of these programs can simulate indoor humidity variations taking into account the effects of coupled heat and moisture transfer at the building envelope. Although attempts have been made to model the moisture adsorption and desorption effects of building materials, some of the models developed are too simplistic to properly account for the involved transport

phenomena whilst the others are either too complicated for practical applications or are in lack of appropriate moisture transport properties data for use with the models (see Section 2.4). These restrict the models from being practically usable and there remains a lot of further improvements and development to be made. The simultaneous effects of intermittent operation and dynamic performance characteristics of air-conditioning systems have not been thoroughly studied and this formed a major objective of this research.

Besides lacking in the ability to simulate moisture transfer, the models in many building energy and system simulation computer software packages have imperfections which need to be improved. First, thermal properties of building materials are often assumed to be of constant values. Thermal conductivity of building materials however vary significantly with moisture content ⁽⁴²⁾ whereas the moisture content within the material will change as a result of changes in the ambient conditions and temperature distribution across the wall. For instance, the thermal conductivity of a lightweight aggregate concrete deviates by more than 10% over the normally assumed moisture content range of 3 to 5% (by volume) for a concrete external wall ⁽⁴³⁾. Second, radiation energy exchange among internal surfaces of a building zone are often estimated by over-simplified approaches (such as environmental temperatures based on a cubical enclosure with black surfaces ⁽⁴⁾). How a reference temperature should be established for simplified calculations however is still subject to argument ^(44,45) and the accuracy of this kind of method is not always good in cases where the actual temperature differences among internal surfaces are large. Third, in most building and plant load simulation packages (e.g. DoE2 ⁽⁴⁰⁾), building thermal load and system performance are calculated in two stages. The building thermal load is estimated first, based on a constant indoor condition, and system performance is then determined based on the load calculated in the first stage. In reality, system performance affects the thermal load in buildings. Accurate estimation therefore needs a simultaneous simulation ^(31,46).

Even though there are some computer software packages which can model building and system response simultaneously (e.g. ESP ⁽³⁵⁾, HVACSIM+ ⁽³⁶⁾, APACHE ⁽⁴⁷⁾), they were not used in this work for several reasons. The major one was that the building models of these simulation programs cannot simulate moisture transfer at the building fabric. Besides, the air-conditioning system component models in some of them are rather limited (e.g. ESP) and some have only steady-state models (e.g. APACHE) or simplified models (e.g. the dynamic cooling and dehumidifying coil model in HVACSIM+) which may not be able to accurately simulate the operating performance of the equipment. Although attempts could be made to modify the relevant component models included in such a software package or to add new program modules into it so that the package could be used for studying the present problem, this was considered not worthwhile because:

- i) Due to the large differences between the nature of the mathematical models to be handled (e.g. the non-linear coupled heat and moisture transfer model compared with the linear heat transfer model), the simulation methods adopted in the program would need to be modified. For instance, the response factor method used in HVACSIM+ ⁽³⁶⁾ would have to be abandoned and replaced by a numerical solution method.
- ii) The changes may lead to fundamental re-structuring of the program which could only be done if the source codes of the program were available but these are seldom provided with the program (e.g. ESP & APACHE), except for public domain softwares (e.g. HVACSIM+).
- iii) Even the source codes are available, to ensure the new modules will be compatible with the main program and with other existing program modules in the software would be a substantial task whereas such work would divert the attention towards the subject area of "software engineering" which is strictly not relevant to the present study.

On the other hand, attempts are being made to develop methodologies through which building and plant simulation programs can be developed based on "objects" and each one of them can be a component model or a mathematical sub-program (e.g. the Energy Kernel System (48,49)). The objectives of developing such methodologies include allowing objects having different calculation methods and data structures be linked together by the user to become a tailor-made simulation program for a specific purpose. When such methodologies are available, the problem on compatibility between program modules and solution methods of different component models can be solved. Therefore, emphasis of this research was focused on developing generic components models as these models may later be converted into objects for wider applications.

1.6 Research Objectives & Work Undertaken

A suitable computer simulation program is required to facilitate the assessment of the complex, simultaneous effects of outdoor weather variations, intermittent air-conditioning, moisture adsorption and desorption of the building fabric and the dynamic performance of the air-conditioning system. With it, these effects can be properly taken into account in design of buildings and systems. As the existing simulation tools do not have these capabilities, the major objective of this research is to develop the methodologies that are required for its development. Other objectives include giving a better insight into the moisture related problems in intermittently air-conditioned buildings in hot and humid climate regions and assessing the importance of dynamic modelling in simulating the humidity control performance of air-conditioning systems. These are achieved by simulation studies using the prototype simulation programs developed in this research. The objectives, in summary are as follows:

- a) To develop a practical model for simulating the coupled heat and moisture transfer in building fabrics based on the theories of simultaneous heat and moisture transfer in porous media.

- b) To develop practical system and equipment models for simulating the dynamic performance of air-conditioning systems based on the theories of heat and mass transfer in air-conditioning processes.
- c) To develop a prototype computer simulation program, integrating the building heat and moisture transfer model and the air-conditioning system model.
- d) To develop the required procedures for numerical solution of the governing equations defining the thermal and moisture behaviour of the building and the system.
- e) To assess the significance of the moisture sorption effects of the building fabric, intermittent air-conditioning and dynamic performance of the air-conditioning system on the indoor environmental conditions and to assess the effectiveness of passive humidity control of air-conditioning systems by using the prototype simulation program.

In this research, two heat and moisture transfer models have been developed for modelling the moisture sorption effect of building walls and slabs of construction that are typical in Hong Kong (where concrete is the predominant construction material). The first one was developed from the governing heat and moisture transfer equations due to Huang ^(50,51) (Chapter 3) and was used in preliminary investigations in this work ⁽⁵²⁾ (see Appendix D.1). It was abandoned in the later part of the work due to its intensive demand on computing effort.

The second model (called the "differential permeability" model, see Chapter 4 and Appendix D.2) is a simplified model and was used in major studies of this research (Chapters 8 & 9). In this model, moisture transfer was assumed to be dominated by vapour diffusion, driven by the vapour pressure gradient, and differential permeability was taken as the moisture transport property of the material. The differential permeability of a material was regarded as a variable dependent on the moisture content

of the material and an equation for its evaluation has been derived. This model has been applied to simulate an experiment on drying of a piece of gypsum board (by Thomas & Burch ⁽⁵³⁾) and the simulated results were found to be in good agreement with the measured results.

Detailed steady-state and dynamic cooling coil models and mathematical models for other components of the air-side system have also been developed. Both steady-state and dynamic coil models have been developed so that the significance of accounting for the dynamic response of the coil when on/off control was adopted could be studied. Both models had been applied to model the steady-state performance of a range of cooling and dehumidifying coils and the results, as compared to manufacturers' performance data, were within acceptable accuracy. The dynamic model has also been applied to model the performance of several coils that had been tested experimentally and the measured results are available from the literature. The model predictions agreed reasonably well with these results.

The differential permeability building heat and moisture transfer model and the system component models have been integrated to become simultaneous building and system simulation programs. An efficient numerical method was adopted to solve the large set of differential and algebraic equations involved. The accuracy of the numerical method in solving an ordinary differential equation and a partial differential equation has been verified against analytical solutions (see Appendix A). A scheme was also proposed to enable different time steps be employed in simulating the building response and the dynamic performance of the air-conditioning system through which a significant reduction in computer execution time was achieved (see Chapter 8).

The integrated building and system models have been applied to study the dynamic heat and moisture transport phenomena in a typical room of a building and in the associated air-conditioning system. The effect of building fabric moisture adsorption and desorption was shown to be significant when there was infiltration of hot and humid air into an intermittently air-conditioned building in that moisture

entering the building during the non-air-conditioned period could be stored within the porous building fabric materials and would be released back to the room air during the air-conditioned period. Passive indoor humidity control performance of the systems with on/off and proportional control were compared and the importance of modelling the dynamic behaviour of the cooling coil was studied. The methodologies developed in this study for modelling indoor moisture transient variations represent significant improvements over those published in the relevant literature and the breadth and depth of the investigations froming this work represent substantial new work.

1.7 Organization and Outline of the Thesis

This thesis comprises ten chapters which may be grouped into five linked parts as shown in the chart at the last part of this chapter. In this chapter (Chapter One), the problem that has been investigated into is outlined first. This is followed by an overview of the climatic conditions, buildings and air-conditioning systems in Hong Kong. The building fabric moisture adsorption and desorption phenomenon and the combined effects, in conjunction with intermittent air-conditioning, on the indoor environment are introduced. Established methods for building thermal response simulation are reviewed followed by criticisms on their deficiencies. The aims of the research and the work done are briefly summarized.

Part two of this thesis comprises three chapters (Chapters 2-4) which are on modelling of heat and moisture transfer at building fabric materials. Chapter Two starts with a review on fundamentals of coupled heat and moisture transfer in porous media. Various theories proposed for description of the phenomena is outlined and published investigations on moisture transfer in buildings are reviewed. This is followed by considerations of the specific characteristics of moisture transfer in concrete, the predominant construction material in Hong Kong. Finally, the approach taken in this work is introduced.

In Chapter Three, the governing equations derived by Huang (50,51) are introduced and the numerical scheme adopted to develop a computer building heat and moisture transfer model from this set of equations is summarized. Application of the model to investigate the relative significance of various driving forces for moisture transfer in concrete is described and the finding that vapour diffusion being the dominant mechanism is reported. This prompted the development of a simpler model for building heat and moisture transfer. In chapter Four, the governing partial differential equations (PDE's) of the "differential permeability" building heat and moisture transfer model, the "self-implicit" numerical scheme for discretization of the PDE's and the solution technique employed to speed up the solution process are detailed, together with the methods adopted to treat boundary conditions. Further explanations on the numerical scheme are given in Appendix A.

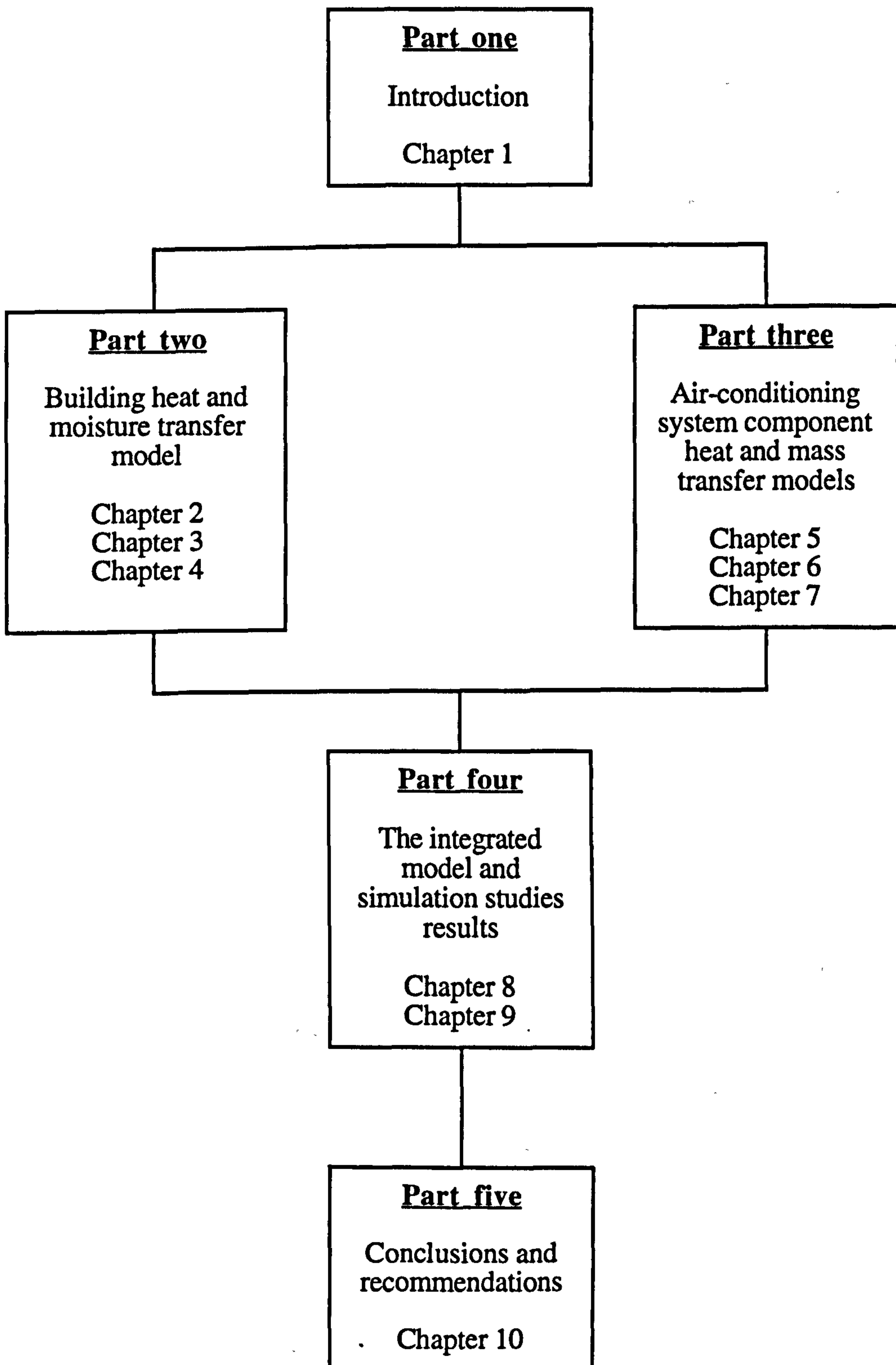
Chapters Five to Seven (part three) are on modelling of air-conditioning system components. Chapter Five consists general descriptions on various air-conditioning system component models developed, covering the controller model, the control valve model, the simple hydraulic system model etc. Appendix B summarizes the step-by-step derivation of the steady-state model (called LMHD model) and Chapter Six shows in detail the derivation of the dynamic finite difference (FD) model for a cooling and dehumidifying coil with corrugated plate fins. Comparisons of predictions of the LMHD steady-state coil model and the FD coil model against manufacturers' performance data and experimental data from the literature are summarized in Chapter Seven.

Chapter Eight describes the methods adopted to integrate the building model with the air-conditioning system models and introduces methods for solving the coupled responses of the building and air-conditioning system. The method adopted to enable different time-step sizes be used in the simultaneous simulation and to co-ordinate the time progress of the two groups of models is explained. Results of numerical experiments carried out by using the integrated building and system models

are summarized and discussed in Chapter Nine. The significance of the moisture effects and the importance of dynamic modelling for air-conditioning system are reported in the this chapter.

Chapter Ten, the last chapter, contains a summary of the findings of application studies done using the integrated models, descriptions on where and how the model should be applied to study moisture problems in buildings and the recommended further work in this subject area which concludes the thesis.

Organization of the thesis



Chapter Two

Modelling Heat and Moisture Transfer in Building Fabrics

To investigate in detail how significantly can moisture adsorption and desorption by porous building materials affect indoor humidity in intermittently air-conditioned buildings requires understanding of the coupled heat and moisture transport processes in porous materials. Although this subject has been studied for more than 50 years and many methods have been proposed for explaining and modelling the phenomena, there is yet no single theory that is universally applicable. Nevertheless, those advanced by Philip & DeVries ⁽⁵⁴⁾, Luikov ⁽⁵⁵⁻⁵⁷⁾, Harmathy ⁽⁵⁸⁻⁶⁰⁾, Berger & Pei ⁽⁶¹⁾, Scheidegger ⁽⁶²⁾ and Whitaker ⁽⁶³⁾ provided much insight into the problem. Heat and moisture transfer models have been applied to study moisture movement in soil (e.g. ⁶⁴) and in drying processes in the chemical industry (e.g. ⁶⁵). Applying the technique to the studies of moisture effects on building materials and on the indoor environment is a recent development.

In this chapter, an overview of fundamental concepts in heat and moisture transfer in porous media is given. Various theories proposed for description of the phenomena and published work on building heat and moisture transfer are reviewed. This is followed by a review of the moisture sorption behaviour of concrete and cement paste. Finally, the approach adopted in this work is introduced.

2.1 Fundamentals of Heat and Moisture Transfer in Porous Media

2.1.1 Equilibrium Moisture Content and Sorption Isotherm

The mechanisms responsible for the detention of moisture within porous solids are highly complicated and are not yet fully understood ⁽⁶⁶⁾. Different solids react differently to changes in moisture content ⁽⁶⁷⁾ - a hygroscopic material (e.g. wood) contains a large amount of physically bound liquid and will shrink or swell as its moisture content changes ⁽⁶⁸⁾ whilst a capillary-porous material (e.g. packed sand) contains a negligible amount of physically bound water and no significant change in volume with moisture content can be observed ⁽⁶⁷⁾. When subjected to a particular steady environment for a sufficiently long time, the porous solid will attain an equilibrium moisture content but value of this will change as the environmental condition changes. A plot of the equilibrium moisture content (m) against relative humidity of the ambient air (RH) under a constant temperature, or the equivalent mathematical expression:

$$m = m(RH) \Big|_{T = \text{const.}} ; \quad RH = \frac{P_v}{P_v^0} \quad (2.1)$$

is generally called the sorption isotherm of the material. This is the most widely accepted way of presenting the moisture sorption characteristics of porous media and is an important piece of information in studies on heat and moisture transfer in porous materials.

Different porous materials may exhibit different shapes of sorption isotherms ⁽⁶⁶⁾ but the S-shaped one (Figure 2.1) is typical among common building materials ⁽⁶⁹⁾. Three regions (Figure 2.1a) can be identified which correspond to different states of moisture that present within the pores ^(58, 69):

- 1) In region I, water is tightly bound to pore surfaces due to forces of attraction between the molecules of the material and the water. Moisture adsorption at this region may be regarded as 'true adsorption' as it is

actually caused by the adsorbent-adsorbate interaction. The range of P_v/P_v^0 covered by this region is from 0 to about 0.4 for many gases/porous material combinations.

- 2) In region II, all pore surfaces are covered by at least one layer of water molecules and more layers of water start to build up. In this region, most water is contained within small capillaries, caused by the formation of curved liquid surfaces in these capillaries, and is relatively more free to move. Capillary condensation is the principal mechanism for accumulation of water in the pores.
- 3) In region III, water is present in the large capillaries, also due to capillary condensation, and therefore the moisture content increases more rapidly with increase in P_v/P_v^0 .

2.1.2 Sorption Hysteresis

In the region of true adsorption (region I in Figure 2.1a), the moisture content in the medium is normally independent of whether the equilibrium state was attained from a higher or lower initial moisture content (concrete and cement paste are exceptions - see 2.4 and Figure 2.1b). In regions II & III, the equilibrium moisture content of a porous solid corresponding to a given environmental condition in general does not have a unique value but is dependent upon whether the solid is adsorbing or desorbing moisture and from which initial condition the sorption process starts. This phenomenon is called sorption hysteresis which may be explained by the "ink-bottle" theory (70,71) and Cohan's "open-pore" theory (72,73) as reviewed by Harmathy (58) and Gregg & Sing (66).

The sorption hysteresis phenomenon leads to problems in the determination of equilibrium moisture content of a porous medium. The biggest hysteresis loop is formed by the adsorption and desorption branches that can be measured by allowing the material to adsorb moisture starting from completely dry to full pore saturation and then

by drying the material back to the completely dry state. For studies involving adsorption or desorption starting from an intermediate moisture content, an 'effective' sorption isotherm, which is normally obtained by scanning tests ^(69,74) (called the scanning curve), has to be used. This scanning curve lies approximately mid-way between the completely dry to fully saturated adsorption and desorption branches and hence may be approximated by an average curve between the two branches (Figure 2.1.b). Since building fabric materials are undergoing repeated cycles of adsorption and desorption due to the periodic changes in outdoor and indoor conditions, an average sorption isotherm may be used in studies of moisture transfer in porous building materials. Pederson ⁽⁷⁵⁾ compared the calculation results obtained by using the average sorption curve against that by using a hysteresis model and concluded that equally good results can be obtained.

2.1.3 Local Thermodynamic Equilibrium

If the hysteresis effect is ignored and an average sorption curve is used as an approximation, the sorption isotherm provides a convenient means for determining the equilibrium moisture content of a porous medium from the knowledge of the value of P_v/P_v^0 or vice versa. However, when the equilibrium condition is upset, exchange of water molecules between the liquid water and the air/vapour mixture within the pores (i.e. evaporation or condensation) will start and transport of moisture from one region to another within the medium or exchange of moisture with the ambient air will follow immediately.

Since deviation from equilibrium is a necessary condition for heat and moisture transfer to take place in a porous medium, it appears therefore that whenever there are heat and moisture transports, the moisture content within the medium could no longer be determined from the equilibrium moisture content relation. This is true if equilibrium of the entire piece of material is concerned. However, based on Kelvin's equation, Claesson ⁽⁷⁷⁾ showed that corresponding to a decrease in ambient relative humidity (or P_v/P_v^0) by just 1%, the reduction in liquid water pressure required to prevent

evaporation whilst maintaining thermodynamic equilibrium within the pores will amount to $13 \times 10^5 \text{ Pa}^*$. The only situation under which a high tension state in the liquid water is possible is when there exists a suitably curved water surface (i.e. surface tension effect). If this cannot be attained, then, the liquid water in the pore will completely evaporate into vapour. Because of the extremely large change in the liquid water pressure in the pores that will result from a small perturbation to the equilibrium condition in a localized region within the medium, the evaporation or condensation process, which will help re-establishing thermodynamic equilibrium in the region, will take place spontaneously. Therefore, the assumption that equilibrium conditions exist in localized regions is valid even during a violent dynamic process.

2.1.4 A Simplified Picture of Moisture Sorption in Porous Media

In reality, the equilibrium condition between the liquid water and water vapour in the pores of a porous medium will be influenced by the presence of salts in the liquid. This gives rise to osmotic pressure which modifies the pressure of the liquid water (77). However, to account for the effects of salts in the liquid within a porous medium will be highly complicated whereas analyses done with such effects ignored provided results that are in good agreement with experimental data (e.g. 1,8,53). Hence, in this work, osmotic effects are ignored. To simplify the analysis further, assumption is made that the substances that present within the pores include only liquid water, water vapour and dry-air. Also, the dry-air is assumed to be a single component gas rather than a mixture of gases (of N_2 , O_2 , etc.); the air/water vapour mixture is assumed to be a binary mixture; and the dry-air, the water vapour and their mixture are all assumed to be perfect gases. Furthermore, the solid phase is assumed to be a single component homogeneous material.

* This abnormally high pressure was purely a theoretical prediction made under simplified assumptions but will not be reached in reality. For example, with the presence of osmotic pressure, the liquid pressure will increase with concentration of the salt in the liquid phase (see also 2.1.4). However, Claesson's analysis points out clearly that there will be large changes in liquid pressure with relative humidity changes.

From equation (2.1) it can be seen that the equilibrium moisture content of a porous material is a function of vapour pressure and temperature, i.e.,

$$m = m(P_v, T) \quad (2.2)$$

Instead of expressing the equilibrium moisture content of porous materials as a function of relative humidity or vapour pressure and temperature, Vassiliou and White (78) proposed that the equilibrium sorption relationship can be expressed as a function of a single parameter, i.e. the mean radius of curvature of liquid surfaces in the pores (r), as follows:

$$m = m(r) \quad (2.3)$$

In conjunction with the Kelvin equation (59,77) which relates the radius of curvature to the vapour pressure and temperature,

$$r = - \frac{\sigma M_w}{\rho_w RT} \frac{2}{\ln \left\{ \frac{P_v}{P_v^0} \right\}} \quad (2.4)$$

a simplified picture of how moisture can be detained within porous media and how it will vary may be seen, albeit the actual mechanisms, as mentioned earlier, are much more complicated:

- 1) Rearranging equation (2.4) in the following form shows that the vapour pressure within the pores is a fraction of the 'flat-surface' or 'free-surface' saturation vapour pressure (P_v^0 , where r is infinity) at the same temperature:

$$\frac{P_v}{P_v^0} = \exp \left\{ - \frac{2 \sigma M_w}{\rho_w r RT} \right\} \quad (2.5)$$

Noting that P_v is the saturation vapour pressure at the surface of a curved liquid surface within the capillary like pores of the medium, it

can be seen that due to capillary (or surface tension) effect, the saturation vapour pressure is much reduced as compared to the 'free-surface' value; the smaller the radius r , the smaller P_v will be. A difference between the vapour pressure in the pores and in the ambient air will cause water vapour to migrate from the higher vapour pressure region to the lower ones. This explains why vapour moisture can migrate into the interstices of the porous medium, condense into liquid phase and that liquid and vapour phases can co-exist within the pores, even when the vapour pressure of the ambient air is much lower than the free-surface saturation value. As the value of r is dependent on the size of the internal pores of porous media, it also explains why the internal pore size distribution has a dominant effect on the equilibrium moisture content and on the transport of moisture in porous media.

- 2) From equation (2.4), it can be seen that parameters affecting the value of r include surface tension, water density, temperature and P_v/P_v^0 (which also equals to the relative humidity of the ambient air with which the medium is in thermodynamic equilibrium). Although the surface tension and the water density are both temperature dependent and there is a temperature term in the equation, because of the log function, P_v/P_v^0 is the dominant parameter. Hence, if the change in temperature in a heat and moisture transfer process is not large, the sorption isotherm with moisture content expressed as a function of P_v/P_v^0 for a given temperature may be used for other temperatures as a reasonably good approximation in studying the moisture sorption behaviour of the material throughout the process.
- 3) The value of P_v^0 is a function of temperature only (and is directly proportional to temperature). Hence, if the porous medium is subjected to the same ambient conditions but its temperature is increased, the value of P_v/P_v^0 will be lowered. Consequently, liquid water within those pores

where the radius of curvature is larger than that given by equation (2.4) will quickly evaporate into water vapour thus increasing P_v within the pores. Because of the large difference in density between the liquid and vapour phases of water, a minute reduction in liquid moisture content will suffice for restoring the local thermodynamic equilibrium condition and this process will take place almost instantaneously. Therefore, before moisture can transport from one region to another, the moisture content (m) at a particular region within the porous material immediately at the start of the transfer process will basically retain its original value and as will the P_v/P_v^0 ratio and r but the values of P_v and P_v^0 are both increased. This gives rise to a difference in vapour pressure between the air-vapour mixture in the pores of the medium and the ambient air and consequently the medium will start giving off moisture to the ambient air. This in fact is the familiar drying process for a porous medium when it is heated and the reverse will happen when there is a drop in temperature of the medium. It can be seen therefore that moisture transport within a porous medium can be established due to the existence of a temperature gradient. It must be pointed out here that the effects of a temperature gradient on moisture transfer referred to in this work relate to the effects as described in this section rather than the Soret effect (79). In this study, Soret effect is ignored.

- 4) Also, if the disturbance to the equilibrium conditions happens only at a localized region in the porous medium, transport of moisture will take place from the disturbed region to the adjacent ones thus upsetting the thermodynamic equilibrium conditions in the nearby regions. Evaporation or condensation therefore will also take place in these regions for restoring equilibrium and the disturbance will propagate through the medium. Hence, it can be seen that moisture can transport

from one region to another within a porous medium through a series of evaporation and condensation processes at the intermediate positions.

2.1.5 Heat of Sorption

Whenever evaporation or condensation occurs in the pores of a localized region within a porous medium, the process has to be sustained by a change in internal energy of the substances in the region including the solid, liquid and the gas mixture within the pores. Assuming that all constituents of the gas mixture may be regarded as perfect gases and that the value of heat of evaporation or condensation (or heat of sorption) does not change significantly, the vapour pressure in the pores may be related to the heat of evaporation by the Clausius-Clapeyron equation (76):

$$P_v = \frac{1}{a} \exp \left\{ -h_{fg} \frac{M_w}{RT} \right\} \quad (2.6)$$

where "a" is an integration constant. Re-arranging (2.6) yields the following equation which may be used for evaluation of the heat of evaporation in porous media:

$$h_{fg} = -\frac{RT}{M_w} \ln \{a P_v\} \quad (2.7)$$

As the Clausius-Clapeyron equation applies both for free and curved water surfaces, in conjunction with the Kelvin's equation, it may be seen that due to the effect of surface tension, the heat of evaporation in porous media is higher compared with that at a free-surface:

$$h_{fg} = h_{fg}^o + \frac{2 \sigma}{\rho_w r} \quad (2.8)$$

2.1.6 Basic Form of Equations Governing Coupled Heat and Moisture Transfer

To model simultaneous heat and moisture transfer in a porous medium is much more complicated than to model sensible heat transfer alone. A mathematical model comprising a set of partial differential equations (PDEs) may be derived starting from

basic principles of mass, momentum and energy conservation ⁽⁷⁹⁾. With reference to an elemental control volume within the porous material and based on the assumption that there exists local thermodynamic equilibrium, one equation of the following form may be derived for each quantity taking part in the transfer process (i.e. the mass, momentum and energy of each substance present in the pores):

Rate of accumulation in the control volume	=	Flux transporting into the control volume	–	Flux transporting out of the control volume	+	Net rate of generation within the control volume	(2.9)
--	---	---	---	---	---	--	-------

Let ϕ_i denotes the i^{th} quantity in transport, the equivalent mathematical expression will be:

$$\frac{\partial \phi_i}{\partial t} = - \nabla \cdot (J_{\phi_i}) + S_{\phi_i} \tag{2.10}$$

where $i = 1, 2, \dots n$ and

n = the number of different quantities taking part in the transfer process

The equations (one for each quantity) are strongly coupled to each other because:

- 1) rate of moisture transfer is affected not only by the gradient of one single state variable (in particular, the temperature gradient has a significant effect on the "driving potentials" of moisture transfer),
- 2) there will be evaporation of liquid water into water vapour and vice versa (this must be duly accounted for in the source term (S_{ϕ}) in both the liquid water and water vapour continuity equations),
- 3) the heat of evaporation or condensation must be accounted for in the energy equation (as the source term), and
- 4) the addition or reduction of moisture content at a local position due to transfer of moisture in turn affects the rate of evaporation or

condensation that will take place to retain local thermodynamic equilibrium and hence the local temperature.

Also, the sorption isotherm is often included to provide a relationship between the local moisture content and the state variables of the liquid and gases in the porous medium. The set of equations is in general highly non-linear because values of the transport properties are strongly dependent on the local moisture content and the sorption isotherm is non-linear. Therefore, analytical solutions are seldom available and numerical methods are normally adopted in solving the equations.

In deriving the moisture conservation equation, a phenomenological equation of the following form needs to be adopted to describe the moisture flux terms (J_v and J_l), similar to the Fourier's Law in heat transfer and the Fick's Law in mass diffusion:

$$\text{Moisture Flux} = \text{Moisture Transport Property in the Material} \times \text{Gradient of the Driving Potential} \quad (2.11)$$

Different state variables (and hence different associated transport properties) have been proposed as the "driving potential" and the major differences between different models (or theories) are primarily in the method adopted to account for this moisture flux term in the equations. However, there is yet no single theory that is universally applicable to heat and moisture transfer processes in a wide range of porous media and under all possible ranges of conditions. Treatments inevitably have to be specific to the situation and be limited in applications.

2.2 Theories of Heat and Moisture Transfer in Porous Media

Much early work in this subject treated the moisture transport phenomenon simply as a liquid diffusion process (80-82). In this theory, moisture transport is driven solely by the concentration gradient of liquid moisture and accordingly, is described by Fick's law. For one-dimensional moisture diffusion with constant diffusivity, the governing equation is:

$$\frac{\partial C}{\partial t} = D \frac{\partial^2 C}{\partial x^2} \quad (2.12)$$

As pointed out by Hougen et al ⁽⁸³⁾, better agreement with experimental results may be achieved by regarding the diffusivity as a variable (a function of moisture content) and thus the equation becomes:

$$\frac{\partial C}{\partial t} = \frac{\partial}{\partial x} \left(D \frac{\partial C}{\partial x} \right) \quad (2.13)$$

This type of model had been applied to predict moisture movement in drying processes ⁽⁸⁴⁾. In this type of simple diffusion model, the diffusion coefficient 'D' is a parameter that needs to be determined experimentally and is used to take account of effects of all the transport mechanisms that take place simultaneously. However, it is clear that the effect of temperature gradient is ignored in this approach.

In other early studies on drying of soil and organic materials, it was postulated that moisture flow is due to surface tension forces or capillary action and hence the gradient of capillary potential ⁽⁸⁵⁾ is regarded as the driving force for moisture movement in unsaturated porous media. Good agreement between results obtained by using this theory and experimental results was found in drying of granular substances, e.g. in the studies of Ceaglske & Hougen ⁽⁸⁶⁾ on drying of sand. Their work also explains the phenomenon that moisture may flow in the direction of increasing concentration.

Hougen et al ⁽⁸³⁾ had pointed out that there are limitations in the diffusion theory, however, moisture may move by vapour diffusion through a solid provided a temperature gradient is established. In the later stage of drying, i.e. the "pendular stage" (where continuous threads of liquid water have been broken up into isolated patches staying inside relatively smaller pores), the mobility of liquid water is greatly reduced and moisture transport takes places predominantly in the form of convection and diffusion in the vapour phase ^(87,88). The liquid water in a capillary pore can migrate to

other pores only after the water has been evaporated into the vapour phase. The evaporation and condensation theory as advanced by Henry ⁽⁸⁹⁾, Gurr et al ⁽⁹⁰⁾ and others is based on the assumption that the pendular state exists and this has been proven to be essentially correct when the system is subject to a temperature gradient ^(90,91).

The diffusion theory, capillary flow theory and evaporation and condensation theory were the three most widely accepted theories on moisture transport in porous media in the 1950's but have been more recently refined and extended (e.g. 54, 55-57, 59 & 61). The major improvements to the previous theories have been in combining contributions to the movement of moisture due to different driving forces. For example, Philip and DeVries ⁽⁵⁴⁾ derived a coupled heat and mass transfer model based on the assumption that moisture moves by both vapour diffusion under the action of a vapour density gradient and capillary flow under a capillary pressure gradient. Instead of the "physical" driving forces, the moisture flux terms (liquid and vapour fluxes) in their equations were expressed in terms of temperature and moisture content gradients:

$$\frac{\partial U}{\partial t} = \nabla \cdot (D_w \nabla U) + \nabla \cdot (D_{wT} \nabla T) \quad (2.14)$$

$$\rho_B C_B \frac{\partial T}{\partial t} = \nabla \cdot (k_T \nabla T) + h_{fg} \nabla \cdot (D_v \nabla U) \quad (2.15)$$

Effects of converting density of water vapour and capillary water pressure within the pores into moisture content and temperature were incorporated into the diffusivity terms (transport properties) in the governing equations.

It can be shown from the theory of irreversible thermodynamics ^(92,93) that the driving potential for moisture transfer in porous media is actually the total water chemical potential (including components of water chemical potentials due to surface tension, hydrostatic pressure, osmotic pressure, gravitational effect, etc.) and temperature ^(56,94,95). Starting from the principles of irreversible thermodynamics, Luikov ⁽⁵⁵⁻⁵⁷⁾ lumped together all the components of total water chemical potential and derived a set of equations similar to that of Philip & DeVries. His model has been

widely referred to in recent publications on this subject. In Luikov's model, total moisture transfer includes flow of both liquid and vapour phases and each of them consists two parts; one due to the total moisture content gradient and the other due to the temperature gradient. The model consists the following PDEs:

$$\frac{\partial T}{\partial t} = \nabla \cdot (K_{11} \nabla T) + \nabla \cdot (K_{12} \nabla U) \quad (2.16)$$

$$\frac{\partial U}{\partial t} = \nabla \cdot (K_{21} \nabla T) + \nabla \cdot (K_{22} \nabla U) \quad (2.17)$$

An additional pressure equation is also included in this model ⁽⁵⁵⁾ to take account of moisture transport due to convection when there exists a significant pressure gradient within the porous material (this kind of flow is also called 'filtration flow' and may be described by the Darcy's law ⁽⁶⁷⁾). The coefficients in the above equations are composed of physical and heat and moisture transport properties of the constituent substances (e.g. densities, specific heats, molecular weights, mass diffusivities, thermal conductivities, etc.), as well as derived parameters relating contributions to the total moisture transfer which include the phase change coefficient and the thermal gradient coefficient ⁽⁵⁵⁾. The phase change coefficient represents the relative contribution of evaporation to an increase in vapour moisture in the pores whereas the thermal gradient coefficient represents the ratio of total (liquid and vapour) moisture transfers due to a temperature gradient to that due to diffusion. These derived coefficients enabled the governing equations be presented in a neat format but created problems because appropriate numerical data of the parameters are difficult to obtain.

To describe mass transfer between two different porous materials that are in contact, Luikov introduced the concept of "mass transfer potential" (M) for use as the driving potential for moisture transfer in and between porous media (instead of moisture content) - analogous to temperature being the driving potential in heat transfer. This is needed when moisture transfer within composite materials is studied (as moisture can migrate from a lower moisture content material to a higher one), but also

makes the required materials data even more difficult to obtain. Mass transfer potential is defined with reference to a standard body (filter paper) and is a function of moisture content and temperature of the material. Its value for a sample porous body is given by the ratio of the moisture content of the reference body when it is in thermodynamic equilibrium with the sample body (U_s) to the maximum moisture content of the reference body achieved in the process of sorption of water steam (U_{sm}), multiplied to 100 "mass transfer degrees" ($^{\circ}M$), viz:

$$M = \frac{U_s}{U_{sm}} \times 100 (^{\circ}M) \quad (2.18)$$

From its definition, it is clear that mass transfer potentials of two pieces of different material that are in thermodynamic equilibrium with each other are of identical value and will be a continuous function across the interface of two adjoining materials where there is mass transfer from one to the other. In Luikov's model, the equilibrium moisture content relation (sorption isotherm) is not explicitly used but the mass transfer potential and the associated phase conversion coefficient, thermal gradient coefficient and moisture diffusion coefficients are all functions of moisture content (and temperature) and these functional relationships corresponding to different porous media need to be determined experimentally (55). However, in some applications of this theory, these coefficients are assumed to be constants (e.g. 57,95,96).

Extending from Krischer's theory (97), Berger & Pei (61) also treated mass transfer in two parts, i.e. flow of liquid due to capillary effect and vapour diffusion due to difference in partial vapour pressure, and used the sorption isotherm to close the set of equations. Berger & Pei's approach differs from Krischer's primarily in that in addition to the sorption isotherm, the maximum sorptional liquid content was assumed to be a function of temperature and that the Clausius-Clapeyron's equation was used to determine partial vapour pressure to cover the initial stage of drying where moisture content is equal to or larger than the maximum sorptional liquid content. This is

important in studies on drying of porous solids starting from saturated state but is not relevant to the present investigation.

Some other researchers started their model formulation from the fundamental principles of irreversible thermodynamics but the water chemical potential was expressed in terms of other thermodynamic properties such as vapour pressure, temperature, moisture content, water vapour mole fraction, etc. (50,51,59,98).

Harmathy (59) derived a set of partial differential equations for simulation of simultaneous heat and moisture transfer in capillary-porous media under the pendular stage (no bulk liquid movement) based on the evaporation and condensation theory and applied his theory to the study of drying of a piece of brick. In this theory, moisture transport is assumed to take place only in the vapour phase but liquid moisture content within the porous medium varies due to evaporation or condensation and this affects the rate of vapour transport. There are three equations representing conservation of mass of moisture, mass of dry air, and conservation of energy. Vapour transport mechanisms modelled include vapour diffusion due to a water vapour concentration gradient, convective flow due to a total pressure gradient, evaporation and condensation, and the effects of a temperature gradient on the moisture transfer driving potentials and the moisture content in the porous medium (through the temperature dependence of P_v^0 and hence r). The sorption isotherm of the material is employed to relate liquid moisture content to thermodynamic states of the air/water vapour mixture within the pores of the medium and thus provide a closed set of equations. Huang (50) and Huang et al (51) also derived a similar set of equations and used them to simulate drying of a concrete slab and a slab of cement paste. Huang (50) attempted to extend his model to cover the "funicular stage" (where continuous water threads exist in the porous medium) by including a liquid diffusion model but how transition from the funicular to the pendular stage can be modelled was unclear.

Whitaker (63) pursued formulation of governing equations for coupled heat and moisture transfer in porous media in a more rigorous way by first deriving conservation

equations for each component substance of the porous systems with each taken as a continuum. A volume averaging technique was then applied to yield the governing equations with state variables all presented in volume averaged form. In this process, the interactions between the solid, liquid and gas phases within a local averaging volume are taken care of by properly imposed boundary and interfacial conditions, and the physical meanings of various transport coefficients are clearly shown. Matsumoto ⁽⁹⁴⁾ has more recently derived a heat and moisture transfer model using directly the water chemical potentials and temperature as the driving potentials for the coupled heat and moisture transfer in porous media. The model has been applied for the analysis of internal moisture condensation and re-evaporation in building walls ^(99,100) and moisture variations in wet soil ⁽¹⁰¹⁾. Unfortunately, the resultant set of equations from these rigorous approaches are much more complicated and the associated transport coefficients are difficult to evaluate.

Although developed independent of each other, Luikov's equations ⁽⁵⁷⁾ and those of Philip & DeVries ⁽⁵⁴⁾ are very similar (compare equations 2.14 & 2.15 with 2.16 & 2.17) and both models should give similar results. Berger & Pei's model ⁽⁶¹⁾ does not seem to offer much innovation over those of Philip & DeVries and Luikov. However, it has been pointed out that due to the assumption of constant "moisture diffusivity" and "specific moisture capacity" (when mass transfer potential is used), there are reservations on the validity of Luikov's theory when applied to non-isothermal conditions ^(61,63). In addition, unavailability of transport properties data remains a significant restriction to widespread application of the theories. The same applies to the approaches of Whitaker ⁽⁶³⁾ and Matsumoto ⁽⁹⁴⁾. Harmathy ⁽⁵⁹⁾ and Huang's ⁽⁵⁰⁾ approach is theoretically rigorous and the required transport properties data are more readily available but is restricted to materials that stay in the pendular state in the heat and moisture transfer process.

Investigations done by various researchers as briefly summarized above show that several mechanisms (or theories) may be used to explain moisture transport in a

porous medium, i.e. liquid diffusion, vapour diffusion, capillary flow, convective transport, and evaporation and condensation, and that the temperature gradient across the medium has significant effects on the moisture flow driving potentials and on the balance of liquid and vapour moisture content in the medium. Also, the moisture transfer is often a combined effect of more than one of these mechanisms - a diagrammatic representation of the moisture transfer in a porous medium is given by Kohonen ⁽⁹⁸⁾ (Figure 2.2). The total moisture transfer therefore may be ascribed to a combination of gradients of properties like moisture concentration, capillary force, vapour pressure and temperature.

2.3 Investigations into Heat and Moisture Transport in Buildings

Notwithstanding that there are uncertainties and limitations in the theories of heat and moisture transfer in porous materials, attempts have been made to apply them in investigations of simultaneous heat and moisture transfer in buildings. In countries with cold weather, accumulation of liquid moisture within building fabrics can give rise to deterioration of building materials or even serious damage to the building structure ⁽¹⁸⁾ and increase the energy consumption for heating ⁽⁵⁾. Therefore, significant work has been done on moisture migration in roofs and external walls of buildings ^(102,103). Most of the work in this area is based on simple, steady-state vapour diffusion theory ^(4,104,105) aimed at the assessment of condensation risk in buildings ^(106,107). There are more rigorous studies which have taken into account the effects of heat and moisture transfer taking place simultaneously ^(99,100,108-113). Since interstitial condensation is not a serious problem for buildings situated in warm and hot climate regions, not much attention has been given to moisture transfer in such buildings until recently, when the impact of moisture adsorption and desorption by building materials on the indoor humidity level and performance of associated air-conditioning systems have been recognized ^(6,7,9,114).

Tsuchiya ⁽⁹⁾ developed a simple model for indoor humidity analysis which is a pioneer work investigated into the effects of wall moisture adsorption and desorption

on indoor air humidity level. In his model, the assumption is made that moisture adsorption or desorption takes place only up to a small depth from the surface of the building fabric material, i.e. in the outermost layer of the solid domain. The rate of moisture adsorption and desorption is proportional to the difference in humidity ratios (kg of water vapour per kg of dry air) between the indoor air and the boundary air film at the surface of the building wall. With reference to wood, a simple equation was proposed by Tsuchiya to relate the humidity ratio in the boundary air layer to the moisture content of the outermost layer of the material:

$$w_i = \frac{w_s}{41} \left(\frac{U_i}{U_o C} T_r - 5.416 \right) \quad (2.19)$$

This is equivalent to making the assumption that the boundary air layer is in thermodynamic equilibrium with the outermost layer of the wall and hence the equation is basically a curve-fit expression for the equilibrium moisture content relation of the wall material. To apply the equation, the average moisture content in the thin outermost layer of the wall ($U_o C$) has to be known and this needs to be determined experimentally. A surface air dew-point probe (SADP) has been developed by Kusuda⁽⁶⁾ which enables the coefficients (called "moisture sorption parameters" by Kusuda) that need to be input into Tsuchiya's model be calculated from the results of measurement using the probe. An infrared reflectance technique has also been used later⁽¹¹⁵⁾ to replace the SADP. Tsuchiya's model is an attractive one due to its simplicity but its practicality and accuracy are doubted because:

- 1) only very limited sorption parameter data have been published. Its validity will be confined, not only to the specific wall materials for which measurements were taken, but also to a limited range of indoor air conditions.
- 2) Tsuchiya's equation includes the room temperature (T_r). It is unclear how this affects the relationship between the wall moisture content and the boundary air layer humidity ratio, and

- 3) this model does not include effects of heat transfer at the building fabric and hence will not be able to simulate temperature effects on moisture transfer in the building materials.

Tsuchiya's model is basically a lumped parameter model. Instead of retaining the thickness of the wall and adjusting the convective mass transfer coefficient, the moisture behaviour of the wall was represented by a thin layer and "actual" convection transfer coefficient is used. The more recently developed effective moisture penetration depth (EMPD) concept ^(116,117) is actually similar to Tsuchiya's approach (see later discussions on the EMPD theory).

The conventional lumped parameter approach has also been employed in many investigations on moisture adsorption and desorption by building envelopes and their effects on indoor humidity. In this approach, details of coupled heat and moisture transfer within the building materials are ignored and the rates of heat and moisture exchange between the building materials and the ambient air zone are assumed to be proportional to the difference in the corresponding representative (lumped) state variables (e.g. temperature or vapour pressure) between the solid and air domains. Based upon this, a set of ordinary differential equations may be derived. This approach has merits in that it is simple to apply and, with certain assumptions made, analytical solutions may be obtained. When the equations are solved in conjunction with appropriate material properties and transport coefficients (such as "effective" vapour resistance ^(111,117) and "effective" convective heat and moisture transfer coefficients, see discussion that follows), this method often leads to the definition of time constants characterizing the rate of response of the material and the air zone ^(108,118,119). The coefficients and material properties are often regarded as constants in studies taking this simple approach.

If the internal moisture transfer resistance of a porous medium is small compared with the surface moisture transfer resistance, the moisture exchange between the medium and the ambient air is controlled by the latter and the moisture content

gradient within the medium will be negligible. In this case, the lumped parameter approach is an accurate and convenient method to describe the moisture sorption behaviour of the medium. This unfortunately is not true for most building materials (120) but the lumped parameter approach may still be applied to materials with significant internal resistances provided the mass transfer coefficients are appropriately adjusted to have this effect taken into account (hence are called "effective" transfer coefficients). However, evaluation of these "effective" coefficients is not simple except under simplified situations and their application will be restricted to limited range of conditions. Therefore, the lumped parameter approach was not adopted in the present investigation.

In more elaborated investigations, a distributed parameter approach is adopted in which the coupled heat and moisture transfer is modelled by partial differential equations (PDEs) and, in general, the set of PDEs are solved by numerical methods. The approach of using a Fick's Law like equation to relate the total moisture flux to either a moisture concentration gradient or a vapour pressure gradient has been applied in studies on the effect of moisture storage of walls on indoor air humidity. For example, Isetti et al (10) related the vapour moisture flux within a wall of an air-conditioned room to the gradient of vapour moisture concentration in the wall and derived a PDE for the description of moisture transients in the room fabric. The vapour moisture diffusivity in their model is a function of the vapour permeability and sorption characteristics (hence the sorption isotherm) of the material. By assuming that the diffusivity is a constant, a linear PDE similar to the Fick's second law (equation 2.12) was obtained. The linear wall moisture equation was coupled to an air-zone moisture mass balance equation and the model was used to analyse the periodic variations of indoor humidity in a room with all sources of moisture and outdoor air humidity variations represented as sinusoidal functions. Their results show that significant damping effect on fluctuations of indoor moisture level is present due to the moisture sorption properties of the building fabric. However, effects of heat transfer across the building fabric was ignored in their analysis and the case studied was based on a

constant indoor temperature which is equivalent to assuming that the air-conditioning system for the room was continuously operated.

The combined effects of wall moisture adsorption and desorption and intermittent air-conditioning has recently been investigated in Hong Kong by Wong ⁽¹⁾ and Wong & Wang ⁽²⁾. Some experimental and site survey findings are also reported in their papers which clearly show the significant effect of intermittent air-conditioning (see Section 1.1). Wong & Wang's model resembles that of Philip & DeVries ⁽⁵⁴⁾ in that the total moisture flux (liquid and vapour) was ascribed to a liquid moisture content gradient and a temperature gradient, each with a different diffusivity, and the relationship between capillary pressure and moisture content was mentioned. In deriving the model, the temperature gradient effect was subsequently neglected on the assumption that the moisture diffusivity associated with the temperature gradient was much smaller than that with the moisture content gradient. Because liquid and vapour moisture diffusion were lumped together and described as total moisture transfer, the liquid-vapour phase change rate term was absent from the moisture flow equation and no account was made of the heat of evaporation or condensation in the porous material in the energy balance equation. Their model therefore is basically a liquid diffusion model. As a consequence, the moisture and heat transfer equations are decoupled at interior nodes in their model but they did take account of the heat of evaporation or condensation at the boundary nodes. In simulation calculations, the moisture diffusivity was assumed to be constant. Due to the serious restrictions imposed by the assumptions made in Wong & Wang's model, their model could only be valid for building materials that are not subjected to a significant temperature gradient.

Shukuya & Saito ⁽⁸⁾ used a controlled volume approach to study the effects of wall moisture adsorption and desorption on indoor humidity changes in a room under step changes of outside air temperature and humidity. Their model is basically a vapour diffusion model with evaporation and condensation. Vapour moisture transfer was assumed to be driven by the gradient of humidity ratio of moist air within the porous

material and no liquid moisture movement was accounted for. Hence the model applies only to the pendular state. Adsorption and desorption coefficients characterizing the moisture sorption properties of the materials were defined with reference to the equilibrium moisture content relation (sorption isotherm) of the materials. By assuming that evaporation and condensation within the porous materials has little effect on local temperature and that the material has constant heat and moisture properties, the energy conservation equation in their numerical model is decoupled from the vapour moisture mass conservation equation but effects of temperature changes on moisture balance are accounted for in the moisture equation. This allows the energy equation be solved first, independent of the moisture equation, and the results then can be used in the solution of the moisture equation.

Originating from the Finite Element Method Application Language Program (FEMALP) developed in Kerestecioglu's PhD work ⁽¹²¹⁾, a model called Moisture Adsorption And Desorption Analysis Method (MADAM) has been developed ^(7,122) in which Luikov's differential equations ⁽⁵⁵⁻⁵⁷⁾ are applied to model the coupled heat and moisture transfer in porous building materials. The model is an elaborate one and has been validated against some experimental data.

For applications in building cooling load analysis, MADAM has been incorporated into the TARP building thermal analysis program ⁽¹²³⁾ and the resultant computer package is called MADTARP ^(7,122). In MADTARP, assumptions are made that:

- 1) only the outermost layer of the building envelope material participates in the moisture adsorption and desorption process;
- 2) the moisture adsorption and desorption behaviour of the layer may be lumped and therefore has a uniform moisture content;
- 3) this layer is always in thermodynamic equilibrium with the boundary air-layer above its surface;

- 4) due to 1) - 3), the moisture conditions in the material's surface layer can be related to the surface air-layer conditions; and
- 5) the moisture exchange between the building fabric and the indoor air (and similarly between the building envelope and the outdoor air) can be fully accounted for by just considering the mass of the surface layer that participates in the moisture adsorption and desorption process, i.e. by artificially varying the dry mass of the building fabric.

Effect of furnishings is to be treated similarly.

It can be seen that assumptions (1)-(4) are similar to those made by Tsuchiya⁽⁹⁾. In MADTARP, it goes further to evaluate (by using MADAM) the depth of the moisture adsorption and desorption layer and uses that to calculate rate of moisture adsorption and desorption at the building materials. This method has later been published separately and called the Effective Moisture Penetration Depth (EMPD) theory⁽¹¹⁶⁾. In MADTARP, MADAM acts as a pre-processor from which the coefficients of expressions correlating the moisture content of the building material to the surface air-layer conditions are calculated and fed to the TARP program for indoor air conditions and cooling load calculations. According to the authors⁽¹²²⁾, predictions from MADTARP have been verified against some experimental findings and good agreement was achieved in those cases.

The building thermal model in the original version of TARP⁽¹²³⁾ is basically a conduction transfer function model⁽⁵⁾ which is valid only for calculations of sensible heat transfer across building envelopes where thermal conductivities of materials are constants. It is not applicable to modelling of coupled heat and moisture transfer across the building envelope given the fact that heat and moisture transfers are coupled and the governing equations are non-linear. In MADTARP, the set of procedures incorporated into the basic TARP program for estimation of moisture exchange between the indoor air and the building envelope appears to be just an added-on routine which would only

affect the water vapour mass balance calculation for the "air-zone" but would not modify the sensible heat transfer within the building envelope calculated by the basic TARP procedures. The MADTARP model therefore would not be a truly simultaneous heat and moisture transfer model.

The concept of EMPD theory is in fact similar to the use of "effective" transfer coefficients in the lumped parameter approach ⁽¹¹⁷⁾. Instead of using the "real" thickness of the material and the "effective" transfer coefficients, an "effective" thickness (the EMPD) and the "real" moisture transfer coefficients are used in this method. This would require less effort in the solution process as compared to solving the PDEs for the coupled heat and moisture transfer. However, the effort for obtaining appropriate values of EMPD may be substantial and different values of EMPD may be required for different operating conditions, particularly in simulations over long periods where there are appreciable changes in moisture content (see Chapter 9). Hence, as the authors of the theory themselves remarked, this concept needs to be used with caution and good judgement. In addition, due to the use of Luikov's theory, not much transport data of materials are available for use with MADAM for generating the required correlations for some building materials that may be encountered in real buildings. For example, even though an extensive survey of available moisture transfer property data has been carried out by Kerestecioglu et al ⁽⁹⁵⁾, data on the coefficients required by Luikov's model for modelling heat and moisture transfer in concrete are missing.

Air-conditioning system performance can also be modelled with MADTARP though the models used to describe the air-conditioning system performance are curve-fit models based on steady-state manufacturers data. Because of the limitations of the EMPD theory and detailed air-conditioning system model is not available, the MADTARP program is not appropriate for the present investigation.

An evaporation and condensation model has also been proposed by Kerestecioglu & Gu ⁽¹²⁴⁾, as an alternative to the Luikov's theory but vapour moisture transfer was assumed to be due to diffusion only, driven by a vapour density gradient.

The moisture diffusivity was related to the molecular diffusivity of water vapour through the use of a "tortuosity" factor which in turn can be related to the permeability of the material. The equation to be solved in this model is slightly more complex than those of Luikov's theory but more material property data (permeability and sorption isotherm) are available (95).

A major difference between this and Huang's model is in that the latter included the treatment of dry air transport within the porous solid, which was considered to have a significant effect on moisture transfer in the material (125). Both the evaporation and condensation models of Huang (50,51) and Kerestecioglu et al (124) have been applied to a single piece of building material but extension of the model for investigation of indoor humidity transients in a building envelope has not yet been made. This formed one of the objectives of this work.

2.4 Moisture Transfer in Concrete and Cement Paste

From the above review on various theories proposed to describe heat and moisture transfer in porous media, it can be seen that because of the assumptions made in their development, there are restrictions to the application of the theories. One theory may be particularly suitable when applied to heat and moisture transfer in a specific kind of material and under a particular range of conditions but may not be equally good for other materials and conditions. As concrete is the major construction material in Hong Kong, it is important in the present investigation to understand the moisture properties of this material so as to determine which method will be the most appropriate.

Concrete is made by mixing cement powder with water and aggregates (sand and stones). It may be regarded as a two phase material with the aggregates dispersed in a matrix of hardened cement paste (h.c.p.) which is formed in the hydration process that takes place after water is added to the cement powder. The aggregates are usually

inert in comparison with the h.c.p. in that they do not hydrate and do not shrink or swell. Hence, most of the properties of concrete derive from the h.c.p. (67).

The h.c.p. has a peculiar microstructure (126,127). Its basic constituent is formed from rolls of sheets of colloidal calcium-silicate hydrate of a thickness of up to a few hundred Å, embedded with crystals of Ca(OH)_2 and some other minor components (58,128). This colloidal mass together with the crystalline particles is called cement gel. Due to its thin sheet structure, cement gel has very large specific surface and very fine pores (called gel pores). The specific surface of h.c.p. is approximately $250 \text{ m}^2/\text{g}$ whereas that of cement powder is only $0.3 \text{ m}^2/\text{g}$ (67). The gel pores are about 15 Å in size and amount to about 28% of the gel volume (58,67). Besides the gel pores, there are also capillary pores in the matrix of h.c.p., which are residues of water-filled spaces in the fresh paste and are much larger in size (approx. 500 Å). The porosity of a slab of h.c.p. therefore may be up to 40% or more depending on the water-cement ratio adopted in making the cement paste.

Due to the existence of pores within the cement gel, water can exist in different states within these pores, including (1) water vapour, (2) free water in the capillaries, (3) adsorbed water on the internal solid surfaces, (4) interlayer water penetrated into the lattice layers of the gel solids and (5) chemically combined water (or water of hydration), and it is impossible to isolate the water of one state from that of any other. In a drying process, it is possible to have desorption and partial dehydration to take place simultaneously and rehydration can occur in a subsequent adsorption process. This is believed to be the cause for the difference between sorption isotherms of h.c.p. from other building materials in that the adsorption and desorption branches remain two distinct curves at $\frac{P_v}{P_v^0} < 0.4$ (58) as shown in Figure 2.1b.

Notwithstanding the peculiarities in internal structure of hardened cement paste, the fundamentals and the methods of describing heat and moisture transport in porous

media as summarized in the preceding sections in general apply to concrete and cement paste. Nevertheless, as Harmathy ⁽⁶⁰⁾ and Huang ⁽⁵⁰⁾ have pointed out:

- a) Due to the exceptionally large specific surface in hardened cement paste, it can hold a substantial amount of moisture in equilibrium with a normal atmospheric environment - the larger is the internal pore surface area in relation to the pore volume, the more moisture can be retained,
- b) consequently, in drying of a cement paste from a high pore saturation, the constant rate period corresponding to the "funicular state" of the medium (where continuous water threads exist in the pores) will quickly end. The cement paste will then reach the so-called pendular state (water threads are broken up) with a substantial amount of liquid water left in the pores.
- c) When in the pendular state, the liquid water has a much lower degree of mobility so that the principle modes of moisture transfer will be diffusion and convection of the gaseous phase induced by pressure gradients, and
- d) transport of moisture in the gaseous phase is possible only if liquid moisture is vapourized first. Hence, evaporation and condensation is the dominant mechanism of liquid moisture transport in the pendular state.

Under normal conditions, concrete walls and slabs and cement plasterings in completed and occupied buildings can seldom be in the funicular state. Hence, capillary flow of moisture, which applies to the funicular state, can be neglected. Also, dehydration of the cement gel in concrete building structures should seldom happen unless subjected to an extraordinarily high temperature environment such as in a fire. The moisture transport in concrete and in cement plastering therefore should be modelled with reference to the pendular state where the pre-dominant mode of transport

is vapour diffusion and filtration flow (convection) with changes in adsorbed liquid moisture effected by evaporation and condensation of liquid water.

2.5 The Methods Chosen for Modelling The Coupled Heat and Moisture Transfer in Concrete Buildings in Hong Kong

To facilitate assessment of the effect of building fabric moisture adsorption and desorption on indoor air humidity variations, which is one of the objectives of this research, heat and moisture transfer in the building fabric has to be properly modelled. To do this, a choice has to be made of which theory, among various theories proposed, is to be used for description of the phenomena. As no single theory will be able to cover all possible kinds of materials and ranges of conditions, a choice can only be made with regard to the specific kind of material to be modelled and to the situation being studied. In this work, focus is put on building materials made from cement and aggregates as these are the predominant construction materials used in Hong Kong.

It has been made clear that any model that neglects the effect of temperature gradient on the moisture transfer driving potential would be inadequate. Vapour diffusion, effects of temperature, and evaporation and condensation, which are the dominant mechanisms for moisture transfer, must be duly accounted for. However, whether or not liquid transport (by diffusion or by capillary effect) is accounted for is unimportant as cementitious building materials normally stay in the pendular stage. The moisture transfer driving potential(s) used in the model must be continuous functions across adjoining layers of different materials as building walls are often composite walls. Furthermore, the building thermal model has to be coupled to detailed air-conditioning system models and a simultaneous solution is essential if the detailed aims of this work are to be addressed. Given the complexity of the problem, a balance amongst the competing factors of model rigour, accuracy and computing efficiency has to be sought.

Amongst various models reviewed, Luikov's theory (55-57), Berger & Pei's theory (61), Harmathy's model (59), Huang's model (50) and various models with vapour diffusion and evaporation and condensation taken into account (e.g. Keresteciogly & Gu (124)) satisfy the abovementioned criteria. It is difficult to tell which one would be the most accurate for studying a particular problem unless the theory has been validated by experimental findings. Unfortunately, up to now, none of the theories has been rigorously and extensively validated by experimental results. Nevertheless, as Kerestecioglu et al (95) pointed out, Luikov's theory and the evaporation and condensation theory appear to be the two most promising ones. Luikov's theory is considered to be a good model because it was developed from fundamental theory of irreversible thermodynamics and its equations are symmetrical to each other and are less complex (as compared to e.g. those of Whitaker (63), Matsumoto (94), Harmathy (59) and Huang (50)). When the equations are solved numerically, they have favourable behaviour in respect of stability and speed of convergence (95). The model is also applicable to a wider range of pore saturation conditions (hence is more general). Wide-spread application of Luikov's model however is restricted by the limited material property data available.

As to models developed from the evaporation and condensation theory, Huang's model (50), amongst others, is the most elaborate one in that evaporation and condensation, vapour diffusion, temperature effects, and filtration flow are all properly modelled, based on sound theoretical backgrounds. The only restriction is that it applies only to moisture transfer in the pendular state. Huang's model is more complex than Luikov's model and will therefore be less efficient in respect of computing time required to obtain a numerical solution. However, property data are more readily available and the method has been applied to studies on heat and moisture transfer in concrete and cement paste (50,51). If it is ascertained that the porous medium stays in pendular state throughout the process, Huang's model should be more appropriate than Luikov's theory because the basic assumption in the latter that moisture transfer takes place both in liquid and vapour phases becomes invalid.

Considering that for concrete buildings, the fabric materials (e.g. structural concrete and cement plastering) are normally in pendular state and that the availability of property data is of vital importance, Huang's model was chosen for preliminary studies on the heat and moisture transport phenomena in concrete walls and slabs of buildings. Knowing that a model developed from the evaporation and condensation theory will be more demanding on computer time, starting from this rigorous model has the advantage that the relative contributions to the total moisture transfer due to various mechanisms can be assessed and any one that has little effect can later be neglected, leading to a simpler model. As detailed experimental data for verification of program predictions are rarely available, simulation results from this rigorous model may be used as a "benchmark" to see whether a simpler model can simulate the heat and moisture transport phenomena with acceptable accuracy. A numerical model was developed based on this theory and coupled to a steady-state air-conditioning system model. A brief summary of Huang's equations, the methods adopted for discretization of the PDEs involved, and the solution techniques adopted is given in Chapter Three.

Chapter Three

The Building Heat And Moisture Transfer Model Based on Huang's Equations

In this chapter, Huang's governing PDEs ⁽⁵⁰⁾ are introduced, the methods adopted to develop a numerical model based upon these PDEs for modelling the heat and moisture transfer in a composite wall or slab are briefly described and the method to treat boundary conditions is outlined. Finally, results of a simulation study on the comparative significance of various moisture driving potentials (in a slab of concrete and a slab of cement paste) are summarized.

Based on the numerical wall/slab models developed from Huang's equations and simple lumped parameters models for a window and for the air enclosed in room, a building heat and moisture transfer model was developed. The building model had also been integrated with a simple air-conditioning system model and then applied in preliminary studies to assess the significance of building fabric moisture absorption and desorption effects on the indoor air humidity ⁽⁵²⁾ (see Appendix D.1). The window model, the room air model and the air-conditioning system model incorporated into the integrated model and the methods used to describe radiant energy exchanges among the walls, slabs and the window of a room are similar to those detailed in Chapter Four.

3.1 Huang's Equations for Coupled Heat and Moisture Transfer

3.1.1 Assumptions

Huang ⁽⁵⁰⁾ derived a set of governing equations for coupled heat and moisture transfer in a porous medium based on the following assumptions:

- i) The multi-phase porous system has isotropic properties and local thermodynamic equilibrium conditions exist in the porous system.
- ii) The solid matrix is rigid and homogeneous.
- iii) Liquid water, water vapour and air are the only substances present in the pores, the air in the pores is a single component gas, and both water vapour and air (and their mixture) are ideal gases.
- iv) The mass of water vapour is negligible in comparison with the mass of liquid moisture content.
- v) The liquid phase of moisture content in the porous system is stationary, i.e. pendular state exists in the medium; and
- vi) the local liquid moisture content may change due to vapour transport, evaporation and condensation, and this in turn affects the vapour transport.

3.1.2 The Governing Equations

The governing partial differential equations due to Huang are:

$$\begin{aligned} A_i \frac{\partial \phi}{\partial t} + B_i \frac{\partial P_g}{\partial t} + C_i \frac{\partial T}{\partial t} &= D_i \frac{\partial^2 \phi}{\partial x^2} + E_i \frac{\partial^2 P_g}{\partial x^2} + F_i \frac{\partial^2 T}{\partial x^2} \\ &+ G_i \left(\frac{\partial \phi}{\partial x} \right)^2 + H_i \left(\frac{\partial P_g}{\partial x} \right)^2 + I_i \left(\frac{\partial T}{\partial x} \right)^2 \\ &+ J_i \left(\frac{\partial \phi}{\partial x} \cdot \frac{\partial P_g}{\partial x} \right) + K_i \left(\frac{\partial \phi}{\partial x} \cdot \frac{\partial T}{\partial x} \right) + L_i \left(\frac{\partial P_g}{\partial x} \cdot \frac{\partial T}{\partial x} \right) \end{aligned}$$

for $i = 1, 2 \text{ \& } 3$.

(3.1)

These three equations represent respectively the conservation equations for mass of moisture (liquid water and water vapour), mass of dry air and energy. Expressions for evaluation of the coefficients A_i to L_i associated with the derivative terms are given in Table 3.1.

It can be seen from these equations that the state variables chosen to describe the transport phenomena include the mole fraction of water vapour in the air/water-vapour mixture (ϕ), the gas mixture total pressure (P_g) and the local temperature (T). This is a good choice because the model can readily be extended to cover multi-layered walls and slabs in buildings as these variables are continuous functions across the interface of two adjoining layers of materials. Component terms of the coefficients A_i - L_i in the equations however include the volume fraction of the gaseous phase (the mixture of water vapour and air) in the porous medium (ϵ_g), which is an additional unknown variable that needs to be solved simultaneously with the other three variables. The sorption isotherm of the medium was employed to provide the additional relationship required to close the set of equations. In Huang's model, the radius of curvature of liquid water surface in the capillary-like pores of the medium (r) was used in the sorption relationship of the medium, viz:

$$\epsilon_l = \epsilon_o - \epsilon_g \quad (3.2)$$

$$\text{where } \epsilon_l = \epsilon_l(r) \quad (3.3)$$

$$\text{and } r = r(\phi, P_g, T) \quad (3.4)$$

Noting the relationship between P_v , P_g and ϕ ($P_v = \phi P_g$, see Section 3.3), equation (3.4) is in fact equivalent to equation (2.4).

In this model, the one-dimensional total moisture flux at an intermediate plane inside a porous medium is given by :

$$J_v = - \rho_g \epsilon_g D \frac{M_a M_v}{M_g^2} \frac{\partial \phi}{\partial x} - \frac{\kappa_g^o}{\mu_g} \zeta_g \rho_g \frac{\partial P_g}{\partial x} \quad (3.5)$$

which is based on the assumption that moisture transfer takes place by virtue of molecular diffusion, driven by a vapour concentration gradient (the first term at RHS of equation 3.5), and filtration flow due to a total gas mixture pressure gradient (the second term). The energy transport modelled includes contributions from heat conduction through the solid, liquid and gaseous phases of substances of the porous system as well as from energy transport associated with mass transport of dry air and water vapour. It also takes into account the heat of evaporation or condensation resulting from the liquid moisture content changes in localized regions in the medium. Being negligibly small as compared to the other modes of energy transport, the energy dissipation due to viscous effect in fluid flow was neglected.

It can also be seen that this set of equations is non-linear and no simple analytical solution is available. A numerical technique therefore has to be used when applying them to model heat and moisture transfer in a porous medium.

3.2 The Finite Difference Model Based on Huang's Equations

A finite difference model for simulating simultaneous heat and moisture transfer in a wall or slab in a buildings was derived based on Huang's equations. It comprises a set of finite-difference nodal equations pertaining to the boundary nodes, the interior nodes and, for a composite wall or slab, the interface nodes.

3.2.1 Interior Nodes

For the interior nodes, the three non-linear partial differential equations (equation (3.1) for $i = 1, 2 \text{ \& } 3$) were each discretised into finite difference form by direct replacement of derivative terms with their corresponding finite difference approximations. The finite differencing scheme used was a backward-in-time, central-in-space scheme as detailed in Table 3.2. The FDEs for interior nodes so obtained are shown as equation (3.6) from which it can be seen that, at both sides of the equation, there are unknown incremental terms of the dependent variables (i.e. $\Delta\phi$, ΔP_g & ΔT which are respectively changes in values of the variables ϕ , P_g & T from the n^{th} to the

$n+1^{\text{th}}$ time step at the interior node under concern (variables at the LHS of equation 3.6) and the nodes adjacent to it at both sides (denoted by subscripts + and -)).

$$\begin{aligned}
& A_i \frac{\Delta\phi}{\Delta t} + B_i \frac{\Delta P_g}{\Delta t} + C_i \frac{\Delta T}{\Delta t} = \\
& \left\{ D_i \left[\frac{\phi_+^n - 2\phi^n + \phi_-^n}{(\Delta x)^2} + \frac{\Delta\phi_+ - 2\Delta\phi + \Delta\phi_-}{(\Delta x)^2} \right] \right. \\
& + E_i \left[\frac{P_{g+}^n - 2P_g^n + P_{g-}^n}{(\Delta x)^2} + \frac{\Delta P_{g+} - 2\Delta P_g + \Delta P_{g-}}{(\Delta x)^2} \right] \\
& + F_i \left[\frac{T_+^n - 2T^n + T_-^n}{(\Delta x)^2} + \frac{\Delta T_+ - 2\Delta T + \Delta T_-}{(\Delta x)^2} \right] \\
& + G_i \left[\left(\frac{\phi_+^n - \phi_-^n}{2\Delta x} \right)^2 + 2 \left(\frac{\phi_+^n - \phi_-^n}{2\Delta x} \cdot \frac{\Delta\phi_+ - \Delta\phi_-}{2\Delta x} \right) \right] \\
& + H_i \left[\left(\frac{P_{g+}^n - P_{g-}^n}{2\Delta x} \right)^2 + 2 \left(\frac{P_{g+}^n - P_{g-}^n}{2\Delta x} \cdot \frac{\Delta P_{g+} - \Delta P_{g-}}{2\Delta x} \right) \right] \\
& + I_i \left[\left(\frac{T_+^n - T_-^n}{\Delta x} \right)^2 + 2 \left(\frac{T_+^n - T_-^n}{2\Delta x} \cdot \frac{\Delta T_+ - \Delta T_-}{2\Delta x} \right) \right] \\
& + J_i \left[\left(\frac{\phi_+^n - \phi_-^n}{2\Delta x} \cdot \frac{P_{g+}^n - P_{g-}^n}{2\Delta x} \right) + \left(\frac{\phi_+^n - \phi_-^n}{2\Delta x} \cdot \frac{\Delta P_{g+} - \Delta P_{g-}}{2\Delta x} \right) + \left(\frac{P_{g+}^n - P_{g-}^n}{2\Delta x} \cdot \frac{\Delta\phi_+ - \Delta\phi_-}{2\Delta x} \right) \right] \\
& + K_i \left[\left(\frac{\phi_+^n - \phi_-^n}{2\Delta x} \cdot \frac{T_+^n - T_-^n}{2\Delta x} \right) + \left(\frac{\phi_+^n - \phi_-^n}{2\Delta x} \cdot \frac{\Delta T_+ - \Delta T_-}{2\Delta x} \right) + \left(\frac{T_+^n - T_-^n}{2\Delta x} \cdot \frac{\Delta\phi_+ - \Delta\phi_-}{2\Delta x} \right) \right] \\
& + L_i \left[\left(\frac{P_{g+}^n - P_{g-}^n}{2\Delta x} \cdot \frac{T_+^n - T_-^n}{2\Delta x} \right) + \left(\frac{P_{g+}^n - P_{g-}^n}{2\Delta x} \cdot \frac{\Delta T_+ - \Delta T_-}{2\Delta x} \right) + \left(\frac{T_+^n - T_-^n}{2\Delta x} \cdot \frac{\Delta P_{g+} - \Delta P_{g-}}{2\Delta x} \right) \right] \left. \right\} \\
\end{aligned} \tag{3.6}$$

Collecting these incremental terms to the left hand side, equation (3.6) may be simplified to (for $i=1, 2 \text{ \& } 3$):

$$\begin{aligned}
& (a_{i1} \Delta\phi_- + a_{i2} \Delta P_{g-} + a_{i3} \Delta T_-) + (b_{i1} \Delta\phi + b_{i2} \Delta P_g + b_{i3} \Delta T) \\
& + (c_{i1} \Delta\phi_+ + c_{i2} \Delta P_{g+} + c_{i3} \Delta T_+) = d_i
\end{aligned} \tag{3.7}$$

and expressions for the coefficients a, b, c and d are as shown in Table 3.3.A.

The set of 3 equations for each interior node can be written in matrix form as follows:

$$\begin{bmatrix} a_{11} & a_{12} & a_{13} \\ a_{21} & a_{22} & a_{23} \\ a_{31} & a_{32} & a_{33} \end{bmatrix} \begin{Bmatrix} \Delta\phi_- \\ \Delta P_{g-} \\ \Delta T_- \end{Bmatrix} + \begin{bmatrix} b_{11} & b_{12} & b_{13} \\ b_{21} & b_{22} & b_{23} \\ b_{31} & b_{32} & b_{33} \end{bmatrix} \begin{Bmatrix} \Delta\phi \\ \Delta P_g \\ \Delta T \end{Bmatrix} + \begin{bmatrix} c_{11} & c_{12} & c_{13} \\ c_{21} & c_{22} & c_{23} \\ c_{31} & c_{32} & c_{33} \end{bmatrix} \begin{Bmatrix} \Delta\phi_+ \\ \Delta P_{g+} \\ \Delta T_+ \end{Bmatrix} = \begin{Bmatrix} d_1 \\ d_2 \\ d_3 \end{Bmatrix} \quad (3.8)$$

or more compactly

$$[a]_k \{\Delta X\}_{k-1} + [b]_k \{\Delta X\}_k + [c]_k \{\Delta X\}_{k+1} = \{d\}_k \quad (3.9)$$

where

$$\{\Delta X\}_{k-1} = \begin{Bmatrix} \Delta\phi_- \\ \Delta P_{g-} \\ \Delta T_- \end{Bmatrix}; \{\Delta X\}_k = \begin{Bmatrix} \Delta\phi \\ \Delta P_g \\ \Delta T \end{Bmatrix}; \{\Delta X\}_{k+1} = \begin{Bmatrix} \Delta\phi_+ \\ \Delta P_{g+} \\ \Delta T_+ \end{Bmatrix}$$

and k = node number in the wall or slab.

3.2.2 Boundary Nodes

By regarding the outermost layer of a wall or slab having a thickness of $\frac{\Delta x}{2}$ as a control volume, the finite difference nodal equation for a boundary node was derived by applying the principles of conservation of mass and energy at the control volume. In that, the mass and energy fluxes from the next interior layer to the layer at the boundary were described in exactly the same way as for mass and energy transfers between adjacent interior nodes whereas appropriate boundary conditions were employed to quantify the mass and energy transfer at the boundary surfaces (see Section 3.3). The boundary node FDEs derived are as follows:

i) *The Moisture equation:*

$$A_1 \frac{\Delta\phi}{\Delta t} + B_1 \frac{\Delta P_g}{\Delta t} + C_1 \frac{\Delta T}{\Delta t} = \frac{2}{\Delta x} \left\{ \frac{RT}{M_v P_g} m_v'' - D_1 \left(\frac{\phi^n - \phi_a^n}{\Delta x} + \frac{\Delta\phi - \Delta\phi_a}{\Delta x} \right) \right. \\ \left. - E_1 \left(\frac{P_g^n - P_{ga}^n}{\Delta x} + \frac{\Delta P_g - \Delta P_{ga}}{\Delta x} \right) \right\} \quad (3.10)$$

ii) *The Energy equation:*

$$A_3 \frac{\Delta\phi}{\Delta t} + B_3 \frac{\Delta P_g}{\Delta t} + C_3 \frac{\Delta T}{\Delta t} = \frac{2}{\Delta x} \left\{ q'' - F_3 \left(\frac{T^n - T_a^n}{\Delta x} + \frac{\Delta T - \Delta T_a}{\Delta x} \right) \right\} \quad (3.11)$$

where A_1 to E_1 and A_3 to F_3 are coefficients identical to corresponding coefficients of the interior nodes and

m_v'' = moisture flux from ambient air to the surface.

q'' = algebraic sum of convective and radiant heat fluxes entering the surface.

Suffix 'a' denotes quantities pertaining to the interior node immediately adjacent to the surface.

iii) *The Air equation:*

One additional boundary condition is required for simultaneous solution of $\Delta\phi$, ΔP_g and ΔT at the surface node which can be obtained by noting the fact that the gas pressure at the boundary is always equal to the ambient air-pressure, i.e.:

$$P_g = P_{atm} \quad (3.12)$$

where P_{atm} = atmospheric pressure which is assumed constant (i.e. the room air would not be subjected to pressurising/depressurising ventilation strategy, hence, $\Delta P_g = 0$).

Re-arranging equations (3.10) to (3.12) gives the following matrix equation for a boundary surface node:

$$\begin{bmatrix} a_{11} & a_{12} & a_{13} \\ a_{21} & a_{22} & a_{23} \\ a_{31} & a_{32} & a_{33} \end{bmatrix} \begin{Bmatrix} \Delta\phi_a \\ \Delta P_{ga} \\ \Delta T_a \end{Bmatrix} + \begin{bmatrix} b_{11} & b_{12} & b_{13} \\ b_{21} & b_{22} & b_{23} \\ b_{31} & b_{32} & b_{33} \end{bmatrix} \begin{Bmatrix} \Delta\phi \\ \Delta P_g \\ \Delta T \end{Bmatrix} = \begin{Bmatrix} d_1 \\ d_2 \\ d_3 \end{Bmatrix} \quad (3.13)$$

and expressions for the coefficients a, b and d are as shown in Table 3.3.B.

3.2.3 Interface Nodes

Finite difference equations for an interface node between two adjoining layers of different materials in a composite wall or slab were derived by first treating the outermost $\Delta x/2$ thick layer in each material as a boundary node based on undetermined fluxes of water vapour, air and energy at the interface surface. The two sets of FDEs were then combined so that the undetermined mass and energy flux terms could be eliminated resulting in a set of FDEs relating parameters at the interface node to those at nodes adjacents to it. The resultant equation can be expressed in the same matrix form as for an interior node (equations 3.8 or 3.9) and the expressions for elements in the matrices are as shown in Table 3.3.C.

3.2.4 Summary of Finite Difference Equations for a Composite Wall or Slab

The matrix equations for various nodal points in a wall or slab were combined to form a finite difference model, expressed as equation (3.14).

The FDEs for boundary nodes of each wall or slab are coupled to the outdoor and indoor conditions as well as to internal surface temperatures at other walls and slabs through equations describing the heat and mass flux terms at the boundary surfaces (which together form a mathematical model for a room in a building).

$$\begin{array}{c|c|c|c|c}
\begin{array}{ccc}
[a]_1 & [b]_1 & \\
[a]_2 & [b]_2 & [c]_2 \\
& [a]_3 & [b]_3 & [c]_3 \\
& & \cdot & \cdot & \cdot \\
& & & [a]_k & [b]_k & [c]_k \\
& & & & \cdot & \cdot & \cdot \\
& & & & & [a]_{N-1} & [b]_{N-1} & [c]_{N-1} \\
& & & & & & [b]_N & [c]_N
\end{array}
&
\begin{array}{c}
\{X\}_1 \\
\{X\}_2 \\
\{X\}_3 \\
\cdot \\
\{X\}_k \\
\cdot \\
\{X\}_{N-1} \\
\{X\}_N
\end{array}
&
=
&
\begin{array}{c}
d_1 \\
d_2 \\
d_3 \\
\cdot \\
d_k \\
\cdot \\
d_{N-1} \\
d_N
\end{array}
&
(3.14)
\end{array}$$

3.3 Convective Heat and Mass Fluxes at Boundary Surfaces

At the surface of a wall (or slab), convective heat flux from the surrounding air to the wall surface, q_c , is described by the Newton's Law of Cooling:

$$q_c = h (T_{sr} - T) \quad (3.15)$$

Similarly, the vapour moisture flux from the surrounding air to the wall surface, m_v'' , is given by:

$$m_v'' = h_m \varepsilon_g (\rho_{v, sr} - \rho_v) \quad (3.16)$$

Here, the assumption is made that the net area over which the wall exchanges moisture with the surrounding air is proportional to the volume fraction of air-vapour mixture in the pores (ε_g) at the surface layer of the wall.

The convective heat and moisture transfer coefficient is assumed to be related by the Lewis relationship:

$$h_m = \frac{h}{\rho C_p} \quad (3.17)$$

where ρ and C_p are based on the moist air, i.e. the mixture of dry air and water vapour.

The driving potential for vapour moisture exchange in equation (3.16) is a density difference. Noting that:

$$\phi = \frac{n_v}{n_v + n_a}$$

whereas

$$\frac{P_j}{\rho_j} = \frac{RT}{M_j}$$

$$\rho_j = n_j M_j \quad \text{for } j = v, a$$

$$\therefore n_j = \frac{P_j}{RT}$$

$$\text{and } \phi = \frac{P_v}{RT} \frac{RT}{P_v + P_a} = \frac{P_v}{P_g}$$

$$\text{or } \phi = \frac{RT}{M_v P_g} \rho_v$$

$$\therefore \rho_v = \frac{M_v P_g}{RT} \phi$$

Using the above, the density difference was converted into a mole-fraction difference and by assuming that the difference in value between T_{sr} and T is small, equation (3.16) becomes:

$$m_v'' = \frac{M_v P_g}{RT} h_m \epsilon_g (\phi_{sr} - \phi) \quad (3.18)$$

where ϕ_{sr} = mole-fraction of water vapour in surrounding air.

When applied to model the heat and mass transfer at the internal surfaces of the walls and slabs (and windows) of an enclosed space (i.e. a room), the radiant heat exchanges amongst the building fabric surfaces must be modelled. Assuming that the internal surfaces behave as gray surfaces, the method can be derived from well established methods for calculating radiant heat exchanges among gray surfaces in an enclosure (e.g. 129). However, for an exterior wall, the effect of solar radiation incident

upon the exposed surface of the wall must be accounted for and, when a window is included, solar radiation transmitted through the window must also be modelled. The methods adopted to model radiation heat exchange in the building are detailed in Chapter Four.

3.4 Comparative Studies on Significance of Driving Forces for Moisture Transfer

3.4.1 Results Obtained by Using The Numerical Model

The numerical studies carried out by Huang ⁽⁵⁰⁾ and Huang et al ⁽⁵¹⁾ on drying of a piece of concrete slab and a slab of cement paste were repeated using the computer model developed. In that model, the conventional successive back-substitution method (with underrelaxation) ⁽¹³⁰⁾ was employed to solve the set of FDEs. The studies were carried out at conditions as summarized in Table 3.4. Simulated results for the two cases studied are as shown in Figures 3.1 and 3.2 which are almost identical to those presented by Huang and Huang et al.

3.4.2 Moisture Flux Components

The moisture flux components due to molecular diffusion (the first term in equation 3.5) and filtration flow (the second term in equation 3.5) were calculated separately based on the results at intermediate time-steps calculated in the above numerical studies so that the relative magnitude of each could be assessed. The contributions of moisture transfer from molecular diffusion and filtration flow calculated from the results of simulation for the concrete slab are shown in Figures 3.3 and 3.4 from which it can be seen that moisture transfer was dominated by diffusion. Over the range of conditions simulated, filtration flow only accounted for less than two percent except when the total moisture flux was extremely small. Similar results were also obtained for the case with cement paste slab.

3.4.3 Correlations Among Various Driving Potentials

As moisture transfer may be ascribed to a combination of different driving potentials (see Section 2.2), the total moisture fluxes calculated in the simulation studies were plotted against each of the following gradients to see which one would provide the best correlation for moisture transfer in concrete and cement paste:

- i) moisture content (Figure 3.5.a);
- ii) total gas pressure (Figure 3.5.b);
- iii) mole fraction (Figure 3.5.c);
- iv) water vapour pressure (Figure 3.5.d); and
- v) temperature (Figure 3.5.e)

From these results, it can be seen that:

- a) The correlations between the total moisture flux and the mole fraction gradient (Figure 3.5.c) and the vapour pressure gradient (Figure 3.5.d) are almost straight lines implying that moisture flux can be ascribed solely to either one of these driving forces.
- b) In a single-layered material, there is a significant correlation between the moisture flux and the moisture content gradient (Figure 3.5.a), but the correlation is not as good as those with other driving forces (except temperature).
- c) The results show that moisture transfer could be in either direction under the same temperature gradient (Figure 3.5.e). This implies that although a temperature gradient could cause moisture to migrate in a porous medium, its effect is indirect in that moisture transfer is established as a consequence of the temperature effect on other driving potentials, particularly on the mole fraction or water vapour pressure in the pores. This effect is given rise to by the relationship between the equilibrium

moisture content and the relative humidity ($\frac{P_v}{P_v^o}$) , i.e. the sorption isotherm relationship (see Section 2.1.4).

3.4.4 Conclusions From The Comparative Studies

The comparative studies showed that molecular diffusion is the dominant mechanism of moisture transfer in concrete and cement paste over the range of conditions simulated in the studies whereas filtration flow (due to a total pressure gradient) only contributed a minimal amount of moisture transfer. As the range of moisture contents in concrete and cement paste in buildings under normal conditions are within those covered in the studies, this conclusion may be applied in simulating heat and moisture transfer in concrete buildings. Furthermore, since the vapour pressure gradient appeared to be a good choice of driving potential for moisture transfer in concrete and cement paste, a simpler model may be developed with moisture transfer ascribed to vapour pressure gradient and with filtration flow neglected. A model making such assumptions was developed (see Chapter 4) and has been shown to be accurate and much more efficient in respect of computing time required in simulation runs as compared with the one developed from Huang's equations.

Chapter Four

A Differential Permeability Model for Simulating Building Heat And Moisture Transfer

A simplified mathematical model has been developed for simulating the coupled heat and moisture transfer in building fabric materials. In this chapter, derivation of the governing partial differential equations (PDEs) is detailed and the methods used to develop the numerical model from the governing PDEs are outlined. A formula is derived for evaluation of the moisture transport property of the material, the differential permeability, associated with this model. Accuracy of this formula was found to be good when compared with results calculated from Huang's model ⁽⁵⁰⁾. This chapter includes also summaries of the methods for modelling the heat and moisture exchanges between the building fabric and its ambient environment (indoor and outdoor), the radiant energy exchanges amongst building fabric surfaces, and the interaction between the indoor air and the air-conditioning system, which are required for the development of a building heat and moisture transfer model. The heat and moisture transfer model developed, which is called the differential permeability model, has also been verified to be accurate when compared with Huang's simulation results ⁽⁵⁰⁾ and with results of an experiment on drying of a piece of gypsum board ⁽⁵³⁾. Descriptions on these comparisons are included in this chapter.

4.1 An Overview of the Differential Permeability Model

The main objective of this research is to develop a coupled building and air-conditioning system model, facilitating in-depth studies on heat and moisture transport phenomena in intermittently air-conditioned buildings. If the building model alone incurs an intensive demand on computer power (like the one developed from Huang's equations, see Chapter 3), then, the coupled building and system model would be extremely time-consuming to develop, debug and use. Thus, it is desirable to have a computationally efficient model for use in investigating the complicated phenomena. This was achieved by neglecting the insignificant moisture transfer mechanism (filtration flow) in deriving the model and by using an efficient numerical scheme (the self-implicit scheme). Like Huang's model ⁽⁵⁰⁾, this model is restricted in application to materials that stay in the pendular state (but many building materials, particularly cementitious materials, are in this category).

Based on the assumption that vapour diffusion is the only moisture transfer mechanism, the material is under the pendular state, and that the liquid moisture content can change due to evaporation or condensation and can affect the rate of moisture transfer (the evaporation and condensation theory), conservation equations describing mass of moisture and heat energy in a piece of building material were derived, resulting in two coupled PDEs (three in Huang's model ⁽⁵⁰⁾). In it, vapour pressure gradient was adopted as the driving force for moisture transfer, differential permeability was adopted as the moisture transport property of the material, and the relationship between temperature and vapour pressure and the heat of condensation associated with changes in liquid moisture content are duly accounted for. The sorption isotherm was used to determine the balance between liquid and vapour moisture contents in the material so as to close the set of equations.

Except in the driving potential and the moisture transport property used, this model resembles in appearance many heat and moisture transfer models developed by others based on the evaporation and condensation theory (e.g. 8,124). Instead of the

conventional numerical methods for solving PDEs (e.g. backward in time, central in space finite differencing scheme and iteration with successive back-substitution and over or under relaxation ⁽¹³⁰⁾), the self-implicit scheme in conjunction with the Runge-Kutta-Merson method ^(131,132) were adopted to solve the set of equations. This numerical method was verified to be accurate and efficient in solving an ODE and a PDE (see Section 4.6 and Appendix A).

4.2 Permeability and Differential Permeability

The conventional method of estimating rate of moisture transfer in building materials ⁽⁴⁾ relates the moisture transfer rate (J_v) to the vapour pressure gradient across the entire thickness of the material as follows:

$$J_v = \delta \frac{P_{vo} - P_{vi}}{L} \quad (4.1)$$

where

P_{vo} & P_{vi} = vapour pressure of ambient air at the two sides of the permeable material.

L = thickness of the slab,

and δ is the transport property of the material, given the name "permeability".

Values of δ (or its reciprocal, $1/\delta$, called vapour resistivity) for a large variety of materials can be found in a wide range of literature (e.g. 4.5). These are normally obtained by standardized measurement methods, such as the "Dry-cup" and "Wet-cup" tests ⁽¹³³⁾.

The method for evaluation of moisture transfer, as given by equation (4.1), is primarily for assessment of the risk of interstitial condensation within building structures and is valid only for steady-state moisture transfer. However, the validity of data of δ in the literature has been questioned ⁽¹³⁴⁾. It was found that there were large

discrepancies between values given in different literature for the same kind of material (which should primarily be due to the different degrees of saturation of the materials and the different environmental conditions under which measurements were carried out).

From the fundamental theories of moisture transfer in porous media, it can be seen that the rate of moisture transfer in a porous material is dependent on its moisture content and the latter in turn is strongly dependent on the ambient vapour pressure and temperature. As there can be significant moisture content variation across a slab of building material, when studying the dynamic moisture transfer in building materials, it is more appropriate to take a differential approach where the moisture transfer rate (one-dimensional) at a given plane within the building wall or slab is related to the gradient of vapour pressure at that plane as follows:

$$J_v = -\mu \frac{\partial P_v}{\partial x} \quad (4.2)$$

The transport property (μ in the above equation), called differential permeability (as opposed to permeability δ ⁽¹³⁴⁾), is a variable and is a function of moisture content, i.e.

$$\mu = \mu(\epsilon_l) \quad (4.3)$$

Assuming the existence of local thermodynamic equilibrium, and ignoring the hysteresis phenomenon, the equilibrium moisture content in an elemental section of the porous medium under a given combination of local vapour pressure and temperature will be given by the material's sorption isotherm (Chapter 2). Then, the dependence of μ may be related to vapour pressure and temperature or simply to the relative humidity,

$$\mu = \mu(RH) \quad (4.4)$$

4.3 Calculation of Differential Permeability

4.3.1 Approximate Formula for Differential Permeability

For one-dimensional moisture transfer in a porous medium having a rigid solid phase and homogeneous and isotropic pore structures (such as concrete and cement paste), the rate of moisture transfer under low pore saturation condition (i.e. in pendular stage) is given by equation (3.5) ⁽⁵⁰⁾. Neglecting the filtration flow term (by assuming $\partial P_g / \partial x$ to be negligible) and by converting the vapour mole fraction (ϕ) in the equation into vapour pressure ($P_v = \phi P_g$), the moisture flux may be approximated by:

$$J_v \approx - \epsilon_g D \frac{M_a M_v}{M_g RT} \frac{\partial P_v}{\partial x} \quad (4.5)$$

Combining the above equation with equation (4.2), the differential permeability may be approximated by:

$$\mu \approx \epsilon_g D \frac{M_a M_v}{M_g RT} \quad (4.6)$$

According to the above equation, differential permeability of a material will increase with ϵ_g , the volume fraction occupied by the mixture of air and water vapour in the porous material. This implies that differential permeability will become smaller when the liquid moisture content of the material increases. This tendency of differential permeability value differs from those of many porous materials (e.g. timber and plywood) determined experimentally. For instance, the permeability of plywood, measured by McLean & Galbraith ⁽¹³⁴⁾, increases with the ambient air relative humidity and rises sharply when the ambient air relative humidity approaches 100%. Nevertheless, there are permeability measurements (e.g. Thomas et al's work on fibre board and gypsum board ⁽¹⁷⁷⁾) which show that, for some materials, their permeability values can exhibit a decreasing trend with increase in relative humidity of the ambient air.

An explanation for the tendency of permeability value implied by equation (4.6) is that for a porous material that stays in the pendular state, vapour diffusion is the dominant mechanism of moisture transport. When there is more liquid water in the material (which is stationary under the pendular state), and hence a larger portion of the pore volume is filled-up with liquid, the "effective" void space through which vapour diffusion can take place will become smaller. Consequently, a lower rate of moisture transfer will result and the permeability of the material becomes smaller. However, when liquid phase transport in the material dominates, which occurs when the material approaches the sorptional saturation state, the permeability should increase with moisture content. Equation (4.6) will therefore be applicable only to materials in the pendular state where vapour diffusion is the dominant mechanism of moisture transfer.

If equation (4.6) is a good approximation of the moisture transport property of a porous material, then, this property (at a given temperature and vapour pressure) can be easily determined when the sorption isotherm and the dry-state porosity of the material are available.

4.3.2 Comparison with Equation in Huang's Model

If equation (4.2) is valid, the moisture transport property of the material (denoted here as μ_{act}) will be given by:

$$\mu_{act} = \frac{J_v}{\left(\frac{\partial P_v}{\partial x}\right)}$$

Hence, values of μ_{act} can be calculated when the vapour flux (J_v) and the corresponding vapour pressure gradient ($\frac{\partial P_v}{\partial x}$) are known. Further, if the right hand side of equation (4.6) is a good approximation of this moisture transport property, a value of μ calculated from it should be close to that of μ_{act} .

By using the intermediate results of the numerical studies on drying of a piece of concrete slab (see Section 3.4), J_v and $\frac{\partial P_v}{\partial x}$ at various interior nodes and intermediate time steps of the simulation study were calculated (the former was calculated from equation 3.5 and the latter was calculated from the vapour mole-fractions and total gas pressures evaluated in the simulation). They were then used to evaluate μ_{act} 's and the results were compared with μ 's calculated from equation (4.6) (based on the corresponding interior node conditions) which showed that the two were in good agreement (Figure 4.1). Equally good agreement was found from a study on cement paste. Equation (4.6) therefore would be able to give a good approximation of differential permeability (the moisture transport property) of concrete and cement paste (and other materials having similar moisture sorptional behaviour, e.g. cement-sand plastering, brick, gypsum board, etc.). This equation has been incorporated into the moisture transfer model for determination of the moisture transport property of materials.

4.4 Governing Equations of the Differential Permeability Model

The following shows, step-by-step, derivation of the governing equations of the differential permeability heat and moisture transfer model.

Denote the rate of one-dimensional moisture transfer across an intermediate plane of a slab of porous material by J_v , then, for an elemental section in the slab, the rate of increase in water vapour concentration (mass per unit volume) is given by:

$$\frac{\partial C_v}{\partial t} = -\frac{\partial J_v}{\partial x} + \dot{e} \quad (4.7)$$

Based on the assumption that moisture transport can only take place in the vapour phase, the addition of vapour moisture due to evaporation from the liquid phase, \dot{e} , must be accompanied by a reduction in liquid water concentration at the same elemental section as described by:

$$\frac{\partial C_l}{\partial t} = -\dot{e} \quad (4.8)$$

Adding (4.7) & (4.8) yields:

$$\frac{\partial}{\partial t} (C_v + C_l) = -\frac{\partial J_v}{\partial x} \quad (4.9)$$

Since $C_v = \rho_v \epsilon_g$ and $C_l = \rho_l \epsilon_l$; and considering that liquid water density is much greater than vapour density and does not vary significantly with pressure and temperature, equation (4.9) may be approximated by:

$$\frac{\partial}{\partial t} (C_v + C_l) \approx \rho_l \frac{\partial \epsilon_l}{\partial t} = -\frac{\partial J_v}{\partial x} \quad (4.10)$$

Applying equation (4.2), the above moisture mass conservation equation becomes:

$$\rho_l \frac{\partial \epsilon_l}{\partial t} = \frac{\partial}{\partial x} \left(\mu \frac{\partial P_v}{\partial x} \right) \quad (4.11)$$

Applying the energy conservation principle and the Fourier's law of conduction, the following energy conservation equation can be derived:

$$(\rho C_p)_B \frac{\partial T}{\partial t} = \frac{\partial}{\partial x} \left(k_B \frac{\partial T}{\partial x} \right) + h_{fg} \rho_l \frac{\partial \epsilon_l}{\partial t} \quad (4.12)$$

In which $(\rho C_p)_B$ is the bulk heat capacity of the material and is given by:

$$(\rho C_p)_B = \rho_s \epsilon_s C_{p_s} + \rho_l \epsilon_l C_{p_l} + \rho_g \epsilon_g C_{p_g} \quad (4.13)$$

whereas the bulk thermal conductivity, k_B , is evaluated using Kingery's empirical formula ⁽⁵⁰⁾ as follows:

$$k_B = [(k_g)^n \epsilon_g + (k_l)^n \epsilon_l + (k_s)^n \epsilon_s]^{1/n} \quad (4.14)$$

where n is an empirically determined coefficient which equals to 0.25.

The last term in equation (4.12) accounts for the amount of condensation heat associated with the change in liquid moisture content. In deriving the energy conservation equation, the assumption was made that thermodynamic equilibrium exists in the elemental section such that the temperature of the solid, liquid and gaseous phases are identical.

Equations (4.11) and (4.12) are the two coupled governing equations describing the heat and moisture transfer in the porous medium. Examining these equations revealed that there are three variables involved, namely, P_v , T and ϵ_l . Hence, one extra equation is required to close the set of equations. The sorption isotherm of the material relating the equilibrium moisture content to vapour pressure and temperature is used for this purpose:

$$\epsilon_l = \epsilon_l (P_v, T) \quad (4.15)$$

and its time derivative is then:

$$\frac{\partial \epsilon_l}{\partial t} = \frac{\partial \epsilon_l}{\partial P_v} \cdot \frac{\partial P_v}{\partial t} + \frac{\partial \epsilon_l}{\partial T} \cdot \frac{\partial T}{\partial t} \quad (4.16)$$

Equations (4.11) and (4.12) therefore can be written as:

$$(\rho_l \frac{\partial \epsilon_l}{\partial P_v}) \frac{\partial P_v}{\partial t} + (\rho_l \frac{\partial \epsilon_l}{\partial T}) \frac{\partial T}{\partial t} = \mu \frac{\partial^2 P_v}{\partial x^2} + \frac{\partial \mu}{\partial x} \frac{\partial P_v}{\partial x} \quad (4.17)$$

$$(-h_{fg} \rho_l \frac{\partial \epsilon_l}{\partial P_v}) \frac{\partial P_v}{\partial t} + [(\rho C_p)_B - h_{fg} \rho_l \frac{\partial \epsilon_l}{\partial T}] \frac{\partial T}{\partial t} = k_B \frac{\partial^2 T}{\partial x^2} + \frac{\partial k_B}{\partial x} \frac{\partial T}{\partial x} \quad (4.18)$$

or alternatively in the form of:

$$a_{11} \frac{\partial P_v}{\partial t} + a_{12} \frac{\partial T}{\partial t} = c_{11} \frac{\partial^2 P_v}{\partial x^2} + c_{12} \frac{\partial P_v}{\partial x} \quad (4.19)$$

$$a_{21} \frac{\partial P_v}{\partial t} + a_{22} \frac{\partial T}{\partial t} = c_{21} \frac{\partial^2 T}{\partial x^2} + c_{22} \frac{\partial T}{\partial x} \quad (4.20)$$

where, the coefficients a's and c's are as defined in Table 4.1.

4.5 Derivatives of the Sorption Isotherm Equation

The coefficients in equations (4.19) & (4.20) involve derivatives of the liquid moisture content in the porous material with respect to P_v and T . These derivatives need to be calculated with reference to the sorption isotherm relationship of the medium. The sorption isotherm relationships for most building materials are presented as functions of relative humidity rather than functions of vapour pressure and temperature (as in (4.15)), i.e.:

$$\epsilon_l = \epsilon_l (RH) \quad (4.21)$$

Since $RH = \frac{P_v}{P_{vs}}$ and $P_{vs} = P_{vs}(T)$ (i.e. the saturation vapour pressure is a function of temperature only), the derivatives of ϵ_l with respect to P_v and T can be evaluated by:

$$\frac{\partial \epsilon_l}{\partial P_v} = \frac{\partial \epsilon_l}{\partial RH} \cdot \frac{\partial RH}{\partial P_v}$$

$$\therefore \frac{\partial \epsilon_l}{\partial P_v} = \frac{1}{P_{vs}} \cdot \frac{\partial \epsilon_l}{\partial RH}, \text{ and;} \quad (4.22)$$

$$\frac{\partial \epsilon_l}{\partial T} = \frac{\partial \epsilon_l}{\partial RH} \cdot \frac{\partial RH}{\partial T}$$

$$\therefore \frac{\partial \epsilon_l}{\partial T} = -\frac{P_v}{P_{vs}^2} \cdot \frac{\partial P_{vs}}{\partial T} \cdot \frac{\partial \epsilon_l}{\partial RH} \quad (4.23)$$

where $\frac{\partial \epsilon_l}{\partial RH}$ can be evaluated directly from the mathematic expression for the sorption isotherm (4.21) and the derivative $\frac{\partial P_{vs}}{\partial T}$ can be evaluated from an empirical equation for

P_{vs} as a function of temperature such as the following one (135):

$$P_{vs} = 2327 \exp \left\{ 6789 \left(3.4112 \times 10^{-3} - \frac{1}{T} \right) - 5.031 \ln \left(\frac{T}{293.15} \right) \right\} \quad (4.24)$$

Hence,

$$\frac{\partial P_{vs}}{\partial T} = \frac{P_{vs}}{T} \left(\frac{6789}{T} - 5.031 \right) \quad (4.25)$$

and

$$\frac{\partial \varepsilon_1}{\partial T} = -\frac{RH}{T} \left(\frac{6789}{T} - 5.031 \right) \frac{\partial \varepsilon_1}{\partial RH} \quad (4.26)$$

These equations were incorporated into the heat and moisture transfer model for evaluation of the coefficients in the governing equations.

4.6 The Numerical Heat and Moisture Transfer Model

4.6.1 The Self-implicit Discretization Scheme and the Runge-Kutta-Merson Method

The governing equations (4.19) & (4.20) are to be solved in conjunction with the sorption isotherm equation when applied to simulate the heat and moisture transfer through a porous material. As these equations are non-linear PDEs, numerical method was adopted for solving them. To apply the numerical solution method, a wall or slab was first discretized into N-1 slices (see Figure 4.2), with the states of these slices represented by variables at the N number of nodal points. In the development of the numerical model, equations (4.19) and (4.20) were partially discretized (in the spatial dimension only) into a set of ordinary differential equations (ODEs) and the Runge-Kutta-Merson ^(131,132) scheme was adopted for solving the ODEs. A self-implicit scheme ⁽¹³⁶⁾ similar to that used by Ewen and Thomas ⁽¹³⁷⁾ was employed in the derivation of the ODEs to approximate the time-derivatives. Further explanations on this numerical scheme are given in Appendix A.

With reference to equation (4.19), how the numerical scheme can be applied is briefly described as follows:

- i) For a variable $\phi(x,t)$, the spatial derivatives of ϕ may be approximated by the following central differences:

$$\frac{\partial^2 \phi}{\partial x^2} \approx \frac{\phi_+ - 2\phi + \phi_-}{(\Delta x)^2} \quad (4.27)$$

$$\frac{\partial \phi}{\partial x} \approx \frac{\phi_+ - \phi_-}{2\Delta x} \quad (4.28)$$

- ii) Following the Crank-Nicolson (C-N) scheme ⁽¹³⁰⁾, for a function $\phi(x,t)$ with time derivative $\frac{\partial \phi(x,t)}{\partial t} = \psi(x,t)$, the time derivative between time t (the n^{th} time-step) and $t+\Delta t$ (the $n+1^{\text{th}}$ time-step) is approximated by:

$$\frac{\partial \phi}{\partial t} \approx \lambda \psi(x,t+\Delta t) + (1-\lambda) \psi(x,t) \quad (4.29)$$

where $0 \leq \lambda \leq 1$. If $\lambda = 0$, the scheme is explicit; if $\lambda = 1$, the scheme is fully implicit (adopted in this work); and the conventional C-N scheme has $\lambda = 0.5$.

Denoting:

$$\Delta P_v = P_v^{n+1} - P_v^n \quad ; \quad \Delta P_{v+} = P_{v+}^{n+1} - P_{v+}^n \quad ; \quad \Delta P_{v-} = P_{v-}^{n+1} - P_{v-}^n$$

where

$$P_v^n = P_v(x,t) \quad ; \quad P_v^{n+1} = P_v(x,t+\Delta t)$$

$$P_{v+}^n = P_v(x+\Delta x,t) \quad ; \quad P_{v+}^{n+1} = P_v(x+\Delta x,t+\Delta t)$$

$$P_{v-}^n = P_v(x-\Delta x,t) \quad ; \quad P_{v-}^{n+1} = P_v(x-\Delta x,t+\Delta t)$$

and applying the C-N scheme with the the spatial derivatives replaced by the finite difference approximations, equation (4.19) may be written as:

$$\begin{aligned} a_{11} \frac{\partial P_v}{\partial t} + a_{12} \frac{\partial T}{\partial t} = & c_{11} \lambda \frac{\Delta P_{v+} - 2\Delta P_v + \Delta P_{v-}}{(\Delta x)^2} \\ & + c_{12} \lambda \frac{\Delta P_{v+} - \Delta P_{v-}}{2\Delta x} \\ & + c_{11} \frac{P_{v+}^n - 2P_v^n + P_{v-}^n}{(\Delta x)^2} + c_{12} \frac{P_{v+}^n - P_{v-}^n}{2\Delta x} \end{aligned} \quad (4.30)$$

iii) Each ΔP_{v+} , ΔP_v & ΔP_{v-} term is multiplied by $\frac{\Delta t}{\Delta t}$ to become:

$$\Delta t \frac{\Delta P_{v+}}{\Delta t} \quad ; \quad \Delta t \frac{\Delta P_v}{\Delta t} \quad \& \quad \Delta t \frac{\Delta P_{v-}}{\Delta t}$$

iv) The $\frac{\Delta P_v}{\Delta t}$ terms are regarded as $\frac{\partial P_v}{\partial t}$ and, after re-arranging, equation (4.30)

becomes:

$$\begin{aligned} & -\lambda \Delta t \left[\frac{c_{11}}{\Delta x^2} - \frac{c_{12}}{2\Delta x} \right] \frac{\partial P_{v-}}{\partial t} + [a_{11} + \lambda \Delta t \frac{2c_{11}}{\Delta x^2}] \frac{\partial P_v}{\partial t} - \lambda \Delta t \left[\frac{c_{11}}{\Delta x^2} + \frac{c_{12}}{2\Delta x} \right] \frac{\partial P_{v+}}{\partial t} \\ & = c_{11} \frac{P_{v+}^n - 2P_v^n + P_{v-}^n}{\Delta x^2} + c_{12} \frac{P_{v+}^n - P_{v-}^n}{2\Delta x} - a_{12} \frac{\partial T}{\partial t} \end{aligned} \quad (4.31)$$

4.6.2 The Merits of The Numerical Scheme

The above numerical scheme was adopted for solving the governing PDEs because:

- the resultant equations become ODEs which are readily solved by methods such as the Runge-Kutta-Merson method;
- by setting $\lambda = 1$ (i.e. fully implicit) the numerical scheme will be stable which will enable larger time-steps be used in the simulation calculations and will thus speed up the solution process;
- although the scheme is fully implicit, the time derivatives of the variables (here P_v 's) at the $n+1^{\text{th}}$ time step are all based on their values at the n^{th} time step (at the right hand side of the equation) and hence can be approximated by solved values of the variables at the n^{th} time step; and
- by applying the Runge-Kutta-Merson scheme, the truncation error of each time step of calculation may be estimated. This can be used as a

guideline for controlling size of time step to be used. Otherwise, the error estimation might involve more steps of calculation (e.g. in a four stage Runge-Kutta scheme (138)).

When applied to solve a simple linear ODE, this scheme was shown to be able to provide accurate results, was able to eliminate the steady error as the dependent variable approached the steady-state solution and was able to gradually enlarge the integration step size while approaching the steady-state solution. The method had also been applied to solve a PDE where analytical solution is available and excellent agreement between the numerical solution and the analytical solution was found (these tests are described in Appendix A).

4.6.3 Finite Difference Equations for Interior Nodes

The ODE for P_v at an interior node obtained by using the above discretization scheme has already been shown in the above. The energy equation in terms of temperature is likewise discretized to become:

$$\begin{aligned} & -\lambda\Delta t \left[\frac{c_{21}}{\Delta x^2} - \frac{c_{22}}{2\Delta x} \right] \frac{\partial T_-}{\partial t} + \left[a_{22} + \lambda\Delta t \frac{2c_{21}}{\Delta x^2} \right] \frac{\partial T}{\partial t} - \lambda\Delta t \left[\frac{c_{11}}{\Delta x^2} + \frac{c_{12}}{2\Delta x} \right] \frac{\partial T_+}{\partial t} \\ & = c_{21} \frac{T_+^n - 2T^n + T_-^n}{\Delta x^2} + c_{22} \frac{T_+^n - T_-^n}{2\Delta x} - a_{22} \frac{\partial P_v}{\partial t} \end{aligned} \quad (4.32)$$

In short form, the partially discretized governing equations for an interior node may be written as:

$$A_{i11} \frac{\partial P_{v-}}{\partial t} + A_{i21} \frac{\partial P_v}{\partial t} + A_{i31} \frac{\partial P_{v+}}{\partial t} = B_{i1} \quad (4.33)$$

$$A_{i12} \frac{\partial T_-}{\partial t} + A_{i22} \frac{\partial T}{\partial t} + A_{i32} \frac{\partial T_+}{\partial t} = B_{i2} \quad (4.34)$$

where the subscript 'i' of coefficients A's and B's denotes the node number; the second subscript of A's ranges from 1 to 3 denoting respectively the node to the left (node i-1),

the current node (node i) and the node to the right (node i+1); and the last subscript of A's and B's is 1 or 2 denoting the pressure and temperature equations respectively.

4.6.4 Finite Difference Equations for Boundary Nodes

At the boundary of the solid domain of a wall or slab, the thickness of the elemental volume is $\frac{\Delta x}{2}$ (see Figure 4.3). At the boundary surface, the material is exchanging heat and moisture with the ambient air at the rates of q'' and m_v'' (per unit area) respectively. Heat and moisture balances for this slice of thickness $\frac{\Delta x}{2}$ at the boundary give the following equations:

$$\frac{\Delta x}{2} \cdot \rho_l \frac{\partial \epsilon_l}{\partial t} = m_v'' + \mu \frac{\partial P_v}{\partial x} \quad (4.35)$$

$$\frac{\Delta x}{2} \cdot (\rho C_p)_B \frac{\partial T}{\partial t} = q'' + k_B \frac{\partial T}{\partial x} + \frac{\Delta x}{2} \rho_l \frac{\partial \epsilon_l}{\partial t} \cdot h_{fg} \quad (4.36)$$

Sub. (4.16) into (4.35) and re-arranging,

$$\rho_l \frac{\partial \epsilon_l}{\partial P_v} \cdot \frac{\partial P_v}{\partial t} + \rho_l \frac{\partial \epsilon_l}{\partial T} \cdot \frac{\partial T}{\partial t} = \frac{2}{\Delta x} m_v'' + \frac{2}{\Delta x} \mu \frac{\partial P_v}{\partial x} \quad (4.37)$$

Similary, (4.36) becomes:

$$\begin{aligned} (\rho C_p)_B \frac{\partial T}{\partial t} &= \frac{2}{\Delta x} q'' + \frac{2}{\Delta x} k_B \frac{\partial T}{\partial x} + h_{fg} \rho_l \frac{\partial \epsilon_l}{\partial P_v} \cdot \frac{\partial P_v}{\partial t} \\ &\quad + h_{fg} \rho_l \frac{\partial \epsilon_l}{\partial T} \cdot \frac{\partial T}{\partial t} \end{aligned} \quad (4.38)$$

Collecting time derivative terms to the LHS, (4.37) and (4.38) become:

$$a_{11} \frac{\partial P_v}{\partial t} + a_{12} \frac{\partial T}{\partial t} = c_{12} \frac{\partial P_v}{\partial x} + d_1 \quad (4.39)$$

$$a_{21} \frac{\partial P_v}{\partial t} + a_{22} \frac{\partial T}{\partial t} = c_{22} \frac{\partial T}{\partial x} + d_2 \quad (4.40)$$

where, the coefficients a's, c's and d's are as defined in Table 4.1.

Following the same discretization scheme and let subscript 'a' denote the node adjacent to the boundary node (either node 2 or N-1) within the wall or slab, equations (4.39) & (4.40) become:

$$[a_{11} + \lambda \Delta t \frac{c_{12}}{\Delta x}] \frac{\partial P_v}{\partial t} - \lambda \Delta t \frac{c_{12}}{\Delta x} \frac{\partial P_{va}}{\partial t} = c_{12} \frac{P_{va}^n - P_v^n}{\Delta x} + d_1 - a_{12} \frac{\partial T}{\partial t} \quad (4.41)$$

$$[a_{22} + \lambda \Delta t \frac{c_{22}}{\Delta x}] \frac{\partial T}{\partial t} - \lambda \Delta t \frac{c_{22}}{\Delta x} \frac{\partial T_a}{\partial t} = c_{22} \frac{T_a^n - T^n}{\Delta x} + d_2 - a_{22} \frac{\partial P_v}{\partial t} \quad (4.42)$$

In short form, the partially discretized governing equations for a boundary node may be written as:

$$A_{i21} \frac{\partial P_v}{\partial t} + A_{ij1} \frac{\partial P_{va}}{\partial t} = B_{i1} \quad (4.43)$$

$$A_{i22} \frac{\partial T}{\partial t} + A_{ij2} \frac{\partial T_a}{\partial t} = B_{i2} \quad (4.44)$$

where the subscript 'i' of coefficients A's and B's here will either be 1 or N; subscript 'j' of A's will either be 1 (if i = N) or 3 (if i = 1); and subscript 'a' denotes the node number of the adjacent node (2 or N-1).

4.6.5 Finite Difference Equations for Interface Nodes

For a composite wall comprising several layers of different materials, the equations for the node at the interface of two adjacent layers of materials may be derived following procedures similar to those described above for a boundary node. That is, equations for a slice of each material can be derived by heat and moisture balance considerations, assuming that the heat and moisture fluxes at the interface plane to be q''_I and J_I respectively (see Figure 4.4). For the left slice of $\frac{\Delta x}{2}$ thick;

$$\frac{\Delta x_-}{2} \rho_l \frac{\partial \epsilon_{l-}}{\partial t} = -J_I - \mu_- \frac{\partial P_v}{\partial x_-} \quad (4.45)$$

$$\frac{\Delta x_-}{2} (\rho C_p)_{B_-} \frac{\partial T}{\partial t} = -q''_I - k_{B_-} \frac{\partial T}{\partial x_-} + \frac{\Delta x_-}{2} \rho_l \frac{\partial \epsilon_{l-}}{\partial t} \cdot h_{fg-} \quad (4.46)$$

For the right slice of $\frac{\Delta x_+}{2}$ thick

$$\frac{\Delta x_+}{2} \rho_l \frac{\partial \epsilon_{l+}}{\partial t} = J_I + \mu_+ \frac{\partial P_v}{\partial x_+} \quad (4.47)$$

$$\frac{\Delta x_+}{2} (\rho C_p)_{B_+} \frac{\partial T}{\partial t} = q''_I - k_{B_+} \frac{\partial T}{\partial x_+} + \frac{\Delta x_+}{2} \rho_l \frac{\partial \epsilon_{l+}}{\partial t} \cdot h_{fg+} \quad (4.48)$$

Adding (4.45) and (4.47) allows the interface moisture flux (which is unknown) to be eliminated and gives:

$$\frac{\Delta x_-}{2} \rho_l \frac{\partial \epsilon_{l-}}{\partial t} + \frac{\Delta x_+}{2} \rho_l \frac{\partial \epsilon_{l+}}{\partial t} = -\mu_- \frac{\partial P_v}{\partial x_-} + \mu_+ \frac{\partial P_v}{\partial x_+} \quad (4.49)$$

Likewise, the interface heat flux is eliminated by adding (4.46) to (4.48):

$$\begin{aligned} \left[\frac{\Delta x_-}{2} (\rho C_p)_{B_-} + \frac{\Delta x_+}{2} (\rho C_p)_{B_+} \right] \frac{\partial T}{\partial t} = & -k_{B_-} \frac{\partial T}{\partial x_-} + k_{B_+} \frac{\partial T}{\partial x_+} + \frac{\Delta x_-}{2} \rho_l \frac{\partial \epsilon_{l-}}{\partial t} h_{fg-} \\ & + \frac{\Delta x_+}{2} \rho_l \frac{\partial \epsilon_{l+}}{\partial t} h_{fg+} \end{aligned} \quad (4.50)$$

Note that:

$$\frac{\partial \epsilon_{l-}}{\partial t} = \frac{\partial \epsilon_{l-}}{\partial P_v} \cdot \frac{\partial P_v}{\partial t} + \frac{\partial \epsilon_{l-}}{\partial T} \cdot \frac{\partial T}{\partial t} \quad (4.51)$$

$$\frac{\partial \epsilon_{l+}}{\partial t} = \frac{\partial \epsilon_{l+}}{\partial P_v} \cdot \frac{\partial P_v}{\partial t} + \frac{\partial \epsilon_{l+}}{\partial T} \cdot \frac{\partial T}{\partial t} \quad (4.52)$$

Sub. (4.51) and (4.52) into (4.49) and (4.50) and re-arranging yields:

$$\rho_l \left\{ \frac{\Delta x_-}{2} \frac{\partial \epsilon_{l-}}{\partial P_v} + \frac{\Delta x_+}{2} \frac{\partial \epsilon_{l+}}{\partial P_v} \right\} \frac{\partial P_v}{\partial t} + \rho_l \left\{ \frac{\Delta x_-}{2} \frac{\partial \epsilon_{l-}}{\partial T} + \frac{\Delta x_+}{2} \frac{\partial \epsilon_{l+}}{\partial T} \right\} \frac{\partial T}{\partial t}$$

$$= -\mu_- \frac{\partial P_v}{\partial x_-} + \mu_+ \frac{\partial P_v}{\partial x_+}, \text{ and} \quad (4.53)$$

$$\begin{aligned} & \left\{ \left[\frac{\Delta x_-}{2} (\rho C_p)_{B_-} + \frac{\Delta x_+}{2} (\rho C_p)_{B_+} \right] - \rho_l \left[h_{fg_-} \frac{\Delta x_-}{2} \frac{\partial \epsilon_{l-}}{\partial T} + h_{fg_+} \frac{\Delta x_+}{2} \frac{\partial \epsilon_{l+}}{\partial T} \right] \right\} \frac{\partial T}{\partial t} \\ & - \left\{ \rho_l h_{fg} \left[\frac{\Delta x_-}{2} \frac{\partial \epsilon_{l-}}{\partial P_v} + \frac{\Delta x_+}{2} \frac{\partial \epsilon_{l+}}{\partial P_v} \right] \right\} \frac{\partial P_v}{\partial t} \\ & = -k_{B_-} \frac{\partial T}{\partial x_-} + k_{B_+} \frac{\partial T}{\partial x_+} \end{aligned} \quad (4.54)$$

Using the coefficients as defined in Table 4.1, equations (4.53) and (4.54) may be written as:

$$a_{11} \frac{\partial P_v}{\partial t} + a_{12} \frac{\partial T}{\partial t} = -\mu_- \frac{\partial P_v}{\partial x_-} + \mu_+ \frac{\partial P_v}{\partial x_+} \quad (4.55)$$

$$a_{21} \frac{\partial P_v}{\partial t} + a_{22} \frac{\partial T}{\partial t} = -k_{B_-} \frac{\partial T}{\partial x_-} + k_{B_+} \frac{\partial T}{\partial x_+} \quad (4.56)$$

Approximating the spatial derivatives by one-sided finite differences as follows:

$$\frac{\partial P_v}{\partial x_-} = \frac{P_v - P_{v-}}{\Delta x_-} = \frac{\Delta P_v - \Delta P_{v-}}{\Delta x_-} + \frac{P_v^n - P_{v-}^n}{\Delta x_-}$$

$$\frac{\partial P_v}{\partial x_+} = \frac{P_{v+} - P_v}{\Delta x_+} = \frac{\Delta P_{v+} - \Delta P_v}{\Delta x_+} + \frac{P_{v+}^n - P_v^n}{\Delta x_+}$$

$$\frac{\partial T}{\partial x_-} = \frac{T - T_-}{\Delta x_-} = \frac{\Delta T - \Delta T_-}{\Delta x_-} + \frac{T^n - T_-^n}{\Delta x_-}$$

$$\frac{\partial T}{\partial x_+} = \frac{T_+ - T}{\Delta x_+} = \frac{\Delta T_+ - \Delta T}{\Delta x_+} + \frac{T_+^n - T^n}{\Delta x_+}$$

and applying the partial discretization and the self-implicit schemes, equations (4.55) and (4.56) become:

$$\begin{aligned}
& [-\lambda\Delta t \frac{\mu_-}{\Delta x_-}] \frac{\partial P_{v-}}{\partial t} + [a_{11} + \lambda\Delta t (\frac{\mu_-}{\Delta x_-} + \frac{\mu_+}{\Delta x_+})] \frac{\partial P_v}{\partial t} - [\lambda\Delta t \frac{\mu_+}{\Delta x_+}] \frac{\partial P_{v+}}{\partial t} \\
& = -\mu_- \frac{P_v^n - P_{v-}^n}{\Delta x_-} + \mu_+ \frac{P_{v+}^n - P_v^n}{\Delta x_+} - a_{12} \frac{\partial T}{\partial t}
\end{aligned} \tag{4.57}$$

$$\begin{aligned}
& [-\lambda\Delta t \frac{k_{B-}}{\Delta x_-}] \frac{\partial T_-}{\partial t} + [a_{22} + \lambda\Delta t (\frac{k_{B-}}{\Delta x_-} + \frac{k_{B+}}{\Delta x_+})] \frac{\partial T}{\partial t} - [\lambda\Delta t \frac{k_{B+}}{\Delta x_+}] \frac{\partial T_+}{\partial t} \\
& = -k_{B-} \frac{T^n - T_-^n}{\Delta x_-} + k_{B+} \frac{T_+^n - T^n}{\Delta x_+} - a_{21} \frac{\partial P_v}{\partial t}
\end{aligned} \tag{4.58}$$

In short form, the partially discretized governing equations for an interface node have the same appearance as the interior nodes as follows:

$$A_{i11} \frac{\partial P_{v-}}{\partial t} + A_{i21} \frac{\partial P_v}{\partial t} + A_{i31} \frac{\partial P_{v+}}{\partial t} = B_{i1} \tag{4.59}$$

$$A_{i12} \frac{\partial T_-}{\partial t} + A_{i22} \frac{\partial T}{\partial t} + A_{i32} \frac{\partial T_+}{\partial t} = B_{i2} \tag{4.60}$$

4.6.6 Summary of Equations

From the above, it can be seen that for a composite wall, the governing equations may be expressed as:

$$\begin{bmatrix} A_{121} & A_{131} \\ A_{211} & A_{221} & A_{231} \\ A_{311} & A_{321} & A_{331} \\ . & . & . \end{bmatrix} \begin{Bmatrix} \overset{\circ}{P}_{v1} \\ \overset{\circ}{P}_{v2} \\ . \\ . \end{Bmatrix} = \begin{Bmatrix} B_{11} \\ B_{21} \\ . \\ . \end{Bmatrix} \tag{4.61}$$

$$\begin{bmatrix} A_{122} & A_{132} \\ A_{212} & A_{222} & A_{232} \\ A_{312} & A_{322} & A_{332} \\ . & . & . \end{bmatrix} \begin{Bmatrix} \overset{\circ}{T}_1 \\ \overset{\circ}{T}_2 \\ . \\ . \end{Bmatrix} = \begin{Bmatrix} B_{12} \\ B_{22} \\ . \\ . \end{Bmatrix} \tag{4.62}$$

Expressions for the elements in the matrices $\{A\}$ and $\{B\}$ pertaining to the interior nodes, boundary nodes and the interface nodes in a composite wall/slab are summarized in Table 4.2. Note that the above matrix equations are both tri-diagonal equations and therefore the efficient tri-diagonal matrix algorithm (TDMA) ⁽¹³⁸⁾ may be employed for solving them. Moreover, the time derivative vectors $\{\dot{P}_v\}$ & $\{\dot{T}\}$ need to be solved by an iterative procedure as the column vector $\{B\}$ at RHS of each equation contains the time derivative of the variable of the other equation (see Table 4.2).

4.7 Heat and Mass Fluxes at Boundary Surfaces

4.7.1 Convective Heat and Mass Fluxes

The methods described in Section 3.3 for modelling convective heat and mass fluxes at boundary surfaces of walls and slabs in the building are applicable to this model. The only change required is in the treatment of the moisture exchange at the boundary surface due to the use of P_v as the moisture driving potential in the differential permeability model. Here, the density difference in equation (3.16) has to be converted into a vapour pressure difference between that at the wall/slab surface and at the room air as follows:

$$\text{Since } \rho_v = \frac{M_v P_v}{RT}$$

$$\text{then } \dot{m}_v = h_m \epsilon_g \frac{M_v}{RT} (P_{v, sr} - P_v) \quad (4.63)$$

in which the assumption is again made that the difference in value between T_{sr} and T is small.

Also, for convenience in calculating mass of vapour moisture in the room air, the vapour density difference term in equation (3.16) is converted into a humidity ratio difference term as follows:

$$\text{Since } \rho_v = \rho_a w$$

$$\therefore \quad \dot{m}_v = h_m \epsilon_g \rho_a (w_{rm} - w) \quad (4.64)$$

From the Lewis relationship (equation 3.17), the convective mass transfer coefficient (h_m) in (4.64) may be expressed in terms of the convective heat transfer coefficient (h) as follows:

$$\dot{m}_v = \frac{h}{C_{p_a}} \epsilon_g (w_{rm} - w) \quad (4.65)$$

As humidity ratio is used in the air-node equations (see Section 4.9), there will be frequent conversions between vapour pressure and humidity ratio in the simulation calculations. The conversion formulae required can be derived from the perfect gas law as follows:

$$P_v V = m_v \frac{R}{M_v} T \quad (4.66)$$

$$P_a V = m_a \frac{R}{M_a} T \quad (4.67)$$

As both the dry-air and water-vapour occupy the same volume (V) and are at the same temperature (T),

$$\therefore \quad \frac{m_v}{m_a} = w = \frac{M_v P_v}{M_a P_a} \quad (4.68)$$

Noting that $P_a = P_{atm} - P_v$ and re-arranging,

$$P_v = w \frac{M_a}{M_v} (P_{atm} - P_v) \quad (4.69)$$

$$\therefore \quad P_v = \frac{\left(\frac{M_a}{M_v}\right) w P_{atm}}{1 + \left(\frac{M_a}{M_v}\right) w} \quad (4.70)$$

4.7.2 Radiation Heat Flux

When there is solar radiation incident upon the external surface of an exterior wall, the amount of solar radiation (short wave) that will be absorbed by the wall surface, q_{ro} , is given by :

$$q_{ro} = \alpha I_t \quad (4.71)$$

where α is the short wave radiation absorptance of wall surface and I_t is the intensity of total solar radiation incident upon the wall surface.

The absorbed solar radiation contributes a heat flow into the exterior wall in addition to the convective heat flow from the outdoor air to the wall surface. The net 'long-wave' radiation exchange between the external surface of the exterior wall and the surrounding may be assumed zero for a vertical surface (5).

At the indoor side, longwave radiation exchange among wall, slab and window surfaces are modelled based on fundamental radiation heat transfer theory for gray surfaces (129) as summarized below:

Let $q_{rl,i}$ be net radiation flux leaving surface i , it follows from the theory of diffuse radiation heat exchange among gray surfaces of an enclosure that:

$$q_{rl,i} = \sum_{j=1}^{N_s} F_{ij} (J_{Ri} - J_{Rj}) \quad (4.72)$$

where N_s is the total number of internal surfaces in the room; F_{ij} denotes the radiation shape factor between surfaces i & j ; and J_{Ri} & J_{Rj} are the radiosities of surfaces i & j respectively.

The radiosities J_{Ri} for $i = 1, 2, \dots, N_s$ need to be found by solving simultaneously the following equations:

$$[R_{ij}]\{J_R\} = \{E_b\} \quad (4.73)$$

where $[R_{ij}]$ is a matrix with elements as follows:

$$\begin{aligned} R_{ij} &= -e_i F_{ij} \quad \text{for } i \neq j \\ R_{ii} &= (1 + \sum_{j=1}^{N_s} e_i F_{ij}) \end{aligned} \quad (4.74)$$

$$\{J_R\} = \begin{Bmatrix} J_{R1} \\ J_{R2} \\ \cdot \\ \cdot \\ J_{RN_s} \end{Bmatrix}$$

$$\{E_b\} = \sigma \begin{Bmatrix} T_1^4 \\ T_2^4 \\ \cdot \\ \cdot \\ T_{N_s}^4 \end{Bmatrix}$$

$$e_i = \frac{1 - \epsilon_i}{\epsilon_i}$$

ϵ_i = emissivity of surface i

σ = Stefan - Boltzmann's constant

When J_R 's are solved, $q_{rl,i}$ can be evaluated using the following formula instead of equation (4.72):

$$q_{rl,i} = \frac{E_{bi} - J_{Ri}}{e_i} \quad (4.75)$$

The total heat flux term, q'' , in equation (4.36) for the external side of the exterior wall therefore is:

$$q'' = \alpha I_t + h_o (T_o - T) \quad (4.76)$$

where h_o is the exposed surface convective heat transfer coefficient and T_o is the outdoor air temperature.

The total heat flux term for an internal surface i is:

$$q''_i = h_i (T_{rm} - T_i) - q_{rl,i} \quad (4.77)$$

4.8 Window Model

The following lumped parameter model was adopted for simulating the thermal behaviour of the window in an exterior wall:

$$\rho_G C_{PG} L_G \frac{dT_G}{dt} = q_{in} \quad (4.78)$$

where T_G is the glass temperature; ρ_G , C_{PG} & L_G are respectively the density, specific heat and thickness of the glass; and q_{in} is the net heat gain due to convective and radiation heat exchange with the surrounding (both indoor and outdoor).

This net heat gain term, q_{in} , in equation (4.78) includes the absorbed portion of solar radiation incident upon it. For the portion that is transmitted through, it was assumed that both the direct and diffuse radiation transmitted through the window glass would be distributed onto other internal wall/slab surfaces as if both were diffuse radiation. In modelling the radiation heat exchange between the window glass and internal walls and slabs, the transmitted solar radiation was treated as an additional source term at the glass surface as follows:

$$J_{RG} = \tau I_t + \epsilon_G E_{bG} + (1 - \epsilon_G) I_{rG} \quad (4.79)$$

where J_{RG} is the radiosity of window glass; τ is the transmittance of glass for solar radiation (short wave); ϵ_G is the emissivity of glass (long wave); E_{bG} is the emissive power of a black surface at temperature T_G ($= \sigma T_G^4$); and I_{rG} is the irradiance upon the window glass. Here, the assumption is made that the window is opaque to longwave radiation.

Since net radiant flux leaving the window glass surface is given by:

$$q_{rl,G} = J_{RG} - I_{rG} \quad (4.80)$$

substituting (4.80) into (4.79) and re-arranging yields:

$$q_{rl,G} = \frac{E_{bG} + \frac{\tau I_t}{\epsilon_G} - J_{RG}}{\left(\frac{1 - \epsilon_G}{\epsilon_G}\right)} \quad (4.81)$$

Note also that

$$q_{rl,G} = \sum_{j=1}^{N_s} F_{Gj} (J_{RG} - J_{Rj}) \quad (4.82)$$

and comparing (4.81) and (4.82) against (4.72) and (4.75), it can be seen that they differ only by the extra source term $(\tau I_t / \epsilon_G)$. Hence, if an apparent emissive power, E'_{bG} , as defined below is used, radiation heat exchange between the window and other wall/slab surfaces, including the transmitted solar radiation, can be solved simultaneously using the procedures described in the previous section.

$$E'_{bG} = E_{bG} + \frac{\tau I_t}{\epsilon_G} \quad (4.83)$$

Using the above result, the heat gain term, q_{in} , in equation (4.78) can be written as:

$$q_{in} = \alpha I_t + h_o (T_o - T_G) + h (T_{rm} - T_G) - (q_{rl,G} - \tau I_t) \quad (4.84)$$

where T_{rm} is the room air temperature and α is the absorptance of glass (short wave).

By noting that $\alpha + \tau + r = 1$, where r is the reflectance (short wave) of the glass,

$$q_{in} = (1 - r) I_t + h_o (T_o - T_G) + h (T_{rm} - T_G) - q_{rl,G} \quad (4.85)$$

From equations (4.78) and (4.85), the ODE for the window is:

$$\frac{dT_G}{dt} = \frac{(1 - r) I_t + h_o (T_o - T_G) + h (T_{rm} - T_G)}{\rho_G C_{PG} L_G} \quad (4.86)$$

Collecting T_G terms at the RHS, (4.86) may be written as:

$$\frac{dT_G}{dt} = -a_G T_G + b_G \quad (4.87)$$

where

$$a_G = \frac{h_o + h}{\rho_G C_{PG} L_G} \quad (4.88)$$

$$b_G = \frac{(1 - r) I_t + h_o T_o + h T_{rm}}{\rho_G C_{PG} L_G} \quad (4.89)$$

Applying the self-implicit scheme, (4.87) is approximated by:

$$\frac{dT_G}{dt} = -\frac{a_G}{1 + a_G \lambda \Delta t} T_G^n + \frac{b_G}{1 + a_G \lambda \Delta t} \quad (4.90)$$

4.9 Air Node Equations

A lumped parameter approach was adopted in deriving the equations for modelling the thermodynamic state of the air in a room. Heat and moisture addition or removal due to internal sources, infiltration, and effects of air-conditioning were included.

4.9.1 Sensible Heat Balance Equation

From a heat balance on the room air, the following lumped equation can be written:

$$\rho_a V_{rm} C_{Pa} \frac{dT_{rm}}{dt} = Q_{int,s} + Q_{inf,s} - Q_{ac,s} - \sum_{i=1}^{N_s} A_i \cdot q_{c,i} \quad (4.91)$$

Note that $Q_{int,s}$ depends on usage condition in the room (e.g. number of occupants and lightings and equipment usage) and may vary according to a certain pattern throughout a day.

The sensible heat gain by the room air due to infiltration is given by:

$$Q_{inf,s} = \rho_a \dot{V}_{inf} C_{Pa} (T_o - T_{rm}) \quad (4.92)$$

where \dot{V}_{inf} = infiltration rate

$$= \frac{V_{rm} \cdot ACR}{3600}$$

ACR = number of air-changes per hour

The rate of sensible heat removal from the room air by the air-conditioning system is given by:

$$Q_{ac,s} = \rho_a \dot{V}_{sa} C_{Pa} (T_{rm} - T_{sa}) \quad (4.93)$$

From equation (3.15), for the surface convection heat transfer,

$$q_{c,i} = h (T_{rm} - T_i) \quad (4.94)$$

4.9.2 Moisture Mass Balance Equation

From balance of mass of water vapour in the room air, the following equation may be written:

$$\rho_a V_{rm} \frac{dw_{rm}}{dt} = \dot{W}_{int} + \dot{W}_{inf} - \dot{W}_{ac} - \sum_{i=1}^{N_s} A_i \cdot m''_{v,i} \quad (4.95)$$

Note that \dot{W}_{int} depends on room usage condition;

$$\dot{W}_{inf} = \rho_a \dot{V}_{inf} (w_o - w_{rm}) \quad (4.96)$$

$$\dot{W}_{ac} = \rho_a \dot{V}_{sa} (w_{rm} - w_{sa}) \quad (4.97)$$

and $m''_{v,i}$'s can be evaluated by using equation (4.65).

4.9.3 The Air-node Model

From equations (4.91) - (4.94), the sensible heat balance equation may be written as:

$$\frac{dT_{rm}}{dt} = -a_{rms} T_{rm} + b_{rms} \quad (4.98)$$

where

$$a_{rms} = \frac{\rho_a \dot{V}_{inf} C_{Pa} + \rho_a \dot{V}_{sa} C_{Pa} + \sum_{i=1}^{N_s} A_i h_i}{\rho_a V_{rm} C_{Pa}} \quad (4.99)$$

$$b_{rms} = \frac{Q_{int,s} + \rho_a \dot{V}_{inf} C_{Pa} T_o + \rho_a \dot{V}_{sa} C_{Pa} T_{SA} + \sum_{i=1}^{N_s} A_i h_i T_i}{\rho_a V_{rm} C_{Pa}} \quad (4.100)$$

From equations (4.95) & (4.96) and using (4.65) for evaluation of m_{vi}'' , the moisture balance equation for the room air may be written as:

$$\frac{dw_{rm}}{dt} = -a_{rmw} w_{rm} + b_{rmw} \quad (4.101)$$

where

$$a_{rmw} = \frac{\rho_a \dot{V}_{inf} + \rho_a \dot{V}_{sa} + \sum_{i=1}^{N_s} \frac{h_i}{C_{Pa}} \epsilon_g A_i}{\rho_a V_{rm}} \quad (4.102)$$

$$b_{rmw} = \frac{\dot{W}_{int} + \rho_a \dot{V}_{inf} w_o + \rho_a \dot{V}_{sa} w_{sa} + \sum_{i=1}^{N_s} \frac{h_i}{C_{Pa}} \epsilon_g A_i w_i}{\rho_a V_{rm}} \quad (4.103)$$

Applying the self-implicit scheme and regarding the b terms as constants, (4.98) and (4.101) are approximated by:

$$\frac{dT_{rm}}{dt} = -\frac{a_{rms}}{1 + a_{rms} \lambda \Delta t} T_{rm}^n + \frac{b_{rms}}{1 + a_{rms} \lambda \Delta t} \quad (4.104)$$

$$\frac{dw_{rm}}{dt} = -\frac{a_{rmw}}{1 + a_{rmw} \lambda \Delta t} w_{rm}^n + \frac{b_{rmw}}{1 + a_{rmw} \lambda \Delta t} \quad (4.105)$$

4.10 Air-conditioning System Operating Conditions

4.10.1 "Perfect" Air-conditioning System:

If the air-conditioning system is assumed to be capable of maintaining a steady room temperature and humidity whenever it is switched on, then,

$$\frac{dT_{rm}}{dt} = \frac{dw_{rm}}{dt} = 0$$

From equations (4.91) and (4.95), the air-conditioning load can be found by:

$$Q_{ac,s} = Q_{int,s} + Q_{inf,s} - \sum_{i=1}^{N_s} A_i \cdot q_{c,i} \quad (4.106)$$

$$\dot{W}_{ac} = \dot{W}_{int} + \dot{W}_{inf} - \sum_{i=1}^{N_s} A_i \cdot m_{v,i} \quad (4.107)$$

4.10.2 "Shut-down" Mode:

When the air-conditioning system is shut down,

$$Q_{ac,s} = \dot{W}_{ac} = 0 \quad (4.108)$$

and these terms can be neglected in solution of equations (4.104) and (4.105) (or equations 4.91 and 4.95).

4.10.3 "Realistic" Air-conditioning System:

In order to properly model variations of indoor air conditions during the air-conditioned period, the rates of heat and moisture removal by the air-conditioning system need to be simulated by an appropriate air-conditioning system model. Such a model should be capable of predicting the supply air conditions (T_{sa} and w_{sa}) under a specific set of operating conditions including for example the on-coil air conditions, supply air flow rate, chilled water supply temperature and flow rate, characteristics of

the cooling coil and control systems etc. More detailed descriptions about the air-conditioning system models developed are given in Chapter 5 and 6.

4.11 Verification of the Differential Permeability Model

To verify that the differential permeability model developed can properly model heat and moisture transfer in porous materials, the model was applied to repeat the simulation study done by Huang ⁽⁵⁰⁾ on drying of a piece of concrete slab (see Section 3.4) and to model the experiment on drying of a piece of gypsum board (by Thomas and Burch ⁽⁵³⁾). Comparison of the simulated results against those of Huang and the experimental data are summarized in the following.

4.11.1 Drying of a Concrete Slab

The simulation study was carried out based on the conditions summarized in Table 3.4. Figure 4.5 shows the moisture content and temperature distributions predicted by the differential permeability model. Variations of moisture contents and temperatures at selected cross sectional planes are plotted together with simulation results of Huang ⁽⁵⁰⁾ for comparison (Figure 4.6).

From Huang's results (see also results simulated by the model developed from Huang's equations as shown in Figures 3.1), it can be seen that within the period simulated, a total gas pressure gradient was built up within the concrete slab (this gradually diminished later in the drying process). However, moisture transfer by filtration flow due to a total gas pressure gradient was ignored in the differential permeability model. Therefore, results predicted by the differential permeability model deviated from Huang's results, particularly at boundary nodes in the early part of the simulated period due to the large total gas pressure gradient established there. In the later part of the simulation, the two sets of results became much closer to each other. This shows that this simpler model is capable of predicting heat and moisture transfer to an acceptable accuracy when compared with a more rigorous model.

4.11.2 Drying of a Piece of Gypsum Board

Thomas and Burch ⁽⁵³⁾ carried out an experiment on drying of a piece of gypsum board in which the moisture desorption rate from the gypsum board was measured. The conditions at which the experiment was conducted are summarized in Table 4.3.

The differential permeability model has been applied to simulate the experiment. In the simulation, the sorption isotherm for gypsum board and the surface convective mass transfer coefficient as given in Thomas & Burch's paper were used but the material moisture transport property was calculated by equation (4.6). The predicted desorption rates at various time intervals are shown in Figure 4.7 together with the measured desorption rates. It can be seen that the results predicted by the model are in good agreement with the experimentally measured data.

Chapter Five

Modelling Air-Conditioning Systems

This chapter starts from outlining the general approach of system modelling. The air-conditioning system component models developed in this work are then described. These include models for cooling and dehumidifying coils, room air temperature control systems, chilled water flow control valves, and a simple water piping circuit. Models for these system components were developed because the operating characteristics of them are the most critical in respect of the control over the indoor environmental conditions which in turn affect the rate of heat and moisture exchange between the indoor air and the building fabric materials. Development of the log-mean enthalpy difference (LMHD) steady-state coil model and the finite difference (FD) dynamic coil model (including the steady-state version of the FD model) are detailed in Appendix B and Chapter Six respectively.

5.1 General Approach of System Modelling

5.1.1 Component and System Modelling

The central air-conditioning system for a building may be divided into several sub-systems, namely the central chiller plant, the chilled water distribution system, the air-handling systems and the air distribution systems. Each of these sub-systems is composed of a number of basic components and sub-components. For example, a chilled water plant (a sub-system) typically includes several chillers (components) and

each chiller is composed of one or more unit(s) of refrigerant compressor, evaporator, condenser and control devices (sub-components). System components are interconnected by piping, ducting, electric cables or mechanical linkages and the performance of one component will affect the operation of other components. In modelling the performance of an air-conditioning system, models for the components of the system have to be established and linked together to form a system model.

From the mathematical point of view, each component model is a mathematical function that represents the relationship between one group of variables and another group of variables and parameters (Figure 5.1). These variables and parameters may include for instance the flow rates, temperatures, pressures, enthalpies, specific heats and concentrations of constituent species of the working fluids. For a given component model, the parameters are related to the geometric configuration of the component and the properties of materials of the component and the working fluids. Among the variables, some have known values (e.g. states and flow rates of fluids arriving at the equipment) but values of other variables will change according to the rates of heat, mass and work transfers taking place at the component (e.g. states of fluids leaving the component). The mathematical model then represents how the dependent variables are related to those given (independent) variables and parameters.

Alternatively, a component may be regarded as a "system" which is subjected to a certain number of inputs, having specific characteristics and, as a result, will output responses according to the input conditions and its intrinsic characteristics ⁽¹³⁹⁾. The entire air-conditioning system is composed of a large number of these components which are inter-related in that outputs from one are inputs to another (or others) via physically connected piping, ducting, cables or mechanical linkages. Hence, once the component model is established, it may be linked to other components, forming a system model. In this model building process, the physical relationships between the component models must be duly accounted for by properly defining the input/output relationships.

5.1.2 Sequential and Simultaneous Modelling

If the relationships between various components in a system are simply a unidirectional sequence of processes (Figure 5.2), the response of the system to a disturbance (the input at the first component in the sequence) can be determined by solving the outputs of the components, one at a time, following the same sequence. The solved output of one component model can be taken as the known input for the next component model with which the output of the latter can be solved. Through this process, the response of the system (the output of the last component) can be found. This is known as sequential modelling (35,139).

In reality, the inter-relationships between system components are much more complicated and are often looped, i.e. some outputs of one component may be the inputs of some preceding components (Figure 5.3). A system comprising closed-loop controls is an example of this. For such a system, the mathematical models of the system components may be put together to form a set of simultaneous equations (each of which may involve several unknown variables) and the whole set of equations need to be solved simultaneously; i.e. simultaneous modelling (35,139). A system model developed from this approach may become very complicated if a large number of component models are involved. It also requires a standardized form of component models and, when changes are made to any one component model, the entire system model may have to be re-established.

Alternatively, the sequential modelling approach can be applied to model a system involving complex relationships among its components (35,139). Since the inputs to a component model may include the outputs of some other component models that have not yet been solved, solving for outputs of such components will have to be based on assumed values of the unknown inputs. By using this approach, simulation calculations may proceed as in the case of straight-forward sequential modelling but the calculations will have to be repeated iteratively, with updating of the assumed inputs by improved estimates before a subsequent round of calculation proceeds, until a

converged solution for the entire system of equations is obtained. Although more tedious and involving more computing effort, this method allows a system model be constructed by putting together component models derived from different approaches and of different forms (because response of each component is solved independently). This is more convenient in building up a mathematical model for a system, and when any one of the component models is changed, the modified model may still be coupled to the other component models in exactly the same manner as before giving flexibility in the development and application of the system model. In this work, the sequential modelling approach was adopted.

5.2 The Air-conditioning System Component Models Developed

In the central air-conditioning system of a building, the air-handling systems serving various air-conditioned rooms are the front-line systems. Their performance have a far more direct and significant impact on the indoor environmental conditions than other parts of the central system. As this research was focused on studying the dynamic heat and moisture exchanges between the building fabric, the indoor air and the air-conditioning system, detailed mathematical models were developed for the major components of the air-handling system.

The air-handling system providing cooling and dehumidification to an individual zone of a building comprises the air-handling equipment (an air-handling unit (AHU) or a fan-coil unit (FCU)), the air-distribution ductwork and the temperature control system (see Figure 5.4). An air-handling equipment basically consists of a fan and a cooling and dehumidifying coil (and other accessories) housed in an insulated metal casing. The coil is connected to a pair of chilled water pipes; one supplies chilled water to the coil and the other returns the chilled water back to the central plant. A control valve is installed at the return chilled water pipe for regulating the rate of chilled water flowing through the coil through which the cooling output of the coil is regulated.

Mathematical models of the air-conditioning system components were developed as far as possible from fundamental principles so that reliance on specific manufacturer's data could be minimized. Mathematical models developed include steady-state and dynamic chilled water coil models, linear and equal percentage control valve models, controller models with on/off and proportional control actions, and a model describing the relationship between chilled water flow rate and pressure losses through elements of the piping system (for modelling changes in flow rate of chilled water through the cooling coil as influenced by opening or closing of the control valve). These mathematical models are described in the following sections. In addition, the method for calculating the properties of the mixture of return room air and outdoor fresh air at the inlet to the cooling and dehumidifying coil is described.

In this study, chilled water control valves were assumed to be two-port valves as such kind of valves is less expensive compared to three-port valves and, for this reason, is widely adopted in large buildings in Hong Kong. Also, the assumption was made that the central chilled water plant would be able to provide chilled water to the air-handling systems at a steady supply temperature but the flow rate would be varying.

5.3 Cooling and Dehumidifying Coil Models

5.3.1 Coil Configuration

A cooling and dehumidifying coil is basically a heat exchanger. Its unique characteristics which make it different from a typical shell-and-tube type heat exchanger include:

- i) heat transfer surface of the coil is normally extended by finned surfaces;
and
- ii) a two-component fluid (mixture of dry-air and water vapour) is handled and condensation of water vapour may occur at the coil surface.

Since chilled water coils constructed from copper tubes with plate aluminium fins bonded to the outer side of the tubes are the most commonly adopted type of cooling coils in central air-conditioning systems, attention was focused on this type of coils. In such coils, the fins are punched to form openings to allow the tubes to pass through and, at each opening, a collar is formed to maintain even spacing between the fins and to ensure good contact between the fins and the tubes (Figure 5.5). The fins may be plane but fins with corrugation patterns (Figure 5.6) are more popular in the air-conditioning industry. With corrugated fins, enhancement of the heat transfer rate by about 30% above that of flat-finned coils is possible ⁽¹⁴¹⁾. Some manufacturers produce coils with perforated fins with even better heat transfer performance ⁽¹⁴²⁾. The tubes are normally arranged in rows (three or more rows are common) and the tube array may be rectangular or triangular (Figure 5.7). The tube ends are connected to form multiple number of chilled water passages (circuits) through the coil (Figure B.2). The inlet and outlets of the tube circuits are connected by header pipes for even distribution of chilled water to the circuits in the coil.

5.3.2 Functions of the Coil Model

In essence, the main function of the mathematical model for a cooling and dehumidifying coil is to facilitate determination of the thermodynamic states of fluids leaving the coil under a given set of operating conditions. Other performance characteristics such as sensible and latent cooling output, moisture removal rate and the total cooling load brought forward to the central plant by the chilled water can be determined when the supply and leaving conditions of the fluids and their flow rates are known. With respect to modelling the state of the indoor environment, (see Sections 4.9 and 4.10) the temperature (T_{sa}) and humidity ratio (w_{sa}) of the supply air from the air-handling equipment to the air-conditioned room need to be determined by using the coil model. Hence, the model may be regarded as comprising the functions ϕ_T and ϕ_w describing T_{sa} and w_{sa} as follows:

$$T_{sa} = \varphi_T (T_{oc}, w_{oc}, \dot{V}_{sa}, T_{cw}, \dot{m}_{cw}) \quad (5.1)$$

$$w_{sa} = \varphi_w (T_{oc}, w_{oc}, \dot{V}_{sa}, T_{cw}, \dot{m}_{cw}) \quad (5.2)$$

These functions are dependent on the design and construction of the coil as well as the thermal properties of the coil materials and the working fluids (air and water). They may form either a steady-state model or a dynamic model depending on whether they are formulated to be functions of time.

In air-conditioning system design, the leaving air conditions from a cooling and dehumidifying coil is often determined based on a parameter called "by-pass factor" or "contact factor" ($= 1 - \text{by-pass factor}$)^(e.g. 3,5) together with the use of a psychrometric chart. The contact factor may be regarded as the fraction of the total rate of air flow through the coil that would be treated by the coil (hypothetically) to the condition of the air-film above the coil surface (corresponding to the apparatus dew point on the psychrometric chart ^(e.g. 3,5)) whilst the remaining fraction of the air-flow is assumed to be untreated and stays at the on-coil condition. The leaving coil air condition is given by the condition of the mixture of the treated and untreated air streams.

The contact factor for a given coil is a function of the air-side surface resistance and velocity ⁽¹⁷⁸⁾ and is fairly constant for all but significant variations in air and water flow conditions. In conjunction with other heat transfer equations, the contact factor may be used to determine the surface temperature of a cooling and dehumidifying coil and a simple method for estimating the performance of cooling and dehumidifying coils may be developed based on such a method ^(e.g. 169). However, the contact factor applies only if condensation is present in a coil ⁽¹⁷⁸⁾ but, in practice, a cooling and dehumidifying coil can become a dry coil in part-load when the chilled water flow rate is reduced to a small value. Once this happens, the coil surface condition can no longer be determined from the contact factor. In this study, it was necessary to have a coil model that would be applicable throughout the entire range of possible chilled water flow rates (from zero to the design maximum flow rate). Hence, although a simple coil

model may be derived by using the contact factor concept, such a method was not adopted.

5.3.3 The LMHD and the Finite Difference Coil Models

Two computer models have been developed for simulating performance of chilled water cooling and dehumidifying coils. The first coil model is a steady-state model which was developed following generally the methods due to McQuiston & Parker ⁽²⁸⁾ (details of the model development are summarized in Appendix B). In applying the model to simulate performance of coils with corrugated fins, the fin-side heat and mass transfer coefficients were first evaluated by using McQuiston's empirical correlations for flat-plate fins ^(143,144) and then corrected by using Beecher & Fagan's empirical correlations ⁽¹⁴¹⁾. The method adopted for determining the location of dry/wet boundary within a cooling and dehumidifying coil followed that outlined in the ASHRAE Handbook ⁽¹⁴⁰⁾. Since this model is basically a steady-state counter-flow heat exchanger model in which the combined heat and mass transfer between the air and the coil surface was modelled by the log mean enthalpy difference (LMHD) method ⁽²⁸⁾, it is called the LMHD model.

The second model is a finite difference numerical model (FD model) developed based on the set of governing differential equations derived from fundamental principles of energy and mass conservation and finite difference method was adopted to solve the equations. Similar to the LMHD model, a cooling and dehumidifying coil was modelled by regarding it as a simple shell-and-tube counter-flow heat-exchanger and the fin-side convective heat and mass transfer coefficients were evaluated based on the empirical correlations due to McQuiston ^(143,144) and Beecher & Fagan ⁽¹⁴¹⁾. This model was developed, in addition to the LMHD model, such that the significance of the dynamic characteristics of the coil can be studied and the differences in results between modelling the coil by a steady-state model (e.g. LMHD model) and by a detailed dynamic model can be compared. Details of development of the FD dynamic coil model are described in Chapter Six.

5.3.4 On-coil Air Condition

Outdoor air is admitted into air-conditioned buildings for providing ventilation. It may be directly ducted to the return air plenum of the air-handling equipment or pretreated (cooled and dehumidified) before it is supplied to the air-handling equipment. Pretreated fresh air may also be directly supplied into the air-conditioned spaces. Except for the last case, the fresh air will be mixed with the return air from the air-conditioned spaces and the conditions of the air entering the coil therefore is that of the mixture of the return room air and the fresh air (pretreated or unpretreated). The mixture conditions with unpretreated fresh air can be evaluated as follows:

$$w_{oc} = \frac{(\dot{m}_{sa} - \dot{m}_{fa})w_{rm} + \dot{m}_{fa} w_o}{\dot{m}_{sa}} \quad (5.3)$$

$$h_{oc} = \frac{(\dot{m}_{sa} - \dot{m}_{fa})h_{rm} + \dot{m}_{fa} w_o}{\dot{m}_{sa}} \quad (5.4)$$

where \dot{m} 's above refer to mass flow rates of dry air of the respective air streams. Also,

$$T_{oc} = \frac{h_{oc} - w_{oc} \cdot h_{fg}}{Cp_d + w_{oc} \cdot Cp_v} \quad (5.5)$$

where h_{fg} is the heat of evaporation of water at 0 °C (see also footnote in 6.3.2)

If the fresh air supply is pre-treated by a fresh-air handling unit to a fixed condition (see Chapter 8 & 9), the on-coil air condition can be evaluated by using the same set of equations but with the outdoor air conditions replaced by the pre-treated fresh air conditons.

5.4 The Temperature Control System

5.4.1 On/Off Control

The control system may include simply a thermostat which will provide an on/off switching action causing the chilled water control valve to open or close. The thermostat may be installed inside the air-conditioned space, typically wall-mounted, or in the return air ducting. On and off settings are preset at the thermostat such that the sensing element within the thermostat will cause the switch to "make" if the room air or return air temperature overshoots the on-setting and to cause the switch to "break" if the off-setting is surpassed (Figure 5.8). This control action is referred to as on/off control. The set-point is (normally) the temperature mid-way between the on and off settings and the difference between the two settings is called control differential or the thermostat dead-band (denoted as D). Letting ϵ be the deviation of the actual room air (or return air) temperature from the set-point value ($\epsilon = \text{setpoint} - \text{actual temperature}$), the output of an on/off controller (denoted as y) may be modelled by:

$$y = 0 \quad \left(\text{for } \epsilon \geq \frac{D}{2} \right) \quad (5.6a)$$

$$y = 1 \quad \left(\text{for } \epsilon \leq -\frac{D}{2} \right) \quad (5.6b)$$

$$y = \text{previous value (either 0 or 1)} \quad \left(\text{for } -\frac{D}{2} < \epsilon < \frac{D}{2} \right) \quad (5.6c)$$

Under on/off control, the valve will stay either at the fully open or the closed position and therefore chilled water supply to the coil will either be at the maximum flow rate or zero. Consequently, the indoor temperature will be fluctuating all the time. The control differential has a direct effect on how frequently the valve will be cycling between fully open and closed positions. Because both the indoor environment and the system take time to react to a switching action between on and off, the range of indoor temperature fluctuation is wider than the control differential (see Figure 5.8). Although there will always be fluctuations in indoor temperature with on/off control, as the cost of this control is much lower than other alternatives, it is widely adopted in Hong

Kong, particularly when FCUs are employed where there are large number of such control devices in a building. The performance of such systems therefore was studied in detail in this work.

5.4.2 P, PI and PID Controls

When a steady room temperature is desirable, controllers that can perform either proportional (P), proportional plus integral (PI) or proportional plus integral plus derivative (PID) control actions need to be adopted ⁽¹⁴⁵⁾. In control systems employing this type of controller, a temperature sensor is used to provide the controller with a feedback signal about the actual indoor air temperature being maintained in the air-conditioned space. The sensor may either be installed inside the air-conditioned space or in the return air ductwork. The controller has a set-point adjustment mechanism through which the desired indoor temperature can be set as the control target. The controller subtracts the feedback value (from the temperature sensor) from the set-point resulting in the error signal (ϵ) which is transduced and amplified into an appropriate electrical or pneumatic signal. This will cause the chilled water control valve to vary its degree of opening thereby regulating the cooling output of the coil. The degree of control valve opening is linearly proportional to the controller output signal (neglecting hysteresis in the valve/signal linkage, see Section 5.7). The relationships between the controller output signal (y) and the error signal (ϵ) for P, PI or PID control actions are as follows:

i) *For P control:*

$$y = 0 \quad \left(\text{for } \epsilon \geq \frac{TR}{2} \right) \quad (5.7a)$$

$$y = 0.5 - G_p \epsilon \quad \left(\text{for } -\frac{TR}{2} < \epsilon < \frac{TR}{2} \right) \quad (5.7b)$$

$$y = 1 \quad \left(\text{for } \epsilon \leq -\frac{TR}{2} \right) \quad (5.7c)$$

where TR = throttling range of the P Controller or
= the difference between values of ϵ for $y=1$ and $y=0$
i.e. 100% and 0% output of the controller
 G_P = proportional gain

Note that $G_P = \frac{1}{TR}$

ii) *For PI control:*

$$y = 0.5 - G_P \epsilon - G_I \int \epsilon \, dt \quad \left(\text{for } -\frac{TR}{2} < \epsilon < \frac{TR}{2} \right) \quad (5.8)$$

where G_I = integral gain and y is always within the range of $0 \leq y \leq 1$.

iii) *For PID control:*

$$y = 0.5 - G_P \epsilon - G_I \int \epsilon \, dt - G_D \frac{d\epsilon}{dt} \quad \left(\text{for } -\frac{TR}{2} < \epsilon < \frac{TR}{2} \right) \quad (5.9)$$

where G_D = derivative gain and y is always within the range of $0 \leq y \leq 1$.

Under P control, as the control valve position is linearly proportional to the error signal, presence of deviations between the indoor temperature and the set-point is inevitable (if the disturbance is a step change, this is called the steady-state error or offset) which is an inherent feature of proportion control (unless the gain, $G_P = \infty$). With PI control, since the error is integrated with time, the output will be varied gradually if the error persists. Consequently, the indoor temperature will eventually attain the set-point value if the disturbance is a simple step function. The additional "D" control action in PID control is meant for improving the promptness of the system in response to rapidly changing disturbances but this is seldom necessary in air-conditioning systems.

In this study, attention was focus on investigating the performance of air-conditioning systems when on/off and proportional controls were adopted. As there

should be no significant differences between the performance of the system when either P, PI or PID was adopted, only P control was studied.

5.5 Control Valve Model

The flow rate of chilled water through the cooling and dehumidifying coil of an air-handling unit is regulated by the associated control valve. The (inherent) flow characteristics of a water flow control valve are described by:

- a) The the flow coefficient (C_v) of the valve when it is fully open:

$$\dot{V}_{wo} = C_v \sqrt{\Delta P} \quad (5.10)$$

where

\dot{V}_{wo} = volume flow rate through the valve when it is fully open

$\sqrt{\Delta P}$ = square root of pressure difference across the control valve.

- b) The flow-rate and degree-of-opening (valve position or stem travel) relationship of the valve when it is partly open.

5.5.1 On-Off Valve

If the flow characteristics of the control valve during times where the valve is opening or closing are ignored, the valve port of an on/off valve will only stay either at the fully open or the closed position. The flow rate of chilled water therefore would be:

$$\dot{V}_w = V_{wo} \text{ for } s = 1 \text{ and } \dot{V}_w = 0 \text{ for } s = 0.$$

In this case, the on/off valve is fully characterized by its C_v .

5.5.2 Linear Control Valve

A control valve is called a linear valve if, when the pressure drop across the valve is kept constant, the water flow rate through it is linearly proportional to the valve position (the linear displacement from the closed position to a partly open position) (145, 146). Hence, the water flow rate through the control valve when the valve is partly open may be found by:

$$\dot{V}_w = \dot{V}_{w0} \cdot \frac{S}{S_0} \quad (5.11)$$

where \dot{V}_w is the flow rate; S is the valve position corresponding to \dot{V}_w ; and S_0 is the valve stroke (at fully-open position).

5.5.3 Equal Percentage Valve

For heating and cooling coils, the reduction of heating or cooling capacity of the coil is not linearly proportional to the flow rate of hot or chilled water through the coil (see Figure 1.2). For achieving an approximately linear relationship between coil output and valve position, "equal percentage" valves are often used for chilled or hot water flow rate control in air-conditioning systems (145,146).

For an equal percentage valve, under a constant ΔP (145,146),

$$\frac{d\dot{V}_w}{dS} \propto \dot{V}_w \quad \text{or} \quad \frac{d\dot{V}_w}{dS} = a \dot{V}_w \quad (5.12)$$

where 'a' is a proportionality constant. Re-arranging the above equation into:

$$\frac{d\dot{V}_w}{\dot{V}_w} = a dS$$

and integrating yields

$$\ln \dot{V}_w = a S + b$$

$$\text{or } \dot{V}_w = c e^{aS} \quad (5.13)$$

where b and c are constants.

At fully open position and under a constant ΔP ,

$$\dot{V}_w = \dot{V}_{w0}$$

It follows that

$$\dot{V}_{w0} = c e^{aS_0} \quad (5.14)$$

$$\therefore c = \dot{V}_{w0} e^{-aS_0} \quad (5.15)$$

Substituting (5.15) into (5.14) yields

$$\dot{V}_w = \dot{V}_{w0} e^{-a(S_0 - S)} \quad (5.16)$$

It should be noted that \dot{V}_w and \dot{V}_{w0} are flow rates through the valve at partly and fully open positions when the pressure difference across the valve are the same in both cases.

Normalizing \dot{V}_w and S respectively by \dot{V}_{w0} and S_0 by defining:

$$v_w = \frac{\dot{V}_w}{\dot{V}_{w0}} \quad (5.17)$$

$$\text{and } s = \frac{S}{S_0} \quad (5.18)$$

(v_w and s are now the fractional flow and fractional opening respectively), equation (5.16) becomes,

$$v_w = e^{-aS_0(1-s)}$$

Since a and S_0 are both constants, they may be combined (using $d = aS_0$) as

$$v_w = e^{-d(1-s)} \quad (5.19)$$

Here, 'd' is a coefficient which needs to be evaluated from a valve characteristic curve provided by the manufacturer of the valve. Its value is not normally a constant throughout the valve stroke range (i.e. from $s = 0$ to $s = 1$). This is evident by observing equation (5.19) in that this equation does not apply when s approaches zero since when $s = 0$, the valve is fully closed and the corresponding value of v_w should be zero. This however requires 'd' to be infinitely large. Hence, in modelling the performance of an equal percentage control valve, its flow characteristics need to be modelled by two or more mathematical expressions, each corresponding to a certain range of s .

Based on the typical curve for equal percentage valves given in ASHRAE Handbook, HVAC Systems & Applications, 1987, Ch. 51 ⁽¹⁴⁶⁾ (shown in Figure 5.9), and assuming a linear relationship between v_w and s for s ranging from 0 to 0.1 the following mathematical model was derived for a control valve:

$$\text{For } 0 \leq s \leq 0.1 \quad v_w = 0.1 s \quad (5.20a)$$

$$\text{For } 0.1 \leq s < 0.3 \quad v_w = 0.005 e^{6.97.s} \quad (5.20b)$$

$$\text{For } 0.3 \leq s \leq 1 \quad v_w = e^{-4.6(1-s)} \quad (5.20c)$$

For some control valves, when the valve is closed ($s=0$), there will be a leakage or "let-by" flow rate of 0.25 - 2% of the full flow (corresponding to $s=1$). In that case, v_w will be a constant when $s=0$.

For a given ΔP , and knowing the C_v of the control valve, \dot{V}_{w0} can be found using equation (5.10). Knowing also s , v_w can be found using one of the above three equations. \dot{V}_w then can be determined by:

$$\dot{V}_w = \dot{V}_{wo} \cdot v_w \quad (5.21)$$

However, in the simulation calculation, ΔP across the valve (and hence \dot{V}_w) is not explicitly known. It is related also to the flow rate and pressure drop at other parts of the chilled water circuit in the system. Moreover, value of s is proportional to the controller output and this is dependent on the type of control action (on/off, P, PI or PID) of the controller and the deviation between the set-point and the instantaneous actual indoor temperature (ϵ). All the unknown variables therefore need be solved simultaneously.

5.6 Hydronic Flow and Pressure Drop Models

In order to determine mass flow rate of chilled water through the coil and the control valve, the relationship between pressure drop and flow rate through various components in the chilled water circuit have to be properly modelled. The water flow rate through each component in the hydraulic circuit (\dot{V}_w) can be related to the pressure drop across the component (ΔP) by a flow conductance (K) as shown in the following equation:

$$\dot{V}_w^2 = K \Delta P \quad (5.22)$$

Hence, for a cooling coil,

$$\dot{V}_w^2 = K_{cc} \Delta P_{cc} \quad (5.23)$$

For a certain length of straight pipe,

$$\dot{V}_w^2 = K_p \Delta P_p \quad (5.24)$$

Likewise, for a control valve,

$$\dot{V}_w^2 = K_{cv} \Delta P_{cv} \quad (5.25)$$

Note that K_{cv} here is a variable which is dependent on C_v and s of the control valve.

Comparing (5.25) with (5.10) and using (5.21), when the valve is fully open,

$$K_{cv} = C_v^2$$

and, when the valve is partly open,

$$K_{cv} = \frac{\dot{V}_w^2}{\Delta P} = \frac{v_w^2 \dot{V}_{w0}^2}{\Delta P} = \frac{v_w^2 C_v^2 \Delta P}{\Delta P}$$

$$\therefore K_{cv} = (v_w C_v)^2 \quad (5.26)$$

For a straight pipe run, the pressure drop per unit length is given by the Darcy formula (30):

$$\Delta P_P = \frac{4fL}{d} \cdot \rho_w \frac{u_w^2}{2} \quad (5.27)$$

and for pipe bends and other fittings (4),

$$\Delta P_f = \zeta \cdot \rho_w \frac{u^2}{2} \quad (5.28)$$

where ζ = pressure loss factor of the fitting.

Alternatively, using the concept of equivalent length (4,5) (L_{eq} , defined as the length of a straight pipe of equal diameter which will give rise to the same pressure drop when conveying the same flow rate) where, for a pipe fitting:

$$L_{eq} = \frac{d}{4f} \cdot \zeta \quad (5.29)$$

the total pressure drop for a piping branch with straight pipes and piping fittings in series can be represented by:

$$\Delta P_P = \frac{4f}{d} (\sum L_{eq}) \cdot \rho_w \frac{u^2}{2} \quad (5.30)$$

$$\text{or } \Delta P_P = \frac{32f}{\pi^2 d^5} (\sum L_{eq}) \cdot \rho_w \dot{V}_w^2 \quad (5.31)$$

Hence,

$$K_P = \frac{1}{\frac{32f}{\pi^2 d^5} (\sum L_{eq}) \rho_w} \quad (5.32)$$

For a branch circuit comprising straight pipes, piping fittings, a cooling coil and a control valve, all in series (Figure 5.10), the total pressure drop is:

$$\Delta P_{b,tot} = \left(\frac{1}{K_P} + \frac{1}{K_{cv}} + \frac{1}{K_{cc}} \right) \dot{V}_w^2 \quad (5.33)$$

Equation (5.33) provides a relationship between the flow rate and the pressure drop across a branch circuit which was used in the system model, in conjunction with the controller model (with input from the air-node model) for determination of chilled water flow rate through the cooling coil.

5.7 Other System Component Characteristics

In modelling the dynamic performance of a system of inter-connected component, there are several system component characteristics which will affect the response of the components to changes in input. These include "transport delay" and "hysteresis" characteristics of certain system components (36,147). If any of these characteristics are known to have significant effects on the performance of the system, they must be properly modelled by the system component model.

A transport delay is the time required for any changes in the state of a fluid at the inlet of a pipe or duct to be reflected at a particular point downstream of the inlet. This depends on the distance between the inlet and the point of concern (usually the outlet), the size of the pipe or duct and on flow rate of the fluid. The effect is significant only when the pipe or duct is of a substantial length and can be neglected in simulating the performance of an air-handling system.

A component exhibits a hysteresis characteristic if its response is not unique when subjected to the same input. Instead of a consistent relationship between the input and the output, the response is dependent upon whether there has been a reversal in the input from an increasing trend to a decreasing trend and vice versa. At a reversal of input (in which the output should ideally respond in a direction opposite to the last one), the component will not react to the change immediately but a corresponding change in its output will take place only after a finite change in input has taken place. The delay in response of an actuator due to the "slack" associated with the actuator mechanism is an example of this kind of situation. In formulating mathematical models for components that have hysteresis characteristics, a delay in response would need to be included whenever the input changes in sign (147).

For on/off controls, the hysteresis characteristic of a valve actuator is modelled by a delay in reversal of action of the control valve. Also, the speed of valve stroke movement is included in the controller model to account for the fact that the valve port will take some time to travel from its last position to that as dictated by the controller. Hysteresis effect for reversal of valve position at an intermediate valve travel however is ignored in this work.

Chapter Six

A Finite Difference Dynamic Model for a Cooling and Dehumidifying Coil

This chapter starts with an overview of the methods for dynamic modelling of a cooling and dehumidifying coil. The relationship between physical parameters of a finned coil and an idealized heat exchanger model is then described. Based on the idealized counterflow heat exchanger model, partial differential equations governing the dynamic heat and mass transfer in a cooling and dehumidifying coil were derived. Derivation of the governing equations and the numerical schemes employed to convert the equations into a numerical coil model are detailed in this chapter.

6.1 The Approach for Modelling the Dynamic Performance of a Cooling and Dehumidifying Coil

Many dynamic heating and cooling coil models have been developed since the mid-sixties (e.g. 36,148-151). The dynamic performance of space heating systems in buildings, such as the stability of the system under part-load operations (e.g. 152,153), have been studied by coupling heating coil models to control system models. Recently developed building energy simulation programs have coil models for simultaneous modelling of thermal performance of the building envelope and the air-conditioning system (e.g. HVACSIM+ ⁽³⁶⁾).

Traditionally, the dynamic performance of a coil was modelled by transfer functions developed based on the Laplace transformation of the governing equations. More recently, Z-transformation and system identification techniques have been used to develop models for applications in systems with direct digital control (DDC) (154). Due to the complex heat and mass transfer processes involved, many transfer function models of heating or cooling coils are simplified models (152,155-157). In most of them, the coil was regarded as a simple counter flow heat exchanger, transient variation of only one parameter (typically the leaving coil air temperature) in response to changes in one other parameter (often the chilled/hot water flow rate) was described and the disturbance was assumed to be a simple time function (e.g. a step function). Few such models include the dehumidification performance of the coil.

Modelling the performance of a chilled water cooling and dehumidifying coil usually involves predicting the changes in the temperature and humidity of the air and the temperature of the water leaving the coil in response to changes in the entering air temperature and humidity, water temperature and flow rates of the air and water. This would require a multi-variable transfer function coil model which could be rather cumbersome to use. In the case of a hot water heating coil, it has been suggested that six transfer functions have to be used (158). For the case of a cooling and dehumidifying coil, the coupled mass transfer must also be modelled and, because of the non-linear nature of the problem, the model will be even more complicated than that of a heating coil. Also, the piecewise linearization of the coil characteristics, which is a necessary approach in deriving the transfer function model for a non-linear system, will restrict applicability of the model to limited ranges of operating conditions.

A simplistic approach was adopted in dynamic modelling of cooling and dehumidifying coils in the HVACSIM+ building systems and equipment simulation program (36). In this model, the dynamic response of a coil is modelled in a somewhat artificial manner in that the transient variations of the leaving coil air temperature and humidity and the leaving coil water temperature are each modelled by a first order

ordinary differential equation (ODE). When the coil is subjected to changes in operating conditions (e.g. the flow rates of the working fluids and their on-coil conditions) over a time-step increment in the simulation, a log-mean enthalpy difference (LMHD) method is first used to predict the steady-state performance of the coil. This steady-state performance is calculated based on the on-coil conditions and the flow rates of the working fluids that correspond to the end of the time-step increment. The transient variations of the leaving-coil air temperature and humidity and the leaving water temperature over this time-step are then modelled by using the ODEs and the initial and the predicted steady-state values of these variables. That is, the assumption is made that the performance of the coil will approach the steady-state performance according to an exponential growth or decay curve. Moreover, the same time constant is used in the three ODEs and the same equations are used irrespective of whether the disturbance is due to a change in on-coil air or water conditions or their flow rates. Therefore, this model can only be regarded as an approximate dynamic coil model.

In this study, a set of coupled partial differential equations that govern the heat and mass transfer performance of a cooling and dehumidifying coil was derived from fundamental principles. It resembles those of Romie ⁽¹⁵⁰⁾ and Tobias ⁽¹⁵⁵⁾ but mass transfer was included and effects of the fin-tube configuration of a coil and effects of fin corrugations were taken into account in this model. The set of equations was solved numerically rather than by Laplace transformation and transfer function methods. This approach was taken because the numerical model developed would be more generally applicable and would involve fewer approximations.

6.2 Idealization of the Coil Construction

To develop a dynamic heat and mass transfer model for a cooling and dehumidifying coil taking detail account of its physical construction and the complex heat, mass and momentum transport phenomena within the coil would be extremely difficult. To simplify, the coil was idealized as a single tube, counter-flow heat exchanger as shown in Figure 6.1. Configuration of the idealized coil at an elemental

section of length δx in the air-flow direction is as shown in Figure 6.2 and its cross-section is as shown in Figure 6.3. Here, the 'tube' of the idealized heat exchanger is composed by two concentric tubes that are in contact with each other. The outer tube, called the 'fin-core' represents the fins and the fin collars of the realistic coil and its total surface area is the heat transfer area of the coil. The inner tube, called the 'tube-core' represents the copper tubes of the realistic coil. In the idealized coil, air flows along the outer side of the fin-core in the axial direction whereas chilled water flows within the tube-core in a direction opposite to the air-flow.

To relate the geometric and flow parameters of a realistic coil to those of the idealized coil, the following parameters are defined:

6.2.1 Geometric Parameters

a) *Heat transfer area and perimeter*

In heat transfer calculations, the total area of all finned surfaces and exposed fin collar surfaces is regarded as the heat transfer area of the coil. Let A be this total heat transfer area, P_o be the outer perimeter length of the fin-core and L be the total length of the coil (in the air-flow direction), they are related by:

$$P_o = \frac{A}{L} \quad (6.1)$$

b) *Air-flow area*

The actual cross-sectional area of the air-passage within a finned coil varies from plane to plane due to presence of the tubes. In the idealized coil, the air-flow area (A_{af}) is defined as:

$$A_{af} = \frac{\text{Total volume of air spaces between fins and tubes}}{L} \quad (6.2)$$

and the total volume of air spaces inside the coil can be calculated using the coil configuration parameters as defined in Appendix B.

c) *Water side heat transfer area and perimeter*

The total water side heat transfer area is the total internal tube surface area of the coil (A_i). Let P_i denotes the inner perimeter length of the tube-core, A_i and P_i are related by:

$$P_i = \frac{A_i}{L} \quad (6.3)$$

d) *Water-flow area*

In a realistic coil, chilled water actually flows in a direction perpendicular to the air-flow. It however also flows from row to row in the direction opposite to the air-flow. For calculating the transport time for chilled water to flow through the coil, a water-flow area (A_{wf}) is defined as follows:

$$A_{wf} = \frac{\text{Total internal volume of tubes}}{L} \quad (6.4)$$

e) *Fin-core cross-sectional area*

In the idealized coil, the cross-sectional area of the fin-core is defined as:

$$A_c = \frac{\text{Total volume of fins and fin collar material}}{L} \quad (6.5)$$

f) *Tube-core cross-sectional area*

Similar to the fin-core, the tube-core cross-sectional area is defined as:

$$A_{tb} = \frac{\text{Total volume of tube material}}{L} \quad (6.6)$$

g) *Tube/Fin-collar contact area and perimeter*

To account for the effect of contact resistance at the interface between the tubes and the fin collars, the contact area (A_{ct}), which is the total external tube surface area, has to be calculated. This is related to the contact perimeter length (P_{ct}) for the idealized coil by:

$$P_{ct} = \frac{A_{ct}}{L} \quad (6.7)$$

6.2.2 Flow Parameters

a) *Air-flow velocity (u_a)*

The air flow velocity varies from plane to plane in a coil with multiple tube rows and finned surfaces. The average velocity, using the definition of flow area A_{af} , is defined as:

$$u_a = \frac{\dot{m}_a}{\rho_a A_{af}} \quad (6.8)$$

b) *Water-flow velocity (u_w)*

Using the definition of water flow area (A_{wf}), the rate of displacement of chilled water in the direction opposite to the air-flow is given by:

$$u_w = \frac{\dot{m}_w}{\rho_w A_{wf}} \quad (6.9)$$

Note must be taken that the above parameters pertaining to the idealized coil are not actual dimensions nor actual flow velocities of fluids in the coil. They are so defined only to facilitate calculation of fluid transport rates and displacements within the coil for calculation of heat exchange at intermediate coil sections. Transport coefficients, such as convective heat and mass transfer coefficients, must be evaluated based on realistic flow velocities (see Appendix B).

6.3 Derivation of Governing Equations of the Coil Model

Based on the parameters defined in section 6.2, governing equations for heat and mass transfers at the coil were derived as summarized in the following in which reference is made to the elemental coil section as shown in Figure 6.2.

6.3.1 Mass Balance on Vapour Moisture in Air-flow

From conservation of mass of water vapour in the elemental coil section, the net rate of increase of water vapour content in the air within the elemental coil section is given by:

$$\rho_a A_{af} \delta x \frac{\partial w_a}{\partial t} = -\rho_a u_a A_{af} \frac{\partial w_a}{\partial x} \delta x - h_d \eta_{ms} P_o \delta x (w_a - w_{so})$$

Dividing throughout by $\rho_a A_{af} \delta x$ yields,

$$\frac{\partial w_a}{\partial t} = -u_a \frac{\partial w_a}{\partial x} - \frac{P_o h_d \eta_{ms}}{A_{af} \rho_a} (w_a - w_{so}) \quad (6.10)$$

6.3.2 Heat balance on air-flow

Considering conservation of heat energy on the air within the elemental coil section yields:

$$\rho_a A_{af} \delta x \frac{\partial h_a}{\partial t} = -\rho_a u_a A_{af} \frac{\partial h_a}{\partial x} \delta x - h_d \eta_{ms} P_o \delta x (h_a - h_{so})$$

Dividing throughout by $\rho_a A_{af} \delta x$,

$$\frac{\partial h_a}{\partial t} = -u_a \frac{\partial h_a}{\partial x} - \frac{P_o h_d \eta_{ms}}{A_{af} \rho_a} (h_a - h_{so}) \quad (6.11)$$

Note that

$$h_a = C_{p_a} T_a + w_a h_{fg} \quad (6.12a) *$$

Hence,

$$\frac{\partial h_a}{\partial t} = C_{p_a} \frac{\partial T_a}{\partial t} + h_{fg} \frac{\partial w_a}{\partial t} \quad (6.12b)$$

$$\frac{\partial h_a}{\partial x} = C_{p_a} \frac{\partial T_a}{\partial x} + h_{fg} \frac{\partial w_a}{\partial x} \quad (6.12c)$$

* h_{fg} is taken to be the specific enthalpy due to evaporation of water at 0 °C and C_{p_a} (for moist air) is assumed constant for the purpose of this work.

Also,

$$h_{so} = C_{p_a} T_{so} + w_{so} h_{fg} \quad (6.13)$$

Substituting (6.12) and (6.13) into (6.11), the heat balance equation for the air in the coil can be written as:

$$C_{p_a} \frac{\partial T_a}{\partial t} + h_{fg} \frac{\partial w_a}{\partial t} = -u_a C_{p_a} \frac{\partial T_a}{\partial x} - u_a h_{fg} \frac{\partial w_a}{\partial x} - \frac{P_o h_d \eta_{ms}}{A_{af} \rho_a} [C_{p_a} (T_a - T_{so}) + h_{fg} (w_a - w_{so})]$$

Multiplying h_{fg} to equation (6.10) and subtracting the resultant equation from the above one yields,

$$\frac{\partial T_a}{\partial t} = -u_a \frac{\partial T_a}{\partial x} - \frac{P_o h_d \eta_{ms}}{A_{af} \rho_a} (T_a - T_{so}) \quad (6.14)$$

From the Lewis relationship (28,129),

$$Le^{2/3} = \frac{h_o}{C_{p_a} h_d}$$

Defining

$$Le_m = Le^{2/3} \quad (6.15)$$

it follows that,

$$h_d = \frac{h_o}{C_{p_a} Le_m} \quad (6.16)$$

Substituting (6.16) into (6.14),

$$\frac{\partial T_a}{\partial t} = -u_a \frac{\partial T_a}{\partial x} - \frac{P_o h_o \eta_{ms}}{A_{af} \rho_a C_{p_a} Le_m} (T_a - T_{so}) \quad (6.17)$$

The above equation is a sensible heat balance equation on the air flowing through a wet coil. For a dry coil, the vapour moisture content of the air stream remains

unchanged across the entire coil and hence there is no need to include equation (6.10). The energy conservation equation for air-flow will then be equation (6.17) with the Le_m term neglected, i.e.

$$\frac{\partial T_a}{\partial t} = -u_a \frac{\partial T_a}{\partial x} - \frac{P_o h_o \eta_s}{A_{af} \rho_a C_{p_a}} (T_a - T_{so}) \quad (6.17a)$$

Here, the surface effectiveness for a wet surface (η_{ms}) is replaced by that for a dry surface (η_s).

6.3.3 Heat Balance on Water Flow

Energy conservation consideration on the chilled water within the elemental coil section yields:

$$\rho_w A_{wf} \delta x C_{p_w} \frac{\partial T_w}{\partial t} = \rho_w u_w A_{wf} C_{p_w} \frac{\partial T_w}{\partial x} \delta x - h_i P_i \delta x (T_w - T_{si})$$

Dividing throughout by $\rho_w A_{wf} C_{p_w} \delta x$,

$$\frac{\partial T_w}{\partial t} = u_w \frac{\partial T_w}{\partial x} - \frac{h_i P_i}{\rho_w A_{wf} C_{p_w}} (T_w - T_{si}) \quad (6.18)$$

6.3.4 Heat Balance on the Tube-core

The tubes in a tube-row in the coil are connected to tubes of adjacent rows by U-bends. Hence, the conduction heat transfer in the air-flow direction through the tube metal can therefore be neglected in the heat balance consideration of the tube-core of the idealized coil. Thus, for the elemental coil section,

$$\rho_{tb} A_{tb} \delta x C_{p_{tb}} \frac{\partial T_{tb}}{\partial t} = -h_i P_i \delta x (T_{si} - T_w) - \frac{P_{ct} \delta x}{R_{ct}} (T_{tb} - T_c)$$

Dividing throughout by $\rho_{tb} A_{tb} C_{p_{tb}} \delta x$,

$$\frac{\partial T_{tb}}{\partial t} = -\frac{h_i P_i}{\rho_{tb} A_{tb} C_{p_{tb}}} (T_{si} - T_w) - \frac{P_{ct}}{\rho_{tb} A_{tb} C_{p_{tb}} R_{ct}} (T_{tb} - T_c) \quad (6.19)$$

6.3.5 Heat Balance on the Fin-core

Noting that the total fin cross-sectional area is very small compared with the total fin surface area, the conduction heat transfer in the air-flow direction within the fin metal therefore can be neglected in the heat balance consideration on the fin-core of the idealized coil. Thus, for the elemental coil section,

$$\rho_c A_c \delta x C_{p_c} \frac{\partial T_c}{\partial t} = -h_d \eta_{ms} P_o \delta x (h_{so} - h_a) - \frac{P_{ct}}{R_{ct}} \delta x (T_c - T_{tb})$$

Dividing throughout by $\rho_c A_c C_{p_c} \delta x$,

$$\frac{\partial T_c}{\partial t} = -\frac{P_o h_d \eta_{ms}}{\rho_c A_c C_{p_c}} (h_{so} - h_a) - \frac{P_{ct}}{\rho_c A_c C_{p_c} R_{ct}} (T_c - T_{tb}) \quad (6.20)$$

Substituting (6.16), (6.12a) and (6.13) into (6.20),

$$\begin{aligned} \frac{\partial T_c}{\partial t} = & -\frac{P_o h_o \eta_{ms}}{\rho_c A_c C_{p_c} C_{p_a} Le_m} [C_{p_a} (T_{so} - T_a) + h_{fg} (w_{so} - w_a)] \\ & - \frac{P_{ct}}{\rho_c A_c C_{p_c} R_{ct}} (T_c - T_{tb}) \end{aligned} \quad (6.21a)$$

For a dry coil, Le_m may be neglected and $w_{so} = w_a$, hence,

$$\frac{\partial T_c}{\partial t} = -\frac{P_o h_o \eta_{ms}}{\rho_c A_c C_{p_c}} (T_{so} - T_a) - \frac{P_{ct}}{\rho_c A_c C_{p_c} R_{ct}} (T_c - T_{tb}) \quad (6.21b)$$

Note that in deriving equations (6.19) & (6.21), the thermal resistances of the fin-collars and the tube walls were neglected based on the assumption that they were very small compared with other thermal resistances. Also, the fin-core surface temperature (T_{so}) in the equations refers to the base temperature of the fins whereas the non-uniformity in fin surface temperature is accounted for by the surface effectiveness (η_{ms}) (see Appendix B). With these assumptions, the coil surface temperature may be regarded as identical to the fin-core temperature and likewise, the inner tube surface temperature may be regarded as same as the tube-core temperature, viz.,

$$T_{so} = T_c$$

$$T_{si} = T_{tb}$$

Moreover, the methods for evaluating the heat and mass transfer coefficients h_o , h_d & h_i and the surface effectivenesses η_{ms} and η_s , as summarized in Appendix B for the steady-state coil model, were assumed to be equally applicable to the dynamic coil model.

6.4 Change of variables

For convenience in solving the governing equations, a non-dimensional spatial dimension, ξ , was defined as follows:

$$\xi = \frac{x}{L} \quad (6.22)$$

Hence,

$$\frac{\partial}{\partial x} = \frac{\partial}{\partial \xi} \cdot \frac{\partial \xi}{\partial x} = \frac{1}{L} \frac{\partial}{\partial \xi} \quad (6.23)$$

Defining also,

$$C_a = \dot{m}_a C_{p_a} = \rho_a u_a A_{af} C_{p_a} \quad (6.24)$$

$$C_w = \dot{m}_w C_{p_w} = \rho_w u_w A_{wf} C_{p_w} \quad (6.25)$$

$$C_c = \rho_c A_c L C_{p_c} \quad (6.26)$$

$$C_{tb} = \rho_{tb} A_{tb} L C_{p_{tb}} \quad (6.27)$$

$$\text{and } Ntu_a = \frac{P_o L h_o \eta_{ms}}{C_a} \quad (6.28)$$

$$Ntu_w = \frac{P_i L h_i}{C_w} \quad (6.29)$$

the governing equations for the cooling and dehumidifying coil can be written as follows:

a) *For a dry coil:*

$$\frac{\partial T_a}{\partial t} = -\frac{u_a}{L} \frac{\partial T_a}{\partial \xi} - \frac{u_a}{L} Ntu_a (T_a - T_c) \quad (6.30)$$

$$\frac{\partial T_w}{\partial t} = \frac{u_w}{L} \frac{\partial T_w}{\partial \xi} - \frac{u_w}{L} Ntu_w (T_w - T_{tb}) \quad (6.31)$$

$$\frac{\partial T_c}{\partial t} = -\left(\frac{C_a}{C_c}\right) Ntu_a (T_c - T_a) - \frac{P_{ct} L}{C_c R_{ct}} (T_c - T_{tb}) \quad (6.32)$$

$$\frac{\partial T_{tb}}{\partial t} = -\left(\frac{C_w}{C_{tb}}\right) Ntu_w (T_{tb} - T_w) - \frac{P_{ct} L}{C_{tb} R_{ct}} (T_{tb} - T_c) \quad (6.33)$$

b) *For a wet coil:*

$$\frac{\partial w_a}{\partial t} = -\frac{u_a}{L} \frac{\partial w_a}{\partial \xi} - \frac{u_a}{L} \frac{Ntu_a}{Le_m} (w_a - w_{so}) \quad (6.34)$$

$$\frac{\partial T_a}{\partial t} = -\frac{u_a}{L} \frac{\partial T_a}{\partial \xi} - \frac{u_a}{L} \frac{Ntu_a}{Le_m} (T_a - T_c) \quad (6.35)$$

$$\frac{\partial T_w}{\partial t} = \frac{u_w}{L} \frac{\partial T_w}{\partial \xi} - \frac{u_w}{L} Ntu_w (T_w - T_{tb}) \quad (6.36)$$

$$\begin{aligned} \frac{\partial T_c}{\partial t} = & -\left(\frac{C_a}{C_c}\right) \frac{Ntu_a}{Le_m} (T_c - T_a) - \left(\frac{C_a}{C_c}\right) \frac{Ntu_a}{C_{p_a} Le_m} h_{fg} (w_{so} - w_a) \\ & - \frac{P_{ct} L}{C_c R_{ct}} (T_c - T_{tb}) \end{aligned} \quad (6.37)$$

$$\frac{\partial T_{tb}}{\partial t} = -\left(\frac{C_w}{C_{tb}}\right) Ntu_w (T_{tb} - T_w) - \frac{P_{ct} L}{C_{tb} R_{ct}} (T_{tb} - T_c) \quad (6.38)$$

6.5 Solution by Finite Difference Method

6.5.1 Discretization Scheme

The set of governing equations for the coil as summarized in the preceding section is a set of coupled partial differential equations. Furthermore, the flow velocities u_a and u_w may both vary as complex functions of time in a realistic air-conditioning system and the relationship between T_c and w_{s0} is non-linear. Hence, to obtain an analytical solution to this set of equations would be very difficult. Thus, a numerical solution using a finite difference method was adopted. To do this, the coil was discretized into N number of segments as shown in Figure 6.4. Nodes at planes 1 and N are referred to as boundary nodes and those at the intermediate planes as interior nodes.

In the finite difference method, the derivative terms in the partial differential equations are to be approximated by finite differences. Conventionally, central differencing is used to approximate the spatial derivatives in the governing PDEs (e.g. the building model in Chapter 4) due to the smaller truncation error that will result compared with one-sided differencing ⁽¹⁵⁹⁾. Because the governing differential equations contain only first order derivatives in the spatial dimension, when central differencing was adopted in conjunction with the self-implicit scheme (see Appendix A), the resultant set of equations, when expressed in matrix form, did not have dominant diagonal elements in the coefficient matrix of the unknown variables. Since the presence of a dominant diagonal is essential for obtaining a numerical solution ⁽¹³⁰⁾, one-sided differencing was adopted in formulating the dynamic coil model.

Because the two working fluids approach the coil from opposite sides (a counter-flow heat exchanger), the known on-coil air and chilled water conditions are associated with different boundary planes of the coil. Therefore, backward differencing was applied for discretizing the moisture and energy equations for the air-flow whilst

forward differencing was applied to the energy equation for the water flow (see equations 6.44a and 6.44b).

The same set of equations would be derived by considering the heat and mass balance on the control volume in each sub-divided region inside the coil and by assuming that the state of the fluid within the control volume of each spatial subdivision in the coil is uniform (i.e. a perfectly mixed system). The latter implies that the states of the fluids leaving the control volume are at the same state as the respective fluid inside the control volume and the state of each fluid entering the control volume will be equal to that in the adjacent upstream node.

6.5.2 Partial Discretization of the Governing PDEs for the Coil

It can be seen that the fluid heat and mass conservation equations (6.30 & 6.31 for a dry coil and 6.34 to 6.36 for a wet coil) are all of the following general form:

$$\frac{\partial \phi}{\partial t} = a \frac{\partial \phi}{\partial \xi} + b (\phi - \psi) \quad (6.39)$$

where $\phi = \phi(\xi, t)$ & $\psi = \psi(\xi, t)$

Also, the energy conservation equations for the fin-core and the tube-core (6.32 & 6.33 for a dry coil and 6.37 & 6.38 for a wet coil) can be written as:

$$\frac{\partial \phi}{\partial t} = c (\phi - \psi_i) + d (\phi - \psi_j) + e (\psi_k - \psi_l) \quad (6.40)$$

Thus, equations (6.39) & (6.40), which represent the general form of the governing equations of the coil, were discretized and later applied to the corresponding equations with the variables ϕ & ψ substituted by the appropriate variables.

Let

$$f(\phi, \psi) = a \frac{\partial \phi}{\partial \xi} + b (\phi - \psi) \quad (6.41)$$

and hence, by referring to equation (6.39),

$$\frac{\partial \phi}{\partial t} = f(\phi, \psi) \quad (6.42)$$

Using the Crank-Nicolson scheme (with $0 \leq \lambda \leq 1$),

$$\frac{\partial \phi}{\partial t} = \lambda f(\phi^{n+1}, \psi^{n+1}) + (1 - \lambda) f(\phi^n, \psi^n) \quad (6.43)$$

where $\phi^n = \phi(\xi, t)$; $\phi^{n+1} = \phi(\xi, t + \Delta t)$

and $\psi^n = \psi(\xi, t)$; $\psi^{n+1} = \psi(\xi, t + \Delta t)$

a) *Interior nodes*

Let $\phi^{n+1} = \phi^n + \Delta \phi$; $\psi^{n+1} = \psi^n + \Delta \psi$

$\phi_+^n = \phi(\xi + \Delta \xi, t)$; $\phi_-^n = \phi(\xi - \Delta \xi, t)$

$\psi_+^n = \psi(\xi + \Delta \xi, t)$; $\psi_-^n = \psi(\xi - \Delta \xi, t)$

The partially discretized form of equations (6.39) & (6.40) for the interior nodes were derived as follows.

Using one-sided differencing, the spatial derivative in equation (6.41) can be replaced by:

$$\frac{\partial \phi}{\partial \xi} = \frac{\phi - \phi_-}{\Delta \xi} \quad (\text{backward}) \quad (6.44a)$$

$$\frac{\partial \phi}{\partial \xi} = \frac{\phi_+ - \phi}{\Delta \xi} \quad (\text{forward}) \quad (6.44b)$$

It follows that:

for the backward differencing scheme,

$$\begin{aligned} \lambda f(\phi^{n+1}, \psi^{n+1}) = & \lambda a \left[\frac{\phi^n - \phi_-^n}{\Delta\xi} + \frac{\Delta\phi - \Delta\phi_-}{\Delta\xi} \right] \\ & + \lambda b (\phi^n - \psi^n) + \lambda b (\Delta\phi - \Delta\psi) \end{aligned} \quad (6.45a)$$

$$\text{and } (1 - \lambda) f(\phi^n, \psi^n) = (1 - \lambda) a \frac{\phi^n - \phi_-^n}{\Delta\xi} + (1 - \lambda) b (\phi^n - \psi^n) \quad (6.46a)$$

for the forward differencing scheme,

$$\begin{aligned} \lambda f(\phi^{n+1}, \psi^{n+1}) = & \lambda a \left[\frac{\phi_+^n - \phi^n}{\Delta\xi} + \frac{\Delta\phi_+ - \Delta\phi}{\Delta\xi} \right] \\ & + \lambda b (\phi^n - \psi^n) + \lambda b (\Delta\phi - \Delta\psi) \end{aligned} \quad (6.45b)$$

$$\text{and } (1 - \lambda) f(\phi^n, \psi^n) = (1 - \lambda) a \frac{\phi_+^n - \phi^n}{\Delta\xi} + (1 - \lambda) b (\phi^n - \psi^n) \quad (6.46b)$$

Substituting (6.45) and (6.46) into (6.43), the latter becomes:

for the backward differencing scheme,

$$\frac{\partial\phi}{\partial t} = a \frac{\phi^n - \phi_-^n}{\Delta\xi} + \lambda a \frac{\Delta\phi - \Delta\phi_-}{\Delta\xi} + b (\phi^n - \psi^n) + \lambda b (\Delta\phi - \Delta\psi) \quad (6.47a)$$

for the forward differencing scheme,

$$\frac{\partial\phi}{\partial t} = a \frac{\phi_+^n - \phi^n}{\Delta\xi} + \lambda a \frac{\Delta\phi_+ - \Delta\phi}{\Delta\xi} + b (\phi^n - \psi^n) + \lambda b (\Delta\phi - \Delta\psi) \quad (6.47b)$$

Adopting the self-implicit scheme of Howells and Marshall ⁽¹³⁶⁾ (see Appendix A), all terms containing $\Delta\phi$ or $\Delta\psi$ are multiplied by $(\Delta t/\Delta t)$. The $(\Delta\phi/\Delta t)$ and $(\Delta\psi/\Delta t)$ terms are then replaced by $(\partial\phi/\partial t)$ and $(\partial\psi/\partial t)$ respectively. In so doing, the equations become:

for the backward differencing scheme,

$$\frac{\partial\phi}{\partial t} = \frac{\lambda a \Delta t}{\Delta\xi} \left[\frac{\partial\phi}{\partial t} - \frac{\partial\phi_-}{\partial t} \right] + \lambda b \Delta t \left[\frac{\partial\phi}{\partial t} - \frac{\partial\psi}{\partial t} \right] + \frac{a}{\Delta\xi} (\phi^n - \phi_-^n) + b (\phi^n - \psi^n)$$

for the forward differencing scheme,

$$\frac{\partial \phi}{\partial t} = \frac{\lambda a \Delta t}{\Delta \xi} \left[\frac{\partial \phi_+}{\partial t} - \frac{\partial \phi}{\partial t} \right] + \lambda b \Delta t \left[\frac{\partial \phi}{\partial t} - \frac{\partial \psi}{\partial t} \right] + \frac{a}{\Delta \xi} (\phi_+^n - \phi^n) + b (\phi^n - \psi^n)$$

which may be re-arranged as:

backward differencing:

$$\begin{aligned} & \left(\frac{\lambda a \Delta t}{\Delta \xi} \right) \frac{\partial \phi_-}{\partial t} + [1 - \lambda \Delta t \left(\frac{a}{\Delta \xi} + b \right)] \frac{\partial \phi}{\partial t} \\ &= \frac{a}{\Delta \xi} (\phi^n - \phi_-^n) + b (\phi^n - \psi^n) - \lambda b \Delta t \frac{\partial \psi}{\partial t} \end{aligned} \quad (6.48a)$$

forward differencing:

$$\begin{aligned} & [1 + \lambda \Delta t \left(\frac{a}{\Delta \xi} - b \right)] \frac{\partial \phi}{\partial t} - \left(\frac{\lambda a \Delta t}{\Delta \xi} \right) \frac{\partial \phi_+}{\partial t} \\ &= \frac{a}{\Delta \xi} (\phi_+^n - \phi^n) + b (\phi^n - \psi^n) - \lambda b \Delta t \frac{\partial \psi}{\partial t} \end{aligned} \quad (6.48b)$$

Similarly, for equation (6.40),

$$\begin{aligned} \frac{\partial \phi}{\partial t} &= \lambda c (\Delta \phi - \Delta \psi_i) + \lambda d (\Delta \phi - \Delta \psi_j) + \lambda e (\Delta \psi_k - \Delta \psi_l) \\ &+ c (\phi^n - \psi_i^n) + d (\phi^n - \psi_j^n) + e (\psi_k^n - \psi_l^n) \end{aligned} \quad (6.49)$$

Applying also the self-implicit scheme,

$$\begin{aligned} \frac{\partial \phi}{\partial t} &= \lambda c \Delta t \left[\frac{\partial \phi}{\partial t} - \frac{\partial \psi_i}{\partial t} \right] + \lambda d \Delta t \left[\frac{\partial \phi}{\partial t} - \frac{\partial \psi_j}{\partial t} \right] + \lambda e \Delta t \left[\frac{\partial \psi_k}{\partial t} - \frac{\partial \psi_l}{\partial t} \right] \\ &+ c (\phi^n - \psi_i^n) + d (\phi^n - \psi_j^n) + e (\psi_k^n - \psi_l^n) \end{aligned}$$

which may be re-arranged as

$$\begin{aligned}
[1 - \lambda \Delta t (c + d)] \frac{\partial \phi}{\partial t} &= c (\phi^n - \psi_i^n) + d (\phi^n - \psi_j^n) + e (\psi_k^n - \psi_l^n) \\
&\quad - \lambda c \Delta t \frac{\partial \psi_i}{\partial t} - \lambda d \Delta t \frac{\partial \psi_j}{\partial t} \\
&\quad + \lambda e \Delta t \frac{\partial \psi_k}{\partial t} - \lambda e \Delta t \frac{\partial \psi_l}{\partial t}
\end{aligned} \tag{6.50}$$

b) *Boundary nodes*

At the boundary nodes, the finite difference equations can be derived directly by applying the heat and mass balance principles to the respective control volume and by making the assumption that the fluid in the control volume is in a perfectly mixed state. The resultant equations are similar to equations (6.48) & (6.50) above but, as the size of the control volume and heat transfer area of the boundary nodes are just half of those of the interior nodes, expressions for the coefficient 'a' in equations (6.48a) and (6.48b) will be twice those for the interior node.

Also, at either of the boundary planes, some variables are of known values, e.g.

at $\xi = 0$, T_a and w_a are known whereas

at $\xi = 1$, T_w is known.

hence, the air moisture and energy balance equations at node 1 and the water energy balance equation at node N can be omitted in the solution processes.

6.5.3 Summary of Partially Discretized Equations

After applying the discretization scheme described above, the governing equations may be written in the summarized form given as follows:

a) *Dry coil*

i) At node 1

$$A'_{122} \frac{\partial T_{w1}}{\partial t} + A'_{123} \frac{\partial T_{w2}}{\partial t} = F'_{12} + E'_{12} \frac{\partial T_{tb1}}{\partial t} \quad (6.51)$$

$$A'_{132} \frac{\partial T_{c1}}{\partial t} = F'_{13} + E'_{13} \frac{\partial T_{tb1}}{\partial t} \quad (6.52)$$

$$A'_{142} \frac{\partial T_{tb1}}{\partial t} = F'_{14} + C'_{14} \frac{\partial T_{w1}}{\partial t} + D'_{14} \frac{\partial T_{c1}}{\partial t} \quad (6.53)$$

ii) At interior nodes 2 to N-1, for $i = 2, 3, \dots, N-1$

$$A'_{i11} \frac{\partial T_{ai-1}}{\partial t} + A'_{i12} \frac{\partial T_{ai}}{\partial t} = F'_{i1} + D'_{i1} \frac{\partial T_{ci}}{\partial t} \quad (6.54)$$

$$A'_{i22} \frac{\partial T_{wi}}{\partial t} + A'_{i23} \frac{\partial T_{wi+1}}{\partial t} = F'_{i2} + E'_{i2} \frac{\partial T_{tbi}}{\partial t} \quad (6.55)$$

$$A'_{i32} \frac{\partial T_{ci}}{\partial t} = F'_{i3} + B'_{i3} \frac{\partial T_{ai}}{\partial t} + E'_{i3} \frac{\partial T_{tbi}}{\partial t} \quad (6.56)$$

$$A'_{i42} \frac{\partial T_{tbi}}{\partial t} = F'_{i4} + C'_{i4} \frac{\partial T_{wi}}{\partial t} + D'_{i4} \frac{\partial T_{ci}}{\partial t} \quad (6.57)$$

iii) At node N

$$A'_{N11} \frac{\partial T_{aN-1}}{\partial t} + A'_{N12} \frac{\partial T_{aN}}{\partial t} = F'_{N1} + D'_{N1} \frac{\partial T_{cN}}{\partial t} \quad (6.58)$$

$$A'_{N32} \frac{\partial T_{cN}}{\partial t} = F'_{N3} + B'_{N3} \frac{\partial T_{aN}}{\partial t} + E'_{N3} \frac{\partial T_{tbN}}{\partial t} \quad (6.59)$$

$$A'_{N42} \frac{\partial T_{tbN}}{\partial t} = F'_{N4} + D'_{N4} \frac{\partial T_{cN}}{\partial t} \quad (6.60)$$

Expressions for coefficients A' , B' , ..., F' are as summarized in Table 6.1.

b) *Wet coil*

Note that the humidity ratio of a sample of saturated moist air (under constant total air pressure) is a function of the air temperature only. At the wet surface of a coil, assuming that the condensate layer and the thin layer of saturated air immediately above

the condensate layer were both at the coil surface temperature, which in turn was assumed to be the fin-core temperature (see section 6.3.5), then,

$$w_{so} = w_{so}(T_c) \quad (6.61)$$

Hence,

$$\frac{\partial w_{so}}{\partial t} = \frac{\partial w_{so}}{\partial T_c} \cdot \frac{\partial T_c}{\partial t} \quad (6.62)$$

The governing equations for the wet coil section can therefore be expressed as follows (where expressions for coefficients A, B, ..., H are as summarized in Table 6.2.):

i) At node 1

$$A_{122} \frac{\partial T_{w1}}{\partial t} + A_{123} \frac{\partial T_{w2}}{\partial t} = F_{12} + E_{12} \frac{\partial T_{tb1}}{\partial t} \quad (6.63)$$

$$A_{132} \frac{\partial T_{c1}}{\partial t} = F_{13} + E_{13} \frac{\partial T_{tb1}}{\partial t} + G_{13} \frac{\partial w_{s01}}{\partial T_{c1}} \frac{\partial T_{c1}}{\partial t} \quad (6.64)$$

$$A_{142} \frac{\partial T_{tb1}}{\partial t} = F_{14} + C_{14} \frac{\partial T_{w1}}{\partial t} + D_{14} \frac{\partial T_{c1}}{\partial t} \quad (6.65)$$

ii) At interior nodes 2 to N-1, for $i = 2, 3, \dots, N-1$

$$A_{i01} \frac{\partial w_{ai-1}}{\partial t} + A_{i02} \frac{\partial w_{ai}}{\partial t} = F_{i0} + G_{i0} \frac{\partial w_{s0i}}{\partial T_{ci}} \frac{\partial T_{ci}}{\partial t} \quad (6.66)$$

$$A_{i11} \frac{\partial T_{ai-1}}{\partial t} + A_{i12} \frac{\partial T_{ai}}{\partial t} = F_{i1} + D_{i1} \frac{\partial T_{ci}}{\partial t} \quad (6.67)$$

$$A_{i22} \frac{\partial T_{wi}}{\partial t} + A_{i23} \frac{\partial T_{wi+1}}{\partial t} = F_{i2} + E_{i2} \frac{\partial T_{tbi}}{\partial t} \quad (6.68)$$

$$A_{i32} \frac{\partial T_{ci}}{\partial t} = F_{i3} + B_{i3} \frac{\partial T_{ai}}{\partial t} + E_{i3} \frac{\partial T_{tbi}}{\partial t} + G_{i3} \frac{\partial w_{s0i}}{\partial T_{ci}} \frac{\partial T_{ci}}{\partial t} + H_{i3} \frac{\partial w_{ai}}{\partial t} \quad (6.69)$$

$$A_{i42} \frac{\partial T_{tbi}}{\partial t} = F_{i4} + C_{i4} \frac{\partial T_{wi}}{\partial t} + D_{i4} \frac{\partial T_{ci}}{\partial t} \quad (6.70)$$

iii) At node N

$$A_{N01} \frac{\partial w_{aN-1}}{\partial t} + A_{N02} \frac{\partial w_{aN}}{\partial t} = F_{N0} + G_{N0} \frac{\partial w_{soN}}{\partial T_{cN}} \frac{\partial T_{cN}}{\partial t} \quad (6.71)$$

$$A_{N11} \frac{\partial T_{aN-1}}{\partial t} + A_{N12} \frac{\partial T_{aN}}{\partial t} = F_{N1} + D_{N1} \frac{\partial T_{cN}}{\partial t} \quad (6.72)$$

$$A_{N32} \frac{\partial T_{cN}}{\partial t} = F_{N3} + B_{N3} \frac{\partial T_{aN}}{\partial t} + E_{N3} \frac{\partial T_{tbN}}{\partial t} + G_{N3} \frac{\partial w_{soN}}{\partial T_{cN}} \frac{\partial T_{cN}}{\partial t} + H_{N3} \frac{\partial w_{aN}}{\partial t} \quad (6.73)$$

$$A_{N42} \frac{\partial T_{tbN}}{\partial t} = F_{N4} + D_{N4} \frac{\partial T_{cN}}{\partial t} \quad (6.74)$$

6.5.4 Fin-core and Tube-core Equations

It can be seen that as a result of neglecting the heat conduction (in the air-flow direction) within the fin-core and the tube-core, the energy conservation equations for the fin-core and the tube-core involve only parameters and their derivatives that are 'local' to the node. Otherwise, there will also be spatial derivatives of these variables. Thus, the fin-core and tube-core equations need only be solved simultaneously with the air and water equations of the same node without involving those at the adjacent nodes. Hence, the governing equations for the fin- and tube-cores (both for a dry coil and a wet coil) can be expressed in terms of the air and water state variables by appropriate substitutions of variables and algebraic manipulations. The equations resulting from this process are shown in the summarized form as follows whereas the expressions for the coefficients associated with these equations are summarized in Tables 6.3 and 6.4.

a) *Dry coil*

i) At inlet node 1

$$\frac{\partial T_{c1}}{\partial t} = K'_{13} \frac{\partial T_{w1}}{\partial t} + L'_{13} \quad (6.75)$$

$$\frac{\partial T_{tb1}}{\partial t} = K'_{14} \frac{\partial T_{w1}}{\partial t} + L'_{14} \quad (6.76)$$

ii) At interior nodes 2 to N-1

$$\frac{\partial T_{ci}}{\partial t} = J'_{i3} \frac{\partial T_{ai}}{\partial t} + K'_{i3} \frac{\partial T_{wi}}{\partial t} + L'_{i3} \quad (6.77)$$

$$\frac{\partial T_{tbi}}{\partial t} = J'_{i4} \frac{\partial T_{ai}}{\partial t} + K'_{i4} \frac{\partial T_{wi}}{\partial t} + L'_{i4} \quad (6.78)$$

iii) At exit node N

$$\frac{\partial T_{cN}}{\partial t} = J'_{N3} \frac{\partial T_{aN}}{\partial t} + L'_{N3} \quad (6.79)$$

$$\frac{\partial T_{tbN}}{\partial t} = J'_{N4} \frac{\partial T_{aN}}{\partial t} + L'_{N4} \quad (6.80)$$

b) *Wet Coil*

i) At inlet node 1

$$\frac{\partial T_{c1}}{\partial t} = K_{13} \frac{\partial T_{w1}}{\partial t} + L_{13} \quad (6.81)$$

$$\frac{\partial T_{tb1}}{\partial t} = K_{14} \frac{\partial T_{w1}}{\partial t} + L_{14} \quad (6.82)$$

ii) At interior nodes 2 to N-1

$$\frac{\partial T_{ci}}{\partial t} = I_{i3} \frac{\partial w_{ai}}{\partial t} + J_{i3} \frac{\partial T_{ai}}{\partial t} + K_{i3} \frac{\partial T_{wi}}{\partial t} + L_{i3} \quad (6.83)$$

$$\frac{\partial T_{tbi}}{\partial t} = I_{i4} \frac{\partial w_{ai}}{\partial t} + J_{i4} \frac{\partial T_{ai}}{\partial t} + K_{i4} \frac{\partial T_{wi}}{\partial t} + L_{i4} \quad (6.84)$$

iii) At exit node N

$$\frac{\partial T_{cN}}{\partial t} = I_{N3} \frac{\partial w_{aN}}{\partial t} + J_{N3} \frac{\partial T_{aN}}{\partial t} + L_{N3} \quad (6.85)$$

$$\frac{\partial T_{tbN}}{\partial t} = I_{N4} \frac{\partial w_{aN}}{\partial t} + J_{N4} \frac{\partial T_{aN}}{\partial t} + L_{N4} \quad (6.86)$$

6.5.5 Solving the Governing Equations for Different Variables in Sequence

The set of nodal equations for a cooling and dehumidifying coil (equations 6.51 - 6.60 for a dry coil or equations 6.63 - 6.74 for a wet coil) may be written in the form of a matrix equation, one for each unknown variable, as shown in equation (6.87).

$$\begin{bmatrix}
 A_{1j2} & A_{1j3} & & & \\
 A_{2j1} & A_{2j2} & A_{2j3} & & \\
 & A_{3j1} & A_{3j2} & A_{3j3} & \\
 & \dots & \dots & \dots & \\
 & & A_{N-1j1} & A_{N-1j2} & A_{N-1j3} \\
 & & & A_{Nj1} & A_{Nj2}
 \end{bmatrix}
 \begin{Bmatrix}
 \dot{\phi}_{1j} \\
 \dot{\phi}_{2j} \\
 \dot{\phi}_{3j} \\
 \vdots \\
 \vdots \\
 \dot{\phi}_{N-1j} \\
 \dot{\phi}_{Nj}
 \end{Bmatrix}
 =
 \begin{Bmatrix}
 R_{1j} \\
 R_{2j} \\
 R_{3j} \\
 \vdots \\
 \vdots \\
 R_{N-1j} \\
 R_{Nj}
 \end{Bmatrix}
 \quad (6.87)$$

where $\dot{\phi}_j$'s are the time derivatives of the variables in the equations;

R_j 's are right hand side of the equations and

for a dry coil, $j = 1, 2$; for a wet coil; $j = 0, 1, 2$. Here, 0, 1 & 2 correspond respectively to the air humidity ratio, air temperature and water temperature.

The above set of equations includes only those pertaining to the states of the air and the water because, with the energy balance equations for the tube-core and fin-core re-arranged as summarized in Section 6.5.4, time derivatives of the fin-core and tube-core temperatures at each coil node can be related to those of the air and water conditions at the same node. In equation (6.87), these are included in the elements of the column vector $\{R\}$ and each element within this column vector is dependent not only on the unknown variable included inside the column vector $\{\dot{\phi}_j\}$ for the corresponding node but also on the other variables (a different j) of the same node. This equation therefore is an implicit equation (with reference to $\dot{\phi}$'s). For instance, element in $\{R\}$ in the air temperature equation for an interior node in a wet coil (equation 6.67) includes the time derivatives of the air temperature, the air humidity ratio and the water temperature and at the same node (equation 6.83). It can be made explicit by appropriately modifying elements in the coefficient matrix $[A]$ and in the column vector $\{R\}$. However, there will still be time derivatives of other variables within the element in $\{R\}$ unless all the equations (for all j 's) are combined but, in that

case, the coefficient matrix will become a large sparse matrix which will complicate the solution process.

By arranging equations for each state variable of the air and water separately as shown in equation (6.87), time derivatives of each variable for all nodal points can be solved, one at a time, independent of equations of other variables but, since the equations (for different j 's) are actually coupled, this necessitates the use of an iterative procedure. When solving for $\{\dot{\phi}_j\}$ for a particular variable (j), the time derivatives of other variables contained within elements in $\{R_j\}$ will need to be treated as known quantities, based either on initial estimates or improved estimates when solutions for them have been found in a previous step of calculation. While solving for the time derivatives of w_a , T_a and T_w , the time derivatives of T_c and T_{tb} for all nodal points will also be evaluated by using equations (6.75) - (6.86) during the solution process.

With this approach, the iterative procedure will be necessary even if a fully explicit solution scheme (in time, i.e. $\lambda = 0$) is employed. The fully-implicit scheme will improve stability and enable a larger time step size be used. Moreover, due to the use of the one-sided differencing scheme, each of the coefficient matrices $[A]$ for $j = 0$ to 2 is simply a bi-diagonal matrix (notwithstanding that they are shown as a tri-diagonal matrix in equation 6.87). For the air equations ($j=0$ & 1), each matrix includes one lower diagonal of elements whereas that for the water equation ($j=2$) has one upper diagonal besides the principal diagonal elements. The solution process therefore will involve a simple backward or forward substitution process and can be done efficiently. The need for solving a set of sparse matrix equations (which would arise if the time derivative terms were all put to the left hand side as unknown quantities) was also avoided.

6.5.6 Coil Surface Conditions

Two different sets of equations with different heat (and mass) transfer coefficients are involved in modelling a dry coil and a wet coil. Whether the coil will be

fully dry, fully wet or partly wet is dependent on the instantaneous coil surface temperature and the dew-point temperature of the on-coil air. However, the coil surface temperature distribution is not known before the relevant equations have been solved. Hence, before solving the equations, and during any intermediate level of calculation, the coil surface temperature at various nodal points must be checked from time to time to see whether there will be condensation of water vapour from the air onto the coil surface. In the solution scheme adopted (self-implicit scheme in conjunction with Runge-Kutta-Merson method), the air temperature, the air humidity ratio and the coil surface temperature at any intermediate level of calculation can be estimated based on values calculated at the last time step and preceding levels of the solution process (the Runge-Kutta-Merson scheme). Hence, the checking procedure can be done conveniently as part of the solution process.

6.6 Steady-state Version of the Finite Difference Coil Model

By setting all time derivative terms in equations (6.30) to (6.38) to zero, the set of governing equations can be converted into a steady-state model for a cooling and dehumidifying coil. The steady-state governing equations can likewise be solved by finite difference method in conjunction with appropriately defined boundary conditions (on-coil air and water conditions and flow rates). The steady-state finite difference coil model was developed primarily for use in setting initial conditions (air temperatures, humidity ratios and water temperatures) at all nodal points based on the given initial on-coil air and water conditions and the initial flow rates of the fluids. The set of finite difference equations obtained for a wet coil are as summarized below:

a) *Mass and Energy Conservation Equations for Air and Water :*

i) At inlet node 1 where w_a & T_a are known,

$$\left(Ntu_w + \frac{2}{\Delta\xi}\right) T_{w1} - \frac{2}{\Delta\xi} T_{w2} = Ntu_w T_{c1} \quad (6.88)$$

ii) At interior nodes, for $i = 2$ to $N-1$,

$$-\frac{1}{\Delta\xi} w_{ai-1} + \left(\frac{1}{\Delta\xi} + \frac{Ntu_a}{Le_m}\right) w_{ai} = \frac{Ntu_a}{Le_m} w_{soi} \quad (6.89)$$

$$-\frac{1}{\Delta\xi} T_{ai-1} + \left(\frac{1}{\Delta\xi} + \frac{Ntu_a}{Le_m}\right) T_{ai} = \frac{Ntu_a}{Le_m} T_{ci} \quad (6.90)$$

$$\left(\frac{1}{\Delta\xi} + Ntu_w\right) T_{wi} - \frac{1}{\Delta\xi} T_{wi+1} = Ntu_w T_{tbi} \quad (6.91)$$

iii) At exit node N where T_w is known,

$$-\frac{2}{\Delta\xi} w_{aN-1} + \left(\frac{2}{\Delta\xi} + \frac{Ntu_a}{Le_m}\right) w_{aN} = \frac{Ntu_a}{Le_m} w_{soN} \quad (6.92)$$

$$-\frac{2}{\Delta\xi} T_{aN-1} + \left(\frac{2}{\Delta\xi} + \frac{Ntu_a}{Le_m}\right) T_{aN} = \frac{Ntu_a}{Le_m} T_{cN} \quad (6.93)$$

b) *Energy conservation equations for the fin-core and tube-core (for $i = 1, 2, \dots, N$):*

$$\begin{aligned} \left(\frac{C_a}{C_c} \frac{Ntu_a}{Le_m} + \frac{P_{ct} L}{C_c R_{ct}}\right) T_{ci} &= \frac{C_a}{C_c} \frac{Ntu_a}{Le_m} T_{ai} - \frac{C_a}{C_c} \frac{Ntu_a}{C_{p_a} Le_m} h_{fg} (w_{soi} - w_{ai}) \\ &\quad + \frac{P_{ct} L}{C_c R_{ct}} T_{tbi} \end{aligned} \quad (6.94)$$

$$\left(\frac{C_w}{C_{tb}} Ntu_w + \frac{P_{ct} L}{C_{tb} R_{ct}}\right) T_{tbi} = \frac{C_w}{C_{tb}} Ntu_w T_{wi} + \frac{P_{ct} L}{C_{tb} R_{ct}} T_{ci} \quad (6.95)$$

For a dry coil, water vapour mass conservation equations (6.89) & (6.92), the term associated with the humidity ratio difference in the right hand side of (6.94) and Le_m can be omitted.

Noting that w_{soi} is a function of T_{ci} and by arranging equations (6.88) - (6.93) into three matrix equations with the fin-core and tube-core temperature terms put to the right hand side vector, an iterative solution procedure similar to that for the dynamic coil model can be adopted for modelling the steady-state performance of cooling and dehumidifying coils.

Chapter Seven

Results of Test-runs with the Log Mean Enthalpy Difference (LMHD) and the Finite Difference (FD) Coil Models

Results of applying the two air-conditioning coil models developed (the LMHD model (Appendix B) and the FD model (Chapter 6)) to simulate the steady-state full-load and part-load and the dynamic performance of chilled/hot water coils are summarized in this chapter. Steady-state coil performance predicted by the models were compared against coil manufacturers' data. The accuracy of predictions by the models were verified and improvements to the coil models were made. Predictions of the FD dynamic model had also been compared against the experimental results due to Stoecker et al (153), Tamm & Green (149) and Maxwell et al (154). Descriptions of these comparisons are included in this chapter.

7.1 Verification of Steady-state Coil Models

To verify and compare the accuracy of prediction of the LMHD model (Appendix B) and the steady-state version of the FD model (Chapter 6), both were applied to simulate steady-state performance of several cooling and dehumidifying coils with corrugated fins and smooth internal tube surfaces (without turbulators - a method used by some manufacturers to enhance the tube-side heat transfer). These coils are

commercial products and their performance data, as given in the manufacturer's catalogue, were used as the basis for the comparison.

The catalogue coil performance data are actually "computed" ratings which have been certified ⁽¹⁷⁹⁾ in accordance with ARI Standard 410 ⁽¹⁸⁰⁾. According to this standard, a coil manufacturer can publish "application ratings" for coils based on heat and mass transfer resistances determined in laboratory "standard rating" tests on a prototype coil of the same surface design and arrangement but may be of different coil size, row depth and operating conditions. In respect of testing requirement for rating chilled and hot water coils, the ARI Standard specifies that the testing procedures and the associated laboratory apparatus and instrumentation shall comply with the ASHRAE Standard 33-78 ⁽¹⁸¹⁾. A method is given in the ARI Standard 410 for reducing the "standard ratings" (test data) for use in determining the application ratings of other coils, without testing each individual unit size of the coils in the same product line.

For compliance with the ARI Standard 410, any coil selected at random will have a total capacity, when tested, not less than 95% of its published total capacity. Hence, the actual coil total capacity should not deviate from the corresponding catalogue data by more than -5%. However, individual conformance of sensible and latent capacities for cooling and dehumidifying coils are not required by the ARI Standard. Notwithstanding the error bands of the sensible and latent capacity data given in the manufacturer's catalogue are unknown, it is reasonable to assume that the data represent, within "acceptable" limits, the actual performance of the coils. Nevertheless, caution was taken of the uncertainty in accuracy of the catalogue data when analyzing the comparison between predictions of the coil models and the catalogue data.

For the coils modelled, the manufacturer provided, in its catalogue, data on total cooling capacities but the sensible and latent cooling capacities of the coils had to be calculated based on given air flow rates and entering and leaving coil air conditions.

A total of 26 different combinations of coil sizes, tube-fin configurations, water circuit arrangements and operating conditions was studied. Characteristics of the coils modelled are as summarised in Table 7.1. The total cooling capacities of the coils modelled ranged from 2.6 kW to 94 kW which correspond to the sizes of coils in air-handling equipment ranging from typical small fan-coil units to large central air-handling units commonly found in commercial buildings in Hong Kong. In addition, the test runs were also aimed at verifying:

- 1) whether performance of coils with corrugated fins can be modelled more accurately by adopting Beecher & Fagan's correlations ⁽¹⁴¹⁾; and
- 2) whether Beecher & Fagan's correlations, which were derived from experiments on dry surfaces, can be applied to both heat and mass transfer.

7.1.1 Effect of Contact Resistance

In both the LMHD and the FD models, the contact resistance arising from imperfect bonding between the fin-collars and the tubes can be included as one of the thermal resistances to heat exchange between the two working fluids. However, the fin-side heat and mass transfer coefficients evaluated by using McQuiston's empirical correlations ^(143,144) should have accounted for the effects of contact resistance. To verify this, preliminary test runs with the coil models were carried out in which the contact resistance was estimated using Eckels's empirical correlation ⁽¹⁶⁰⁾ and included in the evaluation of the U-values of the coils. The simulation results showed that, with the contact resistance additionally included, the two steady-state coil models significantly under-estimated (by more than 10%) both the sensible and the total heat transfer of the coils when compared with the manufacturers' data. Thus, in all subsequent test runs, the assumption was made that the effects of contact resistance were accounted for by the heat and mass transfer coefficients estimated using McQuiston's correlations. The contact resistance term in the LMHD model was

therefore set to zero. However, the same could not be done with the FD model because this would give rise to an overflow error in the computation. Instead, the contact resistance term in the FD model was set to a negligibly small value.

7.1.2 Flat-fins

In the first verification test performed, the coils were assumed to be of flat-plate fins (i.e. without fin corrugation patterns) and Beecher & Fagan's correlations (141) were ignored. Model predictions with this assumed fin geometry would indicate how significant fin-corrugations would be on the performance of a cooling and dehumidifying coil.

By using McQuiston's correlations for flat-plate fins (143,144) to evaluate the fin-side heat and mass transfer coefficients, it was found that for the coils modelled, both models under-estimated the sensible cooling capacity of the coils (Figure 7.1a). Results from the LMHD model deviated from the catalogue data by over 10% whereas the FD model was able to provide marginally better results. On the other hand, both models over-estimated the latent cooling capacity of the coils (Figure 7.1b). The over-estimation in latent cooling capacity compensated for the under-estimation in sensible capacity and hence, both models were able to estimate the total cooling capacities with acceptable accuracy (Figure 7.1c).

Since the total cooling capacities predicted by the models are in good agreement with the manufacturer's data and, should the modelled data be "measured test ratings" of the coils, the coil performance data given in the manufacturer's catalogue would be acceptable as far as compliance with the ARI Standard is concerned. However, given the large deviations in the sensible cooling capacities, which are out of the accuracy that one would expect of data in a manufacturer's catalogue, the flat-fin model cannot be regarded as an acceptable model for coils with corrugated fins. Hence, it is apparent that the effects of fin corrugation must be accounted for in the coil models.

7.1.3 Corrugated Fins with Beecher & Fagan's Correlations Applied to Both Sensible and Total Heat (and Mass) Transfer Coefficients

In the coil models developed, the empirical correlations developed by Beecher & Fagan ⁽¹⁴¹⁾ (B&F) were adopted to account for the effect of fin corrugation on the rates of heat and mass transfer at the fin surfaces. The heat and mass transfer coefficients at corrugated fin surfaces were first calculated based on McQuiston's correlations for flat-plate fins ^(143,144). The coefficients determined were then corrected by applying B&F's correlations. However, because B&F's correlations were derived based on experiments on 'dry' corrugated surfaces, the suitability of the correlations for a wet coil was uncertain.

By applying B&F's correlations to correct both the sensible heat and mass transfer j-factors estimated from McQuiston's correlations, it was found that the sensible cooling capacities of the coils estimated by both models are in good agreement with manufacturers' data (Figure 7.2a). However, both models over-estimated the latent cooling capacity of the coils (Figure 7.2b) and the deviations from catalogue data were slightly larger than those of the preceding case where fins were assumed flat. As a result, both models over-estimated the total cooling capacity of the coils modelled (Figure 7.2c).

7.1.4 Corrugated Fins with Beecher & Fagan's Correlations Applied to Correct the Sensible Heat Transfer Coefficient Only

It was found that by applying Beecher & Fagan's corrections to the sensible heat transfer j-factor only, both the LMHD and the FD coil models were able to give reasonably good estimations of sensible and total cooling capacities of the coils (Figure 7.3 a, b & c). However, the comparison between the model predictions and the manufacturer's data on latent cooling capacities is somewhat disappointing in that the deviations, in many cases, exceeded $\pm 25\%$. Nevertheless, it must be pointed out that the "manufacturer's data" on latent capacities referred to here were actually calculated

data based on the differences between the respective total capacities given and the sensible capacities calculated using the air volume flow rates and on- and off-coil air conditions. The set of latent capacity data used in the comparison therefore is by-itself subjected to a degree of inaccuracy higher than that of the total capacities. For instance, if the total capacity data for a coil is 5% above the actual value whereas the sensible capacity data is 5% below the actual value, for a case where the actual sensible coil load is 70% of the actual total load, the calculated latent load will be 28% above the actual value. Taking into account the inaccuracy of the reference data used in the comparison, the coil models, in which B&F's correlations were applied to correct the sensible heat transfer coefficients only, were adopted in this work for modelling performance of cooling and dehumidifying coils.

7.1.5 Discussions on Comparison of Steady-state Model Predictions

Results of the above simulation studies (Figures 7.1a and 7.3a) show that by adopting corrugated fins, the sensible cooling capacity of cooling and dehumidifying coils could be increased by more than 10%. This however was offset by a corresponding reduction in the latent cooling (dehumidifying) capacity (compare Figure 7.2b with 7.3b) and the resultant total cooling capacity of the coils remained approximately the same as compared to flat-finned coils (compare Figures 7.1c with 7.3c). Experience of cooling load calculations for buildings in Hong Kong (having a hot and humid climate) shows that the room sensible heat ratio (ratio of sensible cooling load to total cooling load) of an air-conditioned space is usually higher than the sensible heat ratio (ratio of sensible to total cooling capacity) of a cooling coil. In conjunction with the practice that the coil capacity output is controlled according to the room air temperature only (i.e. according to sensible room cooling load), the latent cooling capacity of a coil is seldom fully utilized. This sensible cooling effect enhancement therefore is a desirable improvement to the performance of a cooling and dehumidifying coil in that a smaller coil (e.g. less number of rows), and hence a more economical one,

can be used to cope with the same sensible and latent load when compared with a flat-finned coil.

It was found that in general, both models can provide comparatively more accurate performance predictions for coils with medium to large size than smaller size coils. One of the reasons for this is due to the assumptions taken in evaluating the coil parameters such as total finned area, air-flow core area, etc., in which the irregularities of the tube array at the edges were ignored. The effect of this would be more significant for small size coils. It was also found that a majority of cases where there were larger deviations between simulated performance and catalogue data existed with 3-row coils. This showed that the correlation suggested by McQuiston to account for effects of different tube-rows (equation B.33 in Appendix B) might not be able to provide a complete account of the effects. Further, the use of a counter-flow heat exchanger model may be inappropriate for 3-row coils.

Despite the differences in the methods used to simulate the steady-state performance of coils, it can be seen from the simulation results that only small differences existed between the predictions of the LMHD coil model and the steady-state version of the FD coil model. One of the reasons for such differences was due to the effects of variations in the value of the proportionality constant 'C' that was used to evaluate the wet coil surface effectiveness (see Section B.3.3 in Appendix B). In the LMHD model, 'C' was evaluated based on the air-flow exit plane conditions only and the surface effectiveness so determined was applied to the entire wet area of the coil. For the FD model, the values of C and surface effectiveness were calculated on a node-by-node basis with reference to the local coil surface and air conditions at each nodal point. The LMHD model was able to provide slightly better results when an average value of C was used, as suggested by McQuiston & Parker ⁽²⁸⁾, which was obtained by taking the mean value of C based on the on-coil conditions and the leaving coil conditions. However, this was not adopted because more iteration steps would have been required whilst the improvement in accuracy of prediction was insignificant.

The method used in the LMHD model for determining the dry/wet boundary, and hence the dry and wet coil surface areas, should be more accurate than that in the FD model. In the latter, dry/wet areas only change in integral steps according to the number of sub-divisions adopted in solving the governing equations. However, the FD model's ability to account for variations in coil conditions along the air-flow direction (a variable C and, hence, surface effectiveness) is a favourable feature that is absent from the LMHD model. Also, the FD model allows intermediate conditions within the coil to be found but the LMHD model can be used to calculate the overall heat and mass transfer rates only. Nevertheless, if only the steady-state coil performance needs to be modelled, the LMHD model is simpler and computationally more efficient than the FD model (the ratio of computing time required by the two models is about 1:2~4).

7.2 Part-load Performance of a Cooling and Dehumidifying Coil

In a constant air volume (CAV) system, the indoor temperature is controlled by adjusting the mass flow rate of chilled water through the cooling coil. Under design conditions, the latent cooling capacity of a typical cooling and dehumidifying coil accounts for about 30% of the coil's total cooling capacity. When the chilled water flow rate is reduced, both the sensible and latent cooling capacities of the coil will drop but the reduction is larger in latent cooling capacity than in sensible cooling capacity (relative to the respective capacity at the design chilled water flow rate; see Figure 1.2). Consequently, the indoor air humidity will rise as the dehumidification effect of the coil drops.

Although the control over the indoor humidity under part-load conditions may be improved by using different control strategies (e.g. by controlling the cooling coil according to either the indoor temperature or humidity, whichever is deviating further away from the respective set-point, i.e. priority control ^(5,146)) or different system designs (e.g. coil face by-pass system ^(5,146)), these would incur a higher initial cost and possibly a higher running cost (e.g. if re-heat is used in conjunction with the

priority control). Therefore, these methods are seldom used in commercial buildings in Hong Kong (see also Section 1.3). Since an air-conditioning system operates under part-load conditions far more often than under the design load conditions and undesirably high indoor humidity may arise in these circumstances, the ability to properly model the part-load performance of cooling and dehumidifying coils is essential.

Simulating the performance of a cooling and dehumidifying coil may be problematic when the chilled water flow rate is reduced to the extent that the coil surface condition is at the transition between partly wet and completely dry. Under this condition, before arriving at a converged solution, the computer program can encounter extreme values of parameters in the calculation which would give rise to execution errors and adjournment of the solution process. Experience was gained from the test-runs with the models in the course of their development that the value of the proportionality constant 'C' (in equation B.66) could become negative and thus would cause an argument domain error to the square root calculation in the solution of the fin efficiency (see equations B.68 & B.69).

To avoid such failures in simulation, a good initial guess of the leaving coil air and water conditions and of the coil surface temperature was found to be essential. In the LMHD model, initial values of the temperature changes in the two fluids were estimated by apportioning the temperature difference between the two incoming fluids with reference to their respective capacity rates (product of mass flow rate and specific heat). More importantly, the value of the proportionality constant 'C' at the leaving coil plane was checked at every iteration step and if its value was found to be negative, it was set to zero which implied that the coil was assumed to be completely dry. In addition, it was found that, in the solution for surface effectiveness, the surface temperature should be solved first in the iterative process rather than to solve directly the surface effectiveness (see Appendix B, Section B.6).

For the FD model, similar methods were adopted to obtain initial guesses of the leaving coil air and water conditions. Air and water conditions at interior nodes were then evaluated assuming that they were linearly distributed along the air flow direction. Initial coil surface temperatures at all nodal points were then evaluated based on these conditions. In each subsequent iteration step, the coil surface temperatures were checked against the dew-point temperature of the air at corresponding nodes to determine if the surface at the node was dry or wet. Also, the value of 'C' was checked and set to zero (and the coil surface at that node taken as dry) if its value was found to be less than zero.

The part-load performance of a cooling and dehumidifying coil with chilled water flow reduced from 100% down to a few percent of the design flow rate was modelled by the FD steady-state coil model. The cooling coil simulated was the one in the fan-coil unit selected for air-conditioning the model room based upon which test-runs with the building fabric heat and moisture transfer model were carried-out (Chapter 9). Construction details of the coil are given in Table 9.4. In this simulation study, the on-coil air temperature and humidity ratio as well as the on-coil chilled water temperature were held constant. The model predictions are as shown in Figures 7.4a - 7.4c.

It can be seen from the simulated results that the latent cooling capacity of the coil dropped to a very small value (Figure 7.4a) when the chilled water flow rate was reduce to less than 30%. The leaving coil air and water temperatures both rose by about 10 °C (Figure 7.4b) and the leaving coil air humidity ratio approached the on-coil value (Figure 7.4c) over this range of chilled water flow rate reduction. This clearly showed that with reduction in chilled water flow, the temperature rise of the chilled water across the coil was increased which gave rise to an increase in the coil surface temperature and a reduction in the coil's dehumidification capacity. The general trend of cooling capacity variation predicted by the model was similar to the typical coil performance as shown in Figure 1.2.

7.3 Dynamic Performance of a Cooling and Dehumidifying Coil

The dynamic performance of the coil modelled in the study on steady-state part-load performance of a cooling and dehumidifying coil (described in the preceding section) was modelled by using the finite difference (FD) dynamic coil model (Chapter 6). In this simulation study, the chilled water flow rate through the coil was assumed to be controlled by an equal percentage valve and the valve position was proportional to the deviation between the room air temperature and the indoor set-point temperature. The indoor temperature was assumed to vary with time as shown in Figure 7.5a. However, the on-coil air temperature and humidity ratio and the supply chilled water temperature were held constant. For comparison, the steady-state performance of the same coil for the same on-coil air and water conditions at each time interval calculated in the dynamic simulation was also calculated by using the steady-state version of the FD model. Results of the latter would correspond to making the assumption that the coil would be able to attain steady-state instantaneously, as would be the case if quasi-steady air-conditioning system models were used in a dynamic building thermal load simulation.

Simulation results from both models are shown in Figures 7.5b - 7.5d from which it can be seen that a noticeable time delay existed between the coil performance predicted by the dynamic model and those from the steady-state model. This is the effect of the thermal capacity of the coil materials, the transport delay for the fluids to flow across the coil and the rate of valve plug displacement in response to a change in indoor temperature. In detailed studies of how indoor air conditions could be affected by the performance of air-conditioning systems, the coil's dynamic characteristics should be accounted for. As will be seen from results of the simulation studies reported in Chapter 9, there are significant differences in the predicted indoor air humidity level between applying the dynamic and the steady-state models to simulated heat and moisture extraction rates from the room air by an air-conditioning system with on/off control.

7.4 Verification of the FD Dynamic Coil Model

To verify how accurate the FD dynamic coil model can be when it is applied to simulate the dynamic performance of air-conditioning coils, the model was applied to simulate the transient responses of several coils which had been tested experimentally and the measured results are available. In searching for experimental data for verification of the dynamic coil model, it was found that although there are many references in which comparisons of modelled and experimentally obtained coil performance are reported (e.g. 36,147,149,153,154,156), in some of them, the descriptions about the construction details of the coils tested and the operating conditions under which the experiments were conducted were incomplete (e.g. 36,147). Such results are therefore not usable. However, some may still be used if there are only a few parameters missing and the missing data can be replaced by reasonable estimates. In this study, the results of Stoecker et al (153), Tamm and Green (149) and those of Maxwell et al (154) were used for verification of the FD dynamic coil model.

7.4.1 Comparison with Stoecker et al's Experimental Results

Stoecker et al's experiment (153) was on testing the response of a hot water heating coil to a step change in water flow rate. In their paper, the coil construction details and the incoming air and water temperatures were given but data of the flow rates of the two fluids pertaining to the experiment were missing. To circumvent this problem, the air mass flow rate (constant in this case) and the initial and final water mass flow rates (before and after the step change) were estimated by using the steady-state version of the FD coil model. In this, the steady leaving-coil air and water temperatures corresponding to a range of air and water flow rates were evaluated and compared with their respective initial and final steady values in the experiment (obtained from figures 9 and 11 in Stoecker et al's paper). The combination of air and water mass flow rates associated with the set of leaving coil conditions that matched the initial and final steady experimental values were found to be 0.38 kg/s (air mass flow rate), 0.15 kg/s (initial water mass flow rate) and 0.21 kg/s (final water mass flow rates)

respectively. The dynamic coil performance simulation study was based on this set of estimated fluid flow rates.

Based on the given coil construction details, on-coil air and water temperatures and the estimated air and water flow rates, Stoecker et al's experiment on the heating coil, subjected a sudden increase in water flow rate (initially at the rate of 0.0326 kg/s², see the small graph in Figure 7.6), were repeated numerically by using the FD dynamic coil model. Figure 7.6 shows a comparison of the modelled leaving air and water temperatures with the experimental results. Although there is a slight difference between the modelled and the measured results in respect of the coil's rate of response, the two sets of results are, in general, in good agreement with each other.

7.4.2 Comparison with Tamm & Green's Experimental Results

Tamm and Green ⁽¹⁴⁹⁾ performed detailed experiments on the dynamics of multi-row finned hot water heating coils and their results have been used by others for verification of coil models (e.g. ¹⁵⁸). Comprehensive descriptions about the construction details of the coils tested and the experimental conditions are given. The experimental results and the corresponding predictions of their transfer function coil model are shown in the form of Bode plots which represent the responses of the coils to sinusoidal perturbations of varying frequencies. Each set of results are shown by two curves: the amplitude ratio curve and the phase angle curve. In their paper, only the air temperature responses are reported.

In Tamm and Green's experiment, the input used was a complex pulse signal which simulates a sinusoidal function ($f(t)$) comprising five harmonic components (the 1st, 2nd, 4th, 8th and the 16th harmonics):

$$f(t) = \cos \theta - \cos 2\theta + \cos 4\theta - \cos 8\theta + \cos 16\theta$$

where $\theta = \frac{2 \pi t}{T}$; t = time and T = period.

Two fundamental frequencies were used for each set of tests performed; for the low frequency test, the fundamental frequency was $\frac{1}{6}$ cycle per minute (cpm) and that of the high frequency test was $1\frac{1}{3}$ cpm. For convenience in carrying out test runs with the FD dynamic model and in analysis of the results, the input water flow rate functions (for the low and the high frequency tests) were each decomposed into five single harmonic functions (simple cosine functions), and test runs were performed for each component harmonics, one at a time.

According to the above multi-harmonics function, the amplitude of each component harmonics should have been 0.162 times the range of the combined input function (the difference between the maximum and the minimum values of the input variable (the perturbation) which are given in Tamm and Green's paper). However, the amplitudes of the single harmonic functions so determined were very small which made it difficult to determine accurately the amplitudes of the coil response from the modelled results. As the experimental results are in the form of dimensionless amplitude ratios, approximately the same dimensionless frequency response can be obtained by using an input function that has a different amplitude (strictly true only if the coil has a linear response). Hence, in the computer simulation, the amplitudes of the inputs used were twice the amplitudes of the corresponding component harmonics of the combined input used in Tamm and Green's experiment.

The FD dynamic coil model was applied to simulate the frequency response of the coil tested in Test No. 3 and 4 in Tamm and Green's experiment (a four row coil with counterflow arrangement subjected to a water flow velocity perturbation). Based on the input amplitude of the cosine functions determined from the range of hot water flow velocity in the tubes (and magnified) and the frequencies as given in their paper, a time-series of water flow rates was generated for each harmonic component of the input function and the data series were used as the input to the FD dynamic coil model. Other experimental conditions including water supply temperature, air flow rate and on-coil air temperature were mimicked in the numerical simulation. The amplitude ratios were

calculated from the air temperature response (with the transient variations at the initial phase of the coil response ignored), non-dimensionalized by the ratio of steady temperature and steady flow rate and expressed in decibel scale (as in Tamm & Green's paper). The phase lag was determined from the time-shift between the water flow rate input and the air temperature response curves. The results are shown in Bode plot (against the dimensionless frequency), together with the experimental results for comparison (Figure 7.7). The coil response as predicted by Tamm & Green using their transfer function model is also shown. This comparison shows that the dynamic response of the heating coil simulated by the FD model is in good agreement with the experimental results.

7.4.3 Comparison with Maxwell et al's Experimental Results

Maxwell et al ⁽¹⁵⁴⁾ carried out experiments with a cooling and dehumidifying coil to obtain values for the coefficients of their simplified coil model. Their model is an empirical first-order dynamic model which simulates the transient leaving-coil air temperature (the output) in response to changes in the water flow rate (the input). In their model, the dynamic response of a coil is characterized by the time constant, the steady state gain and the temperature offset of the coil, all of which need to be determined experimentally. To account for the non-linear characteristics of a cooling and dehumidifying coil, these empirical coefficients vary with the water flow rate. In their experiment, the coefficients were evaluated by an on-line "recursive least squares identification technique" based on the measured transient response of the coil. In order to make the temperature offset independent of the water flow rate offset, the latter was set to zero and accordingly, the leaving air temperature offset did not correspond to the actual leaving air temperature. The two however are related to each other by:

$$\text{Temp. offset} = \text{Leaving air temp.} + \text{Steady-state gain} \times \text{Water flow rate}$$

where the steady-state gain is the temperature 'drop' of leaving coil air per unit change in water flow rate.

In Maxwell et al's paper, the experimental conditions and some coil construction data are given. However, data about the coil width (W); the number of tubes per row (N_{tpr}), the internal and external tube diameters (D_i & D_x), the tube spacings at the air-flow direction (x_b) and in the transverse direction (x_a) and the fin thickness (y) were missing. In the simulation studies, the following values, which are nominal values for coils of similar size, were assumed:

$$\begin{aligned} W &= 0.762 \text{ m} ; & N_{\text{tpr}} &= 16 ; & D_i &= 16.92 \text{ mm} ; & D_x &= 19.05 \text{ mm} ; \\ x_a &= 38.1 \text{ mm} ; & x_b &= 47.6 \text{ mm} ; & y &= 0.178 \text{ mm}. \end{aligned}$$

Case 1 of Maxwell et al's experiment was repeated numerically in which the cooling coil tested was modelled by the FD dynamic coil model developed. The coil time constants corresponding to various water flow rates were determined from the transient leaving air temperature predicted by the FD coil model. In each step increment in water flow rate, the steady-state temperature drop (from the initial condition to the steady-state condition after the step-change) was noted and the time required for the leaving coil air temperature to reach 0.632 of the steady-state temperature drop was taken as the time constant for that step. The steady-state gain was evaluated by dividing the steady-state temperature drop by the change in water flow rate in that step. The corresponding leaving air temperature offset was calculated based on the water flow rate, the calculated time constant and the simulated leaving coil air temperature.

Comparison of the simulated results with Maxwell et al's experimental data is shown in Figure 7.8. This shows that the deviations in steady-state leaving coil air temperature were more significant at the low water flow rate range. As a result, the coil time constant and the steady-state gain calculated from the simulated coil response over the same water flow rate range were lower than Maxwell et al's results. At a water flow rate of around 0.3 kg/s, the coil was at the transition between partly wet and completely dry and there were significant deviations in the steady-state gain and the leaving coil offset. However, the overall coil performance simulated by the FD coil model was in reasonably good agreement with the experimental results.

Chapter Eight

The Integrated Building and Air-Conditioning System Models

In this chapter, construction of the building and configuration of the air-conditioning system that can be modelled by the component models developed, the inter-relationships between the component models and how the component models were coupled together to form an integrated building and system model are described. The methods used to solve the coupled model equations, to control time-step sizes in the simulation calculation, and to stagger the time progress in the building model and in the system component models to speed-up the solution process are explained. Finally, how weather data and material property data are handled in the integrated model are outlined.

8.1 The Integrated Models

The building heat and moisture transfer model developed from Huang's equations (Chapter 3) was integrated with a simple air-conditioning system model and used in preliminary studies at the early stage of this research ⁽⁵²⁾ (see Appendix D). That air-conditioning system model comprised a steady-state cooling coil model (the LMHD model, see Appendix B), an on/off controller model, a control valve (linear type) model and a simple hydraulic circuit model (Chapter 5). The features of predicting the time of valve position reversal (from open to close and vice versa) and delaying the

valve action when such condition arises (see Sections 5.7 and 8.3.1 below) were not included, and the control valve was assumed to open or close instantaneously. In that model, the conventional successive back substitution method was used to solve the model equations. Because of the complexity of the building model (based on Huang's equations) and the less efficient numerical solution method used (compared with using the self-implicit scheme in conjunction with the Runge-Kutta-Merson method), a large amount of computing effort (and hence, time) needs to be spent when using that integrated model (the ratio of computing time to simulation time (where coil dynamics were ignored) was about 1:1 when a 486PC was used). It was therefore abandoned in further investigations.

The simulation studies reported in Chapter 9 were carried out by using the two integrated models developed from the differential permeability building heat and moisture transfer model (Chapter 4). In the first one, the differential permeability building model was integrated with the steady-state log-mean enthalpy difference (LMHD) coil model (Appendix B) and with models for other components of an air-handling system (Chapter 5). This model therefore is a quasi-steady-state model comprising a dynamic building model and steady-state air-conditioning component models. The second one differs from the first one in that the finite difference (FD) dynamic coil model (Chapter 6) was used instead of the steady-state model. With the two models, the differences in simulation results, with and without accounting for the dynamics of the coil, can be compared (see Chapter 9). The two integrated models were named (and are called in this thesis) as "RKMACC" and "DERMAC" respectively. In the latter, the simulation time progress in the building model and that in the system model were staggered so as to speed up the computing process (see Section 8.3.2).

At present, the two integrated models are both single zone models capable of simulating the heat and moisture transport phenomena in a room located at the perimeter side on a typical floor of a building. Also, the effects of furniture and other hygroscopic materials inside the room (e.g. fibrous materials, books and papers, etc.), which in

reality may also affect the heat and moisture balances in the room air, were not included in the present investigation. Extending the model to a multi-zone model and to account for the effects of hygroscopic materials inside buildings are recommended as further work to be pursued on the basis of the work completed and an outline of how the effects of the latter may be approached is included in Chapter 10.

8.1.1 Construction of the Room

The room that can be modelled is of rectangular shape, enclosed by four walls and two slabs (see Figure 8.1). Each wall or slab of the room may be composed of several layers of different materials. One of the walls (Wall 1) is an exterior wall which is exposed at one side to the outdoor weather conditions. A rectangular window may be included in this wall. The internal partition walls (Wall 2, 3 & 4) and the ceiling and floor slabs (Wall 5 & 6) separate the room from adjacent rooms at the two sides, from the corridor at the side opposite to the exterior wall, and from rooms on floors above and below. The assumption was made that identical conditions exist in all adjacent rooms, including those at both sides of the room and on the floors immediately above and below. The corridor may have a different temperature and humidity (to be specified in the input data file) but they were assumed to be of fixed values.

Based on the assumption that all adjacent rooms would be of construction and subjected to conditions identical to those of the model room, the external surface of each of the partition walls and the floor and ceiling slabs of the model room (and hence an internal surface of an adjacent room) was assumed to be exchanging heat and moisture at exactly the same rates as the corresponding internal surface of the model room. For instance, the rates of heat and moisture transfer at the external surface of Wall 2 were assumed to be identical to those at the internal surface of Wall 4. Likewise, the conditions at the external surface of Wall 4 were assumed to be identical to the internal surface of Wall 2. Wall 5 and 6 were treated similarly.

8.1.2 Configuration of the Air-conditioning System

The room was assumed to be air-conditioned by a constant air volume system which may comprise either a fan coil unit (FCU) or an air-handling unit (AHU) depending on the required size of the equipment to cope with the cooling load of the room to be modelled (Figure 5.4). The cooling and dehumidifying coil in the air-handling equipment was connected to a pair of chilled water supply and return pipes and chilled water supply to the coil was assumed to be at a constant temperature. The flow rate of chilled water through the coil would be regulated by a two-port control valve which would vary its degree of opening according to the command signal from a room air temperature controller. In both the RKMACC and the DERMAC models, choices can be made between the use of an on/off or a proportional controller and of a linear or an equal percentage control valve, by input of appropriate parameters in the input data file for the computer model. Chilled water flow rate through the cooling coil was modelled by a simple piping network model (Chapter 5) based on a constant pumping pressure.

The fresh air supply was assumed to be ducted to the return air plenum of the unit and would be mixed with the return air from the room. The mixed air would then enter the cooling and dehumidifying coil of the air handling equipment and the treated air leaving the coil would be supplied into the room. Duct and fan heat gains and transport delay in the supply ductwork are ignored in the model. The fresh air was assumed to be at the outdoor air conditions though the model could be used to study cases with the fresh air pretreated to a fixed condition (see Chapter 5 & 9).

Infiltration of outdoor air into the room was assumed to be at a constant rate (to be specified in the input data file). An assumption was made that room air would be exhausted at a rate equal to the sum of the rates of fresh air supply and infiltration, i.e. the room air pressure was assumed to be maintained at a constant level at all times and this was assumed to be equal to the atmospheric pressure.

8.1.3 The Inter-relationships of the Component Models

In the integrated building and air-conditioning system models (the RKMACC & DERMAC models), the heat and mass transfer characteristics of the building fabric components, the room air and the components of the air-conditioning system were each described by a mathematical model. The room air model served as a connection through which the component models of the building fabric and the air-conditioning system were coupled together (Figure 8.2). The coupling was provided by the expressions that describe the convective heat and moisture transfer between the room air and the internal boundary surface of each building fabric component, thereby relating the variables (temperature and vapour pressure) pertaining to the internal surface nodes of the building fabric components to those of the room air. The room air model in turn was coupled to the air-conditioning system component models through input-output relationships where the states of the room air (output of the room air model) formed the input variables for the air-conditioning system component models (including the state of the air approaching the cooling coil and the room air temperature signal fed back to the controller). The models for the building fabric components (the walls, slabs and the window) are coupled to each other by the mathematical expressions that describe the rates of radiant heat transfer amongst the internal fabric surfaces (Chapter 3 & 4). Heat and moisture transfer at the external surface of the exterior wall and convective and radiant heat transfer at the window were accounted for in the model so that the room air and air-conditioning system responses to changes in outdoor weather conditions could be properly modelled.

Due to the complex inter-relationships amongst the building and the system component models, the response of each component will be influenced by the state of many other components. The relationships amongst the component models were not a simple unidirectional sequence of inputs and outputs but involved many interactions. There were also recursive loops of input-output relationships where outputs from a downstream component were fed back as inputs to an upstream one (e.g. the control

loop for the indoor temperature). Simultaneous solution of the responses of all the components therefore was required. However, considering the need for the flexibility to allow component models of different mathematical formulations to be integrated to form a combined model, the sequential modelling method (see Chapter 5) was adopted in the integrated building and system model.

8.2 The Numerical Solution Methods Adopted

The heat and mass transfer processes amongst the building and the air-conditioning system components were described by a set of coupled equations including partial differential equations (PDEs), ordinary differential equations (ODEs), and algebraic equations. The PDEs describing the heat and moisture transfer in the building fabric components (Chapter 4) and those of the FD dynamic coil model (Chapter 6) were first converted into a set of ODEs by partial discretization of the governing PDEs in the spatial domain. The resultant set of ODEs (and algebraic equations) was solved by using the Runge-Kutta-Merson (RKM) method (Appendix A). By using the self-implicit scheme (Chapter 4 and Appendix A) in deriving the ODEs for the component models, the implicitly formulated model equations could be solved by the explicit RKM method. More detailed descriptions about the numerical methods adopted in the models are described in Appendix A.

Following the RKM numerical scheme, the changes in the variables of the component models over each time-step in the simulation process were evaluated in five stages. In each of these stages, the time derivatives of the variables were solved first and the incremental changes of the variables over the time-step (the k_i 's in Appendix A) were estimated. Values of the variables at the end of the time-step were then evaluated from the incremental values estimated in the five stages. The truncation error for each variable was then estimated and checked against the tolerance limit. If this was exceeded, the simulation calculation would be brought back to the starting point of the time-step and would proceed with the time-step reduced. Otherwise, the simulation would proceed to the next time-step. The next time-step size used for either onward

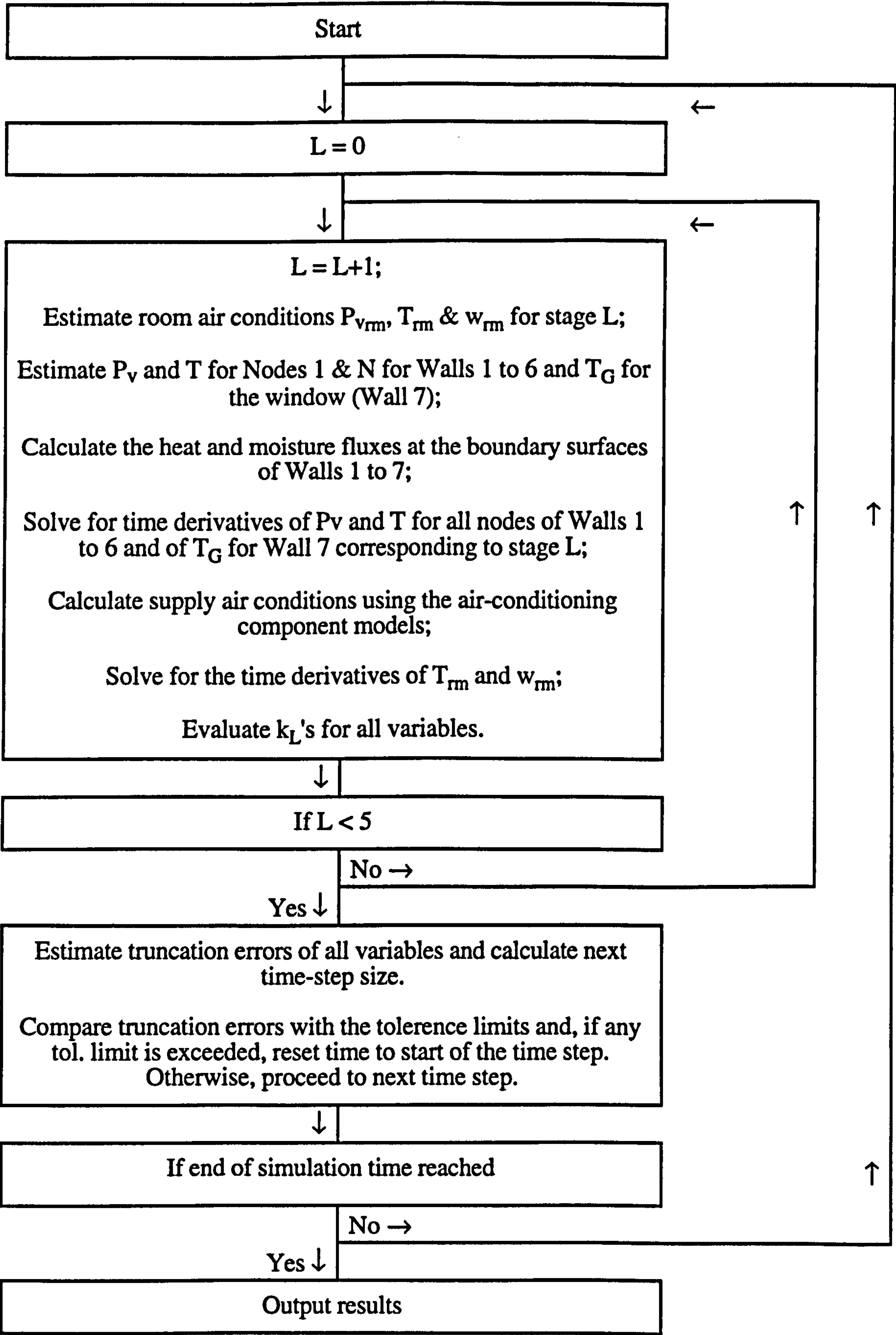
progression or re-calculation with a reduced time-step was determined with reference to the largest estimated truncation error amongst all the variables.

In each of the five stages of calculations in a simulation time-step, the component models were solved sequentially starting from the external wall (Wall 1) and then to the other walls, slabs and the window (Wall 2 to 7), the air-conditioning system and finally to the room air. The solution processes involved are as outlined by the flow chart on the next page.

Due to the coupling amongst the component models (and the use of an implicit scheme), solution of the time derivatives of the variables of a component model required a knowledge of the values of some variables from other components. For instance, in solving for the nodal conditions in a wall, the internal boundary surface temperatures of the other walls and slabs and the room air temperature and vapour pressure should be known. However, they themselves were also unknown variables that need to be solved simultaneously by the iterative procedure.

By employing the self-implicit scheme, the need for iterating round all the component models in each stage of calculation was avoided (iterative calculations however were still required in the solution of variables within certain component models, e.g. the wall and the FD coil models, see Chapter 4 & 6). This was possible because, in this scheme, the variables could be estimated from the known starting values of the variables in a time-step (the expressions at the RHS of the ODEs involved variables at the end of last time-step only). Also, the RKM method allowed the variables at each intermediate stage of a time-step to be estimated from the incremental changes of the variables evaluated at the preceding stage(s) and these could be used to evaluate the coefficients associated with the variables which were dependent on their current values. The heat and mass transfer rates between components could also be estimated based on these estimated intermediate values of the variables (see Appendix A, Section A7). Referring again to the wall model, the estimated room air temperature

A Flow Chart Showing the Solution Processes in the Integrated Model



and vapour pressure in a particular stage of calculation could be used to evaluate the rates of heat and moisture exchange between the boundary surface of the wall and the room air. Likewise, the estimated boundary surface temperatures of the other walls and the slabs could be used to estimate the radiant heat flux at the boundary surface of the wall. Similarly, in solving for the performance of the air-conditioning system, the intermediate stage room air temperature and humidity ratio were used in determining the control valve position (and hence chilled water flow rate through the coil) and the on-coil air conditions. The scheme proved to be very efficient and helped reduce considerably the computational effort required in the simulation studies. Otherwise, at least two to three times the computing time would be required.

8.3 Time Progress Control in the Integrated Model and Staggering of Time Progress in the DERMAC Model

In modelling the dynamic response of a system, the time-step size that can be used in the numerical simulation process is dependent on how sensitive the system is in response to a disturbance (in a first order system, this is characterised by the time constant of the system); the faster the response, the smaller the time-step needed. With large time-steps, the accuracy of the predictions will be poor and the numerical process may become unstable. In a model that simulates the dynamic response of a collection of components having markedly different response rates (the integrated building and system model is one such case), the smallest time-step (for maintaining stability and accuracy) required by the most sensitive component will need to be adopted for the entire simulation. This is referred to as a "stiff" problem (35,36,131,132) in numerical solution of differential equations.

8.3.1 Time-step Size Control

In the adopted numerical scheme (self-implicit + RKM), the size of time-steps used in the simulation process was kept under control by comparing the largest estimated truncation error against the tolerance limit. With this, a small time-step would

be used when the system was excited by a disturbance (as would occur at the start of a simulation or when a sudden change of an input condition was imposed onto the system) but when the system gradually settled down, the time-step would be enlarged. The simulation calculation would be brought back to the starting point and resumed from there with a reduced time-step if the largest estimated truncation error exceeded the tolerance limit.

When simulating cases where on/off control was used, the operating conditions of the coil would be disturbed by the cyclic movement of the control valve between the open and closed positions. In the model, the time ahead where a reversal of control valve opening would be called for was predicted in every time-step of calculation. If the predicted time for this to happen was within the time-step (determined based on the estimated error of the last time-step), the time-step size would be adjusted to end right at this time. Thereafter, the time-step size will be reset to the preset starting value and control over the time-step size would then be dictated by the estimated truncation error. For the RKMACC model, one second was used as the standard starting time-step though this may be changed at the input data file. For the DERMAC model, the time progress in the building and the system models was "staggered" (see the following section) and, hence, two starting time-steps were used; the one for the building model was two seconds and that for the system component models was 0.08 seconds (these may also be changed at the input data file).

8.3.2 Staggered Time Progress in the DERMAC Model

The above time-step size control scheme performed satisfactorily when a steady-state cooling coil model was used (as in the RKMACC model). However, when the dynamic response of the cooling and dehumidifying coil was modelled simultaneously with the building fabric components and the room air, the time-step required by the coil model was found to be less than one second, though, for the building model, experience showed that a time-step of above 100 seconds could be used. When forced to adopt the same time-step size as required by the coil model, the

computing effort became too large to be acceptable (a program execution time greater than twice the simulation time was required).

To circumvent this problem, the component models in the integrated building and system model (DERMAC) were divided into two groups. The first group (the lead-group) consisted of the building fabric component models (Wall 1 to 7) and the second group (the lag-group) consisted of the room air model and the air-conditioning system component models. The time progress in the two groups of models were "staggered" (Figure 8.3) so that different time-steps could be used in each group of components in the simulation.

In a simulation, the changes in the state of the building fabric components over a certain time interval would be predicted first, during which the room air temperature and vapour pressure would be held constant. This would stop when the lead-group time was ahead of the lag-group by more than a preset maximum duration (120 seconds was used). Following that, the response of the room air and the air-conditioning system would be predicted and in this, much smaller time-step sizes (0.8 second at maximum) would be used. This would continue until the simulated time in the lag-group models matched that reached in the lead-group models.

When the air-conditioning system was operating, the time-weighted averages of the indoor air conditions were calculated during the catch-up phase which would be used as the indoor air conditions (constants then) for the next simulation interval for the lead-group models. This enabled the heat and moisture exchanges between the building fabric components and the room air to be calculated based on a steady room air condition as the latter may have short-term fluctuations, especially when on/off control is adopted. In the period where the air-conditioning system is shut-down, the indoor conditions calculated at the end of the catch-up phase would be used.

Because the rate of response of the building fabric to a change in the indoor air condition is much slower than the response of the air to a change in the internal surface

condition of the fabric, assuming that the fabric internal surface conditions remain unchanged throughout the "catch-up" phase is unrealistic. Hence, during the catch-up phase, the internal boundary surface conditions of the building fabric components were assumed to vary between the values at the start and the end of the staggered time interval (already calculated in the lead-group simulation) following a logarithmic growth or decay curve as follows:

- i) if a variable (say the temperature (T); similar applies to the vapour pressure (P_v)) is decreasing in value during the staggered interval,

$$T(t) = T_0 e^{-a(t - t_0)} \quad (8.1)$$

where
$$a = \frac{\ln\left(\frac{T_0}{T_1}\right)}{t_1 - t_0} \quad (8.2)$$

T_0 = value of T at the beginning of the staggered interval,

T_1 = value of T at the end of the staggered interval,

t_0 = the starting time of the staggered interval,

and t_1 = the ending time of the staggered interval.

- ii) if the variable (using T again as an example) is increasing in value during the staggered interval,

$$T(t) = T_0 + (T_1 - T_0)(1 - e^{-a'(t - t_0)}) \quad (8.3)$$

where
$$a' = \frac{\ln\left(\frac{T_1}{T_0}\right)}{t_1 - t_0} \quad (8.4)$$

Using the above equations ensures that the values of the variables at the start and the end of the staggered interval remain the same. In addition, the variation of the variables within the interval is interpolated based on the response of a first order system which resembles the pattern of response of the variables at the internal surfaces of the walls and slabs observed in trial simulations before the staggered-time arrangement was used.

With this staggered arrangement, the integrated building and system model is strictly not a simultaneous simulation model. However, the model should be able to give good predictions if the lead/lag time between the two groups of models was small. When the maximum duration of the staggered interval was set at 120 seconds, there was no noticable difference between results with and without this staggered arrangement.

8.4 Outdoor Weather Input Data

A weather data file was prepared as an input data file for use with the integrated building and system model. The file was compiled from records of Hong Kong weather data supplied by the Royal Observatory of Hong Kong ⁽¹³⁾. Amongst weather data for years from 1978 to 1991, the data of 1980 were chosen for use in the major investigations because weather conditions for this year had been verified to be the most representative for the period from 1979 - 1988 ⁽¹⁶¹⁾. Because frequent access to the weather data file is required in simulating the heat and moisture transfer in buildings, the weather data file was stored in "unformatted" form. This avoided conversion of the input weather data from the text form (ASCII characters) into binary form every time weather data were read from the file.

The weather data file consisted of one year of hourly records of outdoor temperatures, relative humidities, wind speeds, wind directions and global solar radiation intensities. Outdoor temperature, relative humidity and solar radiation intensity data are the major parameters required in calculating heat and moisture transport into buildings. The wind speed and wind direction data are required in estimating the convective heat transfer coefficient (and the mass transfer coefficient through the use of the Lewis relationship) at the exposed surface of the exterior wall and window. Calculation of the convective heat transfer coefficient was based on the empirical correlations due to ASHRAE ⁽¹⁶²⁾ (see Appendix C).

In building heat transfer simulations, both the direct and the diffuse components of solar radiation are required. However, the Royal Observatory of Hong Kong ⁽¹³⁾ measures solar radiation intensities only in the form of global solar radiation (total solar radiation intensity on a horizontal surface). A method was therefore devised to decompose the global solar radiation intensity into direct and diffuse components in which the ratio of the measured global solar radiation intensity to the clear sky total horizontal intensity, and the solar altitude angle were used to estimate intensities of the two components (Appendix C).

Weather data in the input file were hourly records. In order to maintain a smooth variation in weather conditions, data between two hourly records were found by interpolation. In the integrated model, this was done by using cubic spline functions ⁽¹⁶³⁾. The spline function coefficients for each weather parameter were based on six consecutive hourly records and among them, those of the current hour and the next hour were the third and fourth records. When the simulation progressed from one hour to another, the cubic spline function coefficients would be evaluated again. However, spline function coefficients for the preceding hour would still be kept in the computer memory so that if the simulated time was brought back to the starting time of a time-step (due to the estimated error exceeding the tolerance limit) necessitating the last set of coefficients be used again, they could be retrieved.

8.5 Heat and Moisture Transport Property Data

In the integrated building and system model, the heat and moisture transfer in a porous building material can be modelled when the following transport property data are available:

- i) For moisture transfer - the sorption isotherm and the total internal void volume fraction (dry state) of the material; and
- ii) For heat transfer - the density, thermal conductivity, specific heat and surface emissivity.

However, the model was restricted in that the material must be in the pendular state, and moisture transfer by filtration flow is negligible.

At present, sorption isotherm data for five building materials, namely cement paste, cement-sand plastering, concrete, gypsum board and clay brick, are included in the database accompanying the computer models. The data for cement paste and concrete were from Harmathy ⁽⁵⁸⁾. Those for gypsum board were from Thomas & Burch ⁽⁵³⁾ and those for clay brick were from Harmathy ⁽⁵⁹⁾. Sorption isotherms for building materials that are made from a mixture of cement and aggregate materials may be determined from the sorption isotherm of the hydrated cement paste and the mixing ratio between cement and aggregates, based on the assumption that the aggregate materials are non-hygroscopic ⁽⁵⁸⁾. The data for cement-sand plastering was determined by this method. Sorption isotherm and other relevant transport property data for a large collection of building materials are available from various related literatures, e.g. Hansen ⁽⁶⁹⁾ & Kerestecioglu et al ⁽⁹⁵⁾.

Sorption isotherm data of building materials were stored in the data file in the form of a sequence of ordered pairs of equilibrium (volumetric) moisture content and relative humidity values. To facilitate interpolation of moisture content of the material, the cubic spline coefficients corresponding to each relative humidity reading were calculated and included in the data file.

Chapter Nine

Results and Discussion of Simulation Studies

9.1 Simulation Studies Performed

9.1.1 Objectives of the Simulation Studies

The coupled heat and moisture transfer in an intermittently air-conditioned room inside a building in Hong Kong was investigated by computer simulation. The objectives of the investigation are:

- i) to assess how significant the building fabric moisture sorption effect is, in conjunction with intermittent air-conditioning;
- ii) to assess the sensitivity of room humidity to infiltration rate;
- iii) to compare the effectiveness of passive humidity control of air-conditioning systems having different types of control (on/off and proportional);
- iv) to assess the effect of pre-treatment of the fresh air supply; and
- v) to contrast the predicted results between modelling the performance of the cooling and dehumidifying coil by a steady-state model and a dynamic model; and
- vi) to verify the predictive accuracy of the simulation models.

The results summarized in this chapter were obtained by using the DERMAC and RKMACC integrated building and air-conditioning system models (Chapter 8).

9.1.2 Model Room Construction and Characteristics of the Air-conditioning System

Construction of the room modelled is as shown in Figure 8.1. Dimensions of the room were 3 m (W) x 3 m (D) x 3 m (H). The enclosing walls and slabs of the room were all assumed to be constructed of a central core of 100 mm thick concrete and a 13 mm thick cement-sand plastering layer at each surface (Figure 9.1). There was a window (denoted as Wall 7) in the exterior wall (Wall 1) occupying half of the exposed area of the wall. Construction details and material properties of the walls, the slabs and the window are as summarized in Table 9.1. The room was assumed to be air-conditioned between 8:30 am to 5:00 pm, with one occupant and lighting and appliances turned on during the period from 9:00 am to 5:00 pm. The indoor conditions of the room assumed are as summarized in Table 9.2.

In the simulation studies, the external plastering layer, the concrete core and the internal plastering layer of each wall and slab were discretised respectively into 5, 15 & 5 sub-layers. This choice was a compromise between competing factors such as the accuracy of the results, the computing time and the amount of memory (random access memory (RAM)) required in a simulation. In general, with more sub-divisions, the truncation error (given rise by approximating the governing partial differential equations by finite difference equations) will be smaller. However, to achieve this, more RAM spaces and computing time will be required and, because of the larger amount of computations involved, the modelled results will be subjected to higher rounding off errors.

The air-conditioning system was assumed to be a fan-coil system (Figure 5.4). Chilled water supply to the fan-coil unit was assumed to be at a constant temperature of 7 °C. The design cooling load of the room was calculated based on ASHRAE's method (ASHRAE 1989) using Hong Kong weather data for design cooling load calculations.

The result is summarized in Table 9.3. Based on this design cooling load, a fan-coil unit of characteristics shown in Table 9.4 was chosen and all simulation studies reported here were based on this fan-coil unit.

9.1.3 Verification of the Predictive Accuracy of the Integrated Model

The model room described above has a construction and air-conditioning system similar to those of a staff office at the Hong Kong Polytechnic where indoor conditions in hot summer days in August, 1991 had been measured. Indoor conditions predicted by the integrated computer model were compared against the measured indoor conditions in order to provide some limited verification of the model predictions.

More rigorous verification was not carried out because that requires many instruments for measuring all the participating variables (e.g. temperatures and moisture contents in the walls and slabs; heat and moisture fluxes at the wall and slab surfaces; flow rates, temperatures and humidities of air in the room and the air-conditioning system; flow rates and temperatures of chilled water in the piping system; and the pressure losses across the air-conditioning system components; etc.) but, unfortunately, a complete set of such instruments was not available. Moreover, even if such instruments were available, this would require a substantial amount of time for the planning, preparation and execution of the work*. These include to properly set-up the large number of measuring instruments involved (e.g. embedding thermocouples and moisture content sensors into building walls and installing flow rate, temperature and humidity sensors in the air-conditioning system, etc.), to develop a data acquisition system for collecting the measured data, to calibrate these instruments, and to carry out measurements for a long enough period of time. Taking into account the amount of work required for developing the computer models, the measurement work was excluded from the present study.

* A research project proposal covering such measurement work has been submitted to the University and Polytechnic Grants Committee in Hong Kong (the organization responsible for funding allocations, including research funding, to Universities and Polytechnics in Hong Kong) to bid for funding support for the required instruments and manpower. The estimated total cost of the project was about HK\$ 700,000 (£58,000) and the estimated duration of the project was three years.

Nevertheless, attempts have been made to verify individual component models based on experimental data available from various sources (e.g. Thomas and Burch's experimental data ⁽⁵³⁾ for verifying the differential permeability model (Chapter 4), manufacturer's catalogue data for verifying the steady-state coil models (Chapter 7) and published dynamic coil performance data ^(149,153 & 154) for verifying the FD dynamic coil model (Chapter 7)). Also, the simple measurement taken in the Polytechnic staff office provided some data for comparison with predictions of the integrated model.

9.1.4 Cases Studied by Computer Simulation Using the Integrated Model

Three sets of simulation studies were carried out. The first was based on estimated initial moisture content distributions across the walls and slabs (as shown in Table 9.1). Results of this showed that moisture content variations inside the building walls and slabs was a long-term phenomenon (in the order of weeks) and this would significantly affect the short-term (daily) indoor air humidity (also see discussions in Section 9.2.2.2.c).

By repeating the simulation for a number of daily cycles, using the same daily profiles of weather conditions and internal loads, a steady daily pattern of moisture content distribution in the building fabric components could be obtained which could then be used as the starting point for subsequent simulation studies on responses of the building and the air-conditioning system to changes in input conditions (such as varying the infiltration rate, changing the type of control, etc.). However, this approach would require a large amount of computing time and therefore was not taken. Instead, another set of initial moisture contents was estimated, based on the trend of moisture content variations predicted in the first set of simulation studies, and another set of simulation studies was carried out based on the latter set of estimated initial conditions. Results of the latter show that the second set of estimated initial moisture contents was a good estimate in that there were no significant variations, on a daily cycle basis, in the internal moisture contents of the building fabric components (see Section 9.3).

Although the first set of simulation studies was based on a set of "inappropriate" initial moisture contents, the conclusions drawn based on some of the results would still be valid. Therefore, such results are reported in this chapter and studies on those cases were not repeated in the second set of simulation studies. These include results showing:

- i) the trend of moisture content changes inside the building fabric components (which led to the conclusion on the inappropriateness of the assumed initial moisture contents);
- ii) the differences in predictions between the RKMACC and the DERMAC models;
- iii) the indoor air conditions that would arise if moisture adsorption and desorption effect of the building fabric materials was ignored;
- iv) the effects of varying infiltration rates; and
- v) the influence of proportional control (without fresh air supply pre-treatment).

Results of the second set of simulation studies were then compared with those from the first set and further simulation studies were also carried out to investigate:

- i) the effects of pre-treating the fresh air supply to the room; and
- ii) the pull-down operation after a prolonged shut-down period.

The third set of simulation studies was based on the weather conditions corresponding to the period when measured data for the Hong Kong Polytechnic staff office were available, and the results were compared with the measured data to show the predictive accuracy of the model.

The following lists the cases studied by computer simulation with results reported in the following sections of this chapter (the case numbers shown in the list are referred to in descriptions on these studies):

1 The First Set of Simulation Studies (Figures 9.2 - 9.12)

<u>Case No.</u>	<u>Conditions</u>	<u>Simulated Period</u>
1.1	Continuously air-conditioned by a perfect air-conditioning system	0:00 1/7/80 to 8:30 4/7/80
1.2	Continuously air-conditioned by a perfect air-conditioning system	8:30 1/7/80 to 8:30 4/7/80
1.3	Intermittent air-conditioning by LMHD coil model with on/off control	8:30 4/7/80 to 17:00 5/7/80
1.4.a	Intermittent air-conditioning by FD coil model with on/off control	8:30 4/7/80 to 17:00 5/7/80
1.4.b	Intermittent air-conditioning by FD coil model with on/off control	17:00 5/7/80 to 17:00 7/7/80
1.5	Intermittent air-conditioning by LMHD coil model with on/off control and with wall moisture adsorption and desorption ignored	8:30 4/7/80 to 17:00 5/7/80
1.6	Intermittent air-conditioning by LMHD coil model with proportional control	8:30 4/7/80 to 17:00 5/7/80
1.7	Intermittent air-conditioning by LMHD coil model with proportional control, pretreated fresh air and zero infiltration	8:30 4/7/80 to 17:00 5/7/80
1.8.a	Intermittent air-conditioning by LMHD coil model with proportional control, pretreated fresh air and infiltration of 1 air-change per hour	8:30 4/7/80 to 17:00 5/7/80
1.8.b	Intermittent air-conditioning by LMHD coil model with proportional control, pretreated fresh air and infiltration of 1 air-change per hour	17:00 5/7/80 to 17:00 7/7/80

2 The Second Set of Simulation Studies (Figures 9.13 - 9.25)

<u>Case No.</u>	<u>Conditions</u>	<u>Simulated Period</u>
2.1	Intermittent air-conditioning by a perfect air-conditioning system	0:00 1/7/80 to 8:30 4/7/80
2.2.a	Intermittent air-conditioning by LMHD coil model with on/off control	8:30 4/7/80 to 8:30 6/7/80
2.2.b	Intermittent air-conditioning by LMHD coil model with on/off control	8:30 6/7/80 to 17:00 7/7/80
2.3.a	Intermittent air-conditioning by FD coil model with on/off control	8:30 4/7/80 to 8:30 6/7/80
2.3.b	Intermittent air-conditioning by FD coil model with on/off control	8:30 6/7/80 to 17:00 7/7/80
2.4	Intermittent air-conditioning by LMHD coil model with on/off control and with wall moisture adsorption and desorption ignored	8:30 4/7/80 to 17:00 7/7/80
2.5	Intermittent air-conditioning by LMHD coil model with on/off control & pretreated fresh air	8:30 4/7/80 to 17:00 5/7/80
2.6	Intermittent air-conditioning by LMHD coil model with proportional control and pretreated fresh air	8:30 4/7/80 to 17:00 5/7/80
2.7	Intermittent air-conditioning by FD coil model with no air-conditioning for a long period, followed by an air-conditioned period (with on/off control)	8:30 5/7/80 to 8:30 6/7/80, 8:30 6/7/80 to 17:00 6/7/80

3 The Third Set of Simulation Studies - Verification Tests (Figures 9.26 - 9.28)

<u>Case No.</u>	<u>Conditions</u>	<u>Simulated Period</u>
3.1	Intermittent air-conditioning by LMHD coil model with on/off control	0:00 8/8/91 to 7:30 10/8/91
3.2	Intermittent air-conditioning by LMHD coil model with on/off control	7:30 10/8/91 to 24:00 12/8/91

9.2 The First Set of Simulation Studies (Pilot Studies)

9.2.1 Initialization Runs with "Perfect" and Continuous Air-conditioning (Cases 1.1 & 1.2)

Each layer of material in the building fabric elements was initially assumed to be at a uniform temperature and moisture content as shown in Table 9.1. A better set of initial conditions for all nodal points in the building fabric was obtained by performing an initialization run to allow the fabric materials to settle at more realistic profiles of conditions which could be used as the starting conditions for subsequent simulation studies. The initialization run (Case 1.1) was performed with reference to the actual hourly weather conditions in Hong Kong ⁽¹³⁾ at 0:00 hour on 1st July, 1980 till 8:30 on 4th July, 1980 (see Chapter 8). Throughout this period, it was assumed that the indoor air conditions were maintained at the design state, i.e. the air-conditioning system was assumed to be "perfect" and able to cope exactly with the sensible and latent heat loads of the room at all times, and that the system was operated continuously. Simulation results obtained in this initialization run, including the vapour pressure, temperature and moisture content at the internal surfaces of Walls 1, 2, 5, 6 & 7; the heat and moisture gains (by the room air) from these surfaces and the total room sensible, latent and total loads from all sources; and the indoor and outdoor conditions in the simulated period, are shown in Figures 9.2.a, b & c (similar kinds of results are presented for other cases studied).

a) *Weather Conditions in the Simulated Period*

It can be seen (Figure 9.2.c) that throughout this period, the outdoor temperature varied between about 27 °C (300K, occurring at the night time) to about 33 °C (306K, in the afternoon). Solar radiation intensity on the South facing external wall of the room had a peak value of about 300 W/m². The outdoor air humidity ratio was within the range from 0.016 kg/kg to 0.024 kg/kg. These outdoor weather conditions

represent typical diurnal range of outdoor weather conditions in hot summer days in Hong Kong.

b) *Wall Internal Surfaces Conditions and Heat and Moisture Transfer to the Room Air*

Variations in the vapour pressure, temperature and moisture content at the internal surfaces of the walls and slabs and the temperature of the window during this period exhibited cyclic changes (Figure 9.2.a), as a result of the diurnal changes in outdoor weather conditions and internal loads (from occupants and lighting). Due to the much lower thermal capacity of the window glass (Wall 7), changes in its temperature (Figure 9.2.a.ii) followed closely the patterns of outdoor temperature and solar radiation (Figures 9.2.c.i & iii). Conversely, because of the substantial thermal capacity of the wall, internal surface temperature of the external wall (Wall 1) exhibited a cyclic pattern that lagged behind that of the window by about 4 hours (Figure 9.2.a.ii). Under the influence of solar radiation transmitted through the window and the internal loads, there were also cyclic changes in internal surface temperatures of the partition walls and the range of these changes was about 2 °C.

Corresponding to an initial temperature of 300 K (≈ 27 °C) and an initial moisture content of $0.06 \text{ m}^3/\text{m}^3$ in the plastering layer, the initial vapour pressure at the internal surfaces of the walls and slabs was about 1850 Pa. The vapour pressure of room air at the design condition however was around 1570 Pa. Due to this vapour pressure difference, the walls and slabs started to release moisture (Figure 9.2.b.ii) into the room air leading to a drop in moisture content at the wall surfaces (Figure 9.2.a.iii). The rate of moisture desorption gradually dropped as the vapour pressure at the wall surfaces approached that of the room air. Following the increase in wall internal surface temperatures later in the day, the vapour pressure at the wall surfaces rose and as a consequence, the rate of moisture desorption from the walls increased again and the moisture content dropped further. The total heat gain from the wall and window surfaces and the room sensible and latent loads also varied in cyclic patterns as a result

of these changes (Figure 9.2.b). For the room latent cooling load profile, the noticeable step changes were caused by the presence of the occupant (and hence a moisture source) during the occupied period (9:00 - 17:00) and the increased rates of moisture desorption from the walls and slabs.

From the time-plots of the vapour pressure and moisture content at the wall internal surfaces (Figure 9.2.a.i & iii) and of the moisture gains from the walls (Figure 9.2.b.ii), it can be seen that there was a gradual trend of reduction in these variables. To ensure that any moisture desorption from the building fabric material that would be predicted in subsequent simulation studies was not due to the use of unrealistically high initial moisture contents in the building fabric materials (i.e. insufficient pre-conditioning of the building fabric), the simulation run was repeated for two more days. (This however had been proven to be the contrary - see section 9.2.2.2.c below.) The starting time of this simulation (Case 1.2) was set at 8:30 on 1st July, 1980 whereas the conditions of the walls, slabs and the window at 8:30 on 4th July, 1980, as obtained at the end of the preceding simulation (Case 1.1), were taken as the initial conditions. Simulation results of Case 1.2 (Figures 9.3.a & b) show that the cyclic pattern of variations in the internal surface conditions of the building fabric became more steady. States of the walls, slabs and window at end of this simulation were then used as the initial conditions in subsequent simulation studies of the first set.

9.2.2 Simulation of Indoor Air Conditions Under Intermittent Air-conditioning

Simulations starting from 8:30 on 4th July, 1980 were performed to study the effects of intermittent air-conditioning. The simulated time covered an air-conditioned period, a shut-down period and another air-conditioned period. Actual weather conditions of Hong Kong, corresponding to the simulated time, were used and performance of the air-conditioning system was modelled in detail.

The two integrated models, namely RKMACC (where the cooling coil was modelled by the LMHD steady-state coil model) and DERMAC (in which the FD

dynamic coil model was adopted), were both applied so that predictions of these two models could be compared. In both cases, the air-conditioning system was assumed to be controlled by an on/off controller and the control valve was assumed to be a linear valve. An assumption was also made that the control valve would take 30 seconds to move from the fully open to the fully closed position (or vice versa) at a constant speed. The control differential (or dead-band) of the on/off controller was set at 2 °C, i.e. the on and off settings were 1 °C below and above the set-point temperature respectively.

9.2.2.1 Results Obtained by Using Model RKMACC (Case 1.3)

The variations in vapour pressure, temperature, and moisture content at the internal fabric surfaces of the room, the heat and moisture transfer to and from these surfaces, the room cooling load components and changes in the room air conditions over the period from 8:30 on 4th July, 1980 to 17:00 on 5th July, 1980, as predicted by using the RKMACC model (Case 1.3), are shown in Figures 9.4.a, b & c.

a) *The First Air-conditioned Period*

With on/off control in the air-conditioning system, the indoor air temperature was fluctuating about the set-point temperature during the air-conditioned periods (Figures 9.4.a.ii & c.i). The amplitude of fluctuation from the set-point was slightly larger than ± 1 °C because the control valve took a finite time (30 seconds) to open or close in reaction to a command from the controller for reversal of valve position. The proportion of time where the control valve would be fully open depends on the room sensible cooling load - the higher this is, the more frequent the control valve will stay open.

During times when the chilled water supply to the cooling and dehumidifying coil was stopped (and when the flow rate was less than 30% of the design flow rate while the control valve was opening or closing, see Chapter 7), the coil was unable to provide any dehumidification effect and hence, removal of moisture from the room air was intermittent. Consequently, the indoor air humidity ratio (and vapour pressure) that

the air-conditioning system was able to maintain was higher than the design level used in Cases 1.1 & 1.2 where the air-conditioning system was assumed to be "perfect" (0.0104 kg/kg c.f. 0.0098 kg/kg).

The vapour pressure in the room air (Figure 9.4.a.i) exhibited a rapid rise at the start of the simulation run. This lasted for 30 minutes of the simulation time which corresponds to the duration between the time when the air-conditioning system was started (8:30 am) and when the room was occupied and the lighting was turned-on (9:00 am). In this period, the outdoor temperature and the solar intensity were low. As a consequence, the walls and slabs continued to absorb moisture from the room air (Figure 9.4.b.ii) (see also Section 9.2.3). Later in the day, as the room sensible cooling load became larger which led to an increase in dehumidification performance of the FCU, the room air vapour pressure gradually dropped. Coupled with the effect of the increase in internal surface temperatures (Figure 9.4.a.ii), the walls and slabs started to release moisture back to the room air and thus caused a rise in the room latent cooling load (Figure 9.4.b.iii).

b) *The Shut-down Period*

When the air-conditioning system was shut-down, the indoor air temperature quickly rose and approached the outdoor temperature (Figure 9.4.c.i). This was due to the continued injection of heat into the room air due to the heat gain from the walls and window and infiltration of outdoor air. Likewise, a significant rise in the indoor humidity ratio was predicted (Figure 9.4.c.ii) but the rate of rise was much slower than the indoor temperature. The indoor humidity ratio reached at the end of the shut-down period (about 0.014 kg/kg) was still far below the outdoor level (above 0.02 kg/kg). This resulted from the moisture adsorption effect of the porous building fabric materials.

As moisture was continuously transferred into the room air due to infiltration, moisture content of the room air, and hence its vapour pressure, started to rise

immediately after the air-conditioning system was shut-down (Figure 9.4.a.i). When the indoor vapour pressure became higher than that of the moist air inside the voids of the surface layer of materials of the building fabric, moisture transfer from the room air to the building fabric was initiated which significantly slowed down the rate of rise in indoor air moisture content. The majority of the moisture transported into the room was stored within the voids inside the porous building material, giving rise to increases in moisture content at the walls and slabs (Figure 9.4.a.iii).

From the time-plot (Figure 9.4.a.iii) of the moisture content at the internal surface of the floor slab (Wall 6), it can be seen that the rate of rise in its moisture content was initially much slower than the other walls (e.g. Wall 2) and the ceiling slab (Wall 5). This was due to the different convective heat transfer coefficients adopted to evaluate heat convection from a horizontal surface to the air above it. The convection heat transfer rate in this situation is dependent on the direction of heat flow - the heat transfer coefficient for heat flow in the upward direction is higher than that for downward heat flow (4,5,162). With the moisture transfer coefficient related to the heat transfer coefficient by the Lewis relationship (equation 3.17), there was a change in heat and moisture transfer rates when the slab surface temperature changed from below to above the room air temperature. When the surface temperature became higher than that of the room air, the moisture adsorption rate increased causing an increase in moisture content of the slab to a level comparable with the ceiling slab (Wall 5) and other partition walls.

c) *The Second Air-conditioned Period*

When air-conditioning was resumed in the following day, starting from a high indoor temperature and humidity, the fan-coil unit was capable of bringing the indoor temperature back to the controllable range within 15 minutes. It however took about two hours for the indoor air humidity to be lowered to a steady level. Once the indoor air vapour pressure fell below the vapour pressure at internal surfaces of the walls and

slabs, the moisture stored within the walls and slabs during the non-air-conditioned period was released back to the room air (Figure 9.4.b.ii).

When compared with the first air-conditioned period, the rate of moisture gain by the room air from the building fabric was much higher and moisture desorption from the walls and slabs lasted throughout the air-conditioned period. This indicates that the initialization run pre-conditioned the building fabric to a moisture content that is lower than the attainable level when the air-conditioning system was intermittently operated. The moisture desorption reduced gradually to about half of the initial rate towards the end of the air-conditioned period and a corresponding drop in room latent cooling load was predicted. This simulation result clearly demonstrated that indoor air conditions would be significantly affected by the moisture capacity of the building fabric materials.

9.2.2.2 Results Obtained by Using Model DERMAC (Cases 1.4.a & b)

a) *The Simulation Results*

The above simulation study (Case 1.3) was repeated by using the DERMAC model in which the cooling and dehumidifying coil was modelled by the FD dynamic model (Case 1.4.a). The model predictions are shown in Figures 9.5.a to 9.5.c.

By comparing this set of results (Case 1.4.a) against that predicted by the RKMACC model (Case 1.3), it can be seen that although the trends of the variables predicted by both models are similar, significant differences can be identified:

- i) The indoor air humidity ratio (Figure 9.5.c.ii) and vapour pressure (Figure 9.5.a.i) in the air-conditioned periods were significantly higher (c.f. Figures 9.4.c.ii & 9.5.a.i respectively);
- ii) The moisture content at the surfaces of the walls and slabs were higher (Figure 9.5.a.iii c.f. Figure 9.4.a.iii);
- iii) The moisture adsorption by the building fabric in the first air-conditioned period was higher and the moisture desorption from the

building fabric in the second air-conditioning period was significantly lower (Figure 9.5.b.ii c.f. Figure 9.4.b.ii).

b) *Comparison of Model Predictions Between the LMHD Coil Model and the FD Dynamic Coil Model*

By using the steady-state LMHD model to simulate the performance of the cooling and dehumidifying coil, the assumption is made that cooling coil could quickly approach steady-state conditions when subjected to changes in the states and flow rates of the inlet fluids. This is unrealistic when on/off control is adopted. For instance, when the control valve is closed, the coil surface temperature will rise gradually because of the thermal capacities of the coil material and the chilled water retained within the tubes. Once the coil surface temperature rises above the dew point temperature of the air flowing across the coil, no dehumidification effect will be evident. However, the coil will continue to provide a certain rate of sensible cooling until its surface temperature approaches the on-coil air temperature. Conversely, when the control valve is opened and chilled water flow through the coil is resumed, a small time will be taken for purging the residual chilled water out of the tubes and the surface temperature of the coil will drop gradually. The on and off-periods will therefore be longer and there will be a smaller number of such cycles within a given period of time as compared to what would be predicted when a steady-state coil model is used.

Under on/off control, the cooling coil will start removing moisture from the air flowing across it after the control valve has stayed open for some time. With fewer "on-periods", the dehumidification effect predicted by the FD dynamic coil model (which should be the more realistic case) was less than that predicted by the LMHD steady-state model. Consequently, the indoor air humidity predicted was higher and the moisture desorption from the building fabric during the air-conditioned periods was lower. These explain why the predictions by the DERMAC model (Case 1.4.a) were different from those predicted by the RKMACC model (Case 1.3).

To further illustrate these phenomena, the following variables over a short duration in an air-conditioned period were modelled by using both coil models and the corresponding results were overlaid to give a clear comparison between them:

- i) The indoor air temperature and humidity ratio (Figure 9.5.d.i);
- ii) the supply air temperature (Figure 9.5.d.ii) and humidity ratio (Figure 9.5.d.iii);
- iii) the sensible cooling effect (Figure 9.5.d.iv), latent cooling effect (Figure 9.5.d.v) and the total cooling effect (Figure 9.5.d.vi) provided by the coil.

The results clearly show that for the case modelled, the duration of an on/off cycle predicted using the FD dynamic coil model was about 5 minutes but that predicted by using the LMHD steady-state coil model was only about 3.5 minutes (Figure 9.5.d.i). The other distinctive difference between the predictions of the two models was that the sensible cooling effect of the coil as modelled by the FD model did not drop to zero during the off-periods (Figure 9.5.d.iv). This confirmed that the thermal capacitance of the coil maintained a small amount of sensible cooling during the off-periods (and this lengthened the duration of the off-periods). Due to the fewer number of on-periods and the time required for the coil surface temperature to drop during the on-periods, the latent cooling effect of the coil as predicted by the FD coil model was less than that by the LMHD coil model (Figure 9.5.d.v). Consequently, the indoor humidity ratio predicted by the FD model was higher.

Results of the simulation studies clearly show that when on/off control is adopted, the dynamic response of the cooling and dehumidifying coil could significantly affect the performance of an air-conditioning system, particularly in the passive control of indoor humidity. Therefore, when computer modelling is used to assess the performance of the air-conditioning system, the dynamic performance of the

cooling and dehumidifying coil should be modelled in detail. A quasi-steady model could bring about optimistic results which might not be achievable in reality.

c) *Moisture Content in the Walls and Slabs*

It can be seen from the simulation results of Cases 1.3 and 1.4.a (Figures 9.4.b.ii & 9.5.b.ii) that more moisture was adsorbed than released by the walls and slabs over a cycle of air-conditioned and non-air-conditioned periods. Results of a further simulation run (Case 1.4.b) for two more days, by using the DERMAC model, showed that whilst the rate of moisture adsorption during the shut-down period remained approximately the same, the rate of moisture desorption from the building fabric during the air-conditioned periods became much higher and lasted throughout the air-conditioned period (Figure 9.6.b.ii c.f. Figure 9.5.b.ii). Nevertheless, the total amount of moisture adsorbed in the shut-down period was still larger than that released by the building fabric during the air-conditioned period. This implied that there was a net gain of moisture by the building fabric from the room air which should cause an increase in the total moisture content in the walls and slabs of the room.

The predicted moisture content variations at selected nodal positions in Wall 1 and Wall 2 (Figures 9.7.a to d, based on results of Cases 1.4.a & b) indeed showed that there was a significant increasing trend in moisture content at the interior nodes of these walls throughout the simulated period. In each daily moisture adsorption and desorption cycle, there was a net gain of moisture in the building fabric. The net moisture gain at the internal boundary surfaces were transferred towards the inner regions of the walls and slabs. The time required for the moisture content of the walls and slabs to attain steady-state conditions (on a daily cycle basis) could be several weeks. This showed that the indoor air conditions predicted in the short-term simulation run (for several days of simulated time only) might not represent the situations in the room when it was subjected to repeated daily cycles of outdoor weather conditions unless the simulation run is continued for a much longer period of time. Alternatively, the initial moisture contents of the building materials used in the

simulation should be adjusted to correspond to the likely steady levels (as done in the second set of simulation studies).

9.2.3 The Case With Moisture Adsorption and Desorption at the Building Fabric Ignored (Case 1.5)

The simulation results described in the preceding sub-sections showed that, under intermittent air-conditioning, and with the moisture transfer in the porous building fabric materials properly modelled, the building fabric acted as a storage site for moisture. During the non-air-conditioned period, the moisture transported into the room by infiltration was stored within the building materials and was released back to the room air when air-conditioning was resumed. The significance of the moisture adsorption and desorption (MAD) effects of the building fabric can be more clearly seen by comparing the predicted indoor air conditions obtained in the preceding simulation studies with that from a further simulation in which moisture transfer in the building fabric is ignored.

Although the dehumidification capacity of the cooling coil will vary with the room sensible and latent loads, when the air-conditioning system is operating, the difference between the predicted indoor air humidities in the two simulations (one with and the other without the MAD effect modelled) will be small, when compared with that in the non-air-conditioned period. In the latter period, whether the dynamic characteristics of the cooling coil are accounted for in the model will have no significant impact on the simulation results. The RKMACC model, which is a simpler model, therefore was chosen as the basis and was modified into a model with the MAD effects ignored. Predictions of the simulation study (Case 1.5), obtained by using the modified version of the RKMACC model (referred to as model HTRKM), are as shown in Figures 9.8.a to 9.8.c.

In the absence of the moisture capacity of the building fabric, the indoor humidity ratio that could be maintained (Figure 9.8.c.ii) was slightly lower than those predicted in the preceding simulation studies (c.f. Figures 9.4.c.ii & 9.6.c.ii). During

the non-air-conditioned period, the indoor humidity ratio reached the outdoor level about five hours after the air-conditioning system had been shut-down (Figure 9.8.c.ii). This observation however did not agree with the measured results (see Section 9.4) and shows that moisture adsorption and desorption effect of the building fabric materials should not be neglected in modelling thermal response of buildings and systems when the air-conditioning system is intermittently operated.

9.2.4 Effects of Using Proportional Control and Equal Percentage Control Valve (Case 1.6)

The simulation studies described in the foregoing sub-sections were based on the use of an on/off controller (and a linear control valve) in the air-conditioning system. This is a common choice in buildings where fan-coil units (FCUs) with electric valve actuators are employed. However, in large buildings where central air-handling units (each serving a large zone in the building) and pneumatic control are adopted (in which compressed air is used to provide the power for driving the control valve), proportional control is a common choice.

Under on/off control, a coil surface temperature that is low enough to provide dehumidification can be maintained when the valve is fully open and this could still occur when the room sensible cooling load is low, although, under such a condition, the "on-period" will last for a shorter period of time (see also Section 9.2.2.2.b). With proportional control, the chilled water flow rate will be regulated according to the room temperature and will only be a fraction of the design flow rate as the room sensible load is reduced. When there is a large reduction in chilled water flow rate (to less than 30% of the design flow rate), dehumidification effect may not be available until the dew point temperature of the on-coil air subsequently rises above the coil surface temperature. This will occur when there is a reduction in dehumidification effect of the cooling coil leading to a rise in humidity in the room air and consequently in the on-coil air (see Section 1.3 and Figure 1.3).

In order to demonstrate this phenomenon and to contrast the passive humidity control performance of air-conditioning systems using proportional control and on/off control, a simulation study was carried out (Case 1.6) in which the FCU in the model room was assumed to be equipped with a proportional controller and an equal percentage valve (notwithstanding that the use of proportional control for FCUs is uncommon in Hong Kong). Other than for the control system, this simulation study was based on the same set of conditions used before. With this type of control, there would not be rapid fluctuations in chilled water flow rate and in indoor air conditions. Hence, the RKMACC model was employed which should provide similar results as the DERMAC model (confirmed by comparing the results from both models for a short-term simulation) but requiring much less computing effort.

Results of this simulation (Case 1.6) are shown in Figures 9.9.a to 9.9.c. Here, the indoor temperature became very steady but the indoor air humidity ratio during the air-conditioned period was predicted to be about 0.013 kg/kg (corresponding to a relative humidity of 64%) (Figure 9.9.c.ii). This was about 10% higher (approximately 10% higher in relative humidity) than that when on/off control was adopted (c.f. results in Case 1.4.a as shown in Figure 9.5.c.ii). The indoor air humidity ratios reached at the end of the shut-down period were similar in both cases.

From these results, it can be seen that a rise in indoor humidity ratio followed the initial drop at the start of the second air-conditioned period during which there was no occupant in the room nor a significant rate of moisture desorption from the building fabric (Figure 9.9.c.ii). In this period, moisture adsorption by the building fabric following the initial desorption was actually predicted (Figure 9.9.b.ii). This arose because untreated outdoor air was drawn into the system and mixed with the return air from the room before it was cooled and dehumidified by the cooling coil at the FCU. Within the first thirty minutes of the air-conditioned period (8:30 - 9:00), the room sensible load was low which, coupled with the use of proportional control, led to a low chilled water flow rate at the coil. Consequently, the supply air from the FCU actually

added moisture into the room air instead of removing moisture from the room. This can be avoided in practice by pre-treating the fresh air supply to the room by an independent fresh air handling unit which will supply pretreated fresh air to a large number of air-handling units and/or fan-coil units in the same building.

The response of the indoor air to intermittent air-conditioning with pretreated fresh air supply and proportional control was studied by computer simulation. However, since the assumed initial moisture contents within the building fabric components had been found to be inappropriate, this study was repeated in the second set of simulation studies and the results are described in section 9.3.3.

9.2.5 The Cases with No Infiltration (Case 1.7) and Doubled Infiltration Rates (Cases 1.8.a & b)

Except in the first half hour, simulation results summarized above indicate that the air-conditioning system was capable of removing moisture gains from all sources including occupants, infiltration, fresh air intake for ventilation and moisture desorption from the building fabric throughout the air-conditioned period. The phenomenon of moisture storage within the building fabric, as confirmed by the previous simulations, arose because there was infiltration during the non-air-conditioned periods. To verify the significance of infiltration on the moisture storage effect of the building fabric, simulation studies were carried out in which the infiltration rate was suppressed to zero (in Case 1.7; results shown in Figures 9.10.a to c) and increased from half air-change per hour to one air-change per hour (in Cases 1.8.a & b; results shown in Figures 9.11.a to c & 9.12.a to c). Fresh air supply was assumed to be pretreated (to a condition described in section 9.3.3) and proportional control was adopted.

When infiltration was assumed to be absent, the major source of room latent load was that from the occupant. The indoor temperature again rose to the outdoor level after the air-conditioning system was shut down (Figure 9.10.c.i). The indoor air humidity however stayed almost at a constant level (Figure 9.10.c.ii), much lower than in previous cases, and there was very little moisture exchange between the room

surfaces and the room air throughout the air-conditioned and shut-down periods (Figure 9.10.b.ii).

With the infiltration rate increased to one air-change per hour, the moisture adsorption and desorption effects became more significant (Figure 9.12.b.ii). The rate of moisture adsorption, which took place during the shut-down period, was much higher, and the indoor air humidity ratio increased to above 0.016 kg/kg at the end of the shut-down period (Figure 9.12.c.ii). (This would have approached even higher levels, as the moisture contents of the walls and slabs should have been higher than those predicted in this simulation, which were based on a set of under-estimated initial values).

9.3 The Second Set of Simulation Studies

From the results of the first set of simulation studies, more appropriate initial moisture contents in the walls and slabs for hot and humid summer days were identified. These are summarized below (with assumed values for the first set of simulation shown in brackets):

For the exterior wall (Wall 1),

External plastering layer:	0.063 m ³ /m ³	(0.07 m ³ /m ³)
Concrete core:	0.063 m ³ /m ³	(0.06 m ³ /m ³)
Internal plastering layer:	0.058 m ³ /m ³	(0.06 m ³ /m ³)

For other internal partition walls and the ceiling and floor slabs (Wall 2 to 6),

External plastering layer:	0.058 m ³ /m ³	(0.06 m ³ /m ³)
Concrete core:	0.063 m ³ /m ³	(0.06 m ³ /m ³)
Internal plastering layer:	0.058 m ³ /m ³	(0.06 m ³ /m ³)

Although the change made to the moisture content in the concrete core of the walls and slabs was only 5%, there were significant differences in the predicted rate of moisture exchange between the building fabric and the indoor air as can be seen in the

following. These findings under-line the sensitivity of simulation results obtained to initial conditions used.

9.3.1 The Initialization Run (Case 2.1)

Based on the above initial moisture content (and other conditions as shown in Table 9.1), an initialization run (Case 2.1) was performed to allow a proper distribution of conditions across the walls and slabs be attained as starting conditions for further simulation studies. In this, a "perfect" air-conditioning system was again assumed but the indoor air relative humidity was assumed to be at 0.0118 kg/kg (corresponding to a relative humidity of about 60%), which was approximately the indoor condition that the air-conditioning system was able to maintain (see Figure 9.5.c.ii). Also, instead of continuous air-conditioning (as assumed in the initialization run for the first set of simulation studies), the air-conditioning system was intermittently operated so that the building fabric will not be pre-conditioned to a moisture content that is lower than the attainable level when air-conditioning is intermittent. The initialization run covered the period from 0:00 1/7/80 to 8:30 4/7/80 and the results are summarized in Figures 9.13 to 9.15.

From this set of results, it can be seen that the diurnal moisture content variation in the exterior wall (Wall 1) became rather steady (Figure 9.15.b). Although there was still a small increase in moisture accumulation in the internal partition walls (e.g. Wall 2 as shown in Figure 9.15.a), much more steady daily patterns of indoor conditions (Figure 9.13.c) and conditions across the walls and slabs (Figure 9.15) were attained in the last two days in the simulation. The moisture desorption from the walls and slabs (Figure 9.13.b.ii) became much more significant due to their reduced storage capacity resulting from the increased internal moisture content. The indoor air humidity ratio reached in the shut-down period (Figure 9.13.c.ii) now became slightly higher (≈ 0.015 kg/kg).

9.3.2 Intermittent Air-conditioning with On/Off Control (Cases 2.2 & 2.3)

a) *Comparison with Results Obtained in the First Set*

Continuing from the end of the modified initialization run, simulation of the heat and moisture transfer in the room was once again carried out taking into account the performance of the air-conditioning system. The case with on/off control for the period 8:30 on 4/7/80 until 17:00 7/7/80 was studied by using both the RKMACC (Cases 2.2.a & b) and DERMAC models (Cases 2.3.a & b). The results are shown in Figures 9.16 to 9.21.

In both sets of results, the rates of moisture adsorption by the building fabric materials during the shut-down period were similar to those predicted in the first set of simulations but moisture desorption from the building fabric was much higher. The total room latent load during the pull-down period (from the time the air-conditioning system was turned-on to the time the occupant entered the room) was about twice as much as compared to the latent load due to infiltration only. The results predicted by the DERMAC model (with the coil modelled by the FD dynamic model) (Figures 9.19 & 9.20) again showed the less effective dehumidification effect of the coil when its dynamic response was modelled. The indoor humidity ratio during the air-conditioned period as predicted by the RKMACC model (Figure 9.17.c.ii) was about 0.0108 kg/kg (corresponding to 54% in RH) and that by the DERMAC model (Figure 9.20.c.ii) was about 0.0118 kg/kg (corresponding to 59% in RH) which are similar to those values predicted in the first set of studies. No significant rise in internal moisture content in the walls and slabs was predicted by the RKMACC model (Figures 9.18.a & b) whereas there was a small increase in moisture content in the internal partition walls predicted by the DERMAC model (Figures 9.21.b).

b) *Comparison with the Case with Building Moisture Adsorption and Desorption Effect Ignored (Case 2.4)*

The indoor air conditions and the room cooling load when moisture adsorption and desorption effects of the building fabric materials were ignored were simulated

based on the adjusted initial moisture contents in the building fabric. No significant differences between this set of results and earlier results (Section 9.2.3) can be observed.

To show the effects of building fabric moisture adsorption and desorption on the room cooling loads, the new set of results had been plotted together with results predicted by the RKMACC model (Case 2.2.a) for comparison (Figures 9.22.a to d). It can be seen that there were few differences in the predicted indoor air temperature and room sensible load (Figures 9.22.a & c) between the two sets of results. However, a lower indoor air humidity was maintained by the air-conditioning system during the air-conditioned period (Figure 9.22.b). More importantly, this comparison shows that, for the case studied, the room latent load predicted, taking into account the moisture desorption from the building fabric, was about twice as much, compared with the case when such effect is ignored (Figure 9.22.d).

9.3.3 The Cases with Pretreated Fresh Air (Cases 2.5 & 2.6)

To show the effects of pre-treating the fresh air supply to the fan-coil unit (FCU), simulation studies (Cases 2.5 & 2.6) were performed (using the RKMACC model) in which the fresh air was assumed to be pre-treated from the outdoor air condition to a constant temperature and humidity ratio of 16.5 °C and 0.012 kg/kg respectively, by an independent fresh air handling unit before being supplied to the return plenum of the FCU. With this, additional moisture that would be introduced into the room by the fresh air supply would be minimal even when the chilled water supply to the cooling coil was off.

a) *On/Off Control (Case 2.5)*

Simulation results for the period from 8:30 4/7/80 to 17:00 5/7/80, with the air-conditioning system controlled by an on/off controller (Case 2.5), are shown in Figures 9.23.a to c. Comparing this set of results against that without pretreated fresh air (Figures 9.16.a to c), it can be seen that when the fresh air supply is pre-treated, the

air-conditioning system became slightly more effective in dehumidification control as evidenced by the lower indoor air humidity ratio (0.01 kg/kg or 50% RH c.f. 0.0108 kg/kg or 54% RH in Case 2.2 when fresh air was not pre-treated) during the air-conditioning period. As a result, the rate of moisture desorption from the walls and slabs was slightly higher. The overall effect however was not significant. The apparent improvement in stability of indoor temperature (Figures 9.16.a.ii & 9.16.c.i) was due to the overlapped interval of data output and the periodic changes due to the use of on/off control as evidenced by the enlarged time-plot for a shorter interval (Figure 9.23.c).

b) *Proportional Control (Case 2.6)*

Results of simulations (from 8:30 4/7/80 to 17:00 7/7/80) with proportional control (Case 2.6) are shown in Figures 9.24.a to c. In this case, as the fresh air was pre-treated which therefore would not add moisture into the room, a sudden rise in indoor air humidity following the initial drop in the start-up period (Section 9.2.4) was absent. With proportional control, the indoor air humidity ratio that the air-conditioning system was able to maintain increased to 0.0124 kg/kg (an indoor relative humidity (RH) of about 61%) as compared to 0.01 kg/kg (50% RH) in Case 2.5 where on/off control was adopted and fresh air was also pre-treated (Figure 9.24.c.ii c.f. Figure 9.23.c.ii).

9.3.4 The Case of Air-conditioning Following A Prolonged Shut Down Period (Case 2.7)

The foregoing simulation studies showed how significantly indoor air humidity would be affected by moisture adsorption and desorption behaviour of the building fabric when the air-conditioning system was operated in the day time and shut-down in the evening. Over a weekend, the air-conditioning system of a building would not normally be operated throughout the day and hence greater moisture storage within the building fabric will occur. Consequently, a larger dehumidification load would be

imposed on the air-conditioning system when air-conditioning was resumed on the following Monday morning.

To investigate this case (Case 2.7), a simulation run was performed using the DERMAC model. In order that the air-conditioning system model would not be "called-upon" during the "normal" air-conditioned hours (so that the case would correspond to no air-conditioning), the data of starting and ending time of the air-conditioned period in the input data file were set to numerical values that were greater than 24 (hence impossible to occur in the simulation). In this study, the simulated time started from 8:30 on 5th July, 1980 which corresponded to the end of the first shut-down period in Case 2.2.a (described in Section 9.3.2.a). The simulation results at the corresponding time obtained in the latter were adopted as the starting conditions for this simulation run. The simulated time covered one day and one more evening and was then extended to the next air-conditioned period (with the input air-conditioned hours data re-set to the normal values) so that pull-down operation after a long shut-down period could be studied. Results of this simulation study are shown in Figures 9.25.a to c.

Without air-conditioning during the day time, the indoor temperature and humidity ratio continued to rise (Figure 9.25.c). The indoor temperature followed the increasing trend of the outdoor temperature during the day and, due to the thermal capacity of the building fabric and the drop in outdoor temperature in the following evening, the indoor temperature became higher than the outdoor temperature during the evening period. As a consequence, there was heat loss through the window (which had a smaller thermal capacity than the walls and slabs, see Figure 9.25.b). Because of the continued infiltration of hot and humid outdoor air into the room, the humidity ratio and vapour pressure of the room air rose further. Although there were also significant increases in vapour pressure at the internal surfaces of the walls and slabs (resulted from the increase in their temperatures, Figure 9.25.a & c), these were surpassed by the indoor air vapour pressure and hence there was moisture adsorption by the walls and slabs from the room air (Figure 9.25.b). The rate of moisture adsorption during the

evening was, however, slightly lower than that in the preceding evening (c.f. Figure 9.19.b.ii).

When air-conditioning was resumed in the following day, the rate of moisture desorption from the walls and slabs was approximately doubled, and the room latent cooling load during the first several hours of the air-conditioned period was about 1.5 times that when only one evening of shut-down period occurred (Figure 9.25.b.ii c.f. Figure 9.19.b.ii). The rate of moisture release gradually declined towards the end of the air-conditioned period showing that the extra moisture stored within the walls and slabs during the prolonged shut-down period could be extracted and removed by the air-conditioning system. If the shut-down period was longer (e.g. over a long holiday), it might take more than one air-conditioned period to remove the moisture stored inside the building fabric.

9.4 Observations from Results of the Simulation Studies

The following summarizes the observations made from the simulation study results:

- i) The porous building fabric materials can exchange moisture with the indoor air and, thus, significantly affect the indoor air condition when the air-conditioning system is intermittently operated.
- ii) The moisture adsorption and desorption effects are significant when there are sources of moisture, such as infiltration during the shut-down period.
- iii) Under part-load conditions, on/off control is more efficient in maintaining a low indoor air humidity ratio when compared with proportional control.
- iv) To properly model the performance of the air-conditioning system when on/off control is adopted, the dynamic response of the cooling and dehumidifying coil should be modelled in detail. A steady-state coil

model may give optimistic dehumidification performance which could not be achieved in reality.

- v) When proportional control is adopted, the fresh air supply should be pre-treated to avoid the addition of moisture into the air-conditioned space during times when the room sensible load is low (such as during the pull-down period at the start of an air-conditioned period when internal loads are absent).
- vi) The rate of moisture adsorption and desorption and its effect on the indoor air humidity is dependent on the moisture content of the building fabric materials. Although the moisture content of the fabric at the internal boundary surface can change with the daily cycle of indoor air conditions, the total moisture content in the walls and slabs would take a long time to settle down to a steady distribution pattern. This adjustment period might be in the order of weeks for a change of a few percent in the moisture content of the building fabric. Prior to this, the building fabric would continue to act as a sink or source of moisture for the indoor air. Therefore, when there is a sudden change in weather conditions or a change in the operation of the air-conditioning system (e.g. a long shut-down period), this long term moisture storage effect can influence the indoor air humidity during subsequent days.

9.5 Verification of Model Predictions

The simulation results summarized in the foregoing sections demonstrated that the integrated building and system computer models were able to predict the heat and moisture transport phenomena in an intermittently air-conditioned room inside a building constructed of porous building materials (concrete and cement-sand plastering) and subjected to hot and humid weather conditions. The results were, in essence, theoretical predictions but some of the leading results were found to conform to observations made in buildings of similar constructions and usage conditions. In

verifying this, the indoor air conditions in a Hong Kong Polytechnic office room were measured, and these measurements were compared with predictions by the computer models. This comparison however can only be regarded as an illustration of the modelling performance of the computer models rather than a validation of their accuracy, because the room was not equipped with adequate and sufficient measuring instruments to enable accurate and detailed measurements of the heat and moisture transfer at the building fabric and the operating conditions of the air-conditioning system. Moreover, because of the limitations in the present version of the models, they are not able to account for complicated and varied situations that would exist in real buildings. These include the use of various wall, slab and ceiling finishes (e.g. paints, wall paper, carpet, ceiling tiles, etc.), presence of furniture and other hygroscopic materials inside a building (e.g. paper, and other fibrous materials), and disturbances to the operating conditions of the air-conditioning system (e.g. changes in chilled water supply temperature and pressure).

9.5.1 Conditions of the Measurement

The period during which measurements were taken in the Hong Kong Polytechnic staff office covered the 8th August, 1991 (Thursday) to 12th August, 1991 (Monday) and included two normal working days; a weekend and the first working day after the weekend. Throughout the measurement period, there was no occupant in the room. Lighting in the room was turned on at 9:00 and switched off at 17:00 in the normal working days. On the Saturday (10th August, 1991), it was switched on at 9:00 but switched off at 13:00. The lighting remained off on Sunday (11th August, 1991) for the whole day. The air-conditioned hours in these days were:

On 8-8-91 (Thursday), from 7:30 to 17:00

On 9-8-91 (Friday), form 7:30 to 19:00

On 10-8-91 (Saturday), from 7:30 to 13:00

On 11-8-91 (Sunday), no air-conditioning for the whole day

On 12-8-91 (Monday), from 7:30 to 19:00

Throughout the measurement period, the thermostat in the room was set to the minimum level. There were two reasons for this:

- i) There was no temperature scale for the set-point adjustment and it was not possible to set the control differential at the thermostat in the room. Due to the slow response of the temperature and humidity recorder (and the large sampling interval used), it was not possible to record in detail the cyclic variations of the indoor air conditions so as to allow determination of these variables in relation to the data obtained. With the thermostat set to the minimum level, the chilled water control valve would be kept at the fully open position whenever the fan-coil unit was switched on (centrally by a timer-switch). Hence, errors due to improperly chosen control parameters could be avoided by setting correspondingly a low set-point temperature in the air-conditioning system model.
- ii) With a lowered indoor temperature, higher rates of heat and moisture exchange between the room air and the building fabric would take place. This would cause a larger change in indoor conditions which would be more easily measurable to a higher accuracy.

9.5.2 Comparison of Model Predictions with Measured Results

Although the air-conditioning system was installed with an on/off controller, because of the low indoor temperature set-point used, the control valve was at the fully opened position for most of the time. Without frequent changes in the chilled water flow rate through the coil of the FCU, a steady-state coil model should be adequate for modelling its performance and, with this model, less computing time would be required when compared with using the finite difference dynamic coil model. Therefore, the RKMACC model was applied to simulate the heat and moisture transfer in the room. Actual weather data corresponding to the measurement period, obtained from the Royal Observatory of Hong Kong ⁽¹³⁾, were used in the simulation. The indoor air set-point

temperature was set at 19 °C in the model (based on observations of the measured data). The simulated results are shown in Figures 9.26 & 9.27 and comparison of the model predictions against the measured indoor conditions are shown in Figures 9.28.a & b.

The predicted results were similar to those found in the simulation studies described in the foregoing sections. However, instead of fluctuating rapidly about the set-point, the indoor air temperature predicted was very steady over a large portion of the air-conditioned period (Figures 9.26.c.i and 9.27.c.i). This was due to the low indoor air set-point temperature used which gave rise to a large room cooling load during the day time and accordingly, the control valve remained at the fully open position except in the early morning and towards the evening. For the same reason, the predicted moisture desorption and adsorption rates at the building fabric surfaces during the air-conditioned and non-air-conditioned periods were both higher than those in the cases studied previously.

As can be seen from Figures 9.28 a & b, although the model predictions and the measured data are in good agreement in respect of the trend of the variables, there are deviations between them. During the air-conditioned periods, the model underestimated the humidity ratio of the room air. During the non-air-conditioned periods, the model over-estimated the indoor temperature but gave a reasonable estimate of the indoor air humidity ratio (except in the first several hours in this period). The following are believed to be the major reasons for the deviations between the model predictions and the measured data:

- i) The room was actually carpeted and there was a false ceiling made of acoustic tiles and a wooden door. In addition, there were furniture, books and paper in the room. These are hygroscopic materials having both thermal and moisture capacities and are capable of absorbing and desorbing heat and moisture from/to the room air. The effects of these however were neglected in the model.

- ii) There was direct solar radiation transmitted through the window and incident upon the surfaces of the building fabric, the furniture and other materials in the room. In the model, the total amount of solar radiation transmitted through the window was assumed to be diffuse radiation (Chapter 4) and would be distributed onto other fabric surfaces according to the shape factors for radiant energy exchange amongst gray surfaces.
- iii) Air brought into the room due to infiltration was assumed in the model to be at a constant rate (0.5 air-change per hour) and at the outdoor air conditions. In reality, the infiltration rate was unsteady (not measured) and the condition of the air infiltrated into the room was unknown.
- iv) The measurements were taken at one location only but there could be considerable variations in the temperature and humidity at different locations in the room. In the model, such variations cannot be accounted for, as the room air model is a lumped parameter model based on the assumption that the room air is perfectly mixed.

Nevertheless, the comparison provided an illustration that the general pattern of variations in the indoor air conditions in the room as predicted by the model was in agreement with the measured results.

Chapter Ten

Conclusions and Recommended Further Work

In this study, a method was developed for dynamic modelling of the coupled heat and moisture transfer in porous fabric materials of buildings, with particular reference to typical buildings in Hong Kong (i.e. concrete buildings subjected to humid sub-tropical climate and intermittently air-conditioned). The method is in the form of a mathematical model and has been developed into a computer simulation program for predicting heat and moisture transfer in such buildings. Air-conditioning system component models were developed and integrated with the building fabric model. An efficient numerical technique (the self-implicit scheme plus the Runge-Kutta-Merson method) was employed to solve the set of non-linear differential equations involved. The integrated models (the RKMACC and DERMAC models, Chapter 8) were applied to investigate how the indoor environmental conditions, particularly the indoor air humidity, would be affected when moisture adsorption and desorption at the building fabric surfaces were taken into account, together with the influence of the air-conditioning system.

Computer simulation studies were undertaken to reveal the significance of building fabric moisture adsorption and desorption effects when the air-conditioning system was intermittently operated, when infiltration rate was varied, when on/off or proportional control was adopted, when the air-conditioning system was shut-down for a long period of time, and when the cooling and dehumidifying coil in the air-

conditioning system was modelled by a steady-state and a dynamic model. The studies were carried out with reference to a room at the perimeter side of a building which was influenced by the outdoor weather. The methodologies developed for studying indoor moisture transient variations represent significant improvements to those published in the relevant literature and the breadth and depth of the investigations forming this work represent substantially new work.

10.1 Modelling Coupled Heat and Moisture Transfer in Porous Building Materials

Among various methods developed by others for modelling coupled heat and moisture transfer through porous materials (Chapter 2), some are too simplistic to properly account for the transport phenomena that take place in buildings (e.g. 1,2,6,10); some are too complicated for practical applications (e.g. 63,94); and some others are restricted in their applications due to the lack of appropriate moisture transport property data (e.g. 55,95).

Because different porous materials will react differently, and the moisture sorption behaviour of the same material will also vary with different ranges of conditions, there is yet no single theory that is universally applicable to a wide range of porous materials under all possible ranges of conditions. Any method devised to model coupled heat and moisture transfer in porous materials inevitably will be restricted in applications only to a certain range of porous materials and conditions. In this study, attention was focused on the heat and moisture transfer in those porous media that would stay in the pendular stage under the normal range of weather conditions. This should essentially be the case for a material that has a large specific internal pore surface (a large amount of pores with extremely small sizes), and when the material is subjected to a temperature gradient. Concrete and cement products, which are the most common building materials adopted in Hong Kong, are examples of this kind of porous material. In the pendular state, moisture transfer inside this kind of material is dominated by vapour diffusion but evaporation and condensation of the liquid and vapour phases of

water takes place within the capillary pores of the material. In addition, the local liquid moisture content affects the rate of moisture transfer.

To model coupled heat and moisture transfer in such materials, the water vapour pressure inside the pores of the material can be regarded as the driving potential for moisture transfer, with differential permeability taken as the moisture transport property of the material (Chapter 4). The differential permeability of a material varies with its liquid moisture content. In addition, vapour diffusion, evaporation and condensation, and the effect of temperature on the water vapour pressure and liquid and vapour moisture balance in the material must be taken into account in the model. However, moisture transfer by filtration flow, driven by a gradient of total gas pressure (i.e. the total of the partial pressures of the dry air and the water vapour) within the voids of the material, was found to be negligible in the cases of drying of slabs of concrete and cement paste over wide ranges of moisture content and temperature (Chapter 3). Therefore, this mode of moisture transfer can be neglected.

A model making such assumptions have been developed (Chapter 4). In deriving this model, local thermodynamic equilibrium was assumed to hold and, it was assumed that the balance of liquid and vapour moisture content inside localized regions of the porous material would obey the (average) sorption isotherm of the material. Hysteresis in moisture sorption behaviour was ignored. The coupling between heat transfer and moisture transfer, and variations in the thermal conductivity with moisture content of the material, were duly accounted for. In addition, an approximate expression for evaluating differential permeability was incorporated into the model. This expression was derived by relating the adopted moisture flux equation to the rigorous moisture flux expression used by Huang ^(50,51), but with the filtration flow component in the latter ignored (Chapter 4).

The model developed is relatively simple (involving only two partial differential equations) but has been shown to be able to provide predictions that were in good agreement with the experimental results of drying of a piece of gypsum board ⁽⁵³⁾

(Chapter 4). Predictions of this model have also been compared with those of Huang⁽⁵⁰⁾, from a more elaborate model, and good agreement between the two set of results were found (Chapter 4). When compared with other similar models (e.g. 8,121,124), fewer (and more readily available) moisture transport property data of materials are required by the model developed in this work (the data required being the sorption isotherm and the dry-state void volume fraction). In addition, moisture transfer through porous building materials can be modelled with much less computational effort (this was further enhanced by the efficient numerical method adopted). This made possible the analysis of the complicated effects of building fabric moisture adsorption and desorption and intermittent air-conditioning on indoor environmental conditions.

10.2 Modelling Performance of Air-conditioning Systems

The performance of an air-handling system, particularly that of the cooling and dehumidifying coil in an air-handling equipment, has a dominant effect on the indoor humidity that can be maintained in a building. Therefore, detailed performance modelling methods for cooling and dehumidifying coils have been studied in this work. Two coil models have been developed in this work; the first one is a steady-state model based on the log-mean enthalpy difference (LMHD) method (hence called the LMHD model - Appendix B), and the second one is a dynamic model based on three coupled partial differential equations derived from fundamental principles of heat and mass transfer (Chapter 6). In the latter model, the finite difference method was used to solve the governing differential equations (hence called the FD model). In addition, a steady-state version of the FD model has also been developed (Chapter 6). The differences between modelling the performance of a coil, with and without its dynamic characteristics taken into account, have been compared by using these models.

In both the LMHD and the FD models, McQuiston's^(143,144) correlations are used to evaluate the fin-side heat and mass transfer coefficients. The effect of contact resistance, due to imperfect bonding between the fin collars and the coil tubes, has been accounted for in these correlations. However, these correlations are applicable to coils

with flat fins only, whereas, coils with corrugated fins are more common in air-conditioning applications. When the models are applied to simulate coils with corrugated fins, the coefficients evaluated using McQuiston's correlations have to be corrected and, in both the LMHD and the FD models, the empirical correlations due to Beecher and Fagan ⁽¹⁴¹⁾ are used for this purpose.

Since Beecher's Fagan's (B&F's) correlations were derived from experiments on dry surfaces only ⁽¹⁴¹⁾, whether they can be applied to accurately model a cooling and dehumidifying coil was studied by comparing the model predictions against performance data of coils with corrugated fins available from manufacturers' catalogues (Chapter 7). It was found that B&F's correlations should be applied to correct the sensible heat transfer coefficient only, whereas, the latent cooling capacity of the coil would be over-estimated if B&F's correlations were also applied to correct the total heat transfer coefficient. With B&F's correlations applied to sensible heat transfer only, the LMHD model and the steady-state version of the FD model have been verified to be capable of predicting the steady-state performance of a wide range of cooling and dehumidifying coils to an acceptable degree of accuracy, when compared with the manufacturers' data (Chapter 7). Dynamic coil performance predicted by the FD dynamic coil model has also been found to be in good agreement with experimental data available from literature (Chapter 7).

In modelling the part-load performance of cooling and dehumidifying coils, it was found that the numerical model could become unstable when the coil was in transition from being partly wet to completely dry (Section 7.2 in Chapter 7). This problem was overcome by including a checking procedure in the model which monitors the value of the proportionality constant 'C' (which relates the humidity ratio difference to the temperature difference between the air and the coil surface air-film, see equation B.66) and, if 'C' is found to be negative, its value will be set to zero. This means that the coil is assumed to be completely dry when such condition arises. By adopting this method in the LMHD and the FD models, both models are capable of simulating the

part-load performance of cooling and dehumidifying coils when the chilled water flow rate is reduced down to a few percent of the design flow rate.

The finite difference (FD) dynamic coil model (Chapter 6) was developed to facilitate studies on how the performance of the coil would be affected by the thermal capacities of the coil materials and of the chilled water inside the coil tubes, particularly when on/off control was used. The effect on the dehumidification capacity of the coil was of particular interest. This effect was shown to be significant by the results of simulation studies in that the dehumidification capacity of the coil would be lower, leading to a higher indoor air humidity level, when the coil was modelled by the dynamic model instead of the steady-state model (Chapter 9). This implies that, when a steady-state coil model is used in modelling simultaneously the building and the air-conditioning system in which the coil will be subjected to frequent changes in operating conditions (e.g. large fluctuations in chilled water flow rate through the coil that happen when on/off control is used), optimistic dehumidification performance of the system will be predicted which may not be achieved in reality.

Besides the cooling and dehumidifying coil models, models for other components of an air-handling system have been developed and used to investigate the influence of an air-conditioning system on the indoor environmental conditions, coupled with moisture adsorption and desorption by the building fabric. Component models developed include models of controllers with on/off and proportional control actions, chilled water control valves with linear and equal percentage flow characteristics and a simple piping circuit (Chapter 5). To allow the performance of the air-conditioning system to be modelled more realistically, the integrated model has been incorporated with the feature that the control valve will change its degree of opening according to a pre-set speed which simulates the response of a realistic valve actuator designed to avoid water hammer due to sudden opening or closing of valves. When on/off control is used, the time ahead when a reversal of valve-plug position (from fully open to the closed position or vice versa) will be predicted and a time delay is included

when a valve-plug position reversal is called for. This models the delay in response of the valve actuation mechanism due to the existence of "slack".

10.3 The Numerical Method

The numerical method adopted for solving the governing equations of the building fabric component models and the air-conditioning system component models was based on the self-implicit scheme and the Runge-Kutta-Merson (RKM) method (Chapter 4 & Appendix A). This method is efficient and accurate and is particularly suitable for solving a large set of "stiff" differential equations, such as that associated with the integrated building and system model (Chapter 8). The method was first applied to solve a simple, single dependent variable ordinary differential equation (Appendix A), and shown to give accurate results when compared with the analytical solution with negligible steady error and, when the integration progressed towards steady state, was able to allow large time-steps be used without significant loss of accuracy. The accuracy of the numerical method, when applied to solve a partial differential equation (partially discretized into a set of ordinary differential equations), had also been verified (Appendix A) by comparing the numerical solution with an analytical solution available from literature and excellent agreement between the two was found.

In the early stage of this work, an integrated model comprising a building model based on Huang's equations ⁽⁵⁰⁾ (Chapter 3) and simple steady-state air-conditioning system component models was developed. In that model, the conventional successive back substitution method (with under-relaxation) was used to numerically solve the model equations involved. The computing time required in simulation studies (with a 486 PC) using that model was greater than the simulated time ⁽⁵²⁾ (see Appendix D.1). By using the differential permeability model and the more efficient numerical scheme, the ratio between the program execution time and the simulated time (adopting the steady-state coil model, run on a 486 PC) was significantly reduced to about 1:3 for the air-conditioned period when on/off control was used, and about 1:15 for the shut-down

period (the average ratio was about 1 : 6-8). When proportional control was used, the ratio of 1 : 13-15 could be maintained in both periods.

When the dynamic coil model was used (in conjunction with the differential permeability building model and with the self-implicit scheme and the RKM method), it was found that, due to the small time-steps that need to be used (0.8 second at maximum), the required program execution time was about 2.5 times the simulation time. The computational efficiency of the model was significantly improved by incorporating a staggered time arrangement (to become the DERMAC model, see Chapter 8). With this, the program execution time was reduced to about the same as the simulated time, when run on a 486 PC. When implemented in a VAX 6420 computer, only about two hours of CPU time was required to complete a simulation for one day in the modelled room.

10.4 The Integrated Building and System Model and Simulation Results

Simulation studies performed by applying the integrated model to simulate the heat and moisture transfer in a typical perimeter room in a building subjected to hot and humid weather conditions showed that the porous building fabric could exchange moisture with the room air and act as a moisture storage site. The effect of this on the indoor air condition was found to be significant when the air-conditioning system was intermittently operated and when there were sources of moisture (such as infiltration) during the shut-down period.

The ability of the building fabric to adsorb moisture from the room air during the shut-down period can provide a "passive" control on the indoor humidity in that the indoor air can be maintained at a humidity level that is much lower than the outdoor level. However, the adsorbed moisture will be released back to the room air when air-conditioning is resumed and will thus impose an "extra" latent load to the air-conditioning system. In the simulation studies performed, it was found that, during the start-up phase of the air-conditioned period, this "extra" latent load could be as large as

the total latent load from other sources (including infiltration and occupants). If the shut-down period was longer (i.e. more than one evening), the amount of moisture stored within the building fabric could influence the indoor humidity level for several subsequent days.

In the simulation studies, it was found that, for a constant air volume system operating under part-load conditions, on/off control was more effective in maintaining a low indoor air humidity, when compared with proportional control. To properly model the performance of the air-conditioning system when on/off control is adopted, the dynamic response of the cooling and dehumidifying coil should be modelled in detail. When proportional control was adopted, the fresh air supply should be pre-treated to avoid the addition of moisture into the air-conditioned space at times when the room sensible load was low (such as during the pull-down period at the start of the air-conditioned period where internal loads were absent).

The rate of moisture adsorption and desorption and the effect on the indoor air humidity were found to be dependent not only on the moisture content at the surface layer of the building fabric, but also on its distribution across the walls and slabs. Although the moisture content of the fabric at the internal boundary surface could change following the daily cyclic pattern of indoor air conditions, the moisture content distributions across the walls and slabs would take a much longer time to settle down to a steady daily cyclic pattern. This adjustment period could be in the order of weeks for a small change in the average moisture content of the building fabric materials (Chapter 9). Before the steady daily moisture content variation pattern was attained, the building fabric would continue to act as a sink or source of moisture for the indoor air. Therefore, when there was a change in weather conditions (e.g. from a cool and dry condition to a warm and humid condition) or a change in the operation of the air-conditioning system (e.g. a long shut-down period), this long-term moisture storage effect would influence the indoor air humidity balance in subsequent days.

This result shows that the more recently proposed effective moisture penetration depth (EMPD) theory ⁽¹¹⁶⁾ will only be applicable for predicting building fabric moisture adsorption and desorption effects for a short duration within a long period of steady diurnal pattern of outdoor weather conditions, and steady indoor heat and moisture source patterns. When there are changes in either one of these, the EMPD itself will vary and its use can lead to erroneous results. The effort required to obtain the necessary range of EMPD's, sufficient to cover different possible weather changes, will be significant and therefore unlikely to be worthwhile in practice. The same applies to other methods using similar approaches (e.g. Tsuchiya's method ⁽⁹⁾).

The integrated building and system model was applied to simulate the heat and moisture transfer in an office room in the Hong Kong Polytechnic, based on the weather data of August, 1991. During that period, the indoor air temperature and relative humidity of the office room were measured. The simulated indoor air temperature and humidity ratio and the measured data were found to follow similar variation patterns over the air-conditioned and non-air-conditioned periods, but the accuracy of the predictions was not high. The deviations were due to the differences between the model conditions (no furniture, different wall, floor and ceiling finishes, etc.) and the real situation. At present, the required modelling capability to include effects of these is absent from the model. Nonetheless, this comparison showed that the model was capable of predicting the transient variations in indoor environmental conditions that were similar to actual conditions.

Moisture desorption from the fabric materials and other hygroscopic materials inside buildings and poor part-load dehumidification performance of air-conditioning systems were thought to be the causes for complaints about discomfort conditions in certain buildings in Hong Kong (Chapter 1). Support to this conjecture is now provided by the simulation study results obtained and this underlines the need for further research in this subject area.

10.5 Applications of the Models

The primary objective of this research was to develop the required methodologies for the development of a simulation program that can model in detail the heat and moisture transport phenomena in buildings in hot and humid climate regions. This has been achieved by virtue of the methods developed for modelling the building fabric, the air-conditioning system components, and the method for integrating these component models into a simultaneous building and system model, which form a good foundation for the development of such a simulation tool. The integrated building and system model developed still needs further improvements (see Section 10.6 below) before it can accurately predict the thermal and moisture performance of buildings and systems, taking into account the effects of building finishes, furniture and other materials inside buildings, and different designs and controls of air-conditioning systems. Nevertheless, the development of such additional modelling capabilities has to start with a basic model for the building fabric and the air-conditioning components and this model can be applied in this development work.

Despite the restrictions it has, the integrated model, in its present form, may be used to model indoor air humidity transients in buildings without large quantity of hygroscopic materials other than the building fabric (as in the simulation studies performed). With slight modifications to the air-conditioning system component models, it can also be applied to compare the passive humidity control performance of a wider spectrum of air-conditioning system designs (e.g. variable air volume systems, systems with coil face by-pass control, etc.) and to study the effects of varying chilled water supply temperature from the central chiller plant. Besides, the air-conditioning system component models, particularly the cooling and dehumidifying coil models, can be independently applied to study the performance of such components in an air-conditioning system, e.g. the part-load performance of a coil.

When the necessary improvements have been made, the resultant model will facilitate designers of buildings and air-conditioning system to assess the thermal and

moisture performance of the buildings and the systems leading to better designs. The types of building premises that require particular attention include:

- i) buildings that are situated nearby the harbour which are therefore subjected to a more humid ambient environment and higher wind pressure than buildings further away from the harbour and are sheltered from strong wind by nearby buildings;
- ii) buildings that have a high rate of infiltration which may be due to improper sealing at the building envelopes or having open entrances;
- iii) offices with electronic equipments that are sensitive to humidity but are intermittently air-conditioned (if continuous air-conditioning is provided, as in large computer rooms, there should not be a serious moisture problem);
- iv) residential buildings which have more internal moisture sources (e.g. from the kitchens, laundries, bathrooms and toilets, etc.), are air-conditioned less regularly and for shorter time compared with commercial buildings and, while not air-conditioned, are mechanically or naturally ventilated with outdoor air.

10.6 Recommended Further Work

The moisture adsorption and desorption effect of building walls and slabs has been studied in this work together with the influence of certain air-conditioning system components. The effects of furniture, various finishing materials (e.g. carpet, false ceiling, wall paper, wall paints, etc.) and other general objects and furniture that may exist within buildings (e.g. fibrous materials, books, paper, etc.) have not been studied for the following reasons:

- i) Attention was focused on porous fabric materials that have large amount of internal pores with extremely small sizes (e.g. cement products) and would stay in the pendular state. The heat and moisture transfer model

developed is restricted to this kind of materials. However, common furniture and wall, ceiling and floor finishes are made of materials that do not fall in this catalogory. Hence, a different approach will have to be taken to model the moisture sorption behaviour of such materials.

- ii) Because of the irregular geometries of the furniture and the other objects in the room, a detailed treatment, similar to that for the building fabric, will be highly complicated.
- iii) Moisture transport property data for modelling the effects of these objects and materials are at present very limited and more work on determination of moisture transport property of materials is required (e.g. 176). Hence, the study has to be backed-up by experimental work. However, considering the amount of time required to carry out experiments with the large variety of materials involved, these work were excluded from the scope of this study.

To model the moisture sorption behaviour of furniture, a lumped-parameter approach (e.g. the effective moisture penetration depth theory ⁽¹¹⁶⁾) would be a convenient choice, though, as pointed out earlier, such methods may have problems when the materials are subjected to large changes of ambient conditions. This has to be verified by experimental work. The effects of surface finishes may also be model using a lumped parameter model and this is expected to be a good choice as the thickness of finishes is small, compared with the building fabric components. Nevertheless, experimentally measured moisture property data are needed.

Although not included in this study, the moisture sorption behaviour of furniture, finishes and other hygroscopic materials inside buildings may have significant impact on the indoor environmental conditions and hence research into this area is highly important.

From the simulation studies, it was found that the rate of infiltration had a dominant effect on the rate of moisture desorption and adsorption by the building fabric during air-conditioned and non-air-conditioned periods. To accurately predict the rate of infiltration into a particular room in a modern high rise building is complex as the infiltration air will normally pass through a large number of paths (e.g. through window cracks, door gaps, from outdoor direct or through a series of air-conditioned and non-air-conditioned spaces like staircases, lift-shafts, corridors, other rooms etc.). This is further complicated due to the variability of wind pressure, stack effect and pressure differences between adjacent rooms. Methods for accurate estimation of infiltration rates (e.g. 164) and the state of the infiltrated air into rooms therefore is highly important, and requires attention.

The prototype model developed needs to be extended to a multi-zone model for analysing realistic situations in buildings. It needs to be equipped with a larger variety of material property data, and incorporate models for furnitures and other general materials inside a building. Also, models for other air-conditioning system components (e.g. chillers, pumps, hydraulic circuits having many branches, etc.) should be developed so that the performance of the entire central air-conditioning plant can be modelled.

Finally, facilities should also be developed to provide data for the validation of the various component models and the overall accuracy of prediction of the integrated model. However, research into methods for validating computer programs for building energy and plant performance, whilst being actively pursued (e.g. 165), requires much attention.

Table 3.1 Expressions for Evaluation of Coefficients in Huang's Equations

Coef.	i = 1 (Moisture Equation)	i = 2 (Air Equation)	i = 3 (Energy Equation)
A _i	$\bar{Y} \frac{\partial \epsilon_g}{\partial \phi} + \epsilon_g$	$(1 - \phi) \frac{\partial \epsilon_g}{\partial \phi} + \epsilon_g$	$\rho_w h_{fg} \frac{\partial \epsilon_g}{\partial \phi}$
B _i	$\bar{Y} \frac{\partial \epsilon_g}{\partial P_g} + \epsilon_g \frac{\phi}{P_g}$	$(1 - \phi) \bar{O}_P$	$\rho_w h_{fg} \frac{\partial \epsilon_g}{\partial \phi} - \epsilon_g$
C _i	$\bar{Y} \frac{\partial \epsilon_g}{\partial T} - \epsilon_g \frac{\phi}{T}$	$-(1 - \phi) \bar{O}_T$	$\rho_w h_{fg} \frac{\partial \epsilon_g}{\partial T} +$ $[(\epsilon_o - \epsilon_g) \rho_w (C_p)_w +$ $\rho_s (1 - \epsilon_o) (C_p)_s] +$ $\epsilon_g P_g [\phi M_w (C_p)_v +$ $(1 - \phi) M_s (C_p)_s] / (R T)$
D _i	$D \epsilon_g \frac{M_s}{M_g}$	$-D \epsilon_g \frac{M_w}{M_g}$	0
E _i	$\zeta_g \phi \frac{\kappa_g^o}{\mu_g}$	$\zeta_g (1 - \phi) \frac{\kappa_g^o}{\mu_g}$	0
F _i	0	0	k _B
G _i	$-D \bar{O}_\phi \frac{M_s}{M_g}$	$D \bar{O}_\phi \frac{M_w}{M_g}$	0
H _i	$\phi \bar{W}_P \frac{\kappa_g^o}{\mu_g}$	$(1 - \phi) \bar{W}_P \frac{\kappa_g^o}{\mu_g}$	0
I _i	0	0	$\frac{\partial k_B}{\partial \epsilon_g} \frac{\partial \epsilon_g}{\partial T}$
J _i	$D \bar{O}_P \frac{M_s}{M_g} +$ $\frac{\kappa_g^o}{\mu_g} [\phi \frac{\partial \zeta_g}{\partial \epsilon_g} \frac{\partial \epsilon_g}{\partial \phi} + \zeta_g]$	$-D \bar{O}_P \frac{M_w}{M_g} +$ $\frac{\kappa_g^o}{\mu_g} [(1 - \phi) \frac{\partial \zeta_g}{\partial \epsilon_g} \frac{\partial \epsilon_g}{\partial \phi} - \zeta_g]$	0
K _i	$-D \bar{O}_T \frac{M_s}{M_g}$	$-D \bar{O}_T \frac{M_w}{M_g}$	$\frac{\partial k_B}{\partial \epsilon_g} \frac{\partial \epsilon_g}{\partial \phi} -$ $D M_s M_w \epsilon_g P_g \cdot$ $\frac{(C_p)_s - (C_p)_v}{(R T M_g)}$
L _i	$-\phi \bar{W}_T \frac{\kappa_g^o}{\mu_g}$	$-(1 - \phi) \bar{W}_T \frac{\kappa_g^o}{\mu_g}$	$\frac{\partial k_B}{\partial \epsilon_g} \frac{\partial \epsilon_g}{\partial P_g} + (\kappa_g^o \zeta_g P_g) \cdot$ $[M_w (C_p)_v \phi + M_s (C_p)_s (1 -$ $\phi)] / (R T)$

where

$$\bar{O}_\phi = \epsilon_g \frac{M_w - M_s}{M_g} \cdot \frac{\partial \epsilon_g}{\partial \phi} \quad ; \quad \bar{O}_P = \frac{\epsilon_g}{P_g} + \frac{\partial \epsilon_g}{\partial P_g} \quad ; \quad \bar{O}_T = \frac{\epsilon_g}{T} - \frac{\partial \epsilon_g}{\partial T} ;$$

$$\bar{Y} = \phi \cdot \frac{\rho_w R T}{M_w P_g} \quad ; \quad \bar{W}_P = \frac{\zeta_g}{P_g} + \frac{\partial \zeta_g}{\partial \epsilon_g} \frac{\partial \epsilon_g}{\partial P_g} \quad ; \quad \bar{W}_T = \frac{\zeta_g}{T} - \frac{\partial \zeta_g}{\partial \epsilon_g} \frac{\partial \epsilon_g}{\partial T}$$

Table 3.2 The Finite Differencing Scheme Applied to Huang's Equations

For a function $f(x,t)$, let

$$f^n = f(x, t) \quad ; \quad f^{n+1} = f(x, t + \Delta t) \quad ; \quad \Delta f = f^{n+1} - f^n$$

$$f_+^n = f(x + \Delta x, t) \quad ; \quad f_+^{n+1} = f(x + \Delta x, t + \Delta t) \quad ; \quad \Delta f_+ = f_+^{n+1} - f_+^n$$

$$f_-^n = f(x - \Delta x, t) \quad ; \quad f_-^{n+1} = f(x - \Delta x, t + \Delta t) \quad ; \quad \Delta f_- = f_-^{n+1} - f_-^n$$

The temporal and spatial derivatives of the function $f(x,t)$, using the backward in time, central in space differencing scheme, can be expressed as:

$$\frac{\partial f}{\partial t} \approx \frac{\Delta f}{\Delta t} \quad (T.3.2.1)$$

$$\frac{\partial f}{\partial x} \approx \frac{f_+^{n+1} - f_-^{n+1}}{2\Delta x} = \frac{f_+^n - f_-^n}{2\Delta x} + \frac{\Delta f_+^n - \Delta f_-^n}{2\Delta x} \quad (T.3.2.2)$$

$$\frac{\partial^2 f}{\partial x^2} \approx \frac{f_+^{n+1} - 2f^{n+1} + f_-^{n+1}}{(\Delta x)^2} = \frac{f_+^n - 2f^n + f_-^n}{(\Delta x)^2} + \frac{\Delta f_+^n - 2\Delta f + \Delta f_-^n}{(\Delta x)^2} \quad (T.3.2.3)$$

For product of derviatives,

$$\begin{aligned} \left(\frac{\partial f}{\partial x}\right)^2 &= \frac{\partial f}{\partial x} \cdot \frac{\partial f}{\partial x} \approx \left(\frac{f_+^n - f_-^n}{2\Delta x} + \frac{\Delta f_+^n - \Delta f_-^n}{2\Delta x}\right)^2 \\ &= \left(\frac{f_+^n - f_-^n}{2\Delta x}\right)^2 + 2\left(\frac{f_+^n - f_-^n}{2\Delta x} \cdot \frac{\Delta f_+^n - \Delta f_-^n}{2\Delta x}\right) + \left(\frac{\Delta f_+^n - \Delta f_-^n}{2\Delta x}\right)^2 \end{aligned}$$

Neglecting squared term for incremental values (last term in above equation).

$$\left(\frac{\partial f}{\partial x}\right)^2 \approx \left(\frac{f_+^n - f_-^n}{2\Delta x}\right)^2 + 2\left(\frac{f_+^n - f_-^n}{2\Delta x} \cdot \frac{\Delta f_+^n - \Delta f_-^n}{2\Delta x}\right) \quad (T.3.2.4)$$

If g is another variable and g is also a function of x and t , following similar approach,

$$\frac{\partial f}{\partial x} \frac{\partial g}{\partial x} \approx \left(\frac{f_+^n - f_-^n}{2\Delta x} \cdot \frac{g_+^n - g_-^n}{2\Delta x}\right) + \left(\frac{f_+^n - f_-^n}{2\Delta x} \cdot \frac{\Delta g_+^n - \Delta g_-^n}{2\Delta x}\right) + \left(\frac{g_+^n - g_-^n}{2\Delta x} \cdot \frac{\Delta f_+^n - \Delta f_-^n}{2\Delta x}\right) \quad (T.3.2.5)$$

Table 3.3 Expressions for Coefficients in Finite Difference Equations

A) For Interior Nodes (for $i = 1, 2$ and 3):

$$a_{i1} = -\frac{D_i}{(\Delta x)^2} + \frac{2G_i}{2\Delta x} \left(\frac{\phi_+^n - \phi_-^n}{2\Delta x} \right) + \frac{J_i}{2\Delta x} \left(\frac{P_{g+}^n - P_{g-}^n}{2\Delta x} \right) + \frac{K_i}{2\Delta x} \left(\frac{T_+^n - T_-^n}{2\Delta x} \right)$$

$$a_{i2} = -\frac{E_i}{(\Delta x)^2} + \frac{2H_i}{2\Delta x} \left(\frac{P_{g+}^n - P_{g-}^n}{2\Delta x} \right) + \frac{J_i}{2\Delta x} \left(\frac{\phi_+^n - \phi_-^n}{2\Delta x} \right) + \frac{L_i}{2\Delta x} \left(\frac{T_+^n - T_-^n}{2\Delta x} \right)$$

$$a_{i3} = -\frac{F_i}{(\Delta x)^2} + \frac{2I_i}{2\Delta x} \left(\frac{T_+^n - T_-^n}{2\Delta x} \right) + \frac{K_i}{2\Delta x} \left(\frac{\phi_+^n - \phi_-^n}{2\Delta x} \right) + \frac{L_i}{2\Delta x} \left(\frac{P_{g+}^n - P_{g-}^n}{2\Delta x} \right)$$

$$b_{i1} = \frac{A_i}{\Delta t} + \frac{2D_i}{(\Delta x)^2}$$

$$b_{i2} = \frac{B_i}{\Delta t} + \frac{2E_i}{(\Delta x)^2}$$

$$b_{i3} = \frac{C_i}{\Delta t} + \frac{2F_i}{(\Delta x)^2}$$

$$c_{i1} = -\frac{D_i}{(\Delta x)^2} - \frac{2G_i}{2\Delta x} \left(\frac{\phi_+^n - \phi_-^n}{2\Delta x} \right) - \frac{J_i}{2\Delta x} \left(\frac{P_{g+}^n - P_{g-}^n}{2\Delta x} \right) - \frac{K_i}{2\Delta x} \left(\frac{T_+^n - T_-^n}{2\Delta x} \right)$$

$$c_{i2} = -\frac{E_i}{(\Delta x)^2} - \frac{2H_i}{2\Delta x} \left(\frac{P_{g+}^n - P_{g-}^n}{2\Delta x} \right) - \frac{J_i}{2\Delta x} \left(\frac{\phi_+^n - \phi_-^n}{2\Delta x} \right) - \frac{L_i}{2\Delta x} \left(\frac{T_+^n - T_-^n}{2\Delta x} \right)$$

$$c_{i3} = -\frac{F_i}{(\Delta x)^2} - \frac{2I_i}{2\Delta x} \left(\frac{T_+^n - T_-^n}{2\Delta x} \right) - \frac{K_i}{2\Delta x} \left(\frac{\phi_+^n - \phi_-^n}{2\Delta x} \right) - \frac{L_i}{2\Delta x} \left(\frac{P_{g+}^n - P_{g-}^n}{2\Delta x} \right)$$

$$d_i = D_i \left(\frac{\phi_+^n - 2\phi_i^n + \phi_-^n}{(\Delta x)^2} \right) + E_i \left(\frac{P_{g+}^n - 2P_{gi}^n + P_{g-}^n}{(\Delta x)^2} \right) + F_i \left(\frac{T_+^n - 2T_i^n + T_-^n}{(\Delta x)^2} \right)$$

$$+ G_i \left(\frac{\phi_+^n - \phi_-^n}{2\Delta x} \right)^2 + H_i \left(\frac{P_{g+}^n - P_{g-}^n}{2\Delta x} \right)^2 + I_i \left(\frac{T_+^n - T_-^n}{2\Delta x} \right)^2$$

$$+ J_i \left(\frac{\phi_+^n - \phi_-^n}{2\Delta x} \cdot \frac{P_{g+}^n - P_{g-}^n}{2\Delta x} \right) + K_i \left(\frac{\phi_+^n - \phi_-^n}{2\Delta x} \cdot \frac{T_+^n - T_-^n}{2\Delta x} \right)$$

$$+ L_i \left(\frac{P_{g+}^n - P_{g-}^n}{2\Delta x} \cdot \frac{T_+^n - T_-^n}{2\Delta x} \right)$$

B) For Boundary Nodes (for i = 1, 2 and 3):

$$a_{11} = -\frac{2D_1}{(\Delta x)^2}$$

$$a_{12} = -\frac{2E_1}{(\Delta x)^2}$$

$$a_{13} = 0$$

$$a_{21} = a_{22} = a_{23} = 0$$

$$a_{31} = a_{32} = 0$$

$$a_{33} = -\frac{2F_3}{(\Delta x)^2}$$

$$b_{11} = \frac{A_1}{\Delta t} + \frac{2D_1}{(\Delta x)^2}$$

$$b_{12} = \frac{B_1}{\Delta t} + \frac{2E_1}{(\Delta x)^2}$$

$$b_{13} = \frac{C_1}{\Delta t}$$

$$b_{21} = b_{22} = b_{23} = 0$$

$$b_{31} = \frac{A_3}{\Delta t}$$

$$b_{32} = \frac{B_3}{\Delta t}$$

$$b_{33} = \frac{C_3}{\Delta t} + \frac{2F_3}{(\Delta x)^2}$$

$$d_1 = \frac{2}{\Delta x} \left\{ \frac{RT}{M_v P_g} m_v'' + D_1 \frac{\phi_a^n - \phi^n}{\Delta x} + E_1 \frac{P_a^n - P_g^n}{\Delta x} \right\}$$

$$d_2 = 0$$

$$d_3 = \frac{2}{\Delta x} \left\{ q'' + F_3 \frac{T_a^n - T^n}{\Delta x} \right\}$$

C) For Interface Nodes (for i = 1, 2 and 3):

$$a_{i1} = -\frac{D_{i-}}{\Delta x_{-}}$$

$$a_{i2} = -\frac{E_{i-}}{\Delta x_{-}}$$

$$a_{i3} = -\frac{F_{i-}}{\Delta x_{-}}$$

$$b_{i1} = \frac{\Delta x_{-}}{2\Delta t} A_{i-} + \frac{\Delta x_{+}}{2\Delta t} A_{i+} + \frac{D_{i-}}{\Delta x_{-}} + \frac{D_{i+}}{\Delta x_{+}}$$

$$b_{i2} = \frac{\Delta x_{-}}{2\Delta t} B_{i-} + \frac{\Delta x_{+}}{2\Delta t} B_{i+} + \frac{E_{i-}}{\Delta x_{-}} + \frac{E_{i+}}{\Delta x_{+}}$$

$$b_{i3} = \frac{\Delta x_{-}}{2\Delta t} C_{i-} + \frac{\Delta x_{+}}{2\Delta t} C_{i+} + \frac{F_{i-}}{\Delta x_{-}} + \frac{F_{i+}}{\Delta x_{+}}$$

$$c_{i1} = -\frac{D_{i+}}{\Delta x_{+}}$$

$$c_{i2} = -\frac{E_{i+}}{\Delta x_{+}}$$

$$c_{i3} = -\frac{F_{i+}}{\Delta x_{+}}$$

$$d_i = D_{i+} \frac{\phi_+^n - \phi_-^n}{\Delta x_{+}} - D_{i-} \frac{\phi_+^n - \phi_-^n}{\Delta x_{-}} + E_{i+} \frac{P_+^n - P_-^n}{\Delta x_{+}} - E_{i-} \frac{P_+^n - P_-^n}{\Delta x_{-}} + F_{i+} \frac{T_+^n - T_-^n}{\Delta x_{+}} - F_{i-} \frac{T_+^n - T_-^n}{\Delta x_{-}}$$

Notes:

A_{i-} to F_{i-} denote values of A_i to F_i for the material to the LEFT of the interface and

A_{i+} to F_{i+} denote values of A_i to F_i for the material to the RIGHT of the interface.

Likewise, Δx_{-} and Δx_{+} denote respectively the spatial subdivisions in the materials to the LEFT and to the RIGHT of the interface surface.

Table 3.4 Reference Conditions of the Simulation Studies on Drying of a Slab of Concrete and Cement Paste (50,51)

Type of constants	Sym.	Unit	Concrete	Cement
Physical constants				
Universal gas constant	R	J/mol K	8.3149	
Stefan-Boltzmann constant	σ	W/m ² K ⁴	5.676×10^{-8}	
Specific heat of air	C_{p_a}	J/kg K	1.006×10^3	
Specific heat of solid	C_{p_s}	J/kg K	0.879×10^3	
Specific heat of water vapour	C_{p_v}	J/kg K	1.865×10^3	
Specific heat of liquid water	C_{p_l}	J/kg K	4.179×10^3	
Diffusivity of water vapour in air	D	m ² /s	0.256×10^{-4}	
Physical properties				
Emissivity of solid surfaces	ϵ		0.8	
Thermal conductivity of gas	k_g	W/mK	0.02613	
Thermal conductivity of solid	k_s	W/mK	1.4422	
Thermal conductivity of liquid	k_l	W/mK	0.616	
Molecular weight of air	M_a	kg/mol	28.952×10^{-3}	
Molecular weight of water	M_w	kg/mol	18.016×10^{-3}	
Dry porosity	ϵ_o		0.3	0.43
Viscosity of gas	μ_g	kg/ms	1.83×10^{-5}	
Permeability of gas when dry	κ_g^o	m ²	2.5×10^{-14}	
Latent heat of vapouration	h_{fg}	J/kg	2.4418×10^6	
Density of solid (dry)	ρ_s	kg/m ³	2.6×10^3	2.2×10^3
Density of liquid water	ρ_w	kg/m ³	0.9971×10^3	
Geometric constants				
Thickness of slab	L	m	0.1	0.01
Height of slab	H	m	2.0	0.1839
Empirical constants				
Clausius-Clapeyron eqn. const.	a	ms ² /kg	1.2097×10^{-12}	
Exponent in Kingery's equation	n		0.25	
Surface tension at ref. temp.	σ_o	kg/s ²	121.2×10^{-3}	
Temperature coefficient of σ_o	β	kg/s ² K	0.167×10^{-3}	

Table 3.4 (Cont'd)

Type of constants	Sym.	Unit	Concrete	Cement
Initial conditions				
Atmospheric pressure	P_{atm}	Pa	1.01325×10^5	
Initial moisture content	m_{ini}	m^3/m^3	0.096	0.17
Initial temperature	T_{ini}	K	294.8	294.8
Boundary conditions				
LHS ambient air mole fraction	ϕ_1	mol/mol	0.0134	0.003548
RHS ambient air mole fraction	ϕ_2	mol/mol	0.003548	0.003548
LHS ambient air temperature	T_1	K	303.0	298.5
RHS ambient air temperature	T_2	K	294.0	298.5
LHS enclosure temperature	T_{e1}	K	304.0	298.5
RHS enclosure temperature	T_{e2}	K	293.0	298.5

Table 4.1 Coefficients of the Differential Permeability Wall/Slab Heat and Moisture Transfer Model - 1

Coefficients	Interior Nodes	Boundary Nodes	Interface Nodes
a_{11}	$\rho_l \frac{\partial \epsilon_l}{\partial P_v}$	$\rho_l \frac{\partial \epsilon_l}{\partial P_v}$	$\rho_l \left\{ \frac{\partial \epsilon_l}{\partial P_v} \right\}_I$
a_{12}	$\rho_l \frac{\partial \epsilon_l}{\partial T}$	$\rho_l \frac{\partial \epsilon_l}{\partial T}$	$\rho_l \left\{ \frac{\partial \epsilon_l}{\partial T} \right\}_I$
a_{21}	$-h_{fg} \rho_l \frac{\partial \epsilon_l}{\partial P_v}$	$-h_{fg} \rho_l \frac{\partial \epsilon_l}{\partial P_v}$	$-\rho_l \left\{ h_{fg} \frac{\partial \epsilon_l}{\partial P_v} \right\}_I$
a_{22}	$(\rho C_p)_B - h_{fg} \rho_l \frac{\partial \epsilon_l}{\partial T}$	$(\rho C_p)_B - h_{fg} \rho_l \frac{\partial \epsilon_l}{\partial T}$	$\{ \rho C_p \}_I - \rho_l \left\{ h_{fg} \frac{\partial \epsilon_l}{\partial T} \right\}_I$
c_{11}	μ	-	-
c_{12}	$\frac{\partial \mu}{\partial x}$	$\frac{2}{\Delta x} \mu$	-
c_{21}	k_B	-	-
c_{22}	$\frac{\partial k_B}{\partial x}$	$\frac{2}{\Delta x} k_B$	-
d_1	-	$\frac{2}{\Delta x} m_v''$	-
d_2	-	$\frac{2}{\Delta x} q''$	-

where, for the coefficients for the interface nodes,

$$\left\{ \frac{\partial \epsilon_l}{\partial P_v} \right\}_I = \frac{\Delta x_-}{2} \frac{\partial \epsilon_{l-}}{\partial P_v} + \frac{\Delta x_+}{2} \frac{\partial \epsilon_{l+}}{\partial P_v} \quad ; \quad \left\{ \frac{\partial \epsilon_l}{\partial T} \right\}_I = \frac{\Delta x_-}{2} \frac{\partial \epsilon_{l-}}{\partial T} + \frac{\Delta x_+}{2} \frac{\partial \epsilon_{l+}}{\partial T}$$

$$\left\{ h_{fg} \frac{\partial \epsilon_l}{\partial P_v} \right\}_I = h_{fg-} \frac{\Delta x_-}{2} \frac{\partial \epsilon_{l-}}{\partial P_v} + h_{fg+} \frac{\Delta x_+}{2} \frac{\partial \epsilon_{l+}}{\partial P_v}$$

$$\left\{ h_{fg} \frac{\partial \epsilon_l}{\partial T} \right\}_I = h_{fg-} \frac{\Delta x_-}{2} \frac{\partial \epsilon_{l-}}{\partial T} + h_{fg+} \frac{\Delta x_+}{2} \frac{\partial \epsilon_{l+}}{\partial T}$$

$$\{ \rho C_p \}_I = \frac{\Delta x_-}{2} (\rho C_p)_{B-} + \frac{\Delta x_+}{2} (\rho C_p)_{B+}$$

Table 4.2 Coefficients of the Differential Permeability Wall/Slab Heat and Moisture Transfer Model - 2

Coefficients	Interior Nodes
A_{i11}	$-\lambda\Delta t\left[\frac{c_{11}}{\Delta x^2}-\frac{c_{12}}{2\Delta x}\right]$
A_{i21}	$a_{11}+\lambda\Delta t\frac{2c_{11}}{\Delta x^2}$
A_{i31}	$-\lambda\Delta t\left[\frac{c_{11}}{\Delta x^2}+\frac{c_{12}}{2\Delta x}\right]$
B_{i1}	$c_{11}\frac{P_{v+}^n-2P_v^n+P_{v-}^n}{\Delta x^2}+c_{12}\frac{P_{v+}^n-P_{v-}^n}{2\Delta x}-a_{12}\frac{\partial T}{\partial t}$
A_{i12}	$-\lambda\Delta t\left[\frac{c_{21}}{\Delta x^2}-\frac{c_{22}}{2\Delta x}\right]$
A_{i22}	$a_{22}+\lambda\Delta t\frac{2c_{21}}{\Delta x^2}$
A_{i32}	$-\lambda\Delta t\left[\frac{c_{11}}{\Delta x^2}+\frac{c_{12}}{2\Delta x}\right]$
B_{i2}	$c_{21}\frac{T_+^n-2T^n+T_-^n}{\Delta x^2}+c_{22}\frac{T_+^n-T_-^n}{2\Delta x}-a_{22}\frac{\partial P_v}{\partial t}$

Coefficients	Boundary Nodes (i=1)	Boundary Nodes (i=N)
A_{i11}	-	$-\lambda\Delta t\frac{c_{12}}{\Delta x}$
A_{i21}	$a_{11}+\lambda\Delta t\frac{c_{12}}{\Delta x}$	$a_{11}+\lambda\Delta t\frac{c_{12}}{\Delta x}$
A_{i31}	$-\lambda\Delta t\frac{c_{12}}{\Delta x}$	-
B_{i1}	$c_{12}\frac{P_{v2}^n-P_{v1}^n}{\Delta x}+d_1-a_{12}\frac{\partial T_1}{\partial t}$	$c_{12}\frac{P_{vN-1}^n-P_{vN}^n}{\Delta x}+d_1-a_{12}\frac{\partial T_N}{\partial t}$

Table 4.2 Coefficients of the Differential Permeability Wall/Slab Heat and Moisture Transfer Model - 2 (Cont'd)

Coefficients	Boundary Nodes (i=1)	Boundary Nodes (i=N)
A_{i12}	-	$-\lambda\Delta t \frac{c_{22}}{\Delta x}$
A_{i22}	$a_{22} + \lambda\Delta t \frac{c_{22}}{\Delta x}$	$a_{22} + \lambda\Delta t \frac{c_{22}}{\Delta x}$
A_{i32}	$-\lambda\Delta t \frac{c_{22}}{\Delta x}$	-
B_{i2}	$c_{22} \frac{T_2^n - T_1^n}{\Delta x} + d_2 - a_{22} \frac{\partial P_{v1}}{\partial t}$	$c_{22} \frac{T_{N-1}^n - T_N^n}{\Delta x} + d_2 - a_{22} \frac{\partial P_{vN}}{\partial t}$

Coefficients	Interface Nodes
A_{i11}	$-\lambda\Delta t \frac{\mu_-}{\Delta x_-}$
A_{i21}	$a_{11} + \lambda\Delta t (\frac{\mu_-}{\Delta x_-} + \frac{\mu_+}{\Delta x_+})$
A_{i31}	$-\lambda\Delta t \frac{\mu_+}{\Delta x_+}$
B_{i1}	$-\mu_- \frac{P_v^n - P_{v-}^n}{\Delta x_-} + \mu_+ \frac{P_{v+}^n - P_v^n}{\Delta x_+} - a_{12} \frac{\partial T}{\partial t}$
A_{i12}	$-\lambda\Delta t \frac{k_{B-}}{\Delta x_-}$
A_{i22}	$a_{22} + \lambda\Delta t (\frac{k_{B-}}{\Delta x_-} + \frac{k_{B+}}{\Delta x_+})$
A_{i32}	$-\lambda\Delta t \frac{k_{B+}}{\Delta x_+}$
B_{i2}	$-k_{B-} \frac{T_-^n - T_-^n}{\Delta x_-} + k_{B+} \frac{T_+^n - T_+^n}{\Delta x_+} - a_{21} \frac{\partial P_v}{\partial t}$

Table 4.3 Reference Conditions of Thomas and Burch's Experiment on Drying of a Slab of Gypsum Board ⁽⁵³⁾

Type of constants	Symbol	Unit	Gypsum Board
Thickness	L	m	0.0132
Diameter of slab	D	m	0.18
Density	ρ	kg/m ³	670
Specific heat	C _p	J/kg K	1.0894 x 10 ³
Thermal conductivity	k	W/m K	0.1593
Initial moisture content	m _{ini}	m ³ /m ³	0.005293
Surface mass transfer coefficient	$h_m(\frac{\epsilon_g M_v}{RT})$	kg/m ² Pa s	3.2 x 10 ⁻⁸
Ambient air temperature	T _{amb}	K	297.0
Initial ambient air rel. humidity	RH _{ini}	%	74
New ambient air rel. humidity	RH _{amb}	%	26

Table 6.1 Coefficients in Governing Equations for a Dry Coil

i	j	A'_{ij1}	A'_{ij2}	A'_{ij3}
1	1	-	-	-
	2	-	$1 + \lambda \frac{u_w}{L} (\frac{2}{\Delta \xi} + Ntu_w) \Delta t$	$-\frac{2 \lambda u_w \Delta t}{L \Delta \xi}$
	3	-	$1 + \lambda (\frac{C_a}{C_c} Ntu_a + \frac{P_{ct} L}{C_c R_{ct}}) \Delta t$	-
	4	-	$1 + \lambda (\frac{C_w}{C_t} Ntu_a + \frac{P_{ct} L}{C_t R_{ct}}) \Delta t$	-
2 to N-1	1	$-\frac{\lambda u_a \Delta t}{L \Delta \xi}$	$1 + \lambda \frac{u_a}{L} (\frac{1}{\Delta \xi} + Ntu_a) \Delta t$	-
	2	-	$1 + \lambda \frac{u_w}{L} (\frac{1}{\Delta \xi} + Ntu_w) \Delta t$	$-\frac{\lambda u_w \Delta t}{L \Delta \xi}$
	3	-	$1 + \lambda (\frac{C_a}{C_c} Ntu_a + \frac{P_{ct} L}{C_c R_{ct}}) \Delta t$	-
	4	-	$1 + \lambda (\frac{C_w}{C_t} Ntu_a + \frac{P_{ct} L}{C_t R_{ct}}) \Delta t$	-
N	1	$-\frac{2 \lambda u_a \Delta t}{L \Delta \xi}$	$1 + \lambda \frac{u_a}{L} (\frac{2}{\Delta \xi} + Ntu_a) \Delta t$	-
	2	-	-	-
	3	-	$1 + \lambda (\frac{C_a}{C_c} Ntu_a + \frac{P_{ct} L}{C_c R_{ct}}) \Delta t$	-
	4	-	$1 + \lambda (\frac{C_w}{C_t} Ntu_a + \frac{P_{ct} L}{C_t R_{ct}}) \Delta t$	-

Table 6.1 Coefficients in Governing Equations for a Dry Coil (Cont'd)

i	j	B'ij or C'ij	D'ij or E'ij	F'ij
1	1	-	-	-
	2	-	$E'_{ij} = \frac{\lambda u_w Ntu_w \Delta t}{L}$	$-\frac{u_w}{L} \left\{ \frac{2}{\Delta \xi} (T_{w1}^n - T_{w2}^n) + Ntu_w (T_{w1}^n - T_{t1}^n) \right\}$
	3	-	$E'_{ij} = \frac{\lambda P_{ct} L \Delta t}{C_c R_{ct}}$	$-\frac{C_a}{C_c} Ntu_a (T_{c1}^n - T_{a1}^n) - \frac{P_{ct} L}{C_c R_{ct}} (T_{c1}^n - T_{t1}^n)$
	4	$C'_{ij} = \lambda \frac{C_w}{C_t} Ntu_w \Delta t$	$D'_{ij} = \frac{\lambda P_{ct} L \Delta t}{C_t R_{ct}}$	$-\frac{C_w}{C_t} Ntu_w (T_{t1}^n - T_{w1}^n) - \frac{P_{ct} L}{C_t R_{ct}} (T_{t1}^n - T_{c1}^n)$
2 to N-1	1	-	$D'_{ij} = \frac{\lambda u_a Ntu_a \Delta t}{L}$	$-\frac{u_a}{L} \left\{ \frac{1}{\Delta \xi} (T_{a1}^n - T_{a1-1}^n) + Ntu_a (T_{a1}^n - T_{c1}^n) \right\}$
	2	-	$E'_{ij} = \frac{\lambda u_w Ntu_w \Delta t}{L}$	$\frac{u_w}{L} \left\{ \frac{1}{\Delta \xi} (T_{w1+1}^n - T_{w1}^n) - Ntu_w (T_{w1}^n - T_{t1}^n) \right\}$
	3	$B'_{ij} = \lambda \frac{C_a}{C_c} Ntu_a \Delta t$	$E'_{ij} = \frac{\lambda P_{ct} L \Delta t}{C_c R_{ct}}$	$-\frac{C_a}{C_c} Ntu_a (T_{c1}^n - T_{a1}^n) - \frac{P_{ct} L}{C_c R_{ct}} (T_{c1}^n - T_{t1}^n)$
	4	$C'_{ij} = \lambda \frac{C_w}{C_t} Ntu_w \Delta t$	$D'_{ij} = \frac{\lambda P_{ct} L \Delta t}{C_t R_{ct}}$	$-\frac{C_w}{C_t} Ntu_w (T_{t1}^n - T_{w1}^n) - \frac{P_{ct} L}{C_t R_{ct}} (T_{t1}^n - T_{c1}^n)$
N	1	-	$D'_{ij} = \frac{\lambda u_a Ntu_a \Delta t}{L}$	$-\frac{u_a}{L} \left\{ \frac{2}{\Delta \xi} (T_{aN}^n - T_{aN-1}^n) + Ntu_a (T_{aN}^n - T_{cN}^n) \right\}$
	2	-	-	-
	3	$B'_{ij} = \lambda \frac{C_a}{C_c} Ntu_a \Delta t$	$E'_{ij} = \frac{\lambda P_{ct} L \Delta t}{C_c R_{ct}}$	$-\frac{C_a}{C_c} Ntu_a (T_{cN}^n - T_{aN}^n) - \frac{P_{ct} L}{C_c R_{ct}} (T_{cN}^n - T_{tN}^n)$
	4	-	$D'_{ij} = \frac{\lambda P_{ct} L \Delta t}{C_t R_{ct}}$	$-\frac{C_w}{C_t} Ntu_w (T_{tN}^n - T_{wN}^n) - \frac{P_{ct} L}{C_t R_{ct}} (T_{tN}^n - T_{cN}^n)$

Table 6.2 Coefficients in Governing Equations for a Wet Coil

i	j	A _{ij1}	A _{ij2}	A _{ij3}
1	0	-	-	-
	1	-	-	-
	2	-	$1 + \lambda \frac{u_w}{L} \left(\frac{2}{\Delta \xi} + Ntu_w \right) \Delta t$	$-\frac{2 \lambda u_w \Delta t}{L \Delta \xi}$
	3	-	$1 + \lambda \left(\frac{C_a}{C_c} \frac{Ntu_a}{Le_m} + \frac{P_{ct} L}{C_c R_{ct}} \right) \Delta t$	-
	4	-	$1 + \lambda \left(\frac{C_w}{C_t} Ntu_w + \frac{P_{ct} L}{C_t R_{ct}} \right) \Delta t$	-
2 to N-1	0	$-\frac{\lambda u_a \Delta t}{L \Delta \xi}$	$1 + \lambda \frac{u_a}{L} \left(\frac{1}{\Delta \xi} + \frac{Ntu_a}{Le_m} \right) \Delta t$	-
	1	$-\frac{\lambda u_a \Delta t}{L \Delta \xi}$	$1 + \lambda \frac{u_a}{L} \left(\frac{1}{\Delta \xi} + \frac{Ntu_a}{Le_m} \right) \Delta t$	-
	2	-	$1 + \lambda \frac{u_w}{L} \left(\frac{1}{\Delta \xi} + Ntu_w \right) \Delta t$	$-\frac{\lambda u_w \Delta t}{L \Delta \xi}$
	3	-	$1 + \lambda \left(\frac{C_a}{C_c} \frac{Ntu_a}{Le_m} + \frac{P_{ct} L}{C_c R_{ct}} \right) \Delta t$	-
	4	-	$1 + \lambda \left(\frac{C_w}{C_t} Ntu_w + \frac{P_{ct} L}{C_t R_{ct}} \right) \Delta t$	-
N	0	$-\frac{2 \lambda u_a \Delta t}{L \Delta \xi}$	$1 + \lambda \frac{u_a}{L} \left(\frac{2}{\Delta \xi} + \frac{Ntu_a}{Le_m} \right) \Delta t$	-
	1	$-\frac{2 \lambda u_a \Delta t}{L \Delta \xi}$	$1 + \lambda \frac{u_a}{L} \left(\frac{2}{\Delta \xi} + \frac{Ntu_a}{Le_m} \right) \Delta t$	-
	2	-	-	-
	3	-	$1 + \lambda \left(\frac{C_a}{C_c} \frac{Ntu_a}{Le_m} + \frac{P_{ct} L}{C_c R_{ct}} \right) \Delta t$	-
	4	-	$1 + \lambda \left(\frac{C_w}{C_t} Ntu_w + \frac{P_{ct} L}{C_t R_{ct}} \right) \Delta t$	-

Table 6.2 Coefficients in Governing Equations for a Wet Coil (Cont'd)

i	j	B _{ij}	C _{ij}	D _{ij}
1	4	-	$\lambda \frac{C_w}{C_t} Ntu_w \Delta t$	$\lambda \frac{P_{ct} L}{C_t R_{ct}} \Delta t$
2 to N-1	1	-	-	$\lambda \frac{u_a}{L} \frac{Ntu_a}{Le_m} \Delta t$
	3	$\lambda \frac{C_a}{C_c} \frac{Ntu_a}{Le_m} \Delta t$	-	-
	4	-	$\lambda \frac{C_w}{C_t} Ntu_w \Delta t$	$\lambda \frac{P_{ct} L}{C_t R_{ct}} \Delta t$
N	1	-	-	$\lambda \frac{u_a}{L} \frac{Ntu_a}{Le_m} \Delta t$
	3	$\lambda \frac{C_a}{C_c} \frac{Ntu_a}{Le_m} \Delta t$	-	-
	4	-	-	$\lambda \frac{P_{ct} L}{C_t R_{ct}} \Delta t$

Table 6.2 Coefficients in Governing Equations for a Wet Coil (Cont'd)

i	j	E _{ij}	G _{ij}	H _{ij}
1	2	$\lambda \frac{u_w}{L} Ntu_w \Delta t$	-	-
	3	$\lambda \frac{P_{ct} L}{C_c R_{ct}} \Delta t$	$-\lambda \frac{C_a}{C_c} \frac{Ntu_a}{Cp_a Le_m} h_{fg} \Delta t$	-
2 to N-1	0	-	$\lambda \frac{u_a}{L} \frac{Ntu_a}{Le_m} \Delta t$	-
	2	$\lambda \frac{u_w}{L} Ntu_w \Delta t$	-	-
	3	$\lambda \frac{P_{ct} L}{C_c R_{ct}} \Delta t$	$-\lambda \frac{C_a}{C_c} \frac{Ntu_a}{Cp_a Le_m} h_{fg} \Delta t$	$\lambda \frac{C_a}{C_c} \frac{Ntu_a}{Cp_a Le_m} h_{fg} \Delta t$
N	0	-	$\lambda \frac{u_a}{L} \frac{Ntu_a}{Le_m} \Delta t$	-
	3	$\lambda \frac{P_{ct} L}{C_c R_{ct}} \Delta t$	$-\lambda \frac{C_a}{C_c} \frac{Ntu_a}{Cp_a Le_m} h_{fg} \Delta t$	$\lambda \frac{C_a}{C_c} \frac{Ntu_a}{Cp_a Le_m} h_{fg} \Delta t$

Table 6.2 Coefficients in Governing Equations for a Wet Coil (Cont'd)

i	j	F _{ij}
1	0	-
	1	-
	2	$-\frac{u_w}{L} \left\{ \frac{2}{\Delta\xi} (T_{w1}^n - T_{w2}^n) + Ntu_w (T_{w1}^n - T_{t1}^n) \right\}$
	3	$-\frac{C_a}{C_c} \frac{Ntu_a}{Le_m} (T_{c1}^n - T_{a1}^n) - \frac{P_{ct} L}{C_c R_{ct}} (T_{c1}^n - T_{t1}^n) - \frac{C_a}{C_c} \frac{Ntu_a}{Cp_a Le_m} h_{fg} (w_{so1}^n - w_{a1}^n)$
	4	$-\frac{C_w}{C_t} Ntu_w (T_{t1}^n - T_{w1}^n) - \frac{P_{ct} L}{C_t R_{ct}} (T_{t1}^n - T_{c1}^n)$
2 to N-1	0	$-\frac{u_a}{L} \left\{ \frac{1}{\Delta\xi} (w_{ai}^n - w_{ai-1}^n) + \frac{Ntu_a}{Le_m} (w_{ai}^n - w_{soi}^n) \right\}$
	1	$-\frac{u_a}{L} \left\{ \frac{1}{\Delta\xi} (T_{ai}^n - T_{ai-1}^n) + \frac{Ntu_a}{Le_m} (T_{ai}^n - T_{ci}^n) \right\}$
	2	$\frac{u_w}{L} \left\{ \frac{1}{\Delta\xi} (T_{wi+1}^n - T_{wi}^n) - Ntu_w (T_{wi}^n - T_{ti}^n) \right\}$
	3	$-\frac{C_a}{C_c} \frac{Ntu_a}{Le_m} (T_{ci}^n - T_{ai}^n) - \frac{P_{ct} L}{C_c R_{ct}} (T_{ci}^n - T_{ti}^n) - \frac{C_a}{C_c} \frac{Ntu_a}{Cp_a Le_m} h_{fg} (w_{soi}^n - w_{ai}^n)$
	4	$-\frac{C_w}{C_t} Ntu_w (T_{ti}^n - T_{wi}^n) - \frac{P_{ct} L}{C_t R_{ct}} (T_{ti}^n - T_{ci}^n)$
N	0	$-\frac{u_a}{L} \left\{ \frac{2}{\Delta\xi} (w_{aN}^n - w_{aN-1}^n) + \frac{Ntu_a}{Le_m} (w_{aN}^n - w_{soN}^n) \right\}$
	1	$-\frac{u_a}{L} \left\{ \frac{2}{\Delta\xi} (T_{aN}^n - T_{aN-1}^n) + \frac{Ntu_a}{Le_m} (T_{aN}^n - T_{cN}^n) \right\}$
	2	-
	3	$-\frac{C_a}{C_c} \frac{Ntu_a}{Le_m} (T_{cN}^n - T_{aN}^n) - \frac{P_{ct} L}{C_c R_{ct}} (T_{cN}^n - T_{tN}^n) - \frac{C_a}{C_c} \frac{Ntu_a}{Cp_a Le_m} h_{fg} (w_{soN}^n - w_{aN}^n)$
	4	$-\frac{C_w}{C_t} Ntu_w (T_{tN}^n - T_{wN}^n) - \frac{P_{ct} L}{C_t R_{ct}} (T_{tN}^n - T_{cN}^n)$

Table 6.3 Coefficients in the Fin and Tube Core Equations for a Dry Coil

i	j	J _{ij}	K _{ij}	L _{ij}
1	3	-	$\frac{E'_{13} \frac{C'_{14}}{A'_{142}}}{A'_{132} - \frac{E'_{13} D'_{14}}{A'_{142}}}$	$\frac{F'_{13} + E'_{13} \frac{F'_{14}}{A'_{142}}}{A'_{132} - \frac{E'_{13} D'_{14}}{A'_{142}}}$
	4	-	$\frac{C'_{14}}{A'_{142} \frac{D'_{14} E'_{13}}{A'_{132}}}$	$\frac{F'_{14} + D'_{14} \frac{F'_{13}}{A'_{132}}}{A'_{142} - \frac{D'_{14} E'_{13}}{A'_{132}}}$
2 to N-1	3	$\frac{B'_{i3}}{(A'_{i32} - \frac{E'_{i3} D'_{i4}}{A'_{i42}})}$	$\frac{\frac{E'_{i3} C'_{i4}}{A'_{i42}}}{(A'_{i32} - \frac{E'_{i3} D'_{i4}}{A'_{i42}})}$	$\frac{F'_{i3} + \frac{E'_{i3} F'_{i4}}{A'_{i42}}}{(A'_{i32} - \frac{E'_{i3} D'_{i4}}{A'_{i42}})}$
	4	$\frac{\frac{D'_{i4} B'_{i3}}{A'_{i32}}}{(A'_{i42} - \frac{D'_{i4} E'_{i3}}{A'_{i32}})}$	$\frac{C'_{i4}}{(A'_{i42} - \frac{D'_{i4} E'_{i3}}{A'_{i32}})}$	$\frac{F'_{i4} + \frac{D'_{i4} F'_{i3}}{A'_{i32}}}{(A'_{i42} - \frac{D'_{i4} E'_{i3}}{A'_{i32}})}$
N	3	$\frac{B'_{N3}}{(A'_{N32} - \frac{E'_{N3} D'_{N4}}{A'_{N42}})}$	-	$\frac{F'_{N3} + \frac{E'_{N3} F'_{N4}}{A'_{N42}}}{(A'_{N32} - \frac{E'_{N3} D'_{N4}}{A'_{N42}})}$
	4	$\frac{\frac{D'_{N4} B'_{N3}}{A'_{N32}}}{(A'_{N42} - \frac{D'_{N4} E'_{N3}}{A'_{N32}})}$	-	$\frac{F'_{N4} + \frac{D'_{N4} F'_{N3}}{A'_{N32}}}{(A'_{N42} - \frac{D'_{N4} E'_{N3}}{A'_{N32}})}$

Note: Expressions for coefficients A', B', ... , F' are shown in Table 6.1

Table 6.4 Coefficients in the Fin and Tube Core Equations for a Wet Coil

i	j	I_{ij}	J_{ij}
1	3	-	-
	4	-	-
2 to N-1	3	$\frac{H_{i3}}{\left(A_{i32} - \frac{E_{i3} D_{i4}}{A_{i42}} - G_{i3} \frac{\partial w_{soi}}{\partial T_{ci}}\right)}$	$\frac{B_{i3}}{\left(A_{i32} - \frac{E_{i3} D_{i4}}{A_{i42}} - G_{i3} \frac{\partial w_{soi}}{\partial T_{ci}}\right)}$
	4	$\frac{\frac{D_{i4} H_{i3}}{\left(A_{i32} - G_{i3} \frac{\partial w_{soi}}{\partial T_{ci}}\right)}}{A_{i42} - \frac{D_{i4} E_{i3}}{\left(A_{i32} - G_{i3} \frac{\partial w_{soi}}{\partial T_{ci}}\right)}}$	$\frac{\frac{D_{i4} B_{i3}}{\left(A_{i32} - G_{i3} \frac{\partial w_{soi}}{\partial T_{ci}}\right)}}{A_{i42} - \frac{D_{i4} E_{i3}}{\left(A_{i32} - G_{i3} \frac{\partial w_{soi}}{\partial T_{ci}}\right)}}$
N	3	$\frac{H_{N3}}{A_{N32} - \frac{E_{N3} D_{N4}}{A_{N42}} - G_{N3} \frac{\partial w_{soN}}{\partial T_{cN}}}$	$\frac{B_{N3}}{A_{N32} - \frac{E_{N3} D_{N4}}{A_{N42}} - G_{N3} \frac{\partial w_{soN}}{\partial T_{cN}}}$
	4	$\frac{\frac{D_{N4} H_{N3}}{\left(A_{N32} - G_{N3} \frac{\partial w_{soN}}{\partial T_{cN}}\right)}}{A_{N42} - \frac{D_{N4} E_{N3}}{\left(A_{N32} - G_{N3} \frac{\partial w_{soN}}{\partial T_{cN}}\right)}}$	$\frac{\frac{D_{N4} B_{N3}}{\left(A_{N32} - G_{N3} \frac{\partial w_{soN}}{\partial T_{cN}}\right)}}{A_{N42} - \frac{D_{N4} E_{N3}}{\left(A_{N32} - G_{N3} \frac{\partial w_{soN}}{\partial T_{cN}}\right)}}$

Note: Expressions for coefficients A, B, ... , H are shown in Table 6.2

Table 6.4 Coefficients in the Fin and Tube Core Equations for a Wet Coil (Cont'd)

i	j	K _{ij}	L _{ij}
1	3	$\frac{\frac{E_{13} C_{14}}{A_{142}}}{A_{132} - \frac{E_{13} D_{14}}{A_{142}} - G_{13} \frac{\partial w_{sol}}{\partial T_{c1}}}$	$\frac{F_{13} + \frac{E_{13} F_{14}}{A_{142}}}{A_{132} - \frac{E_{13} D_{14}}{A_{142}} - G_{13} \frac{\partial w_{sol}}{\partial T_{c1}}}$
	4	$\frac{\frac{C_{14}}{A_{142} - \frac{D_{14} E_{13}}{(A_{132} - G_{13} \frac{\partial w_{sol}}{\partial T_{c1}})}}}{(A_{132} - G_{13} \frac{\partial w_{sol}}{\partial T_{c1}})}$	$\frac{F_{14} + \frac{D_{14} F_{13}}{(A_{132} - G_{13} \frac{\partial w_{sol}}{\partial T_{c1}})}}{A_{142} - \frac{D_{14} E_{13}}{(A_{132} - G_{13} \frac{\partial w_{sol}}{\partial T_{c1}})}}$
2 to N-1	3	$\frac{\frac{E_{i3} C_{i4}}{A_{i42}}}{(A_{i32} - \frac{E_{i3} D_{i4}}{A_{i42}} - G_{i3} \frac{\partial w_{soi}}{\partial T_{ci}})}$	$\frac{F_{i3} + \frac{E_{i3} F_{i4}}{A_{i42}}}{(A_{i32} - \frac{E_{i3} D_{i4}}{A_{i42}} - G_{i3} \frac{\partial w_{soi}}{\partial T_{ci}})}$
	4	$\frac{\frac{C_{i4}}{A_{i42} - \frac{D_{i4} E_{i3}}{(A_{i32} - G_{i3} \frac{\partial w_{soi}}{\partial T_{ci}})}}}{(A_{i32} - G_{i3} \frac{\partial w_{soi}}{\partial T_{ci}})}$	$\frac{F_{i4} + \frac{D_{i4} F_{i3}}{(A_{i32} - G_{i3} \frac{\partial w_{soi}}{\partial T_{ci}})}}{A_{i42} - \frac{D_{i4} E_{i3}}{(A_{i32} - G_{i3} \frac{\partial w_{soi}}{\partial T_{ci}})}}$
N	3	-	$\frac{F_{N3} + \frac{E_{N3} F_{N4}}{A_{N42}}}{A_{N32} - \frac{E_{N3} D_{N4}}{A_{N42}} - G_{N3} \frac{\partial w_{soN}}{\partial T_{cN}}}$
	4	-	$\frac{F_{N4} + \frac{D_{N4} F_{N3}}{(A_{N32} - G_{N3} \frac{\partial w_{soN}}{\partial T_{cN}})}}{A_{N42} - \frac{D_{N4} E_{N3}}{(A_{N32} - G_{N3} \frac{\partial w_{soN}}{\partial T_{cN}})}}$

Note: Expressions for coefficients A, B, ... , H are shown in Table 6.2

Table 7.1 Summary of Manufacturer's Data of Coils Tested

Cases* Parameters	CB01	CB02	CB03	CB04	CB05	CB06	CB07	CB08	(Units)
A_a	0.1	0.1	0.1	0.58	0.58	0.58	0.58	0.58	(m ²)
W_a	0.49	0.49	0.49	0.8	0.8	0.8	0.8	0.8	(m)
N_r	3	3	3	3	3	3	3	3	-
N_{tpr}	8	8	8	16	16	16	16	16	-
C_n	0.25	0.25	0.25	0.17	0.17	0.17	0.17	0.17	-
Config.	Triangular tube arrays								-
P_d	0.0012	0.0012	0.0012	0.001	0.001	0.001	0.001	0.001	(m)
N_p	4	4	4	4.6	4.6	4.6	4.6	4.6	-
D_o	0.0099	0.0099	0.0099	0.0129	0.0129	0.0129	0.0129	0.0129	(m)
D_i	0.008	0.008	0.008	0.011	0.011	0.011	0.011	0.011	(m)
D_x	0.0095	0.0095	0.0095	0.0127	0.0127	0.0127	0.0127	0.0127	(m)
x_a	0.025	0.025	0.025	0.0316	0.0316	0.0316	0.0316	0.0316	(m)
x_b	0.02	0.02	0.02	0.0275	0.0275	0.0275	0.0275	0.0275	(m)
s	0.002	0.002	0.002	0.002	0.002	0.002	0.002	0.002	(m)
y	0.0002	0.0002	0.0002	0.0001	0.0001	0.0001	0.0001	0.0001	(m)
k_f	0.1731	0.1731	0.1731	0.1731	0.1731	0.1731	0.1731	0.1731	(W/mK)
F_s	18.489	18.489	18.489	25.18	25.18	25.18	25.18	25.18	-
A_o	5.5468	5.5468	5.5468	43.813	43.813	43.813	43.813	43.813	(m ²)
(A_o/A_i)	18.392	18.392	18.392	23.025	23.025	23.025	23.025	23.025	-
(A_f/A_o)	0.939	0.939	0.939	0.9517	0.9517	0.9517	0.9517	0.9517	-
σ	0.5486	0.5486	0.5486	0.5614	0.5614	0.5614	0.5614	0.5614	-
D_h	0.0024	0.0024	0.0024	0.0025	0.0025	0.0025	0.0025	0.0025	(m)
(A_o/A_t)	14.877	14.877	14.877	19.634	19.634	19.634	9.634	19.634	-
(A_o/A_x)	15.439	15.439	15.439	19.943	19.943	19.943	19.943	19.943	-
T_{we}	7	7	7	7	7	7	9	7	(°C)
\dot{M}_w	0.13	0.13	0.13	0.67	0.67	1.83	0.67	0.67	(kg/s)
T_{ac}	24	27	30	27	27	27	27	25	(°C)
T_{wbe}	17	19.5	22	19.5	19.5	19.5	19.5	17	(°C)
\dot{M}_a	0.23	0.23	0.23	1.2	2	1.2	1.2	1.2	(kg/s)
Q_s	2.533	2.962	3.085	12.57	17.23	15.01	11.52	12.22	(kW)
Q_l	0.078	0.302	0.83	4.31	4.88	8.62	2.68	1.28	(kW)
Q_t	2.611	3.264	3.915	16.88	22.11	23.63	14.2	13.5	(kW)

* Data of Cases CB01-CB03 are pertaining to Fan-coil Unit Model 42CMA, Unit 004 of Carrier Corporation, USA.
Data of Cases CB04-CB08 are pertaining to Air-handling Unit Model 40HW, Unit 008 of Carrier Corporation, USA.

Table 7.1 Summary of Manufacturer's Data of Coils Tested (Cont'd)

Cases* Parameters	CA01	CA02	CA03	CA04	CA05	CA06	CA07	CA08	CA09	(Units)
A _a	0.44	0.44	0.44	0.44	0.44	0.44	0.87	0.87	0.87	(m ²)
W _a	0.86	0.86	0.86	0.86	0.86	0.86	1.36	1.36	1.36	(m)
N _r	4	4	4	4	6	6	4	4	4	-
N _{tp}	16	16	16	16	16	16	20	20	20	-
C _n	0.5	1	0.5	1	0.5	1	0.5	1	0.5	-
Config	Triangular tube arrays									-
P _d	0.001	0.001	0.001	0.001	0.001	0.001	0.001	0.001	0.001	(m)
N _p	4.6	4.6	4.6	4.6	4.6	4.6	4.6	4.6	4.6	-
D _o	0.013	0.013	0.013	0.013	0.013	0.013	0.013	0.013	0.013	(m)
D _i	0.011	0.011	0.011	0.011	0.011	0.011	0.011	0.011	0.011	(m)
D _x	0.0127	0.0127	0.0127	0.0127	0.0127	0.0127	0.0127	0.0127	0.0127	(m)
x _a	0.0318	0.0318	0.0318	0.0318	0.0318	0.0318	0.0318	0.0318	0.0318	(m)
x _b	0.0275	0.0275	0.0275	0.0275	0.0275	0.0275	0.0275	0.0275	0.0275	(m)
s	0.0032	0.0032	0.0018	0.0018	0.0032	0.0032	0.0032	0.0032	0.0018	(m)
y	0.0002	0.0002	0.0002	0.0002	0.0002	0.0002	0.0002	0.0002	0.0002	(m)
k _f	0.1731	0.1731	0.1731	0.1731	0.1731	0.1731	0.1731	0.1731	0.1731	(W/mK)
F _s	15.915	15.915	26.892	26.892	15.915	15.915	15.915	15.915	26.892	-
A _o	27.947	27.947	47.222	47.222	41.92	41.92	55.13	55.13	93.154	(m ²)
(A _o /A _i)	14.645	14.645	24.746	24.746	14.645	14.645	14.645	14.645	24.746	-
(A _f /A _o)	0.9231	0.9231	0.9562	0.9562	0.9231	0.9231	0.9231	0.9231	0.9562	-
σ	0.5628	0.5628	0.5415	0.5415	0.5628	0.5628	0.5628	0.5628	0.5415	-
D _h	0.0039	0.0039	0.0022	0.0022	0.0039	0.0039	0.0039	0.0039	0.0022	(m)
(A _o /A _t)	12.388	12.388	20.933	20.933	12.388	12.388	12.388	12.388	20.933	-
(A _o /A _x)	12.685	12.685	21.434	21.434	12.685	12.685	12.685	12.685	21.434	-
T _{we}	7.22	7.22	7.22	7.22	7.22	7.22	7.22	7.22	7.22	(°C)
M _w ^o	0.82	0.66	1.08	0.87	1.12	0.97	1.76	1.52	2.32	(kg/s)
T _{ae}	26.67	26.67	26.67	26.67	26.67	26.67	26.67	26.67	26.67	(°C)
T _{wbe}	19.44	19.44	19.44	19.44	19.44	19.44	19.44	19.44	19.44	(°C)
M _a ^o	1.34	1.34	1.34	1.34	1.34	1.34	2.64	2.64	2.64	(kg/s)
Q _s	14.566	13.222	17.992	16.124	18.14	16.796	30.087	27.859	37.304	(kW)
Q _l	4.424	2.138	7.098	4.066	7.94	5.864	10.823	7.491	16.686	(kW)
Q _t	18.99	15.36	25.09	20.19	26.08	22.66	40.91	35.35	53.99	(kW)

* Data of Cases CA01-CA06 are pertaining to Air-handling Unit Model 39L, Unit 06S of Carrier Corporation, USA.
Data of Cases CA07-CA12 are pertaining to Air-handling Unit Model 39L, Unit 12S of Carrier Corporation, USA.

Table 7.1 Summary of Manufacturer's Data of Coils Tested (Cont'd)

Cases* Parameters	CA10	CA11	CA12	CA13	CA14	CA15	CA16	CA17	CA18	(Units)
A_a	0.87	0.87	0.87	1.59	1.59	1.59	1.59	1.59	1.59	(m ²)
W_a	1.36	1.36	1.36	1.66	1.66	1.66	1.66	1.66	1.66	(m)
N_r	4	6	6	4	4	4	4	6	6	-
N_{tp}	20	20	20	30	30	30	30	30	30	-
C_n	1	1	2	0.5	1	1	2	1	2	-
Config	Triangular tube arrays									-
P_d	0.001	0.001	0.001	0.001	0.001	0.001	0.001	0.001	0.001	(m)
N_p	4.6	4.6	4.6	4.6	4.6	4.6	4.6	4.6	4.6	-
D_o	0.013	0.013	0.013	0.013	0.013	0.013	0.013	0.013	0.013	(m)
D_i	0.011	0.011	0.011	0.011	0.011	0.011	0.011	0.011	0.011	(m)
D_x	0.0127	0.0127	0.0127	0.0127	0.0127	0.0127	0.0127	0.0127	0.0127	(m)
x_a	0.0318	0.0318	0.0318	0.0318	0.0318	0.0318	0.0318	0.0318	0.0318	(m)
x_b	0.0275	0.0275	0.0275	0.0275	0.0275	0.0275	0.0275	0.0275	0.0275	(m)
s	0.0018	0.0032	0.0032	0.0032	0.0032	0.0018	0.0018	0.0032	0.0032	(m)
y	0.0002	0.0002	0.0002	0.0002	0.0002	0.0002	0.0002	0.0002	0.0002	(m)
k_f	0.1731	0.1731	0.1731	0.1731	0.1731	0.1731	0.1731	0.1731	0.1731	(W/mK)
F_s	26.892	15.915	15.915	15.915	15.915	26.892	26.892	15.915	15.915	-
A_o	93.154	82.695	82.695	101.16	101.16	170.93	170.93	151.73	151.73	(m ²)
(A_o/A_i)	24.746	14.645	14.645	14.645	14.645	24.746	24.746	14.645	14.645	-
(A_f/A_o)	0.9562	0.9231	0.9231	0.9231	0.9231	0.9562	0.9562	0.9231	0.9231	-
σ	0.5415	0.5628	0.5628	0.5628	0.5628	0.5415	0.5415	0.5628	0.5628	-
D_h	0.0022	0.0039	0.0039	0.0039	0.0039	0.0022	0.0022	0.0039	0.0039	(m)
(A_o/A_t)	20.933	12.388	12.388	12.388	12.388	20.933	20.933	12.388	12.388	-
(A_o/A_x)	21.434	12.685	12.685	12.685	12.685	21.434	21.434	12.685	12.685	-
T_{we}	7.22	7.22	7.22	7.22	7.22	7.22	7.22	7.22	7.22	(°C)
^oM_w	2	2.13	1.95	3.32	2.93	3.87	3.1	4.04	3.75	(kg/s)
T_{ae}	26.67	26.67	26.67	26.67	26.67	26.67	26.67	26.67	26.67	(°C)
T_{wbe}	19.44	19.44	19.44	19.44	19.44	19.44	19.44	19.44	19.44	(°C)
^oM_a	2.64	2.64	2.64	4.84	4.84	4.84	4.84	4.84	4.84	(kg/s)
Q_s	34.359	35.102	33.457	55.985	52.479	64.942	57.883	65.721	63.043	(kW)
Q_l	12.271	14.488	11.913	21.335	15.781	25.208	14.247	28.329	24.267	(kW)
Q_t	46.63	49.59	45.37	77.32	68.26	90.15	72.13	94.05	87.31	(kW)

* Data of Cases CA07-CA12 are pertaining to Air-handling Unit Model 39L, Unit 12S of Carrier Corporation, USA.
Data of Cases CA13-CA18 are pertaining to Air-handling Unit Model 39L, Unit 21S of Carrier Corporation, USA.

Table 9.1 Material Property of the Composite Walls and Slab of the Model Room

Properties	Concrete	Plastering	Window Glass
Dry density (kg/m ³)	2600	2200	2500
Dry thermal conductivity (W/mK)	1.442	1.442	1.05
Dry porosity (m ³ /m ³)	0.3	0.3	-
Dry specific heat (J/kgK)	879	879	750
Initial moisture content (m ³ /m ³):			
External layer of Wall 1	0.06	0.07	-
Internal layer of Wall 1 and	0.06	0.06	-
Internal and external layers of Wall 2 - 6			
Initial temperature (K)	300	300	300
Emmisivity (long wave radiation)	0.8	0.8	0.8
Absorptance (short wave radiation)	-	-	0.2
Transmittance (short wave radiation)	-	-	0.4
Shading coefficient	-	-	0.53

Table 9.2 Indoor Air and Usage Conditions of the Model Room

Room air Set-point Conditions	Temperature	298 K (25 °C)
	Rel. Humidity	50%
Corridor air condition (fixed)	Temperature	300 K (27 °C)
	Rel. Humidity	65%
Ventilation rate (for one occupant)	7 l/s	
Heat gain from occupant	Sensible	65 W
	Latent	55 W
Infiltration rate (continuous)	0.5 air-changes per hour	
Lighting and appliances load (total)	225 W	

Table 9.3 Design Cooling Load of the Model Room

Peak Time: 14:00 hr. in October

Peak Cooling Load (W)			
Components	Sensible	Latent	Total
Solar	783	0	783
Conduction (Glass)	175	0	175
Conduction (Wall)	263	0	263
Occupants	65	55	120
Lighting	225	0	225
Infiltration	33	129	162
Room Total	1544	184	1728
Ventilation	61	240	301
Block Total	1605	424	2029

Table 9.4 Characteristics of the Fan-coil Unit Serving the Model Room

Supply air flow rate (\dot{V}_{sa})		0.125 m ³ /s (0.15 kg/s)
Chilled water flow rate (control valve open) (\dot{m}_w)		0.12 kg/s
Chilled water supply temperature (fixed) (T_{ws})		280 K (7 °C)
Characteristics of the coil:		
No. of rows (N_r)		3
Fin spacing (s)		2 mm
Face area (A_a)		0.12 m ² (600 mm x 200 mm)
Circuit number (C_n)		1.5
No. of tubes per row (N_{tpr})		10
Diameter of tube (D)		9.53 mm / 8 mm (outer / inner)
Tube spacing:	Transverse (x_a)	20 mm
	Longitudinal (x_b)	20 mm
Fin thickness (y)		0.15 mm
Rated cooling capacity (Q_{cc})		1684 W (sensible) 2196 W (total)

Figure 1.1 Schematic diagram of an air-cooled air-conditioning system

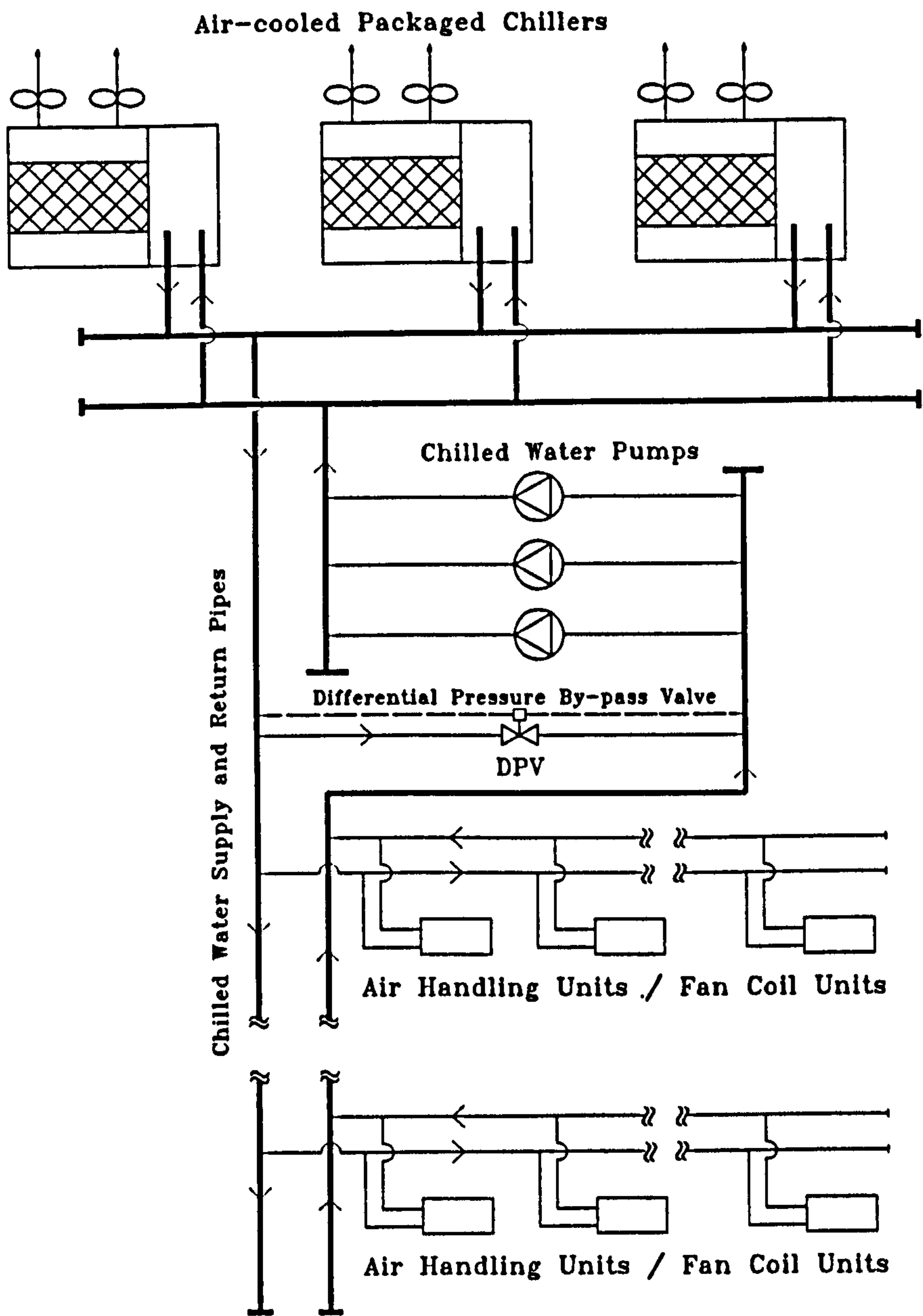


Figure 1.2

Variations of coil sensible, latent and total cooling capacities with chilled water flow rate

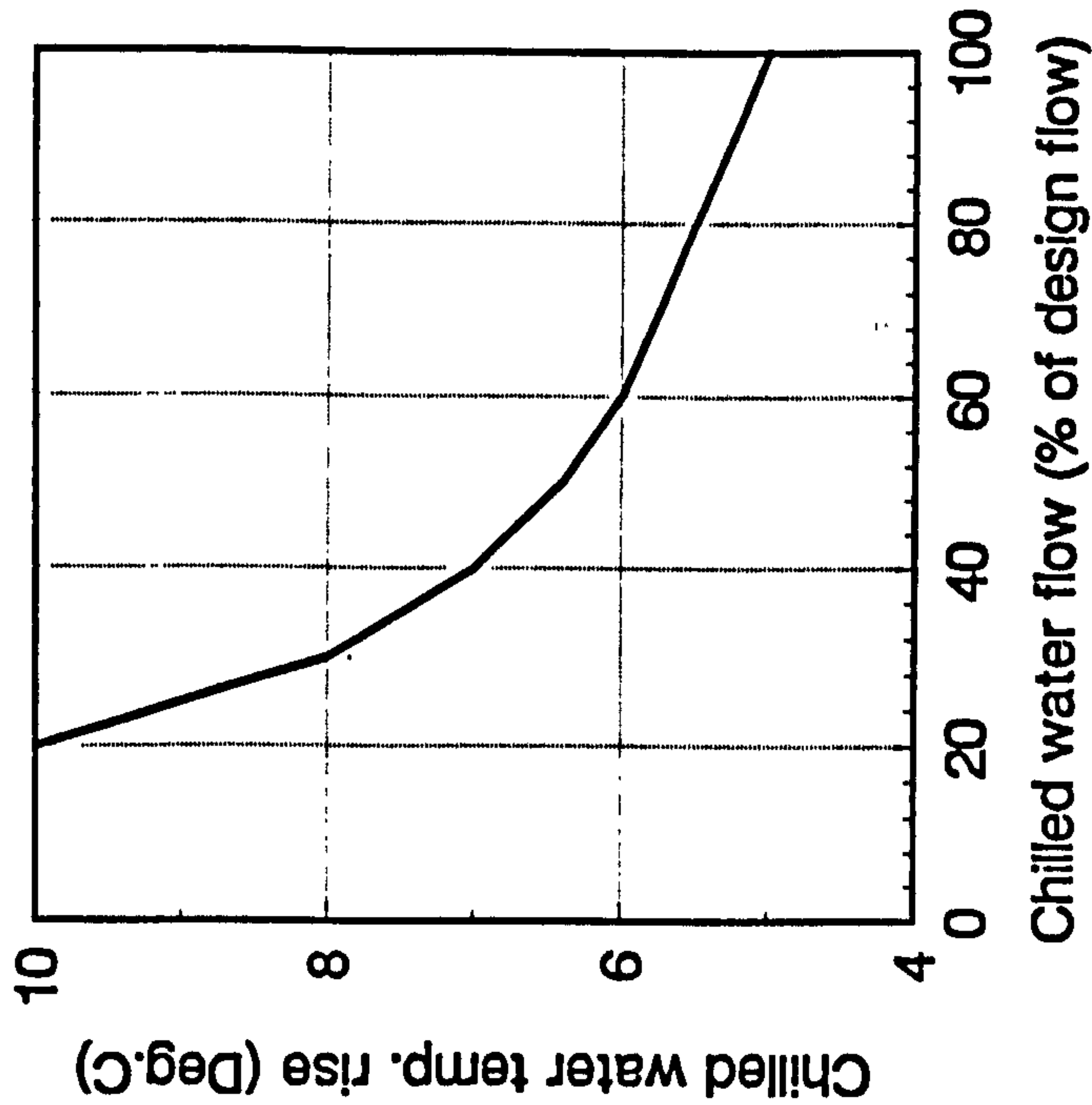
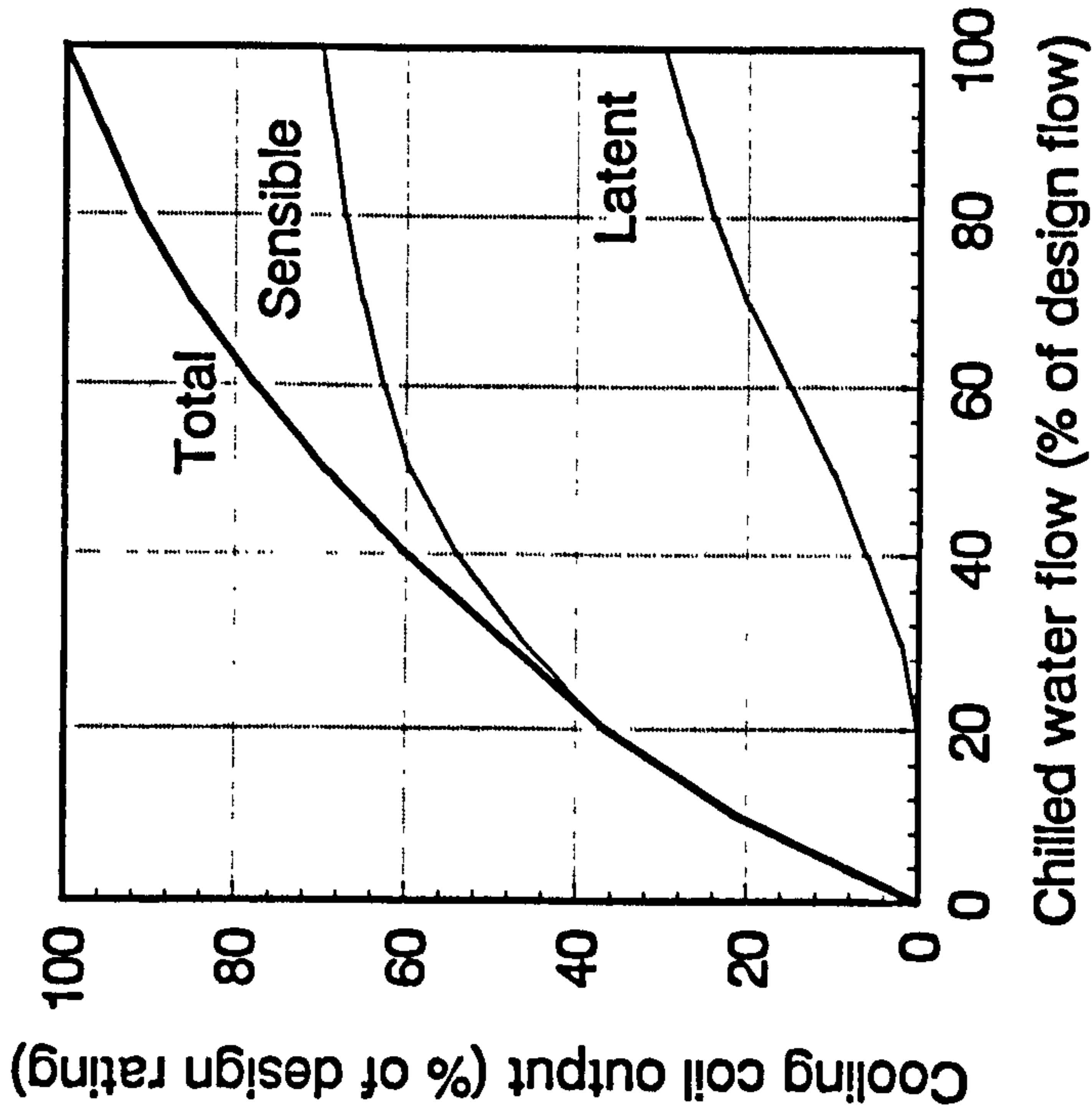
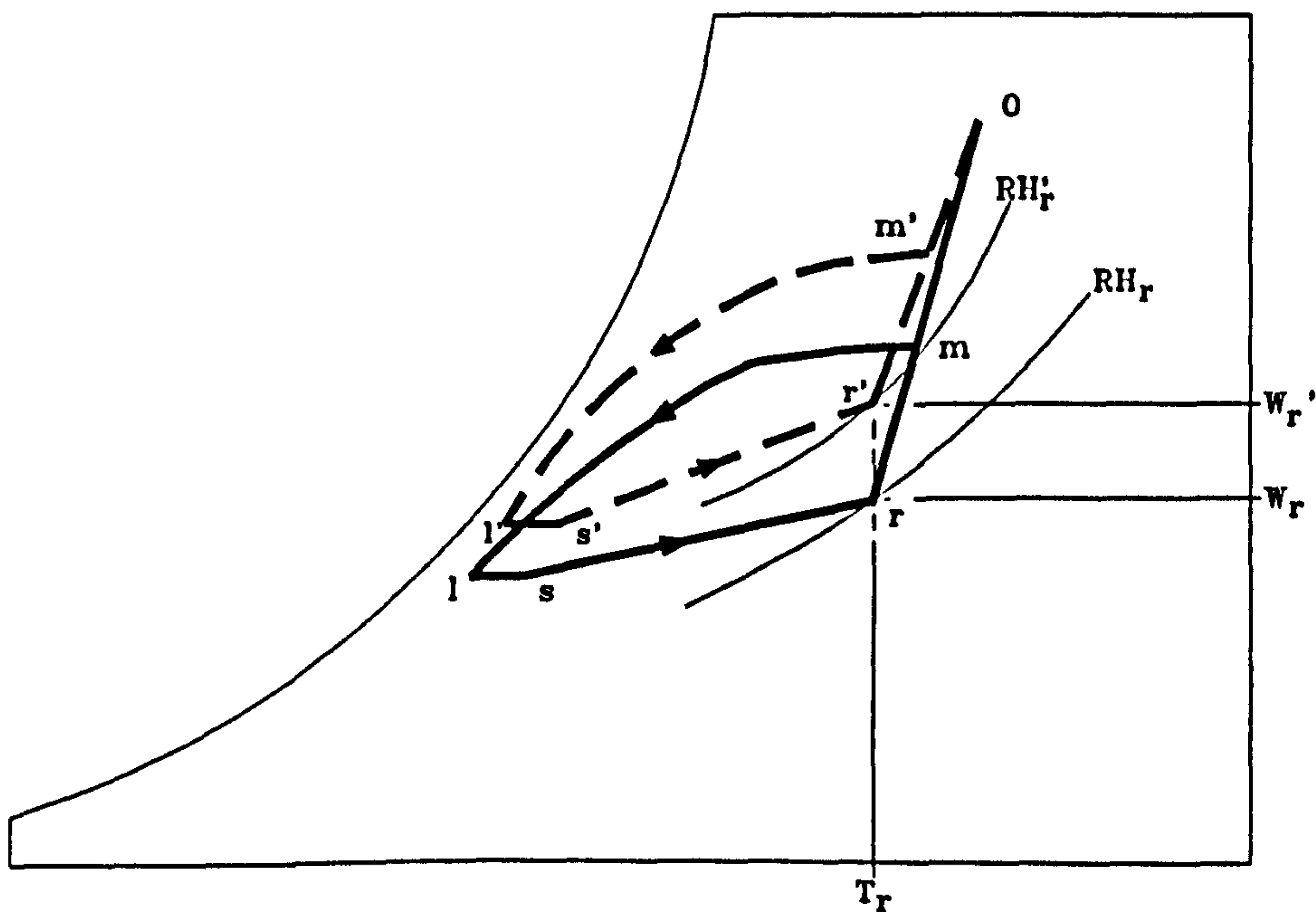


Figure 1.3 Psychrometric cycles of an all-air system at full and part load conditions

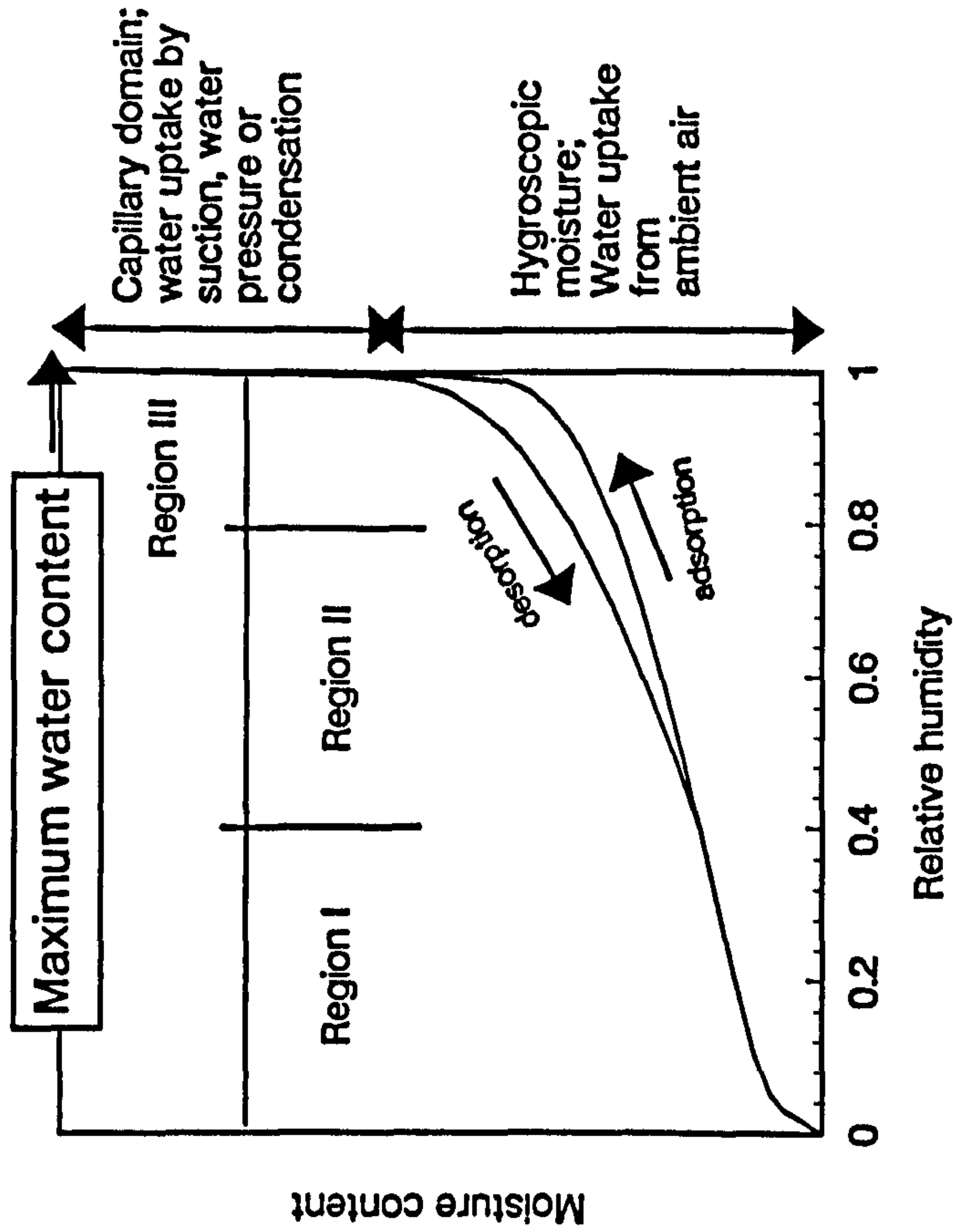


———— Full-load Cycle
 - - - - Part-load Cycle

T_r Room Air Dry Bulb Temperature
 W_r Room Air Humidity Ratio
 RH_r Room Air Relative Humidity
 0 State Point of Outdoor Condition
 m State Point of Mixture Condition
 r State Point of Room Condition
 l State Point of Leaving Coil Condition
 s State Point of Supply Air Condition

Figure 2.1

(a) Typical sorption isotherm of building materials



(b) Sorption isotherm of cement paste

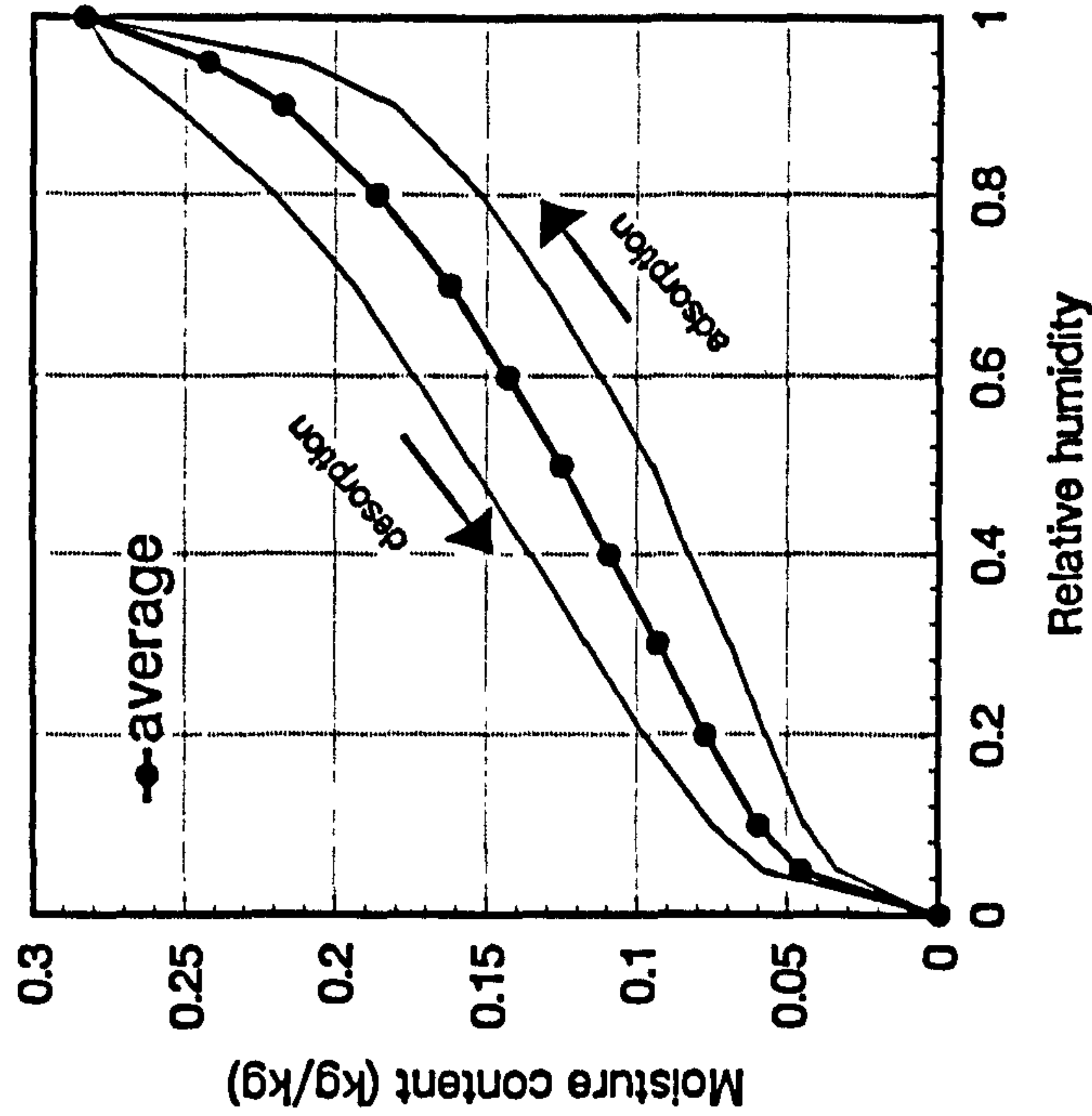


Figure 2.2 A picture of moisture transfer in porous medium

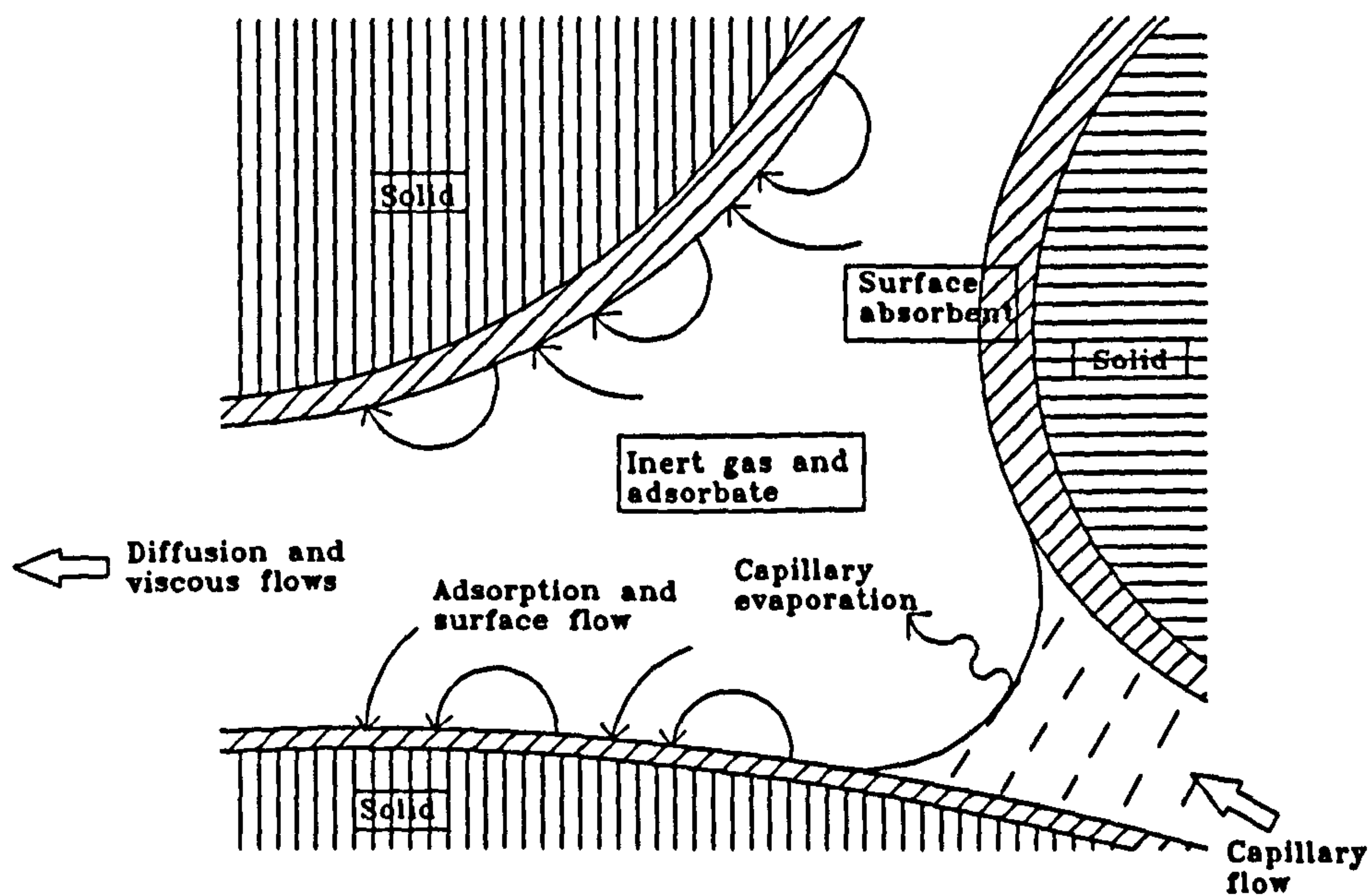


Figure 3.1
Simulation results on drying of a slab of concrete

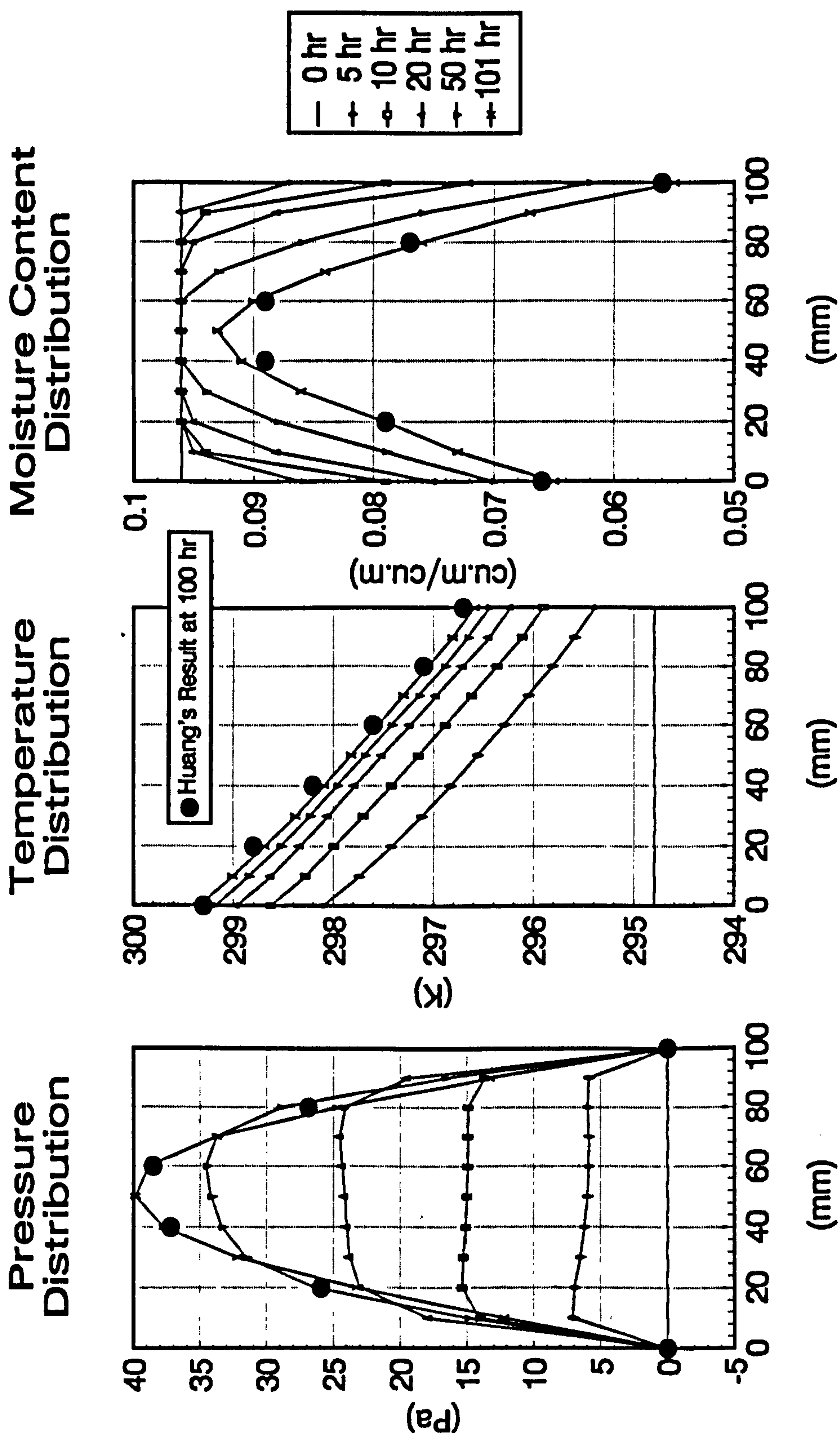


Figure 3.2
Simulation results on drying of a slab of cement paste

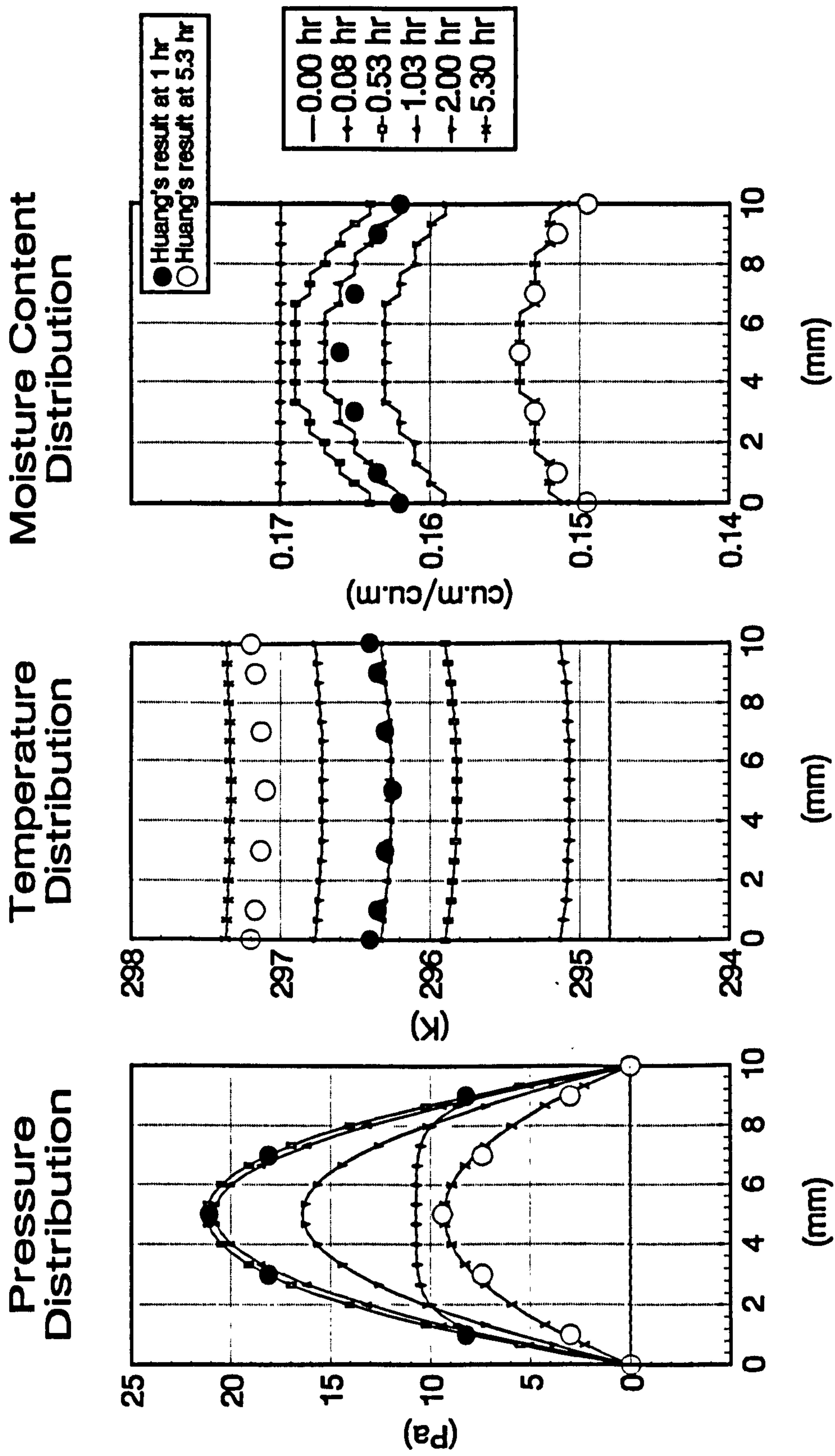


Figure 3.3
Comparison of filtration
flow and diffusion
(drying of a slab of
concrete)

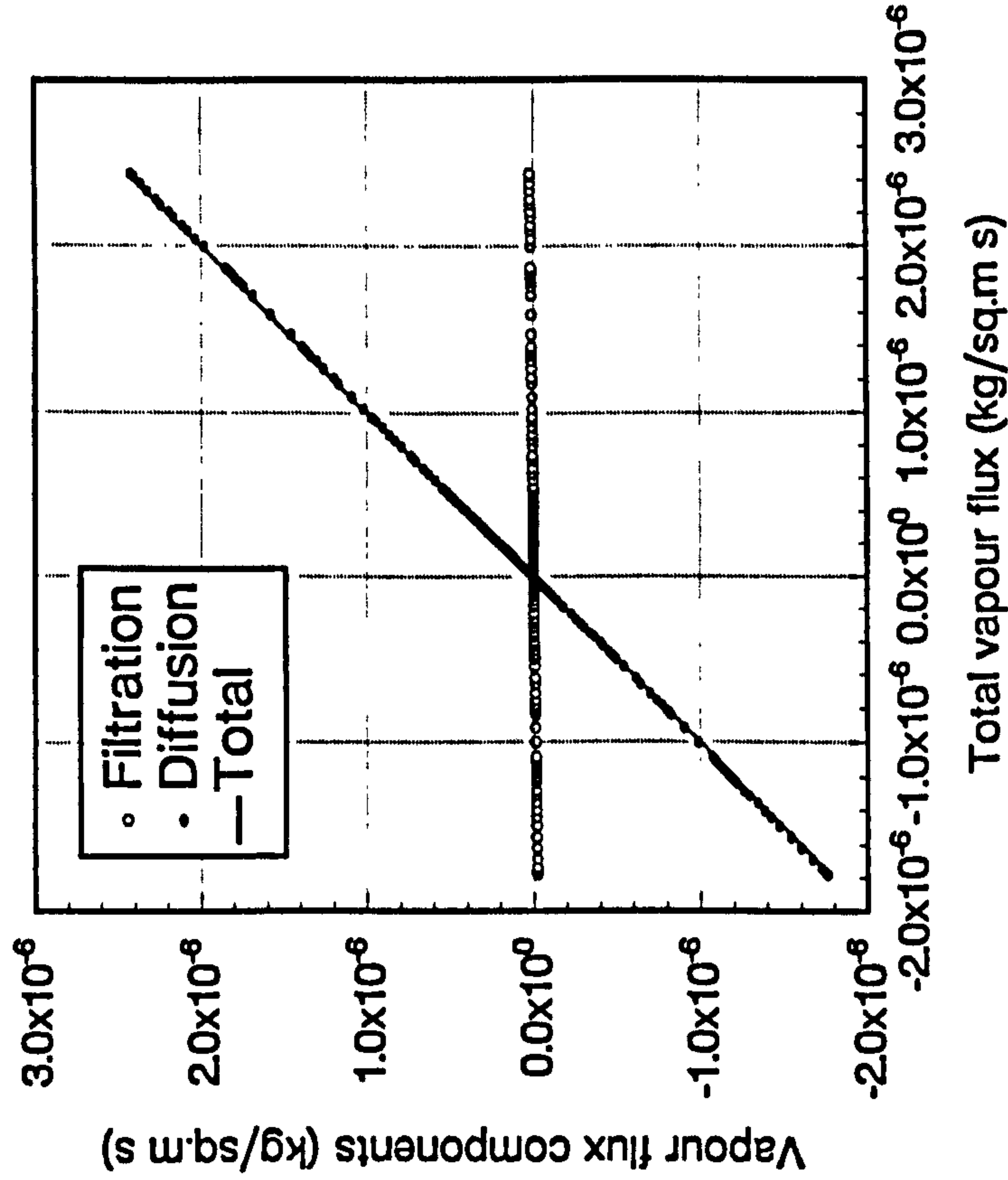


Figure 3.4
Ratio of filtration flow
to total moisture transfer
(%) (drying of a slab of
concrete)

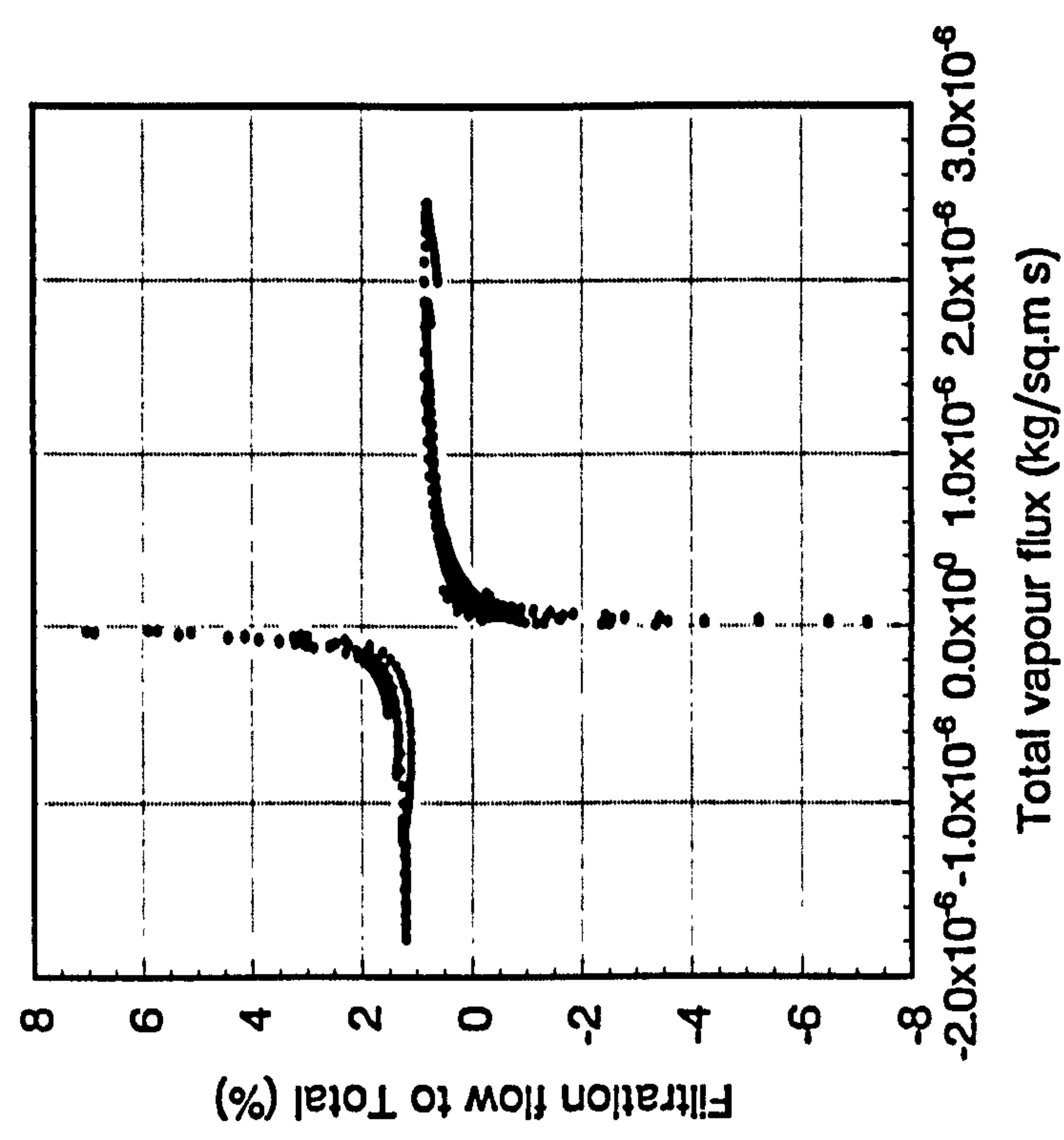


Figure 3.5
Correlations between Vapour flux and gradients of various driving potentials

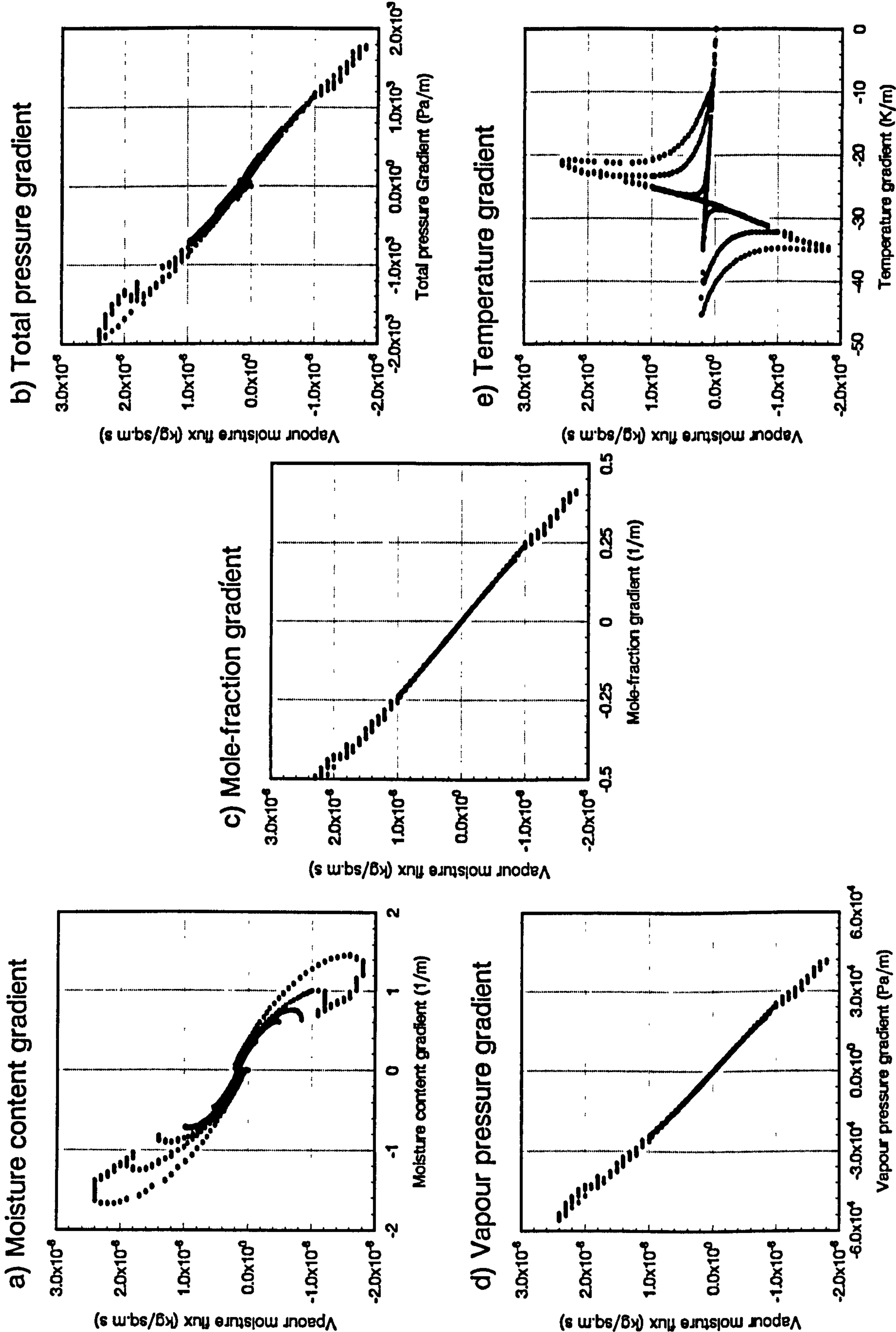


Figure 4.1
Comparison of permeability values based on Huang's
equation and the simplified equation

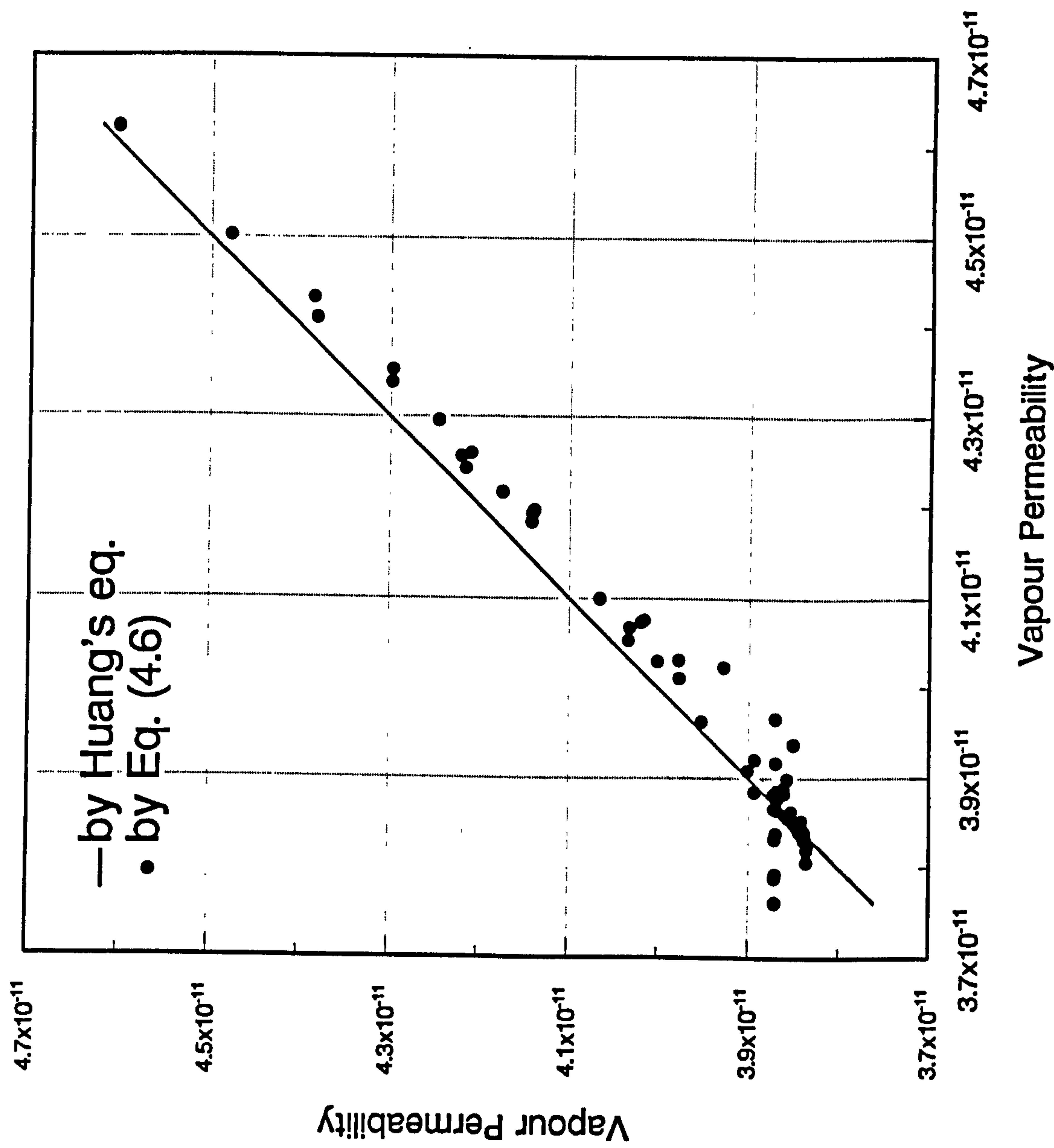


Figure 4.2 Discretization scheme for a wall or slab

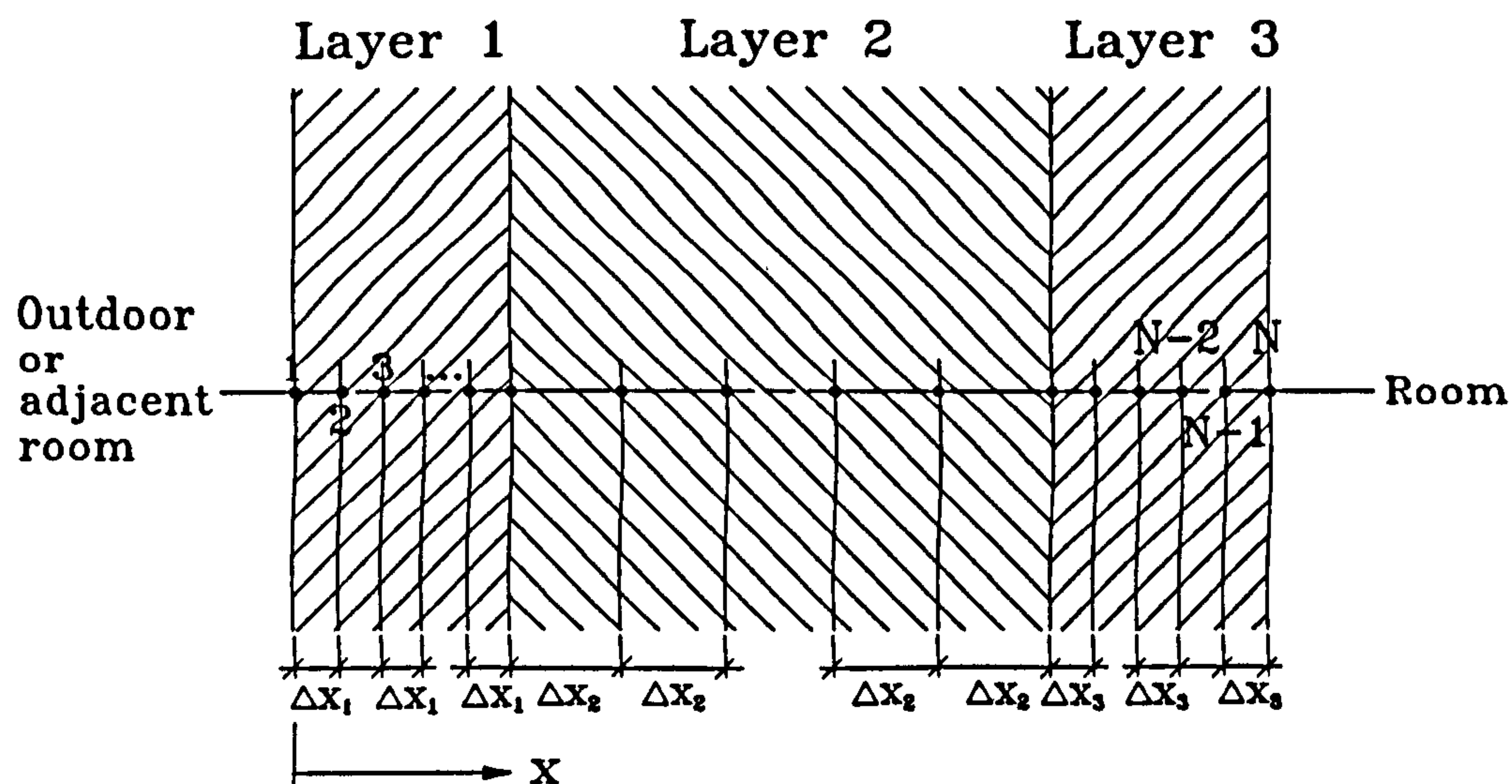


Figure 4.3 Boundary control volume for a wall or slab

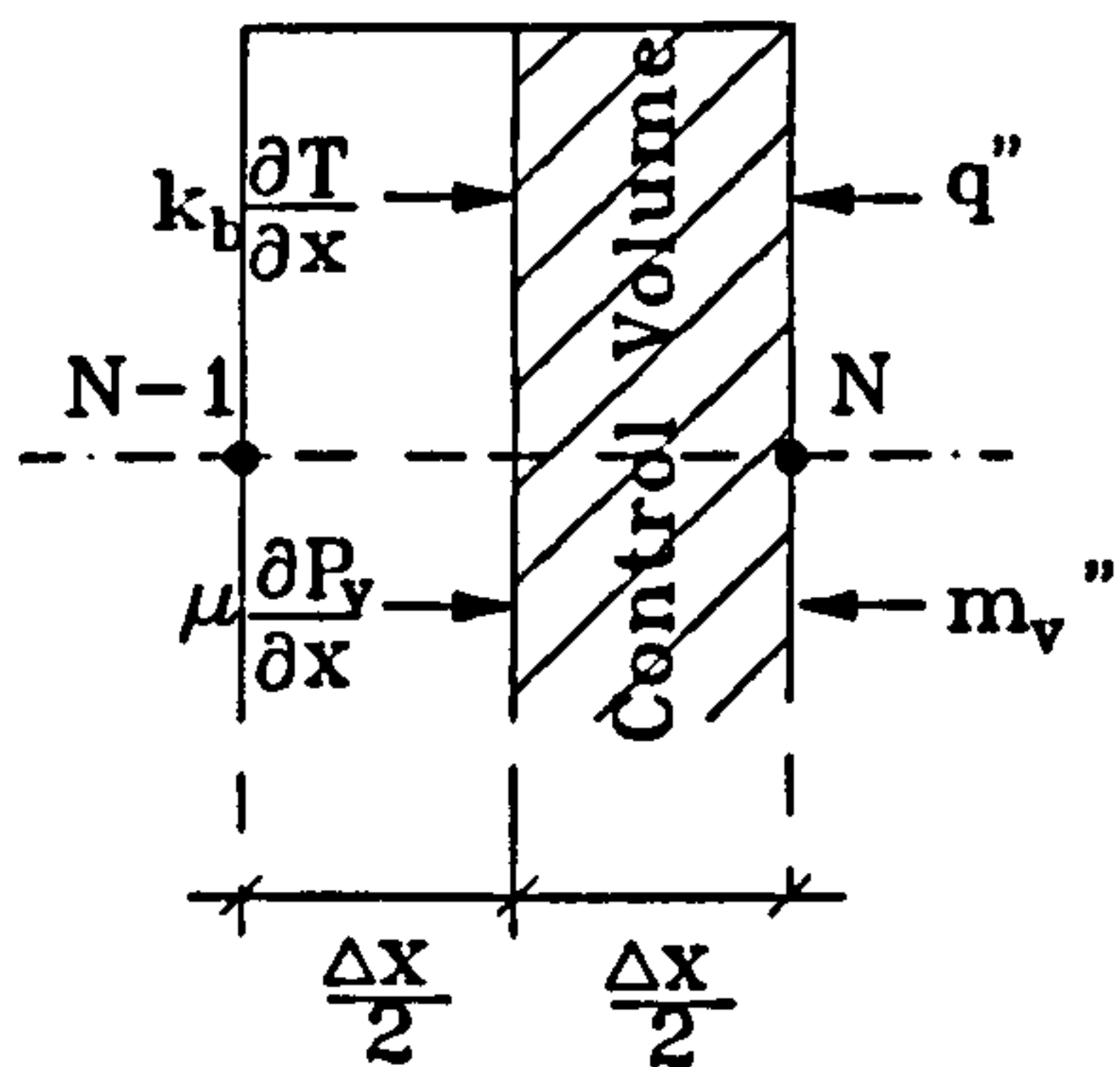


Figure 4.4 Control volume at the interface plane

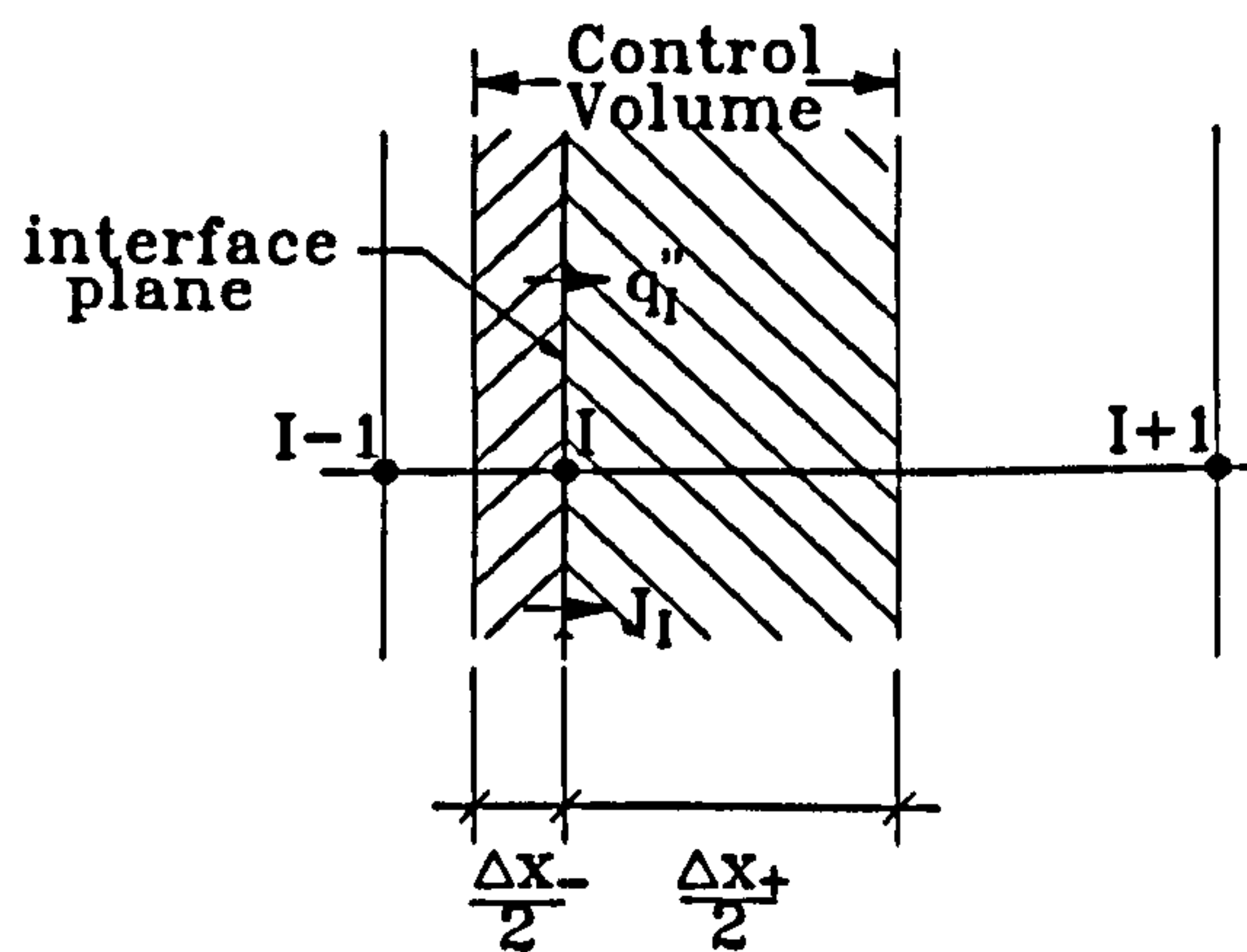


Figure 4.5
Simulation results from differential permeability
model on drying of a slab of concrete

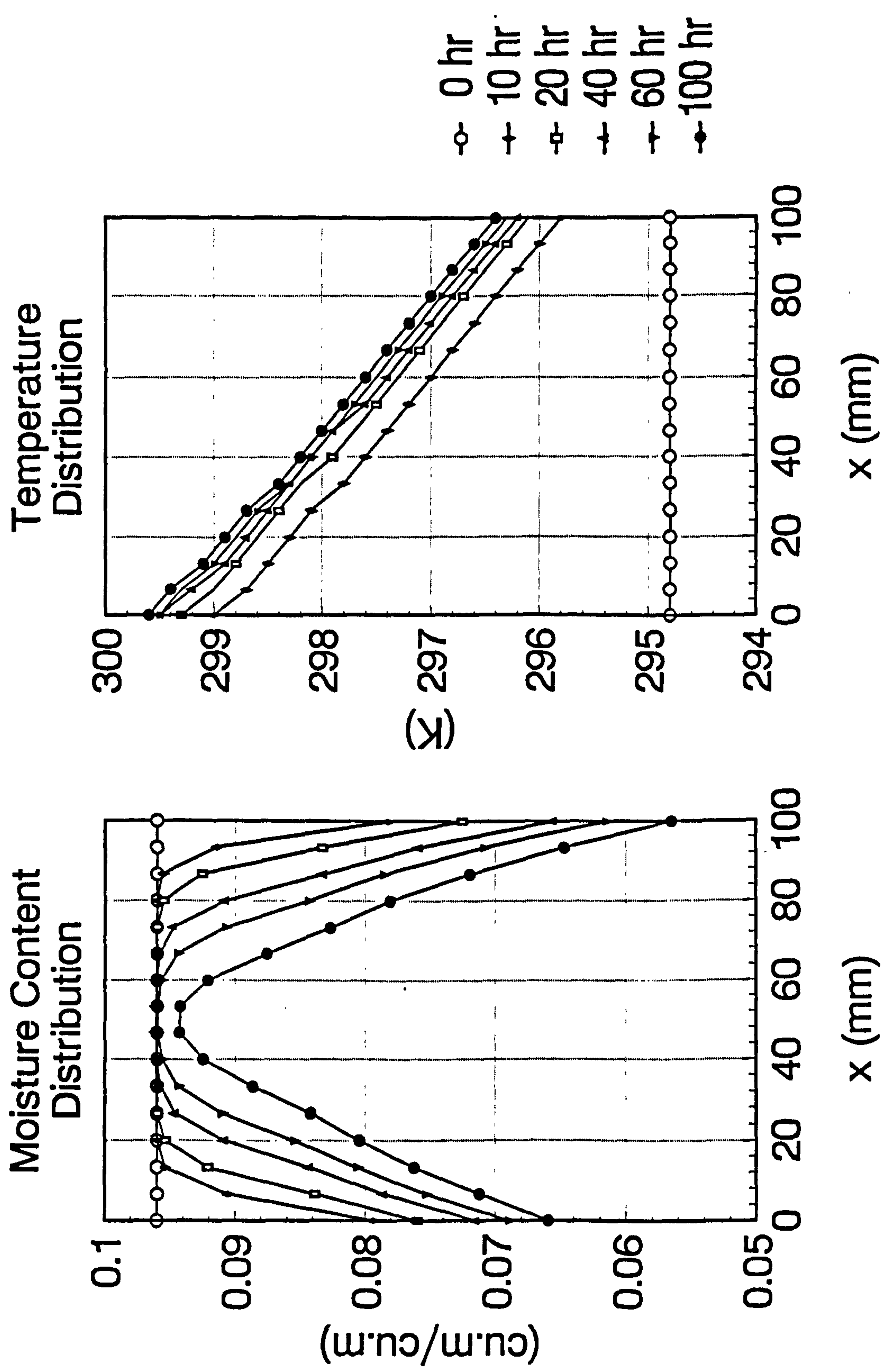


Figure 4.6
Comparison of simulation results between Huang's model
and differential permeability model

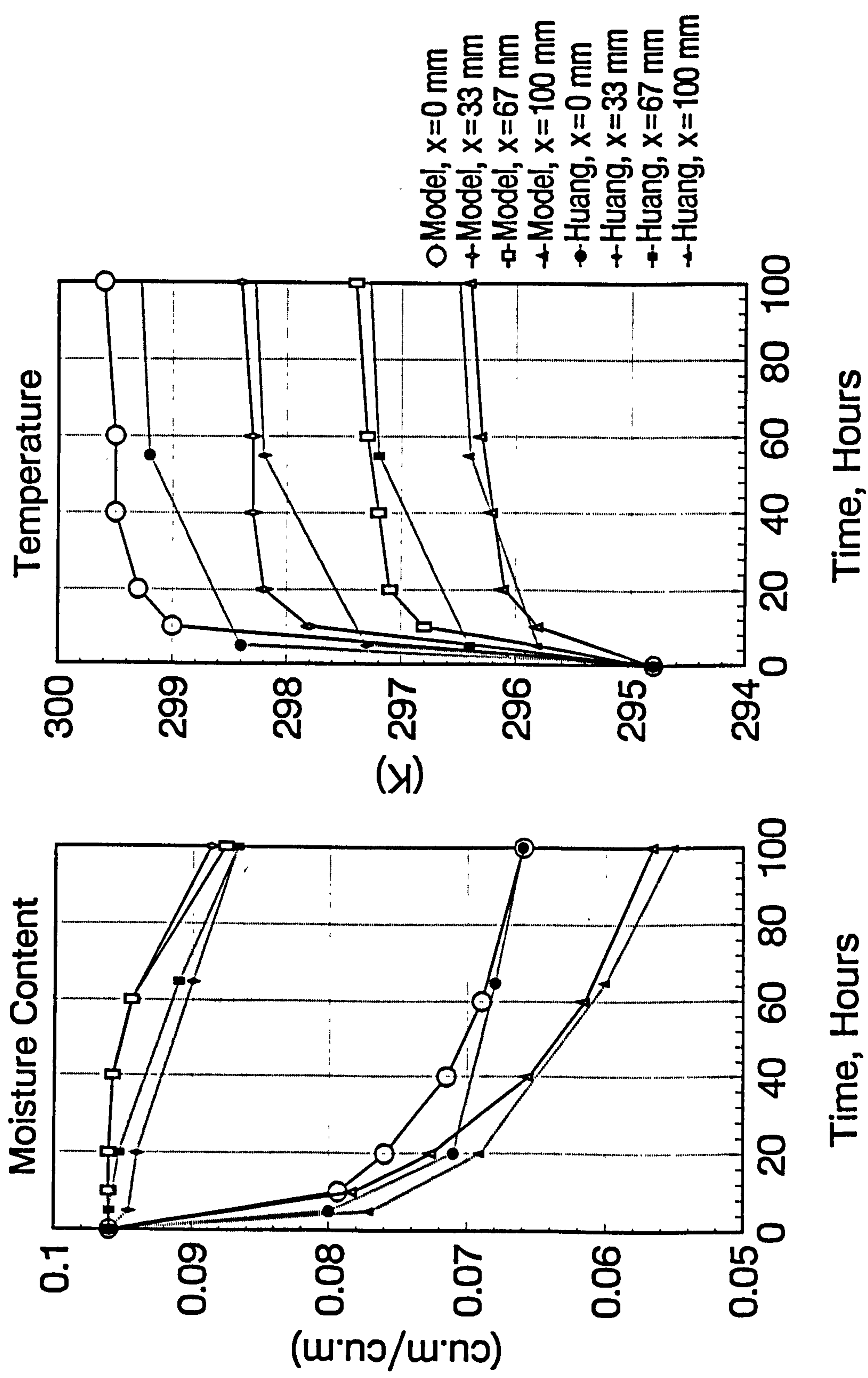


Figure 4.7
 Comparison of moisture desorption rates
 from experiment (by Thomas & Burch 1990) and
 differential permeability model

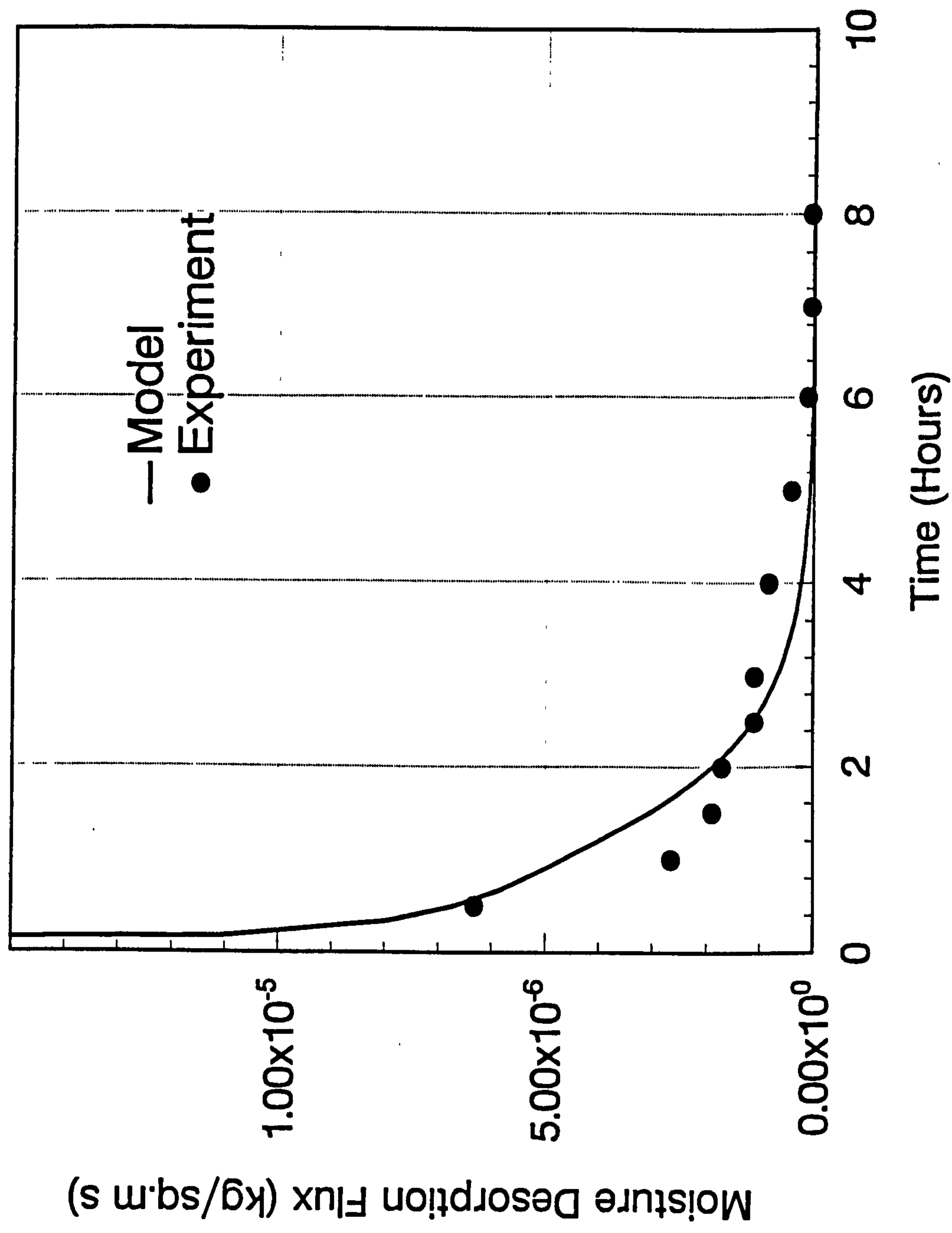


Figure 5.1 Input/output relationship of a component model

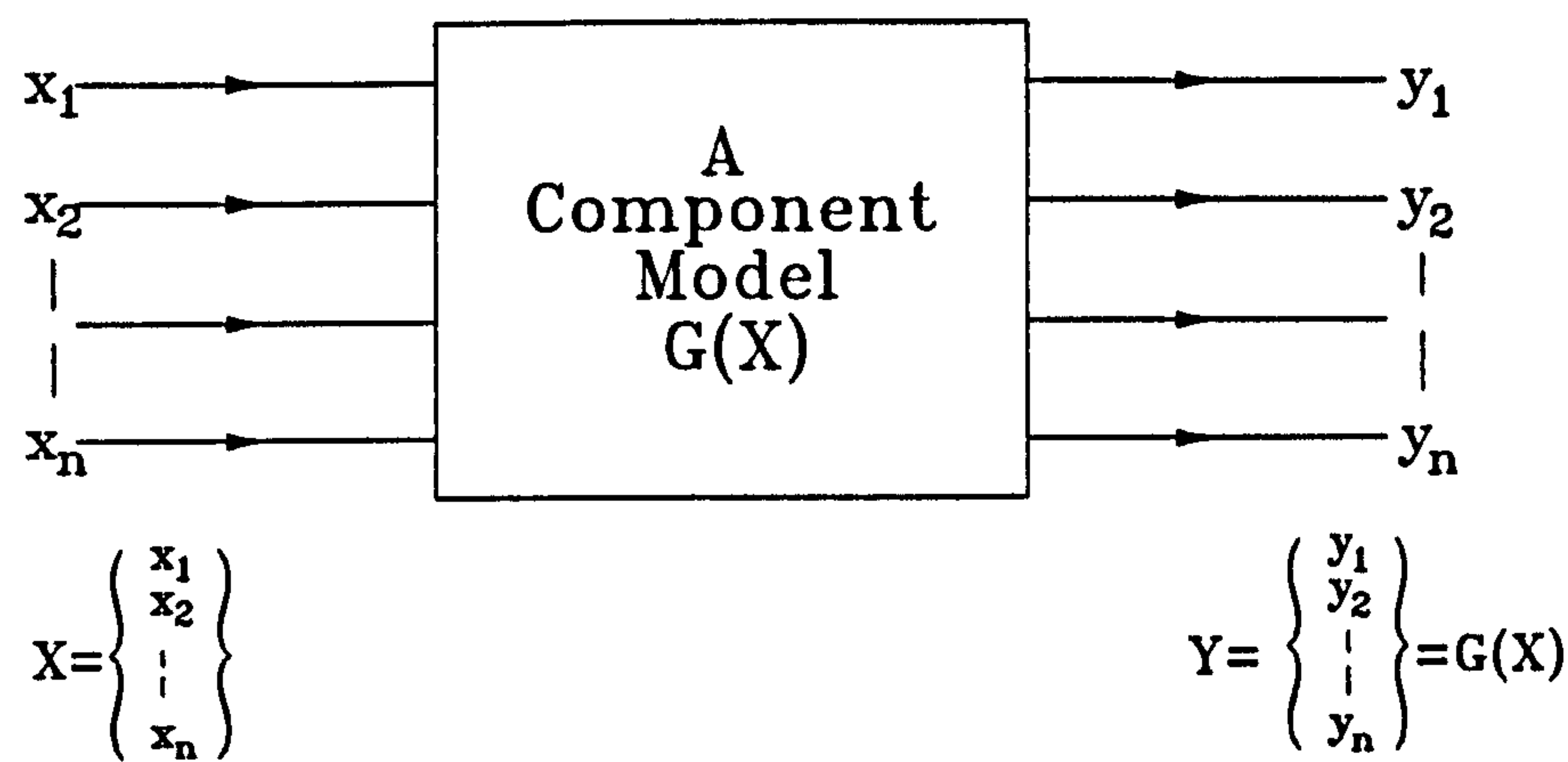


Figure 5.2 A unidirectional sequence of component models

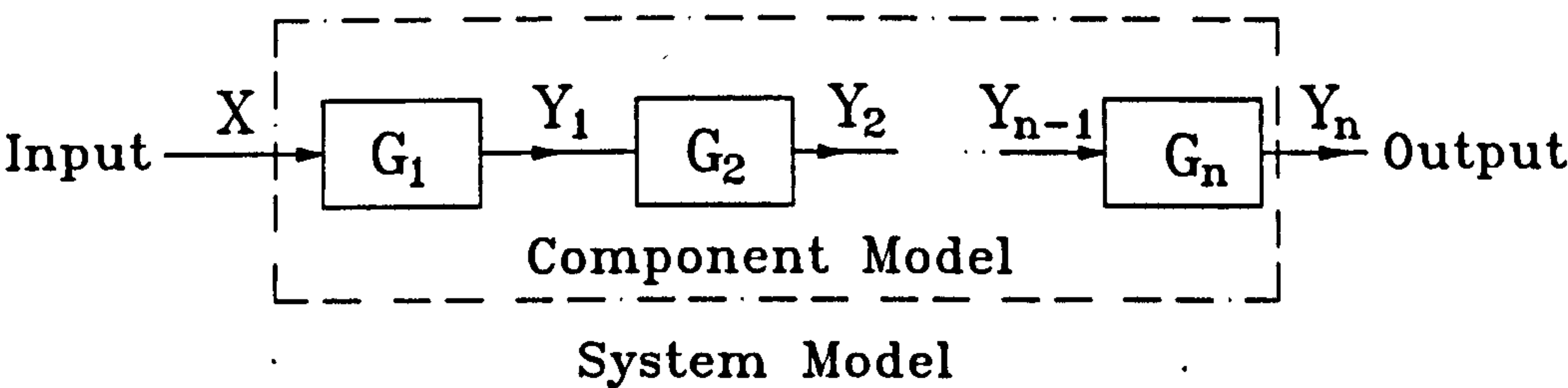


Figure 5.3 Looped relationship of component models

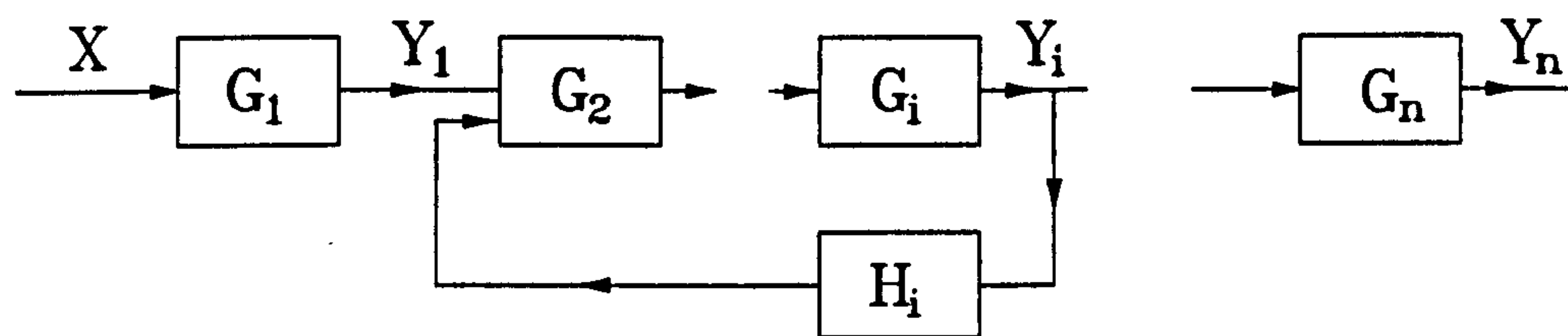


Figure 5.4 Schematic diagram of an air-handling system

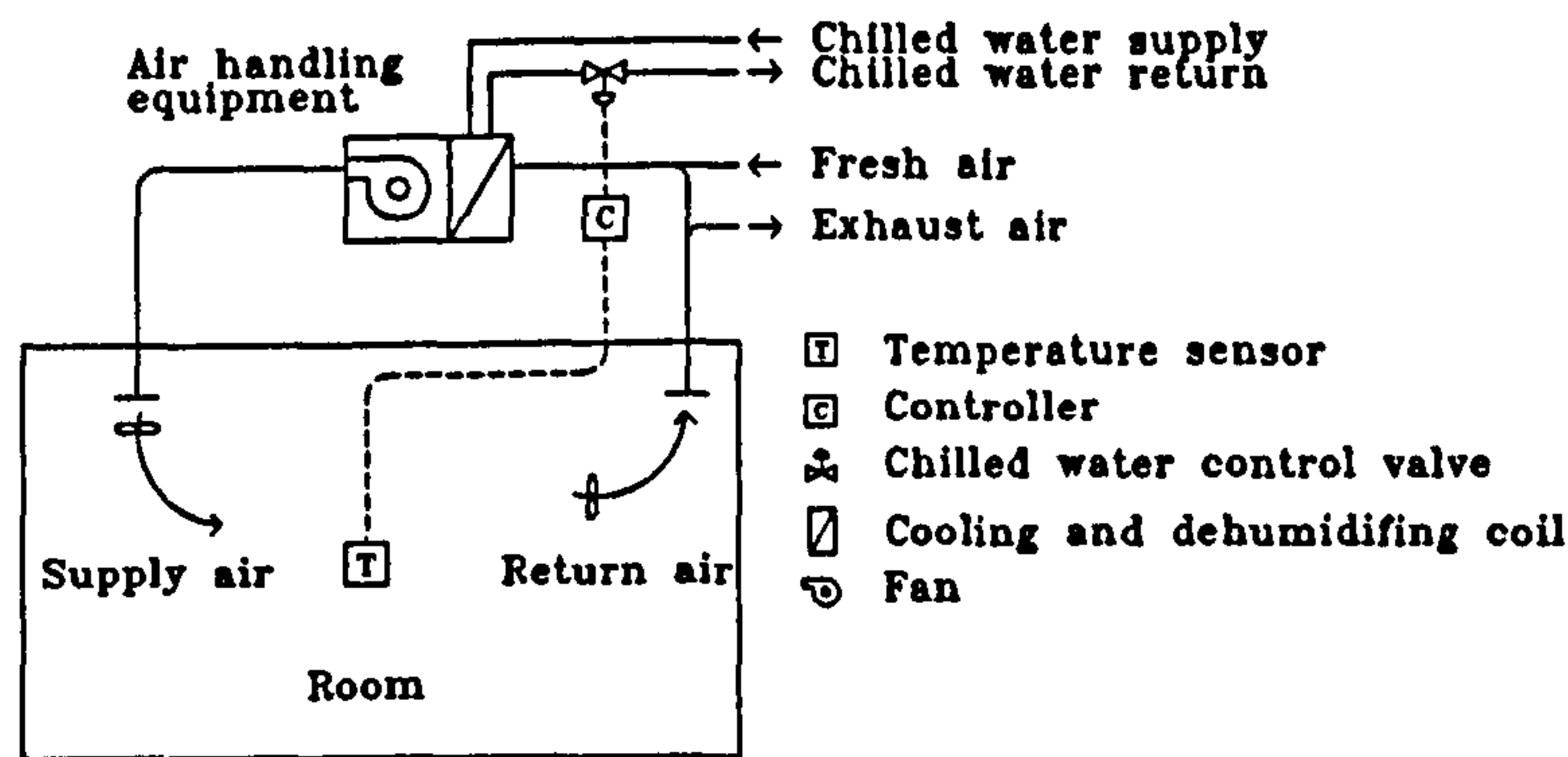


Figure 5.5 Enlarged view of tubes and fins in an air-conditioning coil

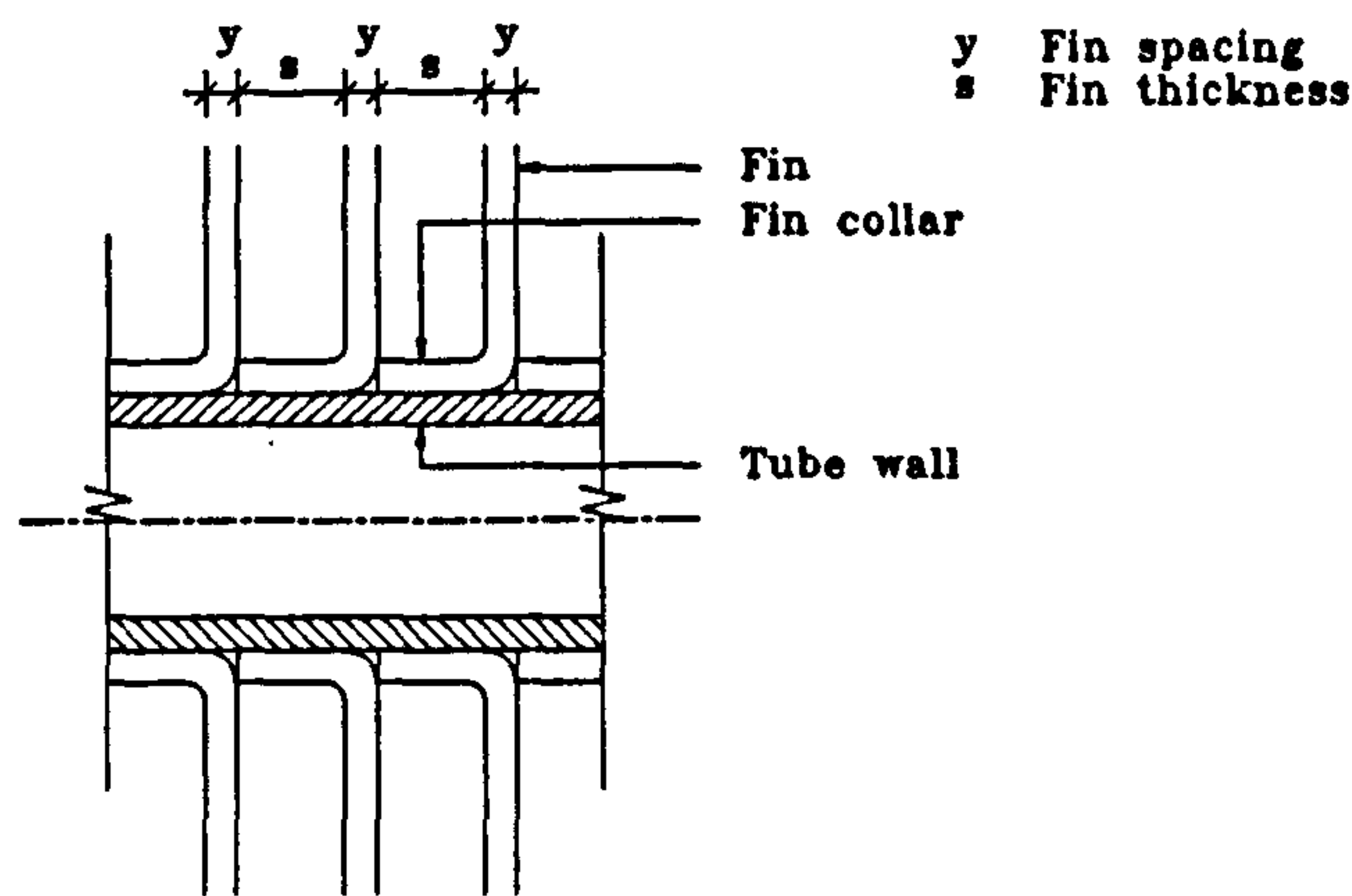


Figure 5.6 Fin corrugation patterns

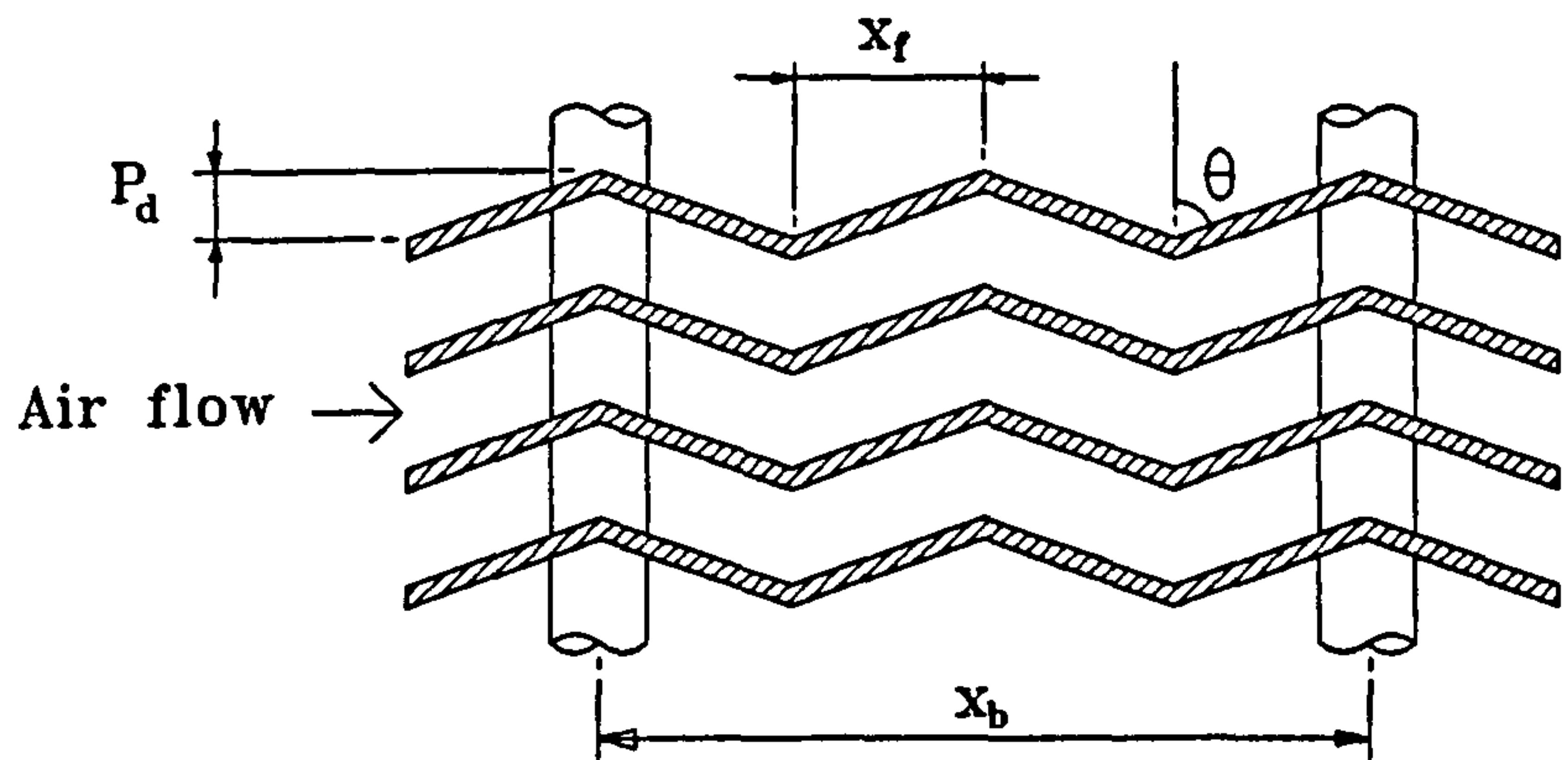


Figure 5.7 Rectangular and triangular tube arrays

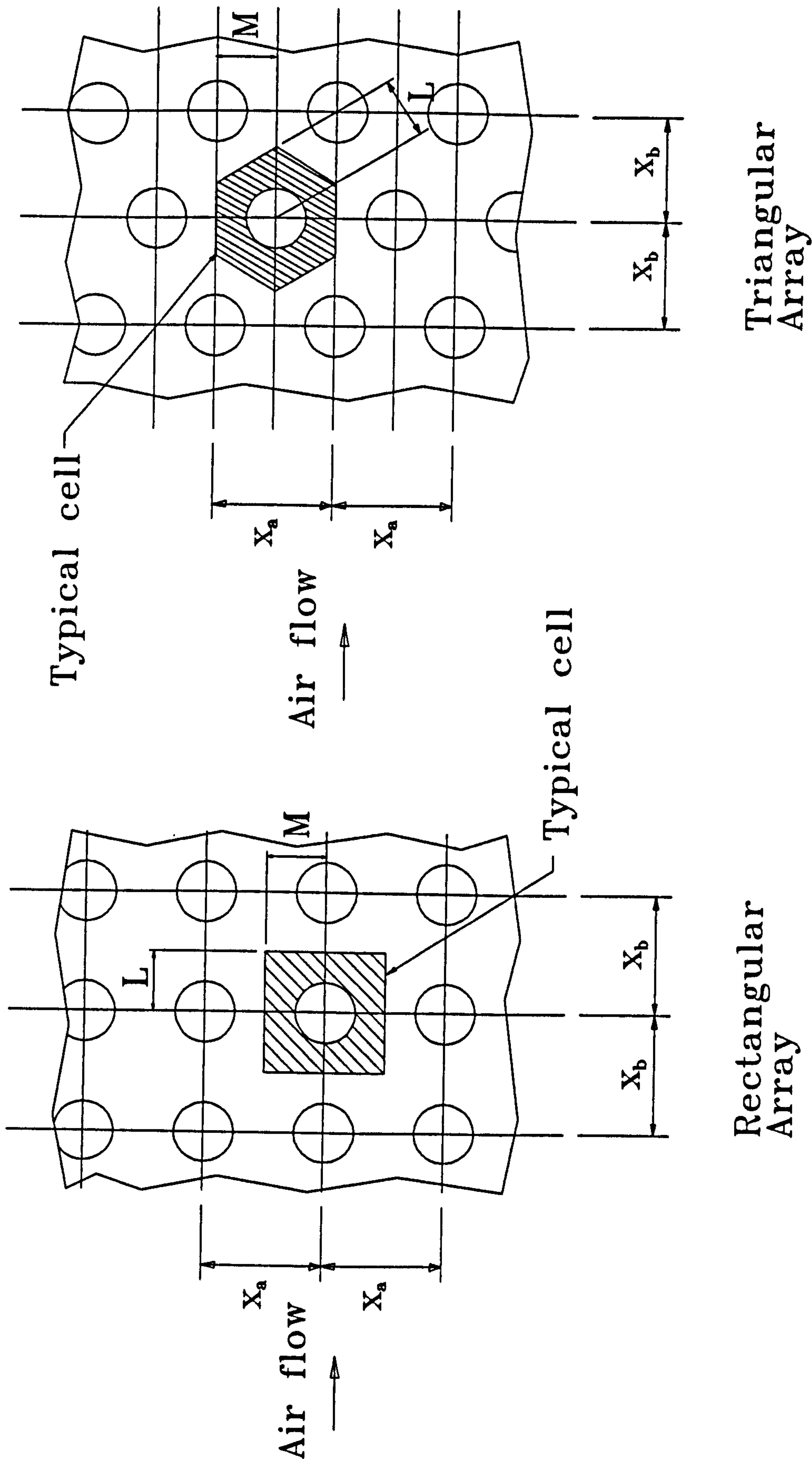


Figure 5.8 Indoor temperature variation pattern with on/off control

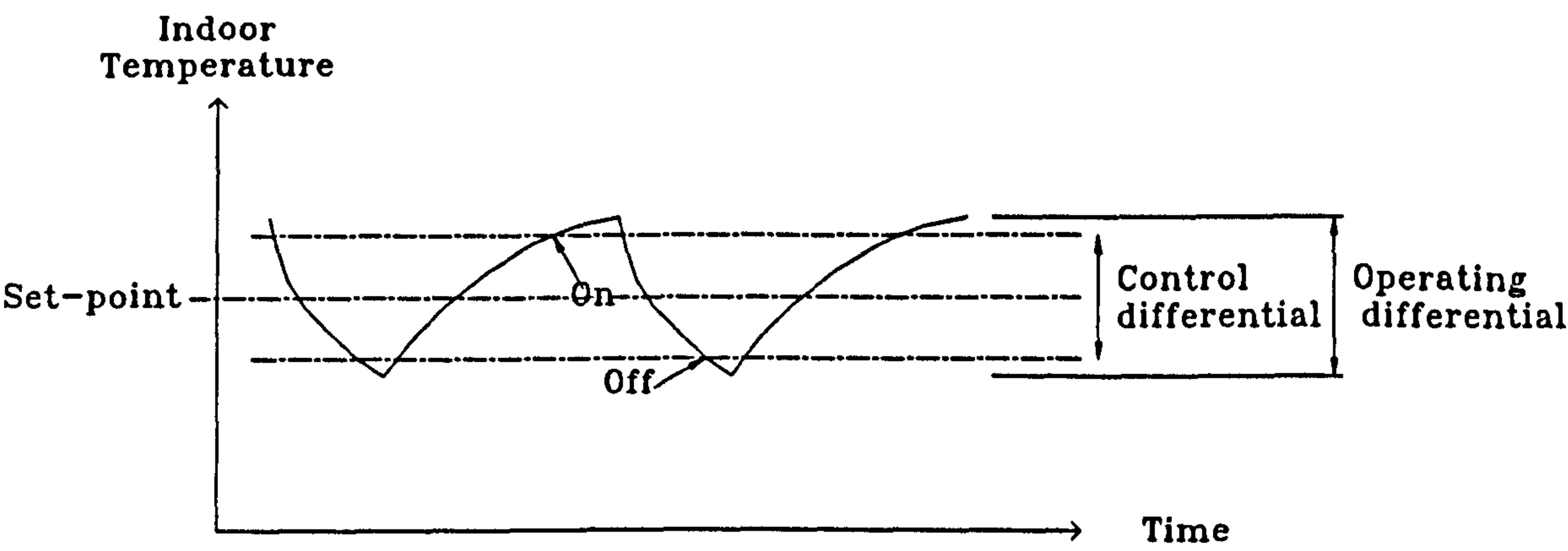


Figure 5.9
Typical inherent characteristics of an
equal percentage valve

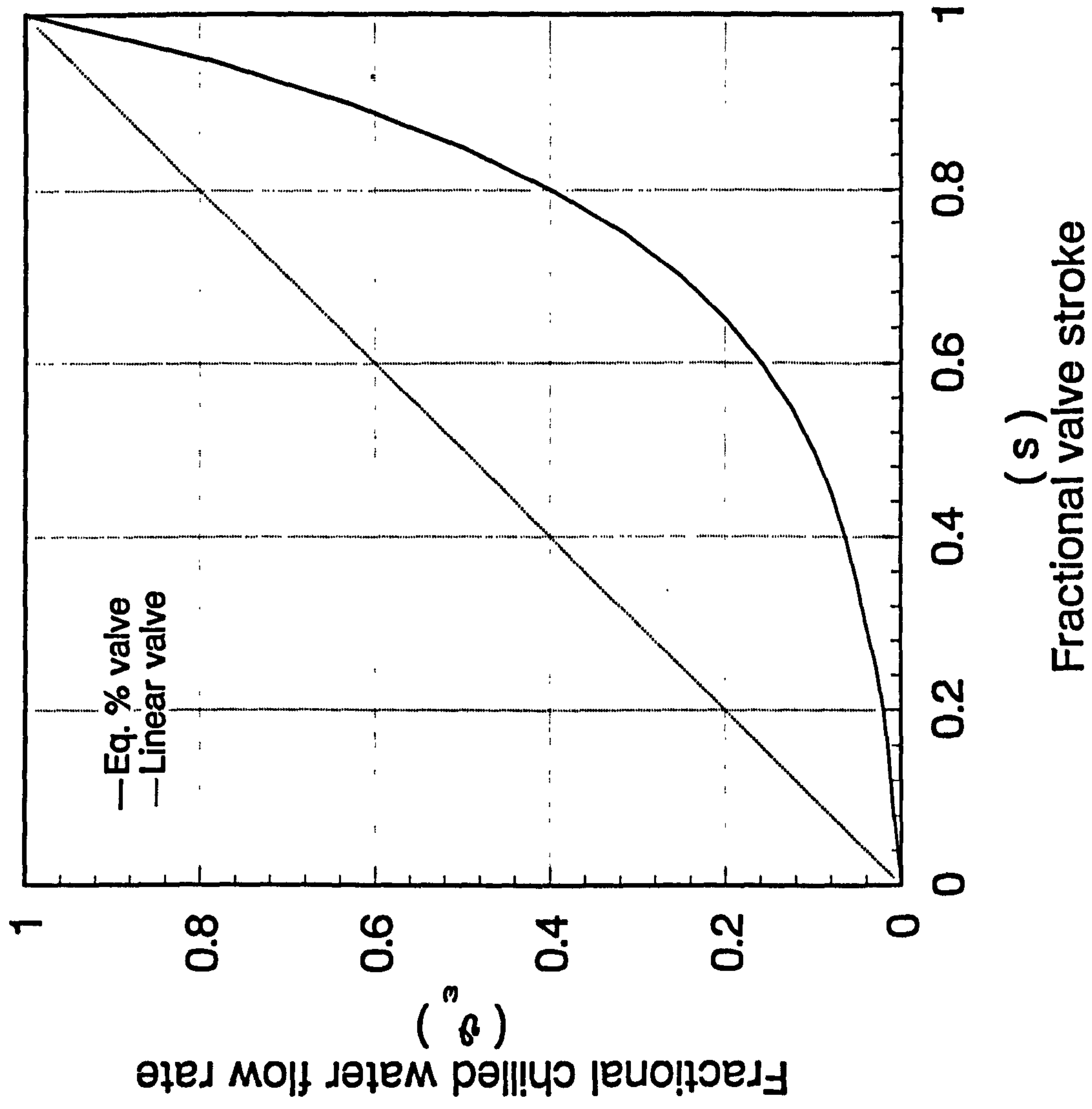


Figure 5.10 Schematic diagram of a branch chilled water circuit

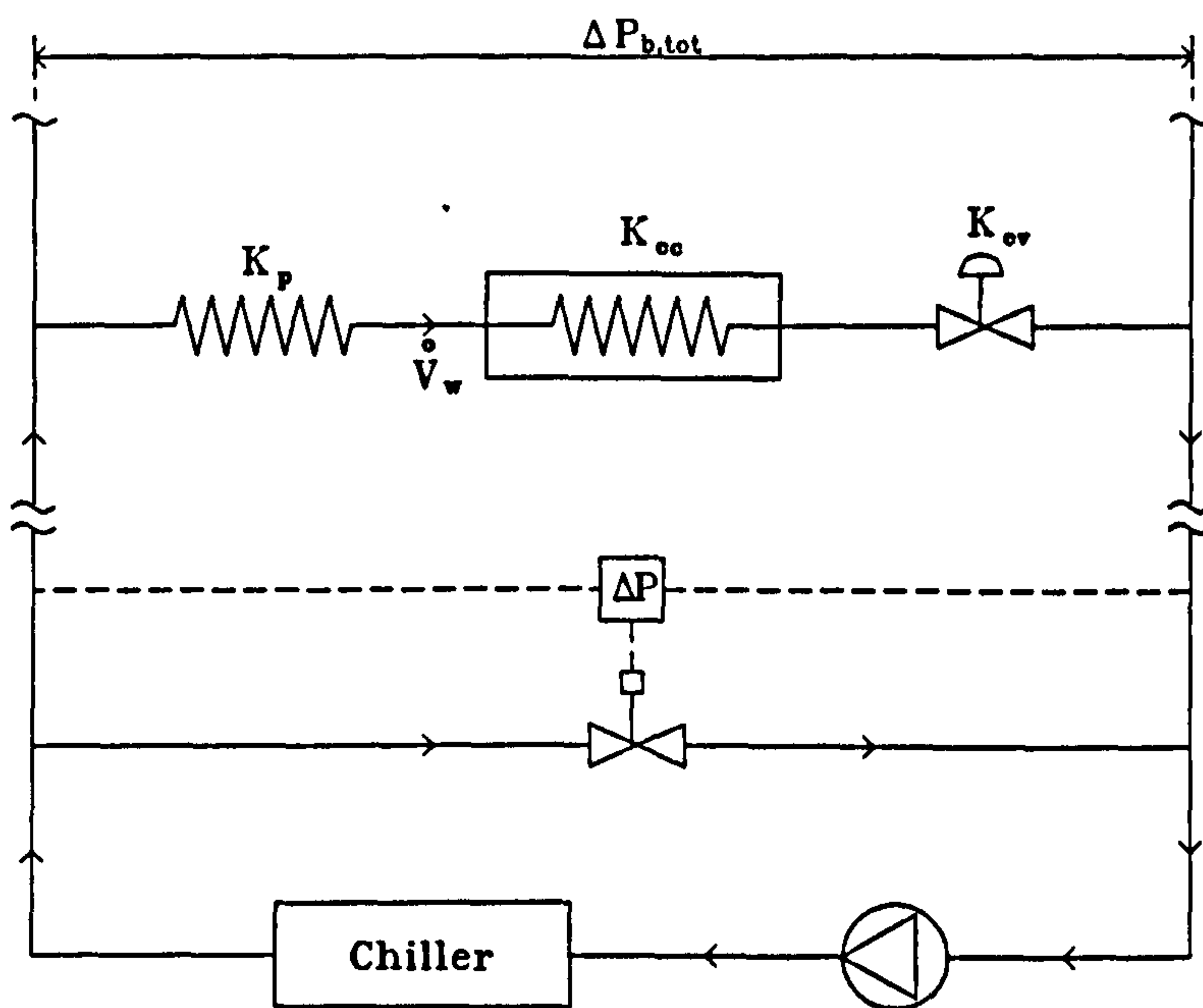


Figure 6.1 Configuration of the single tube, counterflow heat exchange model for a cooling and dehumidifying coil

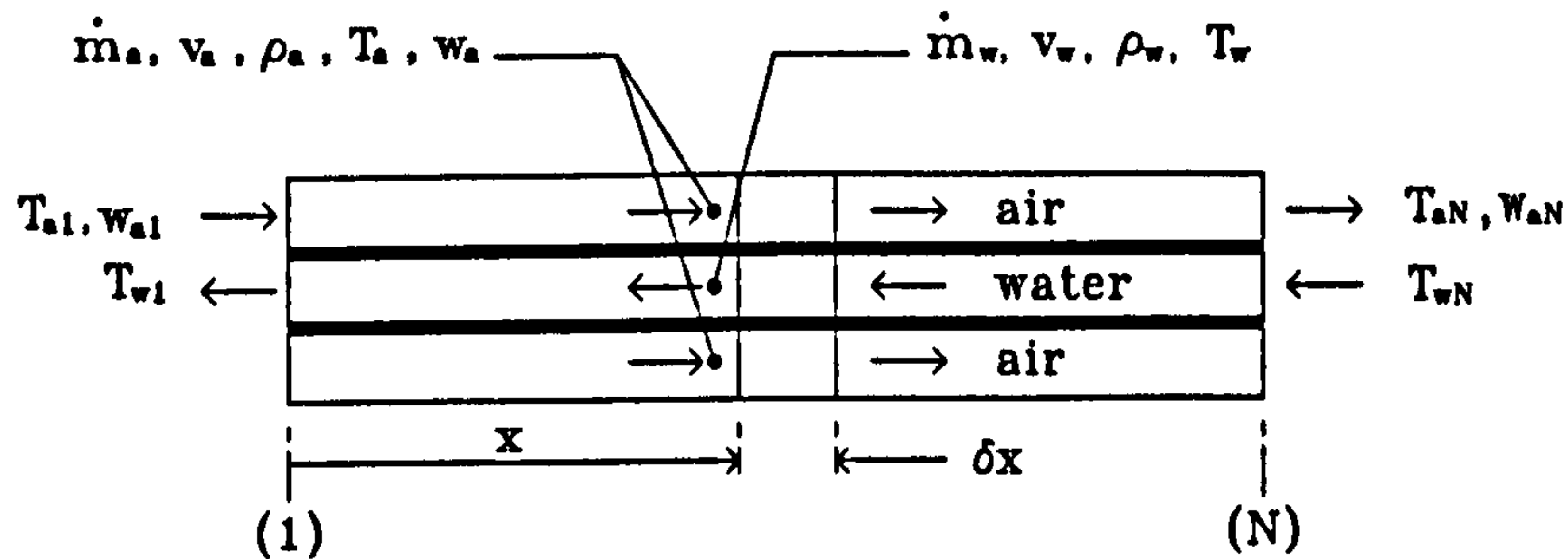


Figure 6.2 Elemental section in the idealized coil

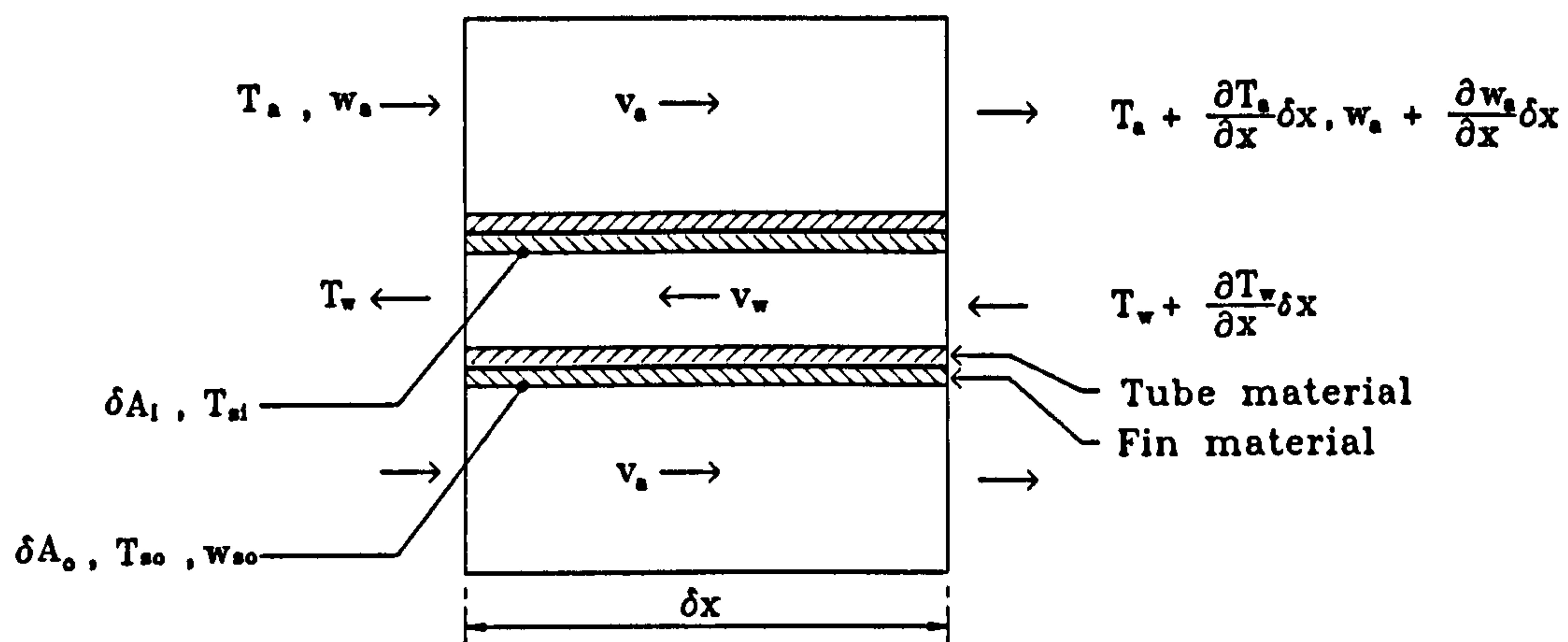


Figure 6.3 Cross-section of the idealized coil

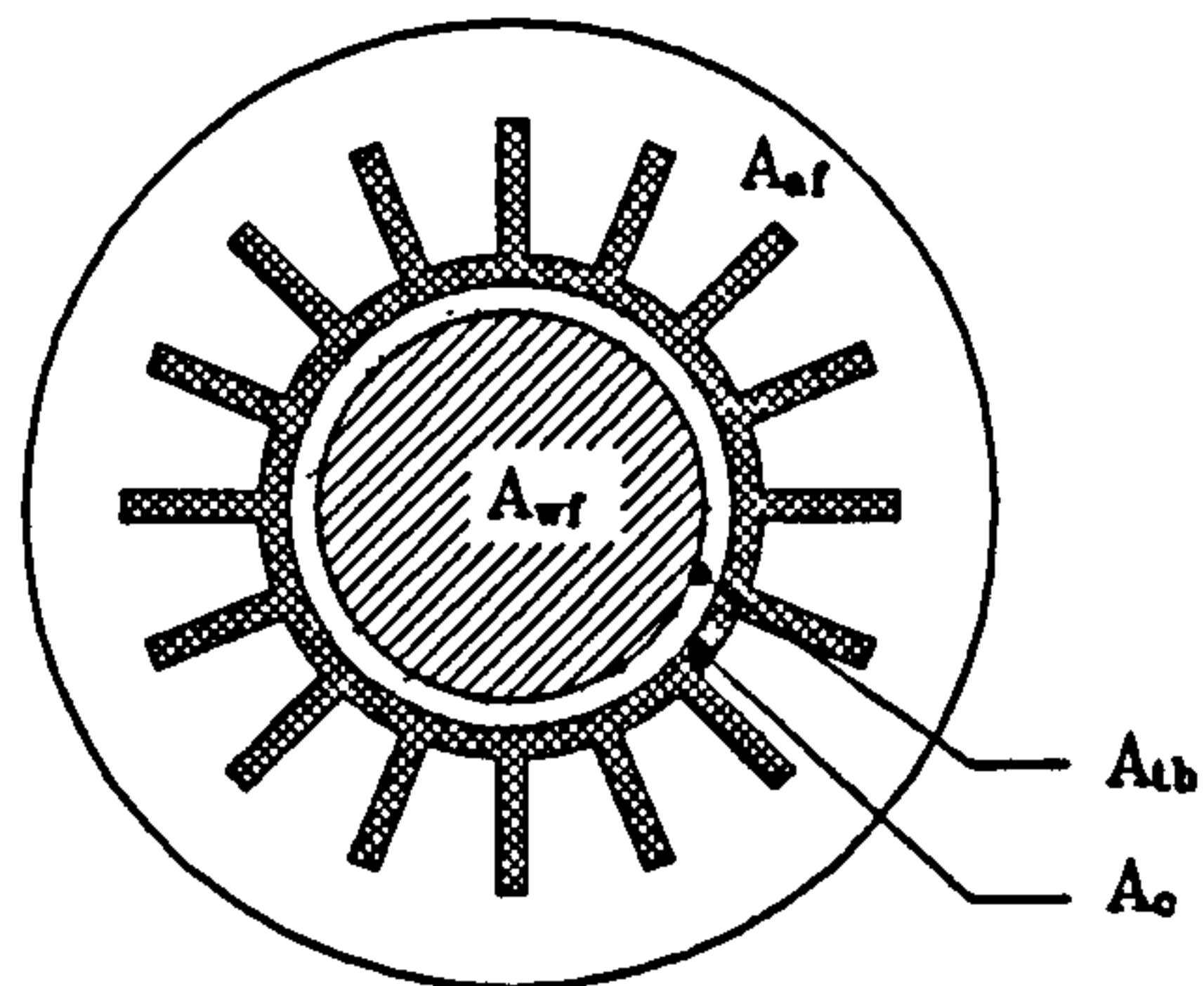


Figure 6.4 Discretization of the idealized coil

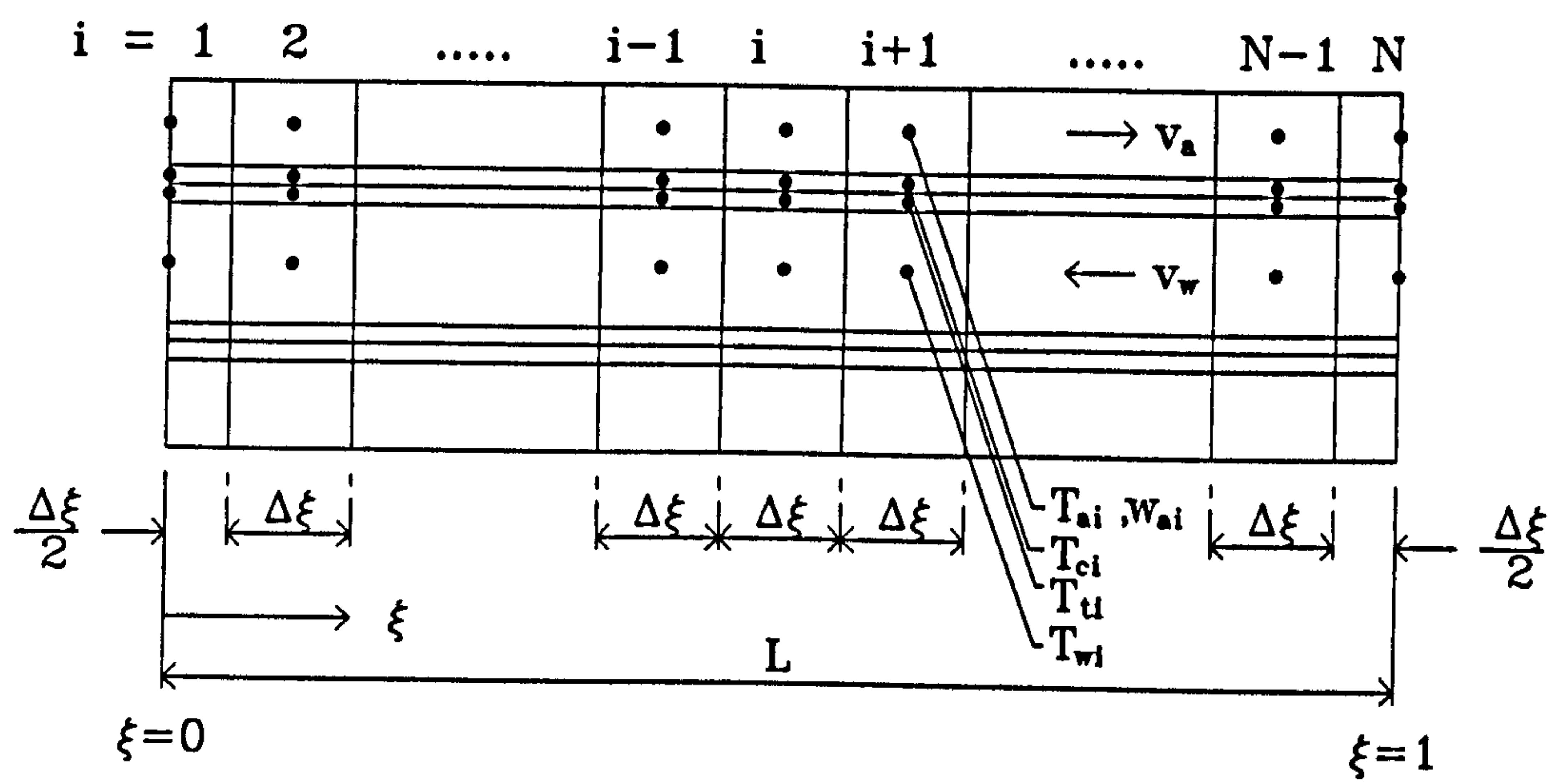


Figure 7.1
Comparison of simulated results with catalogue data
(flat fins)

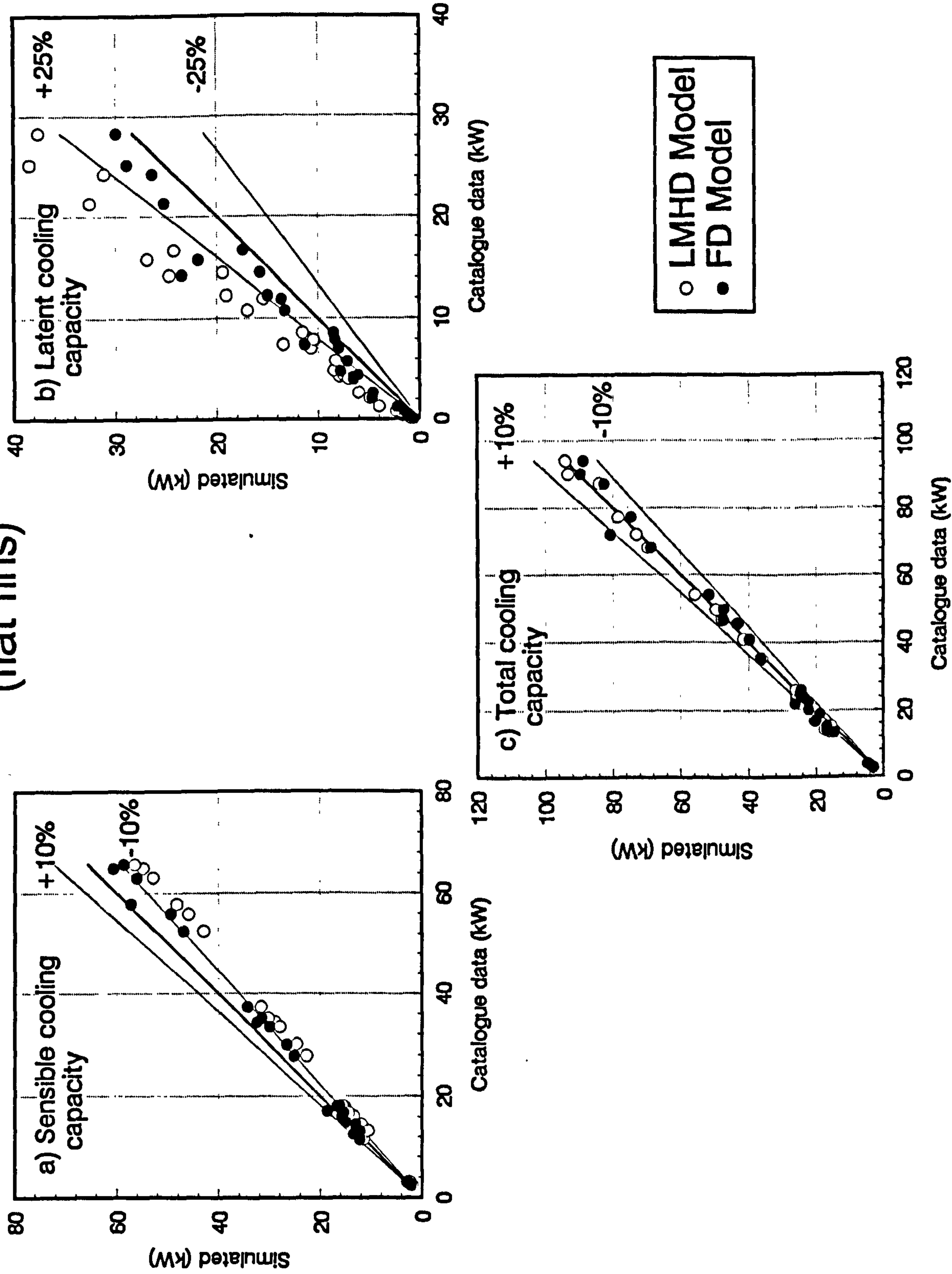


Figure 7.2
Comparison of simulated results with catalogue data
(corrugated fins)

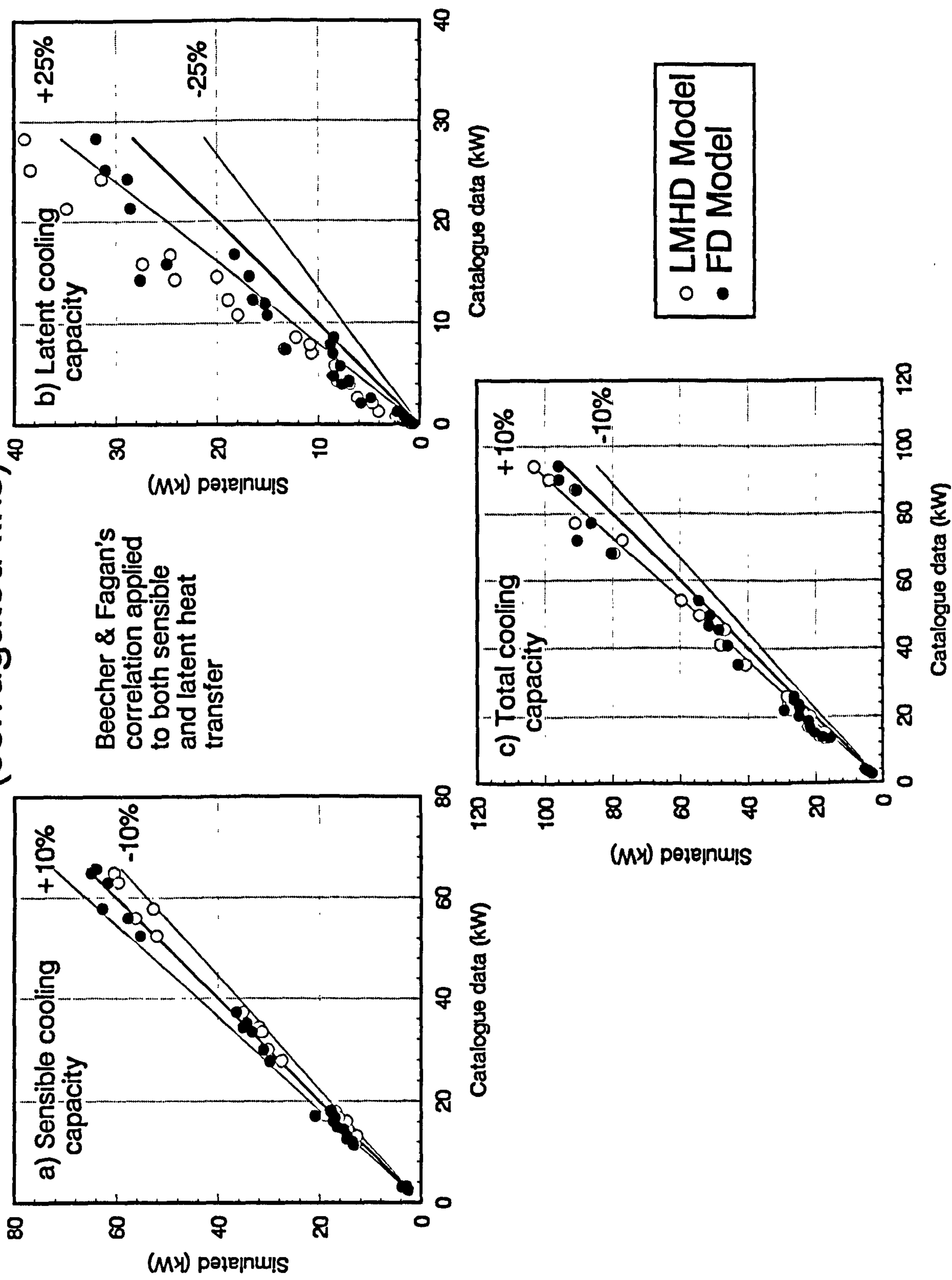


Figure 7.3
Comparison of simulated results with catalogue data
(corrugated fins)

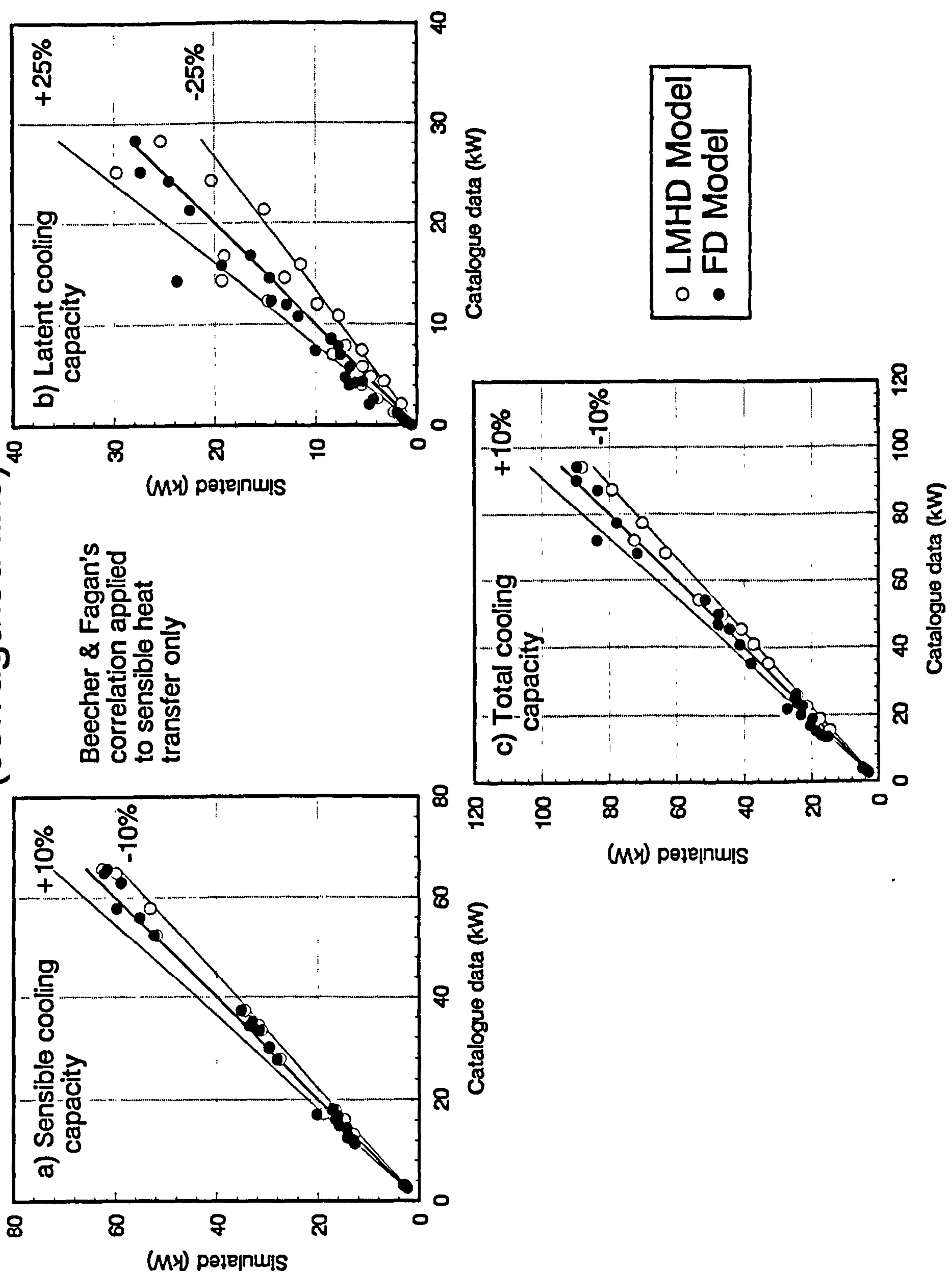
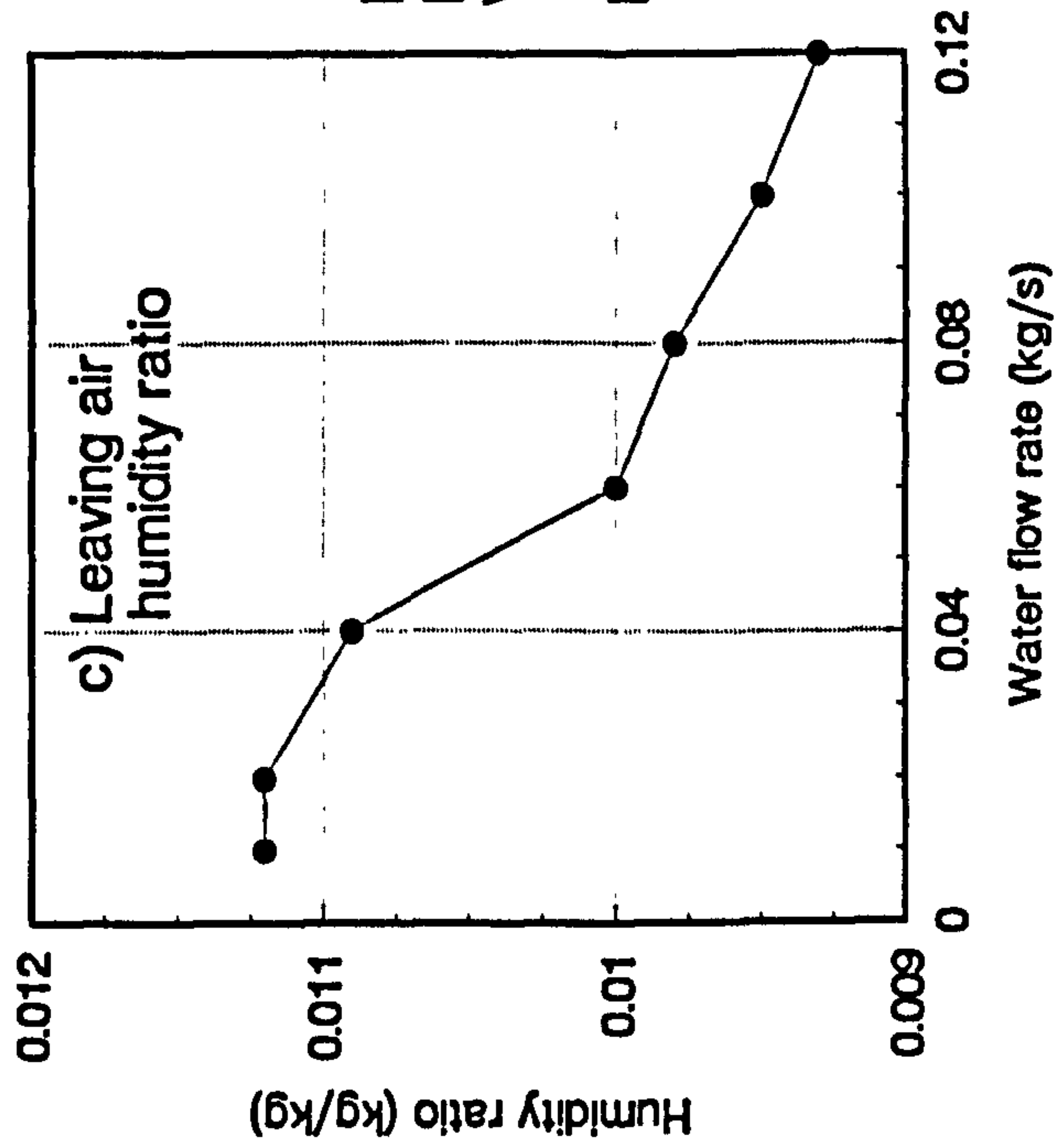
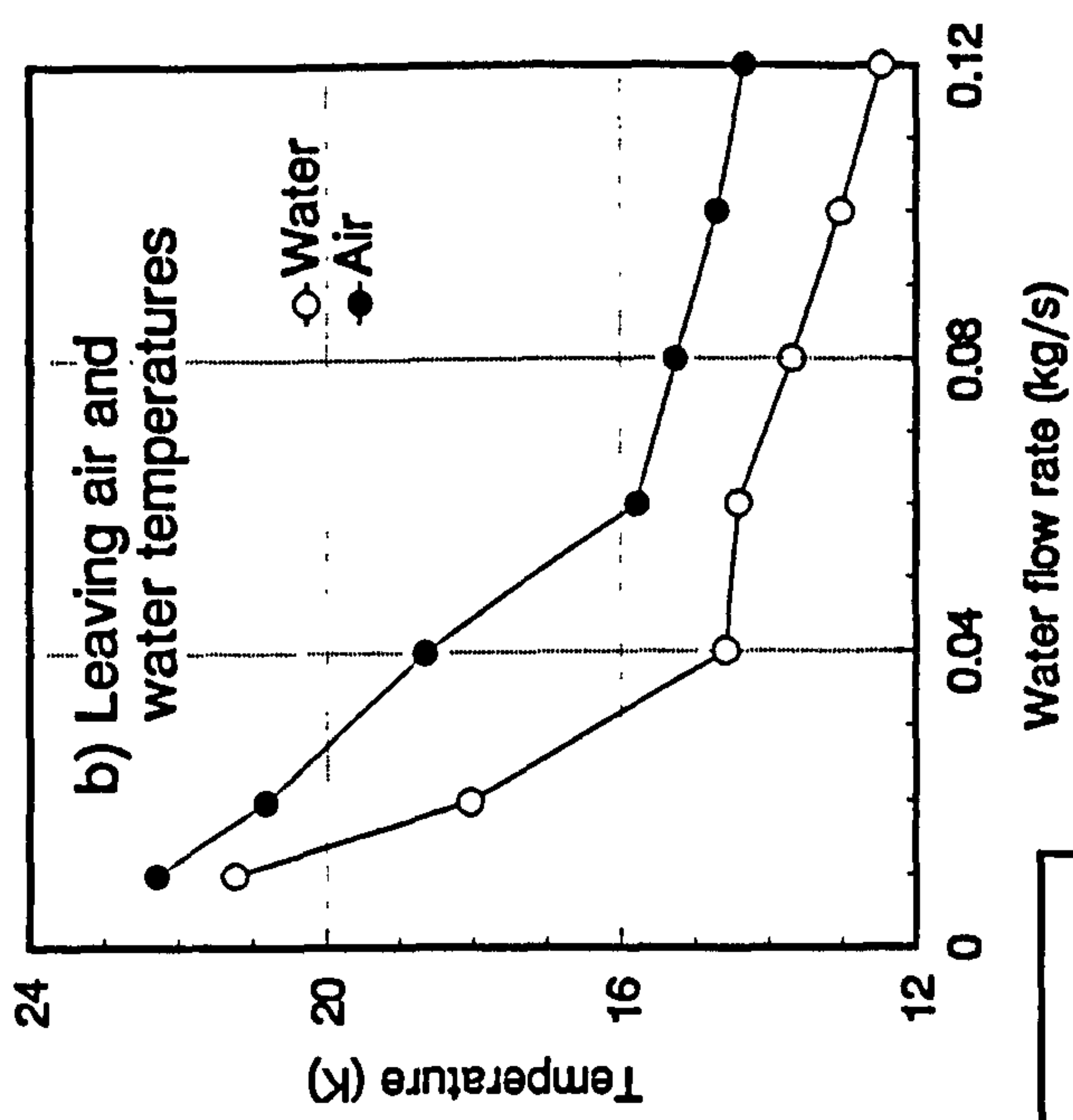
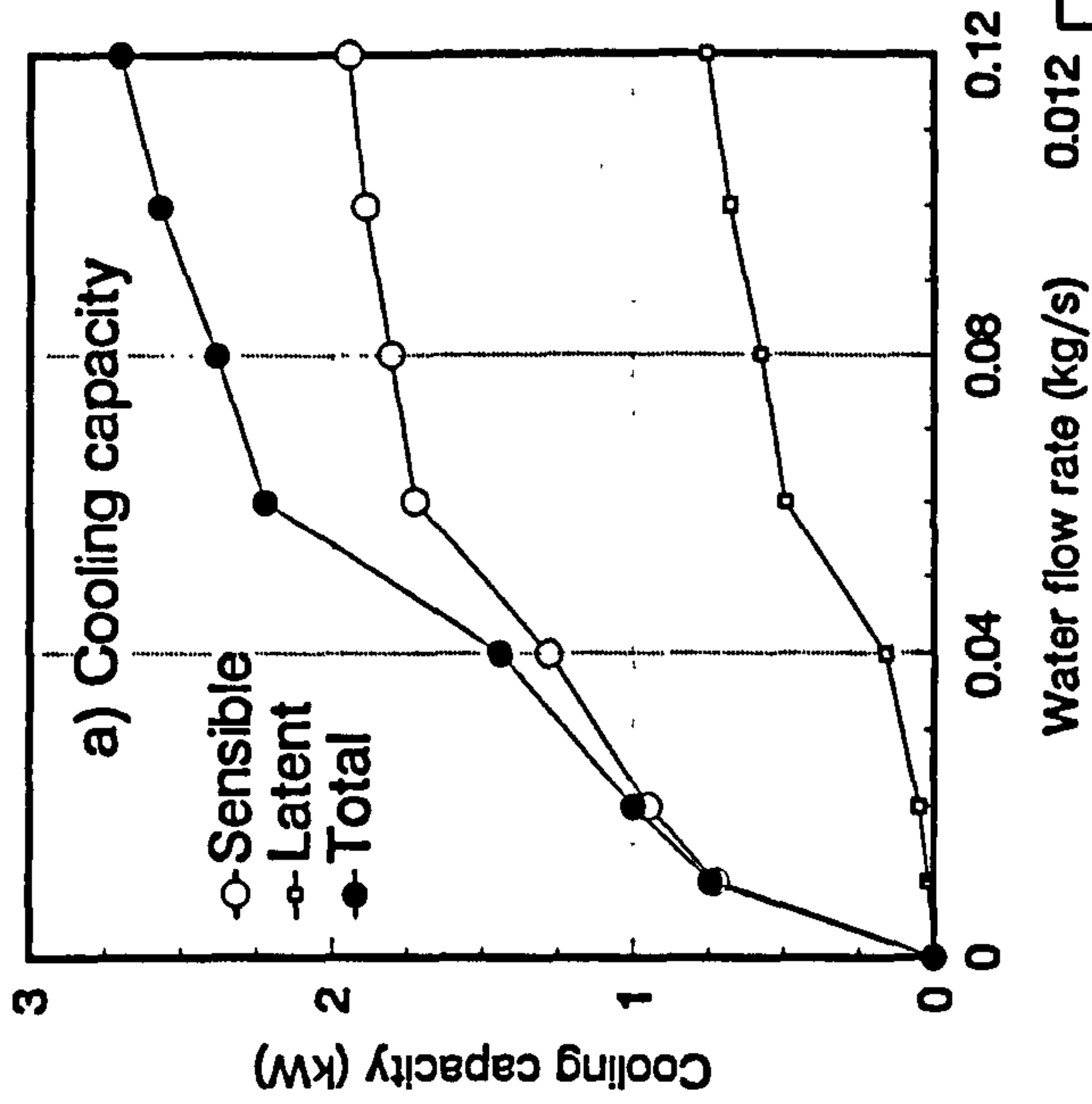


Figure 7.4
Variations of coil performance with chilled water
flow rate



Entering air conditions:
Dry-bulb temp. 27.0 deg.C
Wet-bulb temp. 19.5 deg.C
Entering water temp. 7 deg.C

Figure 7.5
Dynamic performance of a cooling and dehumidifying coil

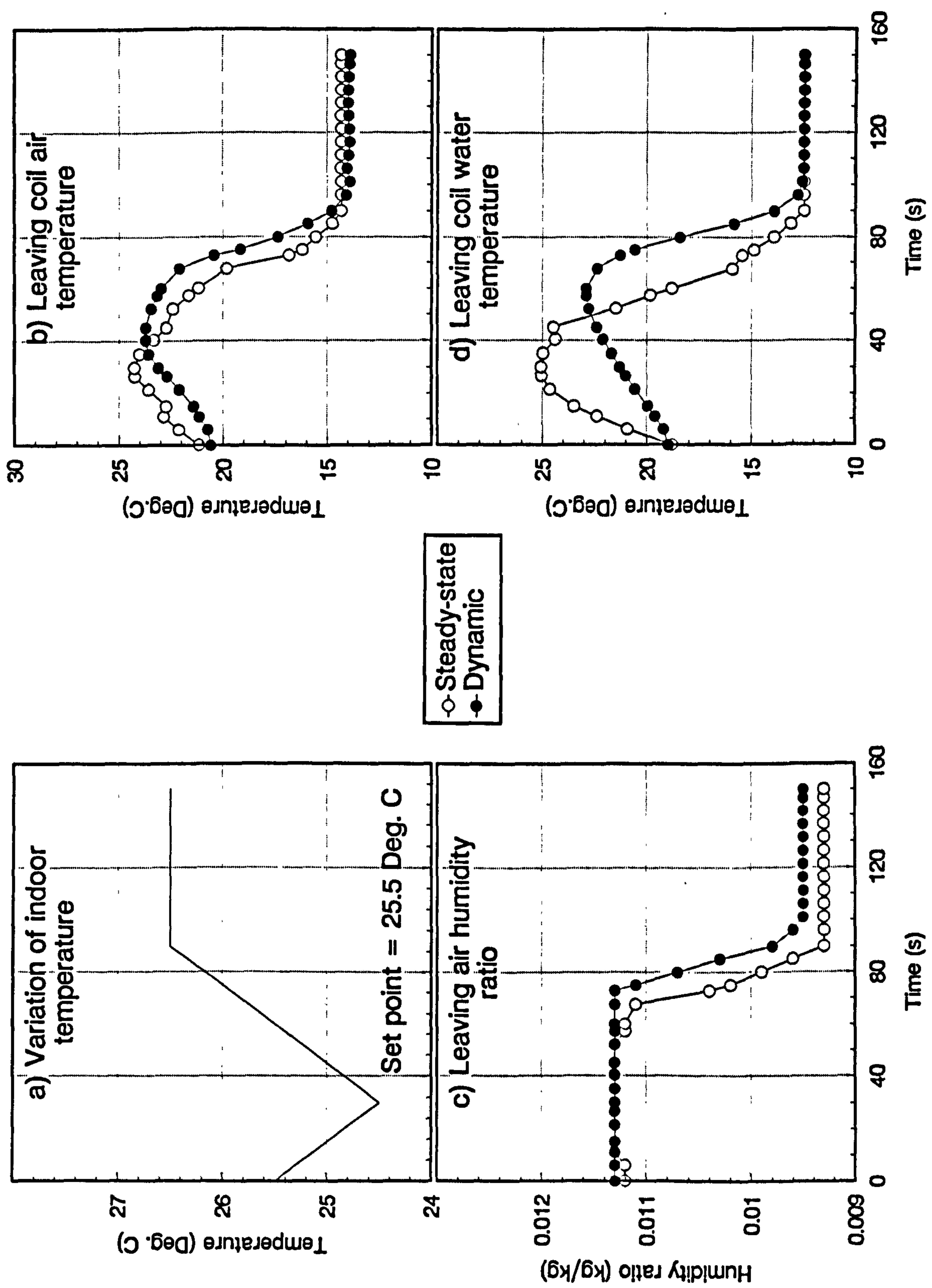


Figure 7.6

Comparison of dynamic coil model predictions with experimental data from Stoecker et al (1978)

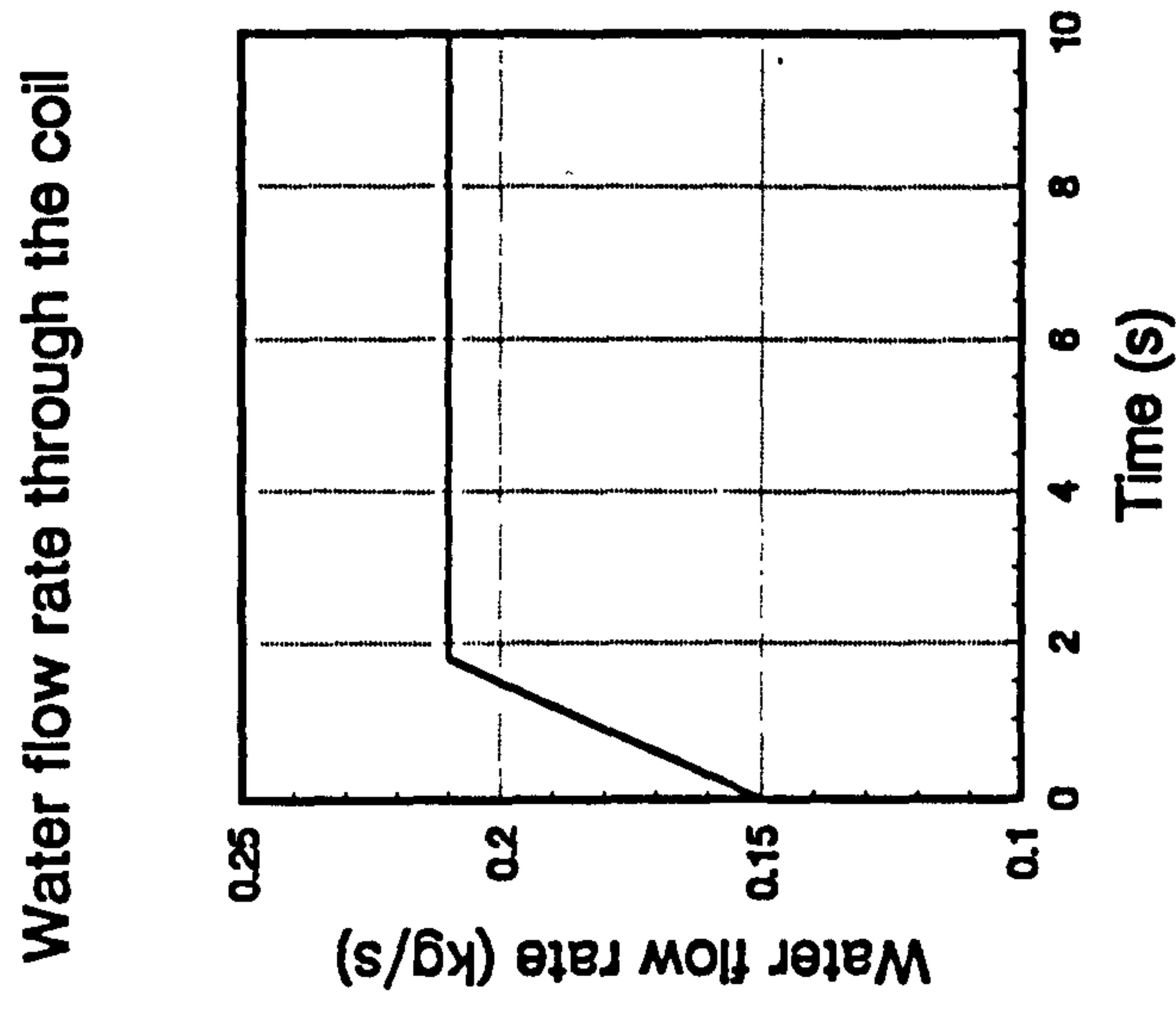
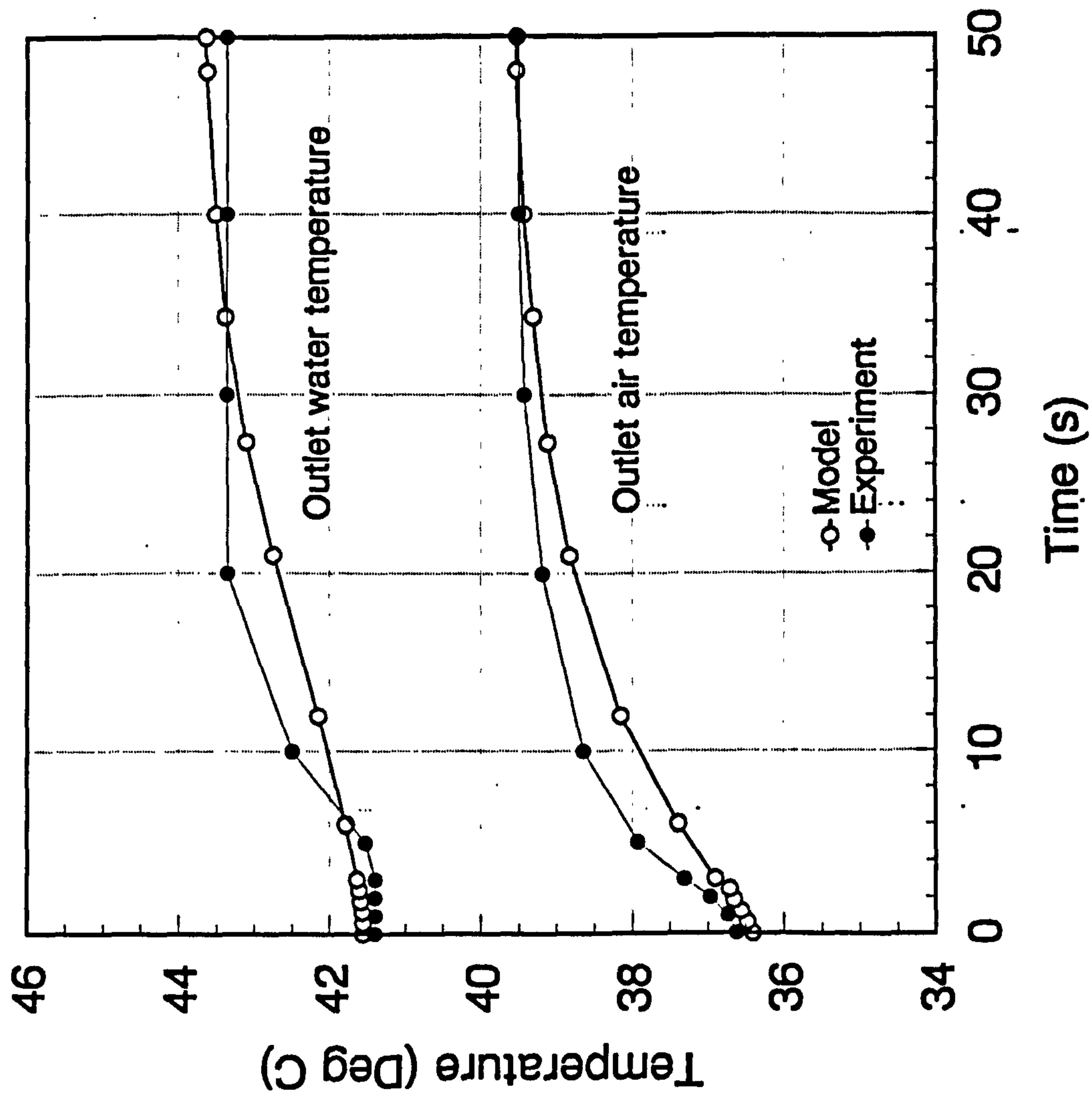


Figure 7.7

Comparison of dynamic coil model predictions with experimental data from Tamm & Green (1973)

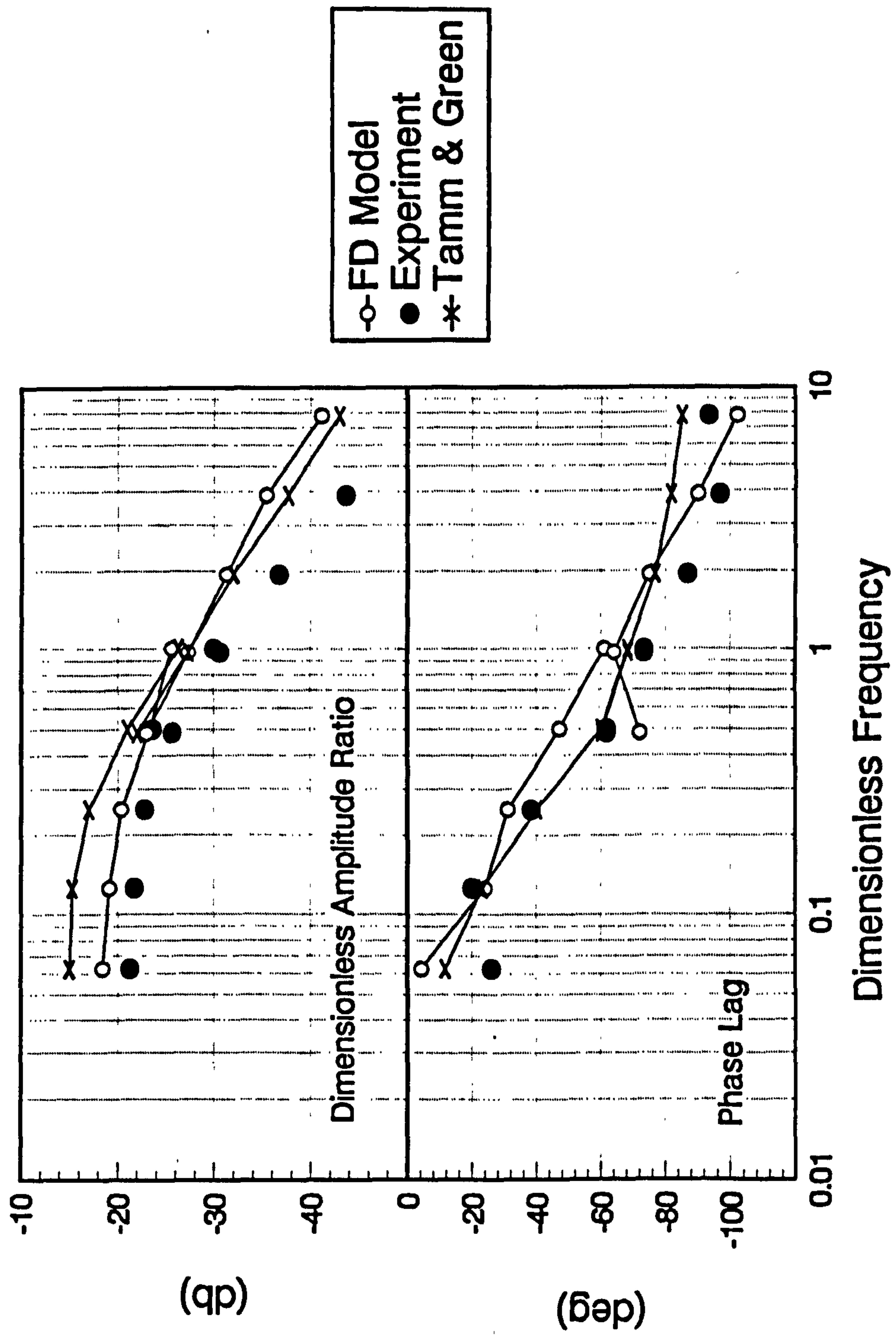


Figure 7.8

Comparison of dynamic coil model predictions with experimental data from Maxwell et al (1989)

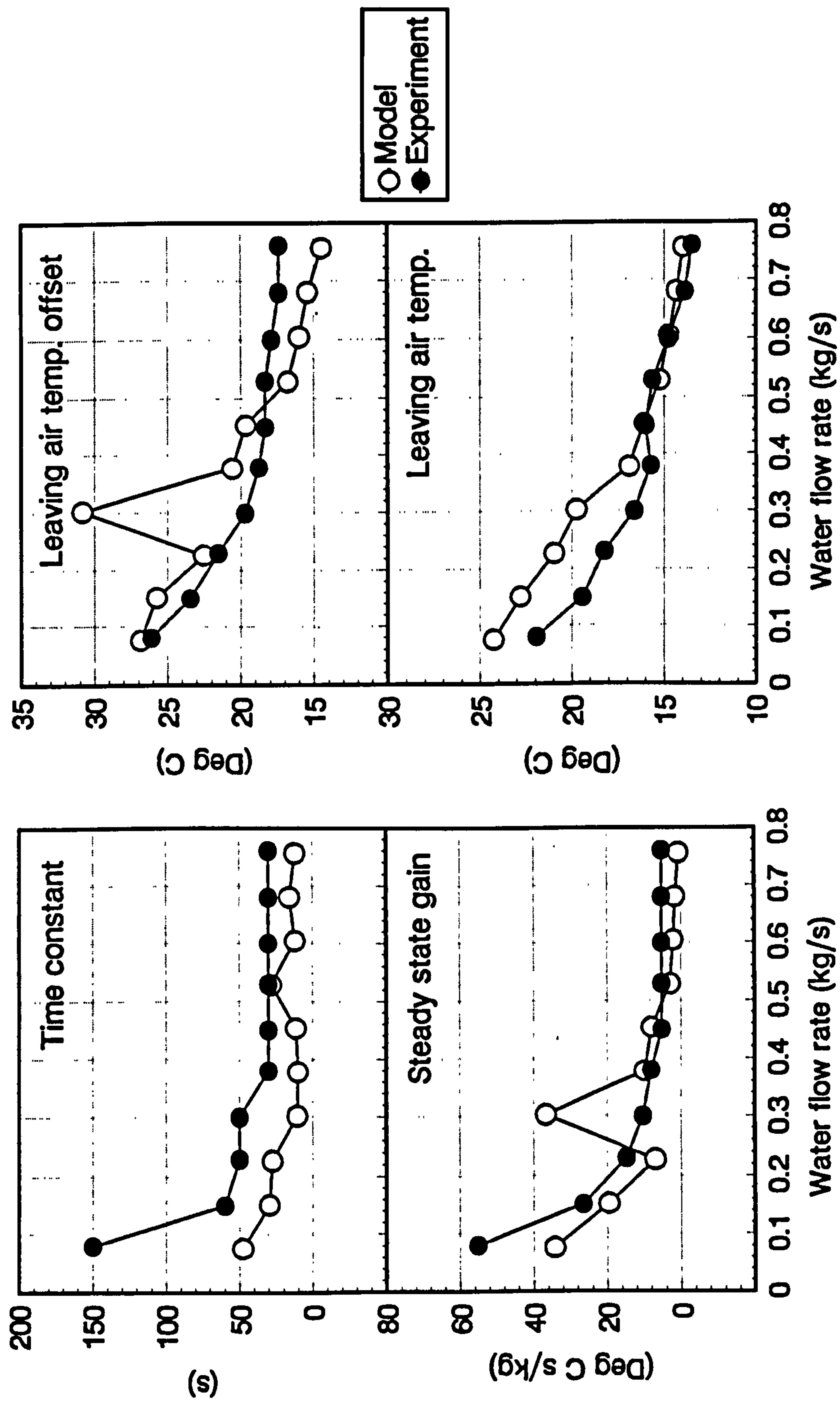


Figure 8.1 Configuration of the room modelled

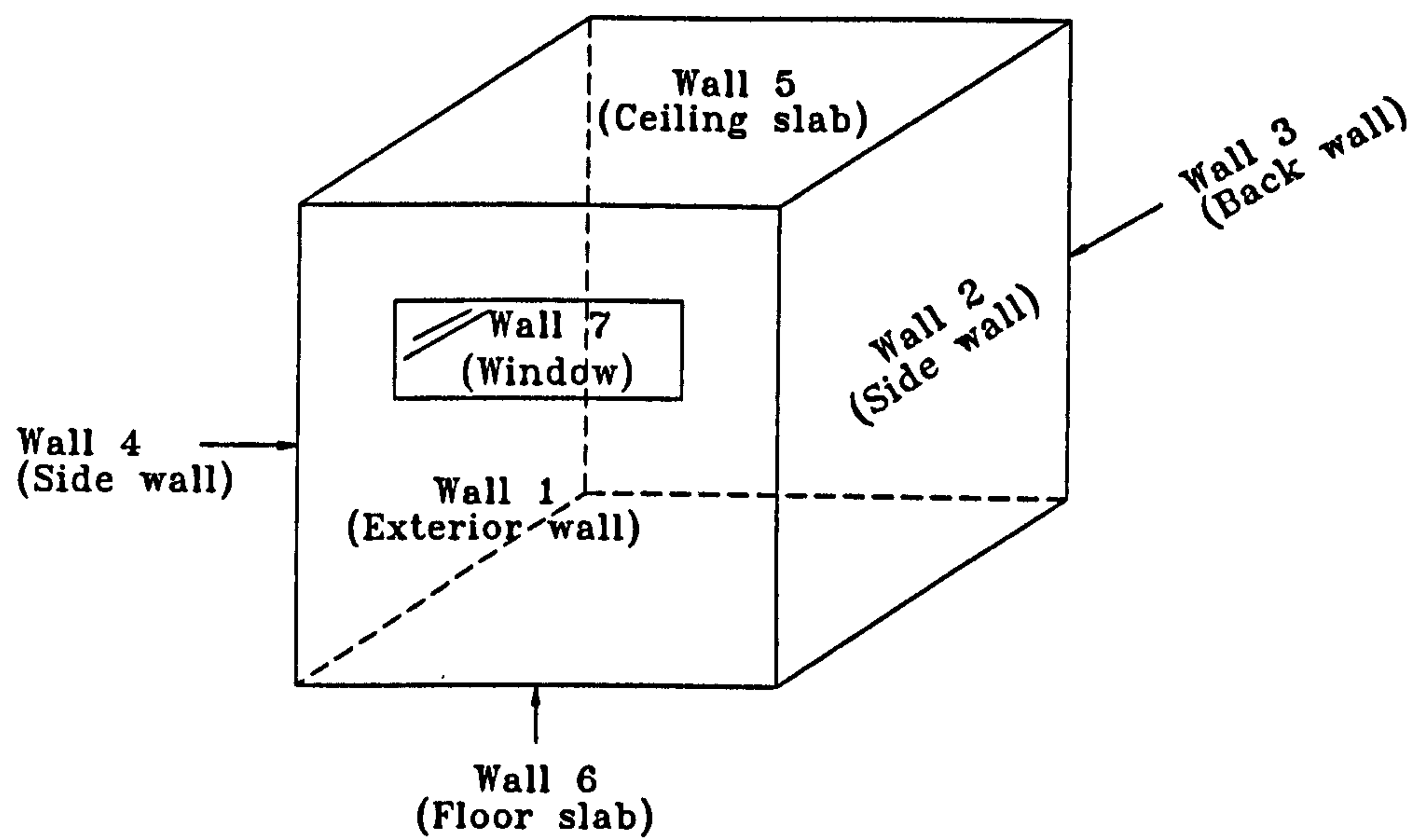


Figure 8.2 Inter-relationships between component models in the integrated model

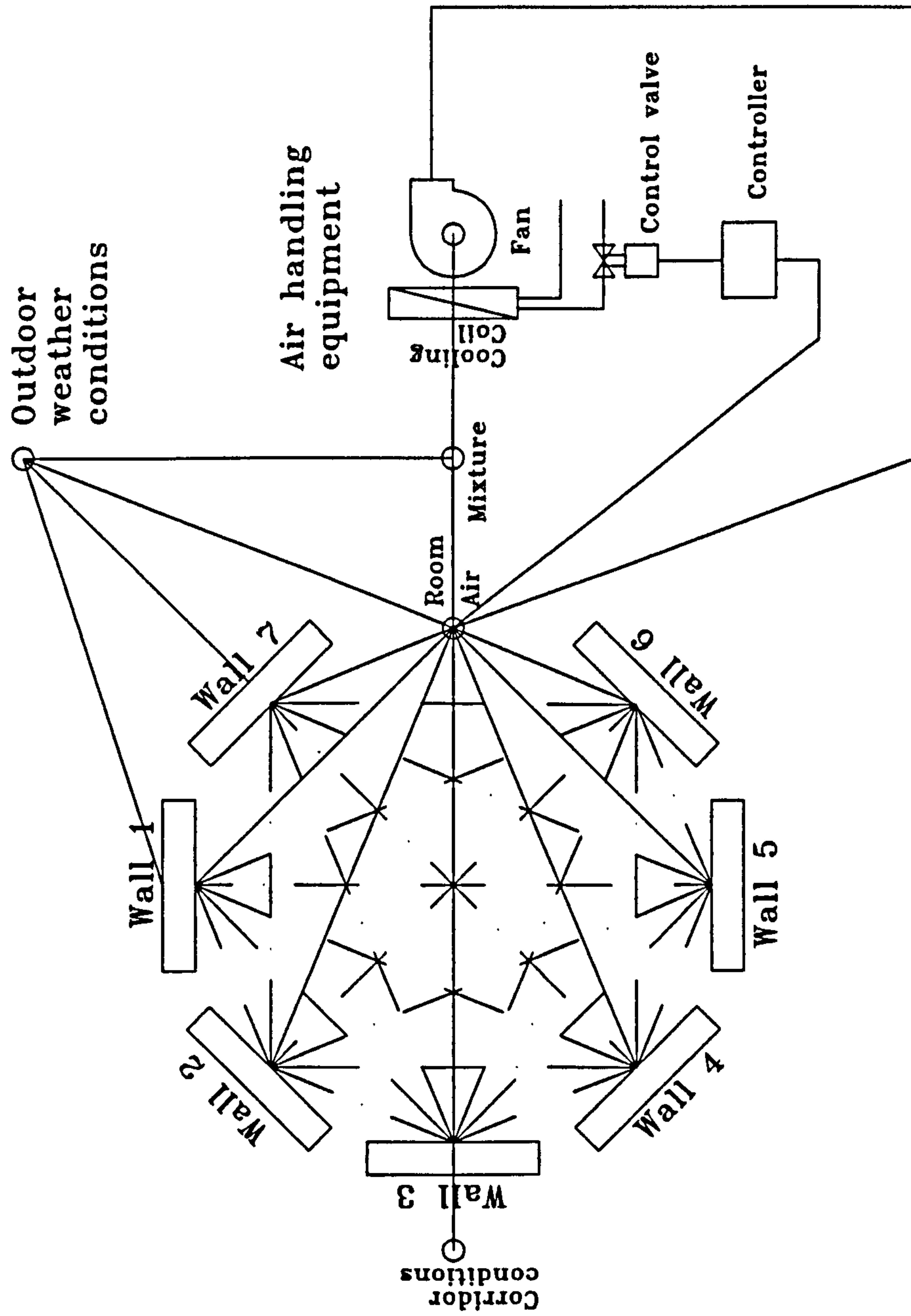


Figure 8.3 Staggered time progress in building and air-conditioning system components

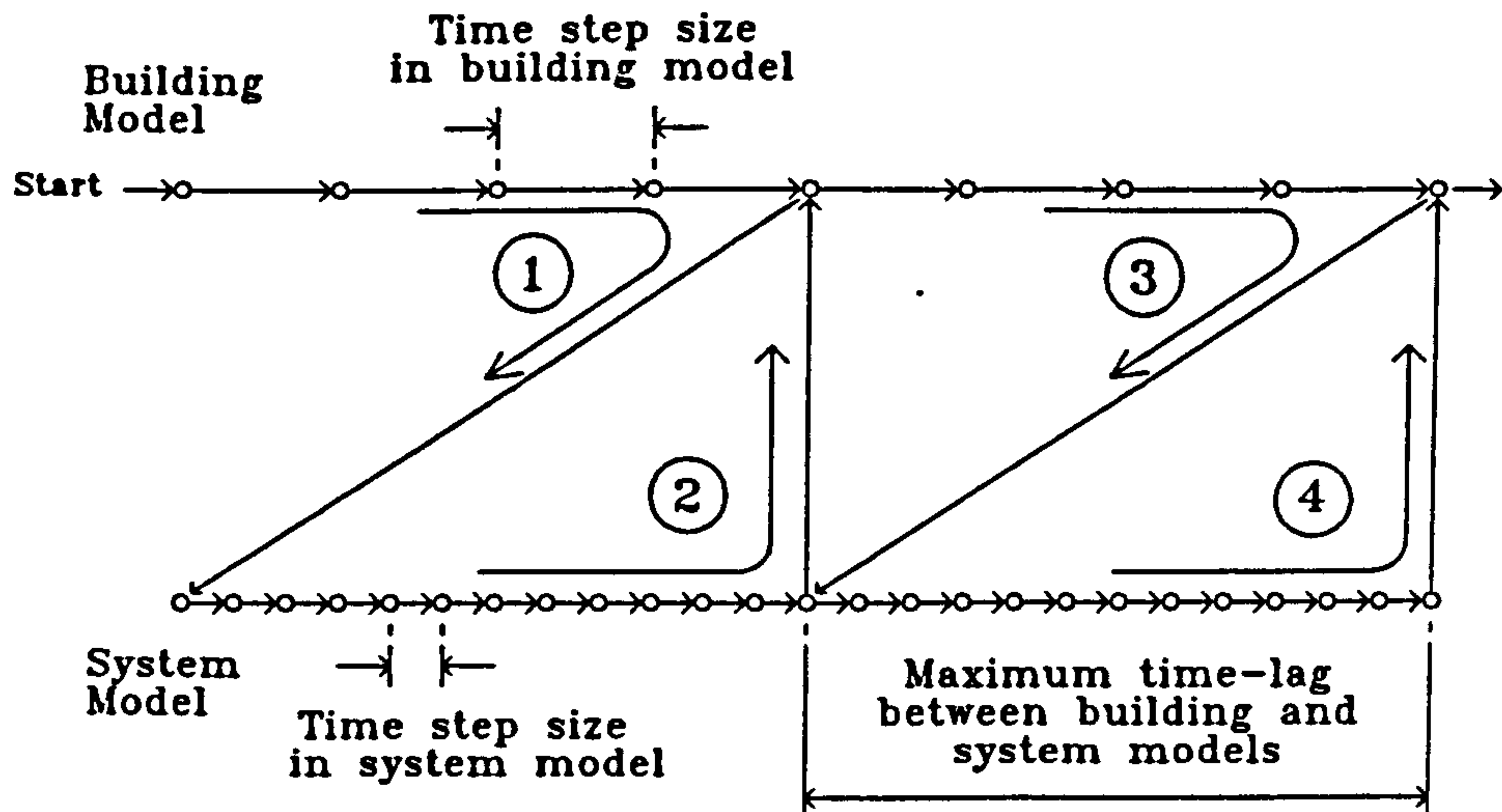


Figure 9.1 Construction of the composite walls and slabs of the model room

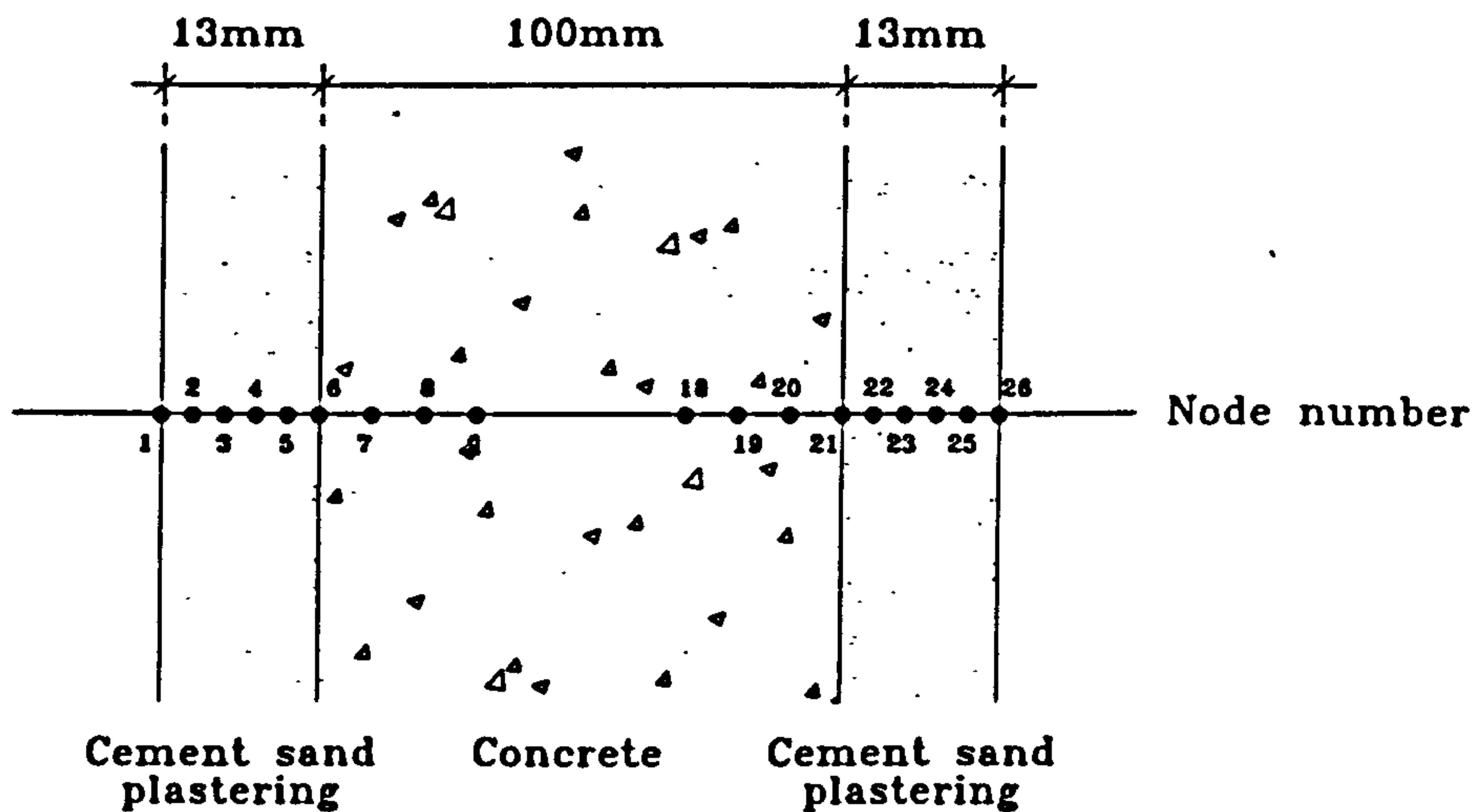
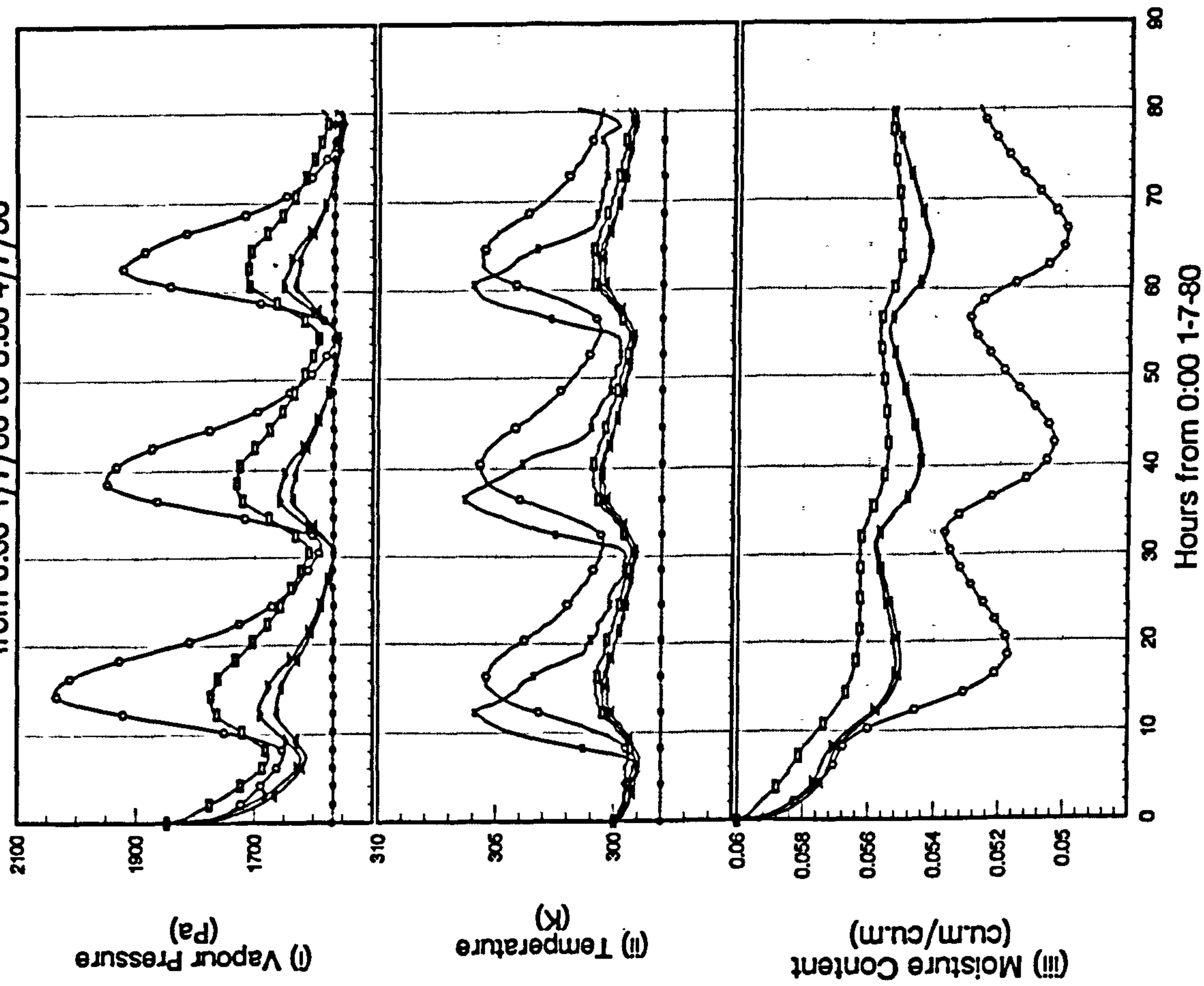


Figure 9.2.a

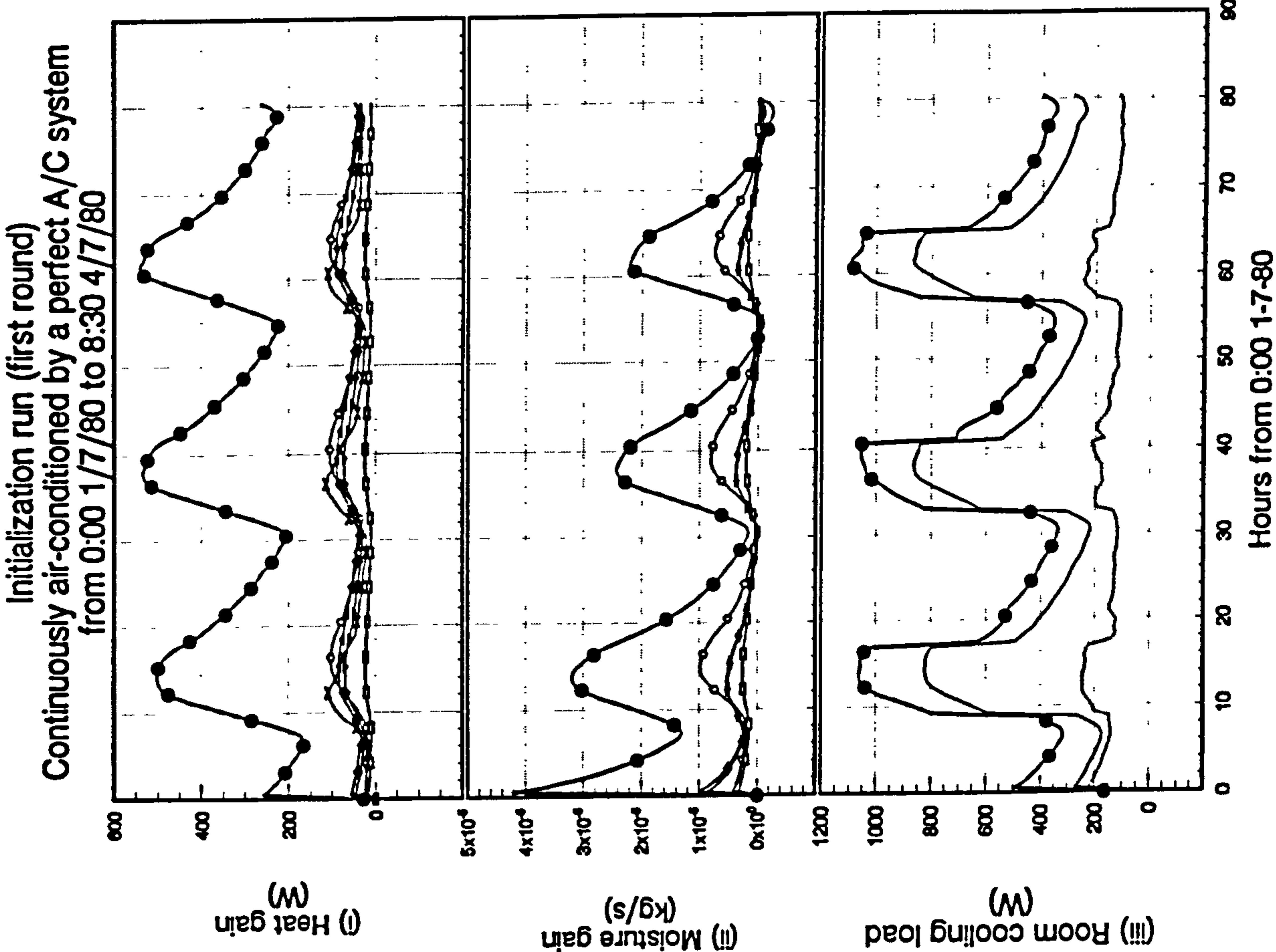
Initialization run (first round)
Continuously air-conditioned by a perfect A/C system
from 0:00 1/7/80 to 8:30 4/7/80



(MODEL: DERMAC)

Heat and Moisture Gains and Room Cooling Load

Figure 9.2.b



(MODEL: DERMAC)

Figure 9.2.c

Initialization run (first round)
Continuously air-conditioned by a perfect A/C system
from 0:00 1/7/80 to 8:30 4/7/80

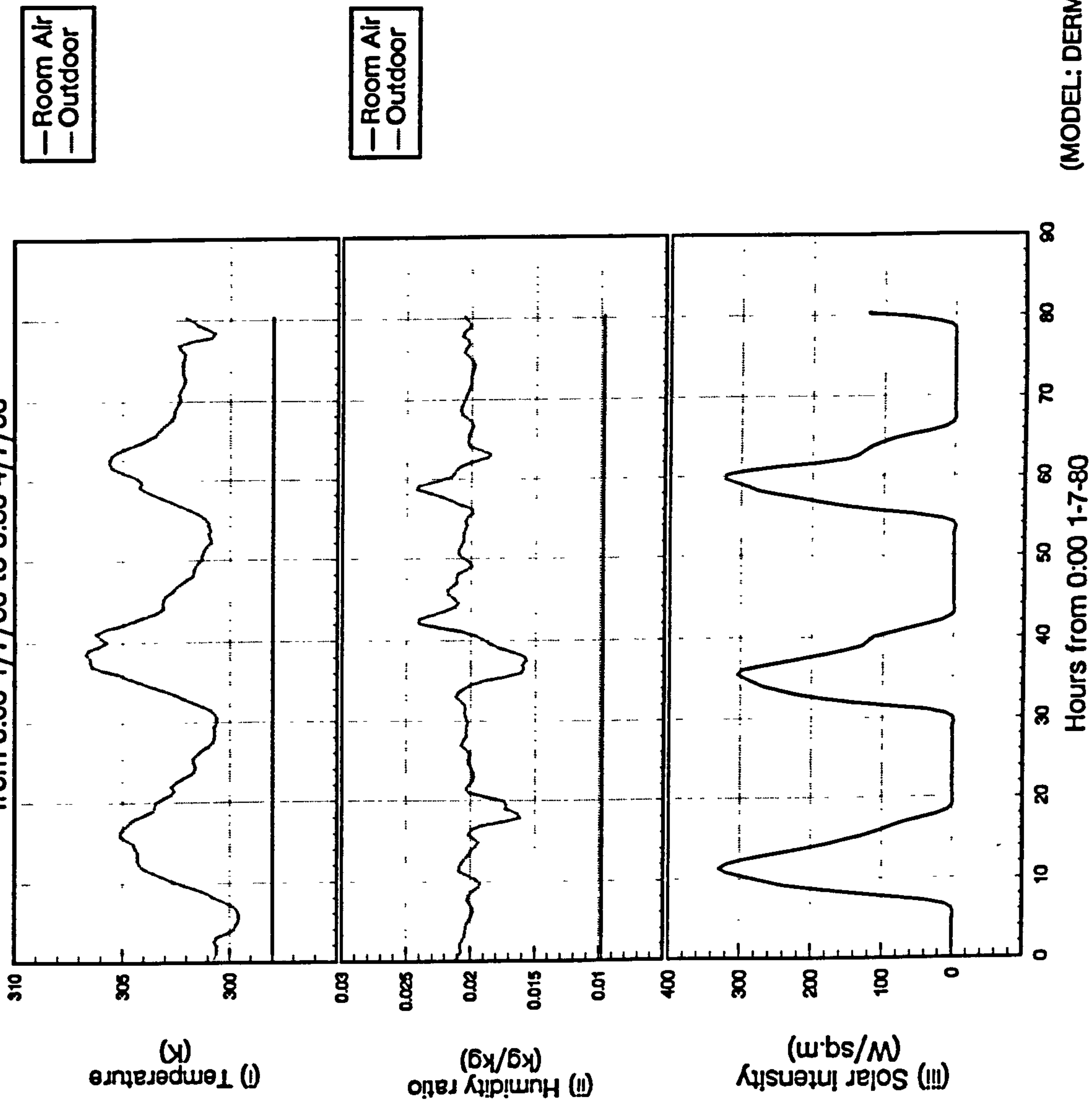
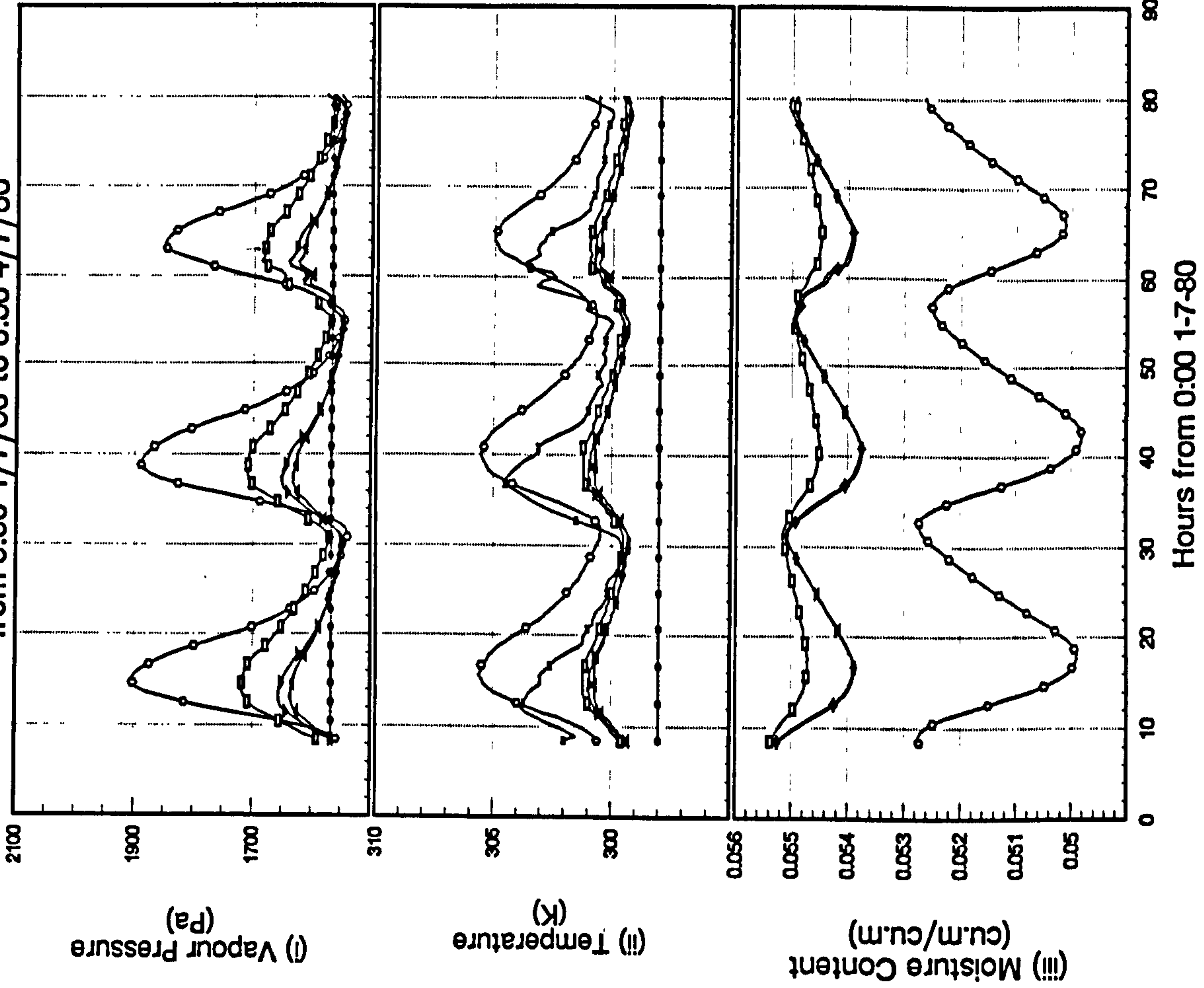


Figure 9.3.a

Initialization run (second round)
Continuously air-conditioned by a perfect A/C system
from 8:30 1/7/80 to 8:30 4/7/80



(MODEL: DERMAC)

Figure 9.3.b

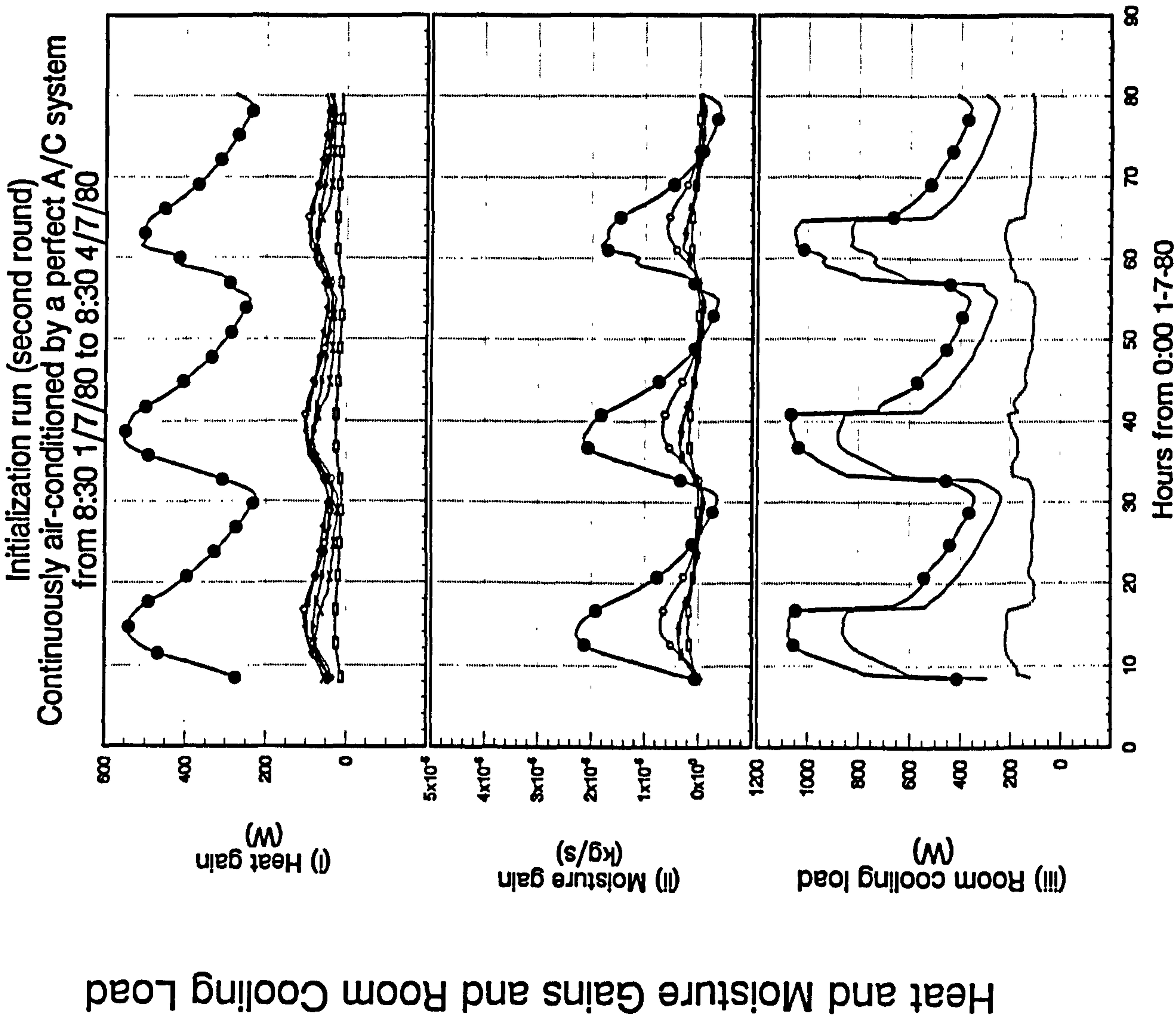
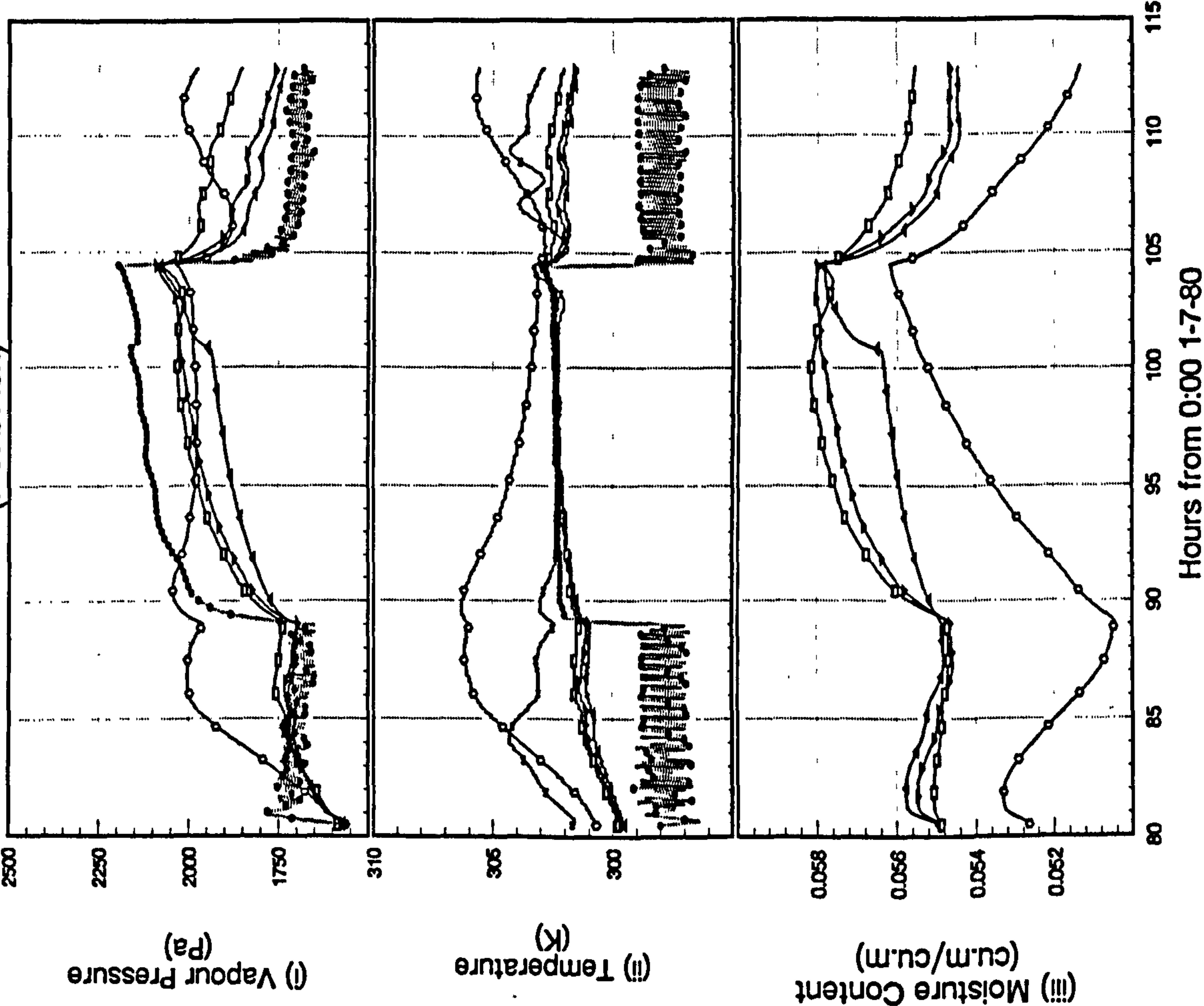


Figure 9.4.a

Intermittent air-conditioning by LMHD coil model
with on/off control from 8:30 4/7/80 to 17:00 5/7/80
(first batch)



(MODEL: RKMACC)

Figure 9.4.b

Intermittent air-conditioning by LMHD coil model
with on/off control from 8:30 4/7/80 to 17:00 5/7/80
(first batch)

Heat and Moisture Gains and Room Cooling Load

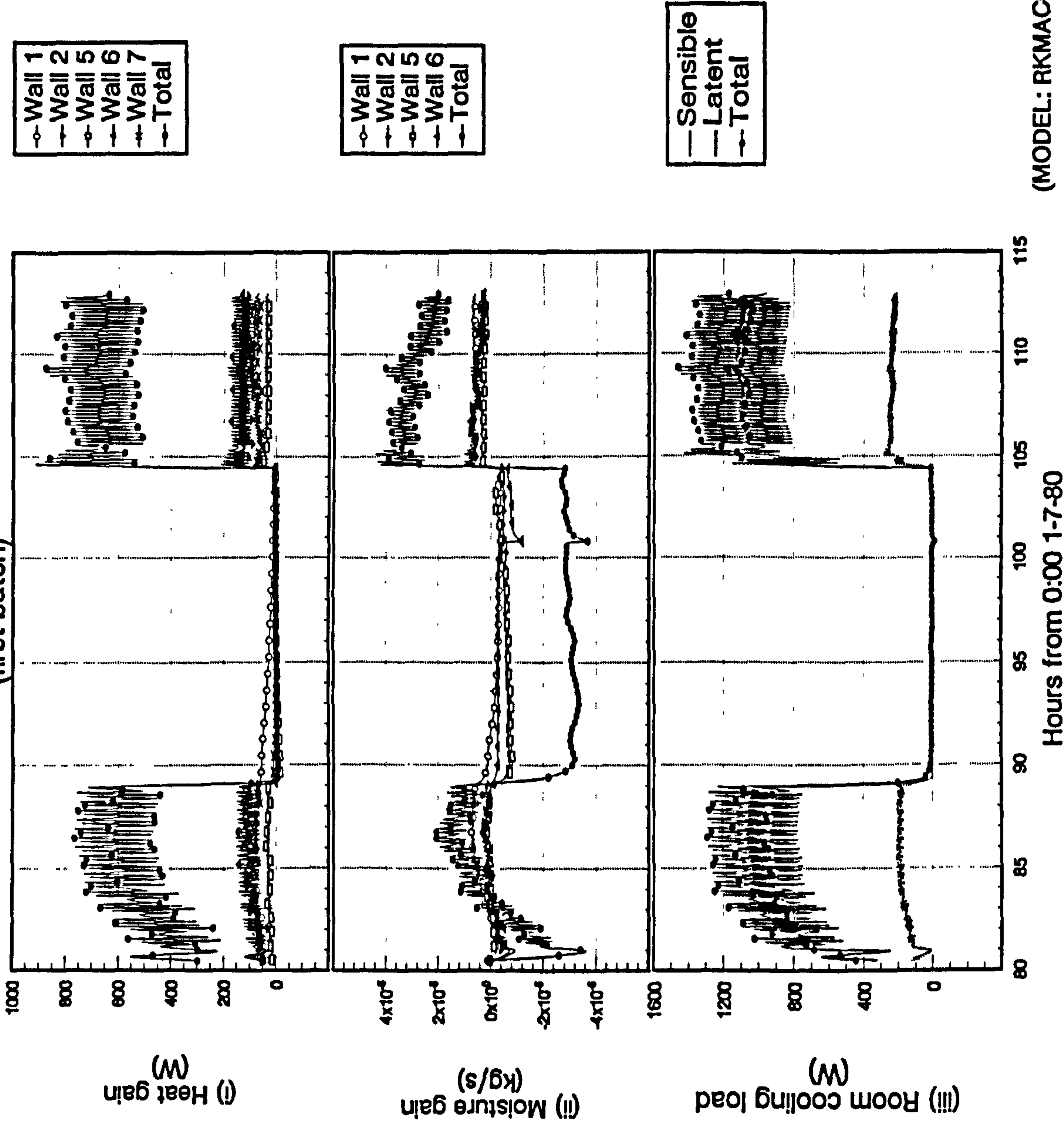
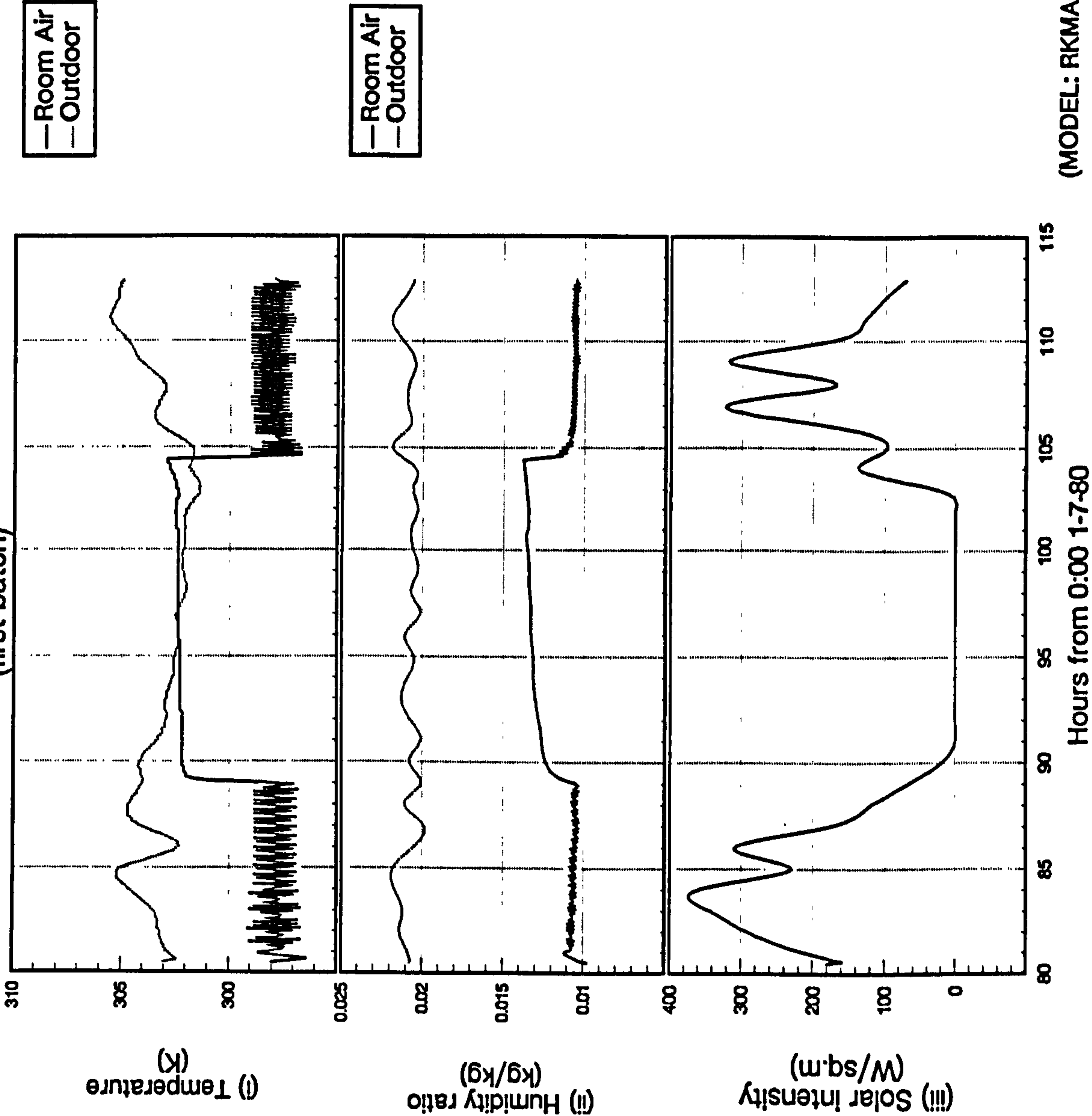


Figure 9.4.c

Intermittent air-conditioning by LMHD coil model
with on/off control from 8:30 4/7/80 to 17:00 5/7/80
(first batch)



(MODEL: RKMACC)

Indoor and Outdoor Conditions

Figure 9.5.a

Intermittent air-conditioning by FD coil model
with on/off control from 8:30 4/7/80 to 17:00 5/7/80
(first batch)

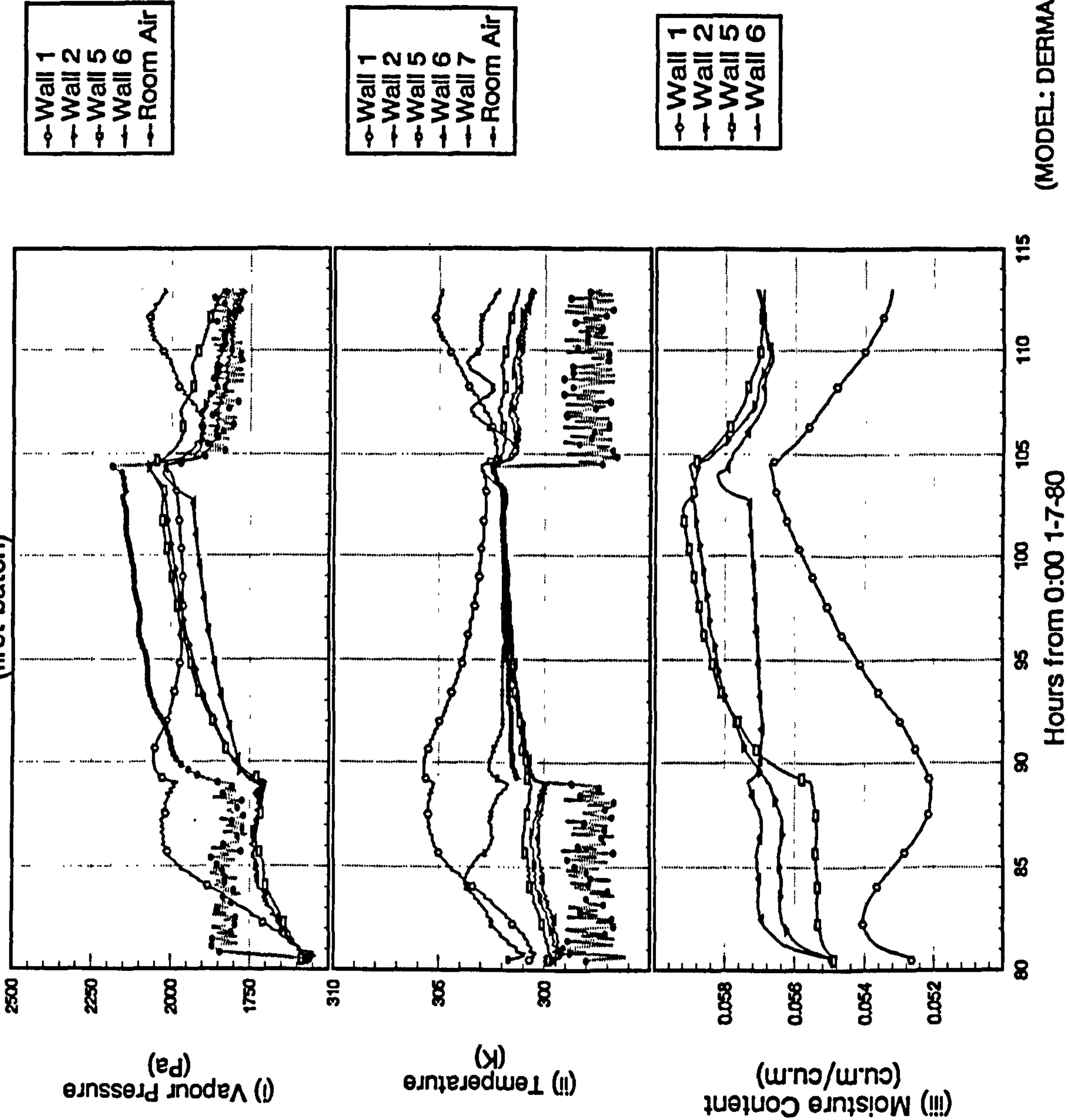


Figure 9.5.b

Intermittent air-conditioning by FD coil model
with on/off control from 8:30 4/7/80 to 17:00 5/7/80
(first batch)

Heat and Moisture Gains and Room Cooling Load

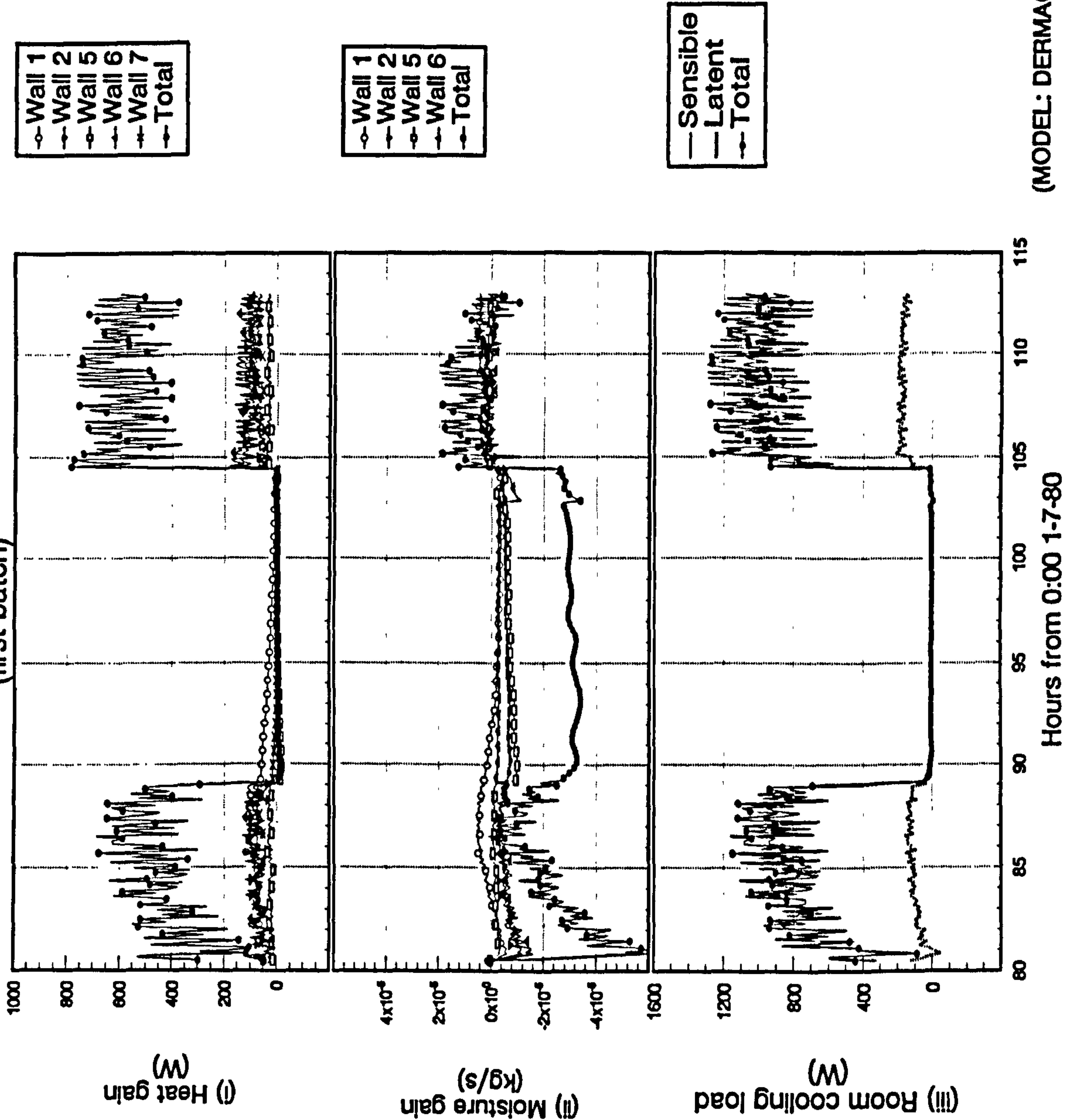
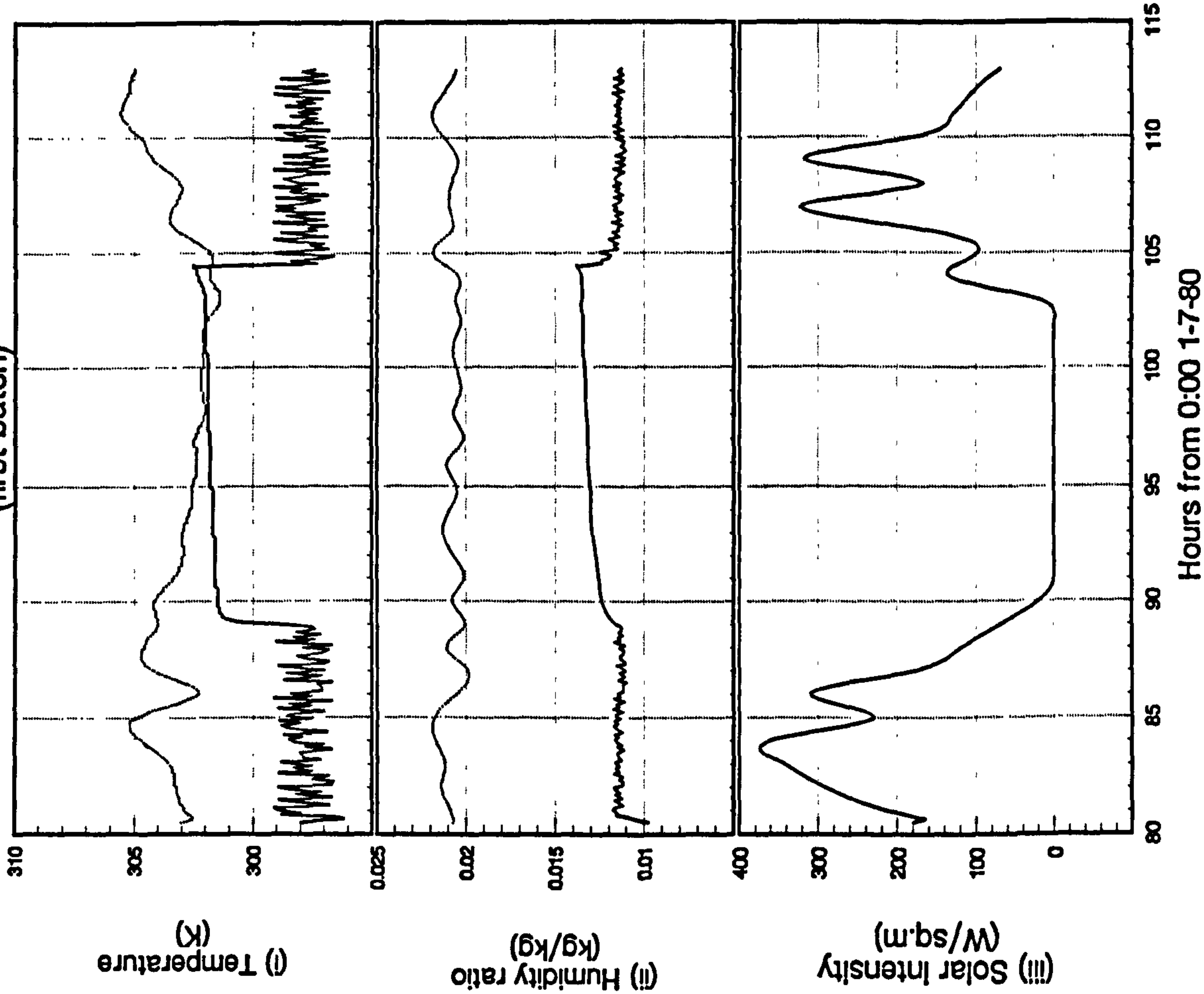


Figure 9.5.c

Intermittent air-conditioning by FD coil model
with on/off control from 8:30 4/7/80 to 17:00 5/7/80
(first batch)



(MODEL: DERMAC)

Figure 9.5.d.i

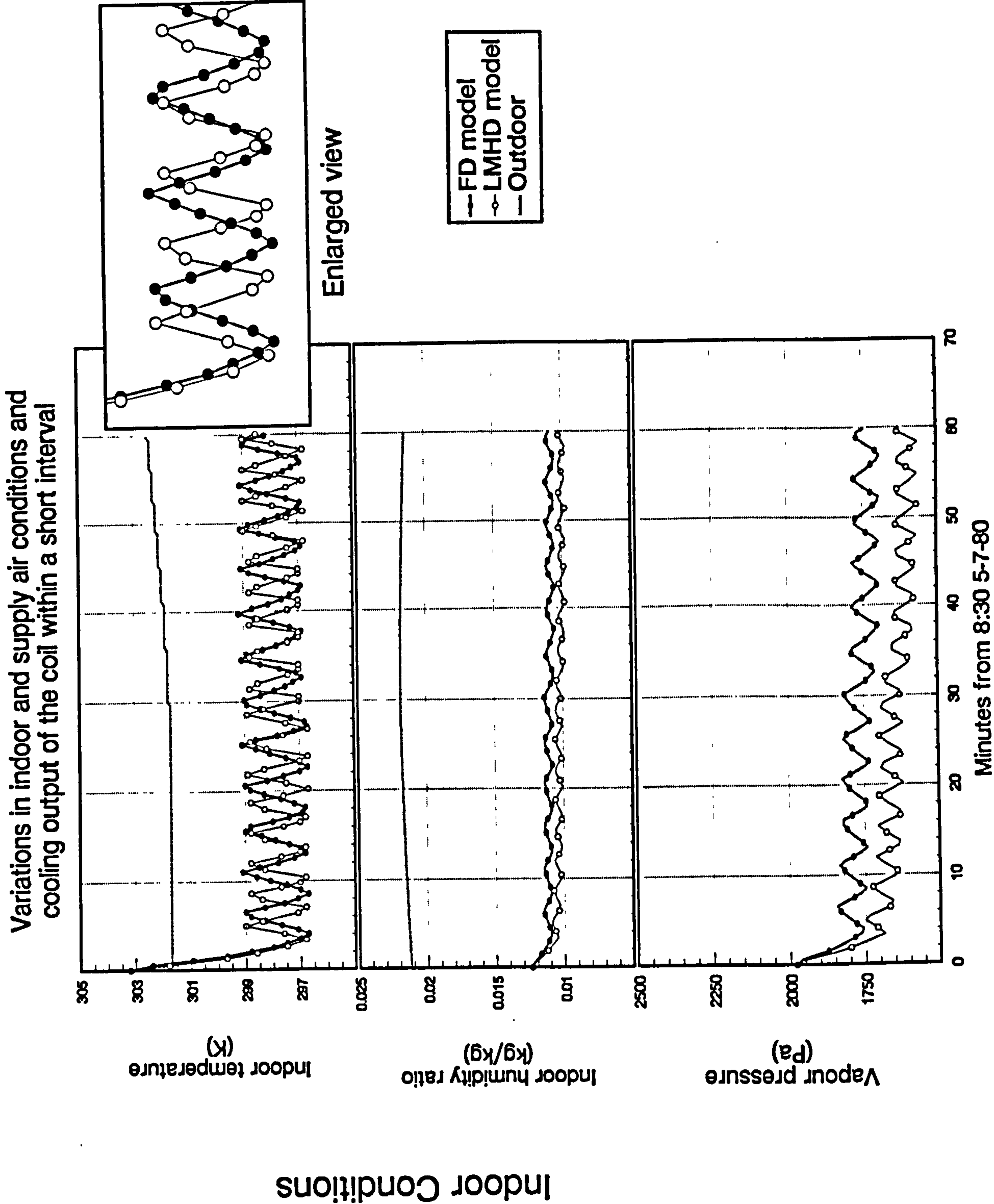


Figure 9.5.d.ii-vi

Variations in indoor and supply air conditions and cooling output of the coil within a short interval

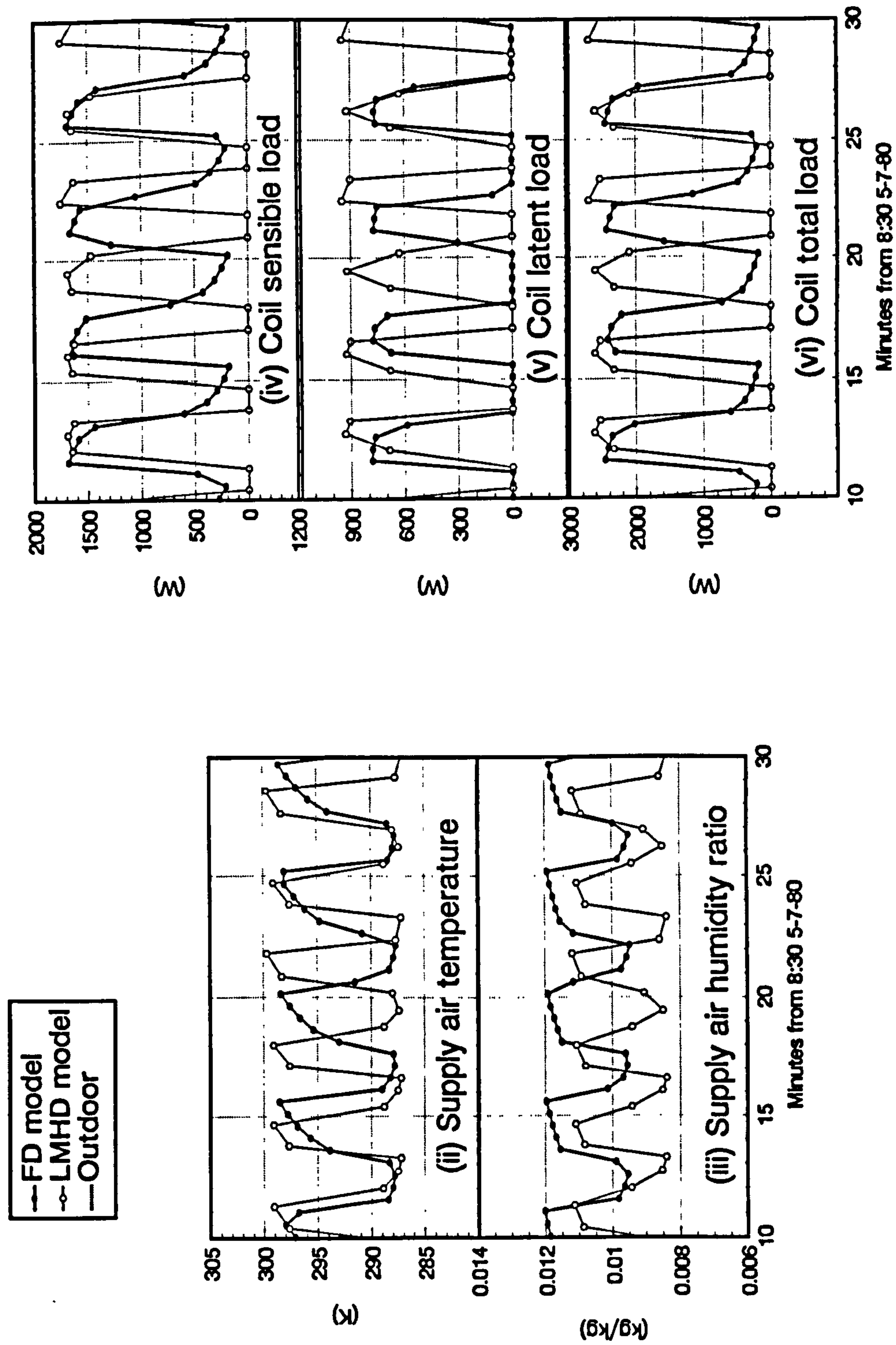
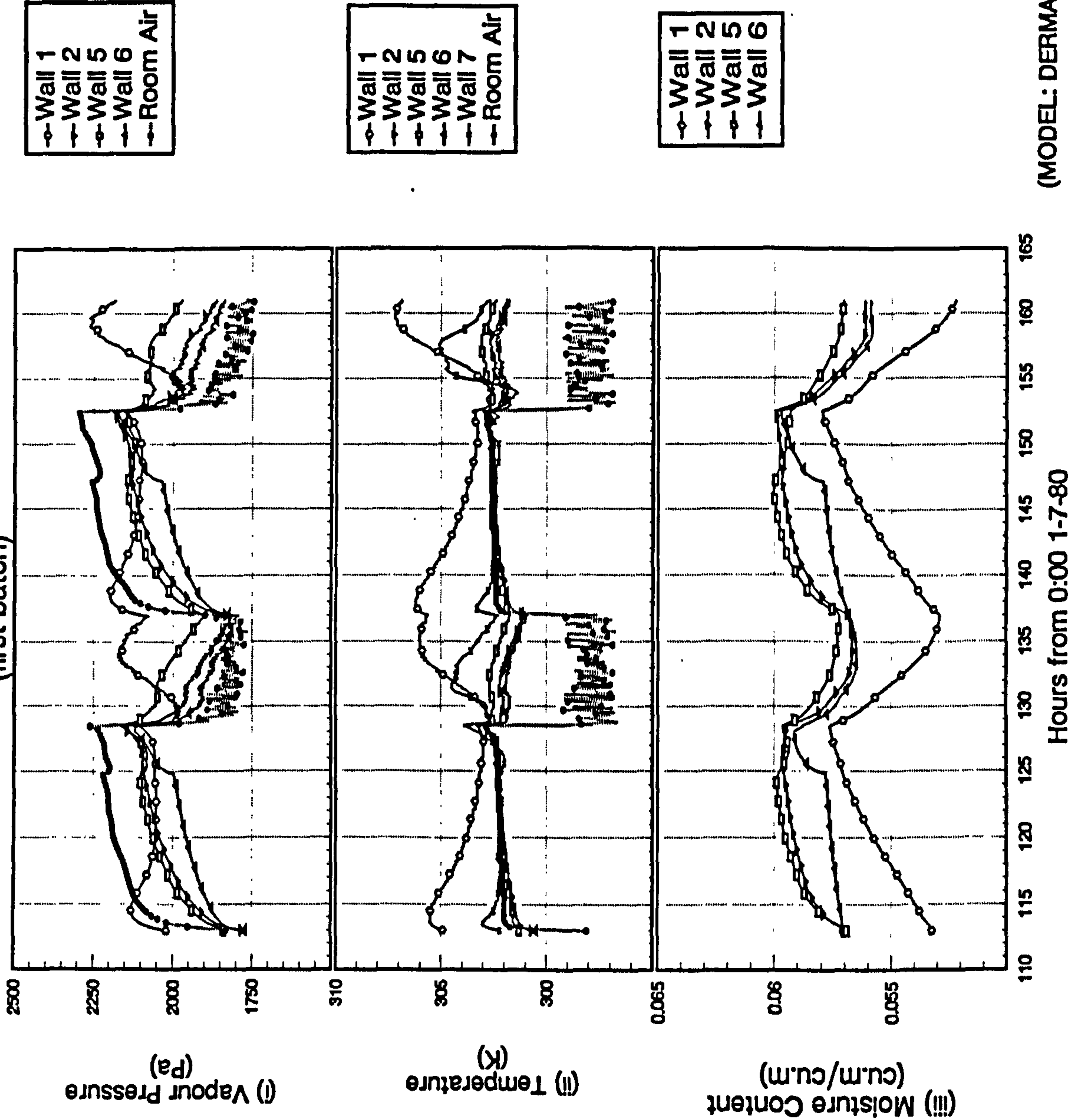


Figure 9.6.a

Intermittent air-conditioning by FD coil model
with on/off control from 17:00 5/7/80 to 17:00 7/7/80
(first batch)



(MODEL: DERMAC)

Heat and Moisture Gains and Room Cooling Load

Figure 9.6.b

Intermittent air-conditioning by FD coil model
with on/off control from 17:00 5/7/80 to 17:00 7/7/80
(first batch)

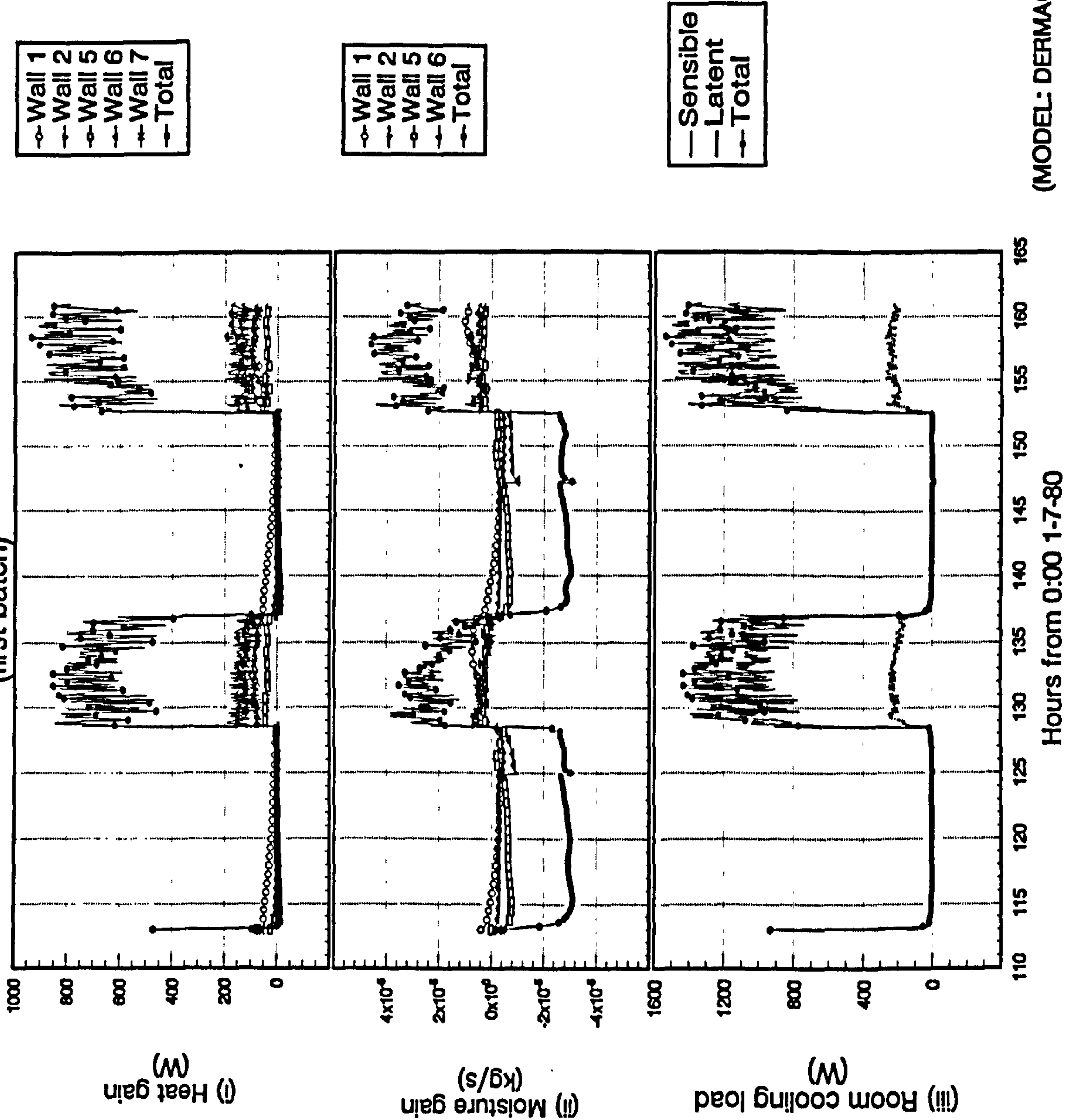
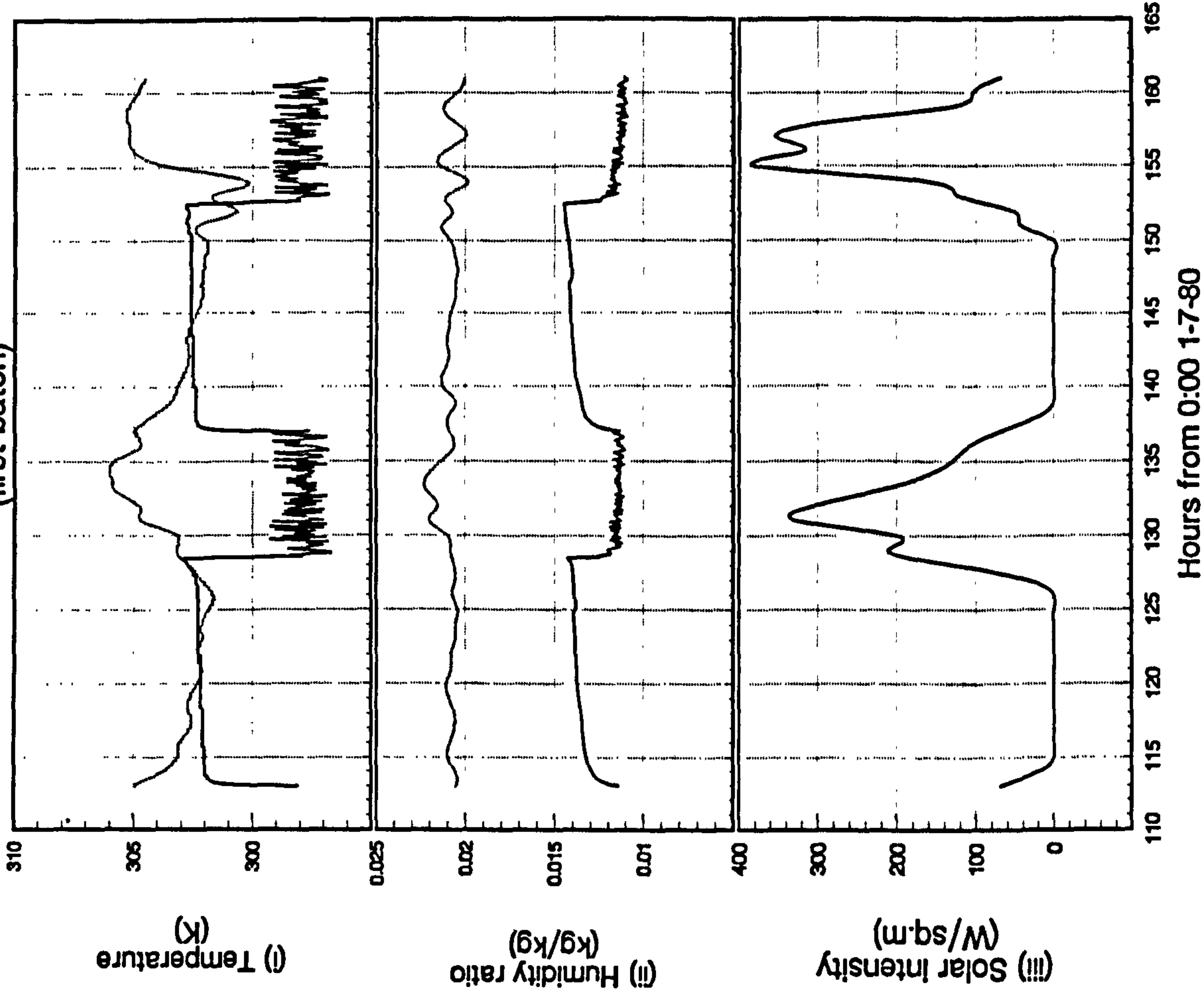


Figure 9.6.c

Intermittent air-conditioning by FD coil model
with on/off control from 17:00 5/7/80 to 17:00 7/7/80
(first batch)



(MODEL: DERMAG)

Figure 9.7

Intermittent air-conditioning by FD coil model
with on/off control from 8:30 4/7/80 to 17:00 7/7/80
(first batch)

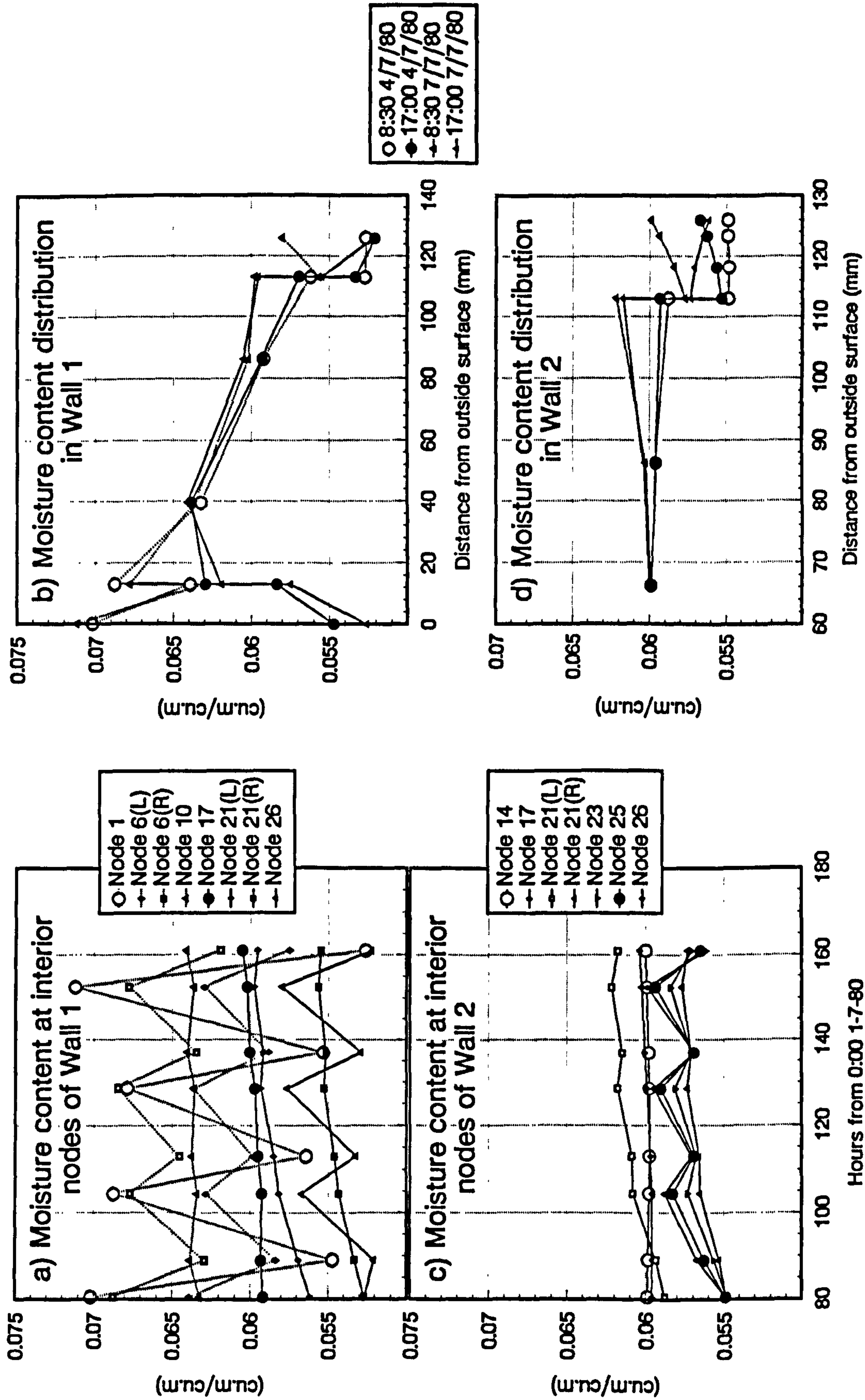


Figure 9.8.a

Intermittent air-conditioning by LMHD coil model
with on/off control from 8:30 4/7/80 to 17:00 5/7/80
and with wall moisture adsorption and desorption ignored
(first batch)

Wall Internal Surfaces Conditions

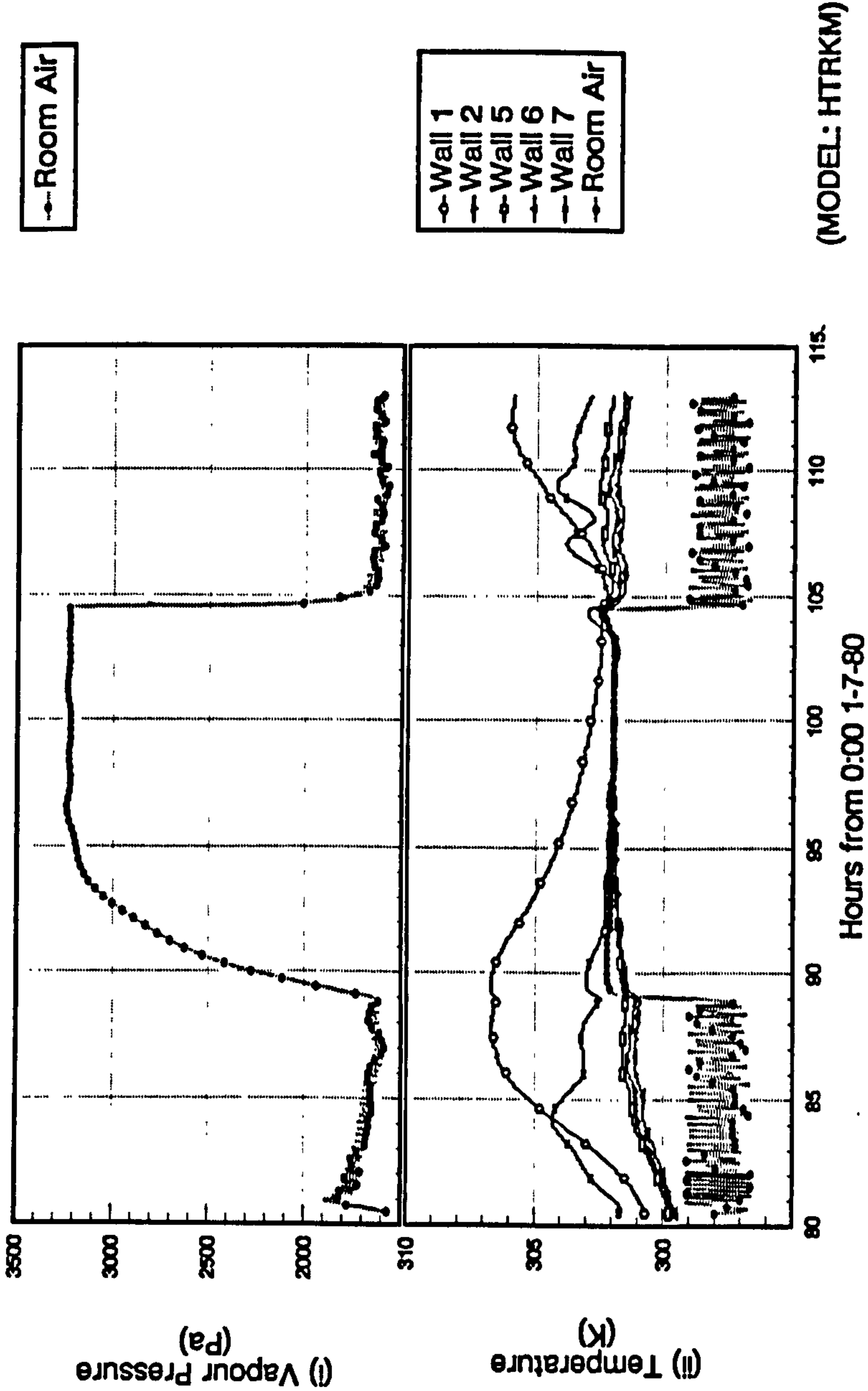


Figure 9.8.b

Intermittent air-conditioning by LMHD coil model
with on/off control from 8:30 4/7/80 to 17:00 5/7/80
and with wall moisture adsorption and desorption ignored
(first batch)

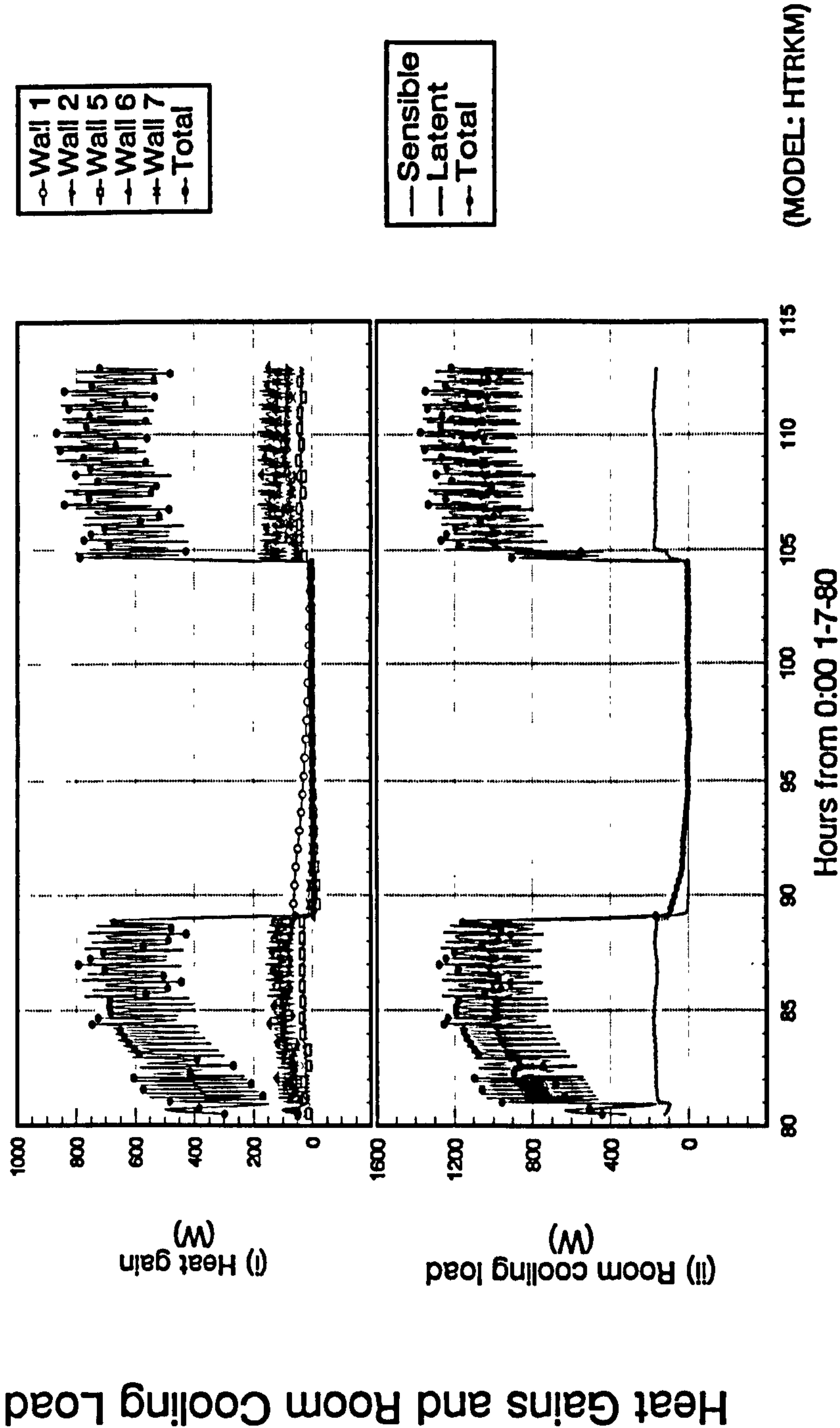


Figure 9.8.c

Intermittent air-conditioning by LMHD coil model
with on/off control from 8:30 4/7/80 to 17:00 5/7/80
and with wall moisture adsorption and desorption ignored
(first batch)

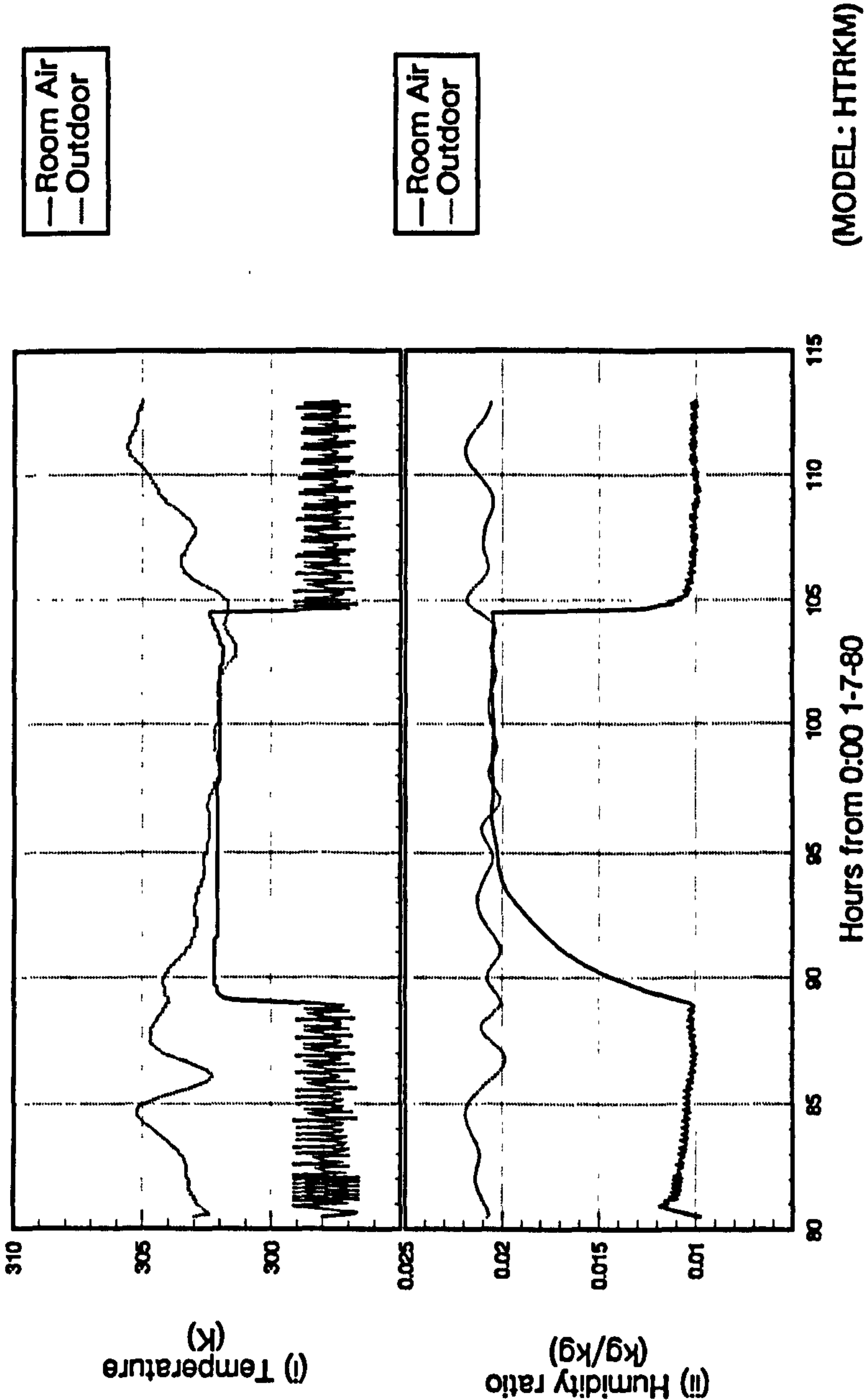


Figure 9.9.a

Intermittent air-conditioning by LMHD coil model
with proportional control
from 8:30 4/7/80 to 17:00 5/7/80
(first batch)

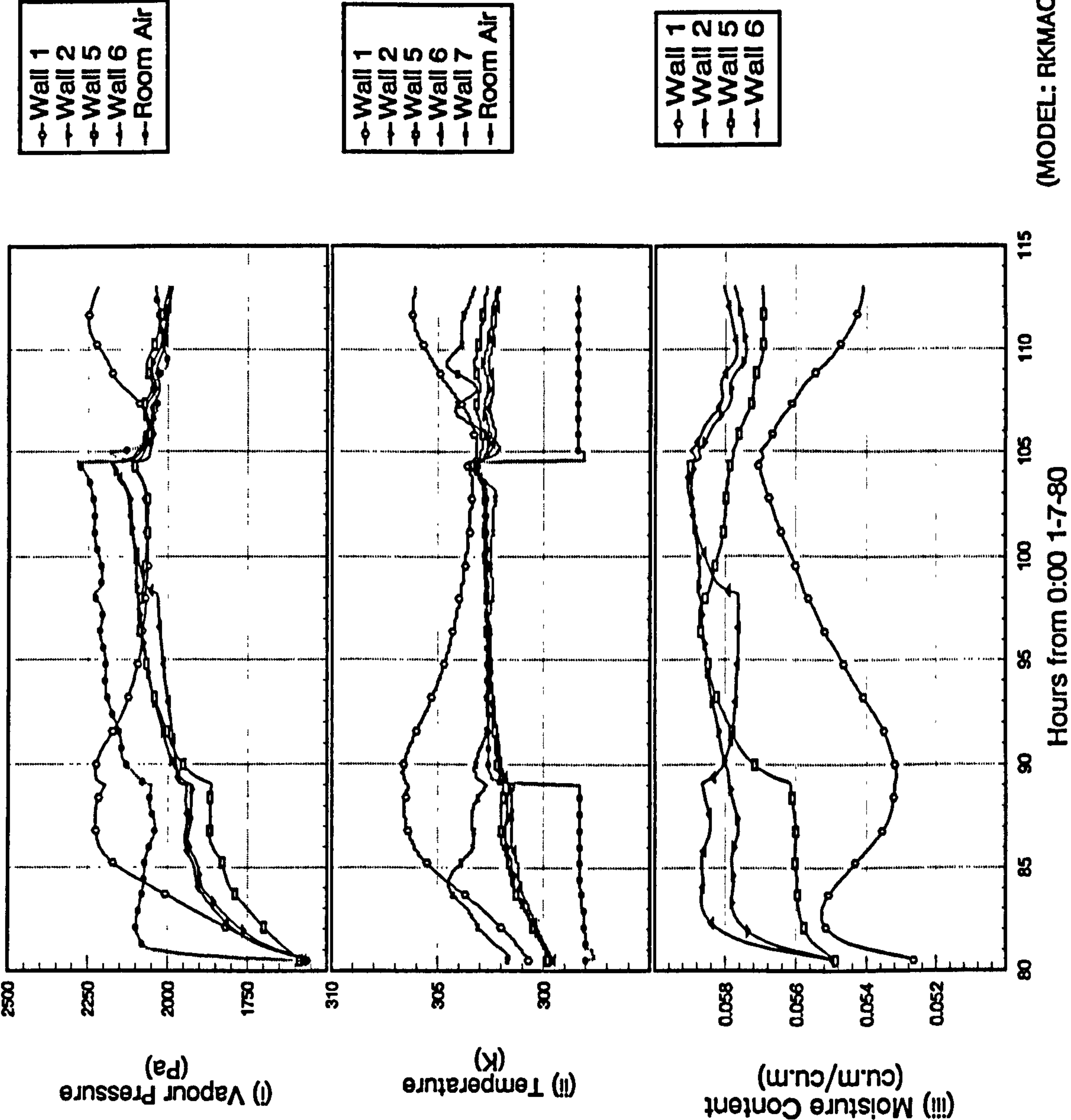
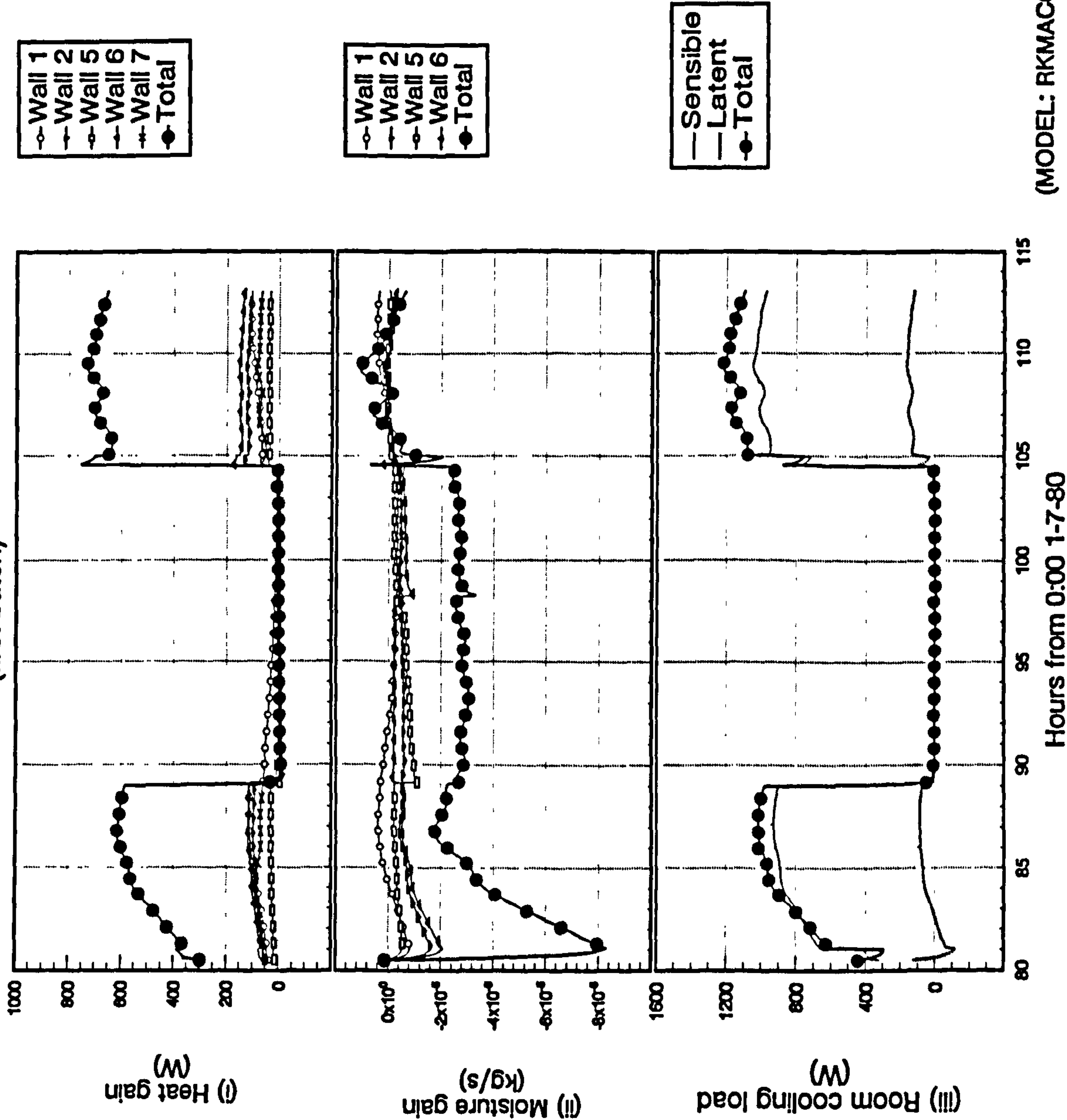


Figure 9.9.b

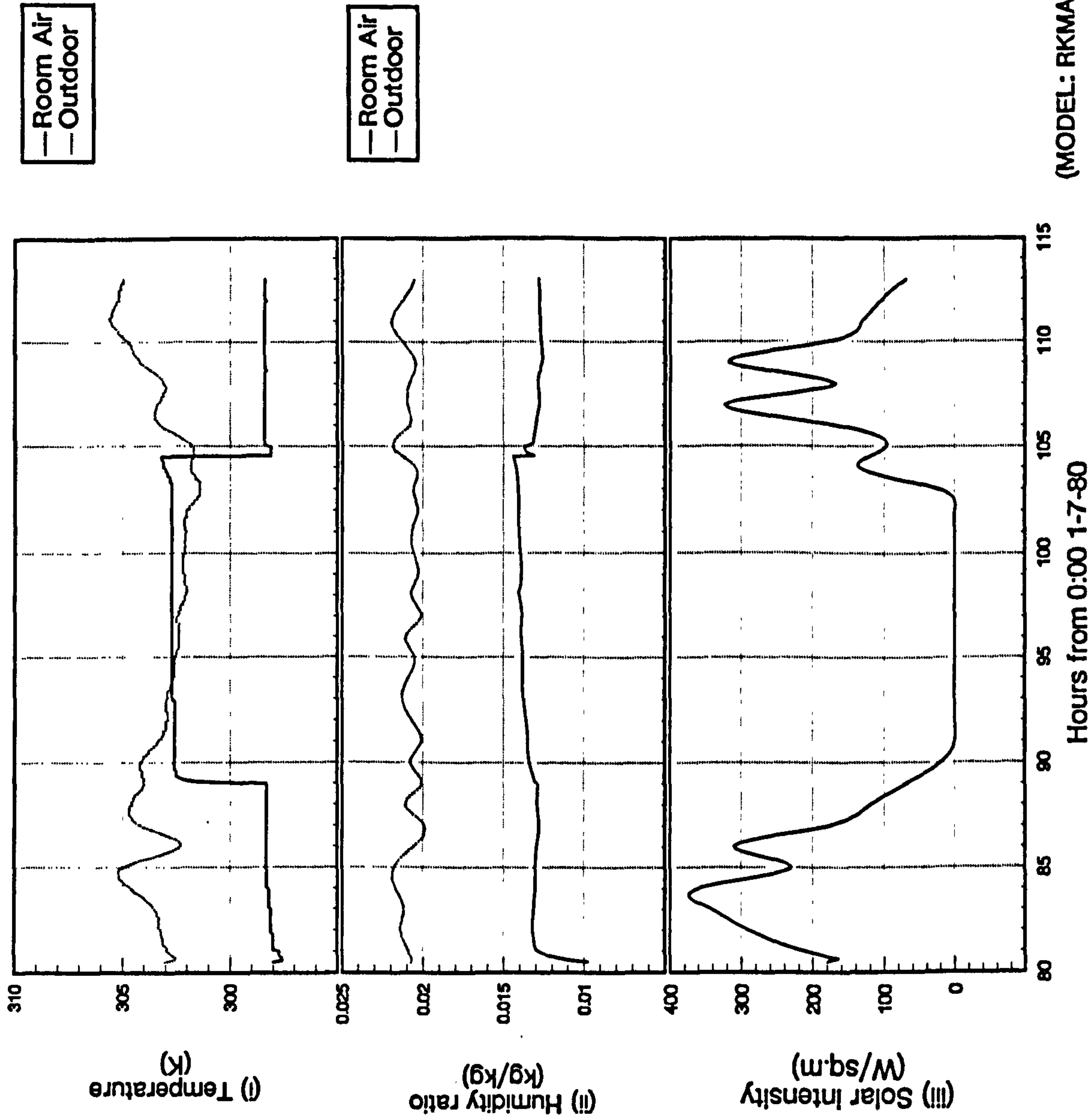
Intermittent air-conditioning by LMHD coil model
with proportional control
from 8:30 4/7/80 to 17:00 5/7/80
(first batch)

Heat and Moisture Gains and Room Cooling Load



Indoor and Outdoor Conditions

Figure 9.9.c
Intermittent air-conditioning by LMHD coil model
with proportional control
from 8:30 4/7/80 to 17:00 5/7/80
(first batch)



(MODEL: RKMAGC)

Figure 9.10.a

Intermittent air-conditioning by LMHD coil model
with P-control, pre-treated FA & zero infiltration
from 8:30 4/7/80 to 17:00 5/7/80
(first batch)

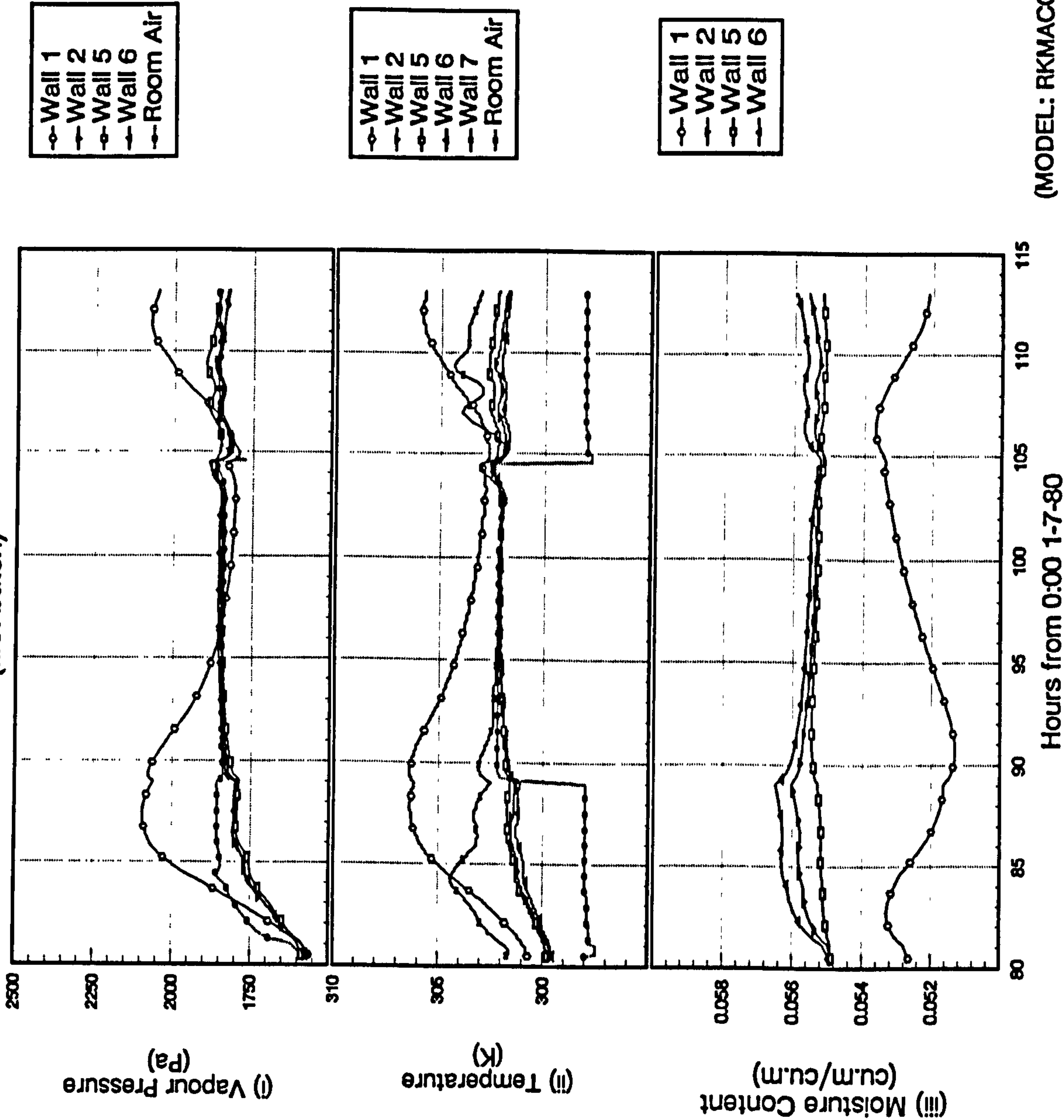
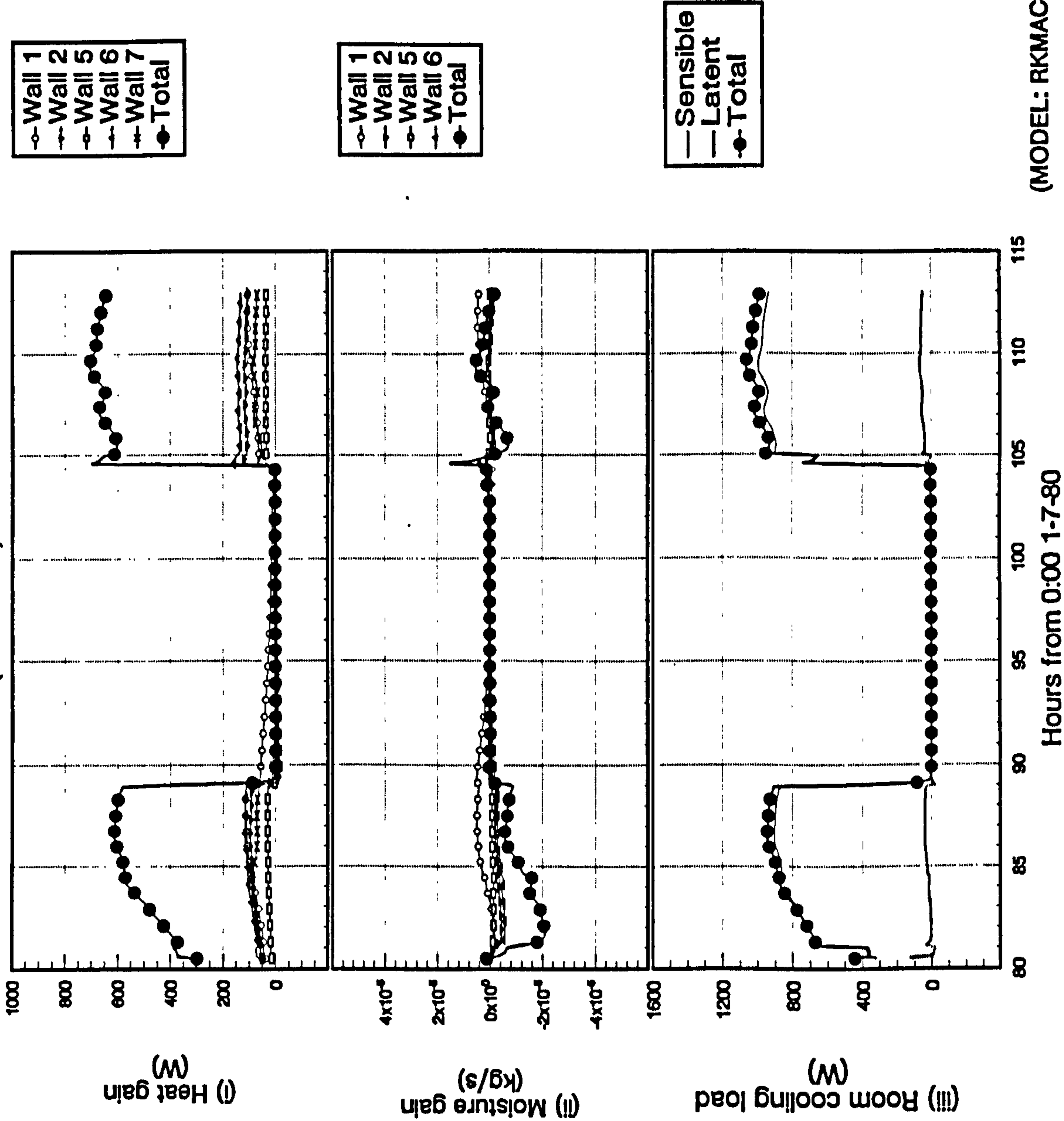


Figure 9.10.b

Intermittent air-conditioning by LMHD coil model
with P-control, pre-treated FA & zero infiltration
from 8:30 4/7/80 to 17:00 5/7/80
(first batch)

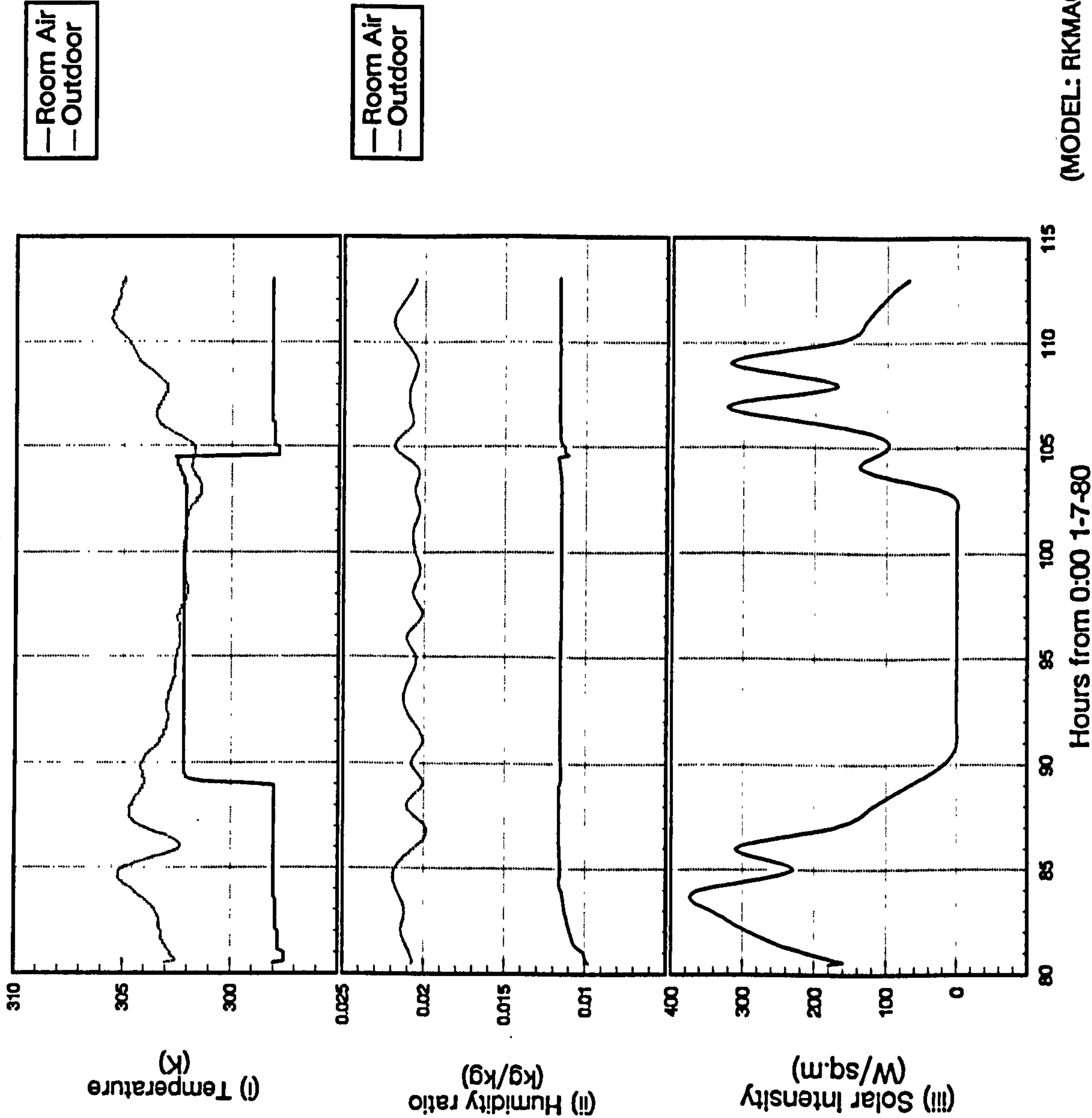
Heat and Moisture Gains and Room Cooling Load



Indoor and Outdoor Conditions

Figure 9.10.c

Intermittent air-conditioning by LMHD coil model
with P-control, pre-treated FA & zero infiltration
from 8:30 4/7/80 to 17:00 5/7/80
(first batch)



(MODEL: RKMACC)

Figure 9.11.a

Intermittent air-conditioning by LMHD coil model
with P-control, pre-treated FA & infiltration of 1 ac/hr
from 8:30 4/7/80 to 17:00 5/7/80
(first batch)

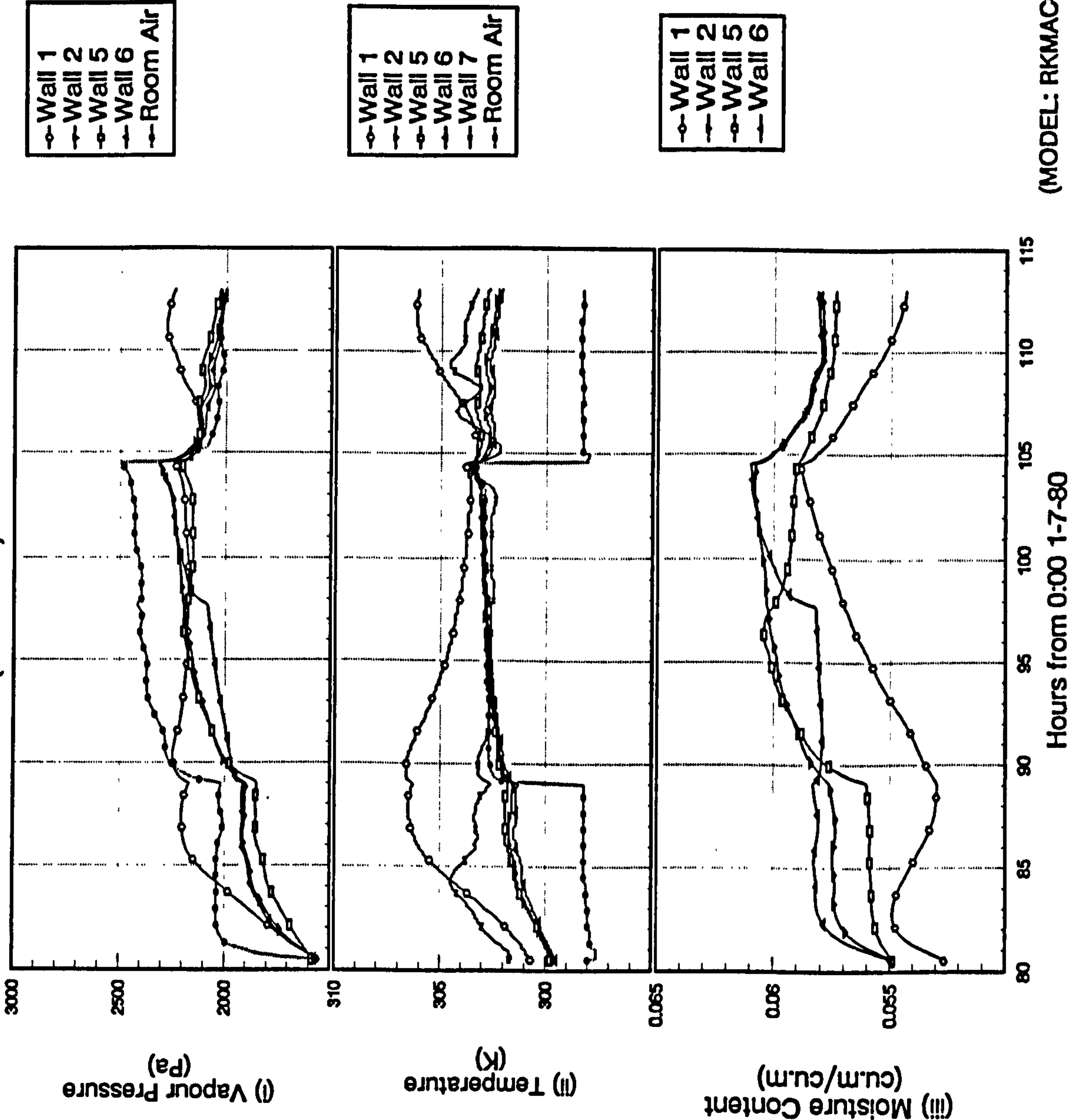
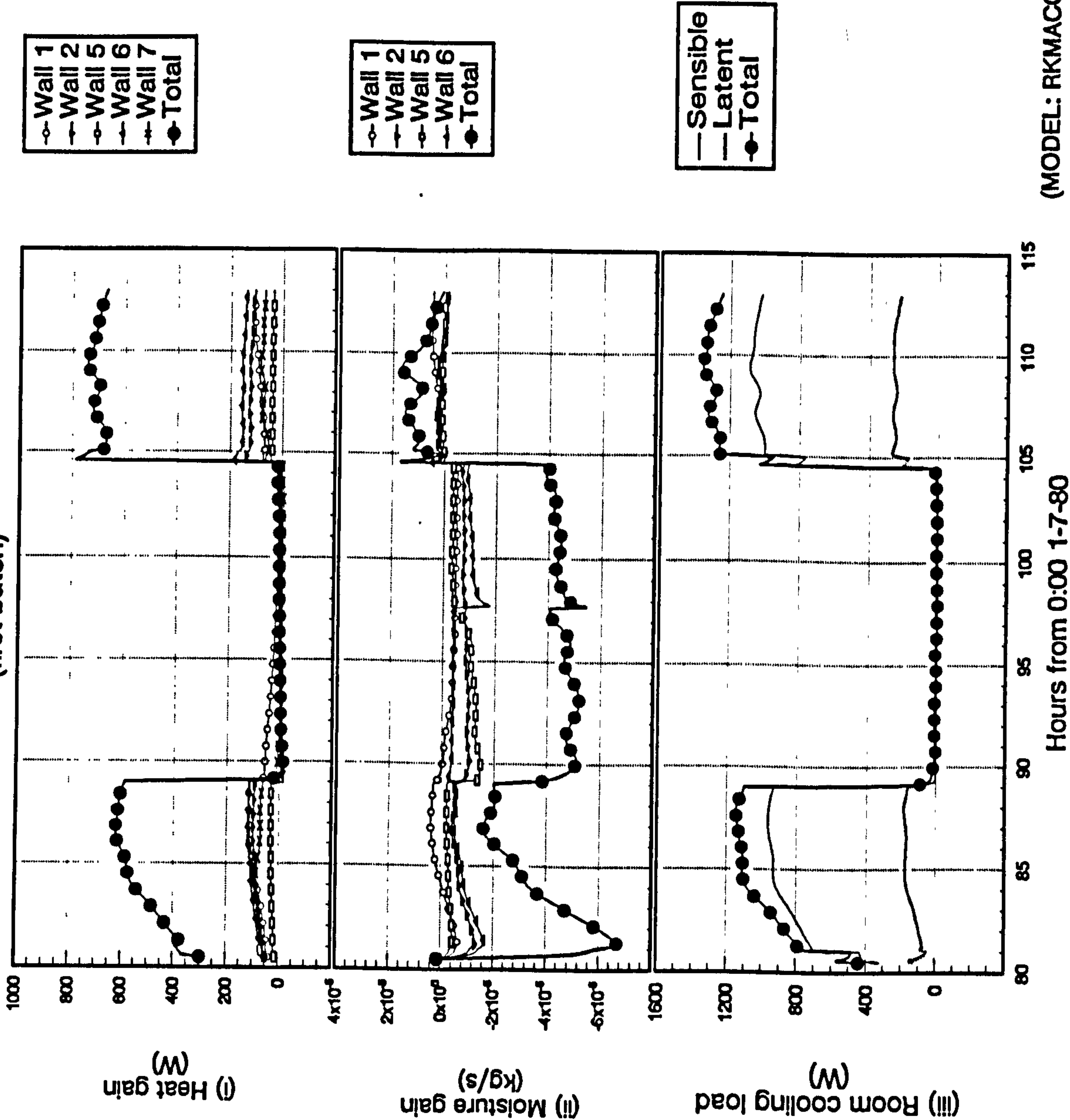


Figure 9.11.b

Intermittent air-conditioning by LMHD coil model
with P-control, pre-treated FA & infiltration of 1 ac/hr
from 8:30 4/7/80 to 17:00 5/7/80
(first batch)

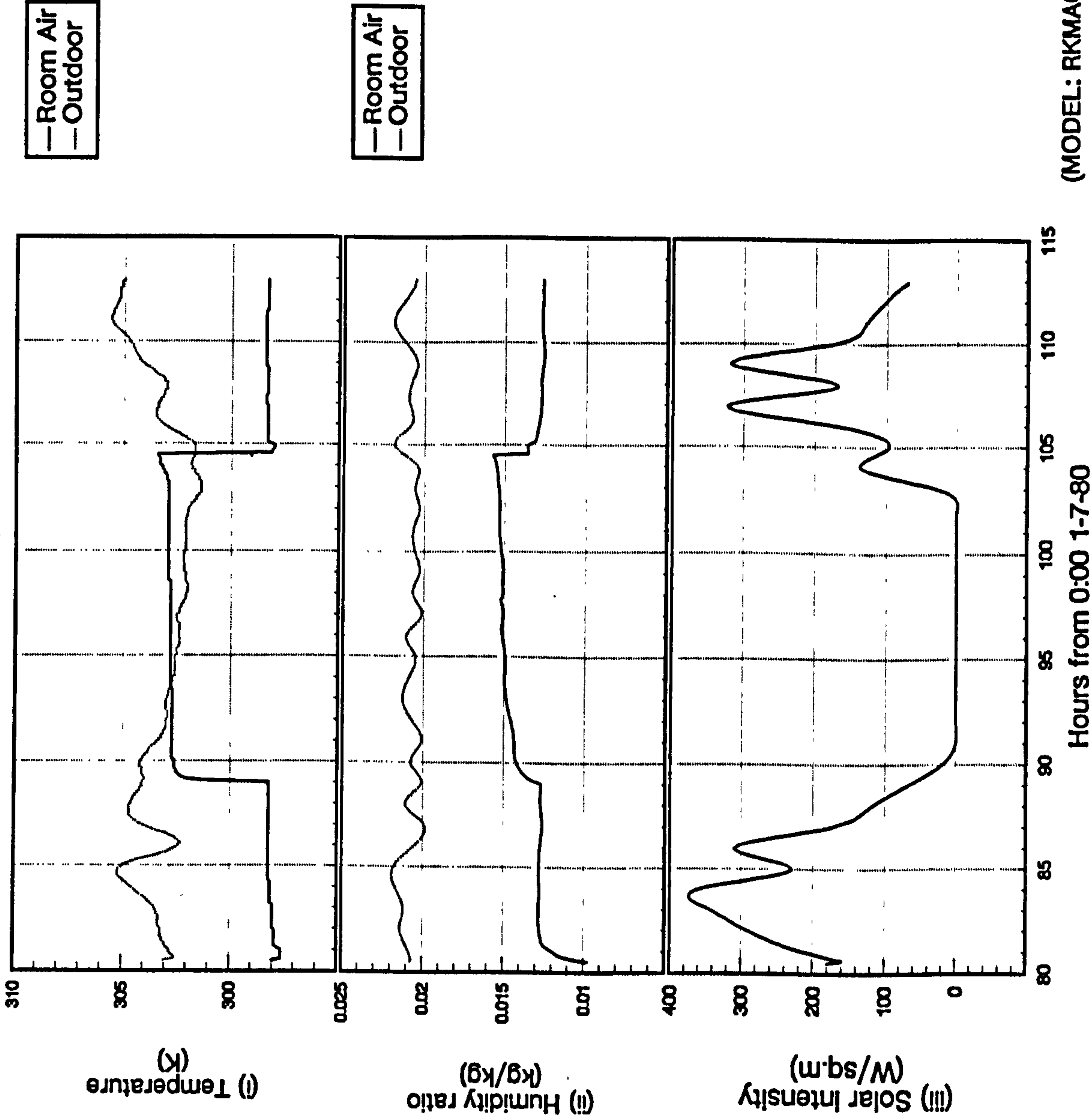
Heat and Moisture Gains and Room Cooling Load



(MODEL: RKMACC)

Indoor and Outdoor Conditions

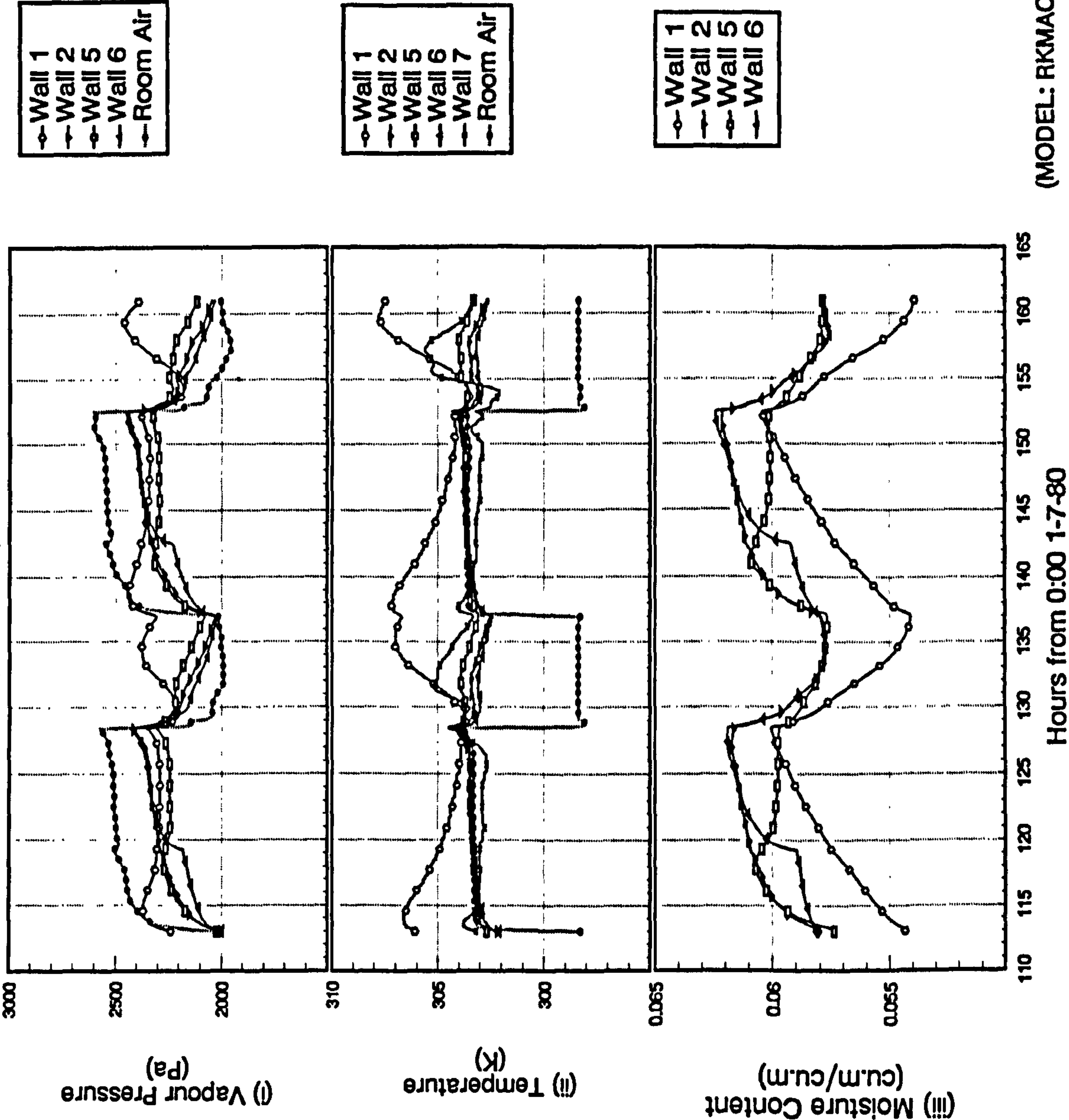
Figure 9.11.c
Intermittent air-conditioning by LMHD coil model
with P-control, pre-treated FA & infiltration of 1 ac/hr
from 8:30 4/7/80 to 17:00 5/7/80
(first batch)



(MODEL: RKMACC)

Figure 9.12.a

Intermittent air-conditioning by LMHD coil model
with P-control, pre-treated FA & infiltration of 1 ac/hr
from 17:00 5/7/80 to 17:00 7/7/80
(first batch)

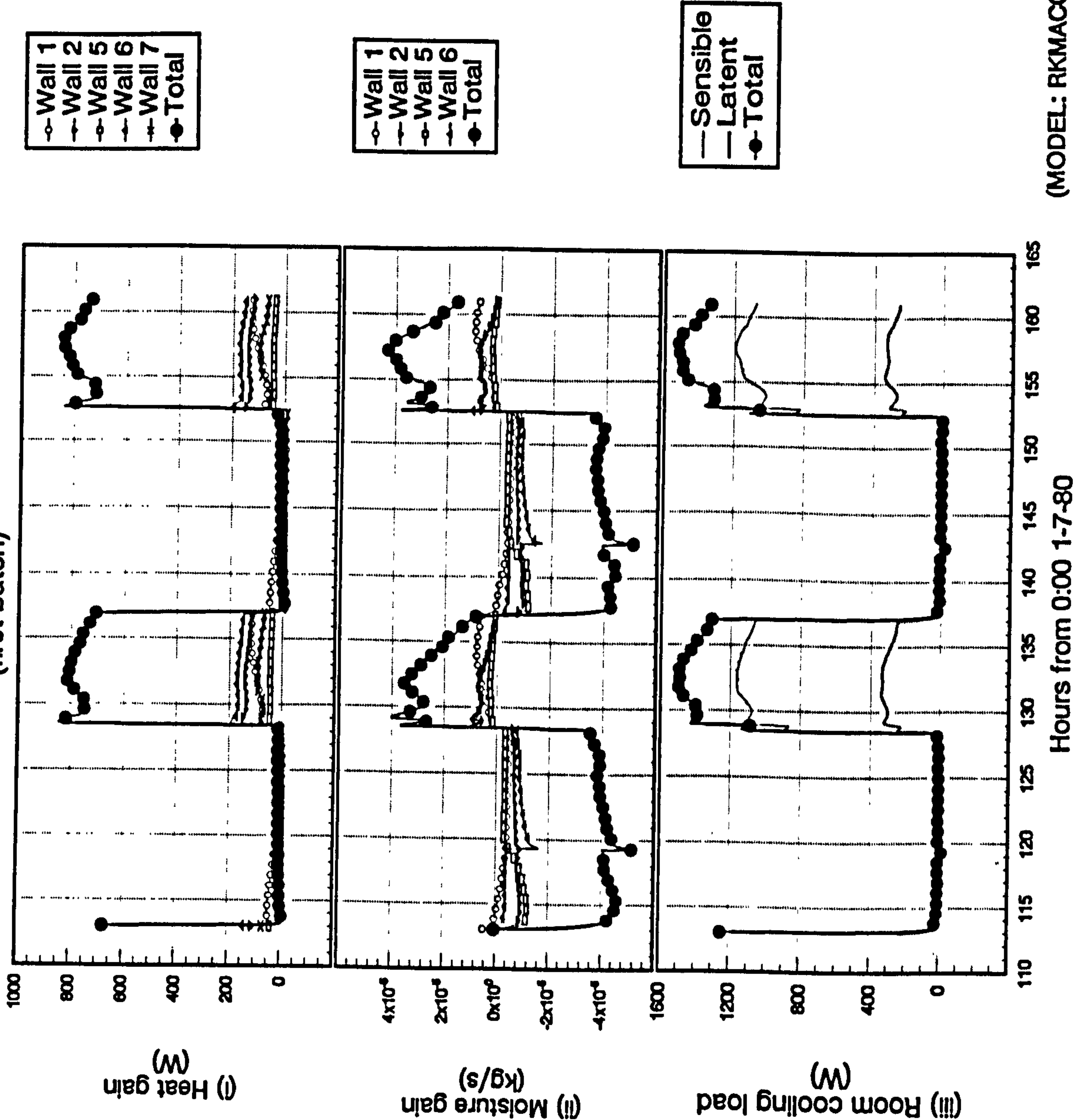


(MODEL: RKMACC)

Figure 9.12.b

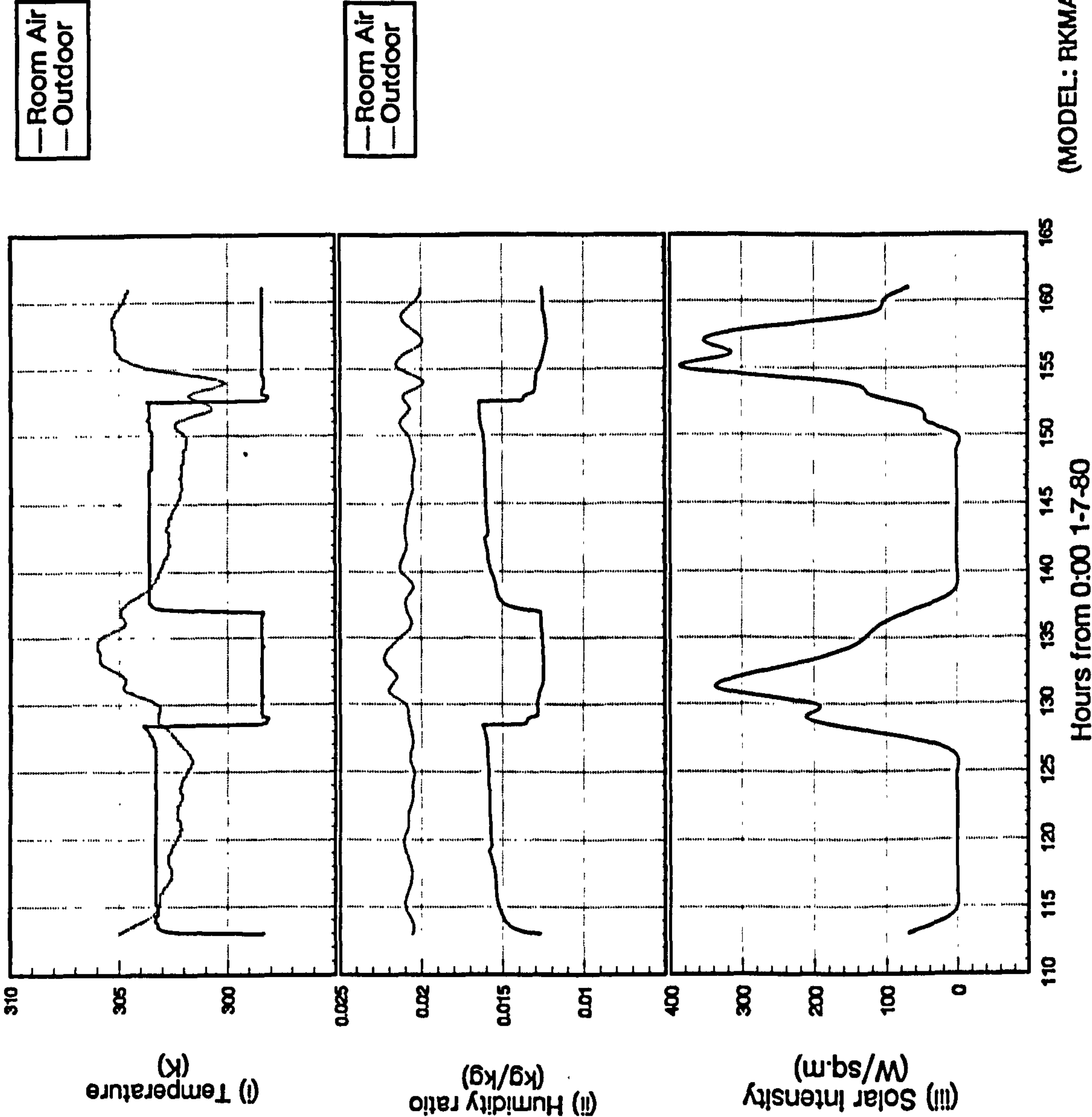
Intermittent air-conditioning by LMHD coil model
with P-control, pre-treated FA & infiltration of 1 ac/hr
from 17:00 5/7/80 to 17:00 7/7/80
(first batch)

Heat and Moisture Gains and Room Cooling Load



Indoor and Outdoor Conditions

Figure 9.12.c
Intermittent air-conditioning by LMHD coil model
with P-control, pre-treated FA & infiltration of 1 ac/hr
from 17:00 5/7/80 to 17:00 7/7/80
(first batch)



(MODEL: RKMACC)

Figure 9.13.a

Initialization run
Intermittent air-conditioning by a perfect A/C system
from 0:00 1/7/80 to 8:30 4/7/80
(second batch)

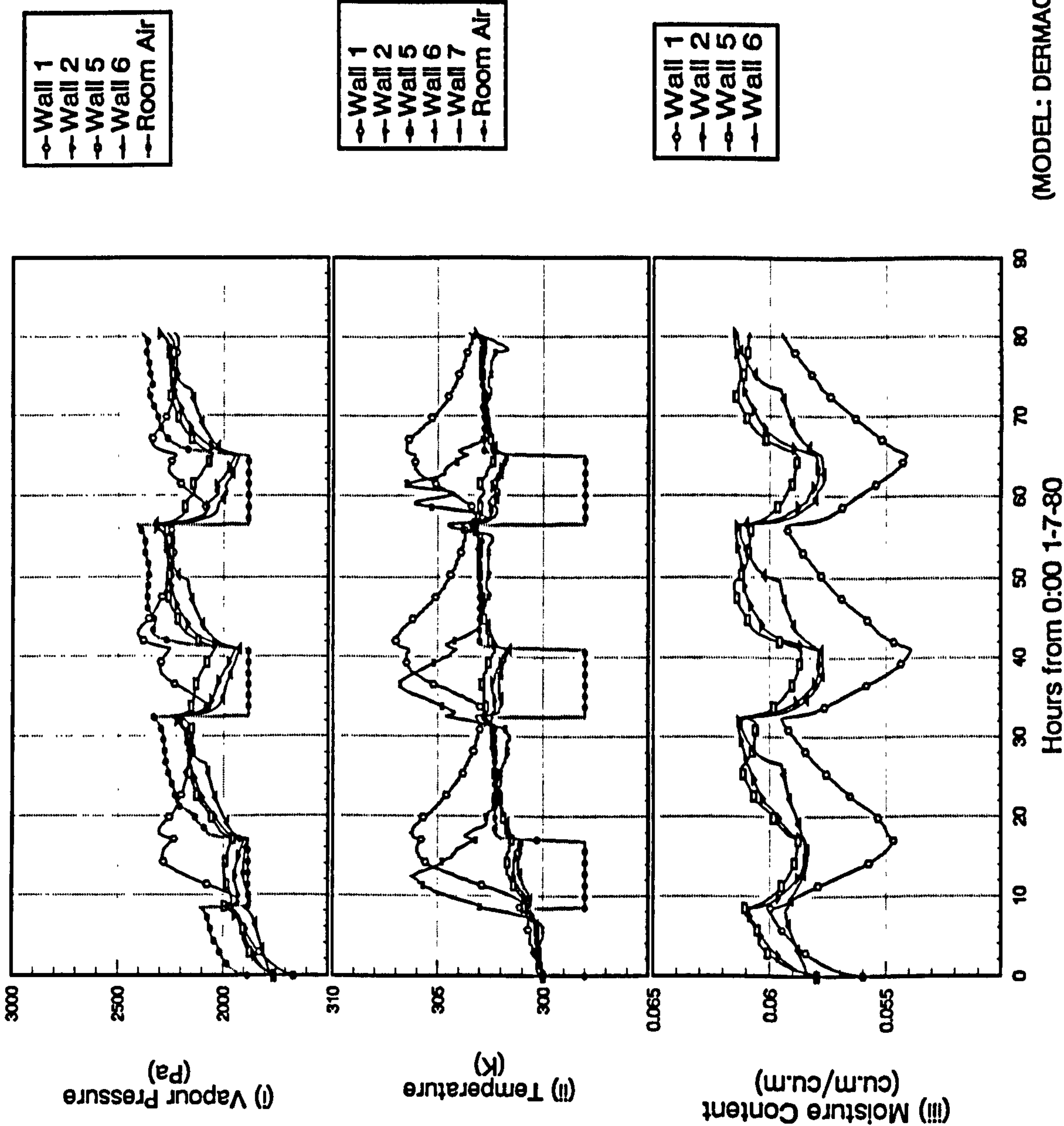


Figure 9.13.b

Initialization run
Intermittent air-conditioning by a perfect A/C system
from 0:00 1/7/80 to 8:30 4/7/80
(second batch)

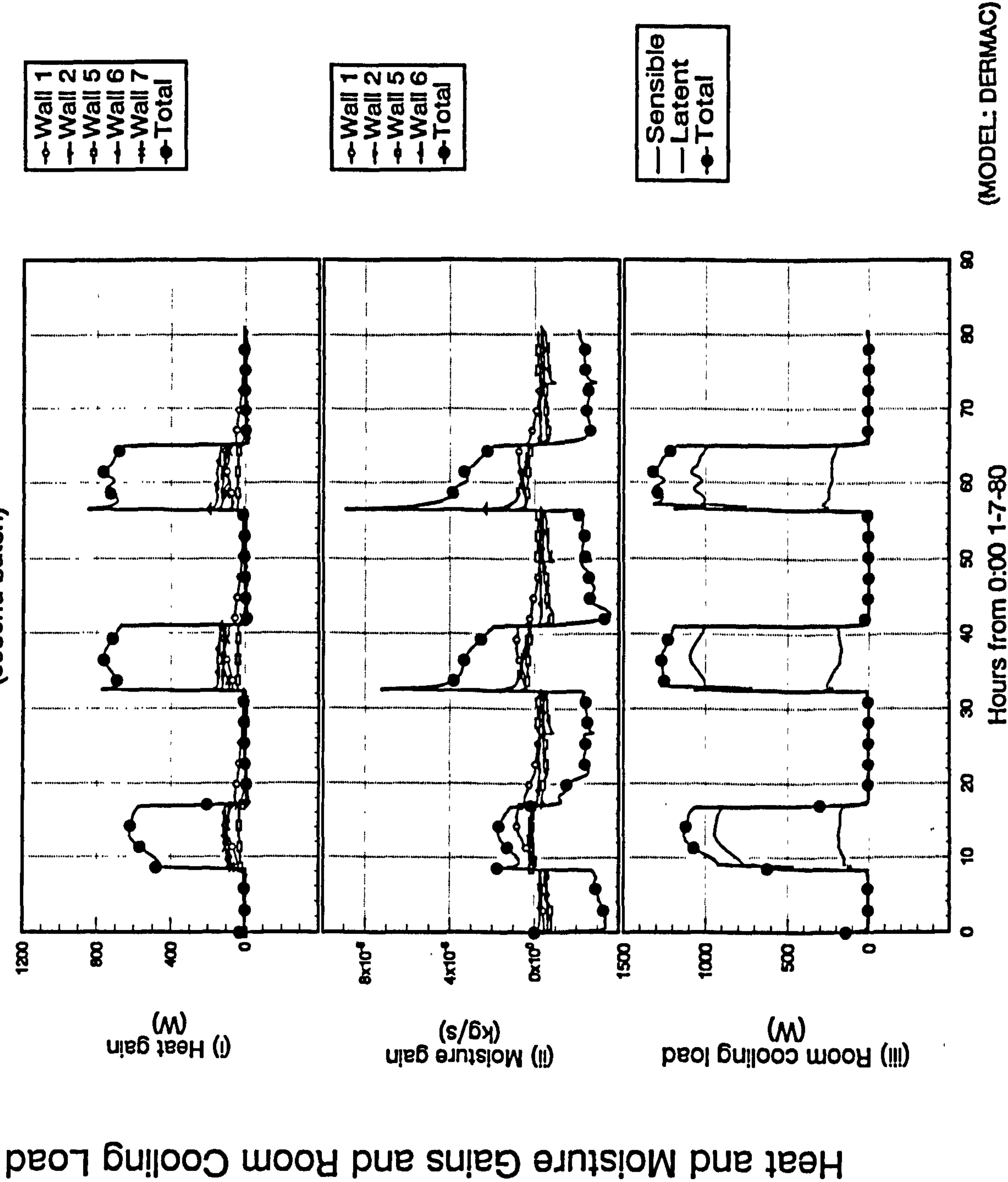
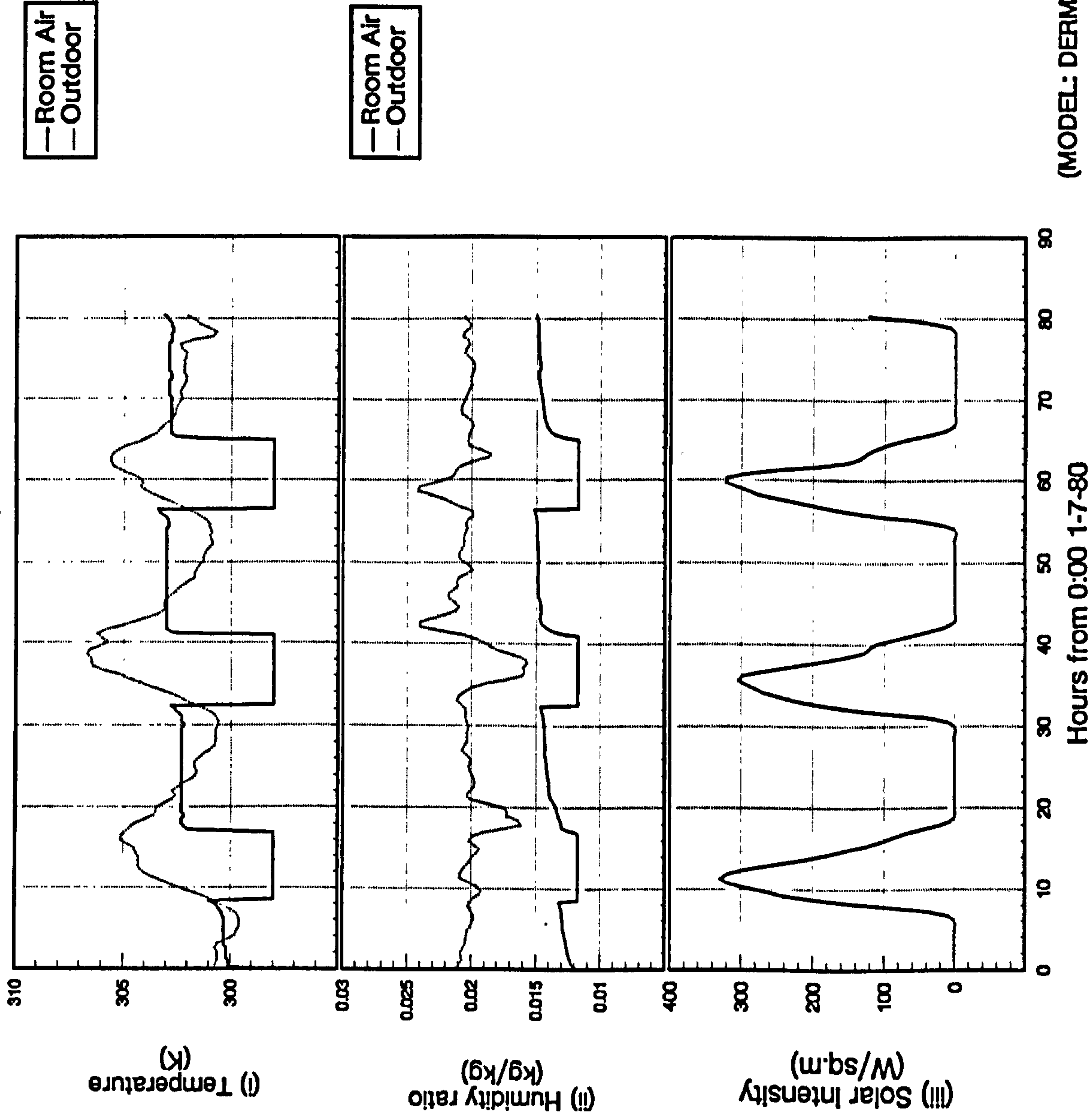


Figure 9.13.c

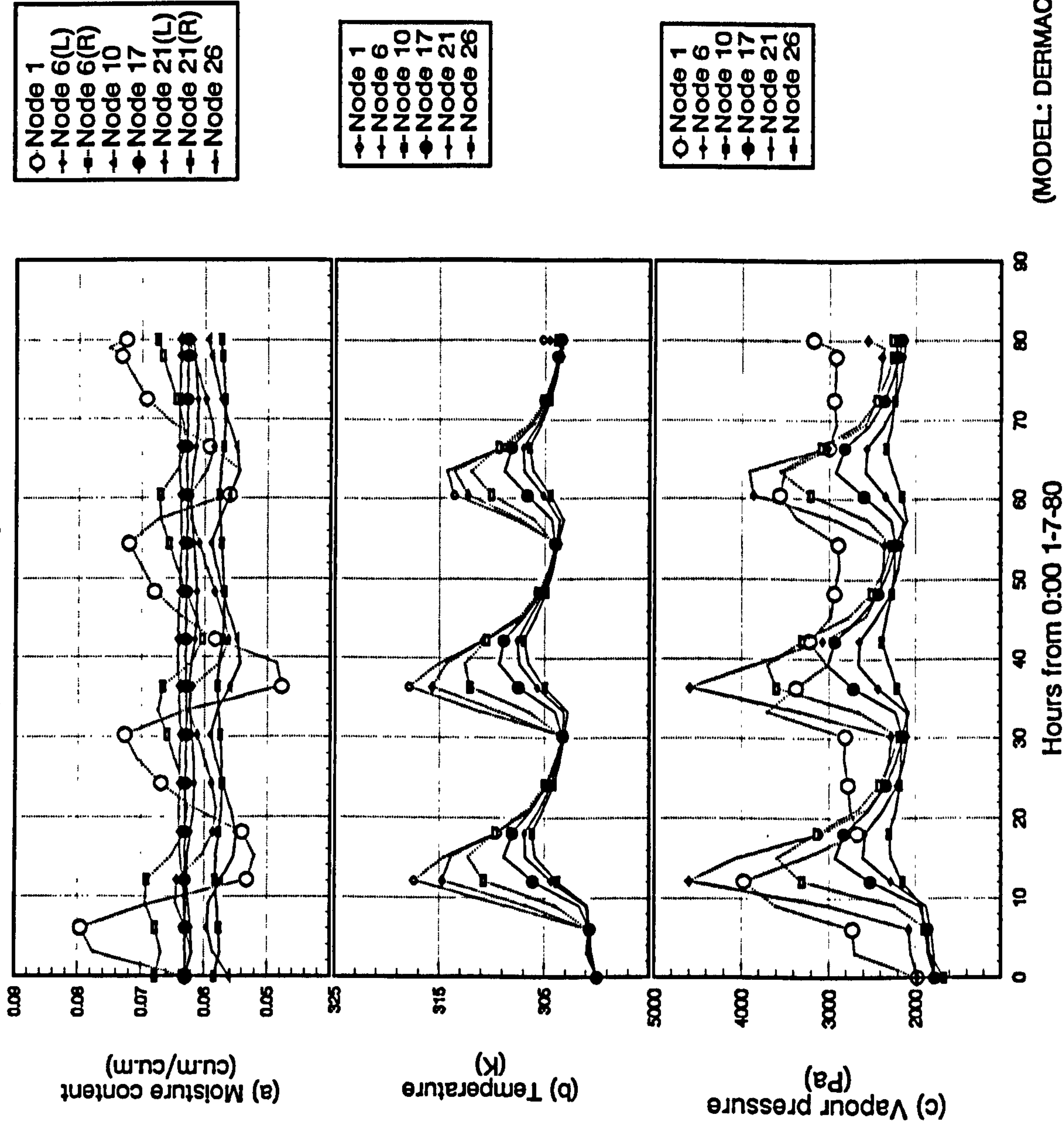
Initialization run
Intermittent air-conditioning by a perfect A/C system
from 0:00 1/7/80 to 8:30 4/7/80
(second batch)



(MODEL: DERMAC)

Figure 9.14

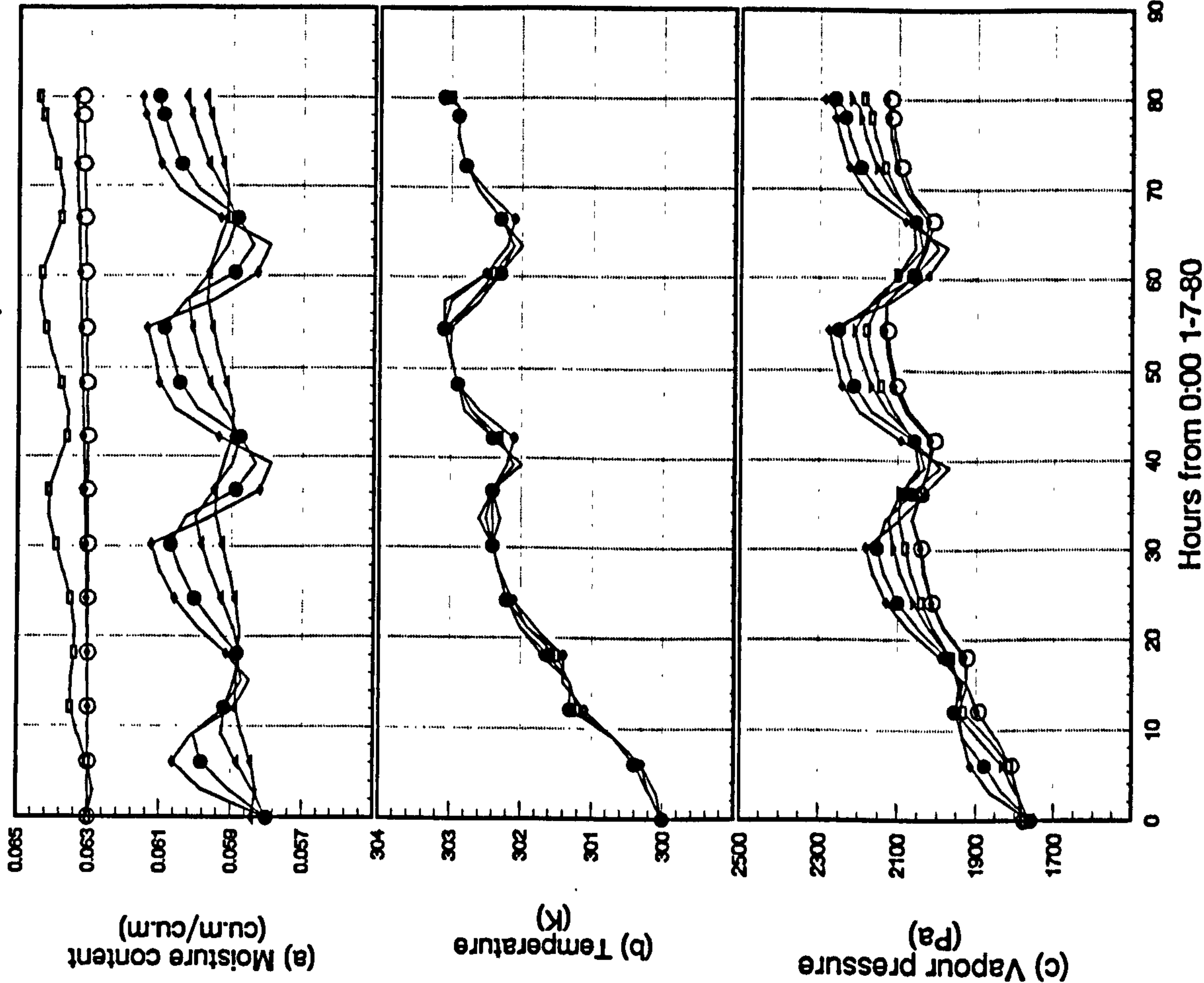
Initialization run
Intermittent air-conditioning by a perfect A/C system
from 0:00 1/7/80 to 8:30 4/7/80
(second batch)



Moisture content, temperature and
vapour pressure at interior nodes
of Wall 1

Figure 9.15

Initialization run
Intermittent air-conditioning by a perfect A/C system
from 0:00 1/7/80 to 8:30 4/7/80
(second batch)



(MODEL: DERMAC)

Figure 9.16.a

Intermittent air-conditioning by LMHD coil model
with on/off control from 8:30 4/7/80 to 8:30 6/7/80
(second batch)

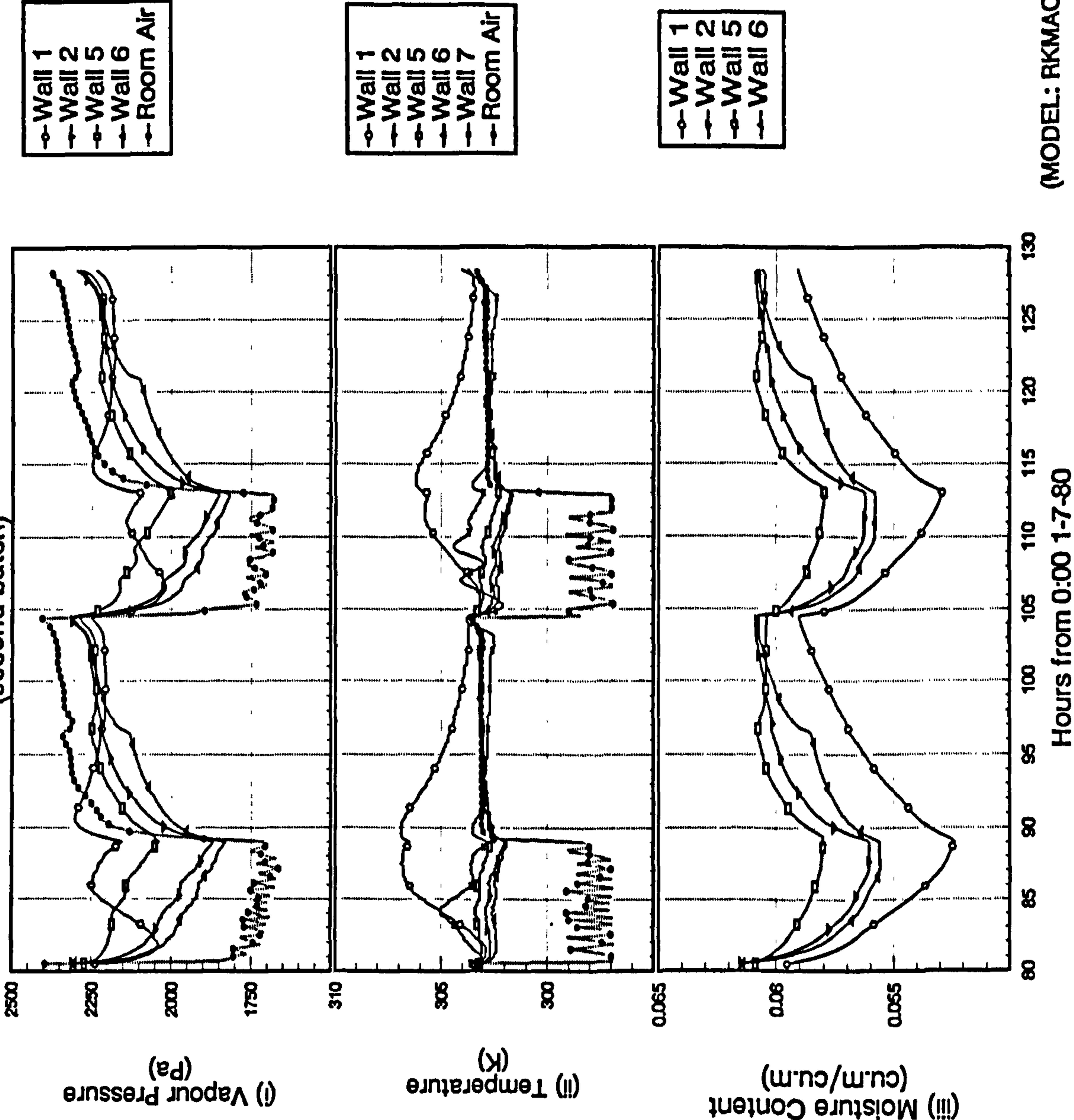
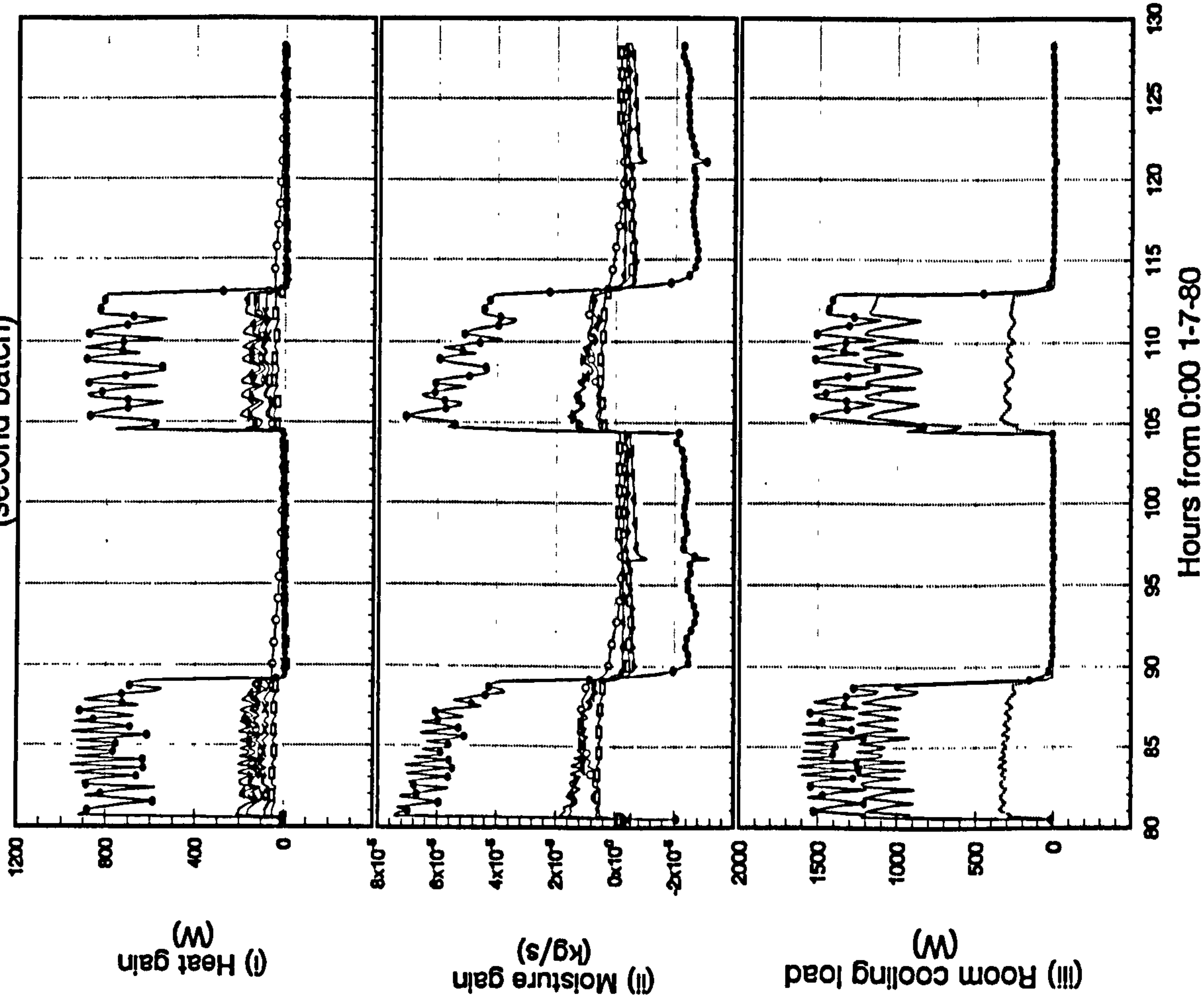


Figure 9.16.b

Intermittent air-conditioning by LMHD coil model
with on/off control from 8:30 4/7/80 to 8:30 6/7/80
(second batch)

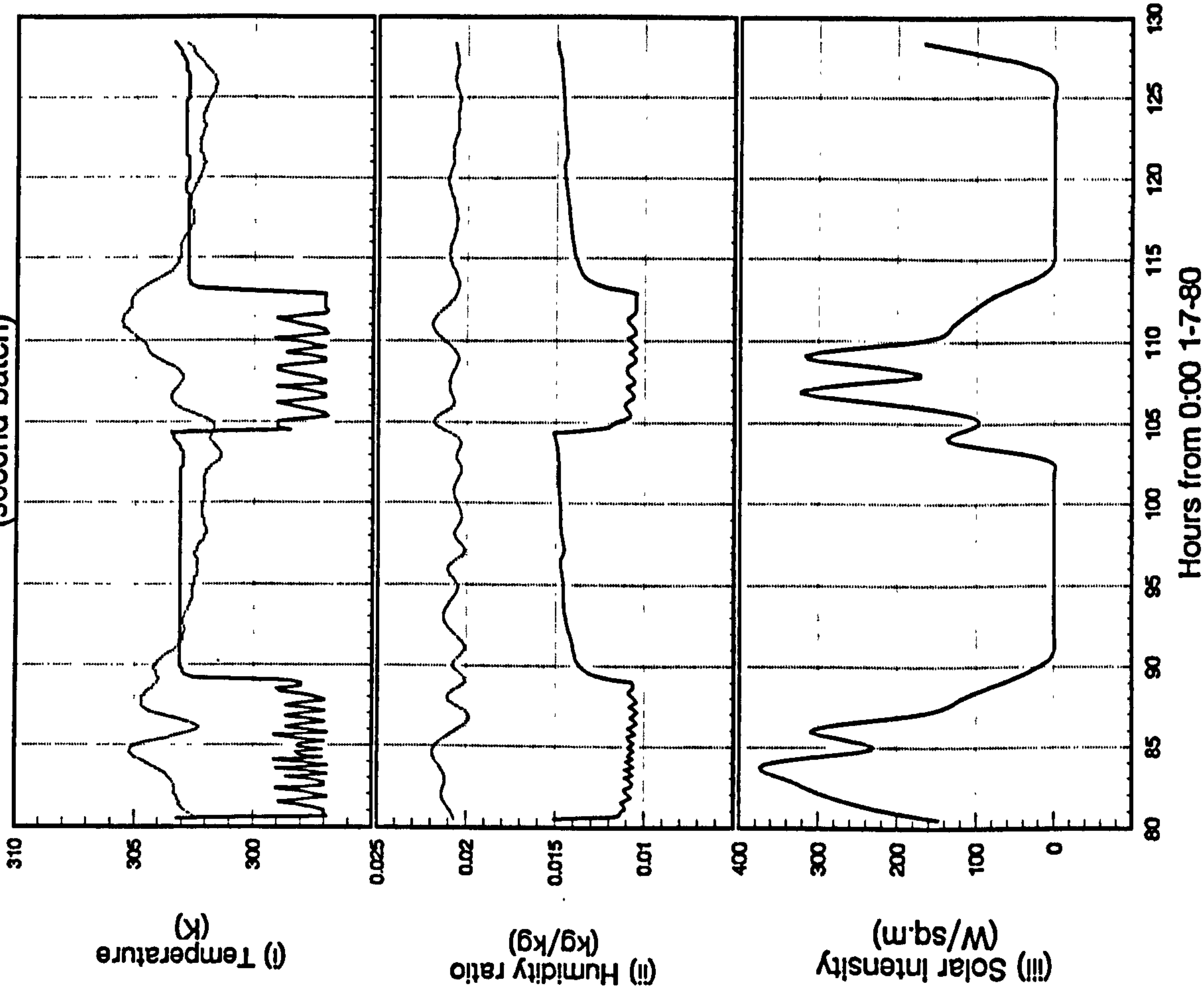
Heat and Moisture Gains and Room Cooling Load



(MODEL: RKMACC)

Figure 9.16.c

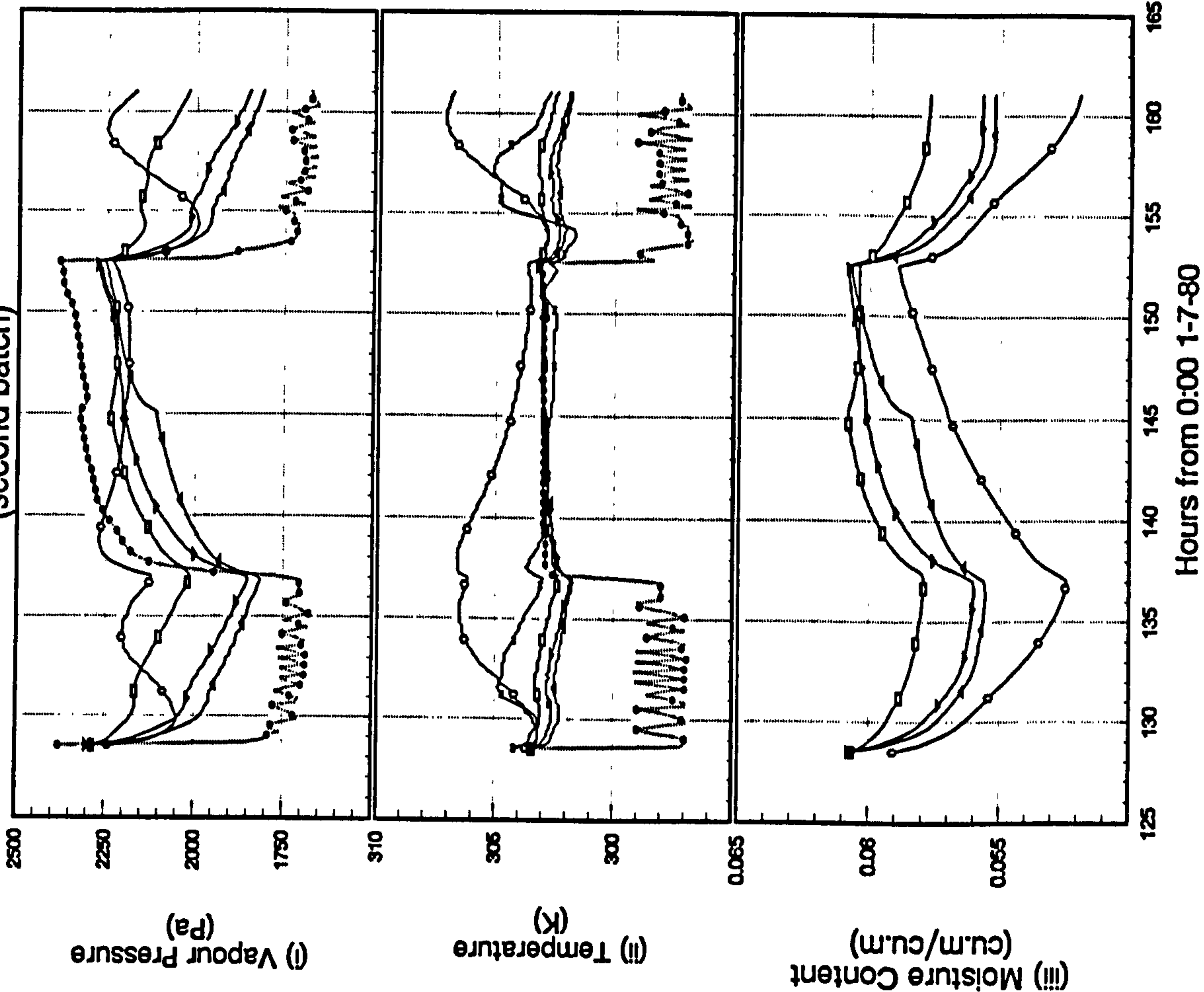
Intermittent air-conditioning by LMHD coil model
with on/off control from 8:30 4/7/80 to 8:30 6/7/80
(second batch)



(MODEL: RKMACC)

Figure 9.17.a

Intermittent air-conditioning by LMHD coil model
with on/off control from 8:30 6/7/80 to 17:00 7/7/80
(second batch)



(MODEL: RKMAOC)

Figure 9.17.b

Intermittent air-conditioning by LMHD coil model
with on/off control from 8:30 6/7/80 to 17:00 7/7/80
(second batch)

Heat and Moisture Gains and Room Cooling Load

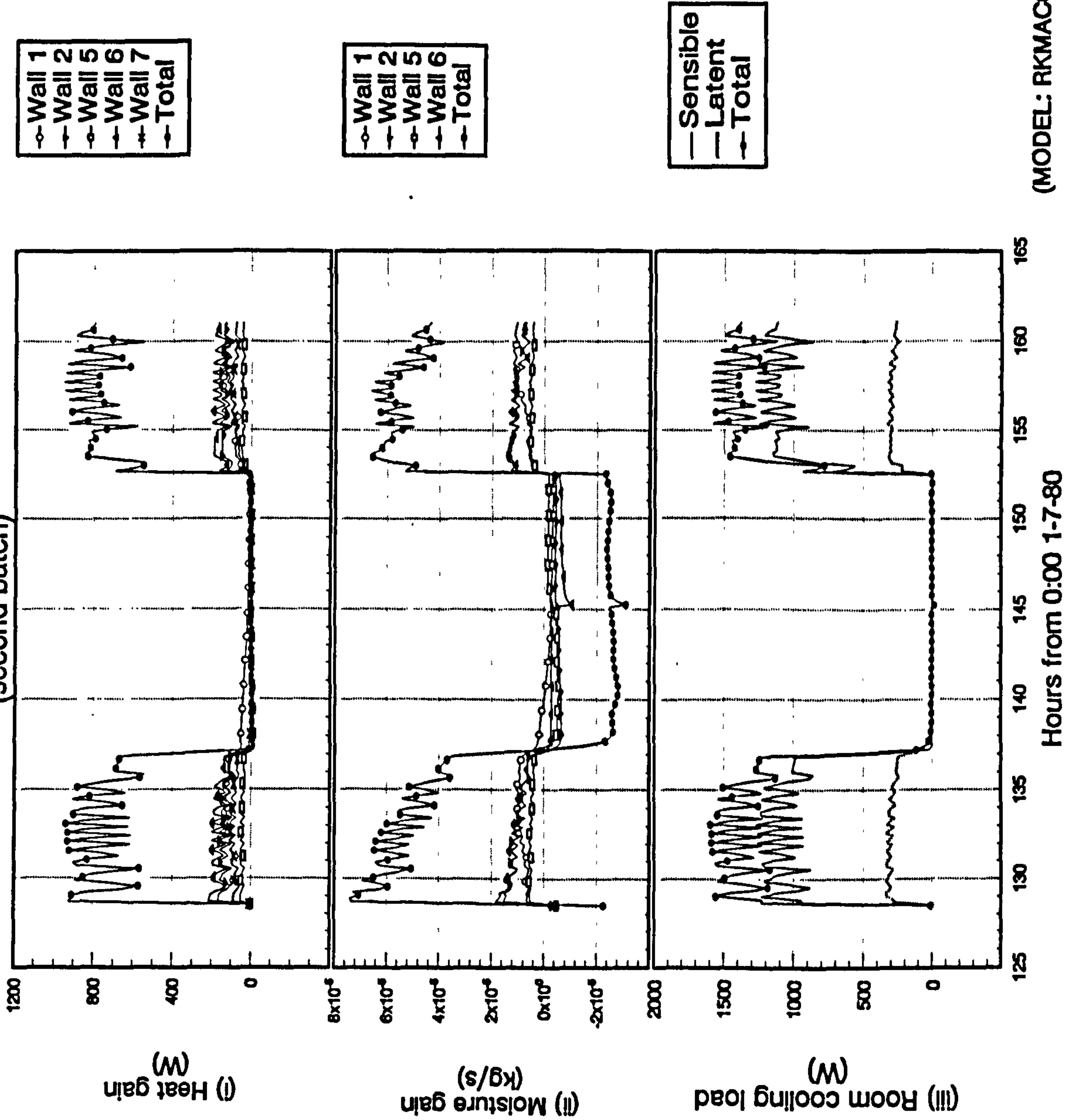
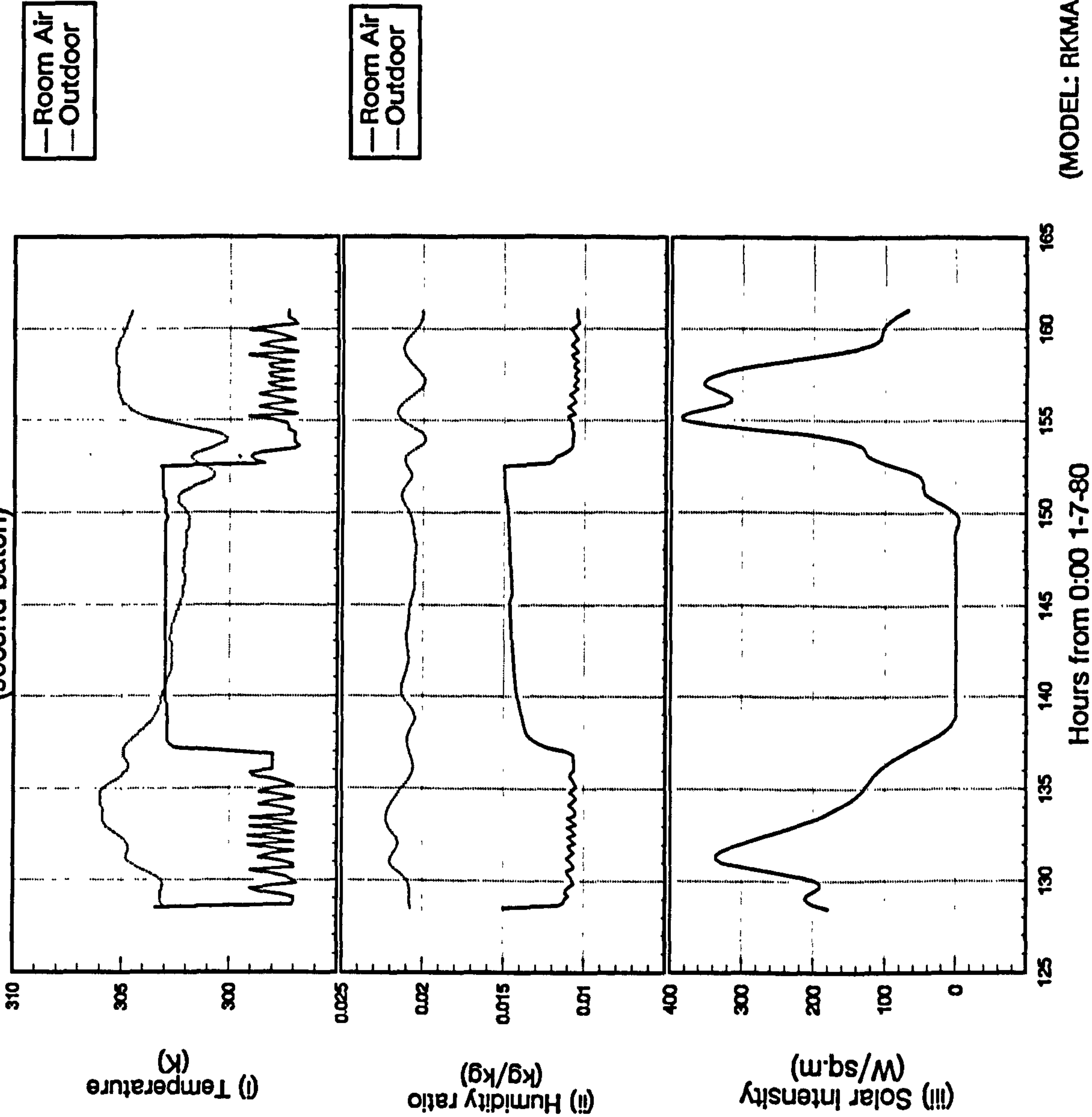


Figure 9.17.c

Intermittent air-conditioning by LMHD coil model
with on/off control from 8:30 6/7/80 to 17:00 7/7/80
(second batch)



(MODEL: RKMACC)

Figure 9.18

Intermittent air-conditioning by LMHD coil model
with on/off control from 8:30 4/7/80 to 17:00 7/7/80
(second batch)

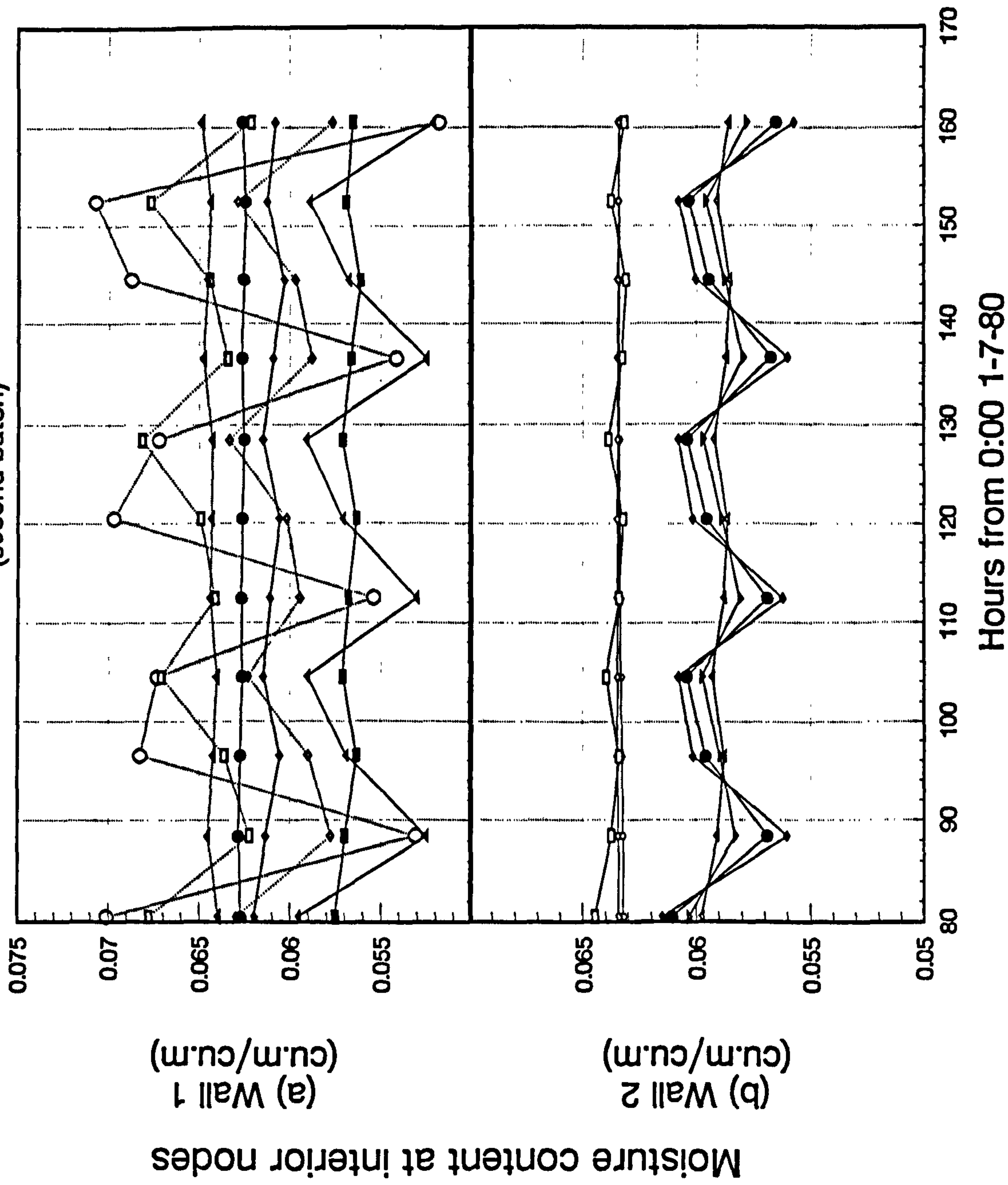
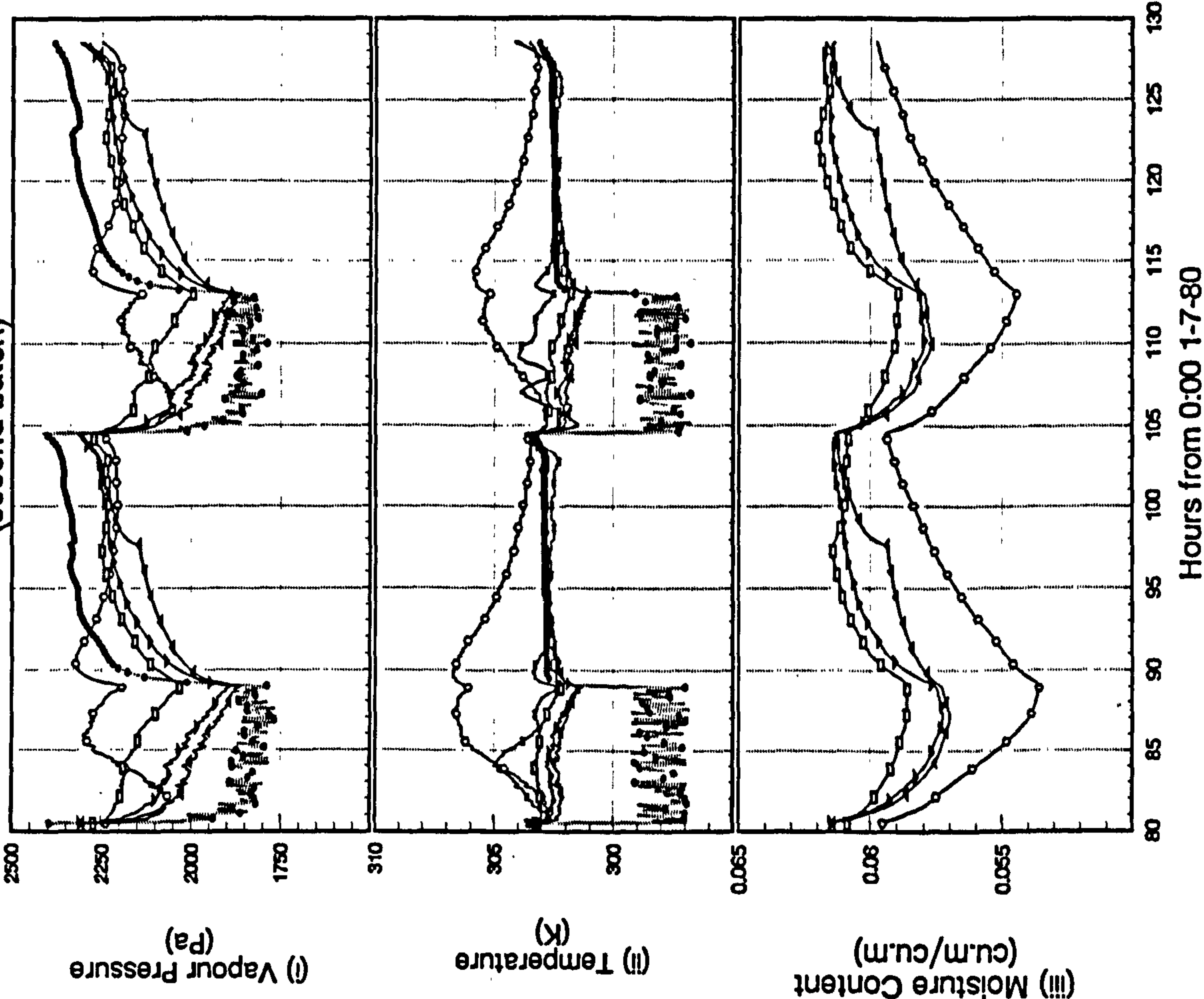


Figure 9.19.a

Intermittent air-conditioning by FD coil model
with on/off control from 8:30 4/7/80 to 8:30 6/7/80
(second batch)

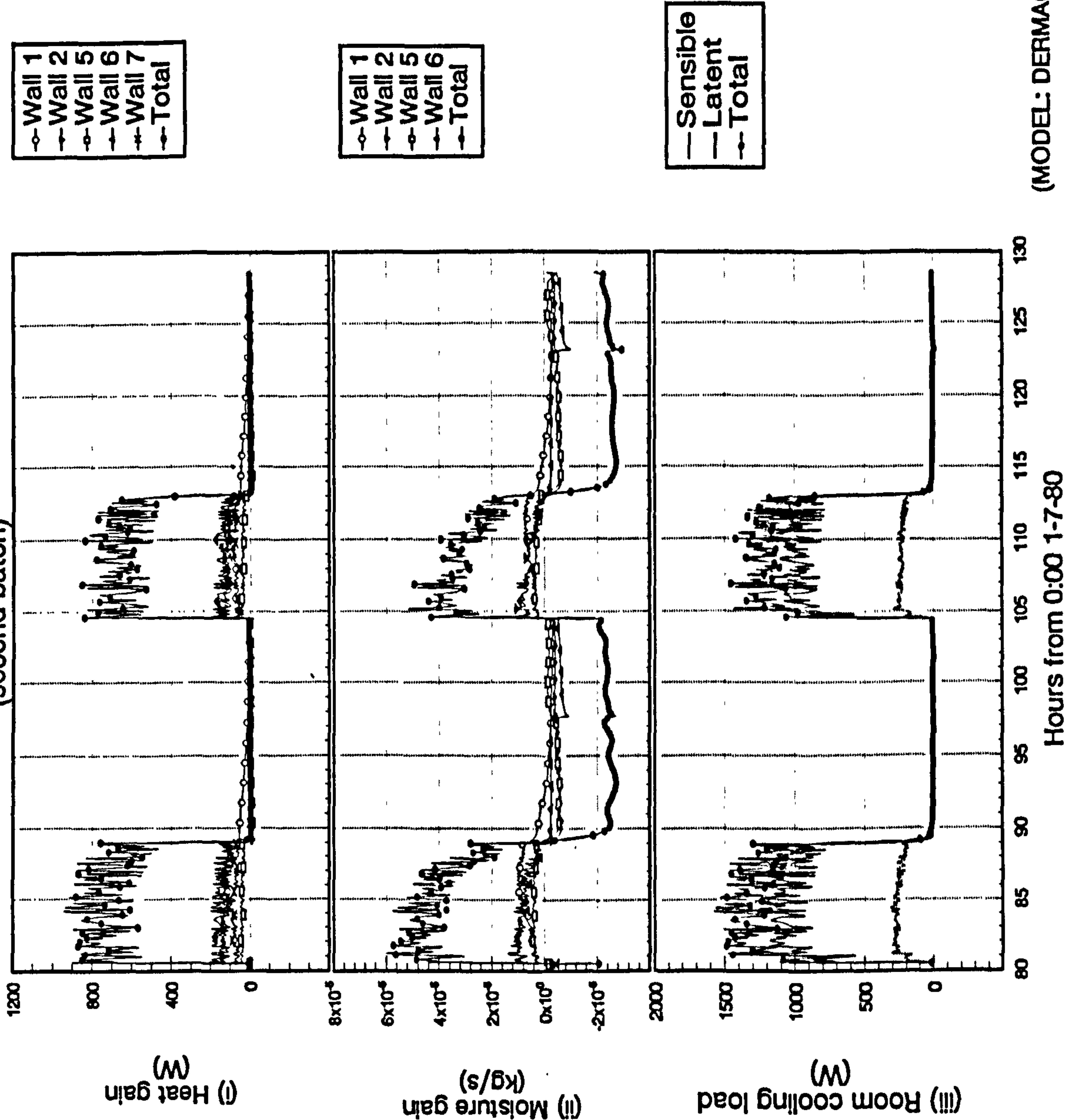


(MODEL: DERMAC)

Figure 9.19.b

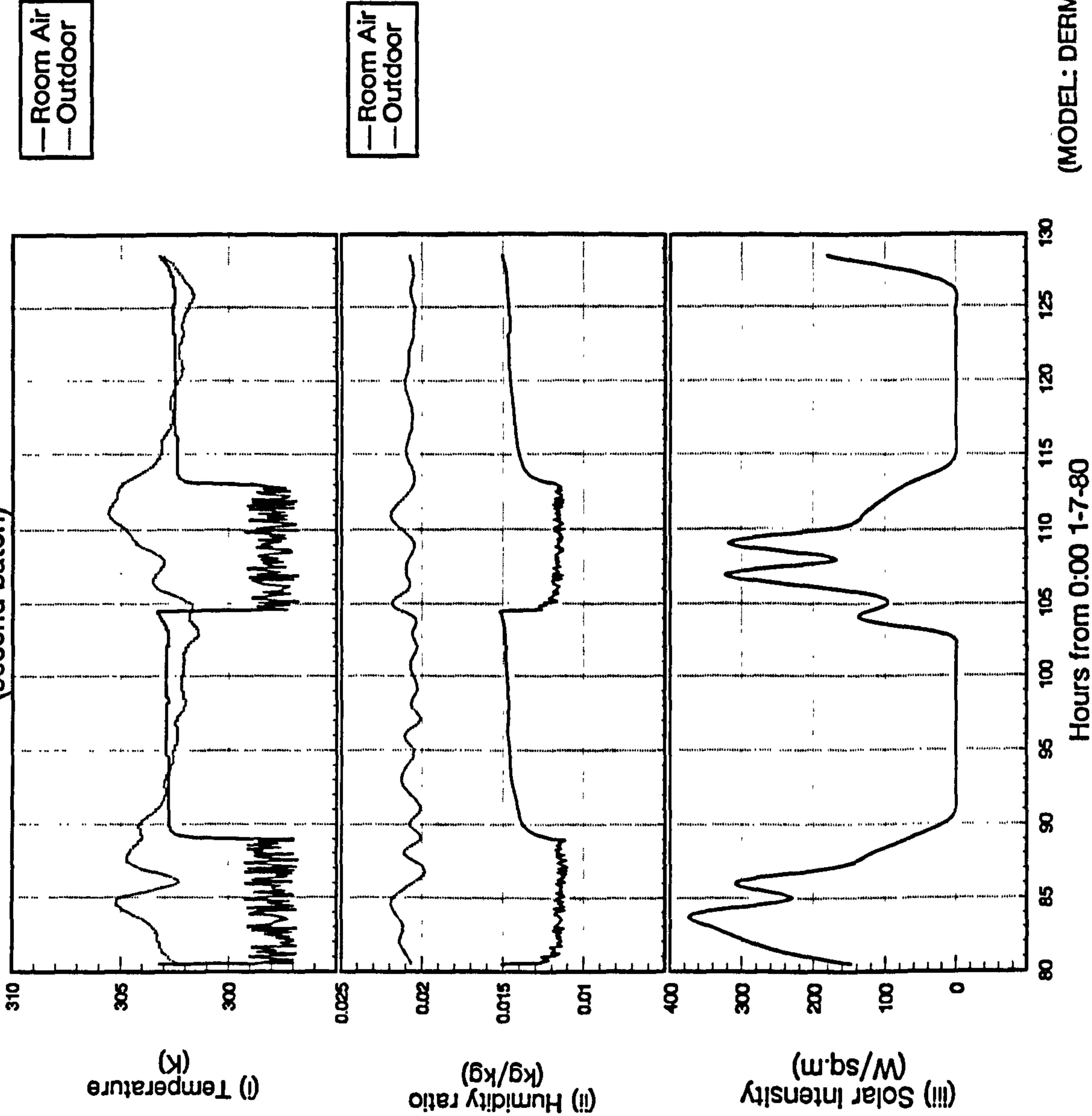
Intermittent air-conditioning by FD coil model
with on/off control from 8:30 4/7/80 to 8:30 6/7/80
(second batch)

Heat and Moisture Gains and Room Cooling Load



Indoor and Outdoor Conditions

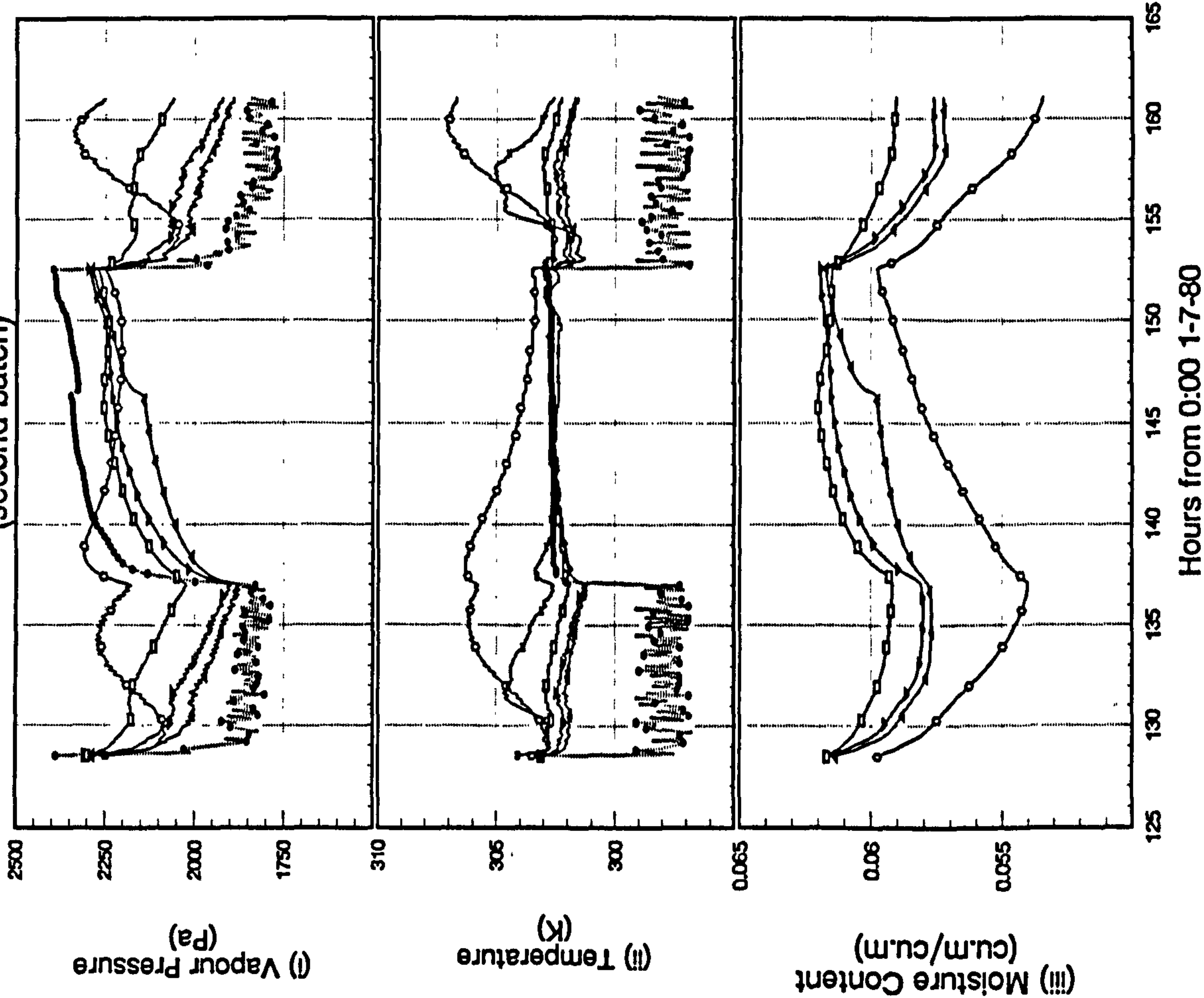
Figure 9.19.c
Intermittent air-conditioning by FD coil model
with on/off control from 8:30 4/7/80 to 8:30 6/7/80
(second batch)



(MODEL: DERMAC)

Figure 9.20.a

Intermittent air-conditioning by FD coil model
with on/off control from 8:30 6/7/80 to 17:00 7/7/80
(second batch)

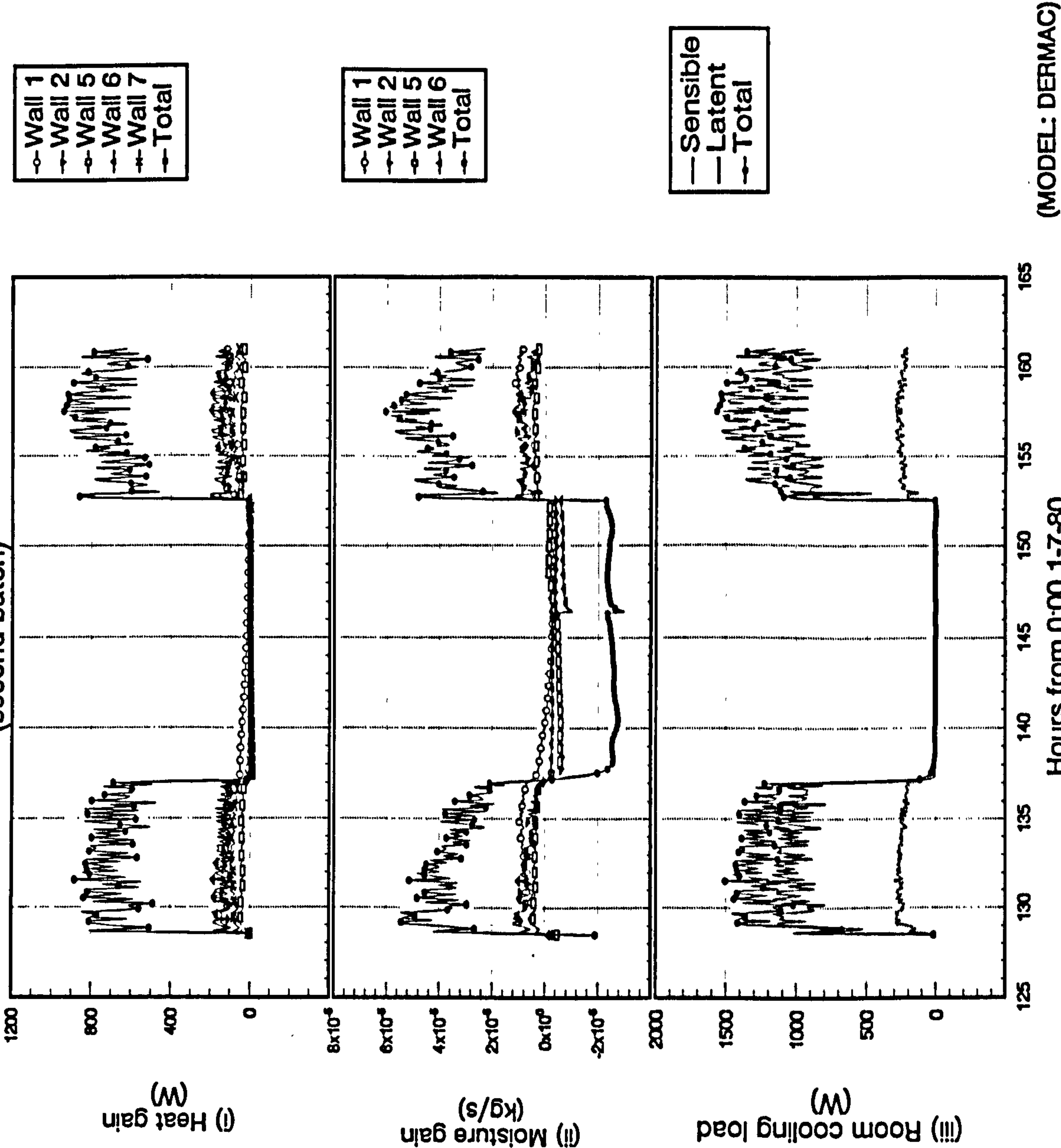


(MODEL: DERMAC)

Figure 9.20.b

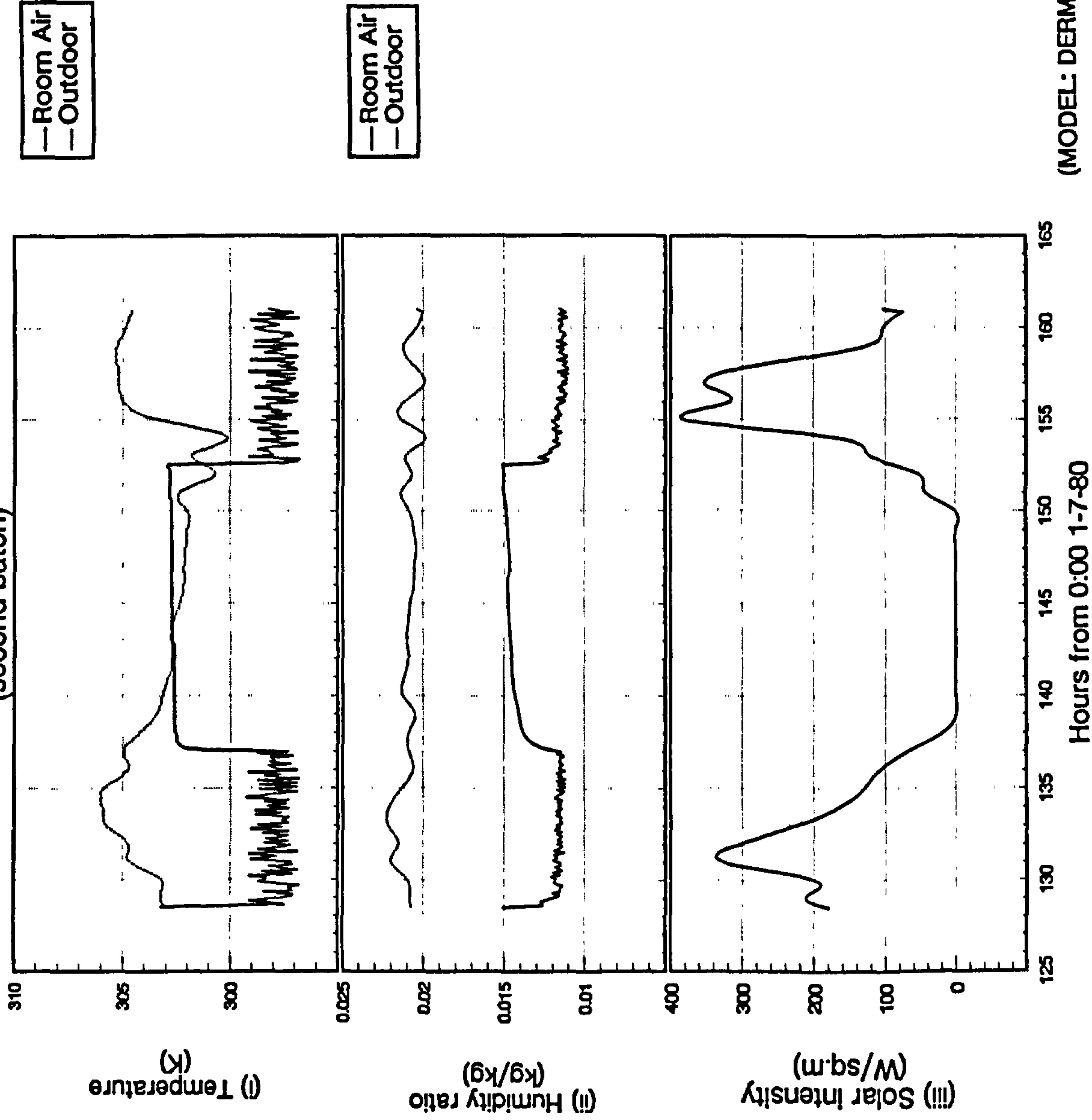
Intermittent air-conditioning by FD coil model
with on/off control from 8:30 6/7/80 to 17:00 7/7/80
(second batch)

Heat and Moisture Gains and Room Cooling Load



Indoor and Outdoor Conditions

Figure 9.20.c
Intermittent air-conditioning by FD coil model
with on/off control from 8:30 6/7/80 to 17:00 7/7/80
(second batch)



(MODEL: DERMAC)

Figure 9.21

Intermittent air-conditioning by FD coil model
with on/off control from 8:30 4/7/80 to 17:00 7/7/80
(second batch)

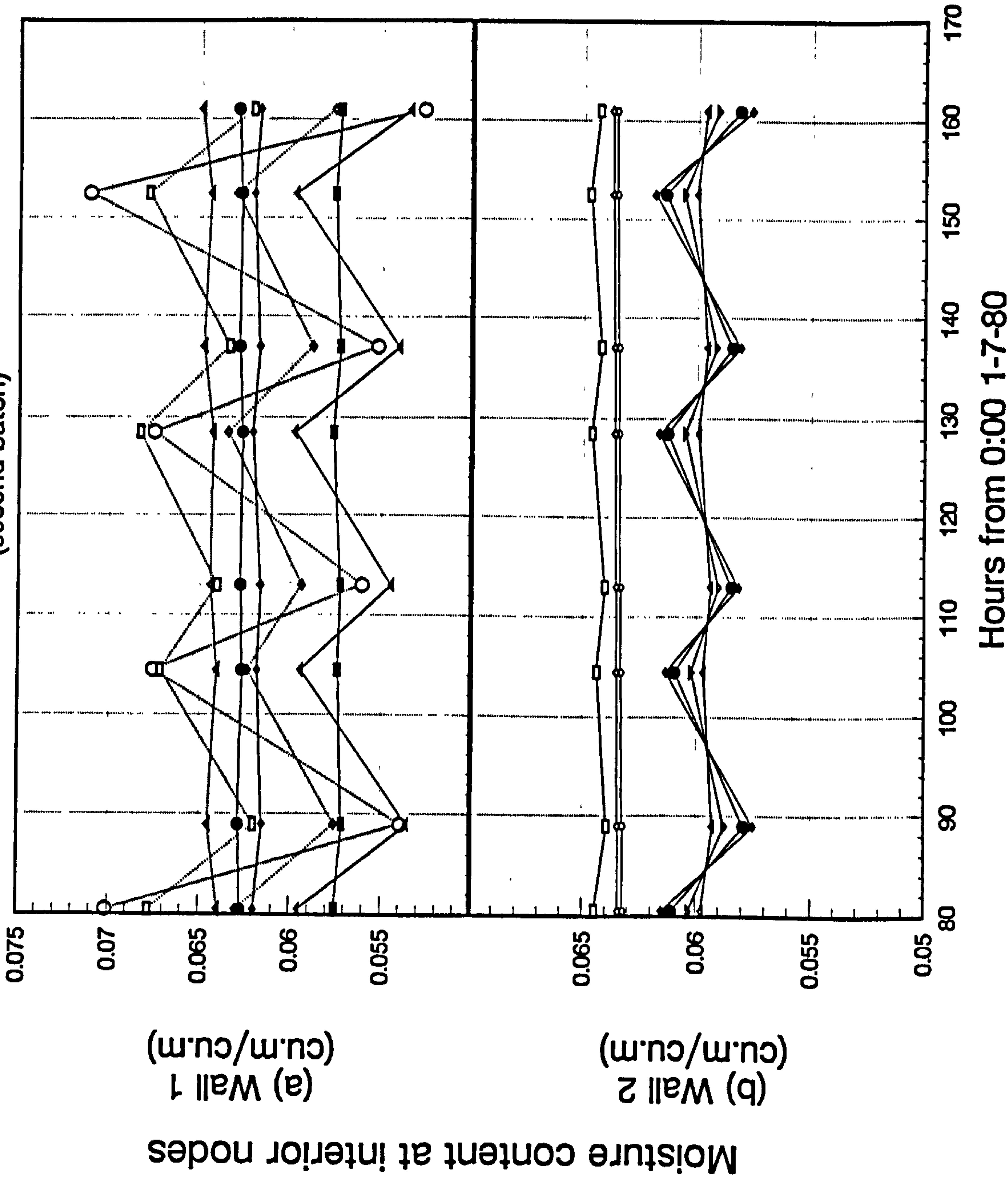


Figure 9.22

Comparison of indoor conditions and room cooling loads with and without moisture adsorption and desorption (MAD) at the building fabric

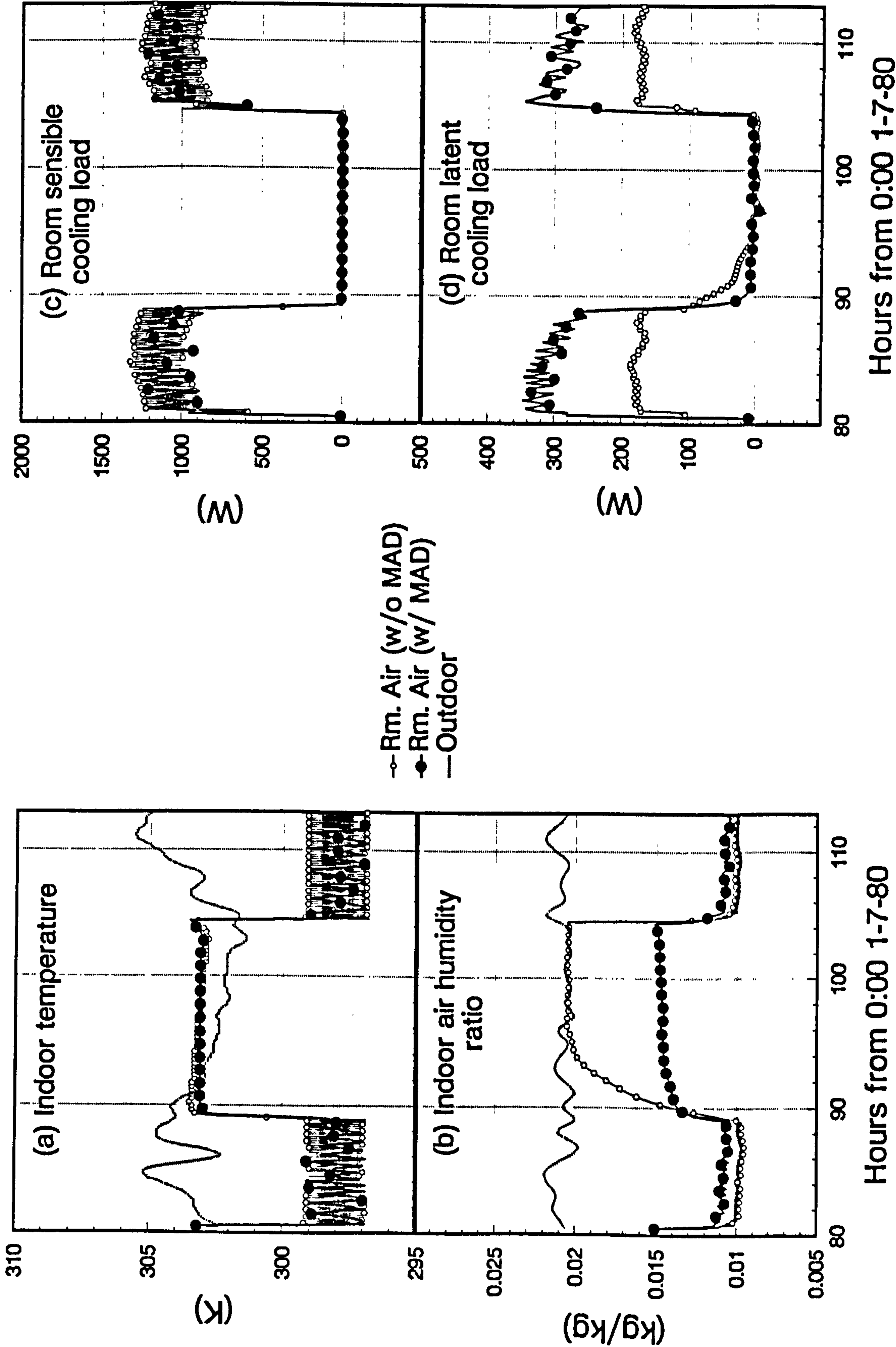
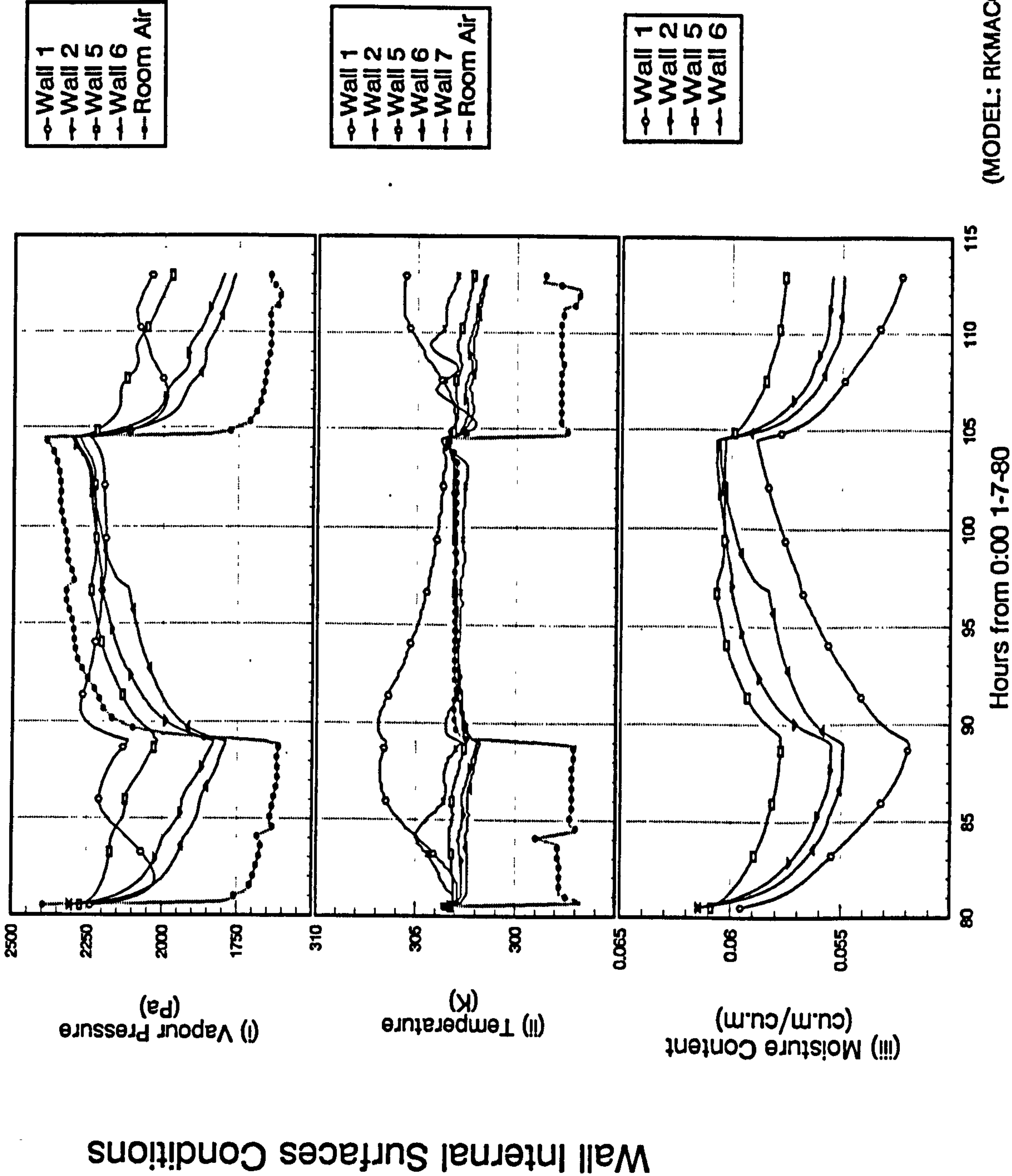


Figure 9.23.a

Intermittent air-conditioning by LMHD coil model
with on/off control and pretreated fresh air
from 8:30 4/7/80 to 17:00 5/7/80
(second batch)



Heat and Moisture Gains and Room Cooling Load

Figure 9.23.b

Intermittent air-conditioning by LMHD coil model
with on/off control and pretreated fresh air
from 8:30 4/7/80 to 17:00 5/7/80
(second batch)

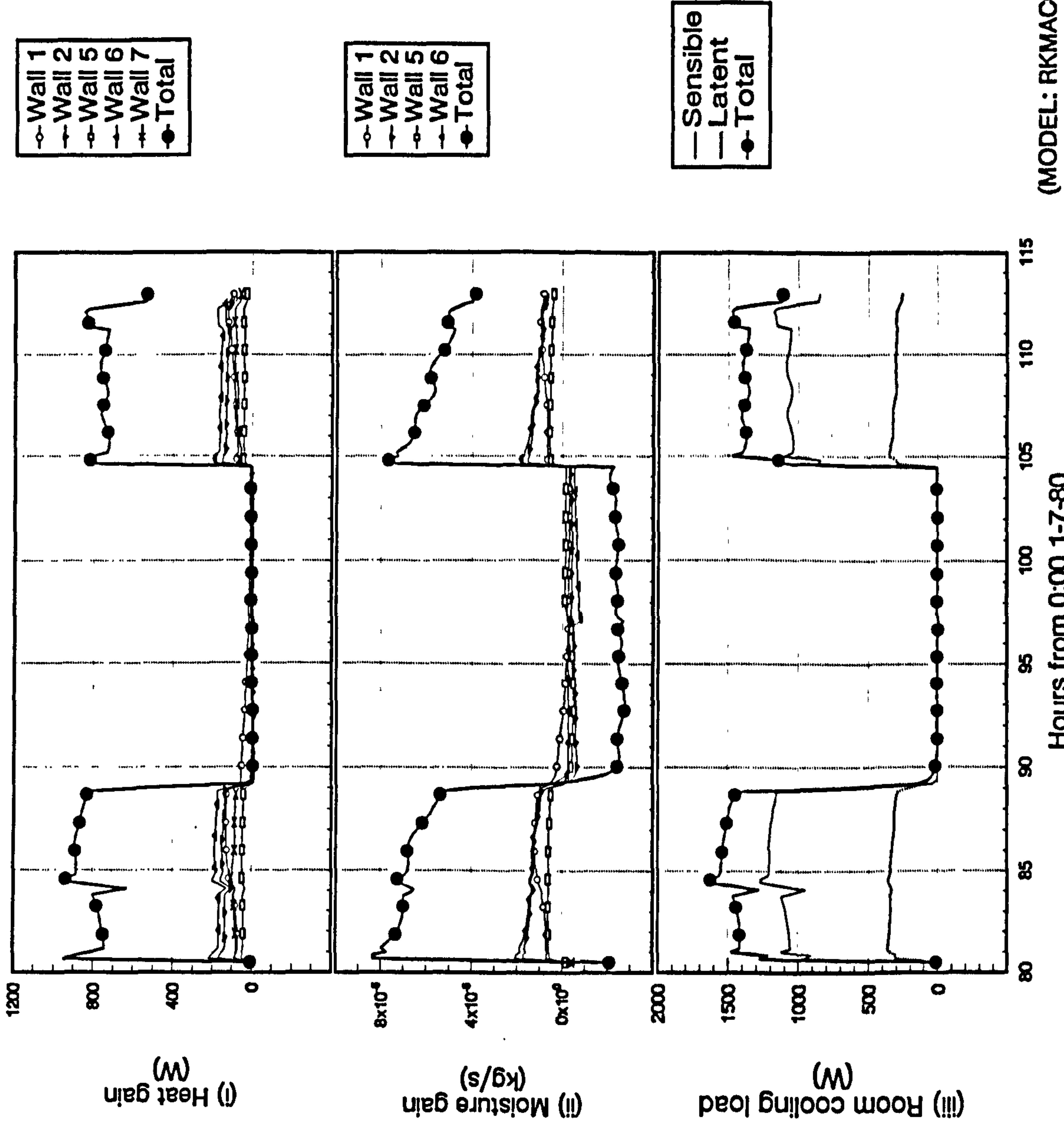
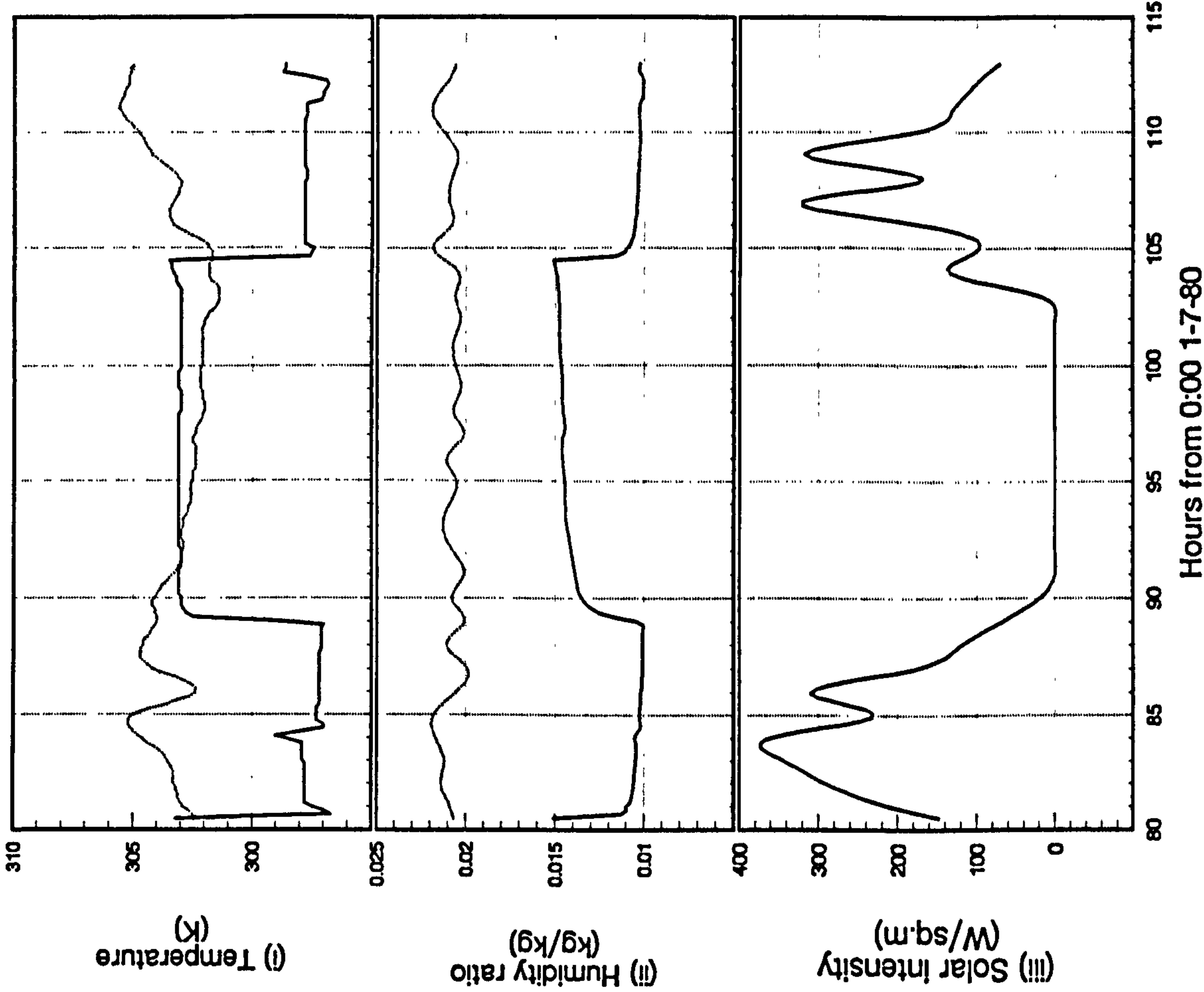
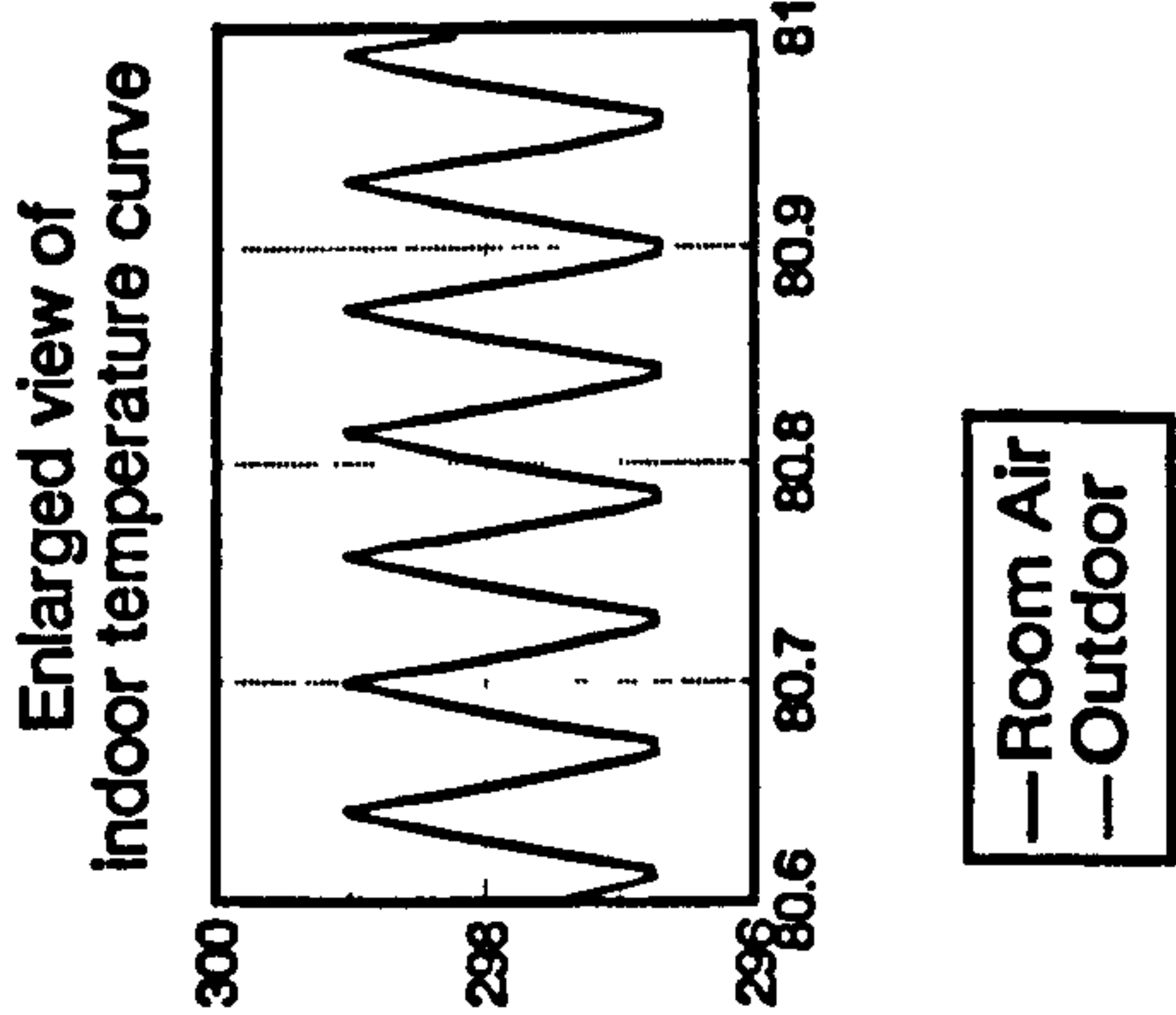


Figure 9.23.c

Intermittent air-conditioning by LMHD coil model
with on/off control and pretreated fresh air
from 8:30 4/7/80 to 17:00 5/7/80
(second batch)



Indoor and Outdoor Conditions

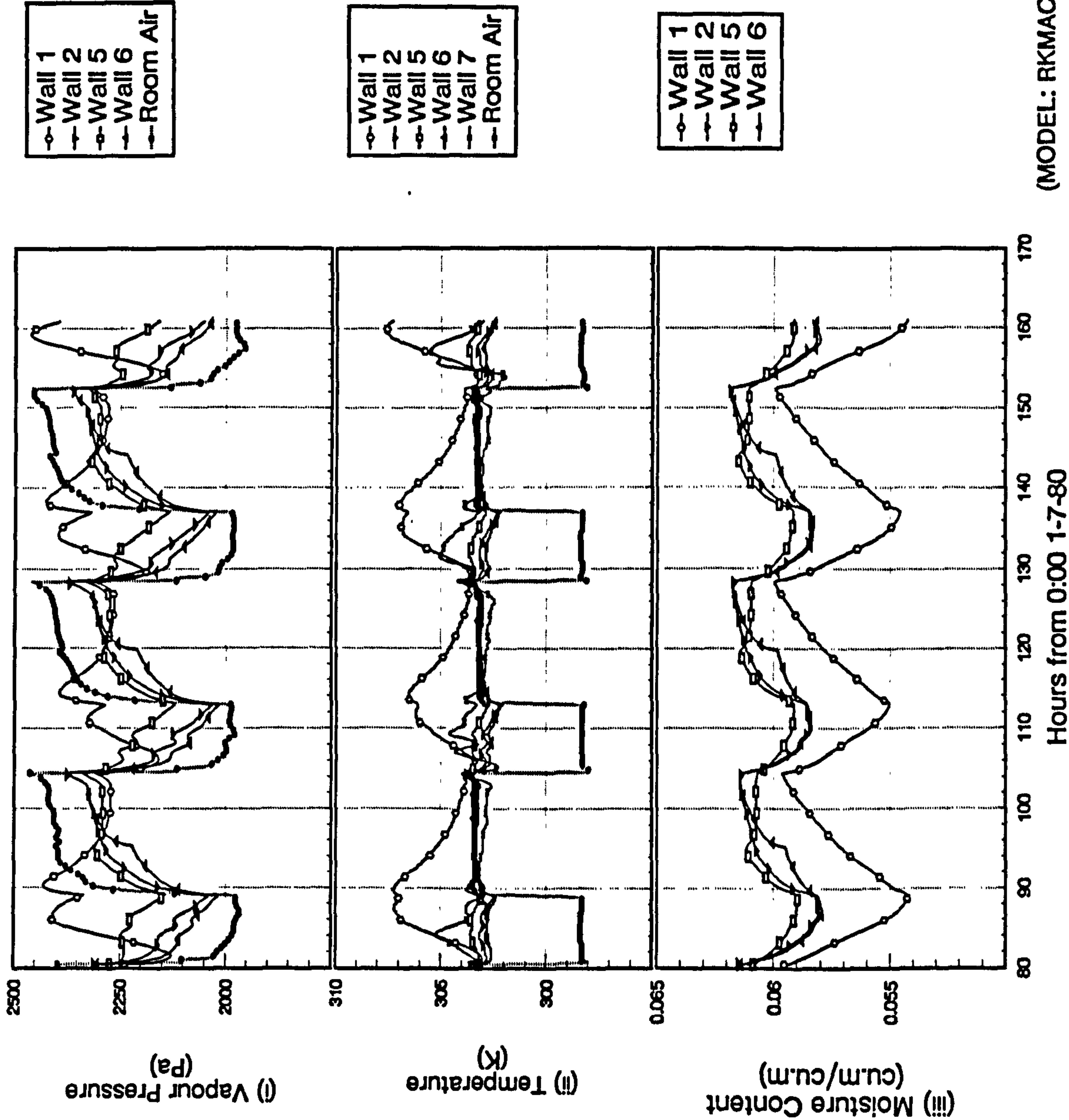


— Room Air
— Outdoor

(MODEL: RKMACC)

Figure 9.24.a

Intermittent air-conditioning by LMHD coil model
with proportional control and pretreated fresh air
from 8:30 4/7/80 to 17:00 7/7/80
(second batch)



Heat and Moisture Gains and Room Cooling Load

Figure 9.24.b

Intermittent air-conditioning by LMHD coil model
with proportional control and pretreated fresh air
from 8:30 4/7/80 to 17:00 7/7/80
(second batch)

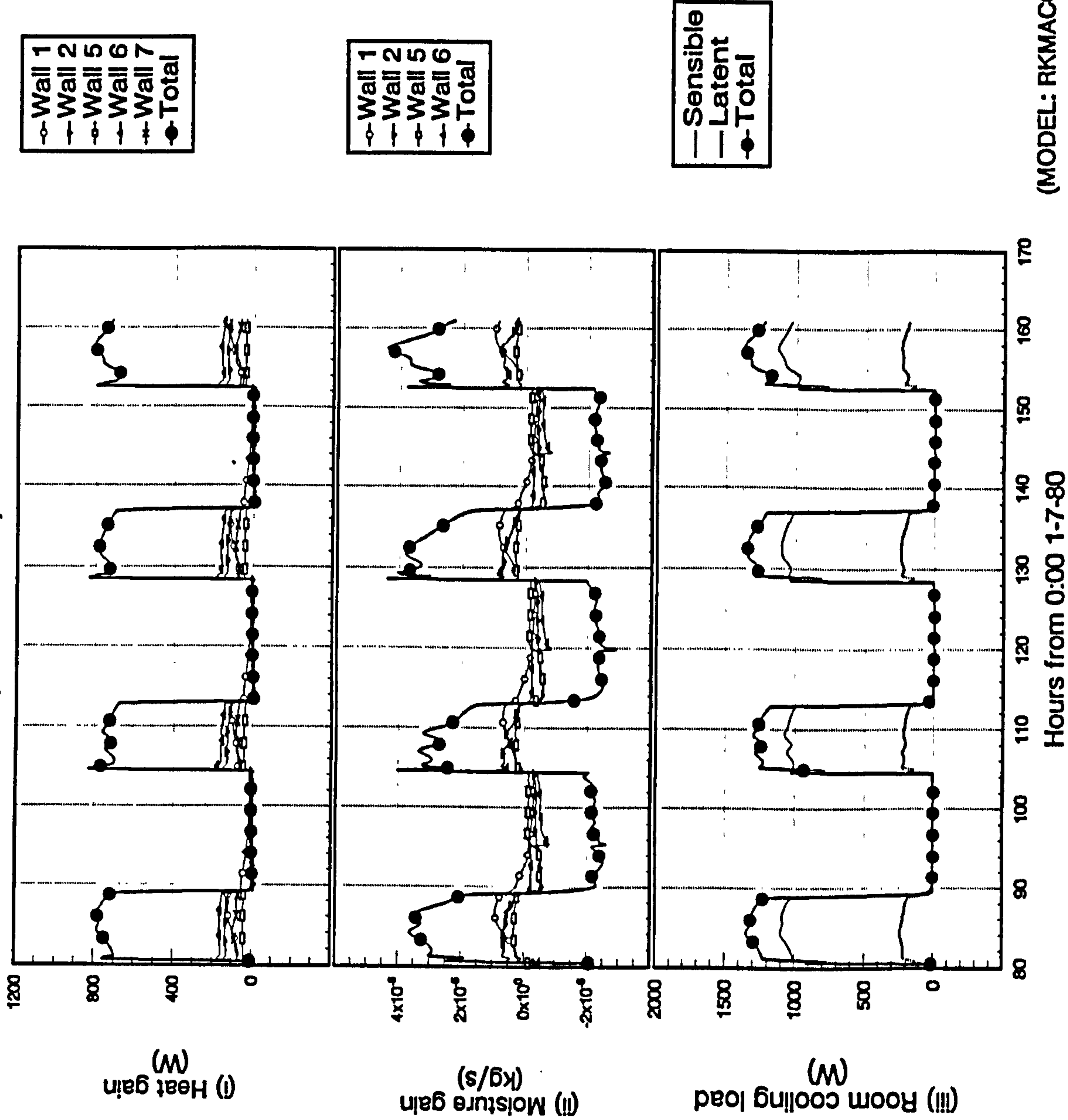
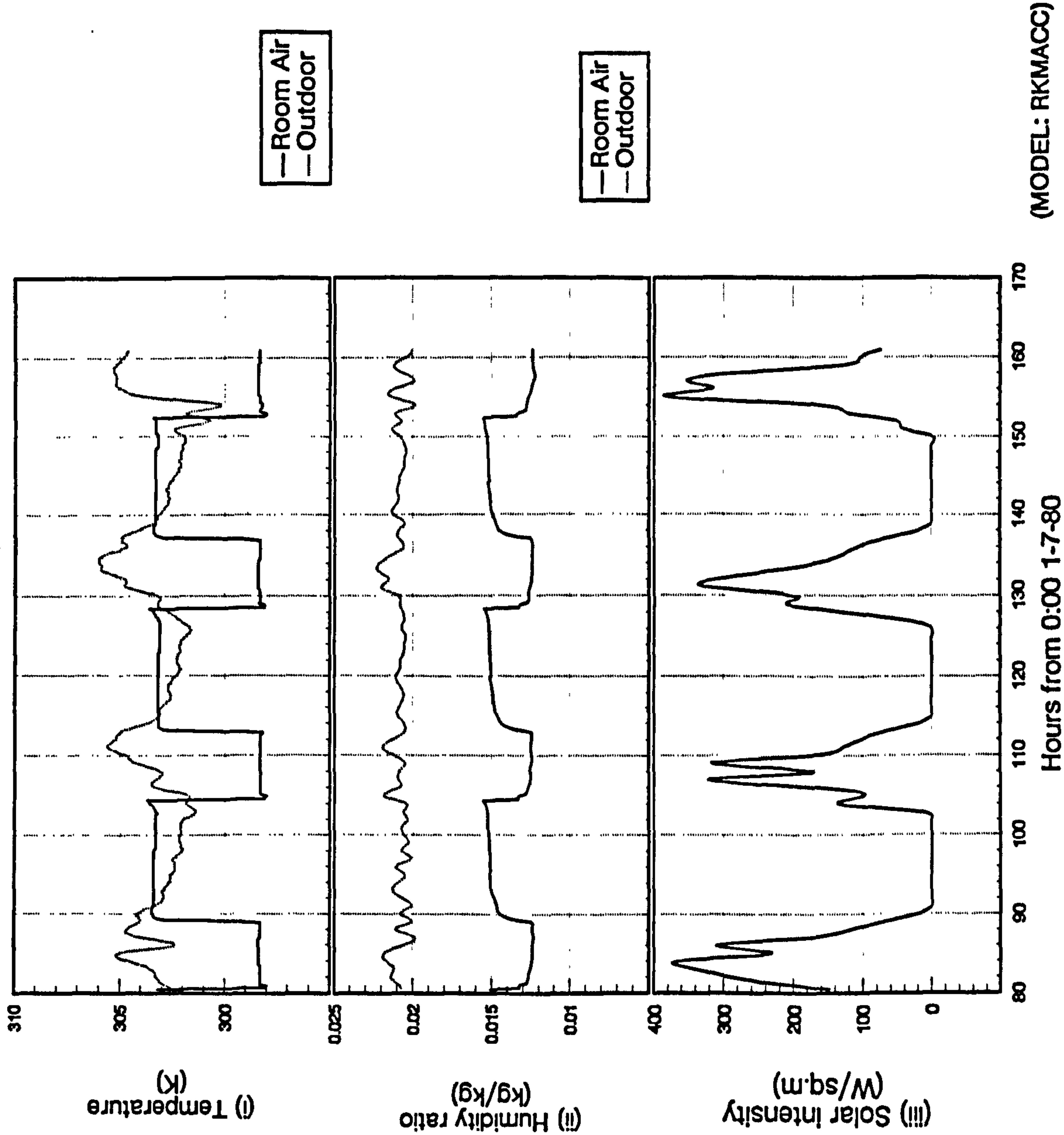


Figure 9.24.c

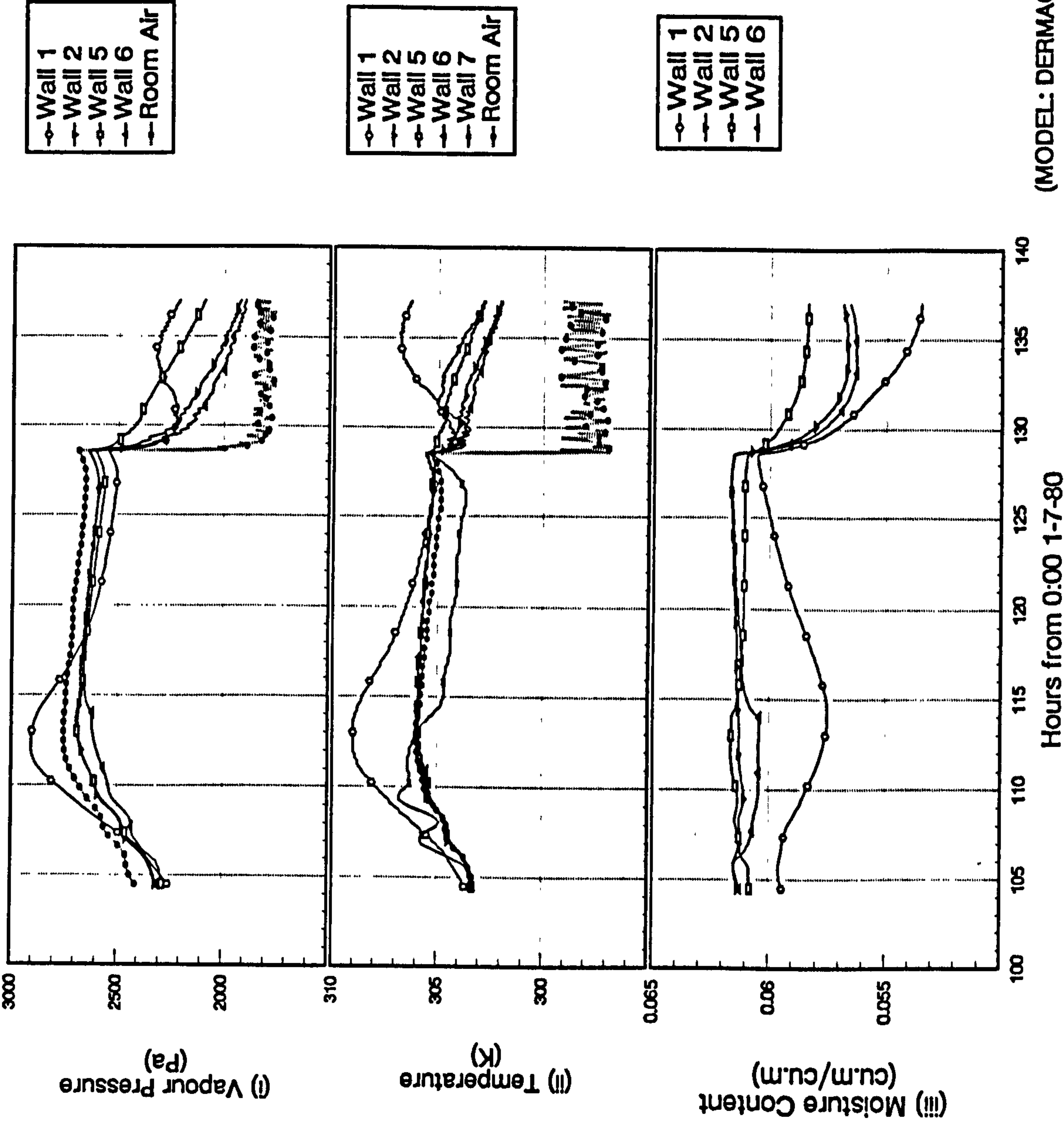
Intermittent air-conditioning by LMHD coil model
with proportional control and pretreated fresh air
from 8:30 4/7/80 to 17:00 7/7/80
(second batch)



Wall Internal Surface Conditions

Figure 9.25.a

Intermittent air-conditioning by FD coil model
with no air-conditioning from 8:30 5/7/80 to 8:30 6/7/80
followed by air-conditioning with on/off control
from 8:30 6/7/80 to 17:00 6/7/80 (second batch)



(MODEL: DERMAC)

Figure 9.25.b

Intermittent air-conditioning by FD coil model
with no air-conditioning from 8:30 5/7/80 to 8:30 6/7/80
followed by air-conditioning with on/off control
from 8:30 6/7/80 to 17:00 6/7/80 (second batch)

Heat and Moisture Gains and Room Cooling Load

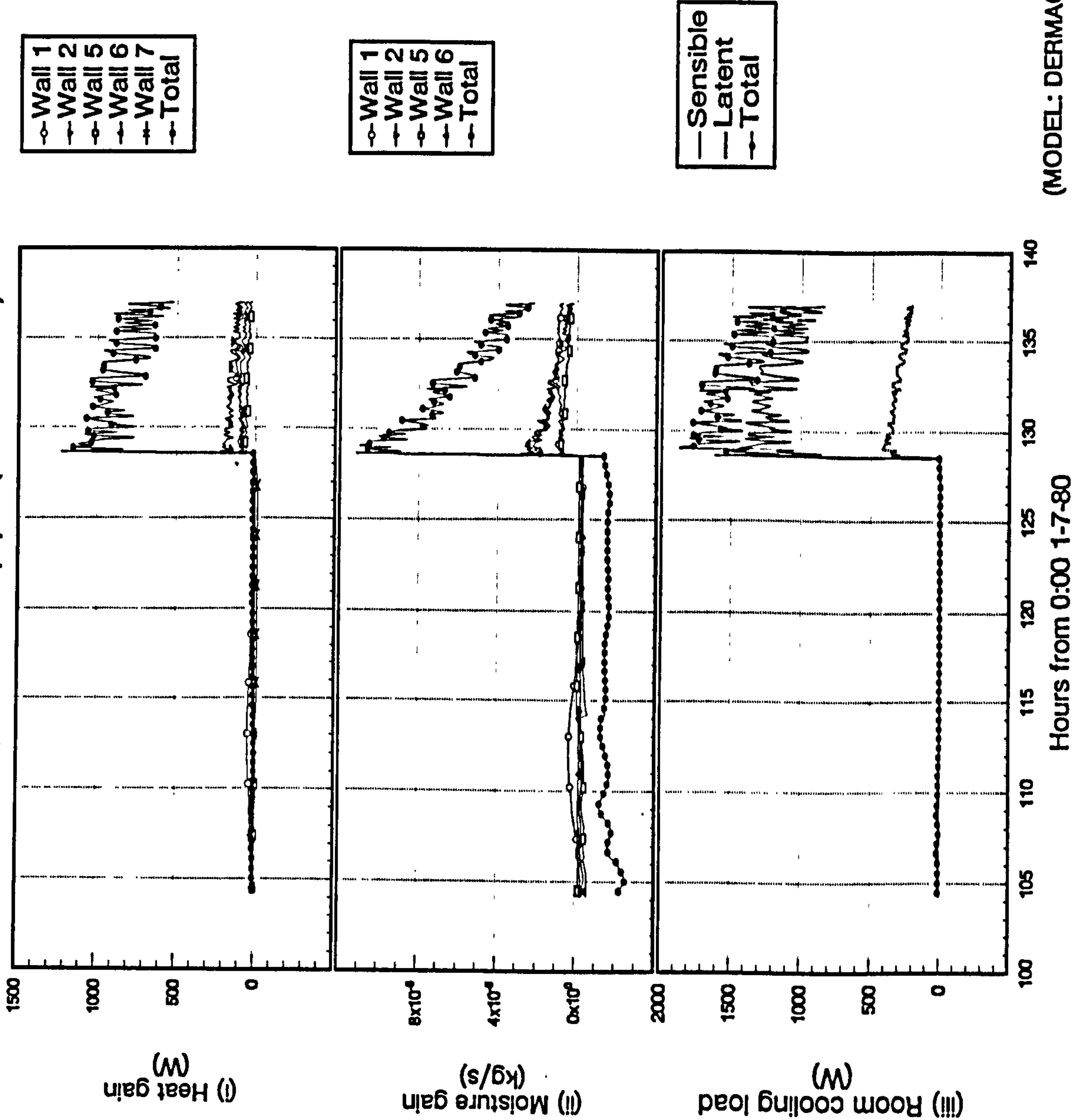
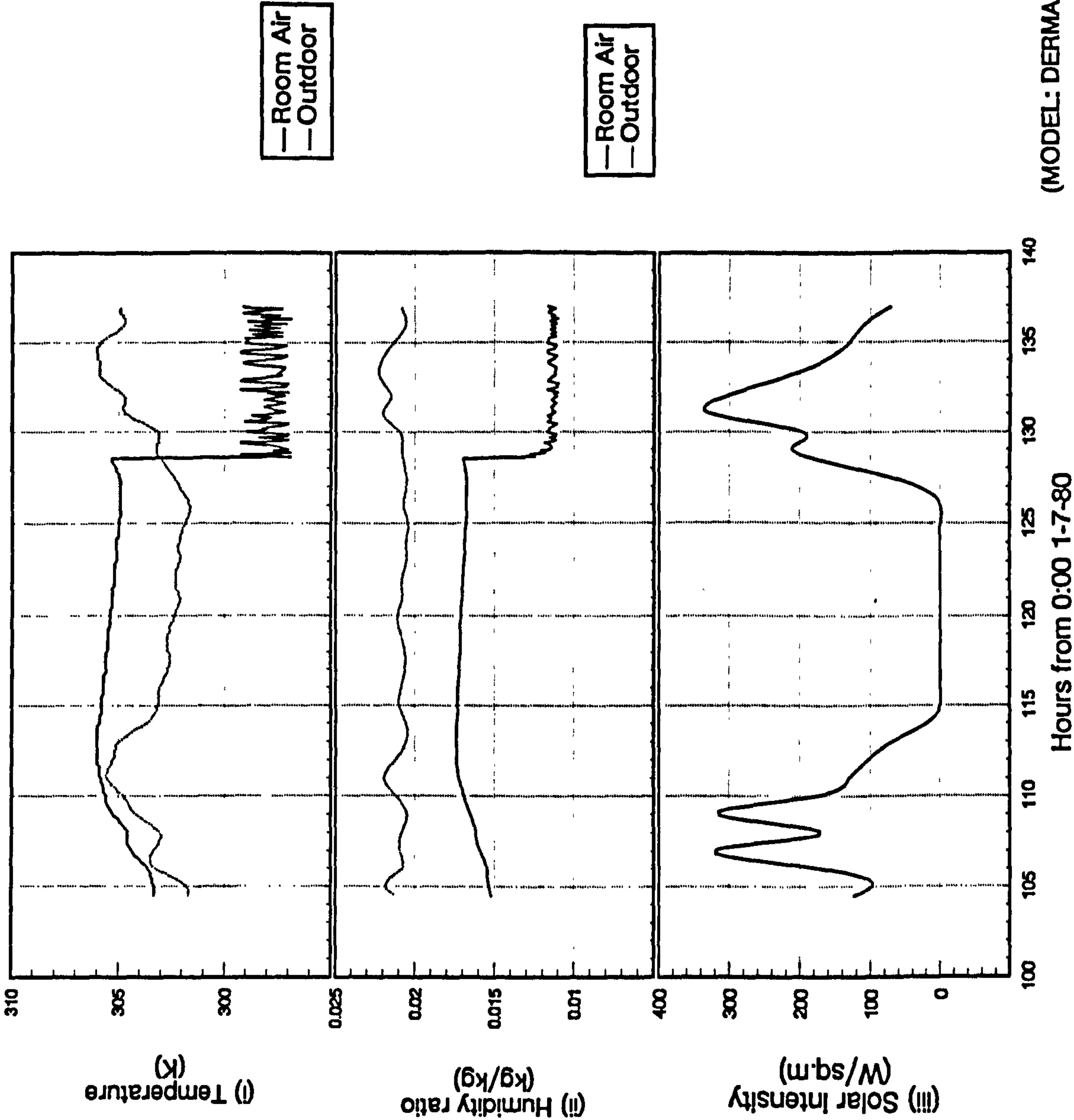


Figure 9.25.c

Intermittent air-conditioning by FD coil model
with no air-conditioning from 8:30 5/7/80 to 8:30 6/7/80
followed by air-conditioning with on/off control
from 8:30 6/7/80 to 17:00 6/7/80 (second batch)

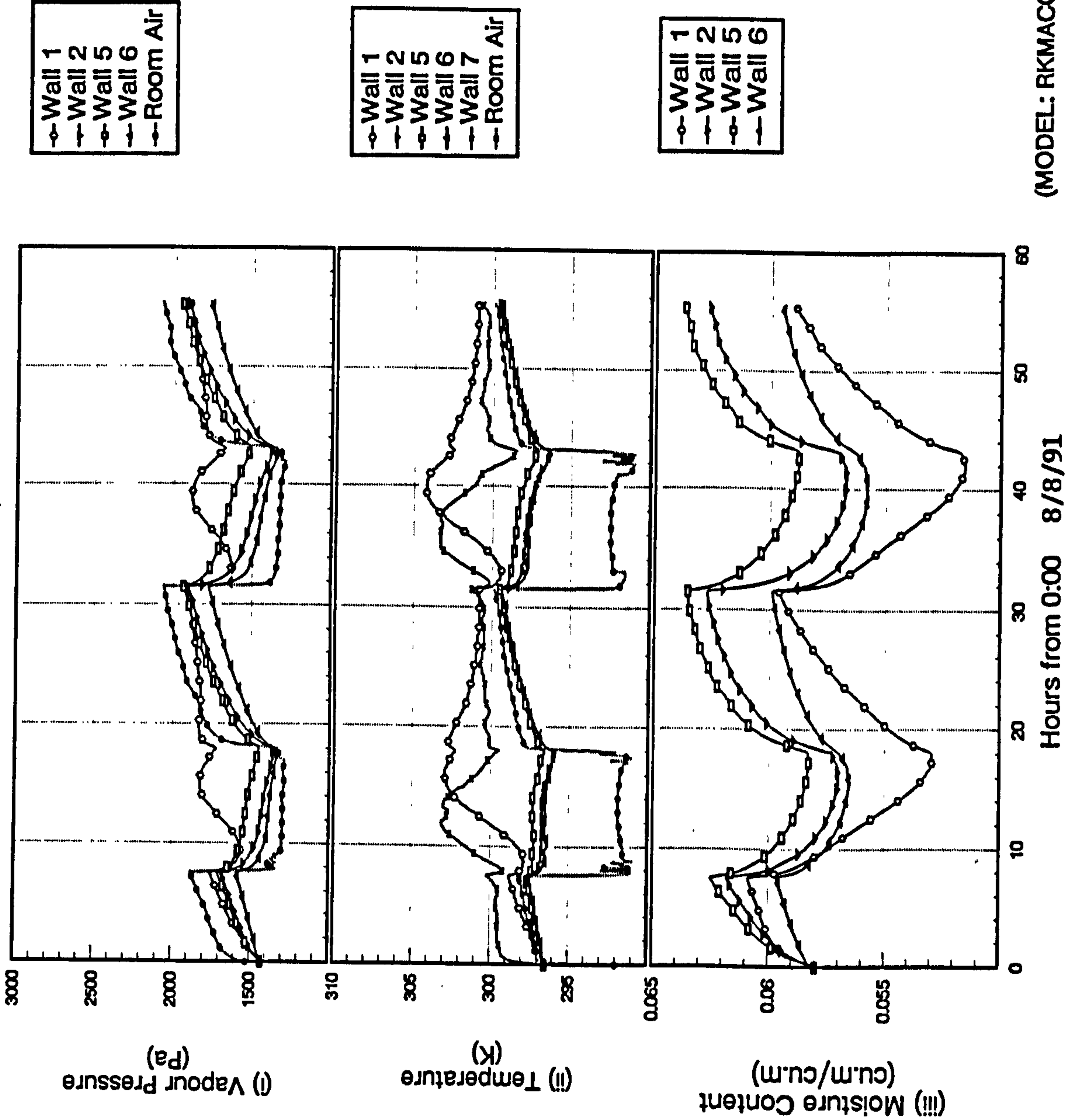


(MODEL: DERMAC)

Indoor and Outdoor Conditions

Figure 9.26.a

Intermittent air-conditioning by LMHD coil model
with on/off control from 0:00 8/8/91 to 7:30 10/8/91
(verification test)

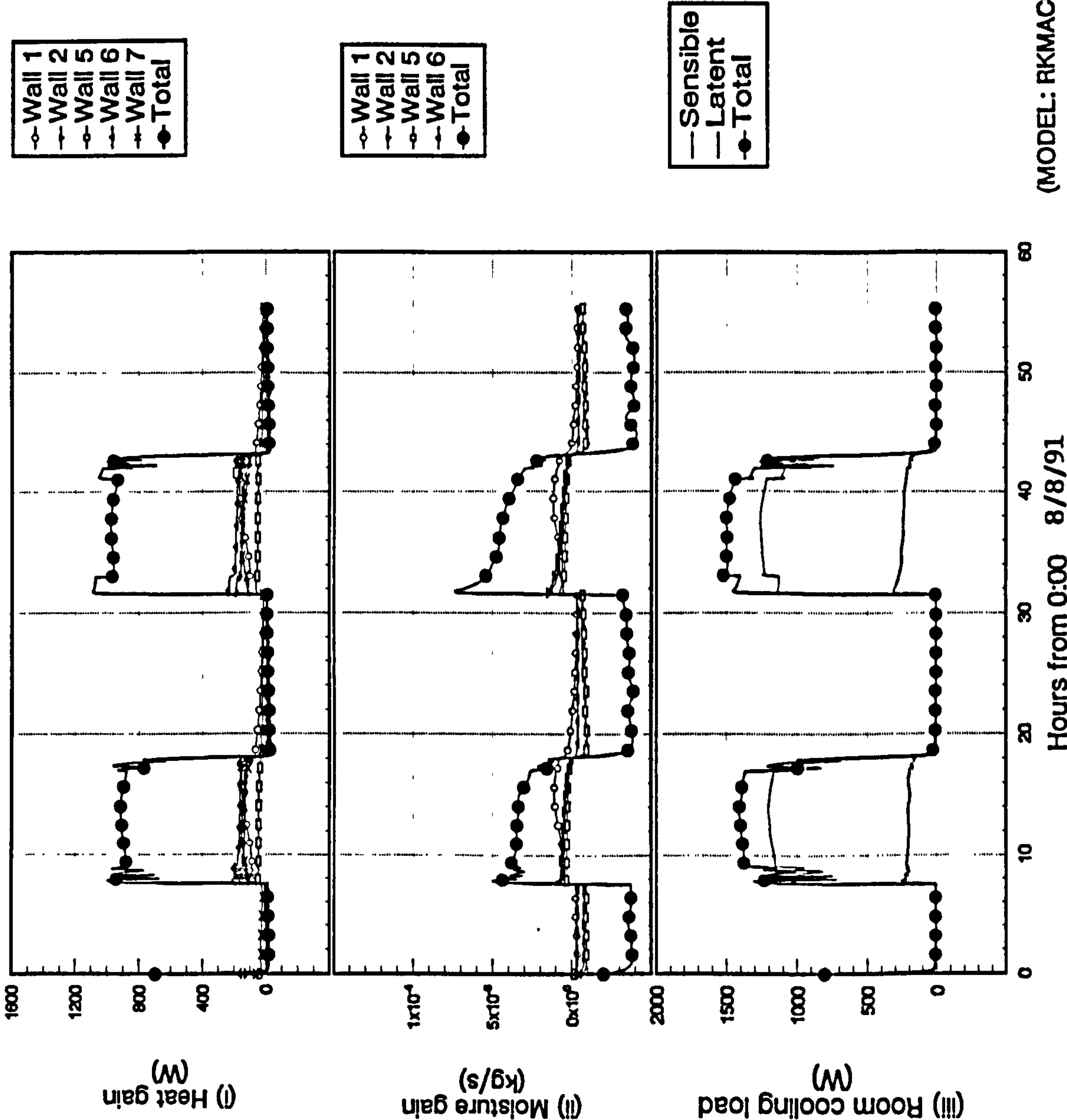


(MODEL: RKMACC)

Figure 9.26.b

Intermittent air-conditioning by LMHD coil model
with on/off control from 0:00 8/8/91 to 7:30 10/8/91
(verification test)

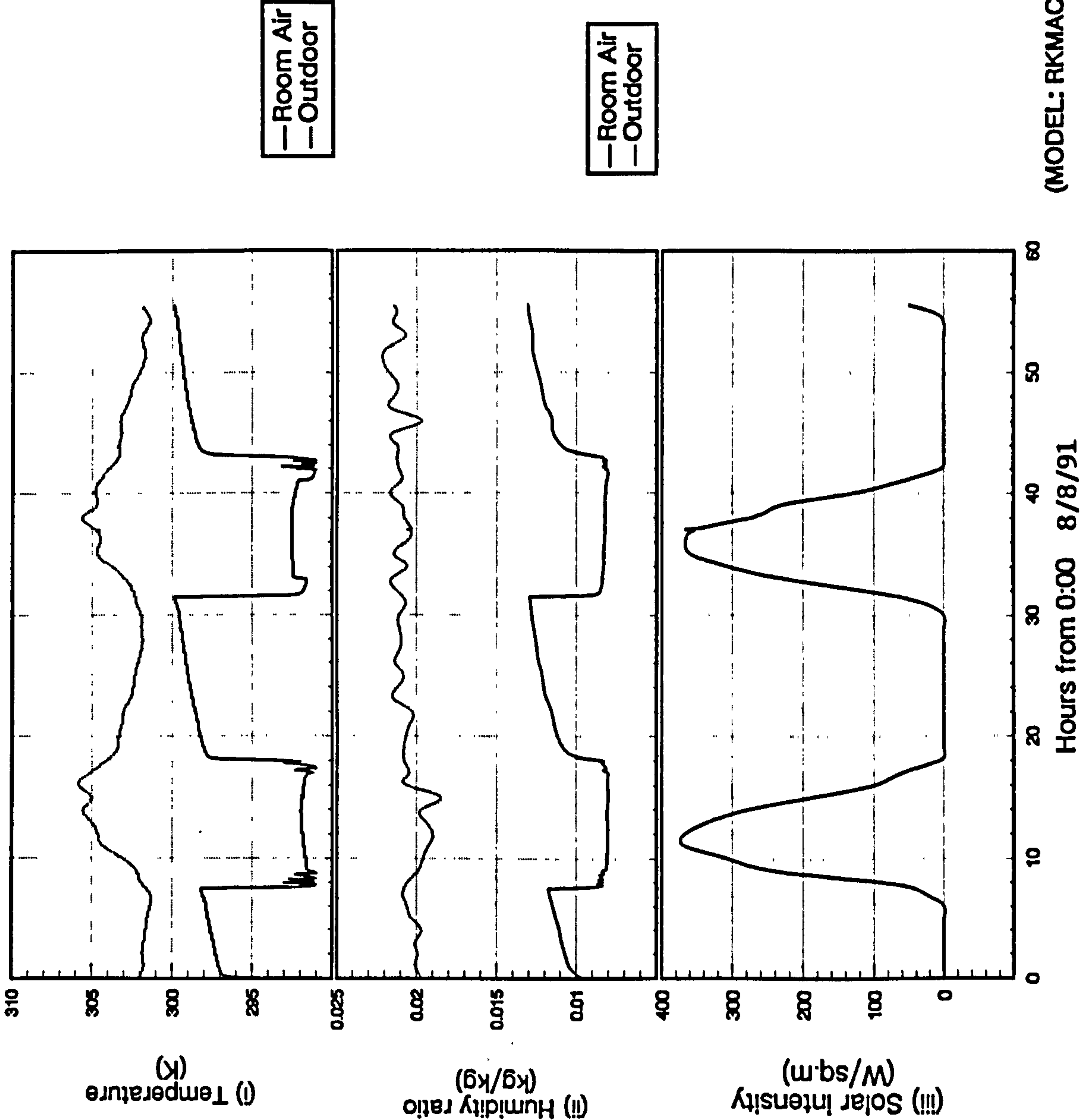
Heat and Moisture Gains and Room Cooling Load



Indoor and Outdoor Conditions

Figure 9.26.c

Intermittent air-conditioning by LMHD coil model
with on/off control from 0:00 8/8/91 to 7:30 10/8/91
(verification test)



Wall Internal Surfaces Conditions

Figure 9.27.a
Intermittent air-conditioning by LMHD coil model
with on/off control from 7:30 10/8/91 to 24:00 12/8/91
(verification test)

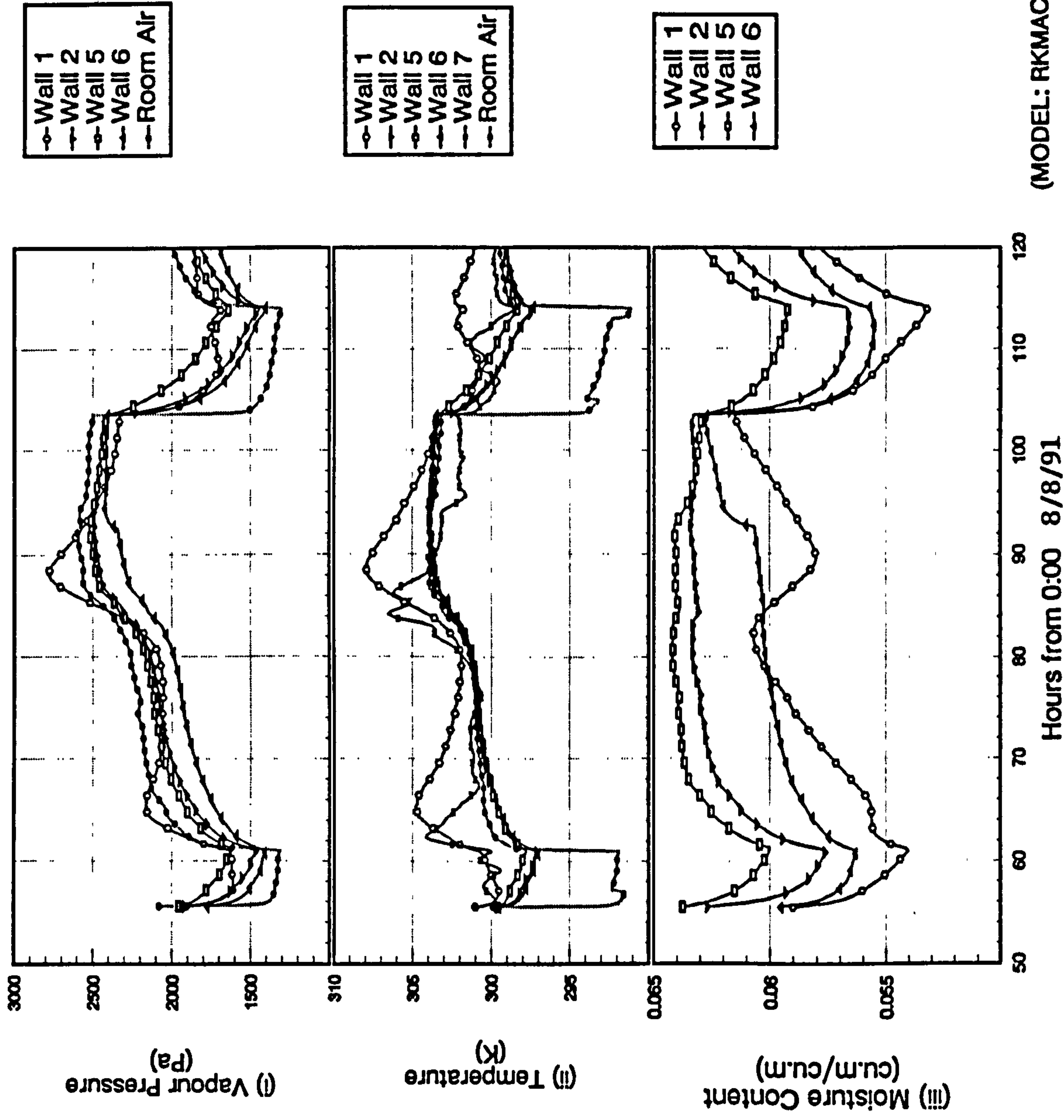
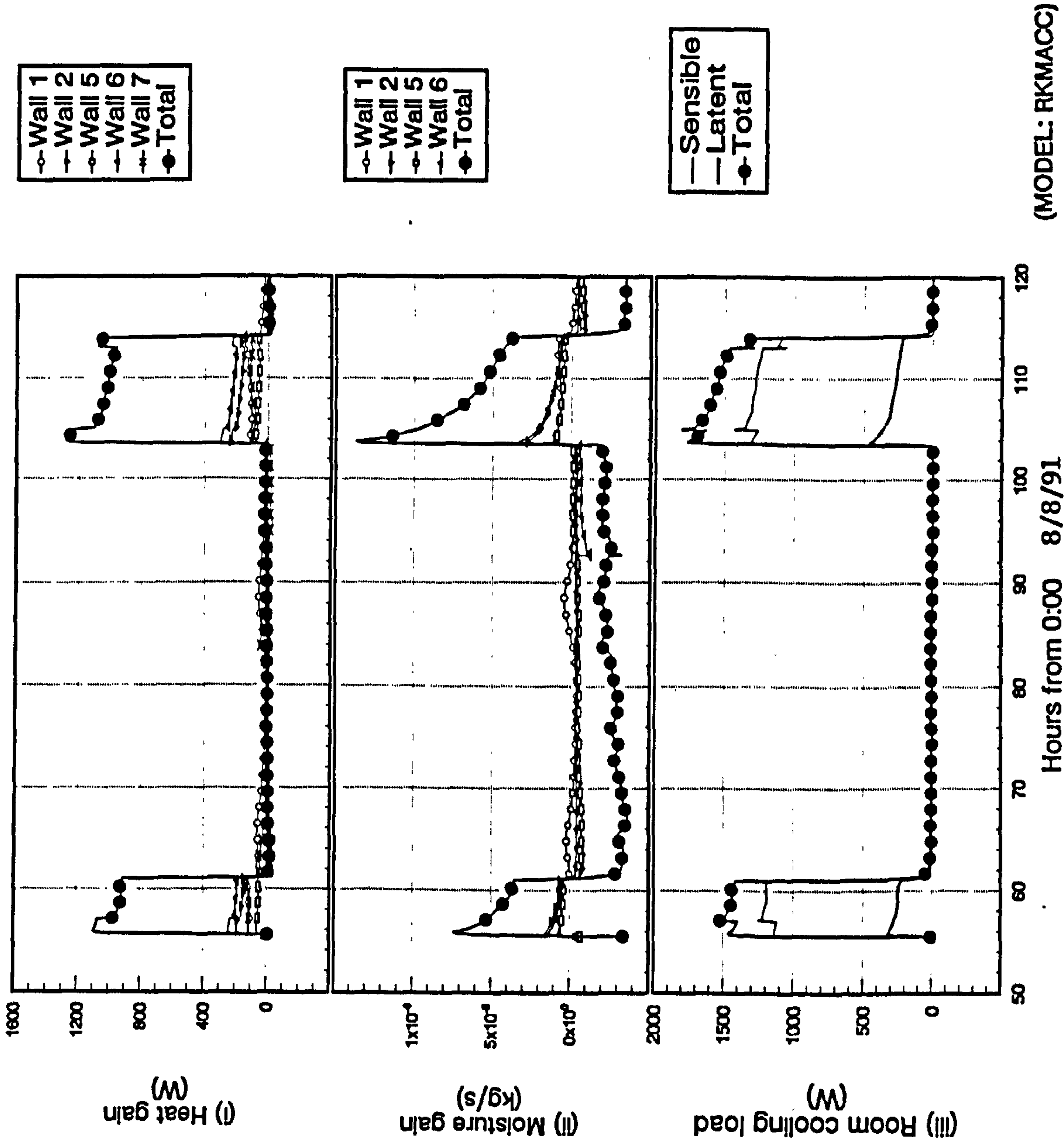


Figure 9.27.b

Intermittent air-conditioning by LMHD coil model
with on/off control from 7:30 10/8/91 to 24:00 12/8/91
(verification test)

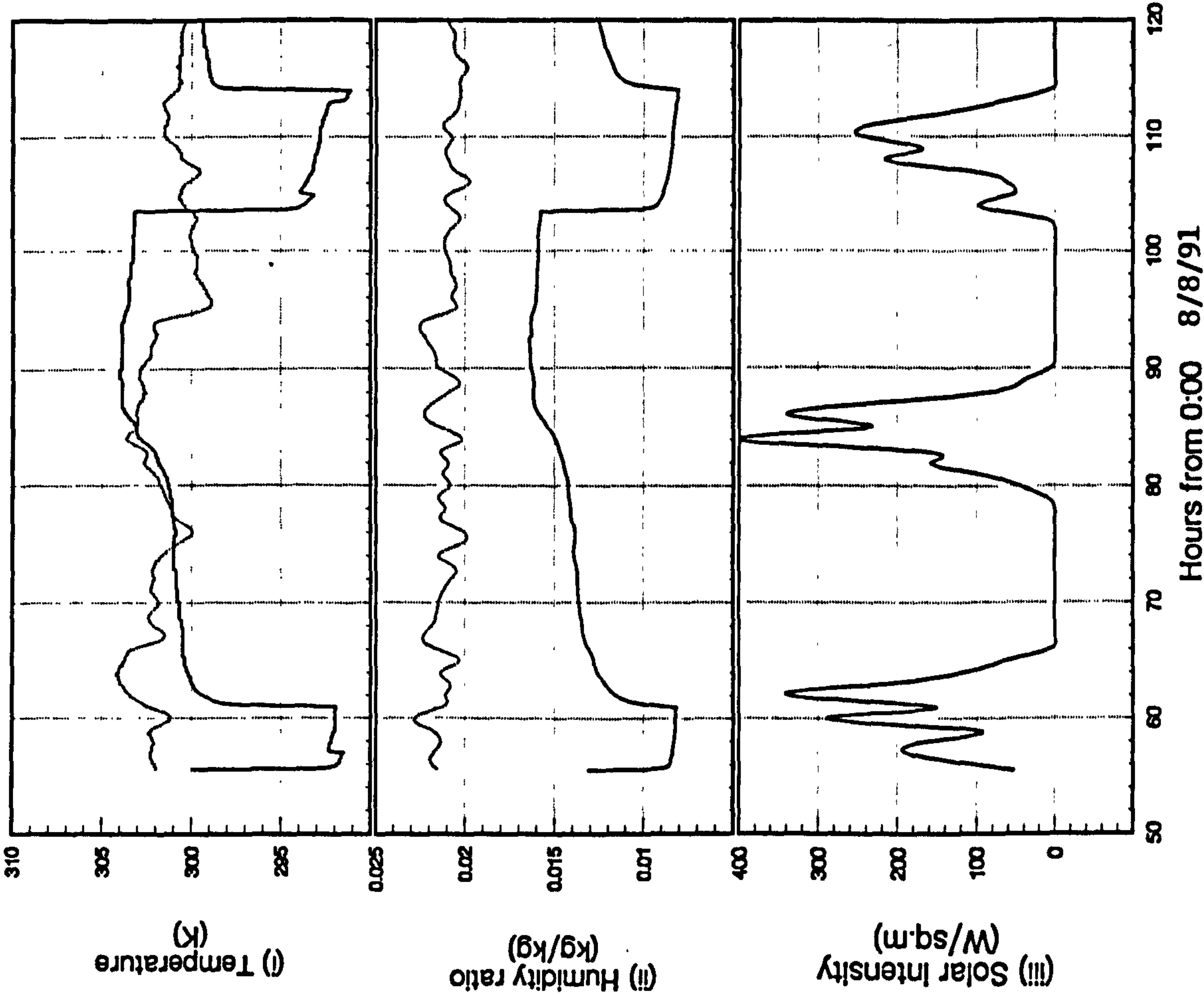
Heat and Moisture Gains and Room Cooling Load



(MODEL: RKMACC)

Figure 9.27.c

Intermittent air-conditioning by LMHD coil model
with on/off control from 7:30 10/8/91 to 24:00 12/8/91
(verification test)



(MODEL: RKMACC)

Figure 9.28.a
Comparison of indoor conditions on 8-9/8/91
Measured and predicted (by RKMACC)

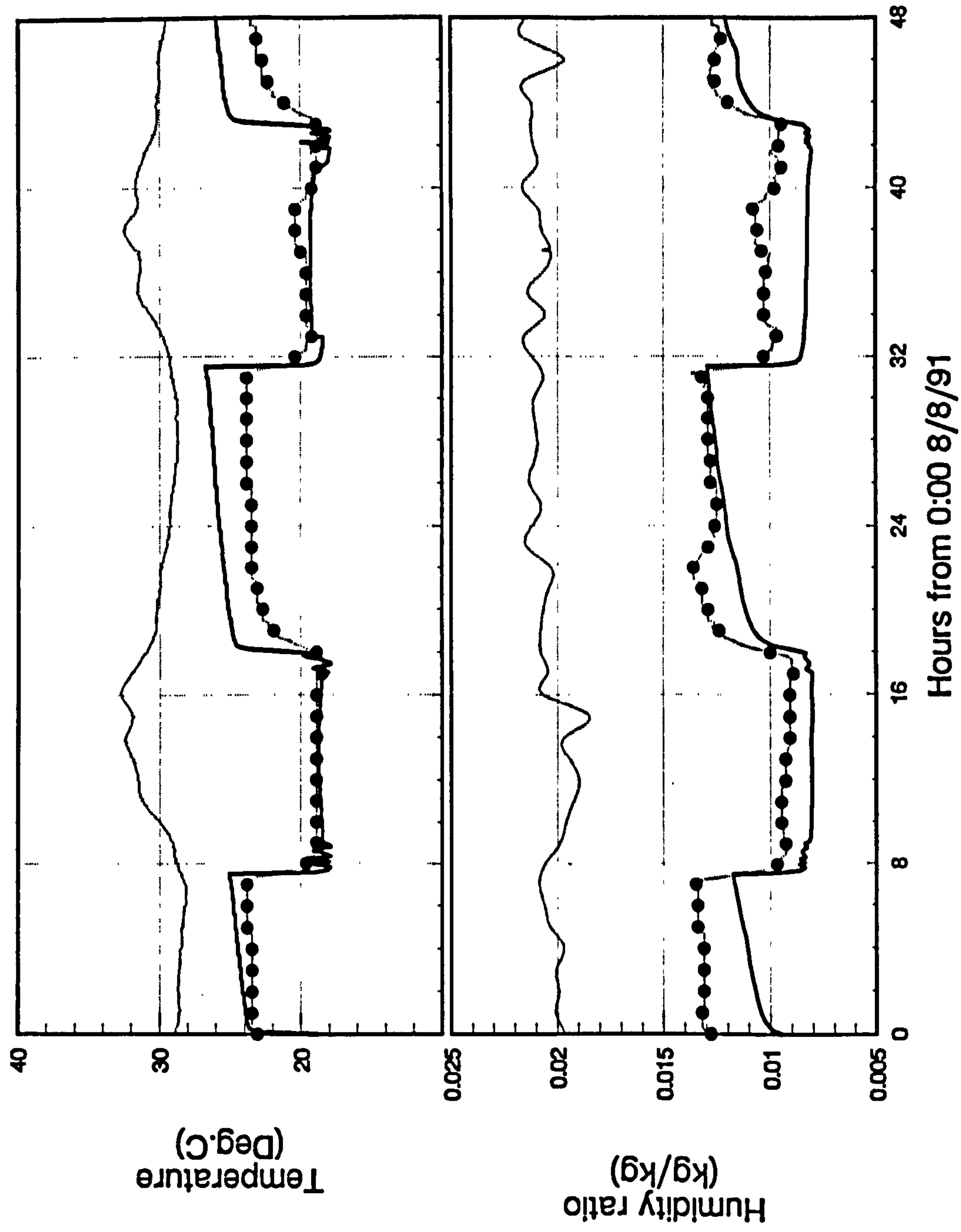
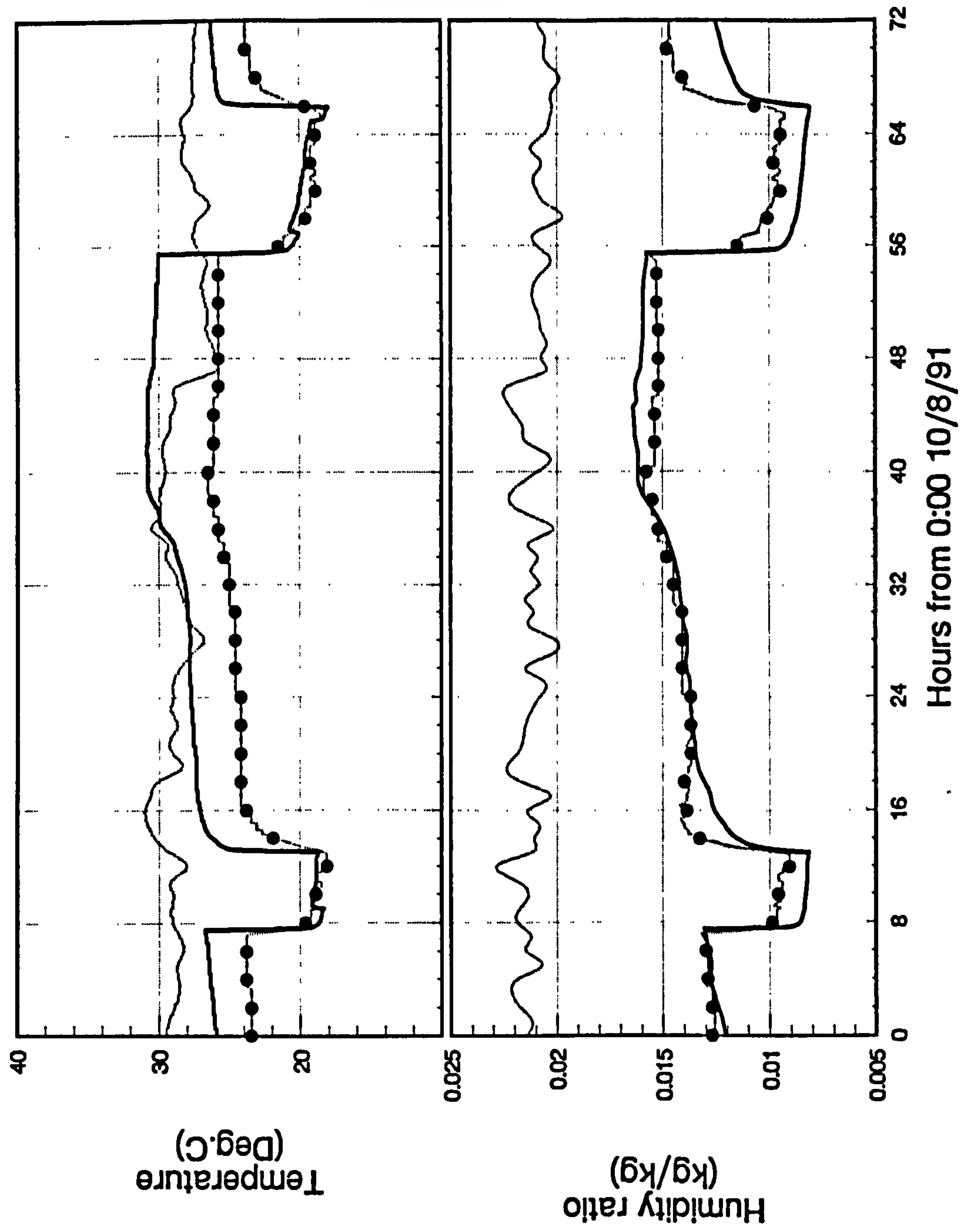


Figure 9.28.b
Comparison of indoor conditions on 10-12/8/91
Measured and predicted (by RKMACC)



List of References

- 1 Wong, S P W, (1990) Simulation of simultaneous heat and moisture transfer by using the finite difference method and verified tests in a test chamber, *ASHRAE Trans.* V.96, Pt 1.
- 2 Wong, S P W, and Wang, S K, (1990) Fundamentals of simultaneous heat and moisture transfer between the building envelop and the conditioned space air, *ASHRAE Trans.* V.96, Pt 2.
- 3 Carrier Air-conditioning Co. (1965) *Handbook of air-conditioning system design*, McGraw Hill.
- 4 CIBSE (1986) *Guide Vol. A*. The Chartered Institution of Building Services Engineers, UK.
- 5 ASHRAE Handbook (1989) *Fundamentals*, ASHRAE, USA.
- 6 Kusuda, T (1983) Indoor humidity calculations, *ASHRAE Trans.* V.89 Pt.2.
- 7 Fairey, P W, and Kerestecioglu, A (1985) Dynamic modelling of combined thermal and moisture transport in buildings: effects on cooling loads and space conditions, *ASHRAE Trans.* V.91, Pt.2A, pp.461-472.
- 8 Shukuya M and Saito M (1990) Simulation of indoor air humidity using control volume heat and moisture balance method, *Energy and Building*, 14(1990) pp. 373 - 384, Elsevier Sequoia.
- 9 Tsuchiya, T (1980) Infiltration and indoor air temperature and moisture variation in a detached residence, *JSHASE Japan*, 54(11), pp.13-19.
- 10 Isetti, C, Laurenti, L and Ponticiello, (1988) Predicting vapour content of the indoor air and latent loads for air-conditioned environments: Effect of moisture storage capacity of the walls, *Energy and Buildings*, 12(1988), pp.141-148.
- 11 Fanger, P O (1972) *Thermal comfort*, McGraw-Hill.
- 12 Chow W K, Burnett, J, Chan, K T, Chung, T M and Yik, F W H (1991) OTTV studies for building envelopes in Hong Kong, *Proc. European Simulation Multiconference*, Copenhagen, Denmark, June 17 - 19, 1991.
- 13 Royal Observatory of Hong Kong, *Meteorological Results, Part 1 - Surface Observations* (published annually), Royal Observatory of Hong Kong.
- 14 Roberts, D (Ed.) (1990) *Hong Kong 1990*, Government Informances Services, Hong Kong.
- 15 Census and Statistics Department, Hong Kong (1990) *Hong Kong energy statistics 1980 - 1990*, Census and Statistics Department, Hong Kong.
- 16 Uyttenbroeck, J and Carpentier, G (1985) Criteria for the avoidance of mould growth in dwellings, *Proc. of the 1985 Internal Symposium on Moisture and Humidity*, ISA.

- 17 Lotz, W A (1989) Moisture problems in buildings in hot humid climates, *ASHRAE Journal*, April 1989, pp.26 - 27.
- 18 Ramson W H (1987) *Building failures: diagnosis and avoidance*, 2nd Ed. E & F N Spon.
- 19 ASHRAE Handbook (1991) *HVAC applications*, ASHRAE, USA.
- 20 Todd, T R and Pate, M E III (1987) Passive humidity control: a comparison of air-conditioning capacity control methods for the humid climate, *Far East Conference on Air Conditioning in Hot Climates*, Singapore, Sept. 1987, pp.170-185, ASHRAE.
- 21 Whiteley, P, Russman H D, and Bishop, J D, (1977) *Porosity of building materials - a collection of published results*, Building Research Establishment Current Paper, CP21/77, Building Research Establishment, Department of the Environment, UK.
- 22 Loudon, A G (1968) *Summertime temperatures in buildings*, IHVE/BRS Symposium, Feb., 1968, BRS Current Paper 47/68, Building Research Establishment.
- 23 Millbank, N O and Harrington-Lynn, J. (1974) Thermal response and the admittance procedure, *BSE*, May 1974, Vol.42, pp.38-51.
- 24 Stephenson, D G and Mitalas, G P (1967) Cooling load calculations by thermal response factor method, *ASHVE Trans.* Vol.73, no.2018.
- 25 Stephenson, D G and Mitalas, G P (1971) Calculation of heat conduction transfer functions for multilayer slabs, *ASHRAE Trans.* Vol.77, Pt.2, pp.117-126.
- 26 Peavy, B A (1978) A note on response factors and conduction transfer functions, *ASHRAE Trans.* Vol.84, pp.688-690.
- 27 Stoecker, W F and Jones, J W (1982) *Refrigeration and air conditioning*, McGraw Hill.
- 28 McQuiston, F C and Parker, J D (1988) *Heating, ventilating, and air-conditioning analysis and design*, 3rd ed., John Wiley and Sons.
- 29 Stoecker, W F (1975) *Procedures for simulating the performance of components and systems for energy calculations*, 3rd Ed., ASHRAE.
- 30 Massey, B S (1970) *Mechanics of fluids*, Van Nostrand Reinhold Company.
- 31 Clarke, J A (1986) Simulation of building energy systems, *Proc. CIB 5th Int. Sym.*, Bath, 1986, pp.118-133, CIBSE, UK.
- 32 Kays, W M and London, A L (1964) *Compact heat exchangers*, 2nd Ed., McGraw Hill.
- 33 McQuiston, F C (1971) Heat transfer and flow friction data for two fin-tube surfaces, *ASME Journal of Heat Transfer*, May, 1971.
- 34 McQuiston, F C (1976) Heat, mass and momentum transfer in a parallel plate dehumidifying exchanger, *ASHRAE Trans.* Vol.82, Pt.2.

- 35 Clarke, J A (1982) *ESP Manual*, ABACUS, University of Strathclyde, Glasgow.
- 36 Clark, D R (1985) *HVACSIM+ building systems and equipment simulation program reference manual*, NBSIR 84-2996, National Bureau of Standards, USA.
- 37 Klein, S A, et al (1981) *TRNSYS: A transient system simulation program*, Report 38-11, Solar Energy Laboratory, University of Wisconsin, Madison.
- 38 Shavit, G and Brandt, S G (1982) Dynamic performance of a discharge air-temperature system with a P-I controller, *ASHRAE Journal*, Sept., 1982, pp.37-41.
- 39 Thompson, J G and Chen, P N T (1979) Digital simulation of the effect of room and control system dynamics on energy consumption, *ASHRAE Trans.* Vol.85, Pt.2, pp.222-237.
- 40 DOE 2 Building Energy Analysis Program - *Reference Manual*, Lawrence Berkeley Laboratory, USA.
- 41 BLAST-3.0 (1986), *Users manual, The building loads analysis and system thermodynamics programme*, Support office, Department of Mechanical and Industrial Engineering, Univerisity of Illinois at Urbana-Champaign, Urbana.
- 42 Loudon, A G (1983) The effect of moisture content on thermal conductivity, *Autoclaved Aerated Concrete, Moisture and Properties*, Amsterdam, Elsevier Scientific Publishing, 131-141.
- 43 Stuckes, A D and Simpson, A (1986) Moisture factors and thermal conductivity of concrete, *BSER&T* 7(2), pp.73-77.
- 44 Uyttenbroeck, J (1990) Building heat loss calculations: choice of internal temperature and of heat exchange coefficient h_i , *BSER&T* 11(2), pp.49-56.
- 45 Davies, M G, (1990) Mean radiant temperature in the CIBSE Guide, *BSER&T* 11(2), pp.69-71.
- 46 Down, P G, Irving, S J and Quick, J P (1981) Energy estimation by system simulation, *New energy conservation technologies and their commercializaton, Proceedings of IEA Conference*, Berlin, 6 - 10 April, 1981.
- 47 *APACHE User Manual* (1988), Facet Ltd., UK.
- 48 Charlesworth P, Clarke, J A, Hammond G, et al (1991) The Energy Kernel System: The way ahead ?, *Proc. of BEP'91* (Cantebury, UK, Apr., 10-11), pp.223-236.
- 49 Wright A J, Clarke, J A, Hammond G, et al (1990) The use of object-oriented programming techniques in the UK Energy Kernel System for building simulation, *Proc. of 1990 European Simulation Multiconference* (Nurembery, June 10-13), pp.548-554.
- 50 Huang, C L D, (1979) Multi-phase moisture transfer in porous media subjected to temperature gradient, *Int. J. Heat Mass Transfer*, Vol. 22, pp. 1275 - 1307.
- 51 Huang, C L D, Siang, H H, and Best, C H, (1979), Heat and moisture transfer in concrete slabs, *Int. J. Heat Mass Transfer*, Vol.22 pp. 257-266.

- 52 Yik, F W H (1991) Dynamic modelling of indoor air humidity, *Proc. of Building Simulation '91 Conference*, Nice, France, The International Building Performance Simulation Association.
- 53 Thomas, W C and Burch, D M (1990) Experimental validation of a mathematical model for predicting water vapor sorption at interior building surfaces, *ASHRAE Trans.* Vol.96, Pt.1.
- 54 Philip, J R, and DeVries, D R, (1957) Moisture movement in porous media under temperature gradients, *Trans. Am. Geophysical Union*, 38(2), pp.222-232.
- 55 Luikov, A V (1964) Heat and mass transfer in capillary porous bodies, *Advances in Heat Transfer*, V.1, Academic Press.
- 56 Luikov, A V (1966) *Heat and mass transfer in capillary porous bodies*, Pergamon Press.
- 57 Luikov, A V (1975) Systems of differential equations of heat and mass transfer in capillary porous bodies (review), *Int. J Heat Mass Transfer*, V.18, pp.1-14.
- 58 Harmathy, T Z (1967) *Moisture sorption of building materials*, Technical Paper No. 242, Division of Building Research, NRCC Canada.
- 59 Harmathy, T Z (1969) Simultaneous moisture and heat transfer in porous systems with particular reference to drying, *I&EC Fundamentals*, 8(1), pp. 92 - 103.
- 60 Harmathy, T Z (1971) *Moisture and heat transport with particular reference to concrete*, Research Paper No. 494, Division of Building Research, NRCC Canada.
- 61 Berger, D, and Pei, D C T, (1973) Drying of hygroscopic capillary porous solids - a theoretical approach, *Int. J. Heat Mass Transfer*, Vol.16, pp.293-302.
- 62 Scheidegger, A E, (1974) *The physics of flow through porous media*, 3rd Ed., University of Toronto Press, Toronto.
- 63 Whitaker, S (1977) Simultaneous heat mass and momentum transfer in porous media: A Theory of Drying, *Advances in Heat Transfer*, Vol 13, pp. 119-203.
- 64 Corey, A T (1977) *Mechanics of heterogeneous fluids in porous media*, Water Resources Publications, Fort Collins, Colorado.
- 65 Satterfield C N (1970) *Mass transfer in heterogeneous catalysis*, MIT Press, Cambridge, Massachusetts.
- 66 Gregg, S J and Sing K S W (1982) *Adsorption, surface area and porosity*, 2nd Ed., Academic Press.
- 67 Illston J M, Dinwoodie, J M and Smith, A A (1987) *Concrete, timber and metals, the nature and behaviour of structural materials*, Van Nostrand Reinhold.
- 68 Skaar, C (1972) *Water in wood*, Syracuse University Press, New York.
- 69 Hansen, K K (1986) *Sorption isotherms, a catalogue*, Building Materials Laboratory, The Technical University of Denmark.

- 70 Kraemer, E O (1931) *A treatise on physical chemistry*, Taylor, H S (ed.) D Van Nostrand.
- 71 McBain, J W (1935) *J. Am. Chem. Soc.*, Vol.57, p.699.
- 72 Cohan, L H (1938) *J. Am. Chem. Soc.*, 60, 433.
- 73 Cohan, L H (1944) *J. Am. Chem. Soc.*, 66, 98.
- 74 Rao, K S (1941) *J. Phy. Chem.*, Vol.45, p.506.
- 75 Pedersen, C R (1991) A transient model for analyzing the hygrothermal behaviour of building constructions, *Building Simulation '91 Conference*, August, 1991, Nice, France, The International Building Performance Simulation Association.
- 76 Atkins, C J (1983) *Equilibrium thermodynamics*, 3rd Ed., Cambridge Univeristy Press.
- 77 Claesson, J (1978) Fundamentals of moisture and energy flow in capillary-porous building materials, *Proc. of Heat Transfer in Building*, ICHMT Internal Seminar 1977, Ed. Hoogendoorn and Afgan, Hemisphere Pub.
- 78 Vassiliou, B and White, J (1948) *Trans. Ceram. Soc.*, Vol.47, p.351.
- 79 Bird, R B, Stewart, W E and Lightfoot, E N (1960) *Transport phenomena*, John Wiley and Sons.
- 80 Lewis, W K (1921) The rate of drying of solid materials, *Ind. Eng. Chem.*, 13, pp.427-432.
- 81 Sherwood, T K (1930) The drying of solids, III, Mechanism of the drying of pulp and paper, *Ind.Chem. Eng.*, Vol.22, pp.132-136.
- 82 Newman, A B (1931) The drying of porous solids: diffusion and surface emission equation, *Trans. Am. Inst. Chem.*, Vol.27, pp.203-220.
- 83 Hougen, O A, McCauley, H J, and Marshall, W R Jr. (1940) Limitations of diffusion equations in drying, *Trans. Am. Inst. Chem. Eng.* 36, pp.183-210.
- 84 Gilliland, E R and Sherwood, T K (1933) The drying of solids VI, Diffusion equations for the period of constant drying rate, *Ind. Eng. Chem*, 25, pp.1134-1136.
- 85 Buckingham, E (1907) Studies on the movement of soil moisture, *US Dept. Agr., Bur. Soils, Bull. 38*.
- 86 Ceaglske, N H and Hougen, O A (1937) Drying granular solids, *Ind. Eng. Chem.*, 29, pp. 805-813.
- 87 Haines, W B (1927) Studies in the physical properties of soils, IV, A further contribution to the theory of capillary phenomena in soil, *J Agric, Sci.*, 17, pp. 264-290.
- 88 Haines, W B (1930) Studies in the physical properties of soils, V, The hysteresis effect in capillary properties and the modes of moisture distribution associated therewith, *J Agric, Sci.*, 20, pp. 97-116.

- 89 Henry, P S H (1939) Diffusion in absorbing media, *Proc. R. Soc.*, Vol.171A, pp.215-241, London.
- 90 Gurr, C G, Marshall, T J and Hutton, J T (1952) Movement of water in soil due to a temperature gradient, *Soil Science*, Vol.74, pp.335-345.
- 91 Kuzmak, J M and Sereda, P J (1957) The mechanism by which water moves through a porous material subjected to a temperature gradient: I, Introduction of a vapour gap into a saturated system, *Soil Sci.*, Vol.84, pp.291-299.
- 92 Onsager, L (1931) *Phys. Rev.*, Vol.37, p.405.
- 93 DeGroot, S R and Mazur, P (1962) *Non-equilibrium thermodynamics*, North Holland, Amsterdam.
- 94 Matsumoto M (1978) Simultaneous heat and moisture transfer in porous wall and analysis of internal condensation, *Proc. of Heat Transfer in Building*, ICHMT International Seminar 1977, Ed. Hoogendoorn and Afgan, Hemisphere Pub.
- 95 Kerestecioglu, A, Swami, M, Dabir, R, Razzaq, N and Fairey, P, (1988) *Theoretical and Computational Investigation of Algorithms for Simultaneous Heat and Moisture Transport in Buildings*, Final Report to US DOE Cotract #DE-FC03-865F16305 and GRI Contract #5087-243-1515, FSEC-CR-191-88.
- 96 Comini, G and Del Giudice, S (1978) Finite element analysis of heat and mass transfer in buildings, *Proc. of Heat Transfer in Building*, ICHMT Internal Seminar 1977, Ed. Hoogendoorn and Afgan, Hemisphere Pub.
- 97 Krischer, O (1963) *Die wissenschaftlichen grundlagen der teoknungstechnik*, Kap IX, Springer, Berlin.
- 98 Kohonen, R (1984) *A method to analyze the transient hygrothermal behaviour of building materials and components*, PhD Thesis, Helsinki Univeristy of Technology, Espoo, Finland.
- 99 Matsumoto, M (1980) Internal condensation and re-evaporation process of moisture in a foam concrete, *The VIth all-union Heat and Mass Transfer Conference*, Vol.7, Minsk.
- 100 Matsumoto, M and Sato, M (1985) Numerical methods in thermal problems, *Int. Conf. on Numerical Methods in Thermal Problems*, 1985.
- 101 Matsumoto, M and Kotera, N (1988) An analysis of the heat storage process in wet soil solved as a coupled problem, *Energy and Buildings*, Vol.11, pp.239-247.
- 102 Loudon, A G (1971) *The effects of condensation and building design factors on the risk of condensation and mould growth in dwellings*, BRE Current Paper CP 31/71, Building Research Establishment.
- 103 BRE (1972) *Condensation*, BRE Digest 110, Building Research Establishment.
- 104 Glaiser, H (1959) A graphical method for the investivation of diffusion processes, *Kaltetechnik*, 11, p.345.

- 105 Kieper G, Caemmerer, W and Wagner, A (1974) A new diagram for technical assessment of moisture protection of building constructions, *Gesundheits - Ingenieur*, 95(8) 214-219.
- 106 Boyd D, Cooper P and Oreszczyn, T (1988) Condensation risk prediction: Addition of a condensation model to BREDEM, *BSER&T* 9(3).
- 107 Letherman, K M (1989) Condensation avoidance in layered structures: Synthesis of designs, *BSER&T* 10(1).
- 108 Cunningham, M J (1983) A new analytical approach to the long term behaviour of moisture concentrations in building cavities - I, Non-condensing cavity, *Building and Envir.* 18(3), pp. 109-116.
- 109 Cunningham, M J (1983) A new analytical approach to the long term behaviour of moisture condensations in building cavities - II, Condensing cavity, *Building and Envir.*, Vol.18, No.3, pp.117-124.
- 110 Cunningham, M J (1984) Further analytical studies of building cavity moisture concentrations, *Building and Envir.*, Vol.19, No.1, pp.21-29.
- 111 Cunningham, M J (1988) The moisture performance of framed structures - a mathematical model, *Building and Envir.* Vol.23, pp.123-135.
- 112 Cunningham, M J (1990) Modelling of moisture transfer in structures - I, A description of a finite-difference nodal model, *Building and Envir.*, Vol.25, No.1, pp.55-61.
- 113 Cunningham, M J (1990) Modelling of moisture transfer in structures - II, A comparison of a numerical model, an analytical model and some experimental results, *Building and Envir.*, Vol.25, No.1, pp.85-94.
- 114 Miller, J D (1984) Development and validation of a moisture mass balance model for predicting residential cooling energy consumption, *ASHRAE Trans.* Vol.90 Pt.2B.
- 115 Kusuda, T and Miki M (1985) Measurement of moisture content for building interior surfaces, *Proc. of the International Symposium on Moisture and Humidity*, ISA, pp. 297 - 312.
- 116 Kerestecioglu, A, Swami, M, and Kamel, A (1990) Theoretical and computational investigation of simultaneous heat and moisture transfer in buildings: Effective penetration depth theory, *ASHRAE Trans.* V.96, Pt.1.
- 117 Cunningham, M J (1992) Effective penetration depth and effective resistance in moisture transfer, *Building and Envir.*, Vol.27, No.3, pp.379-386.
- 118 Becker, R and Jaegermann, C (1982) The influence of permeability of materials and absorption on condensation in dwellings, *Bldg. Envir.* 17(2) pp.125-134.
- 119 Barringer, C G, and McGugan, C A (1989) Development of a dynamic model for simulating indoor air temperature and humidity, *ASHRAE Trans.* Vol. 95 Pt.2, pp. 449 - 460.
- 120 Diasty, R El, Fazio, P and Budaiwi (1993) Dynamic modelling of moisture absorption and desorption in buildings, *Building and Envir.*, Vol.28, No.1, pp.21-32.

- 121 Kerestecioglu, A A (1986) *The detailed mathematical prediction of simultaneous heat and mass transfer in cavities*, PhD Thesis, Florida Institute of Technology.
- 122 Kerestecioglu, A, Fairey, P W and Chandra S (1985) Algorithms to predict detailed moisture effects in buildings, ASHRAE/DOE/BTECC Conference, *Thermal Performance of the Exterior Envelopes of Buildings III*, Dec. 2 - 5, 1985.
- 123 Walton, G (1983) *TARP reference manual*, NBSIR, 83-2655, Washington DC, National Bureau of Standards.
- 124 Kerestecioglu, A, and Gu, L, (1990) Theoretical and computational investigation of simultaneous heat and moisture transfer in buildings: Evaporation and condensation theory, *ASHRAE Trans.* Vol.96, Pt.1.
- 125 Bomberg, M (1974) *Moisture flow through porous building materials*, Report 52, Division of Building Technology, Lund Institute of Technology, Sweden.
- 126 Powers, T C and Brownyard, T L (1948) *Studies of the physical properties of hardened portland cement paste*, Research Laboratories of Portland Cement Association, Bulletin 22, Chicago.
- 127 Powers, T C (1962) *Proc. of the Fourth Int. Sym. on the Chemistry of Cement*, Washington, 1960, Vol.2, p.577, National Bureau of Standards, Washington.
- 128 Neville, A M (1981) *Properties of concrete*, Longman
- 129 Incropera, F P and DeWitt, D P, (1985) *Fundamentals of heat and mass transfer*, 2nd ed., John Wiley and Sons.
- 130 Croft and Lilley (1977) *Heat transfer calculations using finite difference equations*, Applied Science Publishers, UK.
- 131 Gear, C W (1971) *Numerical initial value problems in ordinary differential equations*, Prentice-Hall.
- 132 Lambert, J D (1991) *Numerical methods for ordinary differential systems: The initial value problem*, Wiley.
- 133 BS4370 Pt.2 (1973), *Methods of test for rigid cellular materials*, British Standard Institute.
- 134 McLean, R C and Galbraith, G (1988) Interstitial condensation: applicability of conventional vapour permeability values, *BSER&T* 9(1) pp.29-34.
- 135 Holman, J P (1980) *Thermodynamics*, McGraw- Hill.
- 136 Howells, P B and Marshall, R M (1981) A fast and accurate integration scheme for coupled stiff differential equations, *Proc. Int. Conf. Numerical Methods for Coupled Problems*, pp.45-49, Swansea: Pineridge Press.
- 137 Ewen, J and Thomas, H R (1989) Heating unsaturated medium sand, *Geotechnique*, 39(3).
- 138 Press, W H, Flannery, B P, Teukolsky, S A, and Vetterling, W T (1989) *Numerical recipes - FORTRAN Version*, Cambridge University Press.

- 139 Stoecker, W F (1989) *Design of thermal systems*, McGraw Hill.
- 140 ASHRAE Handbook (1988) *Equipment*, ASHRAE, USA.
- 141 Beecher, D T and Fagan, T J (1987) Effects of fin pattern on the air-side heat transfer coefficient in plate finned-tube heat exchangers, *ASHRAE Trans.* 1987.
- 142 Hatada, T, Ueda, H, Oouchi, T and Shimizu, T (1989) Improved heat transfer performance of air coolers by strip fins controlling air flow distribution, *ASHRAE Trans.* Vol.95, Pt.1, pp.166-170.
- 143 McQuiston, F C (1978) Correlation of heat, mass and momentum transfer coefficients for plate-fin-tube heat transfer surfaces with staggered tubes, *ASHRAE Trans.* Vol. 84 Pt.1.
- 144 McQuiston, F C (1978) Heat, mass and momentum transfer data for five plate-fin-tube heat transfer surfaces, *ASHRAE Trans.* Vol. 84 Pt.1.
- 145 Letherman, K M (1981) *Automatic controls for heating and air-conditioning*, Pergamon Press.
- 146 ASHRAE Handbook (1987) *HVAC systems and applications*, ASHRAE, USA.
- 147 Clark, D R, Hill, C R and Hurley, C W (1985) Dynamic models for HVAC system components, *ASHRAE Trans.* Vol. 91, 1985.
- 148 Gartner, J R and Harrison, H L (1965) Dynamic characteristics of water-to-air crossflow heat exchangers, *ASHRAE Trans.* Vol.71, Pt.1, p.212.
- 149 Tamm, H and Green, G H (1973) Experimental multi-row crossflow heat exchanger dynamics, *ASHRAE Trans.* Vol.79, Pt.2, pp.9-18.
- 150 Romie, F E (1984) Transient response of the counterflow heat exchanger, *ASME Trans.*, Vol.106, pp.620-626.
- 151 Ganesh, R, Sauer, H J and Howell, R H (1989) Part-load simulations of simple air-conditioning systems using a new coil model, *ASHRAE Trans.* Vol.95, Pt.1.
- 152 Hamilton, D C, Leonard, R G, and Pearson, J T (1974) Dynamic response characteristics of a discharge air temperature control system at near full and part heating load, *ASHRAE Trans.* Vol.80, Pt.1, pp.181-194.
- 153 Stoecker, W F, Rosario, L A, Heidenreich, M E and Phelan, T R (1978) Stability of an air-temperature control loop, *ASHRAE Trans.* Vol.84, Pt.2, pp.35-53.
- 154 Maxwell, G M, Shapiro, H N and Westra, D G (1989) Dynamics and control of a chilled water coil, *ASHRAE Trans.* Vol.95, Pt.1.
- 155 Tobias, J R (1973) Simplified transfer function for temperature response of fluids flowing through coils, pipes or ducts, *ASHRAE Trans.* Vol.79, Pt.2, pp.19-22.
- 156 Boot, J L, Pearson, J T and Leonard, R G (1977) An improved dynamic response model for finned serpentine cross-flow heat exchangers, *ASHRAE Trans.* Vol. 83, Pt.1, pp.218-239.

- 157 Pearson, J T, Leonard, R G and McGutchan (1974) Gain and time constant for finned serpentine crossflow heat exchangers, *ASHRAE Trans.* Vol.80, Pt.2, pp.255-267.
- 158 Bhargava, S C, McQuiston F C and Zirkle, L D (1975) Transfer functions for crossflow multirow heat exchangers, *ASHRAE Trans.*, Vol.81, Pt.2, pp.294 - 314.
- 159 Chapra, S C and Canale, R P (1989) *Numerical methods for engineers*, McGraw Hill.
- 160 Eckels, R W (1977) *Contact conductance of mechanically expanded plate finned tube heat exchangers*, Westinghouse Research Laboratories, Science Paper No. 77-1E9-SURCO-P1.
- 161 Ngan, K H (1990) Use of an example weather year in predictions of cooling energy requirement in buildings of Hong Kong, *Research Project Paper No.1.7*, Department of Building Services Engineering, Hong Kong Polytechnic.
- 162 ASHRAE (1975) *Subroutine algorithms for heating and cooling loads to determine building energy requirements*, ASHRAE, USA.
- 163 Jaluria, Y (1988) *Computer methods for engineering*, Allyn and Bacon.
- 164 Jones, P J (1991) The simulation of infiltration rates and air movement in a naturally ventilated industrial building, *Air movement and ventilation control within buildings*, 12th AIVC Conference, Ottawa, Canada, 24-27 Sept., 1991.
- 165 Lomas, K J (1991) Dynamic thermal simulation models of buildings: new method for empirical validation, *BSE&T* 12(1), pp. 25-37.
- 166 Mitchell, A R, and Griffiths, D F (1980) *The finite difference method in partial differential equations*, John Wiley and Sons.
- 167 Smith, G D (1985) *Numerical solution of partial differential equations: finite difference methods*, - 3rd ed., Oxford University Press.
- 168 Constantinides, A (1987) *Applied numerical methods with personal computer*, McGraw Hill.
- 169 Kusuda, T (1960) Coil performance solutions without trial and error, *Air Conditioning, Heating and Ventilating*, January, 1960, pp.73-80.
- 170 Kusuda, T (1969) Effectiveness method for predicting the performance of finned tube coils, *Symposium on Heat and Mass Transfer to Extended Surfaces*, Jan 27-30, 1969, ASHRAE.
- 171 McQuiston, F C (1975) Fin efficiency with combined heat and mass transfer, *ASHRAE Trans.* Vol.81, Pt.1.
- 172 CIBSE (1986) *Guide Vol. C* The Chartered Institution of Building Services Engineers, UK.
- 173 Wang, S K (1987) *Air-conditioning*, Hong Kong Polytechnic.
- 174 Welty, J R (1978) *Engineering Heat Transfer*, John Wiley & Sons.

- 175 Kimura, K I (1977) *Scientific basis of air-conditioning*, Applied Science Publishers Ltd., London.
- 176 Galbraith, G H and McLean, R C (1993) Vapour permeability: Suitability and consistency of current test procedures, *BSER&T* 14(2) pp.67-70.
- 177 Burch, D M, Thomas, W C and Fanney, A H (1992) Water vapour permeability measurements of common building materials, *ASHRAE Trans.*, 1993, pp.486-494.
- 178 Jones, W P (1985) *Air-conditioning Engineering*, Edward Arnhold.
- 179 Carrier Corporation (1989) Product data, 39L Central Station Air Handlers Sizes 03-35, Carrier Corporation, USA.
- 180 ARI Standard 410 (1991) *Standard for forced-circulation air-cooling and air-heating coils*, Air-conditioning & Refrigeration Institute, USA.
- 181 ASHRAE Standard 33-78 (1978) *Methods of testing forced circulation air cooling and air heating coils*, ASHRAE, USA.

Appendix A

The Numerical Scheme Adopted to Solve Differential Equations of the Building and System Models

Many methods for solving ordinary differential equations (ODEs) and partial differential equations (PDEs) can be found in various references on numerical methods (e.g. 131,132,138,166,167). Although methods for solving of PDEs appear to be different from those for ODEs, the latter can also be applied to solve PDEs provided the PDEs are first transformed into ODEs (132). Since a mix of PDEs and ODEs is often found in engineering problems, this approach allows a unified method be used in solving the problem. Among the ODE solution methods, those in the explicit Runge-Kutta family of methods are in widespread use. For simple problems, these methods are satisfactory. However, when applied to solve a set of "stiff" equations, there may be stability problems unless extremely small step-lengths are used in the numerical solution process which will be very time consuming. Although there are sophisticated methods for solving stiff equations (e.g. Gear's multi-step method (131)) the solution procedures involved are much more complicated.

In this work, the "self-implicit" scheme (136,137) was employed. Through this method, an implicit solution scheme (which will be more stable than an explicit scheme) can be implemented in the explicit manner (and therefore computationally more efficient). In applying this method to solve PDEs, each PDE was first partially discretized (or semi-discretized, in the spatial dimension only, (132)) to become a set

of ODEs (one ODE for each spatial node). The Runge-Kutta-Merson (RKM) method (131,132) was then used to integrate the set of ordinary differential equations. This was found to be a simple but efficient and accurate method.

In this appendix, the procedures for implementing this numerical method are exemplified with reference to a simple ODE and a simple PDE. Example calculations and comparison of the numerical solutions with analytical solutions for the differential equations are included.

A.1 The Self-implicit Scheme

In solving a first order ODE, say $y' = f(x,y)$ (where $y' = dy/dx$), by a numerical method, the conventional way is to calculate the derivative of the dependent variable (y') by using the expression at the right hand side of the ODE (in this case, $f(x,y)$). The numerical value of y at the next step (y^{n+1}) is then estimated based on y' and the step-length of the numerical integration, $\Delta x (= x^{n+1} - x^n)$. Starting from a set of initial values of x and y (x^0, y^0) and by repeating this procedure in which the value of x progressively increases (by Δx each time), the value of y corresponding to the desired value of x can be solved. The same applies for solving a system of ODEs simultaneously. For higher order ODEs, they can always be transformed into a set of first order ODEs (138) and solved in the same way. In calculating the value of y' , if the values of x and y used correspond to the current time step, i.e. x^n and y^n , this method is called "explicit", as y' can be found from these known values. However, if values of the variables corresponding to the next step are used, i.e. x^{n+1} and y^{n+1} , the method is called "implicit" and in this case, y' and y^{n+1} need to be solved simultaneously in each step.

In essence, the self-implicit method is an approximate method through which an implicit numerical solution scheme can be implemented explicitly. The procedures involved are illustrated with reference to the following simple ODE:

$$\frac{d\phi}{dt} = -a\phi + b \quad (\text{A.1})$$

where a and b are both positive constants.

Following the Crank-Nicolson scheme, the time derivative, $d\phi/dt$, may be approximated as a weighted sum of $f(\phi^n, t^n)$ and $f(\phi^{n+1}, t^{n+1})$. Using (A.1), this becomes:

$$\frac{d\phi}{dt} \approx \lambda (-a\phi^{n+1} + b) + (1-\lambda)(-a\phi^n + b) \quad (\text{A.2})$$

With $\lambda > 0$, solution for ϕ^{n+1} becomes implicit.

In the self-implicit method, through the use of the approximation:

$$\frac{d\phi}{dt} \approx \frac{\Delta\phi}{\Delta t} \quad (\text{A.3})$$

the value of $\frac{d\phi}{dt}$ in equation (A.2) can still be estimated based on known value of ϕ^n despite that $\lambda > 0$ is used (i.e. implicit). Thus, greater stability of the numerical scheme due to the use of the implicit method can be achieved but the solution procedure is basically that of an explicit method which therefore greatly simplifies the solution process. This can be seen by manipulating with the equation in the following manner:

After substituting ϕ^{n+1} by $\phi^n + \Delta\phi$ and simplifying, equation (A.2) becomes:

$$\frac{d\phi}{dt} \approx -\lambda a \Delta\phi - a\phi^n + b \quad (\text{A.4})$$

Multiplying the term containing $\Delta\phi$ in equation (A.4) by $\Delta t/\Delta t$, it will become:

$$\frac{d\phi}{dt} \approx -\lambda a \Delta t \left(\frac{\Delta\phi}{\Delta t} \right) - a\phi^n + b$$

Using the approximation as shown in equation (A.3), the above equation may be rearranged into:

$$(1 + \lambda a \Delta t) \frac{d\phi}{dt} \approx -a \phi^n + b$$

$$\text{or} \quad \frac{d\phi}{dt} \approx - \frac{a}{1 + \lambda a \Delta t} \phi^n + \frac{b}{1 + \lambda a \Delta t} \quad (\text{A.5})$$

Since the right hand side of equation (A.5) now involves only ϕ^n , $\frac{d\phi}{dt}$ (with $\lambda > 0$) can be estimated based solely on known parameters. For $\lambda = 0$, equation (A.5) reduces back to the explicit formulation (A.1) but, for $\lambda = 1$, the scheme is fully implicit and equation (A.5) becomes:

$$\frac{d\phi}{dt} \approx - \frac{a}{1 + a \Delta t} \phi^n + \frac{b}{1 + a \Delta t} \quad (\text{A.6})$$

A.2 Mathematical Meaning of the Self-Implicit Scheme

From equation (A.6), it can be seen that the derivative $\frac{d\phi}{dt}$ at t^{n+1} is approximated by ϕ at t^n . Using the Taylor series expansion (up to the first order derivative term), ϕ^{n+1} may be expressed in terms of ϕ^n and $\frac{d\phi}{dt}$ as:

$$\phi^{n+1} = \phi^n + \Delta t \frac{d\phi}{dt} + \dots \quad (\text{A.7})$$

If the fully implicit scheme is used, then,

$$\frac{d\phi}{dt} \approx -a \phi^{n+1} + b \quad (\text{A.8})$$

Neglecting the terms involving the second and higher order derivatives in (A.7) (not shown) and substituting (A.8) into (A.7) gives:

$$\begin{aligned} \phi^{n+1} &\approx \phi^n - a \Delta t \phi^{n+1} + b \Delta t \\ \therefore \phi^{n+1} &\approx \frac{1}{1 + a \Delta t} \phi^n + \frac{\Delta t}{1 + a \Delta t} b \end{aligned} \quad (\text{A.9})$$

Substituting (A.9) back into (A.8),

$$\frac{d\phi}{dt} \approx -\frac{a}{1+a\Delta t} \phi^n + \left(1 - \frac{a\Delta t}{1+a\Delta t}\right) b$$

$$\therefore \frac{d\phi}{dt} \approx -\frac{a}{1+a\Delta t} \phi^n + \frac{1}{1+a\Delta t} b \quad (\text{A.10})$$

which is exactly the same as equation (A.6). Hence, it can now be seen that using the self-implicit scheme to evaluate $\frac{d\phi}{dt}$ at t^{n+1} is equivalent to estimating ϕ^{n+1} first, based on ϕ^n (see equation A.9), and this is then used to estimate $\frac{d\phi}{dt}$. Through this, simultaneous solution of $\frac{d\phi}{dt}$ and ϕ^{n+1} by an iterative procedure is avoided.

One may argue that since it is possible to estimate ϕ^{n+1} using equation (A.9), then, evaluation of $\frac{d\phi}{dt}$ appears to be unnecessary. This is true if a one-stage method (e.g. the Euler method ⁽¹⁶⁸⁾) is used to solve the ODE. However, if a multi-stage method (e.g. one of the Runge-Kutta family of methods) is used, then, the time derivatives corresponding to a number of intermediate stages will have to be calculated and this method allows such multi-stage methods be implemented conveniently.

A.3 Stability of a Numerical Scheme Incorporated with the Self-implicit Scheme

In addition to simplifying the procedures for solving an ODE implicitly, the self-implicit scheme can also allow larger time steps be used in the solution scheme. This is explained by the analysis on the stability criteria for solving the following ODE (same as A.1) by using a one-stage explicit method (the Euler method):

$$\frac{d\phi}{dt} = -a\phi^n + b$$

it can be shown that the stability criterion for the one-stage method is (see e.g. Constantinides ⁽¹⁶⁸⁾):

$$\Delta t \leq \frac{2}{|a|} \quad (\text{A.11})$$

With the self-implicit scheme, the ODE can now be written as:

$$\frac{d\phi}{dt} = -a' \phi^n + b \quad (\text{A.12})$$

where $a' = \frac{a}{1 + \lambda a \Delta t}$

Since equation (A.12) is also explicit, the stability criterion therefore will be:

$$\Delta t \leq \frac{2}{|a'|}$$

or, $\Delta t \leq 2 \left\{ \frac{1 + \lambda a \Delta t}{a} \right\}$

Here the absolute sign is ignored as a , λ and Δt are all of positive values. It follows that:

$$a (1 - 2 \lambda) \Delta t \leq 2$$

or $\Delta t \leq \frac{2}{a (1 - 2 \lambda)}$ for $(1 - 2 \lambda) \geq 0$ (A.13.a)

$\Delta t \geq \frac{2}{a (1 - 2 \lambda)}$ for $(1 - 2 \lambda) < 0$ (A.13.b)

Here, λ is within the range of $0 \leq \lambda \leq 1$. The stability criteria therefore become:

- i) For $\lambda = 0$, the stability criterion reduces back to that for explicit solution.
- ii) For $1 \geq \lambda > \frac{1}{2}$, $(1 - 2\lambda) < 0$, from (A.13.b), it can be seen that the solution scheme is unconditionally stable.
- iii) For $0 < \lambda \leq \frac{1}{2}$, $(1 - 2\lambda) \geq 0$ and the criterion shown in (A.13.a) must be obeyed for stability of the numerical solution scheme. Comparing this equation with (A.11), it can be seen that because $(1 - 2\lambda)$ is less than one, the largest value of the time step that can be used with the semi-implicit scheme without violating the stability criterion is greater than what is possible in the conventional explicit method.

Stability criteria for higher order methods (e.g. the classical fourth-order Runge-Kutta method and Runge-Kutta-Merson method) can be found in references on numerical methods for solving ODEs (e.g.¹³²). The application of the criteria however is complicated (involving solution of the eigenvalues of the coefficient matrix of the system of ODEs). In this work, the fully implicit formulation ($\lambda = 1$) was used and therefore the scheme should be stable.

A.4 Implementation of Runge-Kutta-Merson Method with the Self-Implicit Scheme In Solving an ODE

The Runge-Kutta-Merson (RKM) method for solving an ODE (^{131,132}) is as follows:

$$\text{Given } \frac{d\phi}{dt} = f(\phi, t) \quad (\text{A.14})$$

and $\Delta t = \text{time step of integration} = t^{n+1} - t^n$

$$\text{Then, } k_1 = \Delta t f(\phi^n, t^n) \quad (\text{A.15})$$

$$k_2 = \Delta t f\left(\phi^n + \frac{1}{3} k_1, t^n + \frac{\Delta t}{3}\right) \quad (\text{A.16})$$

$$k_3 = \Delta t f\left(\phi^n + \frac{1}{6} (k_1 + k_2), t^n + \frac{\Delta t}{3}\right) \quad (\text{A.17})$$

$$k_4 = \Delta t f\left(\phi^n + \frac{1}{8} (k_1 + 3 k_3), t^n + \frac{\Delta t}{2}\right) \quad (\text{A.18})$$

$$k_5 = \Delta t f\left(\phi^n + \frac{1}{2} (k_1 - 3 k_2 + 4 k_4), t^n + \Delta t\right) \quad (\text{A.19})$$

$$\text{and } \phi^{n+1} = \phi^n + \frac{1}{6} (k_1 + 4 k_4 + k_5) \quad (\text{A.20})$$

Also, the truncation error of this step of calculation can be estimated by (¹³²):

$$\epsilon = \frac{1}{30} (-2 k_1 + 9 k_3 - 8 k_4 + k_5) \quad (\text{A.21})$$

With the RKM method, the error of each integration step can be conveniently estimated by using the above equation. This estimated error can then be used to

control the integration step size to be used in the solution process (see Section A.5) and that is the major reason for using this method in the present study. In using other methods, e.g. the classical fourth-order Runge-Kutta (RK4) method, the error will have to be estimated by repeating the solution process twice (call step-doubling ⁽¹³⁸⁾); in the first, the full-step is used and in the second, two half-steps are used. Since the solution will be more accurate when a smaller step-length is used, the deviation of the solution obtained by using the full-step from that obtained in the two half-steps is then regarded as an indication of the error. The calculation procedures involved however will become more time consuming.

A.5 Numerical Solution Step Size Control

Although the RKM method is a five stage method, its accuracy is only up to order four ⁽¹³²⁾. For an order four method, the truncation error (ϵ) is proportional to $(\Delta t)^5$ ⁽¹³⁸⁾. Therefore, if ϵ_0 is the maximum tolerable error and Δt_0 is the largest time step that will give a truncation error that is equal to ϵ_0 , then,

$$\left| \frac{\epsilon_0}{\epsilon} \right| = \left\{ \frac{\Delta t_0}{\Delta t} \right\}^5 \quad (\text{A.22})$$

$$\text{or,} \quad \Delta t_0 = \Delta t \left| \frac{\epsilon_0}{\epsilon} \right|^{0.2} \quad (\text{A.23})$$

This value of Δt_0 is the desirable step length for minimum computing time. Hence, by comparing the estimated error in a solution step with the tolerance limit, whether the result obtained in this step is acceptable can be determined. If ϵ is smaller than ϵ_0 , the result of the completed step is acceptable and, by using equation (A.23), the step length for the next solution step can be determined. However, if ϵ is greater than ϵ_0 , the result of the completed step is not acceptable. Nevertheless, by using equation (A.23) again, the step length to be used in repeating the calculation can be determined. To be conservative, a scaling of 0.95 was used in the building and system models to scale down the time-step size estimated by equation (A.23) in the next solution step following a successful one and a factor of 0.75 was used to determine

the time-step size to be used in repeating a solution step following an unsuccessful one.

A.6 Comparison of the Numerical Solution with Analytical Solution of an ODE

The numerical scheme was applied to solve the following simple ODE (same as equation A.1) to verify the accuracy of the numerical solution and to test the performance of the scheme:

$$\frac{dy}{dx} = -a y + b \quad (\text{A.24})$$

where a and b are constants.

The analytical solution of equation (A.24) is:

$$y = \frac{b}{a} + \left[(y_0 - \frac{b}{a}) e^{ax_0} \right] e^{-a x} \quad (\text{A.25})$$

where x_0 = the initial value of x

y_0 = the initial value of y at $x = x_0$

The values of the constant coefficients and initial values of the variables assumed in the numerical solution were:

$$a = 1; \quad b = 1; \quad x_0 = 0; \quad y_0 = 0$$

In order to show the effects of using the self-implicit scheme, the explicit RKM method was also applied to solve the ODE. The solutions obtained by using the two numerical methods, together with the analytical solution, are shown in Figure A.1 and the deviations between the numerical solutions from the exact solution are shown in Figure A.2. These graphs show that the explicit method is more accurate than the self-implicit method in the region where x is small and y is rapidly rising. However, there is a consistent error in the explicit solution when x is large but the self-implicit solution becomes indistinguishable from the exact solution when x is larger than ten

(Figure A.2). Figure A.3 shows that at the early stage of the solution process, the numerical integration step sizes used in the self-implicit scheme were smaller than those used in the explicit scheme. However, in approaching to the steady solution, because of the absence of a consistent error, the self-implicit scheme was able to rapidly enlarge the step sizes and therefore was able to complete the solution in less computing time. This comparison shows that the self-implicit scheme is an accurate and efficient numerical scheme for solving an ODE.

Note however must be taken that the error estimated by equation (A.21) is smaller than the actual error of the numerical solutions (Figure A.2) and the latter can exceed the tolerance limit (set at 0.001). This is because:

- i) Due to the approximation made in the self-implicit scheme (equation A.3), the estimated truncation error is not the "true" truncation error of the RKM scheme. Also, as pointed out by Lambert ⁽¹³²⁾ (quoting England's result), equation (A.21) may not always be able to give an accurate estimate of the truncation error.
- ii) The actual error shown in this figure includes also other errors (e.g. the rounding off errors) incurred in the calculations and,
- iii) in this example calculation, the error tolerance was used to determine the integration step size to be used in a following step but the calculation was not repeated even if the estimated error was larger than the tolerance limit (the latter was done in the building and system model). A better result could have been obtained with the self-implicit scheme if the calculation was repeated with a reduced step-length whenever this was encountered.

Hence, the estimated truncation error as given by equation (A.21) can only be regarded as an indicator of the error and be used as a tool for step-length control rather a "true" estimate of the truncation error.

A.7 Solving Partial Differential Equations by the Self-implicit Scheme

The procedure of using the self-implicit scheme and the RKM method to solve a PDE are explained below, with reference to the following PDE:

$$\frac{\partial \phi}{\partial t} = a \frac{\partial^2 \phi}{\partial x^2} + b \quad (\text{A.26})$$

where a and b are constants.

To solve this PDE by the RKM method, its spatial derivative term has to be discretized first such that the PDE becomes a set of ODEs. By using the central difference method, the equation may be semi-discretized into:

$$\frac{\partial \phi_i}{\partial t} \approx a \frac{\phi_{i+1} - 2\phi_i + \phi_{i-1}}{(\Delta x)^2} + b \quad (\text{A.27})$$

Following the Crank-Nicolson method, the time derivative of ϕ_i may be approximated by:

$$\frac{\partial \phi_i}{\partial t} \approx \lambda a \frac{\Delta \phi_{i+1} - 2\Delta \phi_i + \Delta \phi_{i-1}}{\Delta x^2} + a \frac{\phi_{i+1}^n - 2\phi_i^n + \phi_{i-1}^n}{\Delta x^2} + b \quad (\text{A.28})$$

Hence, if there are N nodes in the x dimension, there will be N equations (for $i = 1, 2, \dots, N$) and each may be regarded as an ODE.

Multiplying each of the $\Delta \phi$ terms in equation (A.28) by $\Delta t / \Delta t$, it may be rearranged into:

$$\begin{aligned} \frac{\partial \phi_i}{\partial t} = & \left(\frac{\lambda a \Delta t}{\Delta x^2} \right) \left\{ \frac{\Delta \phi_{i+1}}{\Delta t} - 2 \frac{\Delta \phi_i}{\Delta t} + \frac{\Delta \phi_{i-1}}{\Delta t} \right\} + \\ & \frac{a}{\Delta x^2} \left\{ \phi_{i+1}^n - 2\phi_i^n + \phi_{i-1}^n \right\} + b \end{aligned} \quad (\text{A.29})$$

By approximating the $\left(\frac{\Delta \phi}{\Delta t} \right)$ terms by $\frac{\partial \phi}{\partial t}$ and collecting all these terms to the LHS, equation (A.29) becomes:

$$\begin{aligned}
& - \left(\frac{\lambda a \Delta t}{\Delta x^2} \right) \frac{\partial \phi_{i-1}}{\partial t} + \left(1 + \frac{2 \lambda a \Delta t}{\Delta x^2} \right) \frac{\partial \phi_i}{\partial t} - \left(\frac{\lambda a \Delta t}{\Delta x^2} \right) \frac{\partial \phi_{i+1}}{\partial t} \\
& = \frac{a}{\Delta x^2} \{ \phi_{i+1}^n - 2\phi_i^n + \phi_{i-1}^n \} + b
\end{aligned} \tag{A.30}$$

which may now be written as :

$$A_{i,i-1} \frac{\partial \phi_{i-1}}{\partial t} + A_{i,i} \frac{\partial \phi_i}{\partial t} + A_{i,i+1} \frac{\partial \phi_{i+1}}{\partial t} = f_i(\phi^n) \tag{A.31}$$

Note that $f_i(\phi^n)$ is the explicit formulation of RHS of equation (A.26) and can be evaluated based on the known values of $\phi_{i-1}^n, \phi_i^n, \phi_{i+1}^n, a$ & b .

Denoting $\frac{\partial \phi}{\partial t}$ by ϕ^o , the entire set of equations for all the nodal points, (for $i = 1, 2, \dots, N$) can be written in the following form:

$$\begin{vmatrix}
A_{1,1} & A_{1,2} & & & \\
A_{2,1} & A_{2,2} & A_{2,3} & & \\
& A_{3,2} & A_{3,3} & A_{3,4} & \\
& \dots & \dots & \dots & \\
& \dots & \dots & \dots & \\
& A_{i,i-1} & A_{i,i} & A_{i,i+1} & \\
& \dots & \dots & \dots & \\
& \dots & \dots & \dots & \\
& & A_{N-1,N-2} & A_{N-1,N-1} & A_{N-1,N} \\
& & & A_{N,N-1} & A_{N,N}
\end{vmatrix}
\begin{vmatrix}
\phi_1^o \\
\phi_2^o \\
\phi_3^o \\
\dots \\
\dots \\
\phi_i^o \\
\dots \\
\dots \\
\phi_{N-1}^o \\
\phi_N^o
\end{vmatrix}
=
\begin{vmatrix}
f_1 \\
f_2 \\
f_3 \\
\dots \\
\dots \\
f_i \\
\dots \\
\dots \\
f_{N-1} \\
f_N
\end{vmatrix} \tag{A.32}$$

The set of ODE's resulting from the partial discretization process (equation A.32 above) may be represented in matrix form as follows:

$$[A] \{\phi^o\} = \{f\}$$

and since $[A]$ is a tri-diagonal matrix, $\{\phi^o\}$ can be solved by using the efficient tri-diagonal matrix algorithm (TDMA) ⁽¹³⁸⁾.

In solving an ODE using the RKM method, the time derivatives of the variables ($\{\dot{\phi}\}$'s) at the five intermediate stages need to be evaluated (see equations A.15 - A.19). In this process, the same set of known values of ϕ_i^n at time-step t^n can be used for evaluating the column vector $\{f\}$ in (A.32) in all the stages (and then the k 's), which is an important feature of the self-implicit scheme. However, the values of λ to be used in evaluation of A_{ij} 's in matrix $[A]$ must be adjusted and the values of Δt must be replaced by Δt^* (see equations A.30 and A.31) as follows:

For evaluation of

$k_1,$
 $\lambda = 0$
 $\& \Delta t^* = \Delta t ;$

for
 $k_2,$
 $\lambda = 1$
 $\& \Delta t^* = \Delta t / 3 ;$

for
 $k_3,$
 $\lambda = 1$
 $\& \Delta t^* = \Delta t / 3 ;$

for
 $k_4,$
 $\lambda = 1$
 $\& \Delta t^* = \Delta t / 2 ;$ and

for
 $k_5,$
 $\lambda = 1$
 $\& \Delta t^* = \Delta t$

so that the time derivatives will correspond to the correct time pertaining to each intermediate stage.

Note must also be taken that since basically a fully implicit scheme is implemented for each intermediate step, if the coefficients a and b in the equation are state dependent, (i.e. their values vary with ϕ 's), they should be evaluated at the correspondingly estimated values of ϕ , i.e.:

<u>Stage</u>	<u>Time of the Stage</u>	<u>Value of ϕ for evaluation of a & b</u>
1	$t = t^n$	ϕ^n
2	$t = t^n + \frac{\Delta t}{3}$	$\phi^n + \frac{1}{3} k_1$
3	$t = t^n + \frac{\Delta t}{3}$	$\phi^n + \frac{1}{6} (k_1 + k_2)$
4	$t = t^n + \frac{\Delta t}{2}$	$\phi^n + \frac{1}{8} (k_1 + 3k_3)$
5	$t = t^n + \Delta t$	$\phi^n + \frac{1}{2} (k_1 - 3k_2 + 4 k_4)$

A.8 Comparison of the Numerical Solution with Analytical Solution of a PDE

To verify the accuracy of the numerical solution, it was applied to solve the temperature variations at the central plane of a homogeneous slab of material. The slab was initially at a uniform temperature across its thickness but was suddenly put into a new environment which was at a constant temperature different from the initial temperature of the slab. Assuming the thermal properties of the slab are constants, temperature distribution across the slab is governed by the following PDE (a heat conduction equation):

$$\frac{\partial T}{\partial t} = \alpha \frac{\partial^2 T}{\partial x^2} \quad (\text{A.33})$$

where T is the temperature, t is the time after the slab has been put into the new environment, x is the distance from the central plane of the slab and α is the thermal diffusivity of the material ($\alpha = \frac{k}{\rho C_p}$). Analytical solution of this equation is available

from heat transfer literature (129,135).

In the comparison calculation, the slab was assumed to be a piece of gypsum board having a density (ρ) of 670 kg/m³, a thermal conductivity (k) of 0.1593 W/mK, a specific heat (C_p) of 1.0894x10³ J/kgK and a thickness of 0.0132 m. The initial temperature of the slab was 303 K and the temperature of the ambient air was 293 K. The convective heat transfer coefficient (h) at the two surfaces of the slab was 3.07 W/m²K.

The numerical solution of the problem and the analytical solution are plotted in Figure A.4. It can be seen here that the numerical solution is in excellent agreement with the analytical solution. This shows that the numerical scheme can solve the PDE accurately.

Figure A.1

Comparison of solutions by Explicit and Self-implicit schemes (both used in conjunction with the RKM method) with analytical solution

Solution of $dy/dx = -a y + b$ where $a=1$; $b=1$; $x_0=0$; $y_0=0$
Err. tolerance set at 0.001

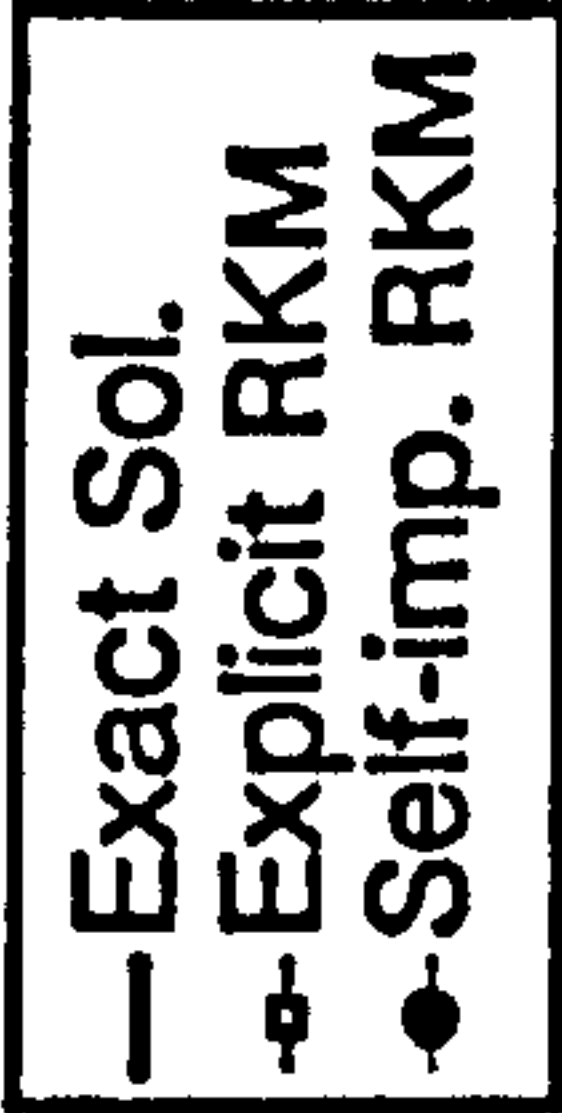
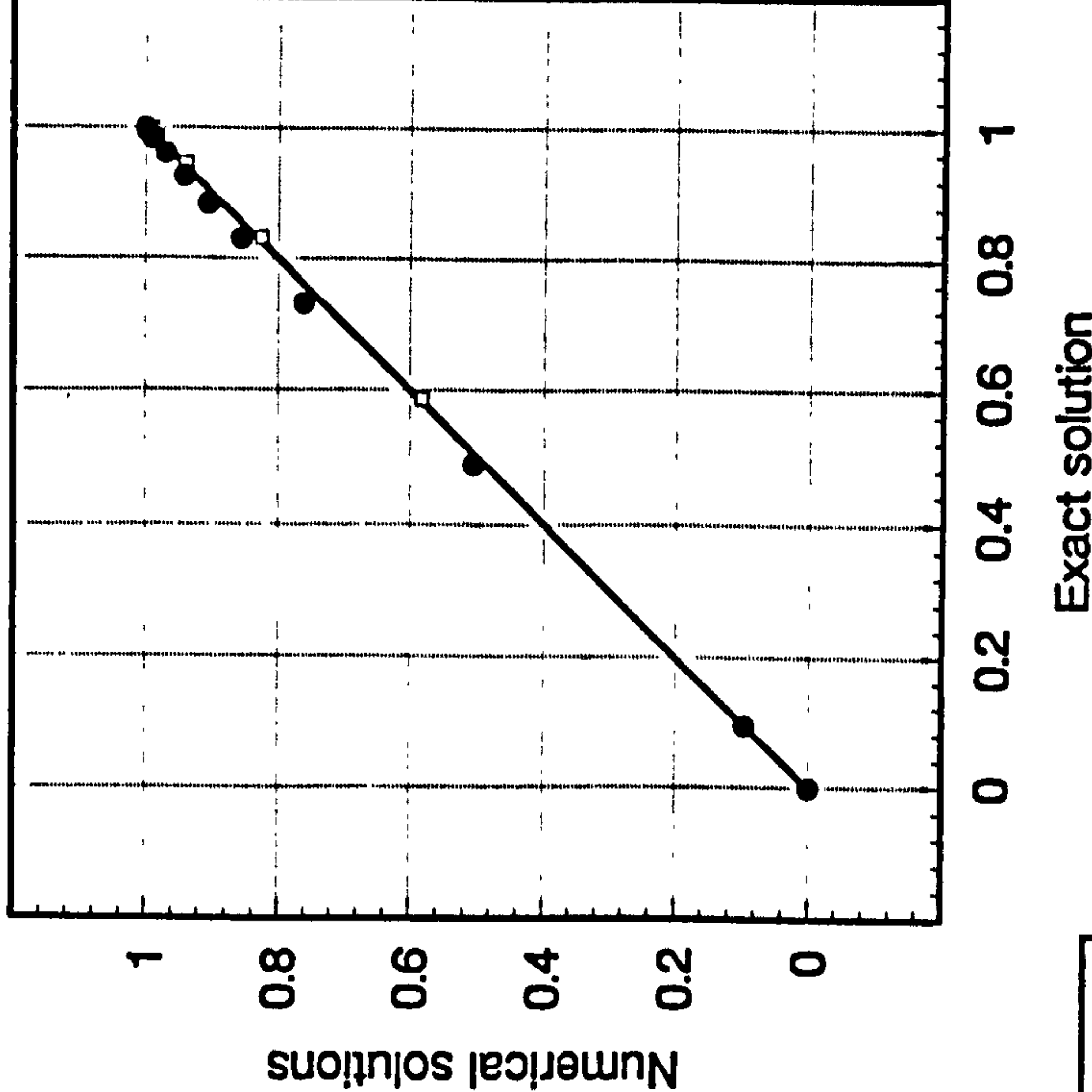
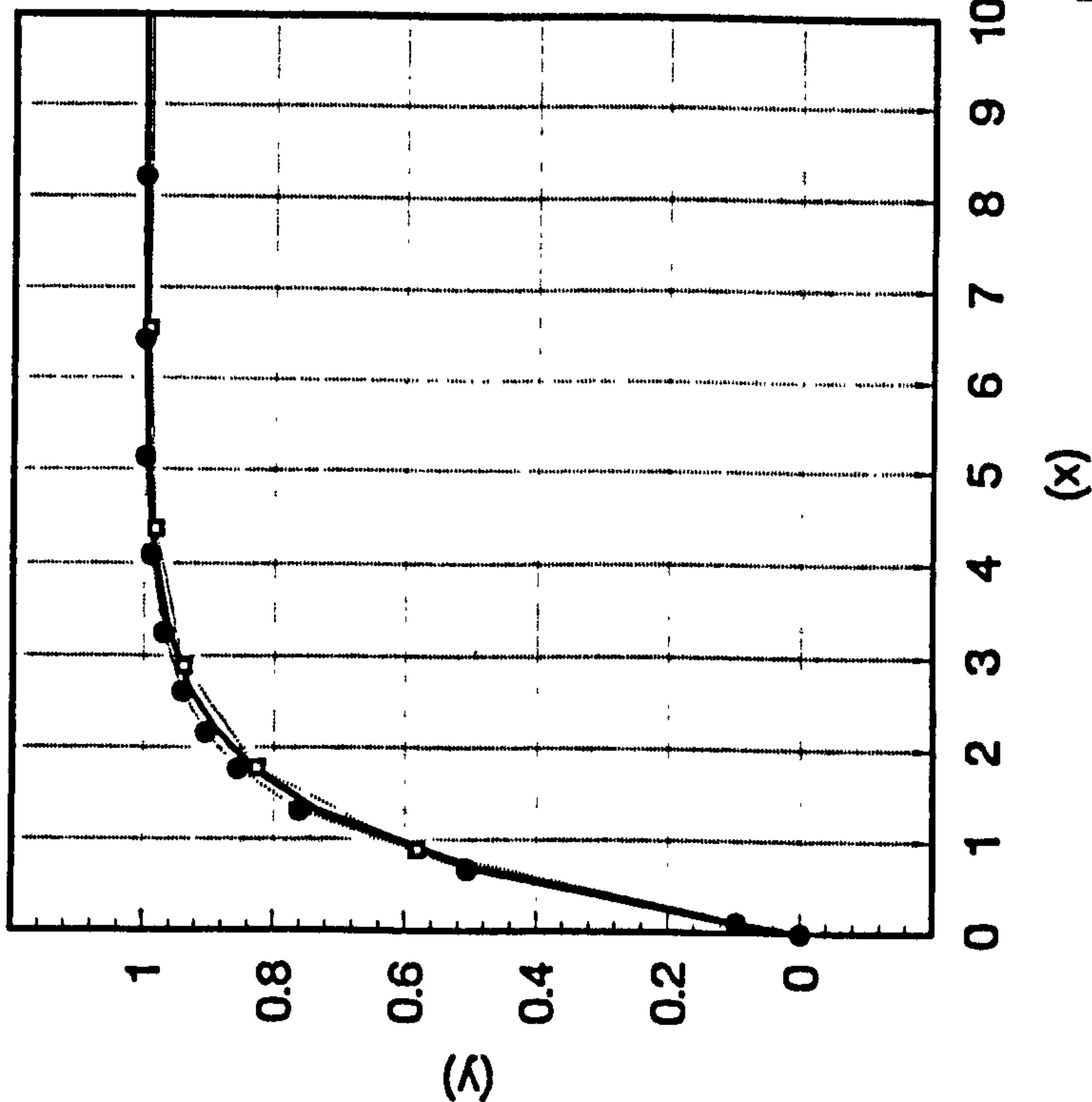
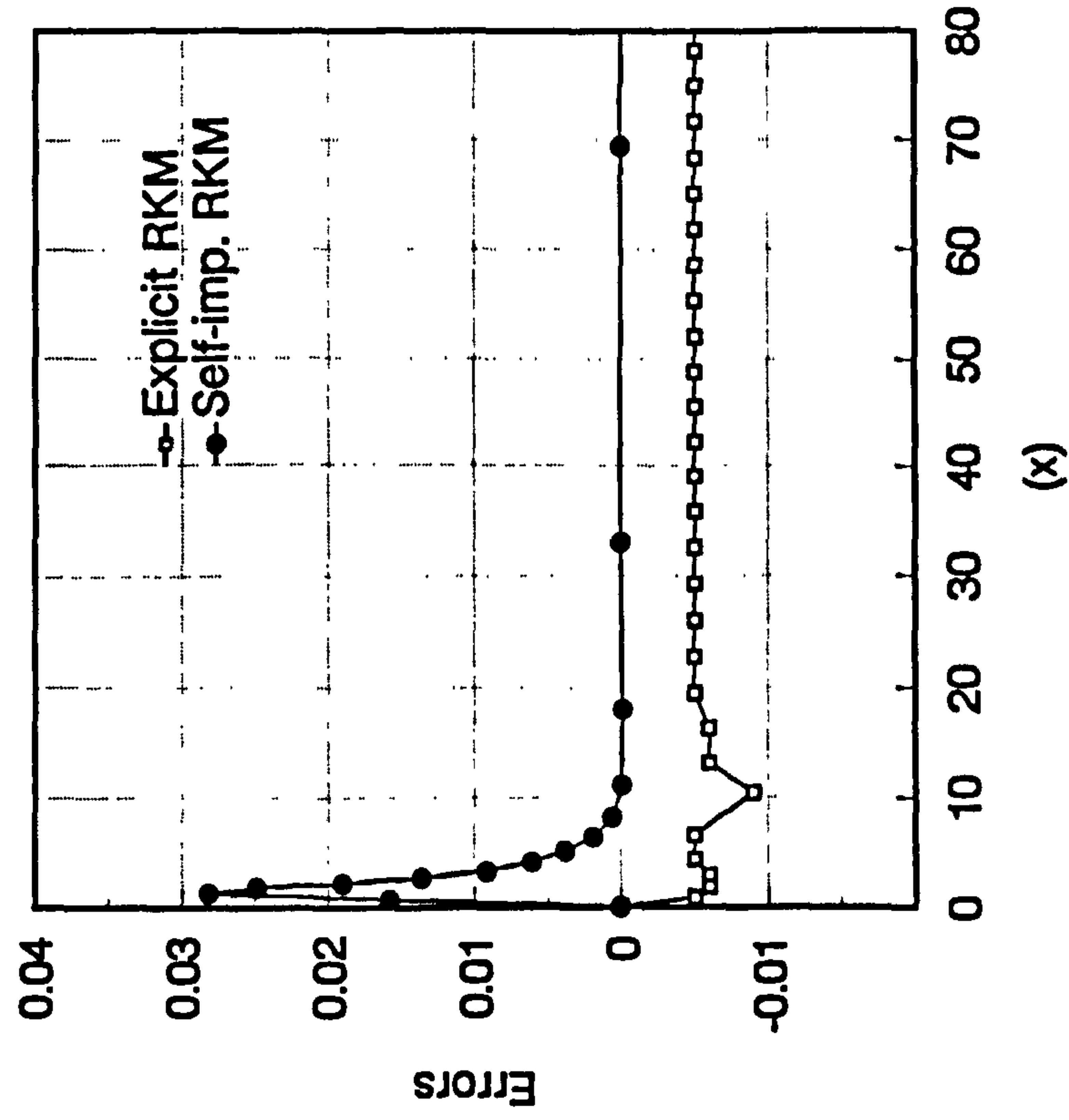


Figure A.2

Comparison of errors
of solutions by
Explicit and Self-implicit
schemes



Solution of $dy/dx = -a y + b$ where $a=1$; $b=1$; $x_0=0$; $y_0=0$
Err. tolerance set at 0.001

Figure A.3

Comparison of integration
step sizes by Explicit
and Self-implicit schemes

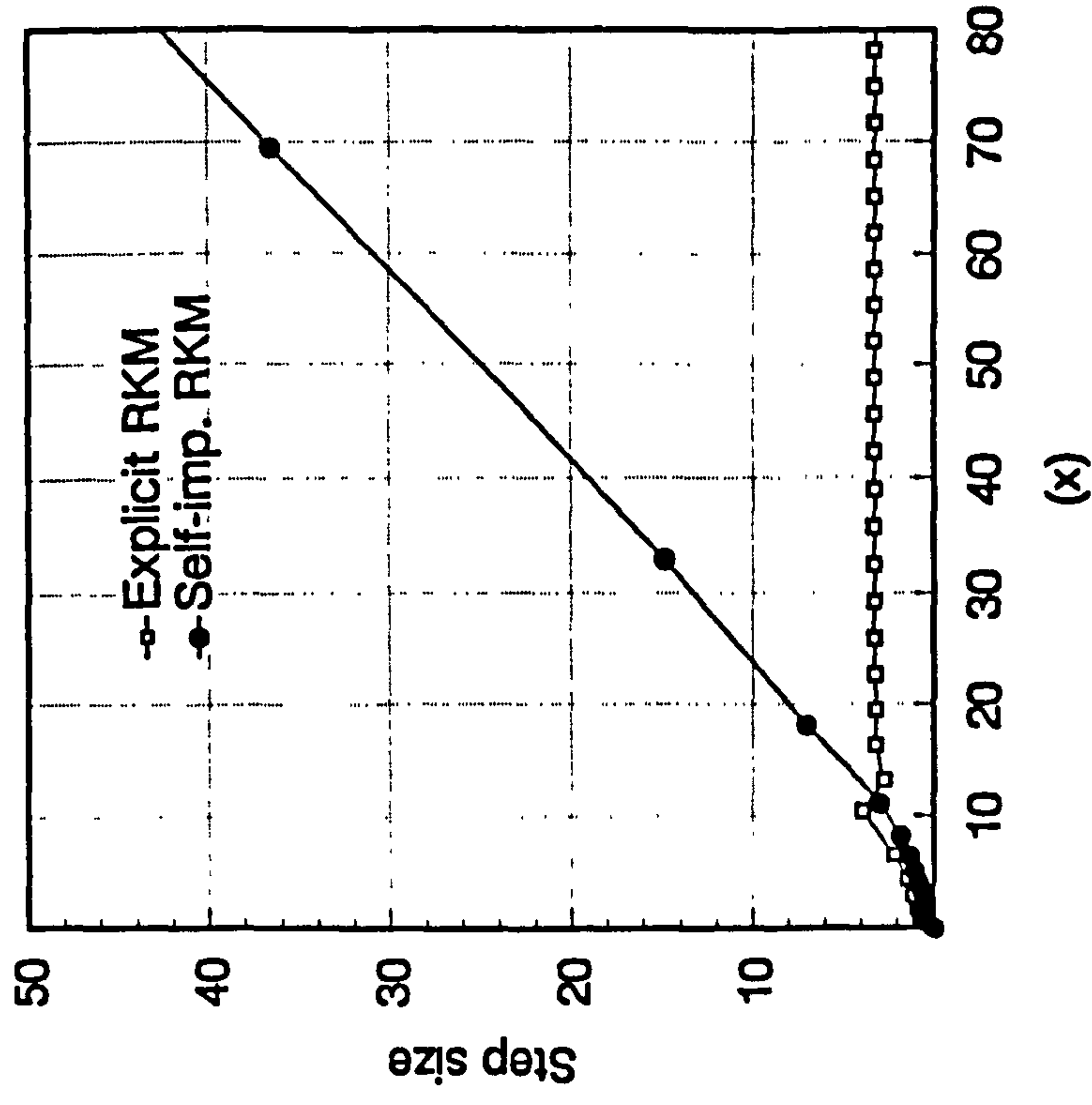
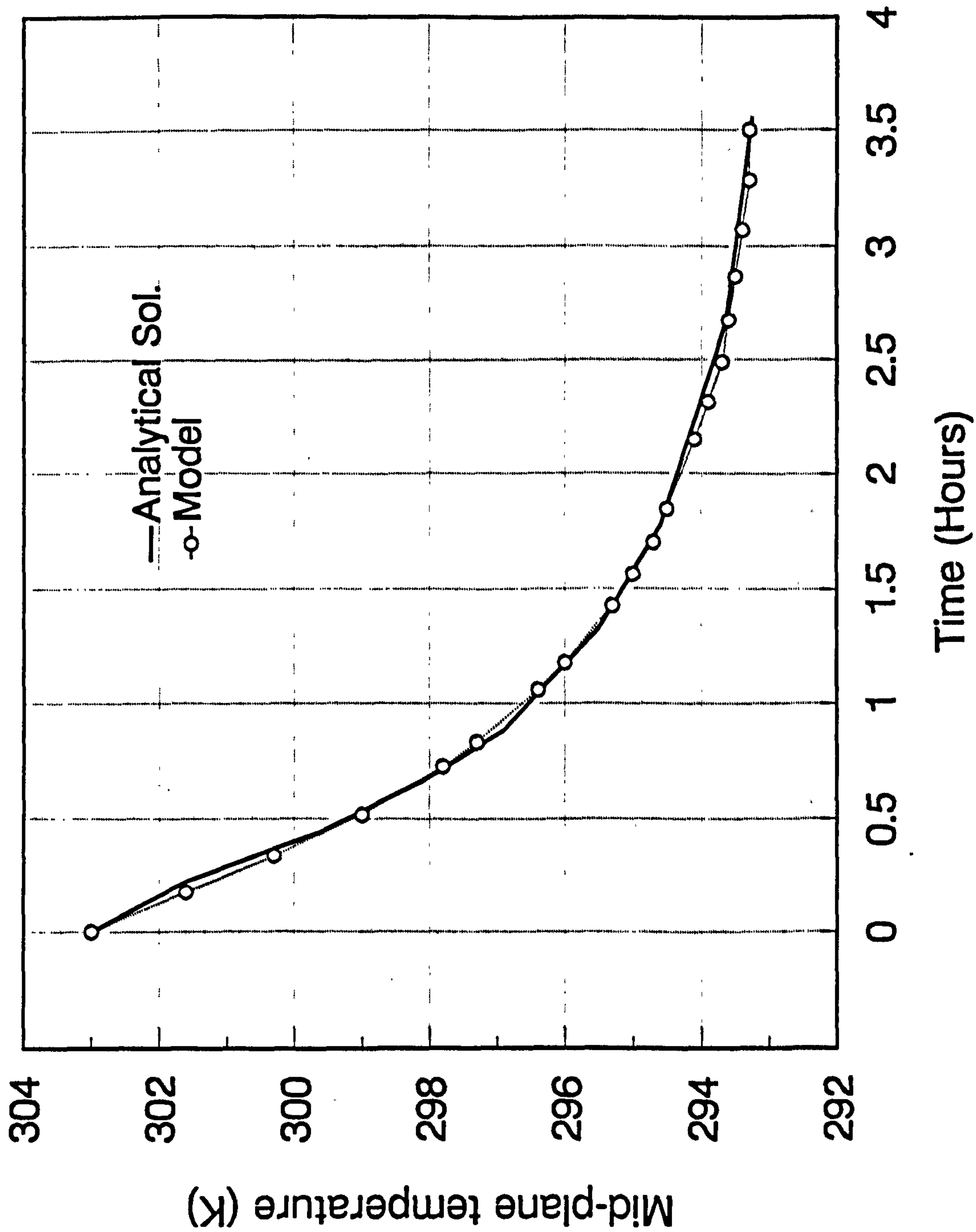


Figure A.4

Comparison of mid-plane temperatures predicted by
numerical model with analytical solution



Appendix B

A Steady-State Cooling and Dehumidifying Coil Model

This appendix describes in detail the methods used in developing the LMHD model (Chapter 5) for simulating steady-state performance of cooling and dehumidifying coils with corrugated fins. First, an overview of the basic heat exchanger theory is given. Following that, mathematical expressions for calculating the parameters required to evaluate the heat transfer area and the overall heat transfer coefficient (U-value) of a sensible cooling coil with flat plate fins are summarized. How these expressions can be modified for applications to a cooling and dehumidifying coil is then described. These methods are based largely on McQuiston's work (28,143,144) but due modifications have been made to account for the effects due to the presence of fin collars. Also, details of how Beecher & Fagan's correlations (141) can be adopted to account for effects of fin corrugations, and the procedures for determining the dry/wet coil surface areas (according to the method given in ASHRAE (140)) are described. Finally, the procedures for setting-up the steady-state coil model are summarized, which include a method for solving for the coil surface air-film conditions. The coil model developed from these methods can predict coil performance to an acceptable accuracy when compared with some manufacturers' catalogue data (see Chapter 7).

B.1 The Approach for Modelling a Cooling and Dehumidifying Coil

B.1.2 Basic Heat Exchanger Model

Despite the complex construction of a cooling or heating coil, its steady state performance can be modelled by the conventional log mean temperature difference (LMTD) method or the Number of transfer units (Ntu) method for shell-and-tube heat exchangers (e.g. Kays & London ⁽³²⁾) provided appropriate modifications are made to cater for the specific coil construction and operating conditions.

a) In the LMTD method, the heat exchange rate (q) is calculated by:

$$q = A U \text{ LMTD} \quad (\text{B.1})$$

where, with reference to a counter-flow arrangement,

$$\text{LMTD} = \frac{(T_{hi} - T_{co}) - (T_{ho} - T_{ci})}{\ln \left\{ \frac{T_{hi} - T_{co}}{T_{ho} - T_{ci}} \right\}} \quad (\text{B.2})$$

Here, T is the temperature of the fluids and subscript 'h' denotes the hot fluid; 'c' denotes the cold fluid; and 'i' & 'o' denote respectively the inlet and outlet conditions of the fluids.

As the expression for the evaluation of LMTD (equation B.2) includes the conditions of the fluids leaving the heat exchanger, which are the unknowns to be solved, determination of heat exchanger performance by this method will involve an iterative procedure.

b) In the Ntu method, the heat exchange rate is given by:

$$q = \epsilon (\dot{m} C_p)_{\min} (T_{hi} - T_{ci}) \quad (\text{B.3})$$

where ϵ is called the effectiveness of the heat exchanger and $(\dot{m} C_p)_{\min}$ is the minimum of the capacity rates (mass flow rate times specific heat) of the two fluids.

For a heat exchanger connected in counter-flow, the value of effectiveness (ϵ), as a function of Ntu, is:

$$\epsilon = \frac{1 - \exp\{-Ntu(1 - CRR)\}}{1 - CRR \exp\{-Ntu(1 - CRR)\}} \quad (B.4)$$

where

$$Ntu = \frac{UA}{\dot{m} C_{p_{\min}}} \quad (B.5)$$

and

$$CRR = \frac{(\dot{m} C_p)_{\min}}{(\dot{m} C_p)_{\max}} = \text{capacity rate ratio of the two fluids} \quad (B.6)$$

For other flow arrangements, expressions or graphs for evaluation of ϵ are available in many references on this topic (e.g. 32).

By using this method, iterative calculation is avoided because the heat exchanger performance is related only to the inlet fluid conditions (and values of U and A).

In applying either method, both the total heat transfer area (A) and the overall heat transfer coefficient (U) of the heat exchanger have to be calculated. For a simple counter flow shell and tube heat exchanger, the heat transfer area (A) may be taken as the total outer surface area of the tube (A_t) whereas the overall heat transfer coefficient (U) can be calculated as follows:

$$U = \frac{1}{\frac{1}{h_o} + \frac{\Delta x_t}{k_t} \frac{A_t}{A_m} + \frac{1}{h_i} \frac{A_t}{A_i} + R_{fi} \frac{A_t}{A_i} + R_{fo}} \quad (B.7)$$

B.1.3 Finned Sensible Cooling Coils

For a finned coil, the fin (extended) surfaces must be taken into account in the evaluation of A and U. The heat transfer area of such a coil is the total of the fin surface area (A_f) and the exposed fin collar surface area (A_o), i.e.,

$$A = A_f + A_o \quad (B.8)$$

When applied to a finned coil, the expression for the evaluation of U needs to be modified because the temperature at the fin surface is in general not uniform and there are additional thermal resistances due to the presence of the collar and the imperfect bonding between the tubes and the inner collar surfaces. The established approach to account for the former is to use the concept of fin surface effectiveness (η_s). In this method, the heat exchange rate is first calculated by assuming that the finned surfaces and the exposed fin collar surfaces are all at a uniform temperature. The actual rate of heat exchange is then calculated as a fraction of the idealistic heat exchange rate through the use of the fin surface effectiveness. The surface effectiveness and the additional thermal resistances can be incorporated into the expression for U (assuming no fin at the inner side of tubes) as follows:

$$U = \frac{1}{\frac{1}{h_o \eta_s} + \frac{\Delta x_t}{k_t} \frac{A}{A_{mt}} + R_{ct} \frac{A}{A_t} + \frac{\Delta x_c}{k_f} \frac{A}{A_{mc}} + \left(\frac{1}{h_i} + R_{fi} \right) \frac{A}{A_i} + R_{fo}} \quad (B.9)$$

In general, the metal thermal resistance terms ($\Delta x_t/k_t$ & $\Delta x_c/k_f$) are very small as compared to other thermal resistance terms and hence can be neglected in modelling the performance of air-conditioning coils. Appropriate empirical correlations and data from relevant literature may be adopted for evaluating the required heat transfer parameters including the convective heat transfer coefficients at the inner tube surface (h_i) and at the finned surface (h_o), the contact resistance (R_{ct}) and the fouling resistances (R_{fi} & R_{fo}).

Having calculated A & U , the total heat exchange rate in a finned coil can be found using the simple heat exchanger equations, based on either the LMTD or the Ntu method, provided no condensation of water vapour occurs on the coil surface. In addition, the corresponding pressure drop incurred by both fluids usually needs to be estimated since these pressure drops will affect the pump and the fan performance and, in turn, the mass flow rates of the fluids and the heat exchange rate. Empirical correlations are also available for finding the friction factor over the dry finned coil surface and over the inner tube wall surface such that the pressure drop incurred by both fluids can be evaluated.

B.1.4 Finned Cooling and Dehumidifying Coils

When the coil surface temperature is sufficiently below the dewpoint temperature of the moist air approaching the plate-finned coil, condensation of water vapour from the air stream onto the coil surface will take place. Moisture will thus be removed from the air stream and this is an essential process (dehumidification) in air-conditioning. With dehumidification, the rate of heat extraction from the air is higher when the same amount of air is cooled by the same temperature drop because the latent heat of condensation must also be removed by the chilled water simultaneously. Due to the presence of a thin layer of liquid water (condensate) on the coil heat transfer surface, the equations for evaluating the heat transfer coefficient and the friction factor for dry coil surfaces have to be modified and the mass transfer coefficient for calculating the rate of condensation needs also be evaluated. By using available empirical equations for evaluating these coefficients, the total heat transfer rate and the mass transfer rate can be estimated by an approach similar to that for a cooling coil with dry fin surface.

An explicit method (no iteration steps involved) has been developed (169,170) for estimating cooling and dehumidifying coil performance by extending the concept of Ntu and effectiveness to latent heat transfer. In this method, assumptions were made that the heat transfer parameters are constants throughout the coil and that the fin side

heat transfer coefficient remains the same irrespective of whether there is condensation in the coil. However, as evidenced by McQuiston's experimental findings (143,144,171), the heat transfer parameters vary from row to row in cooling and dehumidifying coils and there are considerable differences in the sensible heat transfer coefficient of a dry coil from that of a wetted coil. This method therefore was not considered in this work. The model developed was based on the log mean difference approach but, instead of LMTD, the calculation procedure adopted for total heat transfer calculation is based on a log mean enthalpy difference (LMHD) between the air and the air-film above the wet coil surface. Like the LMTD method, an iterative procedure is used.

In a counter flow cooling and dehumidifying coil, chilled water temperature within the coil rises in the direction opposite to the air flow (Figure B.1). At the plane where the air-flow enters the coil, both the chilled water and the air-stream are at their highest respective temperatures. Thus, unless the incoming air is highly humid, the water vapour in the air stream will not condense onto the coil surface once it approaches the coil. Instead, condensation will occur somewhere down stream of the inlet plane where the coil surface temperature is equal to or lower than the air stream dew point temperature. Consequently, there will be a portion of the coil which will stay dry with the other portion wet. Where the dry/wet boundary occurs depends on the air and chilled water conditions at the inlet and exit and is thus an unknown that needs to be solved simultaneously with the exit conditions. In this solution process, the heat exchange rates at the two portions of the coil will also be determined, based on the respective area and heat (and mass) transfer coefficients.

B.2 Heat and Momentum Transfer at Extended Surfaces

B.2.1 Heat Transfer Area Calculation

The total surface area of a finned coil is normally calculated as a multiple of its face area:

$$A = F_s N_r A_a \quad (B.10)$$

where F_s is called the surface factor. Unfortunately, this factor is rarely given in manufacturers' catalogues, but, the total surface area can be approximated based on the known tube array arrangement. For both the rectangular array and the triangular array (Figure 5.7), the fin area of a typical cell in the fin-tube assembly is:

$$\Delta A_f = 2 \left(x_a x_b - \frac{\pi D_o^2}{4} \right) \quad (B.11)$$

The face area (ΔA_a) and the exposed fin collar surface area (ΔA_o) for the same cell are:

$$\Delta A_a = s x_a \quad (B.12)$$

$$\Delta A_o = (s - y) \pi D_o \quad (B.13)$$

Hence, the ratio of total heat transfer area to face area of the typical cell is:

$$\frac{\Delta A}{\Delta A_a} = \frac{2 \left(x_a x_b - \frac{\pi D_o^2}{4} \right) + (s - y) \pi D_o}{s x_a} \quad (B.14)$$

If the irregularities at the fin edges are neglected, the surface factor (F_s) can be approximated by:

$$F_s = \frac{\Delta A}{\Delta A_a} \quad (B.15)$$

from which, the total heat transfer area of a finned coil can be approximated by equation (B.10).

B.2.2 Fin Efficiency and Surface Effectiveness

The fin efficiency, η_f , is defined as:

$$\eta_f = \frac{\text{Actual heat transfer at a fin}}{\text{The heat transfer if the entire fin is at the fin base temp.}} \quad (B.16)$$

If η_f is known, the rate of heat transfer from the fin to the ambient fluid (δq_f) at an elemental section of the coil can be calculated by:

$$\delta q_f = \eta_f \delta A_f h_o (T_{fb} - T_a) \quad (B.17)$$

The fin efficiency (η_f) for plate fins can be calculated from:

$$\eta_f = \frac{\tanh (m r \phi)}{m r \phi} \quad (B.18)$$

$$\text{where } m = \sqrt{\frac{2 h_o}{k_f y}} \quad (B.19)$$

r = the outer radius of the fin collar ($= D_o/2$);

$$\phi = \left(\frac{R_e}{r} - 1 \right) \left[1 + 0.35 \ln \left(\frac{R_e}{r} \right) \right] \quad (B.20)$$

and R_e is to be evaluated as follows:

i) For a rectangular tube array:

$$\frac{R_e}{r} = 1.28 \psi \sqrt{\beta - 0.2} \quad (B.21a)$$

ii) For a triangular tube array:

$$\frac{R_e}{r} = 1.27 \psi \sqrt{\beta - 0.3} \quad (B.21b)$$

where $\psi = \frac{M}{r}$ & $\beta = \frac{L}{M}$; for $L \geq M$ and definitions of L & M are as

shown in Figure 5.7.

Having calculated the fin efficiency (η_f), surface effectiveness (η_s) as defined below, can be calculated:

$$\eta_s = \frac{\text{Actual rate of total heat transfer at the fin surface and the exposed fin collar surface}}{\text{The heat transfer rate if both the fin surface and the exposed fin collar surface are uniformly at the fin base temperature}} \quad (\text{B.22})$$

which can be expressed in terms of the fin efficiency as:

$$\eta_s = 1 - \frac{A_f}{A} (1 - \eta_f) \quad (\text{B.23})$$

The heat transfer between the ambient fluid and the fin (and exposed fin collar surface area) at an elemental section of the coil can therefore be calculated by:

$$\delta q_s = \eta_s \delta A h_o (T_b - T_a) \quad (\text{B.24})$$

B.2.3 Heat Transfer Coefficients

a) *Water side heat transfer coefficient (h_i)*

The heat transfer coefficient at inner surfaces of tubes of the coil can easily be calculated using well established correlations for fluid flow in pipes.

- i) When the flow is turbulent, the Dittus-Boelter equation ⁽¹³⁵⁾ below can be used:

$$h_i = 0.023 \frac{k_w}{D_i} \text{Re}^{0.8} \text{Pr}^n \quad (\text{B.25a})$$

and, $n = 0.4$ when the coil is for cooling; $n = 0.3$ when the coil is for heating.

- ii) For laminar flow, Seider & Tate's correlation ⁽¹³⁵⁾ may be used instead:

$$h_i = 1.86 \frac{k_w}{D_i} \left(\text{Re} \text{Pr} \frac{D_i}{L} \right)^{(1/3)} \left(\frac{\mu_m}{\mu_t} \right)^{0.14} \quad (\text{B.25b})$$

Here, L is the tube length; μ_m is the bulk mean fluid viscosity; and μ_t is the viscosity of the fluid at the tube wall condition.

The water flow velocity in the tubes needs to be determined before either one of the above correlations can be used to evaluate the water side heat transfer. The method for this is described in Section B.2.4 below.

b) *Air-side (fin-side) heat transfer coefficient (h_o)*

From the Chilton-Colburn j-factor analogy, the convective heat transfer coefficient (h_o) can be related to the friction factor (f) through the j-factor as follows:

$$St Pr^{2/3} = j = \frac{f}{2} \quad (B.26)$$

where $St = \text{Stanton Number} = \frac{h_o}{(\rho C_p u)}$

For plate-finned coils, McQuiston ^(143,144) developed an empirical correlation relating the j-factor for sensible heat transfer in finned coil surfaces to another factor, denoted as JP, as follows:

$$j = 0.0014 + 0.2618 JP \quad (B.27)$$

and JP is defined as:

$$JP = Re_{D_o}^{-0.4} \left(\frac{A}{A_{to}} \right)^{-0.15} \quad (B.28)$$

Here, both the Stanton number (St) and the Reynolds number (Re_{D_o}) are evaluated based on the air flow velocity (u_c) at the core area between tubes (A_c).

For air, $Pr^{2/3}$ is very close to one and can therefore be deleted from equation (B.26). Using the definitions of Stanton Number and replacing u by u_c , equation (B2.6) can be modified into the following form:

$$h_o = j \rho_a C_{p_a} u_c \quad (B.29)$$

With this equation, equations B.27 & B.28 for calculating j , and when u_c is known, the heat transfer coefficient h_o can be evaluated.

Following the approach used in heat transfer area calculation, the core area (A_c), the flow velocity at the core area (u_c), and the ratio A/A_{to} can be determined as follows:

Define σ to be the contraction ratio given by:

$$\sigma = \frac{A_c}{A_a} \quad (B.30a)$$

Then, for an elemental cell in the finned coil (Figure 5.7), σ can be approximated by

$$\sigma \approx \frac{\Delta A_c}{\Delta A_a} = \frac{(x_a - D_o)(s - y)}{s x_a} \quad (B.30b)$$

Knowing σ , A_c can be calculated from (B.30a). Let \dot{V}_a be the volume flow rate of air across the coil, then

$$u_c = \frac{\dot{V}_a}{A_c} \quad (B.31)$$

Also,

$$\frac{A}{A_{to}} \approx \frac{\Delta A}{\Delta A_{to}} = \frac{2(x_a x_b - \frac{\pi D_o^2}{4}) + (s-y)\pi D_o}{s \pi D_o} \quad (B.32)$$

Equation (B.27) however is valid for 4-row coils only. For coils with number of rows (N_r) other than four, the following correction needs to be applied (28):

$$\frac{j_n}{j_4} = \frac{1 - 1280 N_r Re_{x_b}^{-1.2}}{1 - 5120 Re_{x_b}^{-1.2}} \quad (B.33)$$

where j_n is the j factor for N_r number of rows and j_4 is that for 4-row coils as from (B.27)

c) *Contact resistance (R_{ct})*

The thermal resistance due to the imperfect contact between the tubes and the fin collar can be estimated by (160):

$$R_{ct} = 3.913 \times 10^6 \left\{ \frac{D_t}{y} \left(\frac{s}{y} - 1 \right)^2 \right\}^{0.6422} \quad (B.34)$$

(This however was verified to be unnecessary as McQuiston's correlations (143,144) already include the effect of contact resistance, see Chapter 7.)

B.2.4 Water Pressure Drop

The water side pressure drop can be calculated using the conventional method for pipe flow calculations as follows:

$$\Delta p_w = \frac{4 f \sum L_{eq} \rho_w u_w^2}{D_i} \quad (B.35)$$

In order to determine the total equivalent length ($\sum L_{eq}$) and the flow velocity of chilled water in the coil tubes (u_w), the circuit arrangement of the coil must be known. In a cooling coil, the straight tube sections are connected by U bends at their ends. The chilled water may be arranged to pass through several straight tube sections (in the same row or in different rows, forming a flow path) when it flows through the coil (Figure B.2) and each of such flow paths is called a water circuit. Water circuit arrangement in a coil can be described by a parameter called "circuit number" (C_n). Instead of a number, this parameter is often given as full, half or quarter circuit, corresponding to $C_n = 1, 0.5$ and 0.25 respectively (some coil manufacturer may use other conventions for describing water circuit arrangements in their coils).

For a coil with N_r number of rows, if a chilled water circuit is composed of N_{pass} number of straight tube sections, the circuit number (C_n) of the coil is then:

$$C_n = \frac{N_r}{N_{pass}} \quad (B.36)$$

Hence, if there are N_{tpr} tubes per row, C_n multiplied by N_{tpr} equals the number of water circuits sharing the total flow rate of chilled water through the coil (\dot{V}_w). Accordingly, the volume flow rate of chilled water per tube (\dot{V}_{pt}) will be:

$$\dot{V}_{\text{pt}} = \frac{\dot{V}_w}{C_n N_{\text{tpr}}} \quad (\text{B.37})$$

It follows that the flow velocity within the tube therefore will be:

$$u_w = \frac{\dot{V}_{\text{pt}}}{\frac{\pi D_i^2}{4}} \quad (\text{B.38})$$

The number of "U-turns" made by the water flow is equal to $N_{\text{pass}} - 1$. If the width of the coil face is W_a and equivalent lengths of the U-bends and the connection piping for supply and return of water to and from the coil are respectively L_{eu} and L_{epc} , the total equivalent length of water flow through the coil can be approximated by:

$$\sum L_{\text{eq}} = L_{\text{epc}} + N_{\text{pass}} W_a + (N_{\text{pass}} - 1) L_{\text{eu}} \quad (\text{B.39})$$

As to the friction factor (f), the well known Colebrook equation ⁽¹⁷²⁾ may be used for its estimation:

$$\frac{1}{\sqrt{f}} = -4 \log_{10} \left\{ \frac{k_s}{3.4 D_i} + \frac{1.255}{\text{Re} \sqrt{f}} \right\} \quad (\text{B.40})$$

where k_s is the roughness of the inner tube surface (for copper tubes, $k_s = 0.015$ mm).

Since f in the Colebrook equation is implicit, solution of f requires an iterative procedure. The following equation ⁽³⁰⁾ is a more convenient alternative:

$$f = 0.001375 \left\{ 1 + \left(20000 \frac{k_s}{D_i} + \frac{10^6}{\text{Re}} \right)^{1/3} \right\} \quad (\text{B.41})$$

If the coil water pressure drop is known from manufacturer's data, the pressure drop at flow rates other than the specified flow rate can alternatively be approximated by:

$$\Delta p_w = \Delta p_{wo} \left(\frac{\dot{V}_w}{\dot{V}_o} \right)^2 \quad (B.42)$$

The above equation however may not be a good approximation if the actual flow rate deviates largely from the specified flow rate \dot{V}_o for which the pressure drop Δp_{wo} is given.

B.2.5 Air-side pressure drop

For plate-finned coils, the air-side pressure drop can be evaluated by (28):

$$\Delta p_a = \frac{(\rho_m u_c)^2}{2\rho_1} \left\{ (1+\sigma^2) \left(\frac{\rho_1}{\rho_2} - 1 \right) + f \frac{A}{A_c} \frac{\rho_1}{\rho_m} \right\} \quad (B.43)$$

where ρ_1 & ρ_2 are respectively the air densities at the coil inlet and outlet and

$$\rho_m = \text{mean density} = \frac{(\rho_1 + \rho_2)}{2}$$

As for the evaluation of the fin side convective heat transfer coefficient, the value of the friction factor (f) needs to be found and this can be based on available correlations obtained from experimental measurements. McQuiston ^(143,144) provided the following correlation for the friction factor of plate-finned coils as a function of a parameter denoted as FP:

$$f = 4.904 \times 10^{-3} + 1.382 (FP)^2 \quad (B.44)$$

where

$$FP = Re_{D_o}^{-0.25} \frac{D_o}{D^*} \left\{ \frac{(x_a - D_o)}{4(s-y)} \right\}^{-0.4} \left\{ \frac{x_a}{D^*} - 1 \right\}^{-0.5} \quad (B.45)$$

and D^* is defined as follows:

$$D^* = D_o \frac{\frac{A}{A_{to}}}{1 + \frac{x_a - D_o}{s}} \quad (B.46)$$

B.3 Heat, Mass and Momentum Transfer at Extended Surfaces

Methods for the evaluation of the heat and mass transfer coefficients and the friction factor for a wetted coil are introduced in this section. In a wetted coil, the mode of condensation could either be 'dropwise' or 'filmwise' (28). However, for aluminum fins, it was found that filmwise condensation could take place only if the surface had been thoroughly cleaned (144). In practice, the dropwise condensation mode should be far more generally applicable. Nevertheless, filmwise condensation is usually assumed to be the case in designing coils as it provides a more conservative estimate of the coil capacity. Therefore, equations for both modes of condensation are included.

B.3.1 Relationship Between Heat and Mass Transfer Coefficients

The Chilton-Colburn analogy adopted to relate momentum transfer to heat transfer, as discussed in B.2.3.b above, can be extended to cover also mass transfer. The rate of moisture transfer between the coil surface and the air stream can be ascribed to the difference in concentration of water vapour (C) between the two as follows:

$$m'' = h_m (C_a - C_s) \quad (B.47)$$

Applying the Chilton-Colburn analogy, the mass transfer coefficient can be related to the heat transfer coefficient as follows:

$$j = j_m = \frac{f}{2} \quad (B.48)$$

where

$$j = \left\{ \frac{h_o}{\rho_a C_{p_a} u} \right\} Pr^{2/3} \quad (B.49)$$

$$\text{and } j_m = \frac{h_m}{v} Sc^{2/3} \quad (B.50)$$

where $Sc = \text{Schmidt number} = \frac{v}{D}$

Since the coil surface is covered by a layer of saturated water (condensate), the layer of air immediately above the coil surface may be assumed to be saturated with water vapour. Also, because only a very thin layer of liquid water can remain attached to the coil surface (otherwise the condensate would drop onto the condensate pan at the bottom of the coil due to gravitational effect), the liquid layer and the coil surface may be regarded as at the same temperature.

For convenience in calculating heat and mass transfer in air-conditioning processes, concentration of water vapour in a moist air is conventionally quantified by humidity ratio (w) (also called moisture content) defined as the mass of water vapour per unit mass of dry air. This relationship is:

$$C = \rho_a w \quad (B.51)$$

Thus, the condensing vapour flux as given by (B.47) is modified to:

$$m'' = h_m \rho_a (w - w_s) \quad (B.52)$$

where w is the humidity ratio of the moist air and w_s is the humidity ratio of the air layer above the surface of the condensate (which is effectively the saturated humidity ratio corresponding to the coil surface temperature).

Defining h_d as the convective mass transfer coefficient when w is taken as the driving potential, the mass flux is then given by:

$$m'' = h_d (w - w_s) \quad (B.53)$$

and h_m & h_d are simply related by:

$$h_d = \rho_a h_m \quad (B.54)$$

Dividing (B.49) by (B.50) and substituting (B.54), the following relationship between h_o and h_d can be found:

$$\frac{h_o}{C_{p_a} h_d} = \left(\frac{Sc}{Pr}\right)^{2/3} = Le^{2/3} \quad (B.55)$$

where Le is the Lewis number and the numerical value of $Le^{2/3}$ is very close to 1 for moist air under normal conditions. Hence, h_d can be evaluated based on a known value of h_o where:

$$h_d = \frac{h_o}{C_{p_a}} \quad (B.56)$$

B.3.2 Heat and Mass Transfer Coefficients for Plate-finned Surfaces

According to the Chilton-Colburn analogy, the j factor for a coil handling sensible cooling only should equally be applicable for modelling the sensible part of the total heat transfer when there is condensation in the coil. However, in McQuiston's investigation ^(143,144) on both dry and wetted plate-finned coils, it was found that the j factor correlation for a dry coil (equation B.27) did not match well with experimental data from coils with wetted surfaces. In this case, the j factor was found to be significantly influenced by the fin spacing (s). Moreover, the sensible and the total (sensible plus latent) heat transfer seemed to be influenced by the fin spacing by different degrees. With a narrow fin spacing (over 8 fins per inch), interaction between the air stream and the condensate was noted and the effect was found to be more severe on the total heat transfer than on the sensible heat transfer. The relationship in (B.56) therefore is not accurate when applied to a 'wetted' coil.

Based on experimental findings, McQuiston ⁽¹⁴³⁾ proposed the following j factor correlations for wetted, (4 row) plate-finned coils:

a) *For sensible heat transfer,*

$$j_s = 0.0014 + 0.2618 (JP) J(s) \quad (B.57)$$

where JP is as defined earlier (B.28) ; and J(s) is a correction term for sensible heat transfer at wetted coil surfaces which is related to the fin spacing (s) and the Reynolds number (Re_s , itself based on fin spacing) as follows:

for filmwise condensation,

$$J(s) = 0.84 + 4.0 \times 10^{-5} Re_s^{1.25} \quad (B.58)$$

for dropwise condensation,

$$J(s) = \left\{ 0.9 + 4.3 \times 10^{-5} Re_s^{1.25} \right\} \left(\frac{s-y}{s} \right) \quad (B.59)$$

b) *For total heat transfer,*

$$j_m = 0.0014 + 0.2618 (JP) J_m(s) \quad (B.60)$$

where $J_m(s)$ is given by:

for filmwise condensation,

$$J_m(s) = \left\{ 0.95 + 4 \times 10^{-5} Re_s^{1.25} \right\} \left(\frac{s}{s-y} \right)^2 \quad (B.61)$$

for dropwise condensation,

$$J_m(s) = \left\{ 0.8 + 4 \times 10^{-5} Re_s^{1.25} \right\} \left(\frac{s}{s-y} \right)^4 \quad (B.62)$$

When j and j_m are known, h_o and h_m (and hence h_d) can then be calculated using equations (B.49) and (B.50) respectively. Since the correlation function for the j factor applies only for 4-row coils, j factors for coils with number of rows other than 4 need to be corrected according to equation (B.33).

B.3.3 Total Heat Transfer and Surface Effectiveness of Wetted Coil

On a wetted surface, it can be shown that the driving potential for total heat exchange (sum of sensible and latent heat exchange) between the surface and the

ambient air can be expressed as the difference in enthalpies between the moist air (h_a), and the saturated air film above the surface (h_s), where h_d is the transport coefficient (28). Over an elemental surface area of a wetted coil, the total heat transfer between the coil surface and the air-stream will therefore be:

$$\delta q = h_d \eta_{ms} (h_a - h_s) \delta A \quad (B.63)$$

where η_{ms} is the surface effectiveness of the wetted heat transfer surface of the coil which is there to account for the fact that the surface temperature (and hence surface air-film enthalpy) is not uniform over the entire fin and exposed fin collar surface.

When integrated over the entire heat transfer area, it can be shown that the total heat transfer is given by:

$$q = A h_d \eta_{ms} \text{LMHD} \quad (B.64)$$

where LMHD is called the log mean enthalpy difference which is given by:

$$\text{LMHD} = \frac{(h_{a1} - h_{s1}) - (h_{a2} - h_{s2})}{\ln \left\{ \frac{h_{a1} - h_{s1}}{h_{a2} - h_{s2}} \right\}} \quad (B.65)$$

where

$h_{a1} - h_{s1}$ = air-stream and surface air film enthalpy difference at entry plane

$h_{a2} - h_{s2}$ = air-stream and surface air-film enthalpy difference at exit plane

Through the use of the following artificially imposed linear equation to relate humidity ratio difference to the corresponding temperature difference between the moist air and the fin surface air film,

$$(w_s - w_a) = C (T_s - T_a) \quad (B.66)$$

where C is assumed to be a constant, McQuiston ⁽¹⁷¹⁾ showed that the fin efficiency for a vertical rectangular fin of a height L over a plane surface can be approximated by the following equation:

$$\eta_f = \frac{\tanh (M L)}{M L} \quad (B.67)$$

where M is given by

$$M = \sqrt{\frac{2 h_o}{k_f y} \left(1 + \frac{C h_{fg}}{C_{p_a}} \right)} \quad (B.68)$$

and h_{fg} = heat of condensation of water vapour

For plate-finned coils, the fin efficiency can be calculated by:

$$\eta_f = \frac{\tanh (M r \phi)}{M r \phi} \quad (B.69)$$

where ϕ is same as that defined for a dry coil (equation B.20) and equation (B.24) can then be applied to find surface effectiveness of a wetted coil from the calculated fin efficiency. However, since equation (B.66) is an artificially imposed relationship to simplify the problem, the value of C is not constant but varies along the air-flow direction through the coil. Its value is particularly sensitive to the on-coil air condition. As an approximation, the average value of C at the entry and exit planes is recommended for use in the evaluation of M .

B.3.4 Air-side Pressure Drop Across a Wetted Coil

Equation (B.43) still applies in estimating the air-side pressure drop across a wetted coil. However, similar to the heat and mass transfer coefficients, the correlation function for evaluating the friction factor (f) has to be modified into the following form:

$$f = 4.094 \times 10^{-3} + 1.382 \left\{ FP F(s) \right\}^2 \quad (B.70)$$

where $F(s)$ is a correction term to account for the effects of presence of condensate on the coil surface and is given by:

for filmwise condensation,

$$F(s) = \left\{ 0.6 + Re_s^{-0.15} \right\} \left(\frac{s}{s-y} \right)^{-3} \quad (B.71)$$

for dropwise condensation,

$$F(s) = \left\{ 0.325 + Re_s^{-0.05} \right\} \left(\frac{s}{s-y} \right)^{-3} \quad (B.72)$$

B.4 Adjustments to Heat, Mass and Momentum Transfer Coefficients for Corrugated Fins

The correlations described in the preceeding sections for evaluating the heat and mass transfer coefficients apply only to flat plate fins. Most coils in air-conditioning systems however have corrugated fins and therefore, in modelling their performance, the coefficients must be modified accordingly. The empirical correlations due to Beecher and Fagan ⁽¹⁴¹⁾ for calculating the heat and mass transfer coefficients for corrugated fins are summarized in this section.

B.4.1 Fin Pattern

The simplest fin corrugation pattern is the triangular wave pattern as shown in Figure 5.6, which is the fin pattern upon which Beecher & Fagan ⁽¹⁴¹⁾ based their experimental studies and developed their empirical correlations. Although fin patterns of actual coils may not be exactly the same, Beecher & Fagan's (B&F's) correlations should provide a reasonably good estimate of the heat and mass transfer coefficients. With the triangular fin pattern, the total fin area (A_f) is increased by a factor of A_{fp}/A_{ff} given by:

$$\frac{A_{fp}}{A_{ff}} = \sec(\theta) \quad (B.73)$$

$$\text{and } \sec(\theta) = \frac{\sqrt{x_f^2 + P_d^2}}{x_f} \quad (\text{B.74})$$

B.4.2 Heat Transfer Correlation Parameters for Patterned Fins

In B&F's correlations ⁽¹⁴¹⁾, the Nusselt number (Nu) is correlated with the Graetz number (Gz) and their definitions are:

$$\text{Nu} = \frac{h_o D_h}{k_a} \quad (\text{B.75})$$

$$\text{Gz} = \frac{\text{Re Pr } D_h}{N_r x_b} \quad (\text{B.76})$$

where D_h is the hydraulic mean depth of the finned coil defined as:

$$D_h = \frac{4 \times \text{Air Volume}}{\text{Total Surface Area}}$$

which can be expressed in terms of the coil configuration parameters as:

$$D_h = \frac{2 s \sigma}{\sigma \sec(\theta) + \frac{2 s}{D_o} (1 - \sigma)} \quad (\text{B.77})$$

The value of Re is calculated based on the flow velocity at the core area (u_c) and the hydraulic mean depth (D_h) (i.e. $\text{Re} = \rho_a u_c D_h / \mu_a$).

The Graetz number (Gz) is a dimensionless measure of the level of flow development. Based on the understanding that the air flow in the narrow spacing between the fins is predominantly developing laminar flow, Gz was chosen by Beecher & Fagan as the correlation parameter and through which good correlation results were obtained with the experimental data.

Substituting (B.77) for D_h in (B.76) and using the definition of Re where $u_c = \frac{u_a}{\sigma}$, Gz may be expressed as:

$$Gz = \frac{4 \rho_a s^2 Pr u_a \sigma}{\mu_a N_r x_b \left\{ \sigma \sec(\theta) + \frac{2s}{D_o} (1 - \sigma) \right\}^2} \quad (B.78)$$

B.4.3 Beecher & Fagan's Correlations for Nu

a) *Nusselt Number Evaluation Based on Arithmetic Mean Temperature Difference*

The temperature difference between the fin surface and the leaving air is usually small in cooling coils. Hence, if the log mean temperature difference (LMTD) calculated from measured temperature readings is used in determining the value of h_o , any inaccuracy in measurement would give rise to large errors to the resultant value of h_o . To circumvent this problem, Beecher & Fagan made reference to the arithmetic mean temperature difference (AMTD) in the determination of the Nusselt number (denoted as Nu_a) instead of that based on the LMTD (denoted as Nu_l) but the two are related by:

$$Nu_l = 0.25 Gz \ln \left\{ \frac{1 + 2 \frac{Nu_a}{Gz}}{1 - 2 \frac{Nu_a}{Gz}} \right\} \quad (B.79)$$

b) *Reference Coil Configuration Parameters*

The basic empirical correlation due to Beecher & Fagan for calculating Nu_a at patterned fin surfaces was based on the following reference coil configuration:

$N_{r,ref} = 3$;	$x_{a,ref} = 1.25 \text{ in. (31.75 mm)}$;
$x_{b,ref} = 1.083 \text{ in (27.5 mm).}$;	$D_{o,ref} = 0.5 \text{ in (12.7 mm).}$;
$s_{ref} = 0.077 \text{ in (1.96 mm).}$;	$N_{p,ref} = 3$;
$P_{d,ref} = 0.038 \text{ in. (0.97 mm)}$	

Additional correlations were developed so that the value of Nu_a based on the reference configuration ($Nu_{a,ref}$) can be corrected for applications to coils with different configurations.

c) *Flat Fins*

The following correlation equations are given by Beecher and Fagan for the evaluation of Nusselt number for flat-finned surface (Nu_{af}) which were derived based on the reference coil configuration except that here, $P_d = 0$:

$$Nu_{af,ref} = 4.17 \left(\frac{Gz}{10} \right)^{0.822} \quad (7 \leq Gz < 15) \quad (B.80a)$$

$$Nu_{af,ref} = 4.37 \left(\frac{Gz}{10} \right)^{0.725} \quad (15 \leq Gz < 30) \quad (B.80b)$$

$$Nu_{af,ref} = 4.64 \left(\frac{Gz}{10} \right)^{0.664} \quad (30 \leq Gz \leq 100) \quad (B.80c)$$

The empirical equations for correcting the Nu_{af} estimated from the above equation for a coil with number of rows, N_r , and a tube spacing ratio $\alpha (= x_b/x_a)$ that are different from the reference coil are as follows:

i) Corrections for different number of rows

$$R_{Nr} = \frac{Nu_{afNr}}{Nu_{af3r}} = \left(\frac{N_r}{3} \right)^{[0.22 (Gz/30)^{0.626}]} \quad (2 \leq N_r \leq 6) \quad (B.81)$$

ii) Corrections for different tube spacing ratios

$$R_{\alpha} = \frac{Nu_{af\alpha}}{Nu_{af\alpha_{ref}}} = \left(1.0332 \alpha \right)^{[0.227 (Gz/30)^{0.163}]} \quad (B.82)$$

The effects of variations in fin spacing (s) on the correlation between Nu_{af} and Gz appeared to be negligible.

d) *Corrugated Fins*

The following set of correlation equations are given for calculating the Nusselt number for corrugated fin surfaces, which were derived based on the reference configuration except for the value of P_d :

$$\text{Denoting } \frac{P_d}{P_{d,ref}} \text{ as } \epsilon_d ,$$

$$Nu_{ap,ref} = 3.31 \epsilon_d^{0.046} \quad (Gz = 7) \quad (B.83a)$$

$$Nu_{ap,ref} = 6.55 \epsilon_d^{0.107} \quad (Gz = 15) \quad (B.83b)$$

$$Nu_{ap,ref} = 11.57 \epsilon_d^{0.182} \quad (Gz = 30) \quad (B.83c)$$

$$Nu_{ap,ref} = 24.68 \epsilon_d^{0.293} \quad (Gz = 80) \quad (B.83d)$$

Correlations given for correcting the estimate to correspond to different number of fin patterns per length of x_b (N_p) are as follows:

$$R_{Np} = \frac{Nu_{aNp}}{Nu_{a3p}} = \left(\frac{N_p}{3}\right)^x \quad (B.84a)$$

where, for $s = 0.077$ in. (mm),

$$x = 0.0942 \epsilon_d^{0.25} \left(\frac{Gz}{30}\right)^y \quad (B.84b)$$

$$y = 3.22 \epsilon_d^{-0.516} \quad (B.84c)$$

and, for $s = 0.094$ in.,

$$x = 0.4354 \left(\frac{Gz}{30}\right)^{0.21} \quad (B.84d)$$

Corrections for different fin spacings (s) are as follows:

$$R_s = A + B \delta_f + C \delta_f^2 \quad (B.85)$$

where

$$\delta_f = \frac{s}{s_{ref}} \quad (B.86)$$

$$A = 6.3440 - 7.3143 R_1 + 1.9632 R_2 \quad (B.87a)$$

$$B = -7.4749 + 10.812 R_1 - 3.3375 R_2 \quad (B.87b)$$

$$C = 2.1239 - 3.4981 R_1 + 1.3743 R_2 \quad (B.87c)$$

and

$$R_1 = 0.829 \epsilon_d^{0.113} \left(\frac{Gz}{10} \right)^{(-0.0315 \epsilon_d^{0.144})} \quad (B.88)$$

$$R_2 = 0.942 \epsilon_d^{0.061} \left(\frac{Gz}{10} \right)^{(-0.006)} \quad (B.89)$$

From the results of Beecher & Fagan, it was shown that the effects of variations in D_o and x_a on the correlation of Nu_a on Gz are minimal and hence, no correction to the calculated value of Nu_a is required for the differences in these parameters.

B.4.4 Application of Beecher & Fagan's Correlations

Since the heat transfer coefficient h_o for flat-finned coils can be evaluated from McQuiston's correlations, the main concern here is to evaluate the ratio of h_o between corrugated and flat fins (Nu_{lp}/Nu_{lf} calculated from the correlations). Hence, the procedures of applying Beecher & Fagan's correlations for determining the effect of fin corrugation are as summarized below:

- a) Based on the actual coil configuration parameters and operating conditions, calculate Gz using on equation (B.78).
- b) Based on Gz calculated, select the appropriate equation in (B.80) to evaluate $Nu_{af,ref}$.
- c) Calculate R_{Nr} & R_α using (B.81) & (B.82) and use them to correct $Nu_{af,ref}$ as follows:

$$Nu_{af} = R_{Nr} R_\alpha Nu_{af,ref} \quad (B.90)$$

(As effects due to variations in N_r and α from the respective reference values should be very similar for both the corrugated and flat fin surfaces, this correction is not necessary if only the ratio of h_o needs to be found.)

- d) As equations for $Nu_{ap,ref}$ are given only for specific values of Gz (see equation B.83), $Nu_{ap,ref}$ corresponding to the case under concern has to be found by interpolating between values from equations corresponding to the next larger and smaller values of Gz (denoted as Gz_j & Gz_i respectively). This is done by linear interpolation between the log-log plot of $Nu_{ap,ref}$ vs Gz and accordingly, the interpolation equation can be expressed as:

$$Nu_{ap,ref} = Nu_{ap,ref,i} \left(\frac{Gz}{Gz_i} \right)^z \quad (B.91)$$

where

$$z = \frac{\ln \left\{ \frac{Nu_{ap,ref,j}}{Nu_{ap,ref,i}} \right\}}{\ln \left\{ \frac{Gz_j}{Gz_i} \right\}} \quad (B.92)$$

and $Gz_j \leq Gz < Gz_i$

- e) Calculate Nu_{ap} by correcting the value of $Nu_{ap,ref}$ using R_{Nr} , R_α , R_{Np} & R_s from equations (B.81), (B.82), (B.84) & (B.85) as follows:

$$Nu_{ap} = R_{Nr} R_\alpha R_{Np} R_s Nu_{ap,ref} \quad (B.93)$$

- f) Convert Nu_{af} & Nu_{ap} into Nu_{lf} & Nu_{lp} by applying equation (B.79) and then calculate the ratio of Nu_{lp} to Nu_{lf} as follows:

$$\frac{h_{op}}{h_{of}} = \frac{Nu_{lp}}{Nu_{lf}} = \frac{\ln \left\{ \frac{1 + 2 \frac{Nu_{ap}}{Gz}}{1 - 2 \frac{Nu_{ap}}{Gz}} \right\}}{\ln \left\{ \frac{1 + 2 \frac{Nu_{af}}{Gz}}{1 - 2 \frac{Nu_{af}}{Gz}} \right\}} \quad (B.94)$$

Having evaluated the above ratio, the heat transfer coefficient at corrugated fins may be calculated by multiplying the ratio by the value of h_o calculated based on McQuiston's correlations for flat finned coils.

B.4.5 Mass Transfer Coefficient and Friction Factor Adjustments

The correlation equations derived by Beecher & Fagan apply only for sensible heat transfer but whether the same correlations would be applicable to combined heat and mass transfer and to the friction factor at corrugated fin surfaces was unknown (to verify this formed one of the objective of this work, see Chapter 7).

B.5 Dry/Wet Boundary Determination

Procedures for determining the location of the dry/wet boundary within a finned cooling and dehumidifying coil are summarized in this section. They were developed based on the methods introduced in the ASHRAE Handbook ⁽¹⁴⁰⁾, with the contact resistance between the tube and the fin collar included in the calculation procedures. However, the metal and fouling resistances were neglected. The latter was neglected so that model predictions can be compared against manufacturers performance data of new coils (though could easily be included in the model).

Assuming there exists a dry/wet boundary in the coil (Figure B.1), the following equations can be set-up:

$$q_{dc} = \dot{m}_a C_{p_a} (T_{a1} - T_{ab}) = \dot{m}_a (h_{a1} - h_{ab}) = \dot{m}_w C_{p_w} (T_{w2} - T_{wb}) \quad (B.95)$$

$$q_{wc} = \dot{m}_a (h_{ab} - h_{a2}) = \dot{m}_w C_{p_w} (T_{wb} - T_{w1}) \quad (B.96)$$

$$q_c = q_{dc} + q_{wc} = \dot{m}_a (h_{a1} - h_{a2}) = \dot{m}_w C_{p_w} (T_{w2} - T_{w1}) \quad (B.97)$$

Define two parameters, Y_r and C_C , as follows,

$$Y_r = \frac{T_{w2} - T_{w1}}{h_{a1} - h_{a2}} \quad (B.98a)$$

and from (B.97),

$$Y_r = \frac{\dot{m}_a}{\dot{m}_w C_{p_w}} \quad (B.98b)$$

also

$$C_C = \frac{T_s - T_w}{h_a - h_s} \quad (B.99)$$

and it is assumed that C_C remains constant over the wet coil.

Note that at an elemental section in the air-flow direction,

$$\delta q_{wc} = \eta_{ms} h_d (h_a - h_s) \delta A_{wc} \quad (B.100)$$

also, if the tube and fin collar thermal resistances and the fouling resistances are neglected, then

$$\delta q_{wc} = \frac{T_s - T_w}{R_{ct} \frac{A_i}{A_t} + \frac{1}{h_i}} \delta A_i \quad (B.101)$$

hence, by equating right hand side of the two equations above and re-arranging, it can be shown that

$$C_C = \eta_{ms} h_d \left(\frac{1}{h_i} \frac{A}{A_i} + R_{ct} \frac{A}{A_t} \right) \quad (B.102)$$

From equation (B.95) which applies over the dry coil portion from the inlet plane up to the dry/wet boundary, solving for h_{ab} yields

$$h_{ab} = h_{a1} - \frac{\dot{m}_w C_{pw}}{\dot{m}_a} (T_{w2} - T_{wb}) \quad (B.103)$$

Using the definition for Y_r ,

$$h_{ab} = h_{a1} - \frac{T_{w2} - T_{wb}}{Y_r} \quad (B.104)$$

It follows that

$$Y_r h_{ab} = Y_r h_{a1} - T_{w2} + T_{wb} \quad (B.105)$$

At the dry/wet boundary, applying equation (B.99),

$$T_{wb} = T_{sb} - C_C (h_{ab} - h_{sb}) \quad (B.106)$$

Since at the dry/wet boundary, condensation just starts to take place and hence the coil surface temperature must be at the dew point temperature of the incoming air-stream, T_{a1}'' . Thus,

$$T_{sb} = T_{a1}'' \quad (B.107)$$

$$\text{and } h_{ab} = h_{a1}'' \quad (B.108)$$

where

h_{a1}'' = enthalpy of saturated air with same moisture content as the incoming moist air

Substituting (B.107) into (B.106) and then substituting T_{wb} from (B.106) into (B.105) and using (B.108), (B.105) may be written as:

$$Y_r h_{ab} = Y_r h_{a1} - T_{w2} + T_{a1}'' - C_C h_{ab} + C_C h_{a1}'' \quad (B.109)$$

Re-arranging,

$$h_{ab} = \frac{T_{a1}'' - T_{w2} + Y_r h_{a1} + C_C h_{a1}''}{C_C + Y_r} \quad (B.110)$$

From the above equation, the moist air enthalpy at the dry/wet boundary can be calculated. If there is actually a dry/wet boundary, the following inequality will hold:

$$h_{a1} > h_{ab} > h_{a2} \quad (B.111)$$

However, if the coil is fully wet,

$$h_{a1} < h_{ab} \quad (B.112)$$

or, if the coil is fully dry,

$$h_{a2} > h_{ab} \quad (B.113)$$

The above method determines whether the coil is fully dry, fully wet or partly dry, and by the same process, the air and water conditions at the dry/wet boundary can be determined. Hence, the coil sensible and total heat transfer can then be calculated accordingly.

B.6 Procedures for Simulating Performance of a Cooling and Dehumidifying Coil

The procedures by which a steady-state cooling and dehumidifying coil model has been developed are summarized in this section and in the flow chart that follows. Here, the mass flow rates of air and chilled water, their respective entering conditions and the physical characteristics of the coil are assumed to be known. The function of the model is to evaluate the leaving conditions of the air and the chilled water as well as the total and sensible heat transfer rates. Following that, the air and water side pressure drops can also be determined. At the start of the solution process, the initial assumption is made that the coil is partly dry and partly wet.

Step Descriptions of calculations involved

- 1 Calculate basic parameters – coil heat transfer area, air and water flow areas, contact resistance, hydraulic mean diameter, etc.
- 2 Assign assumed leaving conditions – make an initial estimate of leaving air and chilled water conditions and determine the respective mean bulk temperatures of the fluids in the coil.
- 3 Calculate transport properties of the fluids – based on bulk mean temperature of the respective fluid evaluated from known inlet and assumed outlet conditions.

A bank of transport properties data of the fluids must be available for this and the required data can be found from standard transport properties databooks.

- 4 Calculate j factors, heat and mass transfer coefficients and corrections required. The value of h_i at the tube side can be evaluated using either the Dittus-Boelter correlation (B.25a) or the Seider & Tate correlation (B.25b), based on the velocity of water flow within the tubes, the type of flow (laminar or turbulent) and the transport properties of water found in step 3.

Based on results of steps 1 to 3, the fin side heat and mass transfer coefficients can be evaluated by using McQuiston's j -factor correlations (see Section B.2 & B.3), with corrections for wet surface effects and for number of rows made accordingly. Having calculated the j -factor for sensible heat transfer for the dry coil surface and the j -factor for sensible and total heat transfer for the wet coil surface, the heat transfer coefficient h_o for the dry coil portion and the heat and mass transfer coefficients h_o and h_d for the wet coil portion can be evaluated using equations (B.29 or B.49, B.50 & B.54). Following the method described in Section B.4, the coefficients can be corrected to account for any fin corrugation effects.

- 5 Calculate the coil surface temperature at the exit plane and the wet fin surface effectiveness. The fin effectiveness for both the dry and wet coil surfaces can be calculated based on h_o at the fin side found in step 4 according to the procedure described in Section B.2.2 & B.3.3. In calculating the surface effectiveness for the wet coil portion, the coil surface air-film conditions have to be known. An evaluation of the latter in turn depends on a known value of coil effectiveness. Both therefore need to be solved for simultaneously. The procedures developed for calculating the fin surface effectiveness were based on the conditions at the air exit plane (plane 2) where the off-coil air conditions have been assumed and the water entering temperature is known. Details of the procedures involved are as follows:

a) Equations required for solving T_{s2} are as follows:

- i) The saturated humidity ratio (w_{sat}) of a moist air sample may be related to its corresponding temperature (T) using the cubic polynomial (173):

$$w_{sat} = a_0 + a_1 T + a_2 T^2 + a_3 T^3$$

$$\text{where } a_0 = 3.7658 \times 10^{-3}$$

$$a_1 = 3.0517 \times 10^{-4}$$

$$a_2 = 4.648 \times 10^{-6}$$

$$a_3 = 3.787 \times 10^{-7}$$

for w_{sat} in kg/kg-dry air and T in °C. Hence,

$$w_{s2} = a_0 + a_1 T_{s2} + a_2 T_{s2}^2 + a_3 T_{s2}^3 \quad (B.114)$$

- ii) The enthalpies of air (h_a) and of the saturated air-film above the coil surface (h_{s2}) are given by:

$$h_{a2} = C_{p_d} T_{a2} + w_2 (C_{p_s} T_{a2} + h_{fg}) \quad (B.115)$$

$$h_{s2} = C_{p_d} T_{s2} + w_{s2} (C_{p_s} T_{s2} + h_{fg}) \quad (B.116)$$

Here, h_{a2} is based on the assumed leaving coil conditions and hence is a known value within this process of solving for T_{s2} .

- iii) The value of C from equation (B.66) is:

$$C = \frac{w_{s2} - w_2}{T_{s2} - T_{a2}} \quad (B.117)$$

- iv) The relationship between coil surface temperature and enthalpy difference at an elemental section in the wet coil portion (from equation B.106) is given by:

$$T_{s2} = T_{w2} + C_C (h_{a2} - h_{s2}) \quad (B.118)$$

in which C_C may be evaluated from equation (B.102):

$$C_C = \eta_{ms} h_d \left(\frac{1}{h_i} \frac{A}{A_i} + R_{ct} \frac{A}{A_t} \right)$$

and η_{ms} can be evaluated by using equations given in Sections B.2.2 & B.3.3 based on value of C calculated above.

b) Re-arranging the equations.

Substituting (B.114) into (B.116) and then substitute the resultant expression for h_{s2} (a function of T_{s2}) into (B.118) and re-arranging, the following equation can be obtained:

$$C_0 + C_1 T_{s2} + C_2 T_{s2}^2 + C_3 T_{s2}^3 + C_4 T_{s2}^4 = 0 \quad (B.119)$$

where

$$C_0 = T_{w2} + C_C (h_{a2} - a_0 h_{fg})$$

$$C_1 = 1 + C_C (Cp_d + a_0 Cp_s + a_1 h_{fg})$$

$$C_2 = C_C (a_1 Cp_s + a_2 h_{fg})$$

$$C_3 = C_C (a_2 Cp_s + a_3 h_{fg})$$

$$C_4 = C_C a_3 Cp_s$$

which is a fourth order polynomial of T_{s2} containing the term C_C which is also a function of T_{s2} . Hence, T_{s2} can then be found by solving this implicit non-linear equation using an appropriate method (e.g. Newton-Raphson method (159)).

c) The solution procedure for in summary is as follows:

- i) Assume a coil surface temperature (\hat{T}_s);
- ii) calculate C and η_{ms} based on \hat{T}_s ;

- iii) calculate C_C based on η_{ms} ;
- iv) solve (B.119) with this value of C_C ;
- v) compare the value of T_{s2} with \hat{T}_s and repeat, with \hat{T}_s updated in each round of iteration, until a converged solution is obtained.

The surface effectiveness η_{ms} can therefore be calculated in this process.

- 6 Compute U values – based on surface effectiveness from step 5, for both the dry and wet portions of the coil.
- 7 Find the dry/wet boundary and the corresponding dry and wet coil surface areas. The value of moist air enthalpy at the dry-wet boundary can be calculated following the procedures described in Section B.5. This value is then compared with the entering air enthalpy and the enthalpy corresponding to the assumed leaving air conditions for determining whether the coil is fully dry, fully wet or partly dry and partly wet.
 - a) If the coil is partly dry and partly wet, the dry part heat transfer can be calculated based on the inlet and the dry/wet boundary temperatures. The areas of the dry and the wet portions can also be found accordingly. Knowing the wet coil area, the sensible and total heat transfer at the wet portion can be evaluated using the LMHD between the air stream and the air-film above the coil surface (see Section B.3.3).
 - b) If the entire coil surface is wet, the surface effectiveness of the coil has to be re-calculated, with the value of the coefficient C used in calculating the effectiveness replaced by average of the two coefficients (according to equation B.66) at the inlet and exit planes. If the assumption is made that the coil characteristic (C_C) based on the leaving air condition does not change significantly throughout the wetted portion of the coil, then

iteration steps can be avoided in the re-calculation of fin effectiveness. Knowing the effectiveness of the coil surface, the U value and hence the total and sensible heat transfer can be evaluated.

- c) If the entire coil surface is dry, the sensible heat exchange can be calculated based on the surface effectiveness and the Ntu method (no iteration required).

8 Calculation of leaving air and water conditions. Knowing the heat transfer rates (sensible and latent), the leaving air and water conditions can be calculated based on the heat transfer rates and the mass flow rates of the two fluids.

9 Compare assumed and calculated leaving conditions. Leaving conditions evaluated in step 8 are to be compared with those assumed initially. If they differ by a significant extent, the calculated values become the assumed values, and steps 3 to 12 are repeated until convergence.

10 Calculation of pressure drops. Having found the dry/wet coil surface areas and the friction factors for each portion of the coil, the air side and water side pressure drops can be determined using the equations introduced in Sections B.2.4 & B.3.4.

A Flow Chart Showing the Procedures for Modelling Steady-state Performance of a Cooling and Dehumidifying Coil

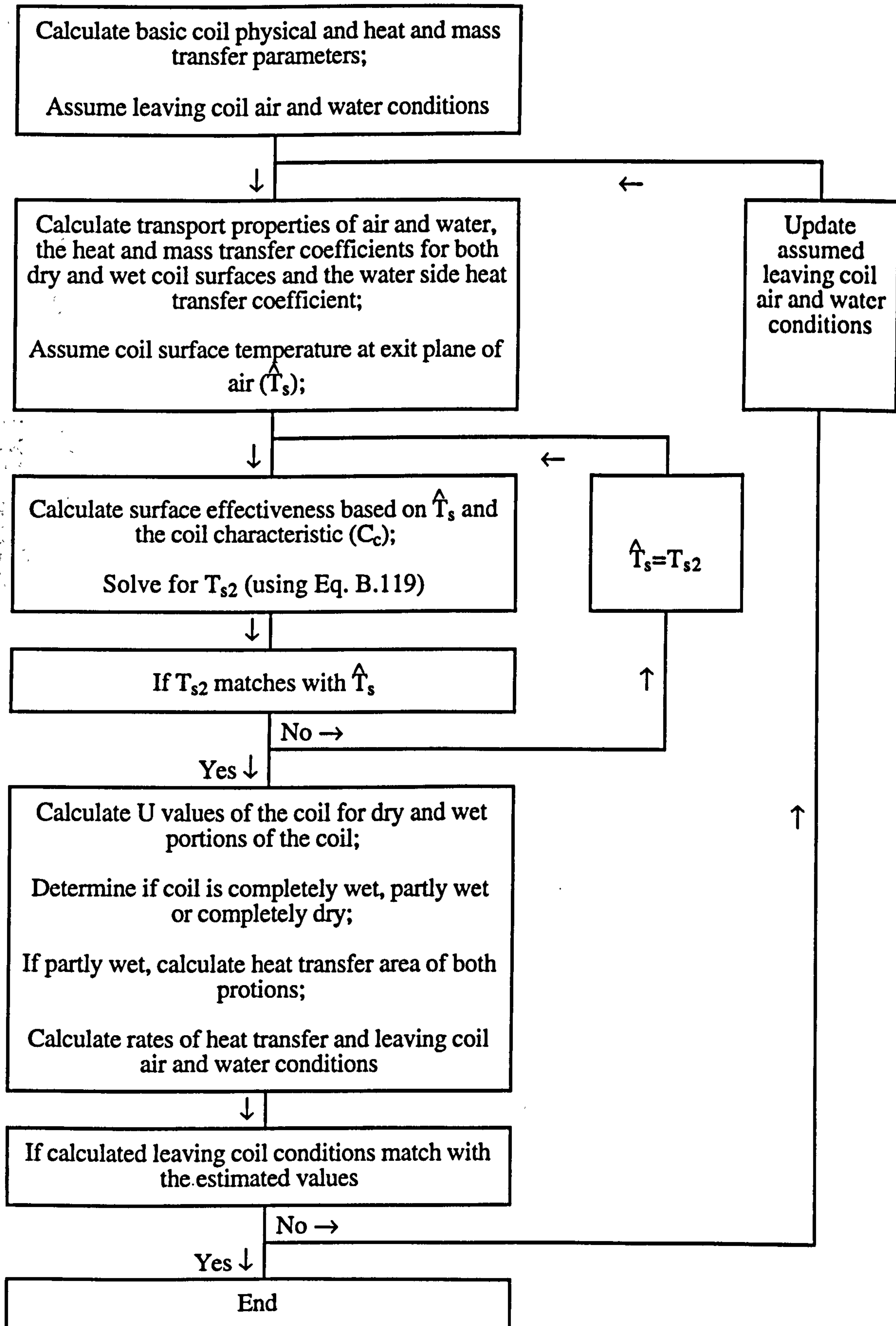


Figure B.1

Air and water temperature profiles in
a cooling and dehumidifying coil

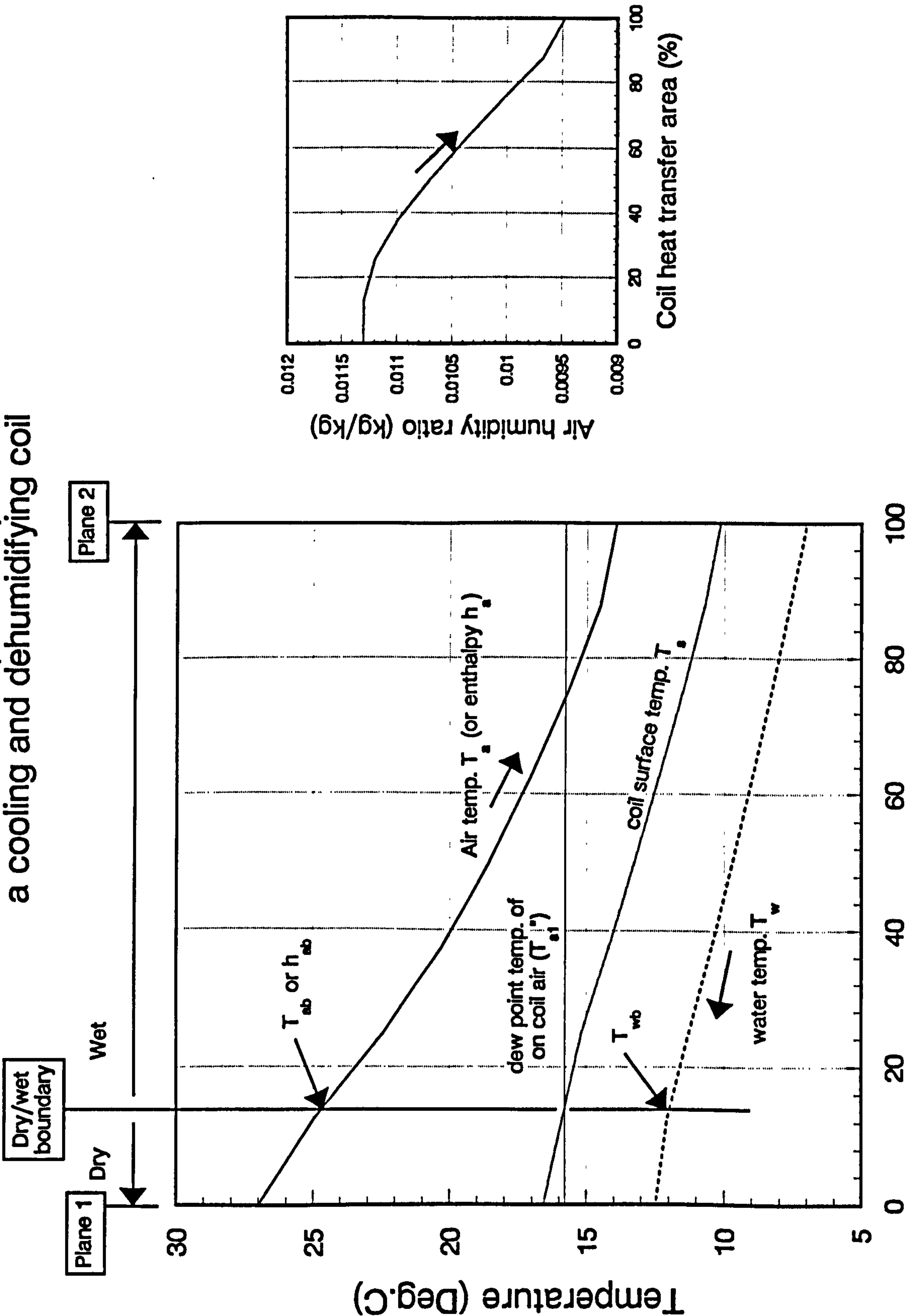
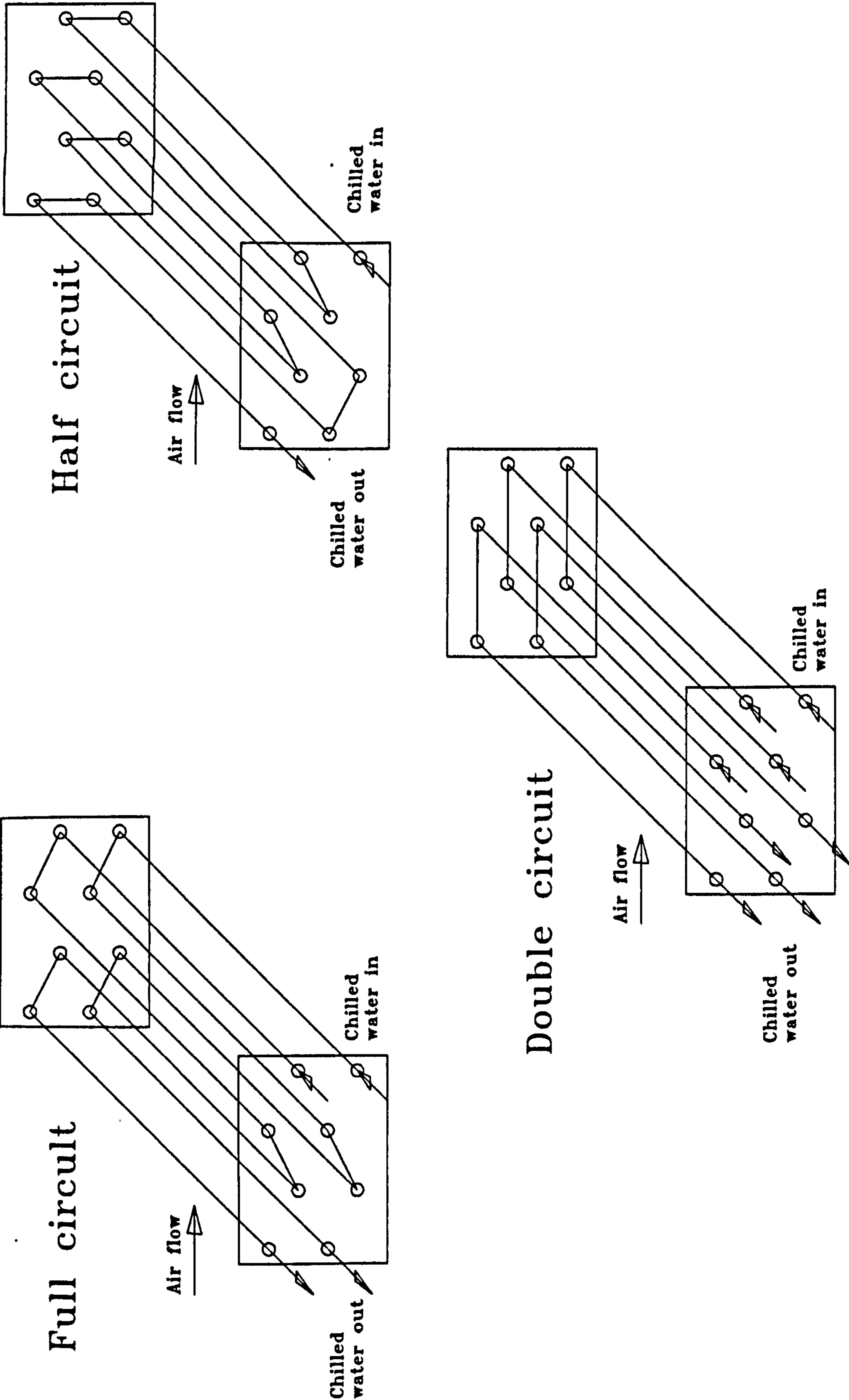


Figure B.2 Water circuit arrangement in a coil



Appendix C

Miscellaneous Methods Used in the Building Model

Contents

	Page
C.1 Radiation Shape Factors	C 2 - C 4
C.2 Convective Heat Transfer Coefficients at Wall and Slab Surfaces	C 5 - C 6
C.3 Decomposition of Global Solar Radiation into Direct and Diffuse Components	C 7 - C 8

C.1 Radiation Shape Factors

The method for modelling the radiant energy exchange between internal surfaces of the walls, slabs and the window of the model room has been outlined in Chapter Four. In applying the method, the radiation shape factor (F_{ij}) between each pair of surfaces (i & j) has to be evaluated. The methods for calculating shape factor between surfaces of an enclosure can be found in many references (e.g. 31, 129, 135, 174). The methods adopted in the building heat and moisture transfer model developed in this work are summarized below.

C.1.1 Perpendicular and Parallel Surfaces

For the six enclosing surfaces of a rectangular enclosure, the shape factor for each pair of surfaces can be evaluated by using the following formulae ⁽¹²⁹⁾ for two surfaces that are parallel and perpendicular to each other:

- i) Two identical rectangular planes parallel to each other (Figure C.1):

$$F_{ij} = \frac{2}{\pi xy} \left\{ \ln \sqrt{\frac{(1+x^2)(1+y^2)}{1+x^2+y^2}} + x \sqrt{1+y^2} \tan^{-1}\left(\frac{x}{\sqrt{1+y^2}}\right) + \right. \\ \left. y \sqrt{1+x^2} \tan^{-1}\left(\frac{y}{\sqrt{1+x^2}}\right) - x \tan^{-1}(x) - y \tan^{-1}(y) \right\} \quad (C.1)$$

- ii) Two rectangular planes perpendicular to each other and with a common edge (Figure C.2):

$$F_{ij} = \frac{1}{\pi w} \left\{ w \tan^{-1}\left(\frac{1}{w}\right) + h \tan^{-1}\left(\frac{1}{h}\right) - \sqrt{h^2+w^2} \tan^{-1}\left(\frac{1}{\sqrt{h^2+w^2}}\right) + \right. \\ \left. \frac{1}{4} \ln \left[\frac{(1+w^2)(1+h^2)}{1+w^2+h^2} \left(\frac{w^2(1+w^2+h^2)}{(1+w^2)(w^2+h^2)} \right)^{w^2} \left(\frac{h^2(1+h^2+w^2)}{(1+h^2)(h^2+w^2)} \right)^{h^2} \right] \right\} \quad (C.2)$$

For two rectangular surfaces of different dimensions that are parallel or perpendicular to each other but do not have a common edge (such as the window in the exterior wall

(Wall 1, see Figure 8.1) and the other wall and slab), the shape factor between the two surfaces can be calculated by first extending the surfaces into the standard form as shown in Figure C.1 or C.2 and then using the shape factor algebra technique (174). This method however is rather cumbersome. The alternative is to numerically integrate the fundamental shape factor integral equation for two arbitrary plane surfaces (129,174) A_i and A_j as shown in Figure C.3:

$$F_{ij} = \frac{1}{\pi A_i} \int_{A_i} \int_{A_j} \frac{\cos \phi_i \cos \phi_j}{r_{ij}} dA_i dA_j \quad (C.3)$$

iii) For two rectangular parallel planes with parallel edges (Figure C.4), the numerical formula is:

$$F_{12} \approx \frac{\Delta A_1 \Delta A_2}{\pi A_1} \left\{ \sum_{i=1}^{N_{x1}} \sum_{j=1}^{N_{y1}} \sum_{k=1}^{N_{x2}} \sum_{l=1}^{N_{y2}} \frac{(z_b - z_a)^2}{[(x_k - x_i)^2 + (y_l - y_j)^2 + (z_b - z_a)^2]^2} \right\} \quad (C.4)$$

where N_{x1} , N_{y1} , N_{x2} , N_{y2} denote the number of subdivisions of the two plane surfaces in the two directions (parallel to the edges of the planes). Other symbols used are as defined in the figure.

iv) For two rectangular, perpendicular planes (Figure C.5), the numerical formula is:

$$F_{12} \approx \frac{\Delta A_1 \Delta A_2}{\pi A_1} \left\{ \sum_{i=1}^{N_{x1}} \sum_{j=1}^{N_{y1}} \sum_{k=1}^{N_{x2}} \sum_{l=1}^{N_{y2}} \frac{(z_b - z_a)(x_i - x_b)}{[(x_b - x_i)^2 + (y_k - y_j)^2 + (z_l - z_a)^2]^2} \right\} \quad (C.5)$$

In the building model, the shape factor between the six enclosing surfaces of the room were calculated by using equations C.1 & C.2 whereas those between the window (Wall 7) and the other walls and slabs were calculated using the numerical integral equations (C.4 & C.5). Shape factor between Wall 1 (the exterior wall) and

other walls and slabs (F_{1j} for $j=2,3,...,6$) were evaluated by using the following shape factor relationship:

$$A_1 F_{1j} = A_8 F_{8j} - A_7 F_{7j} \quad (C.6)$$

where A_8 is the total area of Wall 1 and Wall 7 ($= A_1 + A_7$) and F_{8j} denotes the shape factor between the total surface of Wall 1 and Wall 7 and another wall or slab j .

C.1.2 Transformation of Coordinate System

In using the above equations to calculate shape factors in a computer program, the geometric relationship between each pair of surfaces has to be properly defined with reference to the coordinate system based upon which the equations were derived. This was done by a linear transformation including a translation of the origin point of the coordinates and rotation(s) of the coordinate axis. For instance, if the lower left corner of the exterior wall (viewed from inside the room to the wall) is chosen as the origin (0,0,0) of the co-ordinate system, Figure C.5 shows the geometric relationship between the window (Wall 7) and the floor slab (Wall 6). The origin will have to be translated to the top right corner of Wall 1 and the coordinate system will have to be rotated by 180° about the x axis (normal to the exterior wall pointing into the room) to bring it correspond to the relationship between the window and the ceiling slab (Wall 5).

Calculation of shape factors needs to be done only at the first time a particular room is modelled. The shape factors will be stored in a data file for re-use in subsequent simulation studies with the same room.

C.2 Convective Heat Transfer Coefficients at Wall and Slab Surfaces

C.2.1 Internal Surfaces

Values of the convective heat transfer coefficient at internal surfaces of the walls and slabs used in the building model were adapted from ASHRAE (162). Its value depends on the direction of heat flow (horizontal or vertically upward or downward):

Heat Flow Direction	Value of Convective Heat Transfer Coefficient (h) (W/m ² K) (162)
Upward	4.04
Horizontal	3.07
Downward	0.92

It can be seen that there is a large difference between the convective heat transfer coefficients for upward and downward heat flow. For the ceiling and the floor slab, the direction of heat flow can be reversed depending on the temperatures of the slab surface and the room air. If a sudden change in the value of the coefficient h occurs within a solution step, it would cause problems to the numerical solution process. To overcome this, the convective heat transfer coefficient used in the building model had an interpolated value between those for upward and downward heat flow situations (with referene to the temperature difference between the slab surface and the room air) when a switch over in heat flow direction was detected.

C.2.2 External Surfaces

As is well known, the convective heat transfer coefficient at a solid surface is dependent on the flow velocity of the fluid above it (129,135,174). For the internal wall

and slab surfaces (and the window), a steady indoor air movement may be assumed but for the external surfaces, the outdoor air movement varies from time to time depending on the wind speed and the wind direction relative to the wall. The method used in the model for determining the heat transfer coefficients at the external side of the exterior wall and the window was based on the empirical formulae due to Kimura (1975):

i) For a windward surface:

$$\text{if } U > 2 \text{ (m/s),} \quad u = 0.25 U;$$

$$\text{if } U \leq 2 \text{ (m/s),} \quad u = 0.5 U$$

ii) For a leeward surface:

$$u = 0.3 + 0.05 U$$

where U = wind speed above the building

u = wind speed near the building

and the heat transfer coefficient is given by:

$$h = 3.5 + 5.6 u \text{ (W/m}^2\text{K)} \quad (\text{C.7})$$

Determination of whether a surface is at the windward or the leeward side is based on the incident angle (γ) of the wind velocity vector relative to the normal vector from the surface (Figure C.6). If γ is less than 90° , the wall is at the windward side, otherwise, the wall is at the leeward side.

C.3 Decomposition of Global Solar Radiation into Direct and Diffuse Components

In calculating heat transfer into a building due to solar radiation incident upon the external surfaces of the building, the total intensity of solar radiation incident upon each external surface of the building has to be determined. The total intensity of solar radiation is composed of two components, the direct component and the diffuse component. The intensity of the direct component upon a surface is dependent on the incident angle of the direct solar radiation onto the surface. Thus, the total intensity of solar radiation upon a surface can be determined only if the direct and diffuse intensities and the position of the sun relative to the surface are known.

Relative position between the sun and an arbitrary surface can be determined from the sol-earth geometric relationships and the direction of the surface relative to the latitudes and longitudes of the earth and the horizontal plane (the earth's surface) (5,175). However, in Hong Kong, the Royal Observatory of Hong Kong measures only the global solar radiation (13), i.e. the total intensity on a horizontal surface. Therefore, a method for decomposing the global solar radiation intensity into direct and diffuse intensities is required for building heat transfer modelling. The method adopted in this work was based on Kimura's work (175) as follows:

The direct horizontal intensity under a cloudy sky (I_{DH}^*) may be approximated by:

$$I_{DH}^* = I_{DH} - \frac{1 - P}{1 - Y} I_{TH} \quad (C.8)$$

where

I_{DH} and I_{TH} are respectively the direct horizontal and total horizontal intensities under a clear sky which can be determined by using the method detailed in the ASHRAE Handbook (5);

P is the ratio of cloudy sky total horizontal radiation (the global solar radiation) to the clear sky total horizontal radiation, viz.:

$$P = \frac{I_{DH}^*}{I_{DH}} \quad (C.9)$$

Y is dependent on the solar altitude angle (β) as follows (175):

$$Y = 0.309 - 0.137 \sin (\beta) + 0.394 \sin^2 (\beta) \quad (C.10)$$

Knowing I_{DH}^* , the direct normal intensity under a cloudy sky (I_{DN}^*) can be determined by:

$$I_{DN}^* = \frac{I_{DH}^*}{\sin (\beta)} \quad (C.11)$$

and the diffuse horizontal intensity (I_{SH}^*) can be determined by:

$$I_{SH}^* = I_{TH}^* - I_{DH}^* \quad (C.12)$$

Having determined the direct normal intensity and the diffuse horizontal intensity, the solar intensity upon an arbitrary surface can then be determined following the methods as given in the ASHRAE Handbook (5).

Figure C.1 Two identical rectangular planes parallel to each other

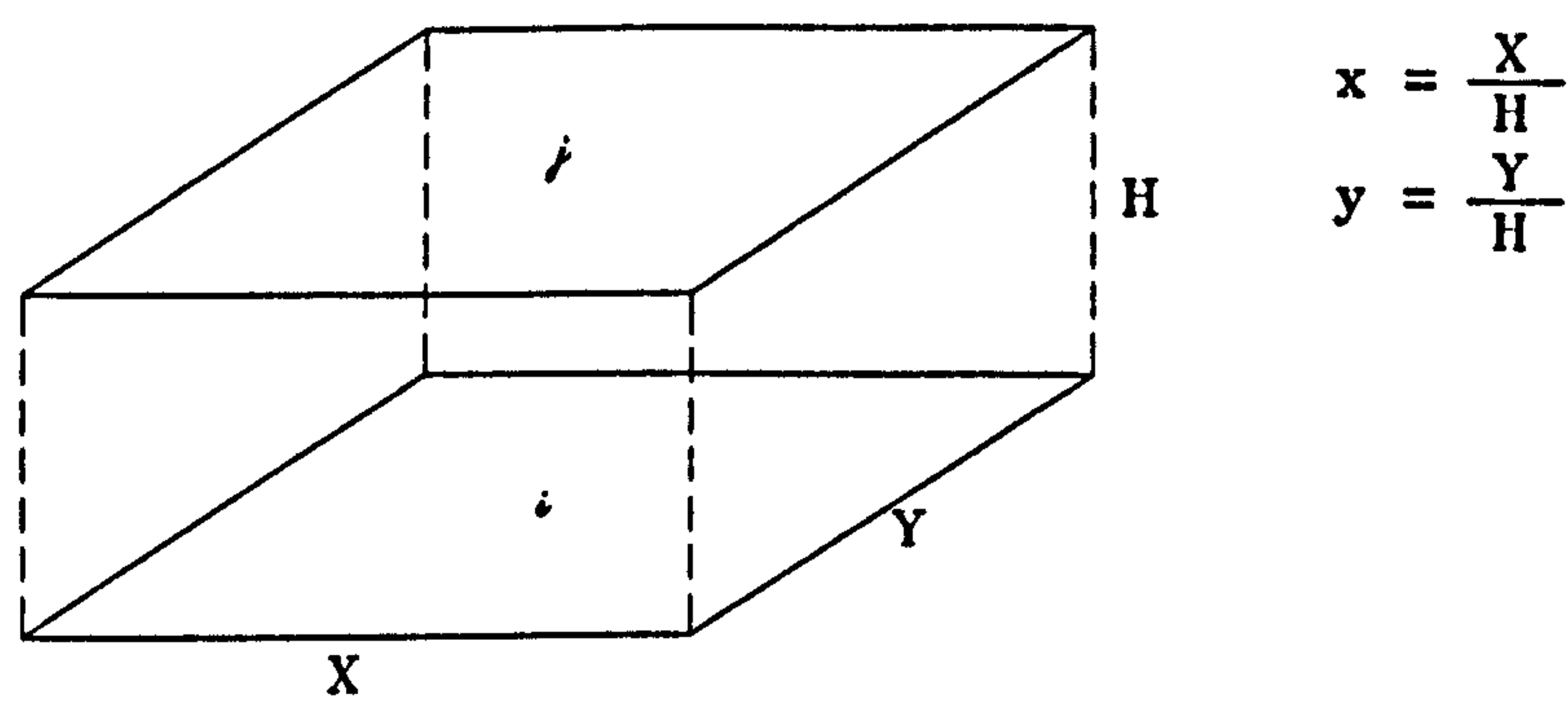


Figure C.2 Two rectangular planes perpendicular to each other and with a common edge

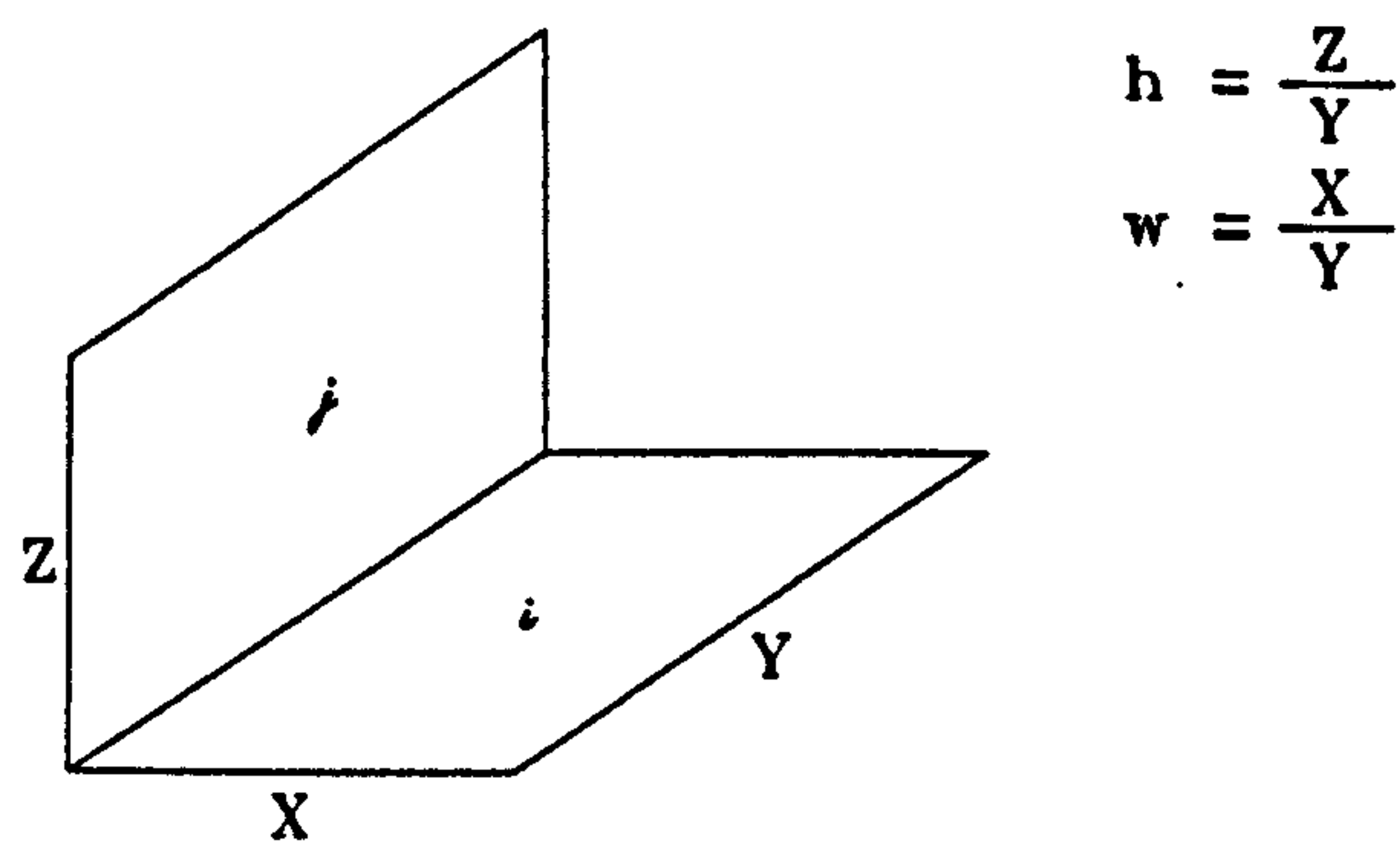


Figure C.3 Two arbitrary planes

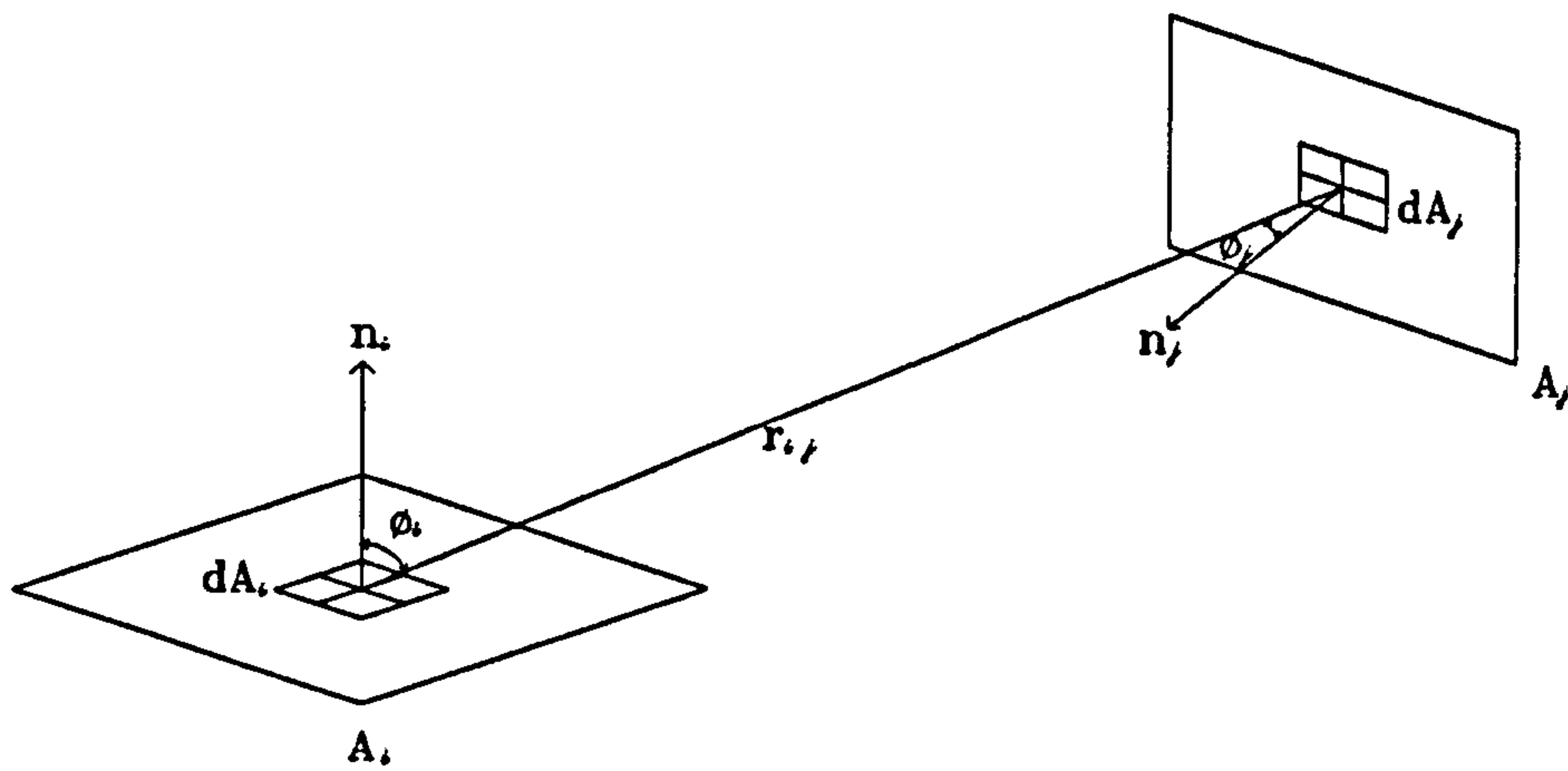


Figure C.4 Two parallel planes with parallel edges

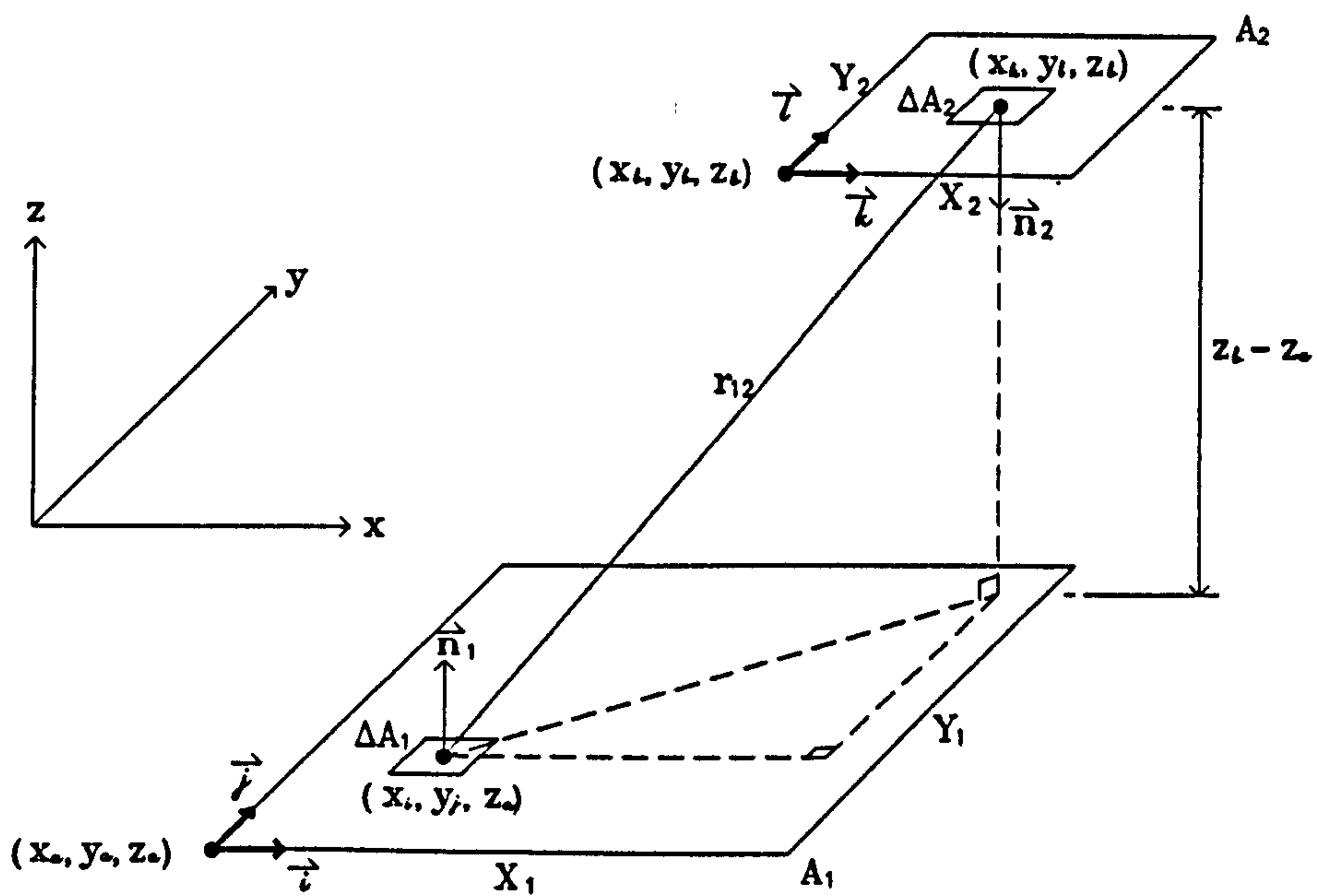


Figure C.5 Two perpendicular planes

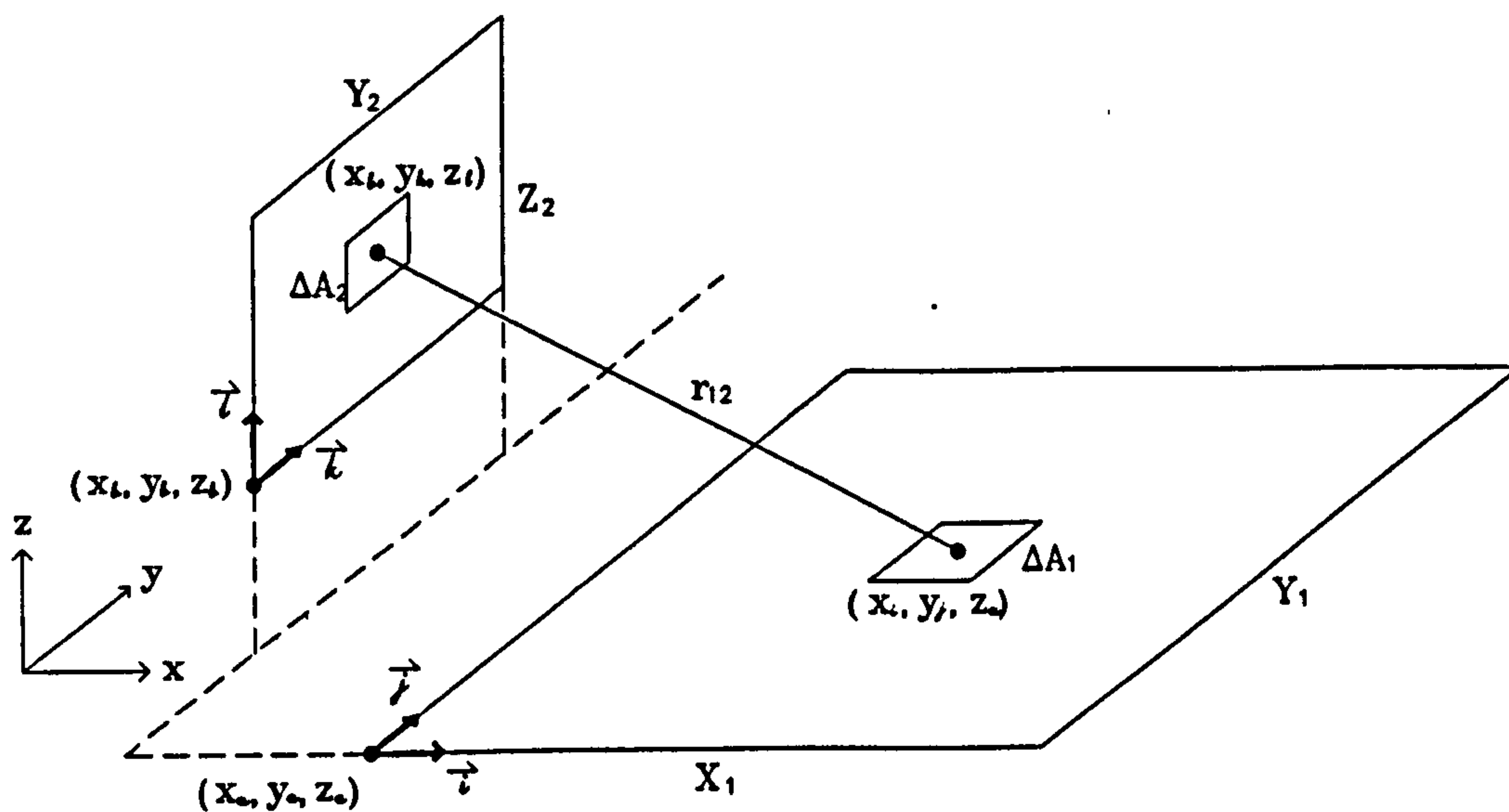
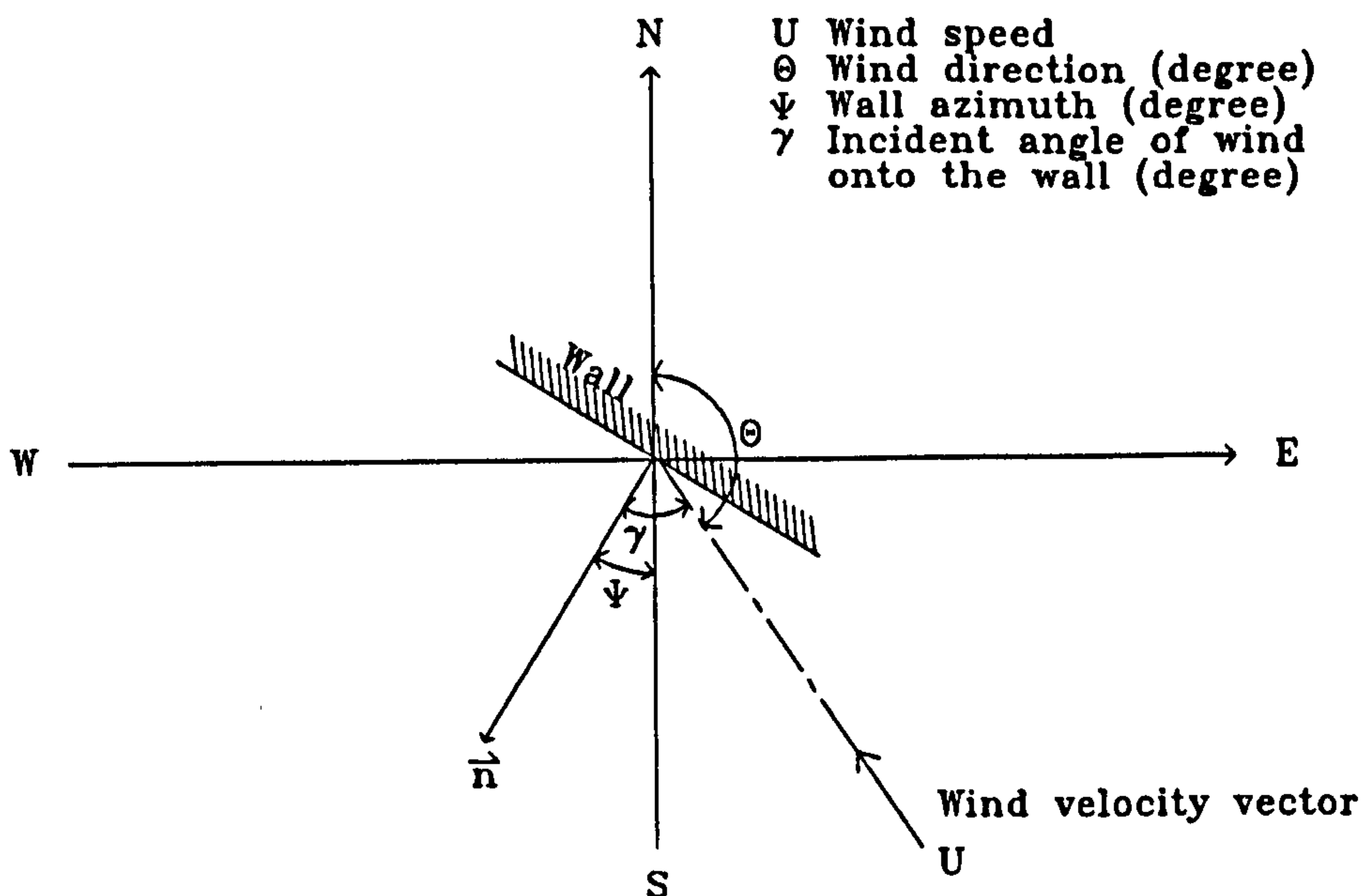


Figure C.6 Wind direction relative to a wall



Appendix D

Publications Originated from this Work

Contents

	Page
D.1 Dynamic Modelling of Indoor Air Humidity	D 2 - D 9
Proc. of Building Simulation '91 Conference, August, 1991, Nice, France, The International Building Performance Simulation Association.	
D.2 A Differential Permeability Model for Simulating Building Heat and Moisture Transfer	D10 - D18
Clima 2000 conference, November, 1993, London, CIBSE.	

DYNAMIC MODELLING OF INDOOR AIR HUMIDITY

F. W. H. Yik

Senior Lecturer

Department of Building Services Engineering
Hong Kong Polytechnic, Hunghom, Hong Kong.

ABSTRACT

This paper describes a computer simulation program being developed at the Hong Kong Polytechnic for dynamic modelling of heat and moisture transport in buildings. At present, the program can simulate simultaneous heat and moisture transfer in the walls and slabs of a room and its effect on the room temperature and humidity. Effects of outdoor weather and air-conditioning are simultaneously simulated. Presented in this paper include: discussions on why indoor humidity modelling is needed; a review of relevant works reported in various literatures; descriptions of the models incorporated into the program; and simulation results obtained by using the room and system models that have been developed.

INTRODUCTION

It is well known that humidity level affects occupants' comfort and performance of air-conditioning systems. When indoor humidity in an air-conditioned room is high, occupants would feel uncomfortable (Fanger 1970) and would try to lower the thermostat set-point so as to retain comfort. This would increase the space heat gain and hence more energy would be consumed for air-conditioning. Besides, prolonged high indoor humidity (>70%) would promote growth of molds and mildews at wall and furniture surfaces which might affect health of occupants and cause deterioration of materials in buildings. When the cooling load or the room sensible heat ratio in an air-conditioned room is low, indoor relative humidity rising above 70% is not uncommon in buildings situated in a place with humid weather like Hong Kong. High indoor humidity will also arise when the air-conditioning system is intermittently operated while there exist moisture sources (e.g. infiltration) during the shut-down period. Moisture adsorption and desorption effects of building materials also play an important role in indoor moisture content changes.

As most building materials like concrete, wood, wall finishes, etc. are porous materials (Whiteley et al. 1977), moisture can migrate into or out of the interstices of the material. This provides a storage capacity for indoor moisture, similar to the thermal storage effect for sensible heat. Part of the moisture brought into or generated within the air-conditioned space will be adsorbed by walls and furnitures which will be released back to the room air when the air-conditioning system is restarted after a night shut-down period. Wong & Wang's measurement (1990) showed that the latent load of an air-conditioned office building and a library in Hong Kong were both over ten times higher than what could be possible due to infiltration and internal sources during the morning start-up period. Since this extra latent load on the air-conditioning systems is seldom accounted for in system design, this may explain why complaints often arise from occupants about insufficient cooling during the morning hours in buildings in Hong Kong.

To address to the increasing user requirements in respect of higher standard of comfort, more stringent specifications of

environmental conditions for process work and the demand for more efficient use of energy, building and air-conditioning system designers must be able to accurately predict the performance of the designed building and systems to ensure that the requirements will be met. The design processes often involve comparison of several alternative designs and selection of the optimal one from them. This is particularly important when innovative design ideas are employed to provide a solution whereas its economic viability needs to be justified. Detail analysis and evaluation of building and systems involve large amount of calculations which need to be carried-out with the aid of a computer and a good simulation program. At present, many building energy calculation and air-conditioning system simulation packages are available, both for commercial use and for research purposes. Unfortunately, except a few that are for research use (see next section), none of them can properly simulate indoor humidity variation due to the simultaneous effects of moisture adsorption and desorption of the building fabric and moisture extraction by the air-conditioning system.

Besides lacking in moisture modelling capability, these packages also have short comings in one way or the other. First, in these packages, values of thermal properties of building materials are often assumed to be constant values. Thermal conductivity of building materials however vary significantly with moisture content whereas the moisture content within the material also varies. For example, the thermal conductivity of a light weight concrete deviates by more than 10% over the normally assumed moisture content range of 3 to 5% (by volume) for a concrete external wall (Stuckes & Simpson 1986). This deviation in thermal property, if not taken into account, could give rise to over or under estimation of the heat flow through the building envelop and thus could lead to wrong sizing of equipment or even wrong choice of system selection. Second, building thermal load is normally calculated first, based on a constant indoor condition, and system performance are then determined based on the load calculated in the first stage. In reality, system performance affects the thermal load in buildings. Accurate estimation of them therefore needs a simultaneous solution (Clarke 1986). Third, radiation energy exchange among internal surfaces of a building zone are often estimated by over-simplified approaches (such as environmental temperatures based on a cubical enclosure with black surfaces (CIBSE 1986)). How a reference temperature should be established for calculation however is still subject to argument (Uyttenbroeck 1990, Davies 1990) and the accuracy of this kind of method is not always good in cases where room configuration is non-typical or when the actual temperature differences among internal surfaces are large.

To address to the local need for an appropriate simulation tool for thermal load and indoor humidity analysis, attempt is being made at the Hong Kong Polytechnic to develop a computer program that can properly model the heat and moisture exchange between the indoor air and the building envelop, and the

heat and moisture extration rate of the air-conditioning system when it is in operation. At present, a simulation program has been developed which is an intermediate result of the work. The theories and approach adopted in development of models in the program are introduced and results of studies obtained by using this program are discussed in the following sections.

SIMULTANEOUS HEAT AND MOISTURE TRANSFER IN BUILDING MATERIALS

As moisture adsorption and desorption at porous building materials has a significant effect on indoor humidity variations, it must be properly modelled in the development of a simulation program for predicting indoor heat load and humidity variations. To do this, the theory of simultaneous heat and moisture transfer in a porous medium has to be employed in the program formulation.

Studies on simultaneous heat and moisture transfer in porous media have been actively pursued by engineers and scientists for more than 50 years and a number of theoretical models had been proposed for its description. Among the earlier works in this subject, those of Philip & DeVries (1957), Luikov (1964, 1966, 1975), Harmathy (1969), Berger & Pei (1973) and Whitaker (1977) provided much insight into the problem. However, to mathematically describe simultaneous heat and moisture transfer in a porous medium and to solve the resultant equations are much more difficult than to model sensible heat transfer alone. First, there are several possible mechanisms (and theories) of moisture transport in porous media, such as liquid diffusion, vapour diffusion, capillary flow, convective transport and evaporation and condensation, and it is well known that temperature gradient across the medium has a significant effect on the moisture flux (Luikov 1966, Harmathy 1969, Whitaker 1977). However, which mechanism is the dominant one in a particular material under a specific set of conditions is often unknown and it is possible that the moisture transport is a combined effect of more than one of these mechanisms. In fact, there is yet no single theory or explanation that is known to be universally adaptable for modelling moisture transfer in porous solids. Second, the moisture transport phenomenon depends also on the pattern of pore size and shape distributions that exist in the porous system and on how the voids are inter-connected but it is extremely difficult to accurately describe these for a real porous solid (Scheidegger 1974). Due to these complications, models invariably are full of hypothesis and assumptions which limit their generality of application.

The other difficulty that is often faced by modellers is the lack of material properties data for use with the moisture transfer models. Value of some transport properties vary drastically with moisture content in the medium, e.g. the moisture diffusivity of simple Fick's Law like models (Bomberg 1974) and the permeability of materials in simple vapour diffusion models (McLean and Galbraith 1988), but precise data are generally lacking or insufficient in the literatures. Also, the kind of required data differs between models developed based on one theory to another and in general they are not inter-convertable.

A comprehensive summary of different theories proposed by various researchers can be found in the report by Kerestecioglu et al (1988). In appendix A of that report, the model equations of the liquid diffusion, capillary flow, and evaporation and condensation theories and those of Luikov's, Philip and DeVries's and Berger and Pei's theories are described. It must also

be mentioned that material properties data and sorption isotherm data for a collection of building materials for use with these models are summarised in another appendix of this report. Data like these for a much wider range of building materials are highly necessary.

Notwithstanding there are still uncertainties in the theories, attempts have recently been made to apply them in investigations of simultaneous heat and moisture transport in buildings. Among various attempts made, the lumped parameter approach appeared to be a popular choice due to its simplicity and analytical solution can be obtained in some simple cases (e.g. Becker & Jaegermann 1982, Cunningham 1983). Tsuchiya (1980) developed a simple model for indoor humidity analysis which was an early attempt. In his model, assumption was made that moisture adsorption and desorption took place only in a thin layer at the building fabric surface. The humidity ratio in the air film at the room fabric surface was related to the moisture content at the surface layer of the material by a simple equation which actually was a piecewise linear fit of the sorption isotherm of the material. The average moisture content at room surfaces however need to be determined experimentally. Kusuda (1983) developed a surface probe for measuring the coefficients for use with Tsuchiya's model. This model is an attractive one due to its simplicity but unfortunately, not much corresponding materials data have been published.

The approach of using a Fick's Law like equation to relate moisture flux to either a moisture concentration or a vapour pressure gradient has been applied in studies on effect of moisture storage of walls on indoor air latent load (e.g. Isetti et al 1988, Wong 1990 and Wong & Wang 1990). Cunningham (1990) has also developed recently a 3-D model using vapour pressure gradient as the driving potential for moisture movement in solids. Problem with this approach is in availability of appropriate data of diffusivity or permeability and they are strongly dependent on the moisture content. Often, constant values were assumed in analyses (e.g. Wong & Wang 1990).

Fairey & Kerestecioglu (1985) have developed a finite element model called MADAM, based on Luikov's differential equations (1964, 1966, 1975), for simulation of simultaneous heat and moisture transfer in building materials. The model is an elaborated one and has been validated against some experimental data. Unfortunately, due to the use of 'Mass Transfer Potential' (Luikov 1964) as the driving potential for moisture movement, not much transport data of materials are available for use with this model. Kerestecioglu, Swami & Kamel (1990) further proposed the 'Effective Moisture Penetration Depth' (EMPD) theory to simplify the analysis. With it, the simple lumped parameter approach can be used and thus would require less effort in the solution process. Unfortunately, the effort for obtaining appropriate values of EMPD could be substantial. Further, as the authors themselves remarked, this concept need to be used with caution and good judgement and different values of EMPD may be required for different operating conditions.

The evaporation and condensation theory has been adopted to formulate mathematical models for describing moisture transport in building materials. Such a model has been proposed by Kerestecioglu & Gu (1990), as an alternative to the Luikov's theory. The equation to be solved is slightly more complex than those of Luikov's theory but more material properties data are available for this type of model (Kerestecioglu et al 1988).

Harmathy (1969) derived a set of partial differential equations for simulation of simultaneous heat and moisture transfer in a porous medium during the pendular stage (no bulk liquid movement) and used them to study drying of a piece of brick. Huang (1979) and Huang et al (1979) also presented similar equations (see next section) and used them to simulate drying of a concrete slab and a slab of cement paste. Their equations were derived based on conservation of mass of vapour moisture and dry air and conservation of energy, resulting in three non-linear partial differential equations. Moisture transport was assumed to take place only in the vapour phase but liquid moisture content within the porous medium would vary due to evaporation or condensation and would affect the rate of vapour transport. Vapour transport mechanisms modelled included vapour diffusion, convective flow, evaporation and condensation and effect of a temperature gradient. The sorption isotherm of the material was employed to relate liquid moisture content to thermodynamic states of the water vapour/air mixture within the pores of the medium and thus provided a closed set of equations.

THE HEAT AND MOISTURE TRANSFER SIMULATION PROGRAM DEVELOPED

General Features

A simulation program is being developed at the Hong Kong Polytechnic for dynamic modelling of simultaneous heat and moisture transport in buildings. At present, the program can be used to simulate variations of indoor temperature and humidity in a simple rectangular room due to the heat and moisture exchanges between the room air and the enclosing walls and slabs (a single-zone model). Simultaneous effects of outdoor weather and air-conditioning on the room fabric and indoor air conditions can be simulated. The room comprises four walls, one ceiling slab and one floor slab. One of the walls can be an external wall with a window on it (see Figure A), which is exposed to incident solar radiation and outdoor air. The wall opposite to the external wall is assumed to be a partition wall separating the room and a corridor with constant air temperature and humidity which may be different from those in the room. The room being modelled is assumed to be a typical cell in a building with identical cells at both sides and at above and below.

Mathematical Models

Wall/Slab Model In the simulation program, heat and moisture transport in individual layers of materials within the walls or slabs are modelled based on the set of non-linear partial differential equations developed by Huang (1979) based on Harmathy's theory (1969). This model is chosen due to its sound theoretical grounds, the variables chosen as heat and moisture transfer driving potentials are continuous across adjoining layers of different materials (and hence the model is readily adaptable to multi-layer analysis), and data for use with this model is relatively more easy to obtain from literatures (Kerestecioglu et al 1988). The equations of the model are of the form as follows:

$$A_i \frac{\partial \phi}{\partial t} + B_i \frac{\partial P}{\partial t} + C_i \frac{\partial T}{\partial t}$$

$$= D_i \frac{\partial^2 \phi}{\partial x^2} + E_i \frac{\partial^2 P}{\partial x^2} + F_i \frac{\partial^2 T}{\partial x^2} + G_i \left(\frac{\partial \phi}{\partial x} \right)^2 + H_i \left(\frac{\partial P}{\partial x} \right)^2 + I_i \left(\frac{\partial T}{\partial x} \right)^2 + J_i \left(\frac{\partial \phi}{\partial x} \cdot \frac{\partial P}{\partial x} \right) + K_i \left(\frac{\partial \phi}{\partial x} \cdot \frac{\partial T}{\partial x} \right) + L_i \left(\frac{\partial P}{\partial x} \cdot \frac{\partial T}{\partial x} \right)$$

for $i = 1, 2 \text{ \& } 3$, denoting respectively conservation equations for mass of vapour, mass of air, and energy; where ϕ is the mole-fraction of vapour in the moist air; P is the moist air pressure; and T the temperature. A_i to L_i are coefficients with values dependent on the local state of the medium, the transport properties of the medium, and the local equilibrium moisture content as governed by the sorption isotherm of the material. Mathematical expressions for evaluation of these coefficients are detailed in Huang's paper (1979).

The set of non-linear partial differential equations has been discretised into a set of algebraic equations using an implicit, backward-in-time finite difference scheme. The set of nodal equations (three algebraic equations for each nodal point) constitutes a finite difference model for the room envelop. The finite difference model has been formulated to enable multi-layered walls and slabs be simulated using the program.

Convective Heat and Moisture Transfer at Wall/Slab Boundary Surfaces Rate of convective heat exchange between the outdoor or room air and the boundary surface of a wall or slab is evaluated using the Newton's Law of Cooling. The convective heat transfer coefficient is determined by using equations given by ASHRAE (1975). For the outdoor side of the external wall, the coefficient is evaluated with reference to the wind speed and direction whereas the indoor side coefficient is determined with reference to the direction of heat flow. Similar to heat transfer, moisture exchange at wall surfaces is calculated based on the surface to air vapour mole fraction difference and a mass transfer coefficient which is determined based on the convective heat transfer coefficient and the Lewis' relationship (Kerestecioglu et al 1988).

Solar Radiation Model Intensities of direct and diffuse solar radiation incident upon the external wall and window is determined based on global solar radiation (total horizontal intensity) data contained in the weather data file. The global solar radiation is first decomposed into direct normal and diffuse components using Kimura's model (1977) and intensities on the external wall are then calculated based on the incident angle at the corresponding time.

Internal Surfaces Radiation Exchange Long wave radiation exchange among internal surfaces in the room are modelled following basic principles of radiation heat transfer among gray surfaces (Incropera and DeWit 1985). To simplify the calculation, both direct and diffuse solar radiation transmitted through the window is assumed to be diffuse radiation which will be distributed to other internal wall or slab surfaces according to the radiation shape factor between the window and individual wall/slab surfaces, as for the long wave radiation.

Window Model The window glass is modelled by a lumped equation (an ordinary differential equation) derived from heat balance at the window glass and backward-in-time finite difference was applied to obtain a numerical model for the window.

Air-conditioning System Model In the program, the air-conditioning system model includes a cooling and dehumidifying

coil model, a control valve model and a simple pipe flow model. The coil model was developed based on detailed theory of heat and moisture transfer between the air stream through the coil and the surface in a finned coil (McQuiston 1989, ASHRAE 1988). Effects of heat capacitance of the coil material and water held in the tubes are at present neglected. Options are available for the valve to be either controlled by an ON/OFF or a Proportional controller. In the present version of the program, time-lag in controller output is also neglected. When proportional control is used, the valve characteristics is assumed to be an equal percentage valve. Flow rate of chilled water through the cooling coil is determined based on hydraulic principles under the condition of a given pump head and pressure losses through the chiller, the pipings, the coil and the control valve corresponding to the flow. Supply chilled water temperature is assumed constant.

Air-node Model The room air condition is also modelled by a lumped parameter approach. Two ordinary differential equations, one for the air-node temperature and the other for the humidity ratio, that were derived respectively from heat and moisture balance in the room air, are used to simulate the air-node condition changes. They are both discretised into finite difference form by backward-in-time finite difference and solved in conjunction with equations for the walls and slabs, the window and the air-conditioning system.

Weather Data A weather data file containing actual hourly records of Hong Kong weather data in Year 1980 has been prepared for use with the simulation program. Outdoor weather parameters include temperature, relative humidity, wind speed and direction and global solar radiation intensity.

Other modules of the program include those for calculating radiation shape factors, radiation heat exchanges among internal wall and slab surfaces, those for psychrometric calculations and general mathematical routines for solution of a non-linear equation, a system of equations and for interpolation of weather data and materials' sorption isotherm data. Cubic spline functions are used in such interpolations.

Numerical Solution of the Mathematical Models

Numerical Solution Scheme Guass-Seidal iteration scheme with under relaxation is employed to solve simultaneously the set of coupled equations for the walls, slabs, the window, the air-conditioning system and the air-node.

Time Step Size Control The equations to be solved by the numerical scheme is a set of highly non-linear equations. Although an implicit finite difference scheme has been used, there is still a limit on time step size (and grid size in walls and slabs) whereas the criterion for its determination is not easy to work out and it also changes with progress of simulation (Huang 1979). In the program, a variable time step control scheme has been incorporated into the program to minimize chances of divergence and to speed up the calculation when the conditions become stabilised. From trial runs with the program, it was found that the time-step size needs to be small at the start of a simulation or after the occurrence of a change of condition like starting/stopping of the air-conditioning system (in the order of minutes when the room is air-conditioned and in the order of seconds when the system is shut-down) but can be larger as the simulation proceeds. In the program, the time step can be lengthened during the simulation run at the user specified rate until the time step reaches the maximum

value specified by the user. When convergence is not achieved after a maximum number of iterations, the time step size will be halved and this continues until convergence is achieved or when the time step size is reduced to the minimum size in which case simulation time will be brought backward by a number of time steps and simulation will be resumed from there starting with the minimum time step size. This adaptive time step size control worked reasonable well in the trial runs.

SIMULATION STUDIES USING THE PROGRAM

General

The simulation program had been used to model dynamic heat and moisture transfer in a typical room at the perimeter of a hypothetical building situated in Hong Kong. Geometric configuration of the room was as shown in Figure A.

Construction, Material Properties and Initial and Operation Conditions The model room was 3m (W) x 3m (D) x 3m (H) in size with a 3m (W) x 1.5m (H) window at the South-facing external wall (wall 1). All walls and slabs were composite walls, each constructed of 100mm thick concrete with 13mm cement plastering at each side. The window was of 6mm thick single pane glass. Properties and initial conditions of the wall/slab materials and window glass used in the calculations were as summarized in Table 1.

The indoor set-point conditions, conditions in the corridor (outside of Wall 3, fixed) and indoor design parameters were assumed to be:

Room air set-point condition	temperature	:	298 K
	rel. humidity	:	50%
Corridor air condition (fixed)	temperature	:	300 K
	rel. humidity	:	65%
Number of occupant	:	1 person	
Ventilation rate	:	7 l/s	
Infiltration rate	:	1/2 air-change per hour (continuous)	
Lighting load	:	225 W	
Air-conditioned hrs.	:	8:30 to 17:00	
Occupied hrs.	:	9:00 to 17:00 (occupants in and lights on)	

Discretisation of Walls/Slabs In the numerical simulation study with the model room, the external plastering, the concrete core and the internal plastering layer of each wall and slab were discretised respectively into 5, 15 and 5 sub-layers resulting in a total of 26 nodal points for each wall/slab and a total of 156 wall nodes for the entire room. Node number 1 and 26 are surface nodes whereas node number 6 and 21 are interface nodes between the plastering layers and the concrete core.

Design Cooling Load of the Room Design cooling load of the model room had been calculated according to ASHRAE's cooling load calculation method (ASHRAE 1989) and design data for Hong Kong. U-values used in the calculation were determined based on thermal conductivities of the wall and slab materials, with liquid moisture content as given in Table 1. This effective thermal conductivity was evaluated based on Kingery' empirical formula (see Huang's paper 1979).

Results of the calculation were as follows:

Peak Time : 14:00 Oct.

Peak Cooling Load (W):

Components	Sens.	Lat.	Total
Solar	783	0	783
Conduction (Glass)	175	0	175
Conduction (Wall)	263	0	263
Occupants	65	55	120
Lighting	225	0	225
Infiltration	33	129	162
Room Total	<u>1544</u>	<u>184</u>	<u>1728</u>
Ventilation	61	240	301
Block Total	<u>1605</u>	<u>424</u>	<u>2029</u>

Table 1 Properties and initial conditions of wall materials of the model room

Properties	Concrete	Plastering	Glass
Dry density (kg/m ³)	2600	2200	2500
Dry thermal conductivity (W/mK)	1.44	1.44	1.05
Porosity (m ³ /m ³)	0.3	0.43	-
Dry specific heat (J/kgK)	879	879	750
Permeability of air at dry state (m ²)	2.5x10 ⁻¹⁴	2.5x10 ⁻¹⁴	-
Initial moisture content (m ³ /m ³)	0.05	0.15	-
Initial temperature (K)	300	300	300
Emmisivity of surface (long wave radiation)	0.8	0.8	0.8
Absorptance (short wave radiation)	-	-	0.2
Transmittance (short wave radiation)	-	-	0.4
Shading coefficient	-	-	0.53

Air Conditioning System Based on the design load calculation result, a fan-coil unit was selected for the model room. Charateristics of the selected unit were as follows:

Supply air flow rate	:	0.125 m ³ /s
Chilled water supply flow rate (valve open)	:	0.12 kg/s
Chilled water supply temperature (assumed)	:	280 K

Coil characteristics:-

No. of rows :	3
Fin spacing :	2 mm
Face area:	0.12 m ² (600 mm x 200 mm)

No. of circuits :	1.5
No. of tubes per row :	10
Dia. of tubes :	9.53 mm / 8 mm (outer/inner)
Tube spacing :	20 mm / 20mm (transverse/longitudinal)
Fin thickness :	0.15 mm
Rated sensible cooling capacity :	1684 W
Rated total cooling capacity :	2196 W

Fresh air supply at outdoor condition was assumed to be ducted to the return plenum of the fan-coil units at which it would mix with the return air. Chilled water flow through the fan-coil unit was assumed to be controlled by an ON/OFF controller with on/off settings at ± 1 °C about the set-point.

Simulation Results

Results of three simulation runs are presented here. Before that, a simulation run had been performed over the period of 0:00 on 1st July to 8:30 on 4th of July, with the room air conditions fixed at the set-point conditions, to allow the room fabric to attain relatively steady conditions. The first simulation run started from 8:30 on 4th July till 17:00 of the same day but with the room air-conditioned by the fan-coil system with ON/OFF control. This was for investigating effect of air-conditioning on the indoor conditions during the normal operating hours. The second run started from 17:00 till 8:30 on 5th July with no air-conditioning, for investigating rate of moisture build-up during the shut-down period. The third run continued from ending time of the second run till noon time of the same day, for investigating effectiveness of the air-conditioning system during the pull-down operation.

Run No.1 (Normal Operation) During the normal operating hours, the air-conditioning system was able to limit the room temperature from rising or falling outside of the control differential of 298 ± 1 K (Figure B.1) while the moisture content in indoor air was kept rather steadily at a level of about 0.0105 kg/kg (Figure B.2). Expanding the time scale showed that both the room temperature and moisture content actually were not as steady but were fluctuating due to the effects of ON/OFF control (Figure B.3 & B.4).

Run No.2 (Shut-down Period) When the air-conditioning system was shut-down, the room temperature quickly rose to about 302 K in 15 minutes (Figure C.1). The indoor air moisture content also started to rise but at a rate that was much slower than temperature (Figure C.2). The increase in room temperature steadied-down in about an hour after air-conditioning was stopped (Figure C.3) but indoor moisture content continued to rise steadily to about 0.0125 kg/kg just before re-starting time of the air-conditioned period in the following day (Figure C.4). Due to sun rise in the early morning whilst air-conditioning was only started at 8:30, the indoor temperature further rose to above 303 K during this period (Figure C.3).

Run No.3 (Pull-down Period) When air-conditioning resumed in the next day, the room temperature dropped quickly from around 303 K back to within the controlled range but fluctuated rather rapidly, which was the result of the ON/OFF control (Figure D.1). The moisture content also dropped rather rapidly at the start but it slowed down after the first several minutes from re-starting of the air-conditioning system (Figure D.2). In contrast to the room temperature which remained rather steady

after the first 30 minutes (Figure D.3), it took about two hours for moisture content to attain a steady level (Figure D.4).

DISCUSSIONS

From the simulation results, the effects of moisture storage at building walls and slabs were found to be significant. In the shut-down period, the results (run No.2) demonstrated that the indoor moisture content only rised by a small extent. Had there been no adsorption of moisture at wall surfaces, the indoor moisture should have risen quickly to a level close to the outdoor condition due to the continued infiltration of humid outdoor air into the room. The adsorbed moisture were released from wall surfaces back into the room air when the air-conditioning was re-started in the next day. As opposed to thermal storage, effects of moisture storage on indoor air moisture content was much slower and the pull-down period required to bring indoor conditions back to the desired range took a much longer time than to bring temperature alone back to the controllable range (run No.3). If this moisture adsorption and desorption effect is not accounted for in predicting indoor conditions and evaluating performance of the air-conditioning system, erroneous results will be obtained.

The results demonstrated that analyses of indoor air humidity transients can be carried-out with the program developed and further analyses including conditions in days with more humid or colder weather, effects on energy for air-conditioning, effects of other type of control systems etc. can also be investigated by using the program. The method adopted in describing the moisture adsorption and desorption effects of the walls and slabs (Huang's equations) however appeared to be too complicated for long term simulation analysis as it took a very large computational effort in the simulation calculations. In the simulation studies reported here, the CPU time required (using a 486 machine) was as long as the simulated time. A simpler model for use in year-round simulation studies is therefore necessary but the detailed model is still a valuable tool for detailed, storter term studies and could serve as a reference model for checking accuracy of the simpler model.

ACKNOWLEDGEMENT

The work reported here was sponsored by the Hong Kong Polytechnic as a staff development program for the author. The work was registered as a research degree programme at the Newcastle Upon Tyne Polytechnic, UK. The author thanks Dr. C. P. Underwood, Dr. A. J. Newall, Dr. W. K. Chow, Dr. J. Burnett and his colleagues in the Department of Building Services Engineering, Hong Kong Polytechnic, for their kind support towards his work.

REFERENCES

- ASHRAE (1975) Subroutine Algorithms for Heating & Cooling Loads to Determine Building Energy Requirements, ASHRAE, USA.
- ASHRAE Handbook (1988) Equipment, ASHRAE, USA.
- ASHRAE Handbook (1989) Fundamentals, ASHRAE, USA.
- Becker, R and Jaegermann, C (1982) The Influence of Permeability of Materials and Absorption on Condensation in Dwellings, Bldg. Envir. 17(2) pp.125-134.
- Berger, D, and Pei, D C T, (1973) Drying of Hygroscopic Capillary Porous Soilds - A Theoretical Approach, Int. J. Heat Mass Transfer, Vol.16, pp.293-302.
- Bomberg, M (1974) Moisture Flow Through Porous Building Materials, Report 52, Division of Building Technology, Lund Institute of Technology, Sweden.
- CIBSE (1986) Guide Vol. A. The Chartered Institution of Building Services Engineers, UK.
- Clarke, J A (1986) Simulation of Building Energy Systems, Proc. CIB 5th Int. Sym., Bath, 1986, pp.118-133, CIBSE, UK.
- Cunningham, M J, (1983) A New Analytical Approach to the Long Term Behaviour of Moisture Concentrations in Building Cavities - I Non-condensing Cavity, Bldg Envir. 18(3), pp. 109-116.
- Cunningham, M J, (1990) Modelling of Moisture Transfer in Structures - I. A Description of a Finite-Difference Nodal Model, Bldg Envir. 25(1), pp. 55-61.
- Davies, M G, (1990) Mean Radiant Temperature in the CIBSE Guide, BSER&T 11(2), pp.69-71, CIBSE, UK.
- Fairey, P W, and Kerestecioglu, A (1985) Dynamic Modelling of Combined Thermal and Moisture Transport in Buildings: Effects on Cooling Loads and Space Conditions, ASHRAE Trans. V.91, Pt.2A, pp.461-472.
- Fanger, P O (1970) Thermal Comfort Analysis and Applications in Environmental Engineering, McGraw-Hill Book Company.
- Harmathy, T Z, (1969) Simultaneous Moisture and Heat Transfer in Porous Systems with Particular Reference to Drying, I&EC Fundamentals, 8(1), pp. 92 - 103.
- Huang, C L D, (1979) Multi-phase Moisture Transfer in Porous Media Subjected to Temperature Gradient, Int. J. Heat Mass Transfer, Vol. 22, pp. 1275 - 1307.
- Huang, C L D, Siang, H H, and Best, C H, (1979), Heat and Moisture Transfer in Concrete Slabs, Int. J. Heat Mass Transfer, Vol.22 pp. 257-266.
- Isetti, C, Laurenti, L and Ponticiello, (1988) Predicting Vapour Content of the Indoor Air and Latent Loads for Air-conditioned Environments: Effect of Moisture Storage Capacity of the Walls, Energy and Buildings, 12(1988), pp.141-148.
- Incropera, F P and DeWitt, D P, (1985) Fundamentals of Heat and Mass Transfer, 2nd ed., John Wiley & Sons.
- Kerestecioglu, A, Swami, M, Dabir, R, Razzaq, N and Fairey, P, (1988) Theoretical and Computational Investigation of Algorithms for Simultaneous Heat and Moisture Transport in Buildings, Final Report to US DOE Cotract #DE-FC03-86SF16305 and GRI Contract #5087-243-1515, FSEC-CR-191-88.
- Kerestecioglu, A, Swami, M, and Kamel, A (1990) Theoretical and Computational Investigation of Simultaneous Heat and Moisture Transfer in Buildings: "Effective Penetration Depth" Theory, ASHRAE Trans. V.96, Pt.1, ASHRAE USA.
- Kerestecioglu, A, and Gu, L, (1990) Theoretical and Computational Investigation of Simultaneous Heat and Moisture Transfer in Buildings: 'Evaporation and Condensation' Theory, ASHRAE Trans. Vol.96, Pt.1, ASHRAE USA.
- Kimura, K I (1977) Scientific Basis of Air-conditioning, Applied Science Publishers Ltd., London.
- Kusuda, T (1983) Indoor Humidity Calculations, ASHRAE Trans. V.89 Pt.2, ASHRAE, USA.
- Luikov, A V (1964) Heat and Mass Transfer in Capillary Porous Bodies, Advances in Heat Transfer, V.1, Academic Press.

Luikov, A V (1966) Heat and Mass Transfer in Capillary Porous Bodies, Pergamon Press.

Luikov, A V (1975) Systems of Differential Equations of Heat and Mass Transfer in Capillary Porous Bodies (review), Int. J Heat Mass Transfer, V.18, pp.1-14.

McLean, R C and Galbraith, G (1988) Interstitial Condensation: Applicability of Conventional Vapour Permeability Values, BSER&T 9(1) pp.29-34, CIBSE, UK.

McQuiston, F C and Parker, J D (1988) Heating, Ventilating, and Air-conditioning Analysis and Design, 3rd ed., John Wiley & Sons.

Philip, J R, and DeVries, D R, (1957) Moisture Movement in Porous Media under Temperature Gradients, Trans. Am. Geophysical Union, 38(2), pp.222-232.

Scheidegger, A E, (1974) The Physics of Flow Through Porous Media, 3rd Ed., University of Toronto Press, Toronto.

Stuckes, A D and Simpson, A (1986) Moisture Factors and Thermal Conductivity of Concrete, BSER&T 7(2), pp.73-77, CIBSE, UK.

Tsuchiya, T (1980) Infiltration and Indoor Air Temperature and Moisture Variation in a Detached Residence, JSHASE Japan, 54(11), pp.13-19.

Whitaker, S (1977) Simultaneous Heat Mass and Momentum Transfer in Porous Media: A Theory of Drying, Advances in Heat Transfer, Vol 13, pp. 119-203.

Whiteley, P, Russman H D, and Bishop, J D, (1977) Porosity of Building Materials - a Collection of Published Results, Building Research Establishment Current Paper, CP21/77, Building Research Establishment, Department of the Environment, UK.

Wong, S P W, (1990) Simulation of Simultaneous Heat and Moisture Transfer by Using the Finite Difference Method and Verified Tests in a Test Chamber, ASHRAE Trans. V.96, Pt 1, ASHRAE, USA.

Wong, S P W, and Wang, S K, (1990) Fundamentals of Simultaneous Heat and Moisture Transfer Between the Building Envelop and the Conditioned Space Air, ASHRAE Trans. V.96, Pt 2, ASHRAE, USA.

Uyttenbroeck Ir, J (1990) Building Heat Loss Calculations: Choice of Internal Temperature and of Heat Exchange Coefficient h_i , BSER&T 11(2), pp.49-56, CIBSE, UK.

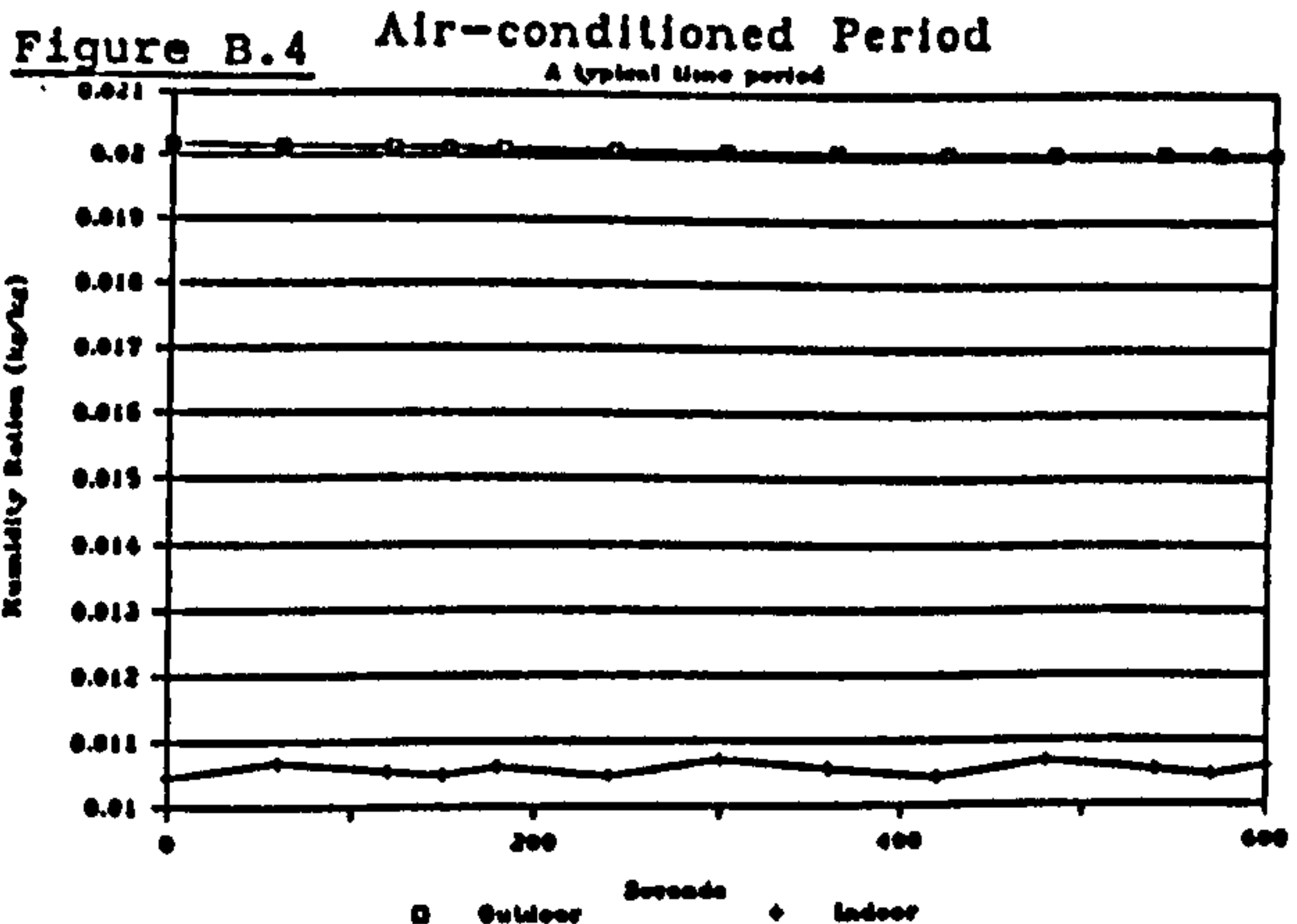
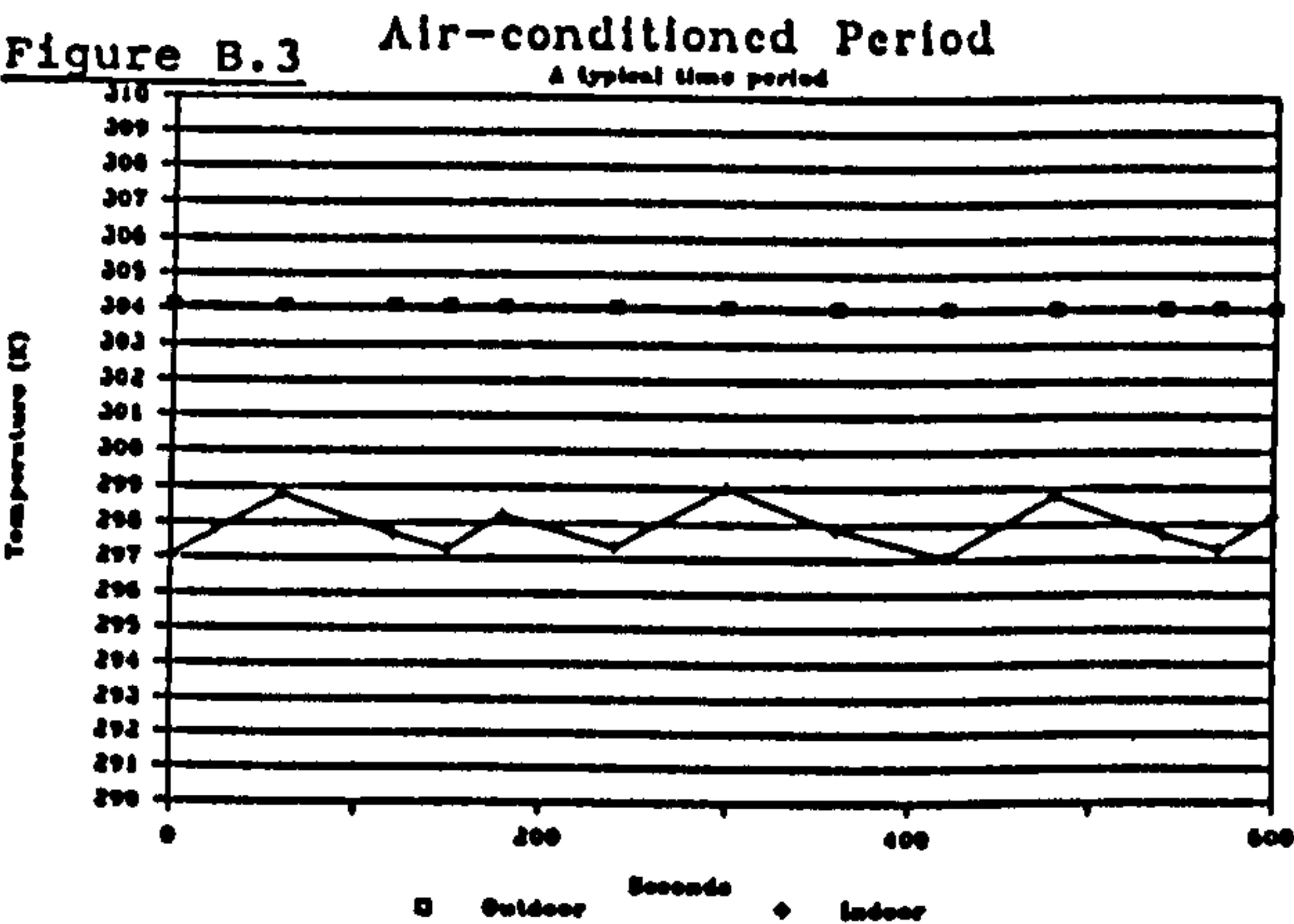
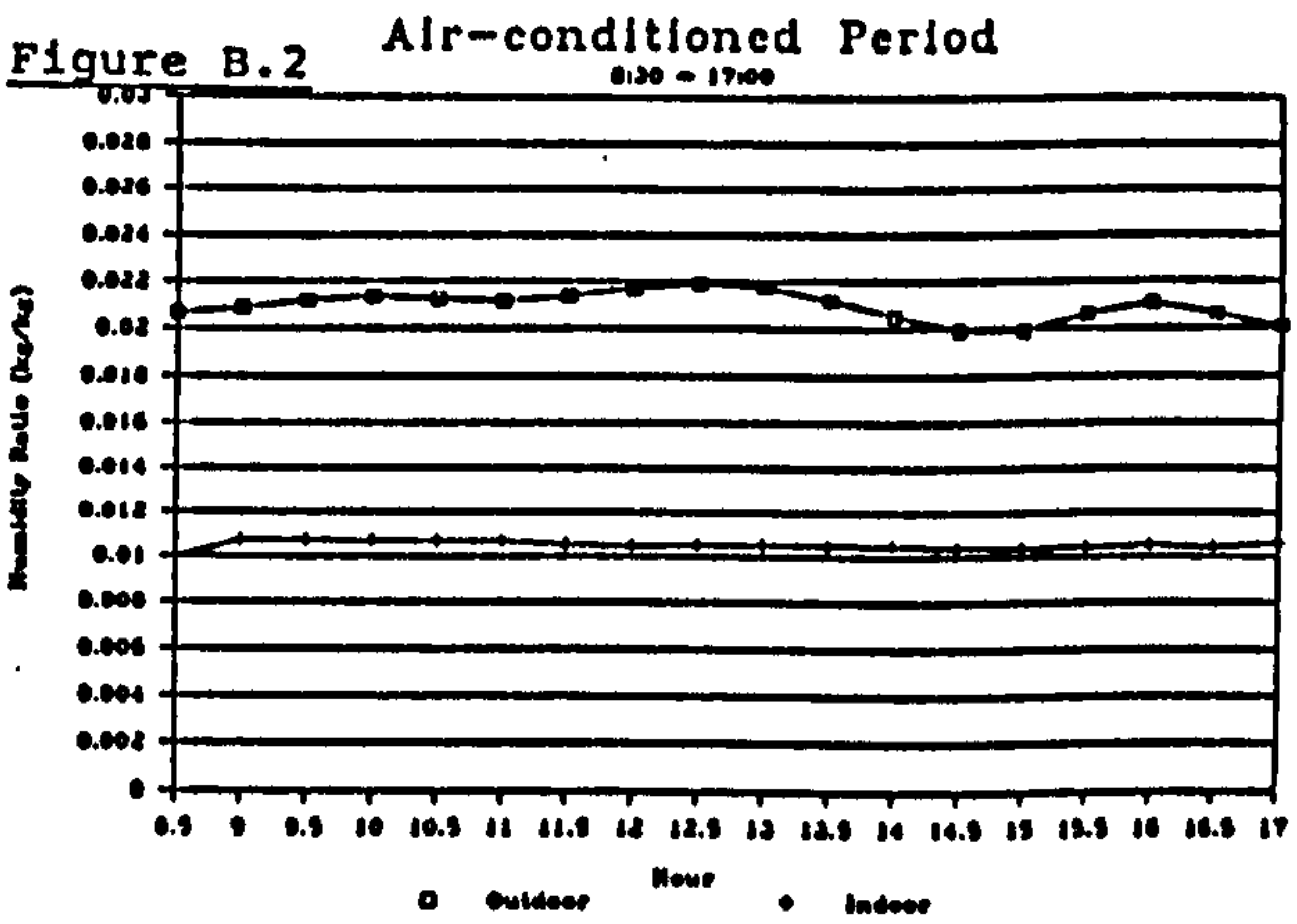
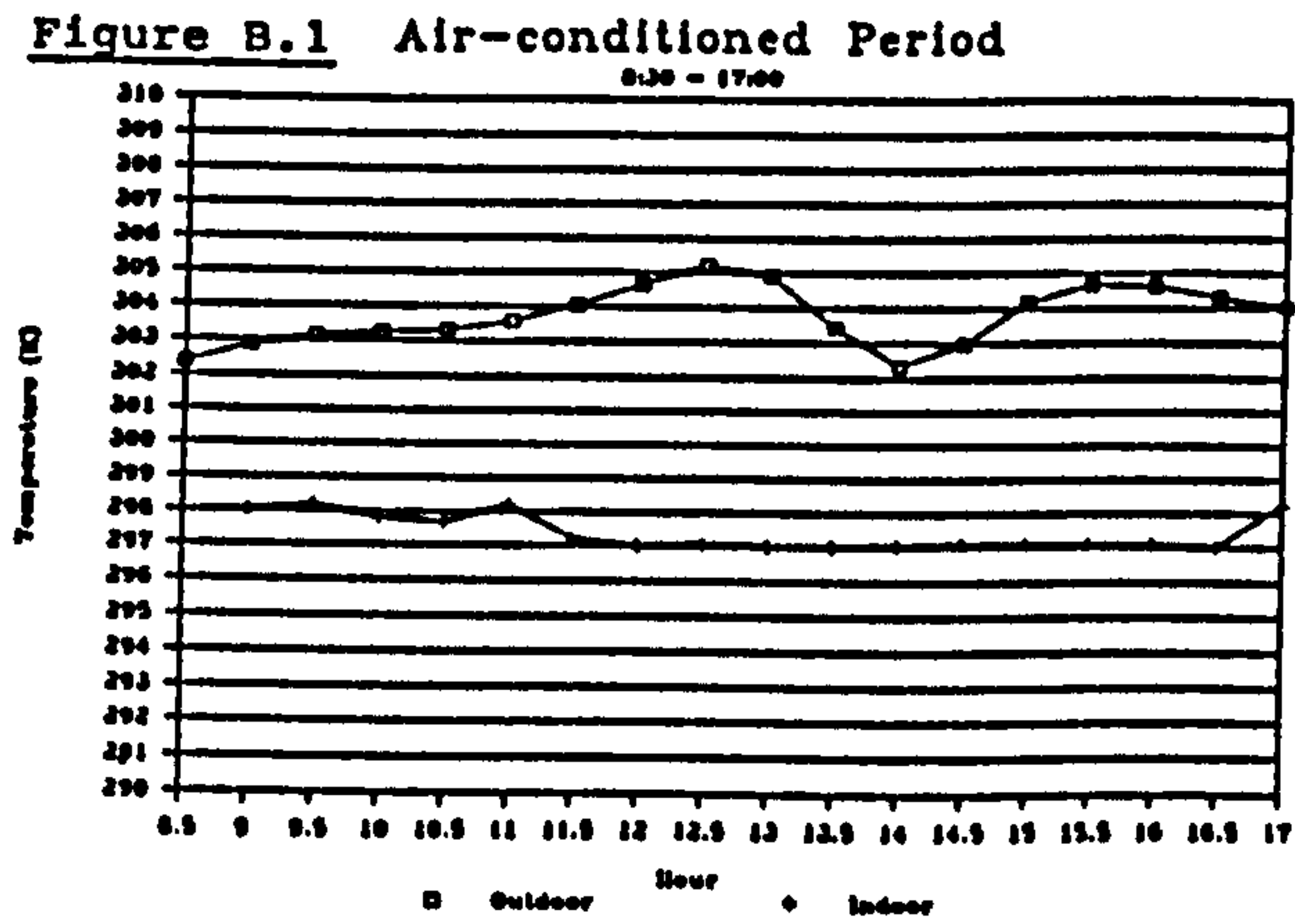
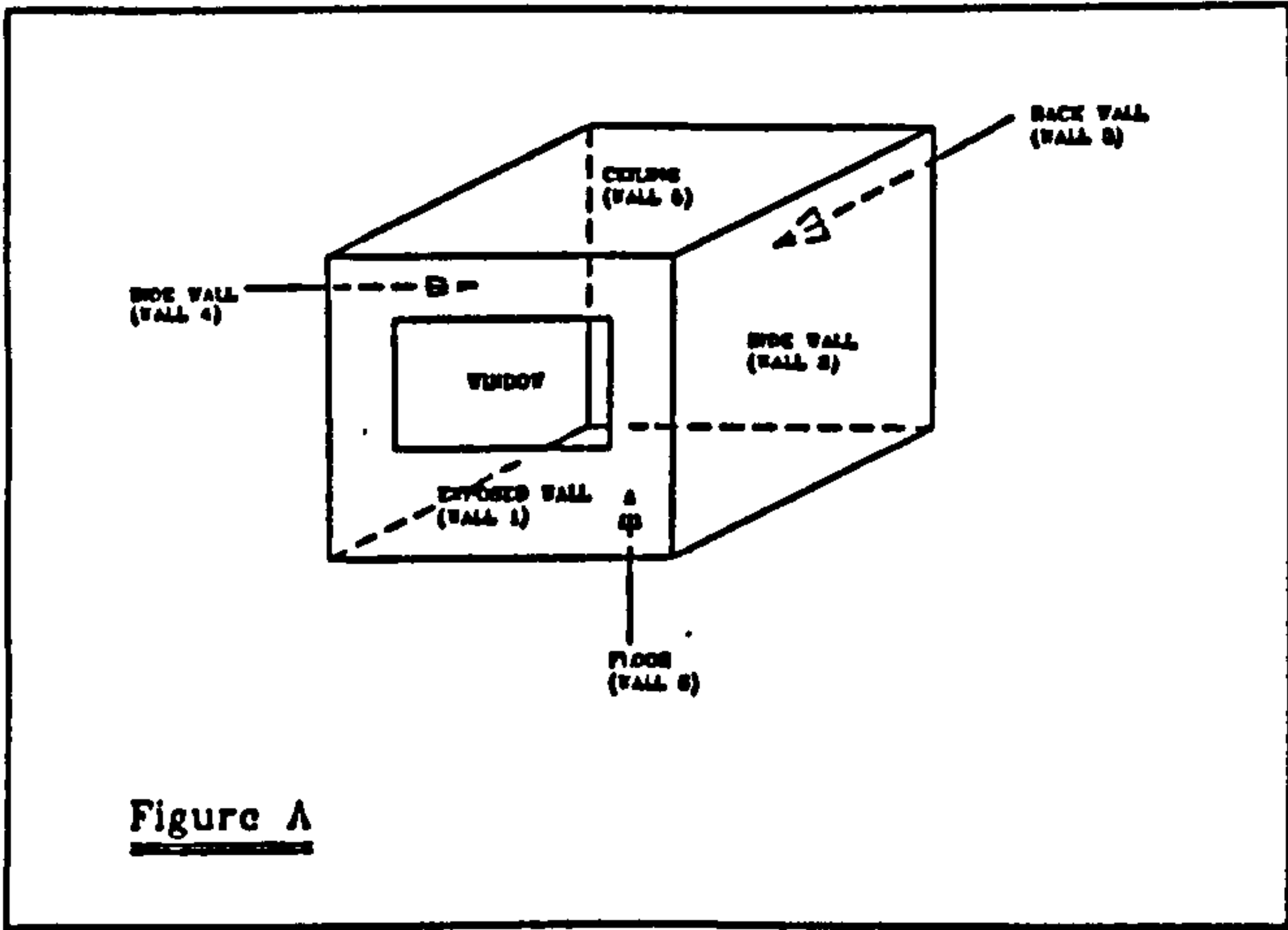


Figure C.1 Shut-down Period
17:00 - 17:30

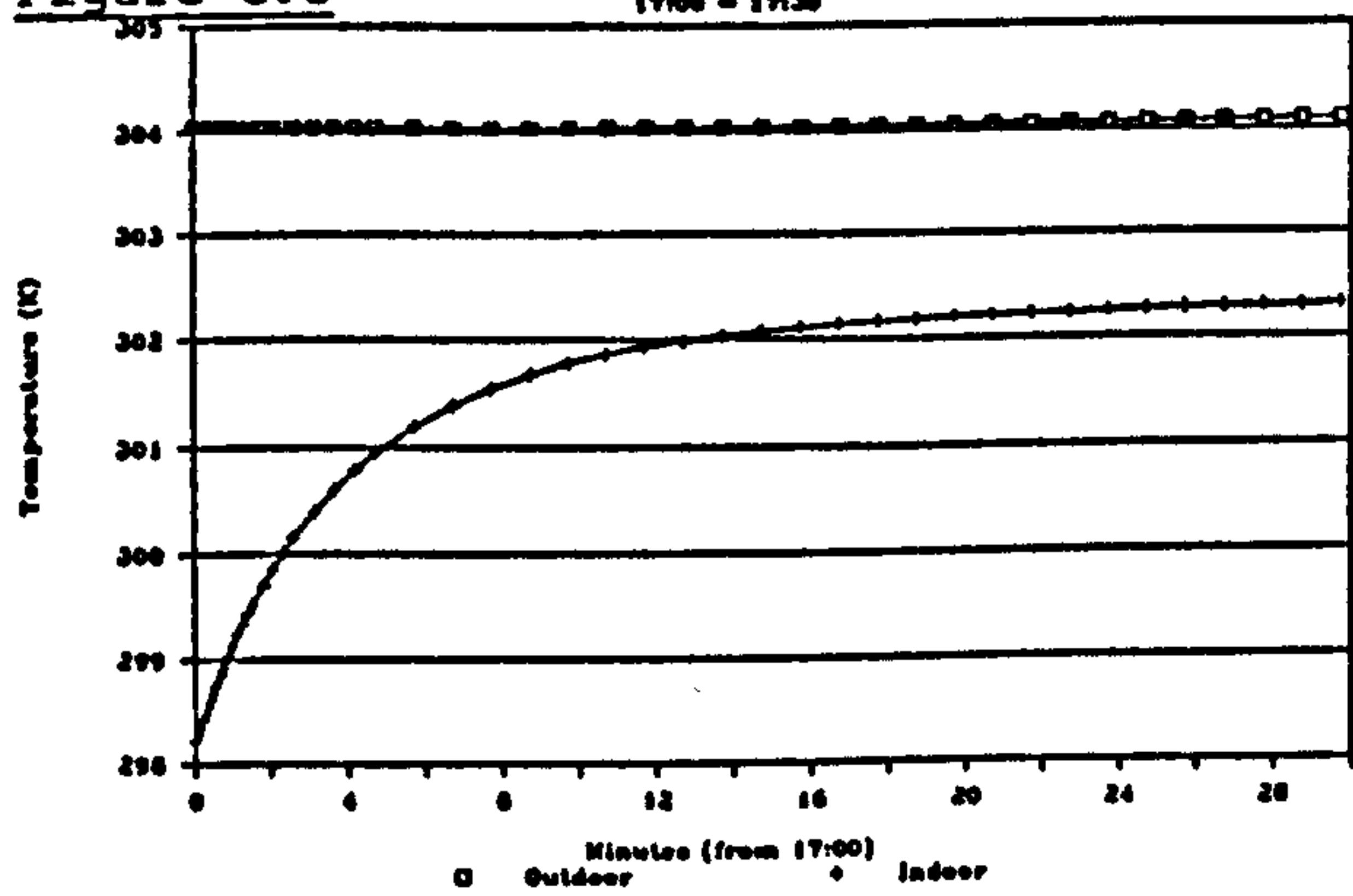


Figure C.2 Shut-down Period
17:00 - 17:30

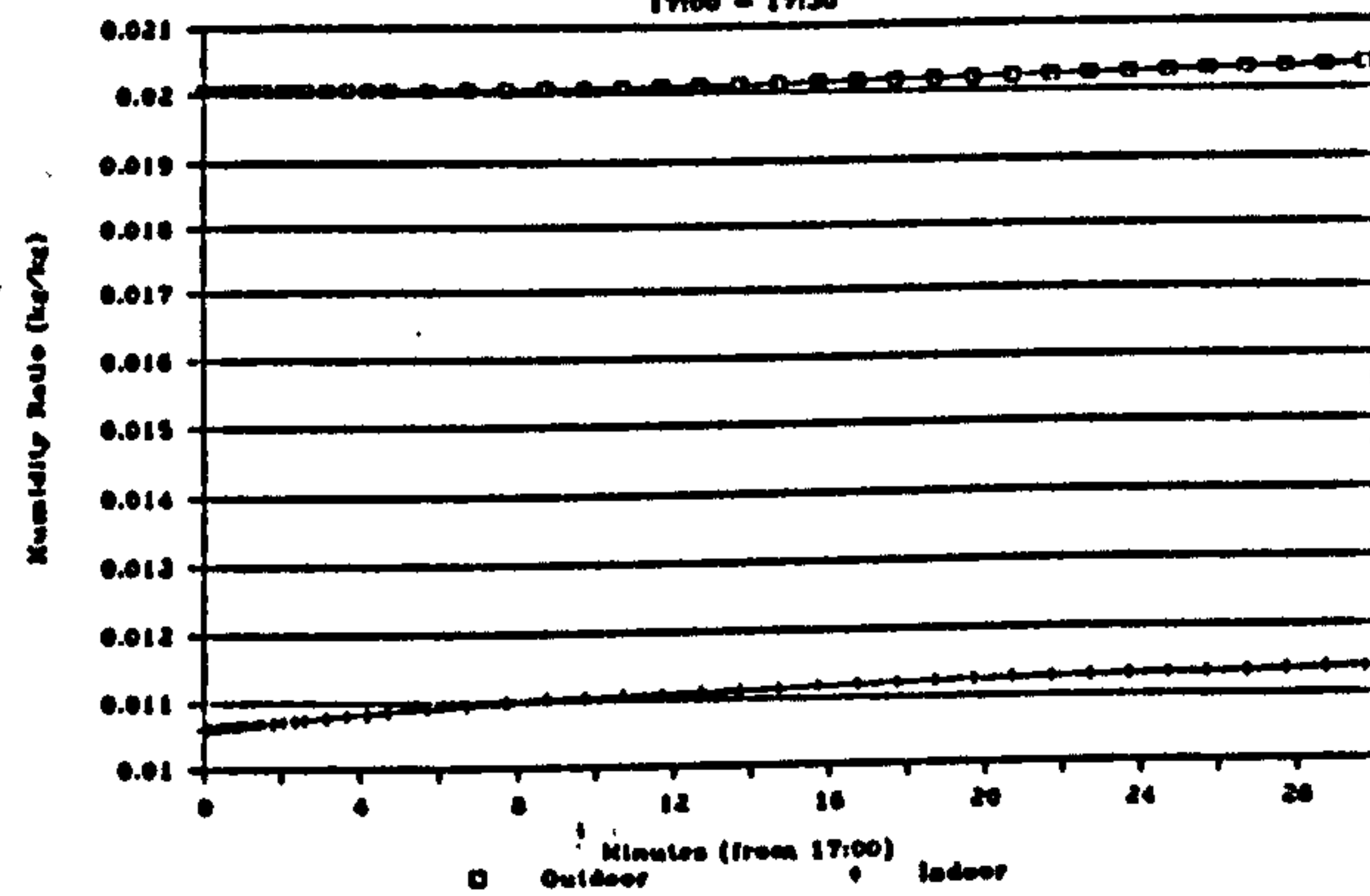


Figure C.3 Shut-down Period
17:30 - 8:00

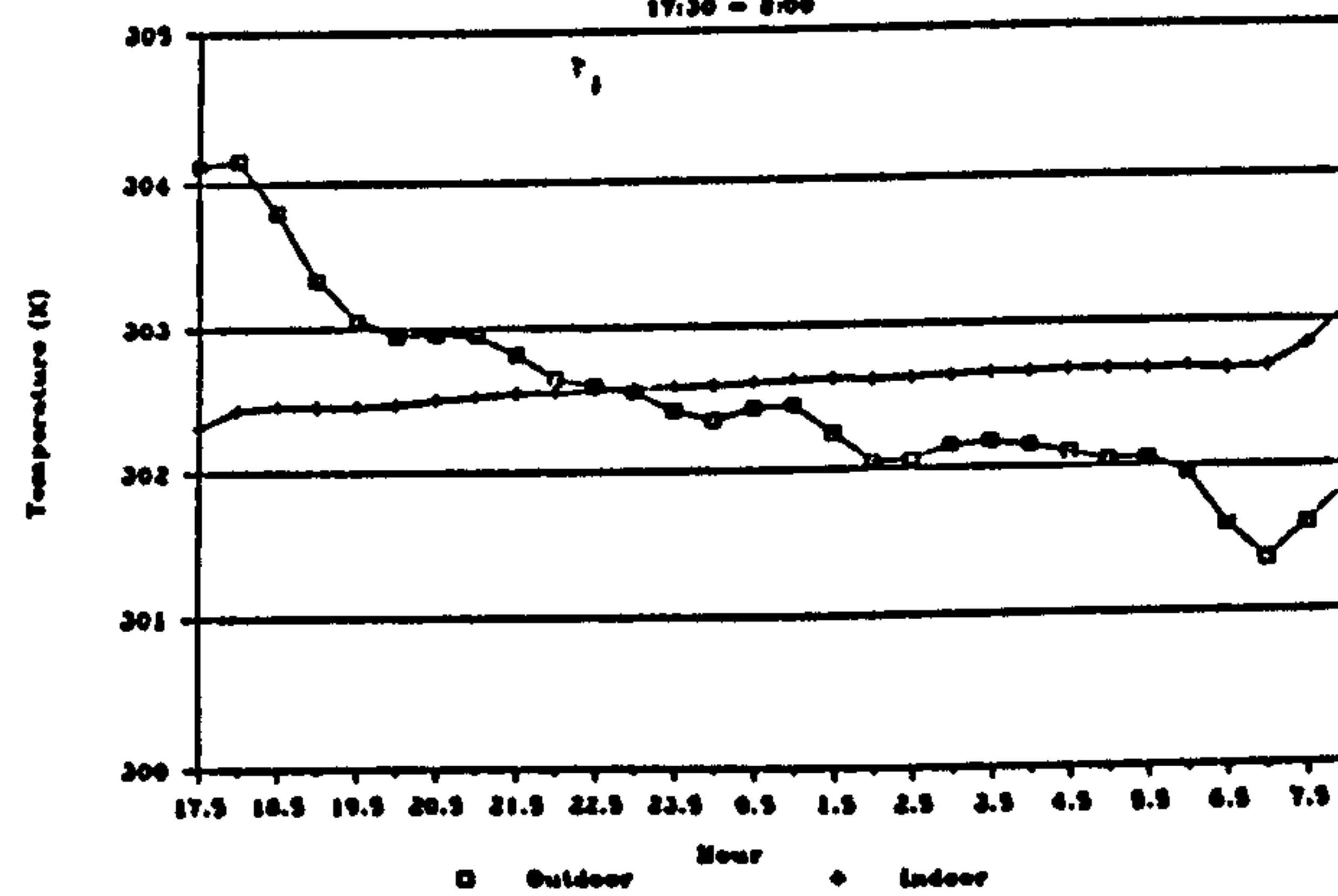


Figure C.4 Shut-down Period
17:30 - 8:00

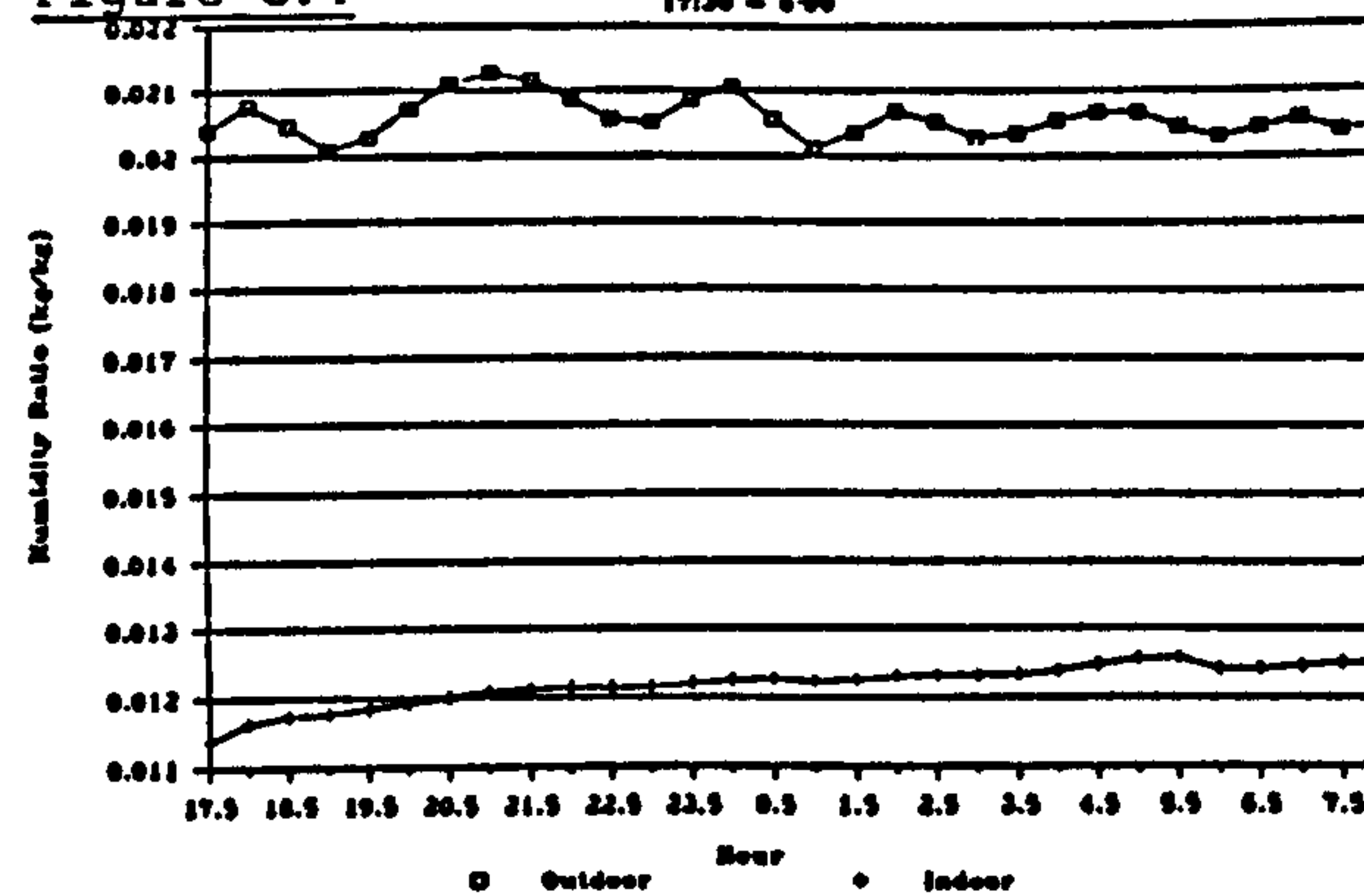


Figure D.1 Pull-down Period
8:30 - 9:00 5th July

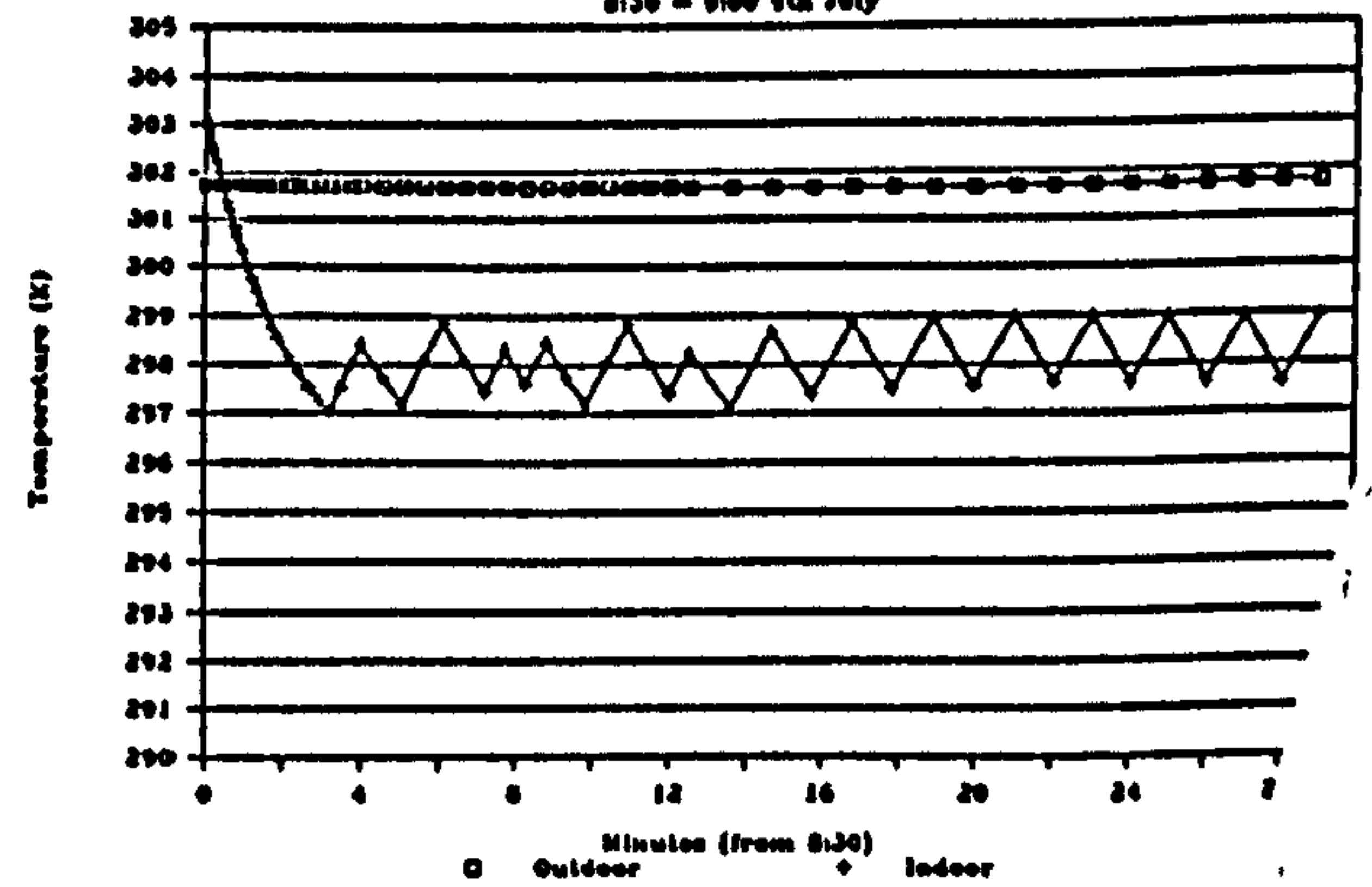


Figure D.2 Pull-down Period
8:30 - 9:00 5th July

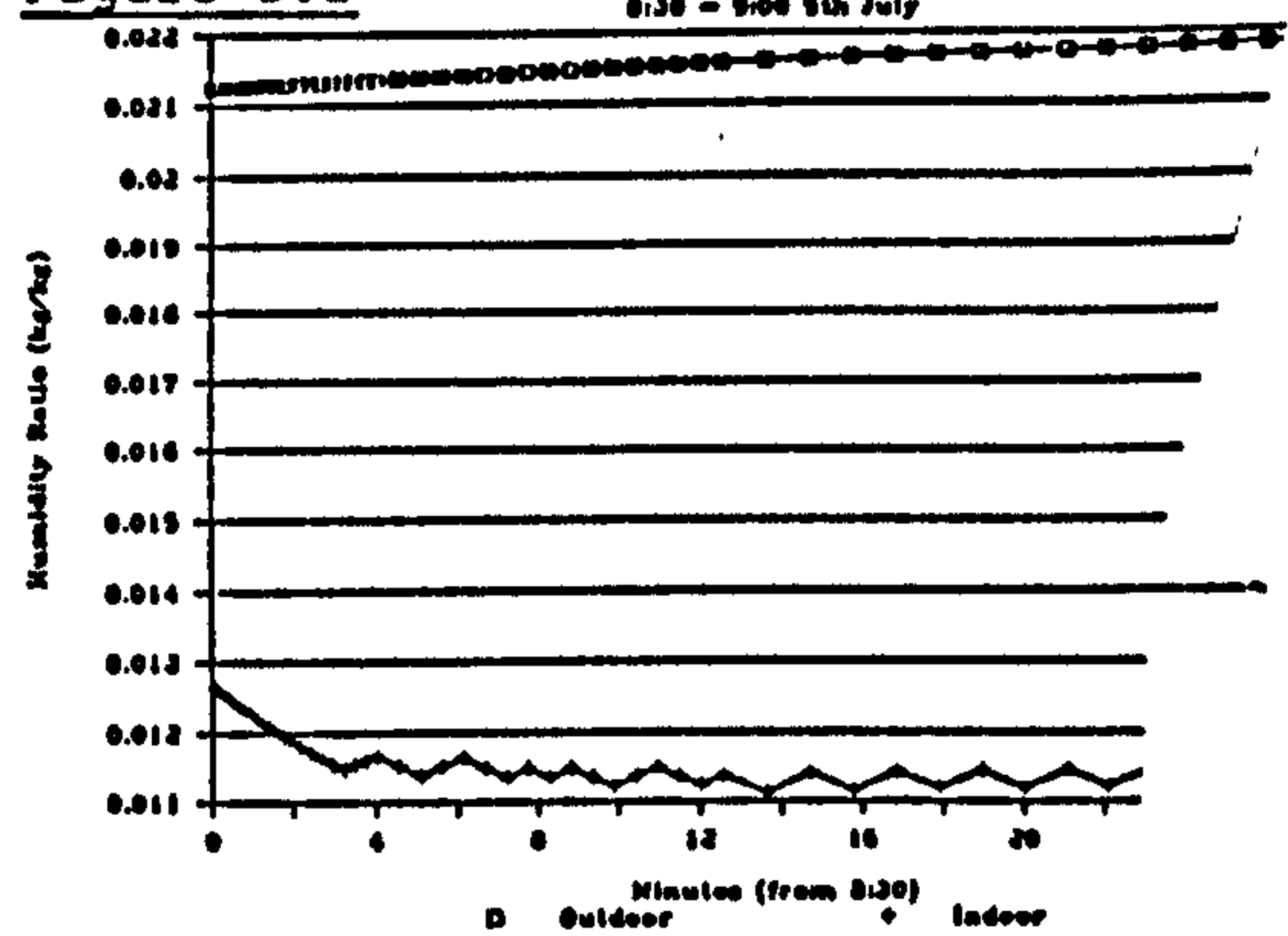


Figure D.3 Air-conditioned Period
9:30 - 12:00 5th July

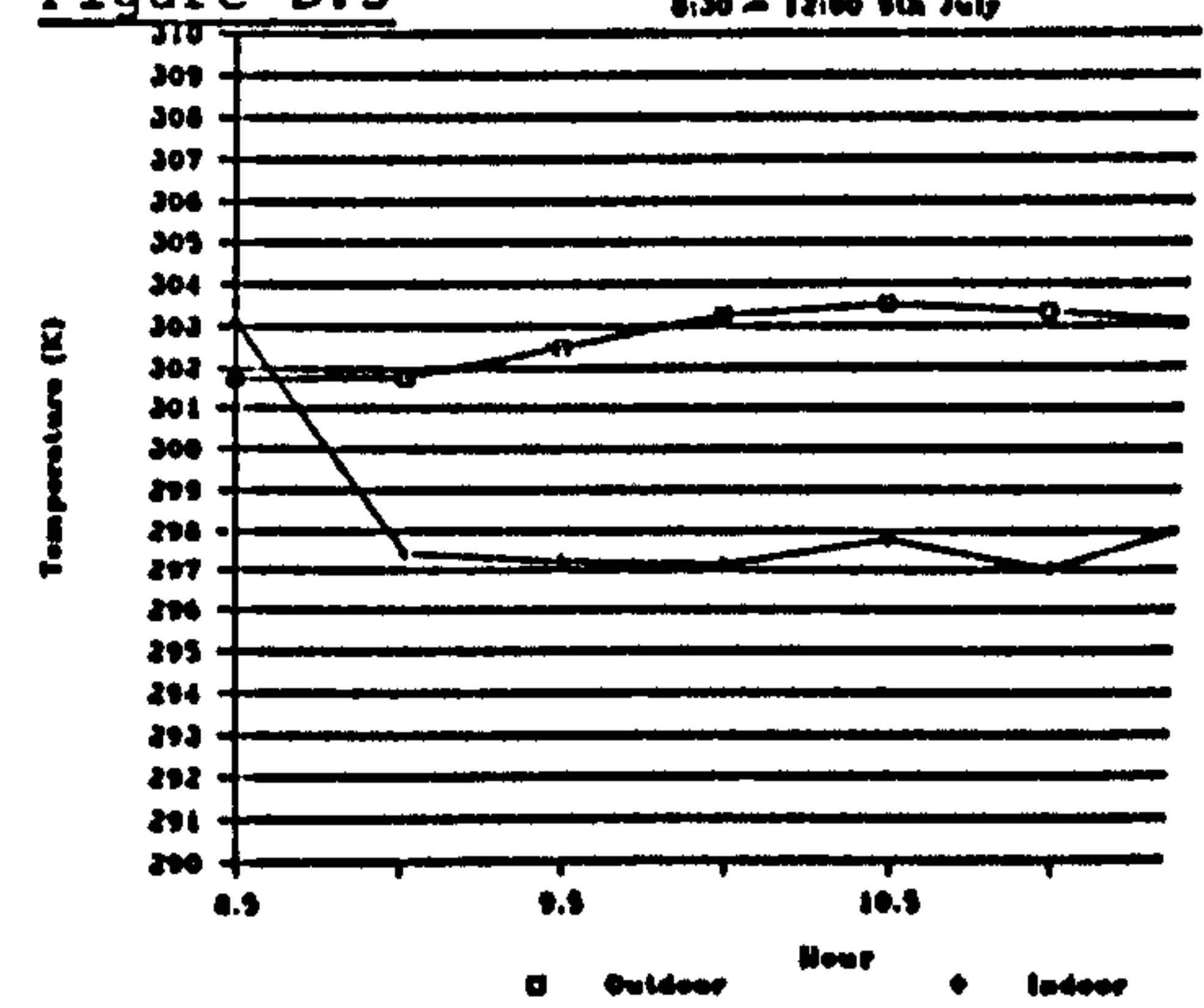
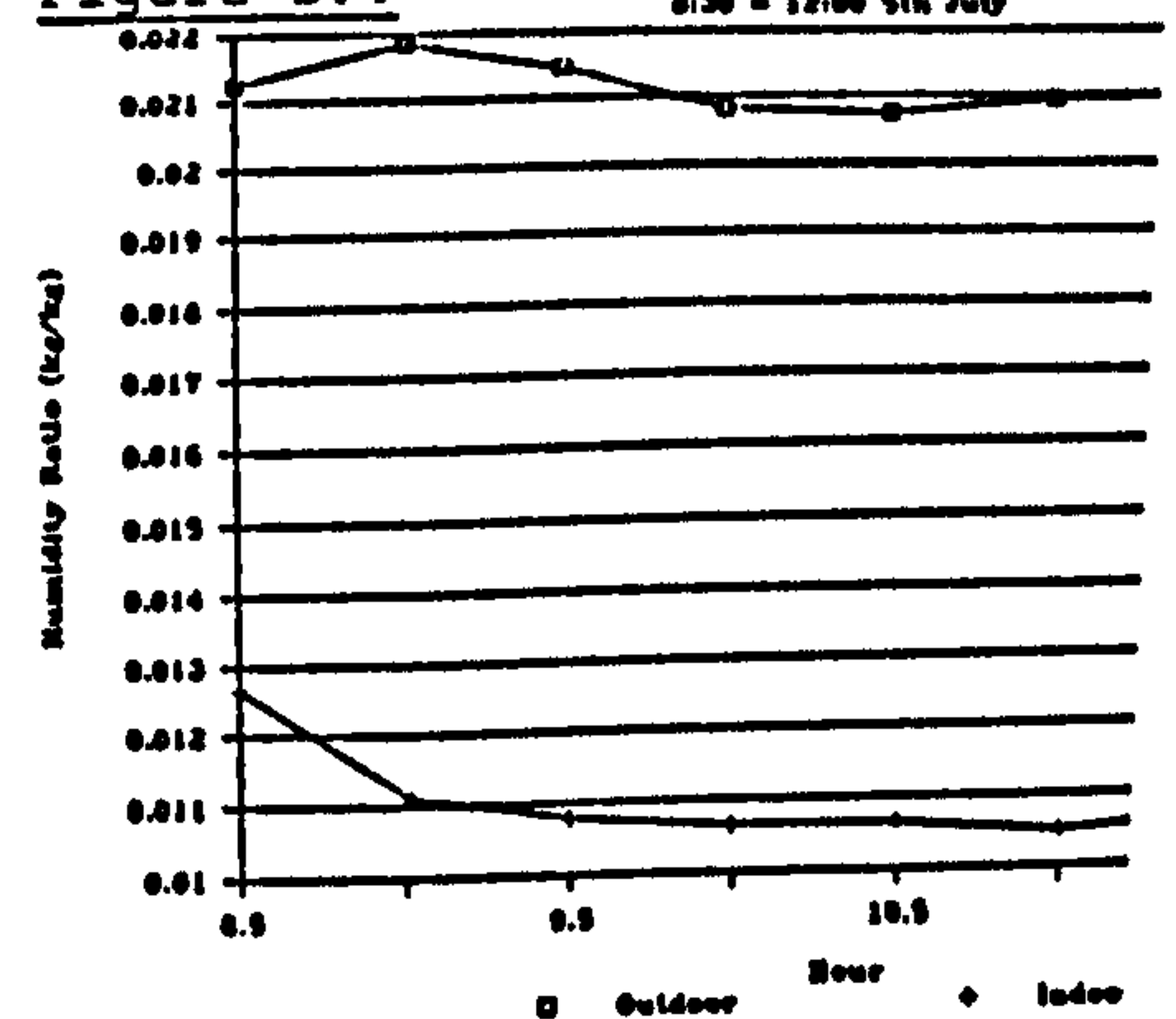


Figure D.4 Air-conditioned Period
9:30 - 12:00 5th July



Summary This paper presents a simplified dynamic model for simulating the coupled heat and moisture transfer in fabrics of concrete buildings. Assumptions were made that (1) moisture transfer in the wall is dominated by vapour diffusion and is driven by vapour pressure gradient with differential permeability being the moisture transport property; (2) evaporation and condensation theory applies; and (3) the materials are in pendular state, with reasons explained. The impact of moisture adsorption and desorption at building fabrics on indoor air humidity under intermittent air-conditioning was studied in an earlier paper by using a more rigorous approach. The study was repeated by using this model which gave predictions with similar accuracy but required much less computing time. Besides a simpler model, a more efficient numerical scheme was also used. Both the model and the numerical scheme are introduced and simulation results are presented.

A differential permeability model for simulating building heat and moisture transfer

Francis W H Yik BSc(Eng), MSc(Eng), CEng, MCIBSE, MIMechE, MHKIE

Department of Building Services Engineering, Hong Kong Polytechnic, Hong Kong

Nomenclature

C	mass concentration (kg/m ³ of bulk volume)
C _p	specific heat (J/kg K)
D	diffusivity (m ² /s)
\dot{e}	evaporation rate (kg/m ³ s)
h _{fg}	heat of evaporation or condensation (J/kg)
J _v	vapour flux (kg/m ² s)
k	thermal conductivity (W/mK)
L	thickness (m)
m _v ["]	moisture flux at boundary surface (kg/m ² s)
M	molecular weight of the gas or component (kg/mol)
P _v	vapour pressure (Pa)
q ["]	heat flux at boundary surface (W/m ²)
R	universal gas constant (J/mol K)
RH	relative humidity
t	temporal dimension (s)
T	temperature (K)
x	spatial dimension (m)

Subscripts

+	the node to the right adjacent to the current node
–	the node to the left adjacent to the current node
g	gas mixture (dry-air and water vapour)
l	liquid
s	solid or saturated state
v	vapour

Greek symbols

δ	permeability (kg/Pa ms or s)
μ	differential permeability (kg/Pa ms or s)
ε	volume fraction (m ³ /m ³)
κ _g [•]	permeability of the gas when the porous system is dry
ζ _g	relative permeability when there is liquid moisture in the porous system

η _g	viscosity of the gas (kg/ms)
ρ	density (kg/m ³)
φ	mole fraction of water vapour in a dry-air/water vapour mixture

Introduction

To facilitate assessment of condensation risk in buildings in cold climate countries, lots of effort have been paid to investigate moisture migration in building fabrics (e.g. [1-4]). Since interstitial condensation is not a serious problem for buildings situated in warm and hot climate regions, not much attention has been given to moisture transfer in buildings in these places until recently when the impact of moisture adsorption and desorption by building materials on the indoor humidity level and performance of air-conditioning systems has been recognized. For instance, the work reported in [5-11] showed the significance of this phenomenon.

Most building materials are porous materials within which moisture can stay in their internal voids and, when there exist a gradient of vapour pressure or temperature, moisture can migrate through the porous materials. Consequently, the building fabric materials can adsorb moisture from or release moisture to the indoor air thus giving rise to a moisture storage effect similar to the thermal storage effect in sensible heat transfer in buildings. To study this effect, the coupled heat and moisture transfer in the building fabric materials has to be properly modelled taking into account the heat and moisture balance in the air-zone. When there is air-conditioning, performance of the air-conditioning system needs to be modelled also but this effect has not been studied in detail.

In the development of a building model, an appropriate theory has to be adopted to model the coupled heat and

moisture transfer in the porous building materials. Although there is yet no single theory proven to be universally applicable, amongst the various theories proposed, it has been pointed out that Luikov's theory and the evaporation and condensation theory are the two most promising ones [12]. Since most buildings in Hong Kong are concrete buildings, the present study is focused on heat and moisture transfer in concrete and cement plastering. Due to the peculiar structure of cement gel, there are extremely large number of fine pores in concrete and cement plastering, disconnected by larger-sized capillary pores [13]. Hence, a significant amount of moisture can be detained in these materials under normal environmental conditions but the liquid water stays primarily in the fine pores and are highly immobile. Thus, moisture migration takes place predominantly by vapour diffusion and the liquid moisture cannot move from one location to another unless first evaporated into vapour state. Therefore, under normal environmental conditions, the material is under the so called pendular state [13-15] and the evaporation and condensation theory is a valid model for moisture transfer in concrete and cement plastering. Besides the physical validity of the theory, consideration must also be given to availability of transport properties data required for use in conjunction with the model. In this respect, there are much more data available for the evaporation and condensation theory as compared to Luikov's model [12]. Furthermore, as the building thermal model is to be coupled to detailed air-conditioning system models and a simultaneous solution is required, a balance amongst theoretical rigour, accuracy and computing efficiency has to be sought.

A computer model was developed by the author [16] for modelling the dynamic indoor temperature and humidity changes taking into account the effects of building fabric moisture adsorption and desorption and the effects of intermittent air-conditioning. The numerical model for the building fabric was developed based on the set of detailed differential equations due to Huang [14], which is based on the evaporation and condensation theory and is valid for the pendular state. The model had also been coupled to simple air-conditioning system models. Predictions by the model showed that the moisture adsorption and desorption effect was significant in intermittently air-conditioned concrete buildings in Hong Kong but the test runs also showed that with this rigorous approach, the ratio between the required computing time and the simulated time duration was as high as 1:1 when a 486 PC was used. Comparative analyses by using the model and repeating Huang's studies [14,15] showed that moisture transfer in a concrete slab and in a slab of cement paste were dominated by vapour diffusion whereas filtration flow only accounted for less than 2 percent of the total rate of moisture transfer. With this finding, the model for concrete structure (and similar materials) of buildings can be simplified by neglecting the bulk transport of dry-air and vapour mixture due to filtration flow and thus moisture transfer can be ascribed solely to vapour diffusion.

Based on the vapour diffusion model and the evaporation and condensation theory, conservation equations on mass of moisture and heat energy in a piece of building material were derived, resulting in two coupled partial differential equations. In this model, the concept of "differential permeability" [17] is adopted. The simplified heat and

moisture transfer model is presented in this paper together with simulation results obtained by using the model. A method for evaluation of differential permeability is also given.

The differential permeability model

Permeability and differential permeability

The conventional model of moisture transfer in building materials [17,18] is:

$$J_v = \delta \frac{P_{vo} - P_{vi}}{L} \quad (1)$$

Data of δ , called permeability, or its reciprocal ($1/\delta$), called vapour resistivity, for a large variety of materials can be found in lots of literatures, e.g. [18,19]. Their values are normally obtained by standardized measurement methods, such as the 'Dry-cup' and 'Wet-cup' tests [20].

The method for evaluation of moisture transfer, as given by equation (1), is obviously valid only for steady-state moisture transfer. Hence, the validity of applying the same model and the same set of permeability data for the studies of dynamic moisture transfer in building materials is doubtful. Moreover, the validity of data of δ in the literatures has also been questioned [17]. It was found that there were large discrepancies between values given by different literatures for the same kind of material which should primarily be due to the different degree of saturation of the materials and the different environmental conditions under which measurements were carried out. Improved method has been suggested to provide more appropriate permeability data [17].

The rate of moisture transfer in a porous medium is dependent on its moisture content and, in turn, the equilibrium moisture content in the medium is dependent on the ambient vapour pressure and temperature. As there can be significant moisture content variation across a slab of building material, in studying the dynamic moisture transfer in buildings, it is more appropriate to take a differential approach where the moisture transfer rate at a given plane within the building wall or slab is related to the gradient of vapour pressure at that plane as follows:

$$J_v = -\mu \frac{\partial P_v}{\partial x} \quad (2)$$

whereas the transport property (μ in the above equation), called differential permeability (as opposed to permeability δ [17]), should be a variable which is a function of moisture content, i.e.

$$\mu = \mu(\epsilon_l) \quad (3)$$

Assuming the existence of local thermodynamic equilibrium in an elemental section of the porous medium and ignoring the hysteresis phenomenon, there will be a unique equilibrium moisture content for a given combination of vapour pressure and temperature at a local position within the medium. Then, the dependence of μ may be related to vapour pressure and temperature or simply to the relative humidity,

$$\mu = \mu(RH) \quad (4)$$

Calculation of differential permeability

For one-dimensional moisture transfer in a porous medium with a rigid solid phase and homogeneous and isotropic pore structures (such as concrete and cement paste), the rate of moisture transfer under low pore saturation condition (i.e. in pendular stage) is given by [14]:

$$J_v = -\frac{\kappa_g^0}{\eta_g} \epsilon_g \rho_g \frac{\partial P_g}{\partial x} - \rho_g \epsilon_g D \frac{M_a M_v}{M_g^2} \frac{\partial \phi}{\partial x} \quad (5)$$

In this model, moisture transfer mechanisms taken into account included vapour diffusion and filtration flow (i.e. bulk convection of the dry-air and water vapour mixture). Neglecting the filtration flow term by assuming the total gas pressure gradient to be negligible and by converting ϕ to vapour pressure ($\phi = P_v/P_g$),:

$$J_v = -\epsilon_g D \frac{M_a M_v}{M_g RT} \frac{\partial P_v}{\partial x} \quad (6)$$

Comparing (6) with (2), the differential permeability therefore may be approximated by:

$$\mu = \epsilon_g D \frac{M_a M_v}{M_g RT} \quad (7)$$

Governing equations

Assuming equation (2) applies, then for an elemental section in the slab, the rate of increase in water vapour concentration is given by:

$$\frac{\partial C_v}{\partial t} = -\frac{\partial J_v}{\partial x} + \dot{e} \quad (8)$$

Further assuming that the material is in pendular state, the addition of vapour moisture due to evaporation from the liquid phase, \dot{e} , must be accompanied by a reduction in liquid water concentration in the pores as described by:

$$\frac{\partial C_l}{\partial t} = -\dot{e} \quad (9)$$

Adding (8) & (9) yields:

$$\frac{\partial}{\partial t} (C_v + C_l) = -\frac{\partial J_v}{\partial x} \quad (10)$$

Since $C_v = \rho_v \epsilon_g$ & $C_l = \rho_l \epsilon_l$ and considering the liquid water density is much larger than the vapour density, equation (10) may be approximated by:

$$\frac{\partial}{\partial t} (C_v + C_l) \approx \rho_l \frac{\partial \epsilon_l}{\partial t} = -\frac{\partial J_v}{\partial x} \quad (11)$$

Applying equation (2), the above moisture mass conservation equation becomes:

$$\rho_l \frac{\partial \epsilon_l}{\partial t} = \frac{\partial}{\partial x} \left(\mu \frac{\partial P_v}{\partial x} \right) \quad (12)$$

Applying the energy conservation principle and the Fourier's law of conduction, the following energy conservation equation can be derived:

$$(\rho C_p)_B \frac{\partial T}{\partial t} = \frac{\partial}{\partial x} \left(k_B \frac{\partial T}{\partial x} \right) + h_{fg} \rho_l \frac{\partial \epsilon_l}{\partial t} \quad (13)$$

in which $(\rho C_p)_B$ is the bulk heat capacity of the medium given by:

$$(\rho C_p)_B = \rho_s \epsilon_s C_{ps} + \rho_l \epsilon_l C_{pl} + \rho_g \epsilon_g C_{pg} \quad (14)$$

and the bulk thermal conductivity, k_B , is evaluated using Kingery's empirical formula [14] as follows:

$$k_B = [(k_g)^n \epsilon_g + (k_l)^n \epsilon_l + (k_s)^n \epsilon_s]^{1/n} \quad (15)$$

where n is an empirically determined coefficient which equals to 0.25.

The last term in equation (13) accounts for the amount of condensation heat associated with the change in liquid moisture content. In deriving the energy conservation equation, assumption has been made that there exists thermodynamic equilibrium in the elemental section such that the temperature of the solid, liquid and gaseous phases are identical.

Equations (12) and (13) are the two coupled governing equations describing the heat and moisture transfer in the porous medium. Examining these equations reveals that there are three variables involved, namely, P_v , T and ϵ_l . Hence, one extra equation is required to close the set of equations. The sorption isotherm of the material relating the equilibrium moisture content to vapour pressure and temperature is used for this purpose:

$$\epsilon_l = \epsilon_l(P_v, T) \quad (16)$$

$$\therefore \frac{\partial \epsilon_l}{\partial t} = \frac{\partial \epsilon_l}{\partial P_v} \cdot \frac{\partial P_v}{\partial t} + \frac{\partial \epsilon_l}{\partial T} \cdot \frac{\partial T}{\partial t} \quad (17)$$

Equations (12) and (13) therefore can be written as:

$$\begin{aligned} \left(\rho_l \frac{\partial \epsilon_l}{\partial P_v} \right) \frac{\partial P_v}{\partial t} + \left(\rho_l \frac{\partial \epsilon_l}{\partial T} \right) \frac{\partial T}{\partial t} = \\ \mu \frac{\partial^2 P_v}{\partial x^2} + \frac{\partial \mu}{\partial x} \frac{\partial P_v}{\partial x} \end{aligned} \quad (18)$$

$$\begin{aligned} \left(-h_{fg} \rho_l \frac{\partial \epsilon_l}{\partial P_v} \right) \frac{\partial P_v}{\partial t} + [(\rho C_p)_B - h_{fg} \rho_l \frac{\partial \epsilon_l}{\partial T}] \frac{\partial T}{\partial t} = \\ k_B \frac{\partial^2 T}{\partial x^2} + \frac{\partial k_B}{\partial x} \frac{\partial T}{\partial x} \end{aligned} \quad (19)$$

or alternatively in the form of:

$$a_{11} \frac{\partial P_v}{\partial t} + a_{12} \frac{\partial T}{\partial t} = c_{11} \frac{\partial^2 P_v}{\partial x^2} + c_{12} \frac{\partial P_v}{\partial x} \quad (20)$$

$$a_{21} \frac{\partial P_v}{\partial t} + a_{22} \frac{\partial T}{\partial t} = c_{21} \frac{\partial^2 T}{\partial x^2} + c_{22} \frac{\partial T}{\partial x} \quad (21)$$

The sorption isotherm equation

The sorption isotherm relationship for most building materials are presented as a function of relative humidity rather than functions of vapour pressure and temperature:

$$\varepsilon_l = \varepsilon_l(RH) \quad (22)$$

Since $RH = P_v/P_{vs}$ and $P_{vs} = P_{vs}(T)$, the derivatives of ε_l with respect to P_v and T can be evaluated by:

$$\begin{aligned} \frac{\partial \varepsilon_l}{\partial P_v} &= \frac{\partial \varepsilon_l}{\partial RH} \cdot \frac{\partial RH}{\partial P_v} \\ \therefore \frac{\partial \varepsilon_l}{\partial P_v} &= \frac{1}{P_{vs}} \cdot \frac{\partial \varepsilon_l}{\partial RH} \end{aligned} \quad (23)$$

$$\begin{aligned} \frac{\partial \varepsilon_l}{\partial T} &= \frac{\partial \varepsilon_l}{\partial RH} \cdot \frac{\partial RH}{\partial T} \\ \therefore \frac{\partial \varepsilon_l}{\partial T} &= -\frac{P_v}{P_{vs}^2} \cdot \frac{\partial P_{vs}}{\partial T} \cdot \frac{\partial \varepsilon_l}{\partial RH} \end{aligned} \quad (24)$$

where $\partial \varepsilon_l / \partial RH$ can be evaluated directly from the mathematical expression for the sorption isotherm (22) and the derivative $\partial P_{vs} / \partial T$ can be evaluated from an empirical equation for P_{vs} as a function of temperature such as the following one [21]:

$$P_{vs} = 2327 \cdot \exp\{6789(3.4112 \times 10^{-3} - \frac{1}{T}) - 5.031 \ln(\frac{T}{293.15})\} \quad (25)$$

Hence,

$$\frac{\partial P_{vs}}{\partial T} = \frac{P_{vs}}{T} \left(\frac{6789}{T} - 5.031 \right) \quad (26)$$

$$\frac{\partial \varepsilon_l}{\partial T} = -\frac{RH}{T} \left(\frac{6789}{T} - 5.031 \right) \frac{\partial \varepsilon_l}{\partial RH} \quad (27)$$

The finite difference scheme

The governing PDEs (eq. 20 & 21) were first partially discretized (in the spatial dimension only) into a set of ODEs and then solved by adopting the Runge-Kutta-Merson [22] scheme. In the derivation of the ODEs, a semi-implicit scheme similar to that used in [23] was employed to approximate the time-derivatives. With reference to equation (20), the numerical scheme adopted is as briefly described in the following:

- i) The spatial derivatives of $P_v(x,t)$ may be approximated by:

$$\frac{\partial P_v}{\partial x} \approx \frac{P_{v+} - P_{v-}}{2\Delta x} \quad (28)$$

$$\frac{\partial^2 P_v}{\partial x^2} \approx \frac{P_{v+} - 2P_v + P_{v-}}{(\Delta x)^2} \quad (29)$$

- ii) Following the Crank-Nicolson (C-N) scheme, for a function $\phi(x,t)$ with time derivative $\partial \phi(x,t) / \partial t = \psi(x,t)$, the time derivative is approximated by:

$$\frac{\partial \phi}{\partial t} \approx \lambda \psi(x, t+\Delta t) + (1-\lambda) \psi(x, t)$$

where $0 \leq \lambda \leq 1$. Applying the C-N scheme and substituting the finite difference approximations of the spatial derivatives, equation (20) may be written as:

$$\begin{aligned} a_{11} \frac{\partial P_v}{\partial t} + a_{12} \frac{\partial T}{\partial t} = & c_{11} \lambda \frac{P_{v+} - 2P_v + P_{v-}}{(\Delta x)^2} + \\ & c_{12} \lambda \frac{P_{v+} - P_{v-}}{2\Delta x} + \\ & c_{11} \frac{P_{v+}^n - 2P_v^n + P_{v-}^n}{(\Delta x)^2} + \\ & c_{12} \frac{P_{v+}^n - P_{v-}^n}{2\Delta x} \end{aligned} \quad (30)$$

- iii) Each ΔP_{v+} , ΔP_v & ΔP_{v-} term is multiplied by $\Delta t / \Delta t$ to become:

$$\Delta t (\Delta P_{v+} / \Delta t); \Delta t (\Delta P_v / \Delta t) \text{ \& \; } \Delta t (\Delta P_{v-} / \Delta t).$$

- iv) The $(\Delta P_v / \Delta t)$ terms are regarded as $(\partial P_v / \partial t)$ and, after re-arranging, equation (30) becomes:

$$\begin{aligned} -\lambda \Delta t \left[\frac{c_{11}}{2} - \frac{c_{12}}{2\Delta x} \right] \frac{\partial P_{v-}}{\partial t} + [a_{11} + \lambda \Delta t \frac{2c_{11}}{2}] \frac{\partial P_v}{\partial t} \\ - \lambda \Delta t \left[\frac{c_{11}}{2} + \frac{c_{12}}{2\Delta x} \right] \frac{\partial P_{v+}}{\partial t} = \\ c_{11} \frac{P_{v+}^n - 2P_v^n + P_{v-}^n}{\Delta x^2} + c_{12} \frac{P_{v+}^n - P_{v-}^n}{2\Delta x} - \\ a_{12} \frac{\partial T}{\partial t} \end{aligned} \quad (31)$$

The merits of using the above numerical scheme include:

- the resultant equations become ODEs which are readily solvable by methods for solving systems of ODEs such as the Runge-Kutta-Merson method;
- by setting $\lambda = 1$ (i.e. fully implicit) the numerical scheme will be stable;
- although the scheme is fully implicit, at the right hand side, the time derivatives of the variables (here P_v 's) are all based on the n^{th} time step and hence can be approximated by solved values of the variables at the n^{th} time step; and
- by applying the Runge-Kutta-Merson scheme, the error of each time step of calculation may also be estimated which may be used as a guide-line for controlling size of time step to be used without repeating the calculations twice with the time step halved.

The above numerical scheme is applied to discretize the governing equations for interior nodes, the boundary nodes and interface nodes of a multi-layer composite wall and the resultant finite difference equations are as summarized in

Table 1. The set of equations for a composite wall may also be expressed as:

$$[A_1] \{P_v\} = \{B_1\} \quad (32)$$

$$[A_2] \{T_v\} = \{B_2\} \quad (33)$$

and $[A]$'s are tri-diagonal matrices. Note that the $\{B\}$ vector in each equation actually contains the time derivatives of the variable in the other equation and hence the time derivative vectors $\{P_v\}$ & $\{T_v\}$ actually need to be solved for simultaneously by an iterative procedure.

Results and discussions

The simulation runs described in the earlier paper [16] were repeated by using the differential permeability model and the numerical scheme described above. The study was about a typical room of 3m (W) x 3m (D) x 3m (H), constructed of concrete walls and slabs with plastering at both sides and with a window at the exposed wall (Figure 1 & 2). The room was air-conditioned intermittently by a fan-coil system with On/Off control during the period from 8:30 am to 5:00 pm. Initial conditions of the walls and slabs, the indoor design conditions, properties of the wall and slab materials, characteristics of the air-conditioning system and the date and time of the simulated period were identical to those in [16]. Weather conditions used were actual weather data of Hong Kong in July 1980.

Simulation results of the earlier study for a shut-down period and a following air-conditioned period are shown in Figure 3 and the results obtained in the present study are shown in Figure 4. It can be seen that predictions of temperature and humidity ratio in the room obtained by both models are very close to each other. Another simulation run with the moisture adsorption and desorption effect of the building fabric ignored gave the results as shown in Figure 5 which clearly show that when this effect is ignored, the indoor humidity ratio would quickly approach the outdoor value during the shut-down period due to continued infiltration of humid outdoor air into the room - this does not match with experience and therefore demonstrates the significance of the problem. The moisture released from the walls and slabs during the pull-down period increased the dehumidification load on the air-conditioning system and prolonged the time required for the air-conditioning system to bring the indoor humidity back to the normal range. These phenomena should be duly accounted for in air-conditioning system design.

The simplified model and the new numerical scheme are effective in reducing the required computing time. For the shut down period, the ratio of computing time to simulated time was about 1:10 and for the air-conditioned period, the ratio was about 1:6. For the simulation run with moisture effect ignored, the ratio was 1 to above 300.

References

- 1 Loudon, A G (1971) *The effects of condensation and building design factors on the risk of condensation and*

- mould growth in dwellings*, BRE Current Paper CP 31/71, BRE.
- 2 BRE (1972) *Condensation*, BRE Digest 110, Building Research Establishment.
- 3 Boyd D, Cooper P & Oreszczyn, T (1988) *Condensation risk prediction: Addition of a condensation model to BREDEM*, BSER&T 9(3), CIBSE.
- 4 Letherman, K M (1989) *Condensation avoidance in layered structures: Synthesis of designs*, BSER&T 10(1), CIBSE.
- 5 Tsuchiya, T (1980) *Infiltration and indoor air temperature and moisture variation in a detached residence*, JSHASE Japan, 54(11).
- 6 Kusuda, T (1983) *Indoor humidity calculations*, ASHRAE Trans. Vol.89 Pt.2.
- 7 Miller, J D (1984) *Development and validation of a moisture mass balance model for predicting residential cooling energy consumption*, ASHRAE Trans. Vol.90 Pt.2B.
- 8 Fairey, P W & Kerestecioglu, A (1985) *Dynamic modelling of combined thermal and moisture transport in buildings: Effects on cooling loads and space conditions*, ASHRAE Trans. Vol. 91 Pt. 2A.
- 9 Shukuya, M & Saito, M (1990) *Simulation of indoor air humidity using control volume heat and moisture balance method*, Energy and Building, 14(1990), Elsevier, Sequoia.
- 10 Wong, S P W (1990) *Simulation of simultaneous heat and moisture transfer by using the finite difference method and verified tests in a test chamber*, ASHRAE Trans. Vol.96 Pt.1.
- 11 Wong, S P W & Wang, S K (1990) *Fundamentals of simultaneous heat and moisture transfer between the building envelope and the conditioned space air*, ASHRAE Trans. Vol.96, Pt.2.
- 12 Kerestecioglu, A, Swami, M, Dabir, R, Razzaq, N & Fairey, P (1988), *Theoretical and computational investigation of algorithms for simultaneous heat and moisture transport in buildings*, Final Report to US DOE, FSEC-CR-191-88.
- 13 Harmathy, T Z (1971) *Moisture and heat transport with particular reference to concrete*, Research paper # 494, Division of building research, NRCC, Ottawa, Canada.
- 14 Huang, C L D (1979) *Multi-phase moisture transfer in porous media subjected to temperature gradient*, Int. J. Heat Mass Transfer, Vol.22.
- 15 Huang, C L D, Siang, H H & Best, C H (1979) *Heat and moisture transfer in concrete slabs*, Int. J. Heat Mass Transfer, Vol.22.
- 16 Yik, F W H (1991) *Dynamic modelling of indoor air humidity*, Proceedings of Building Simulation '91 Conference, Nice, France, The international building performance simulation association.

17 McLean, R C & Galbraith, G (1988) *Interstitial condensation: Applicability of conventional vapour permeability values*, BSER&T 9(1), CIBSE.
18 CIBSE (1986), CIBSE Guide, Volume A, CIBSE.
19 ASHRAE (1989) ASHRAE Handbook, Fundamentals Volume.
20 BS4370 Pt.2 (1973), *Methods of test for rigid cellular materials*, Bristish Standard Institute, UK.

21 Holman, J P (1980) *Thermodynamics*, McGraw- Hill.
22 Lambert, J D (1991) *Numerical methods for ordinary differential systems: The initial value problem*, Wiley.
23 Ewen, J & Thomas, H R (1989) *Heating unsaturated medium sand*, Geotechnique, 39(3).

Figure 1

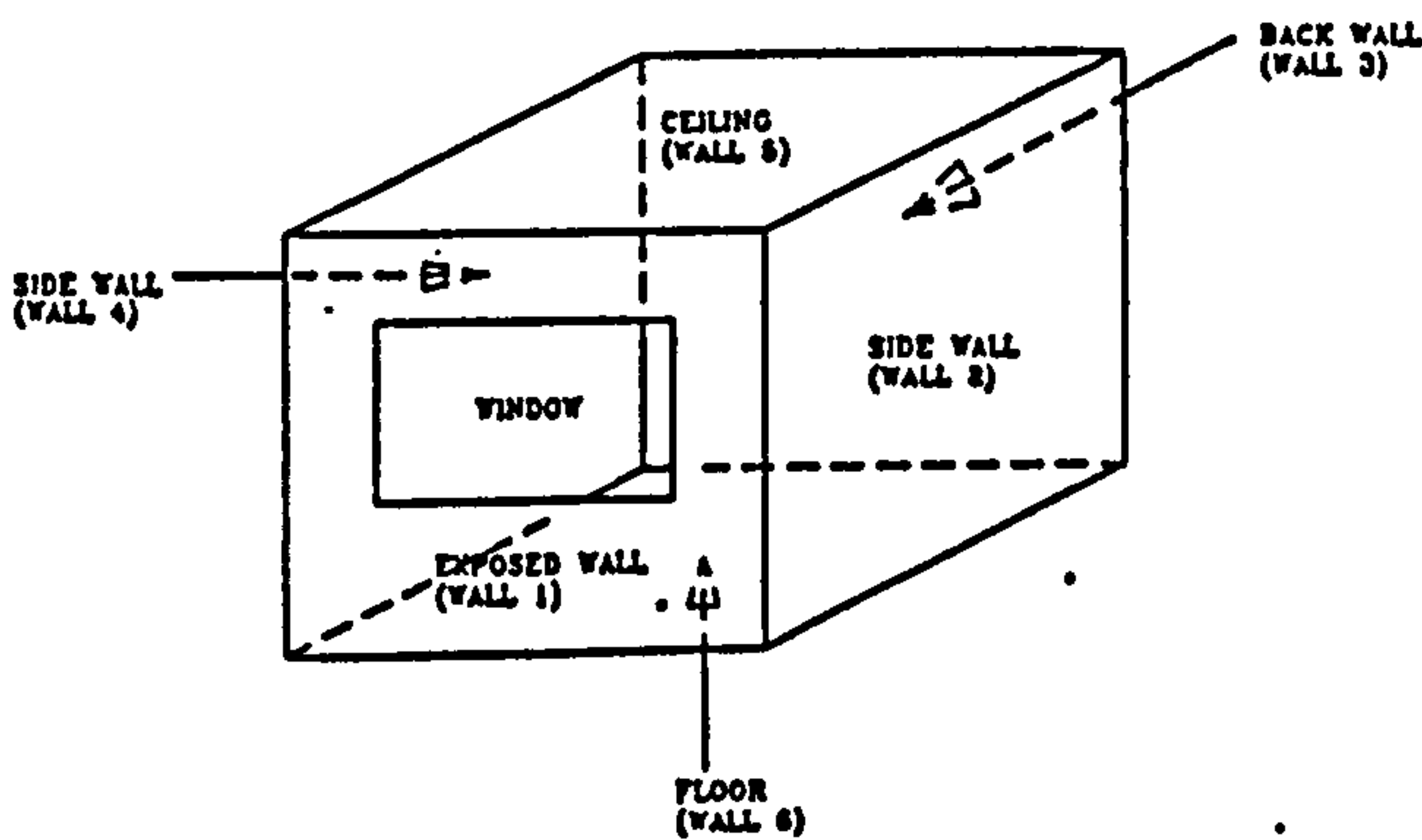


Figure 2

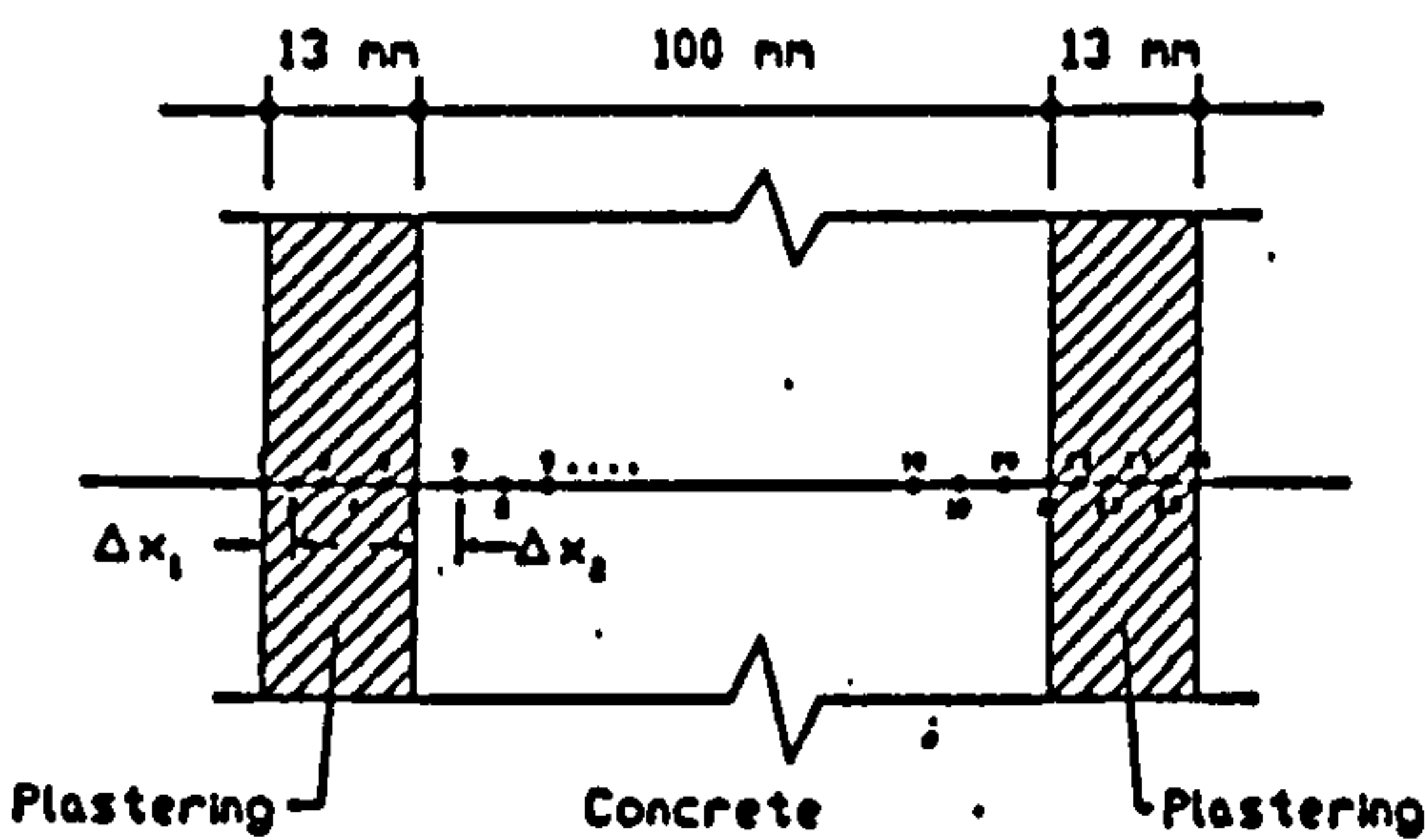


Figure 3

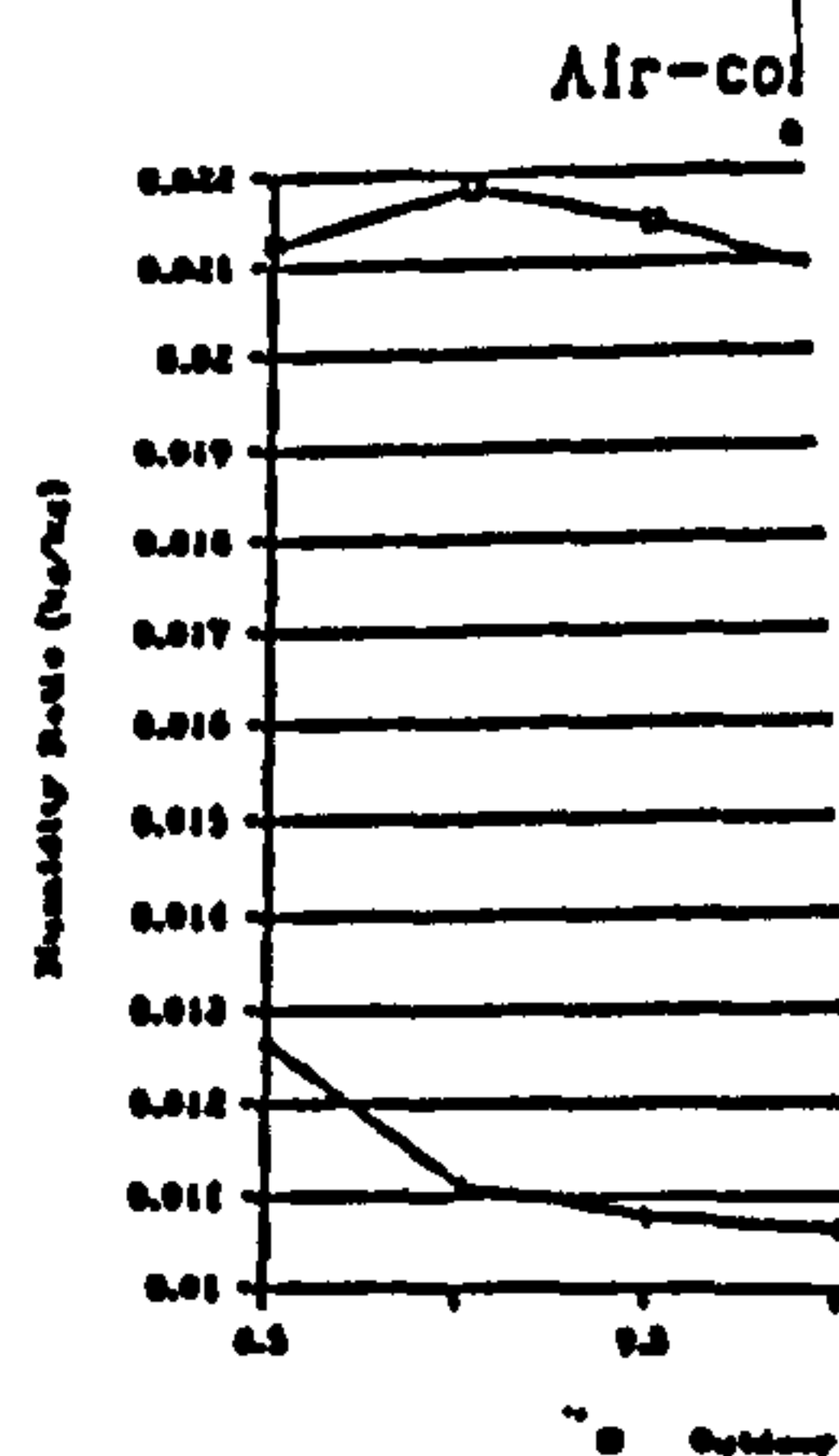
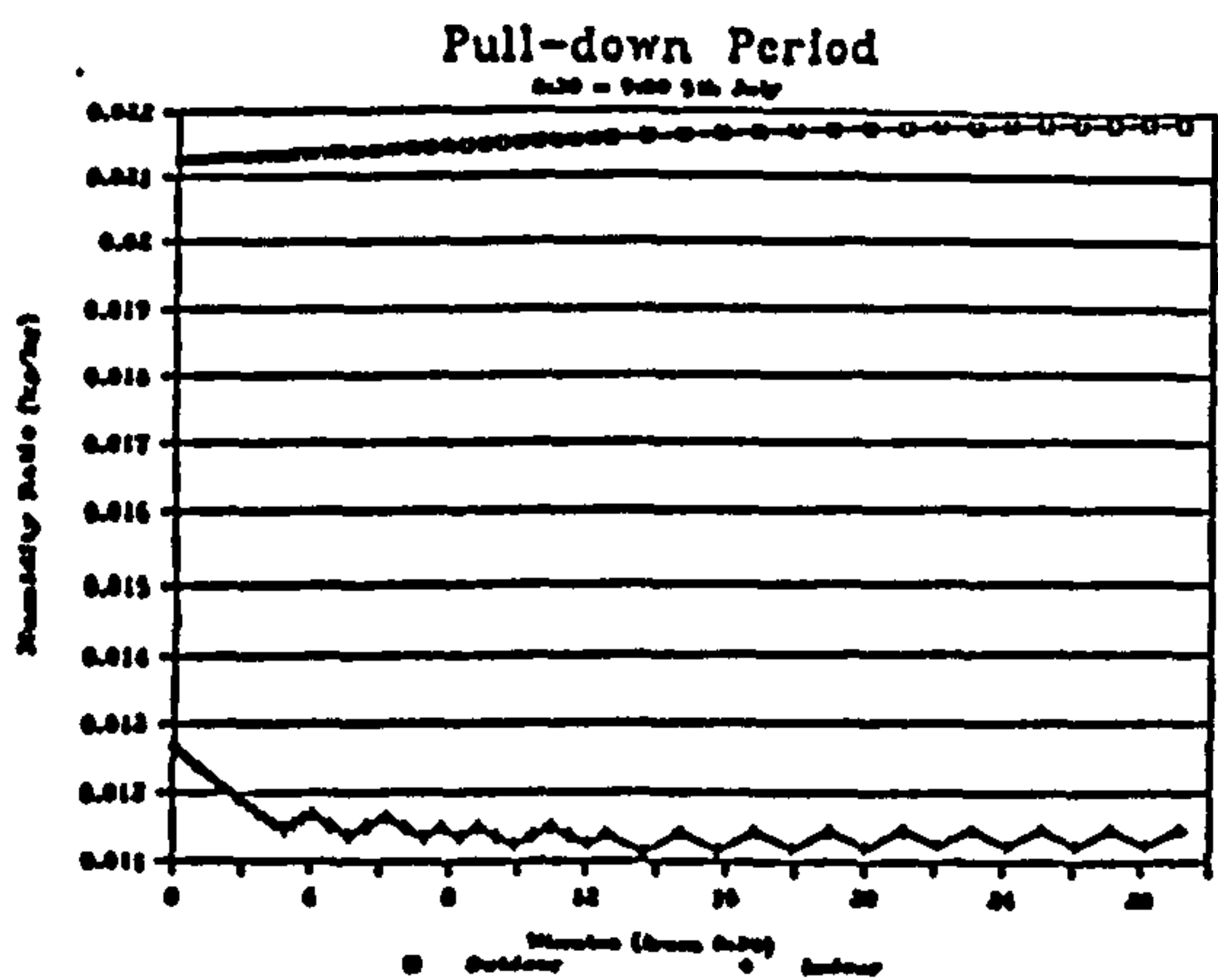
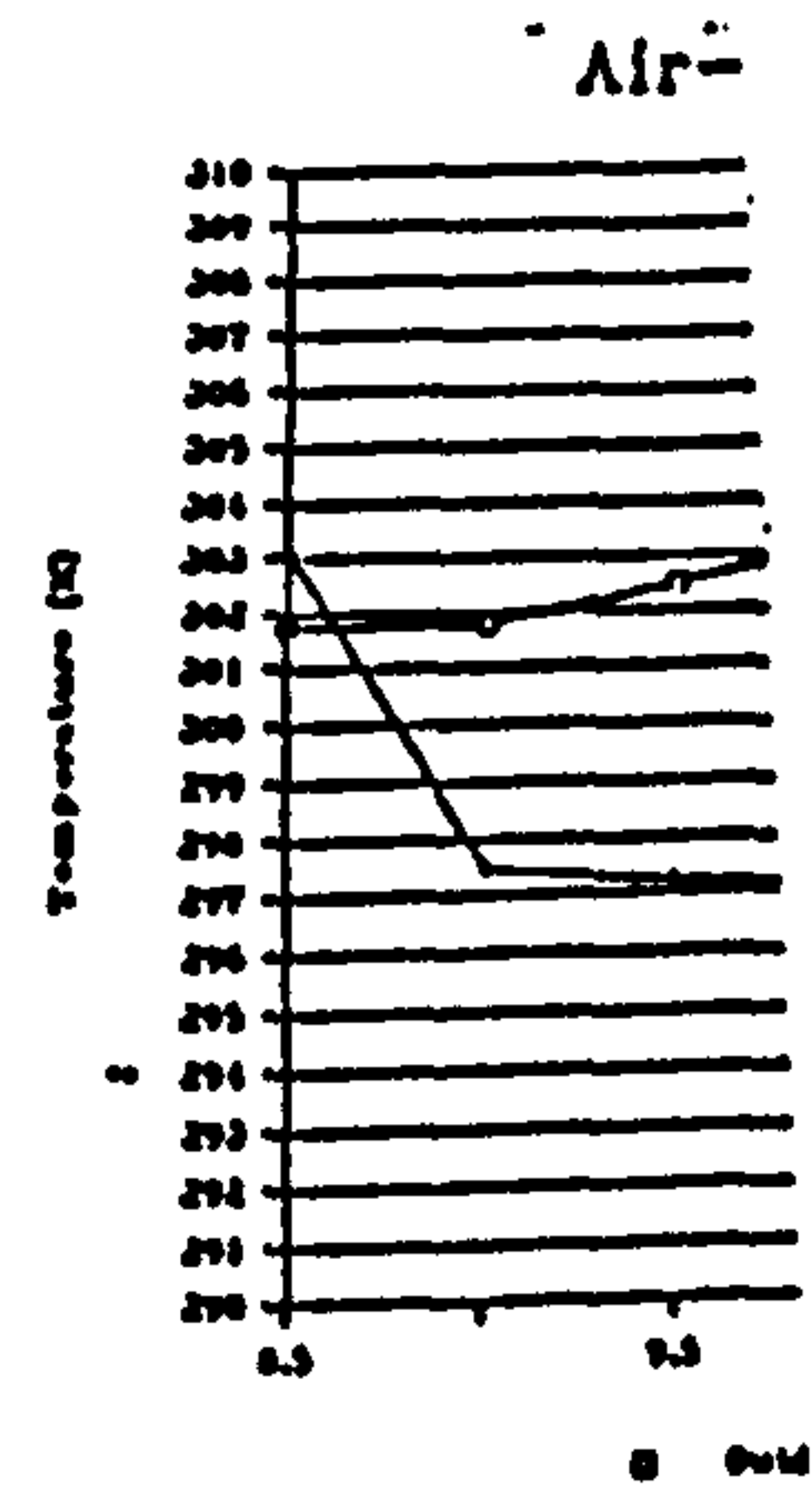
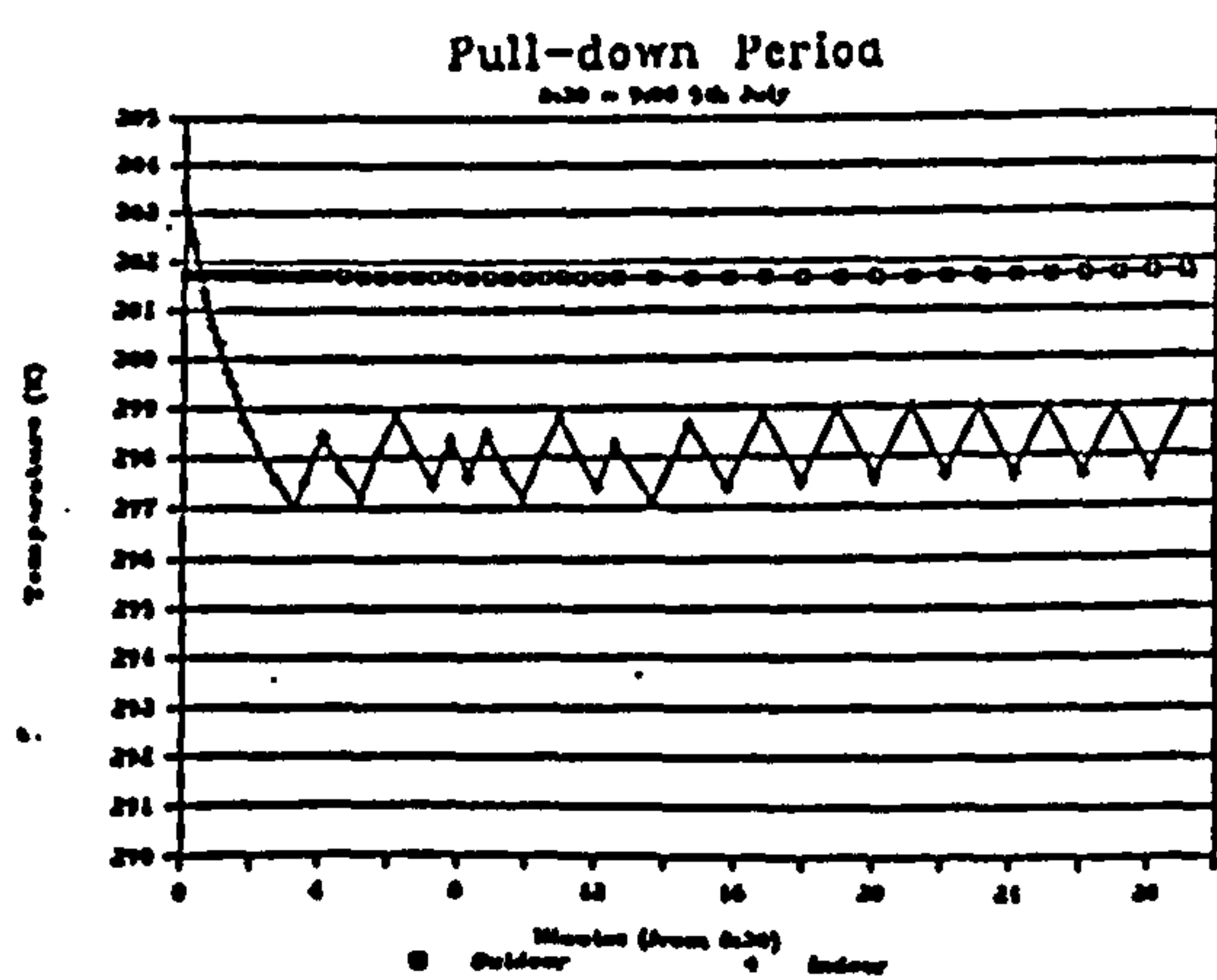
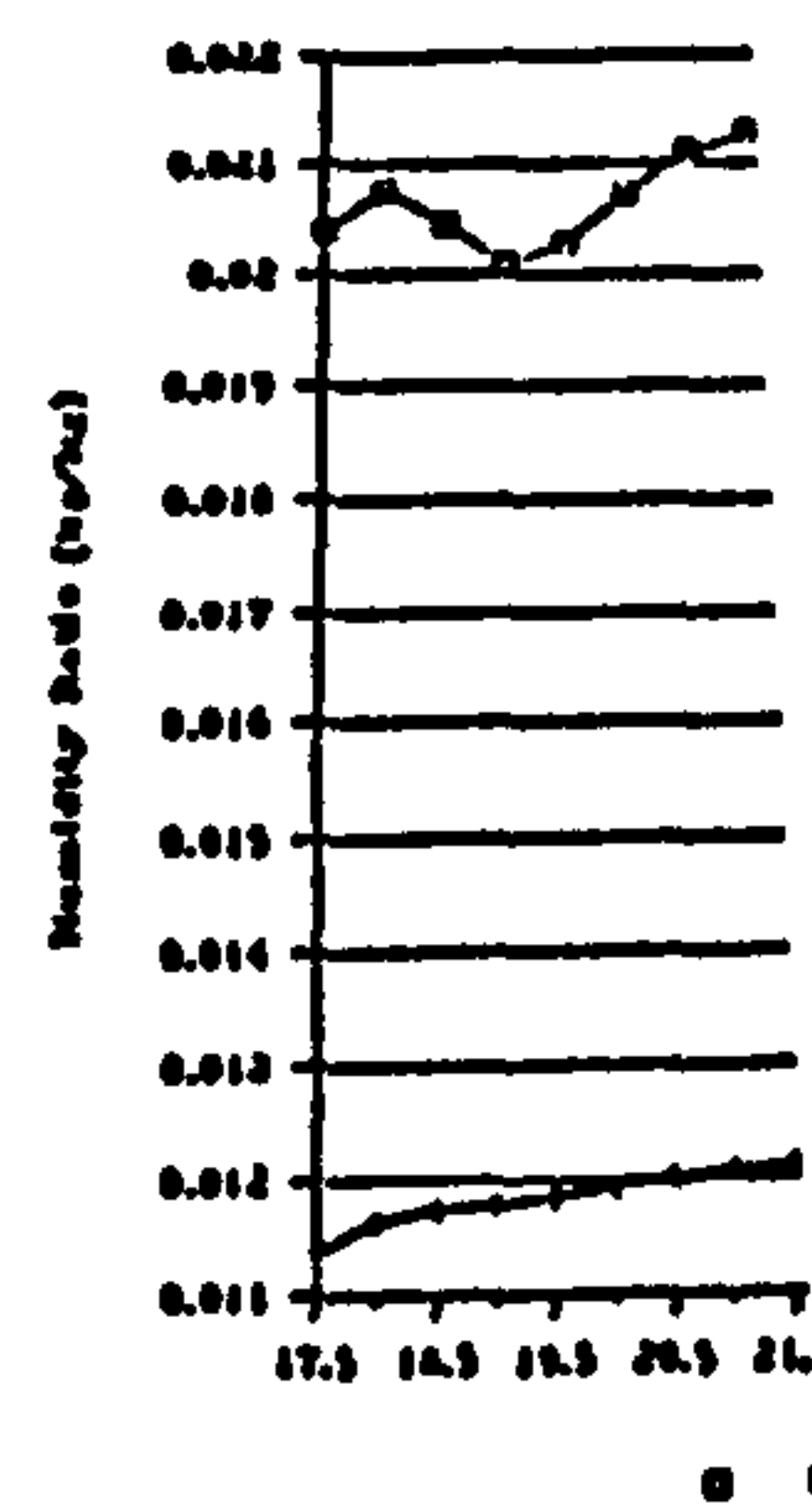
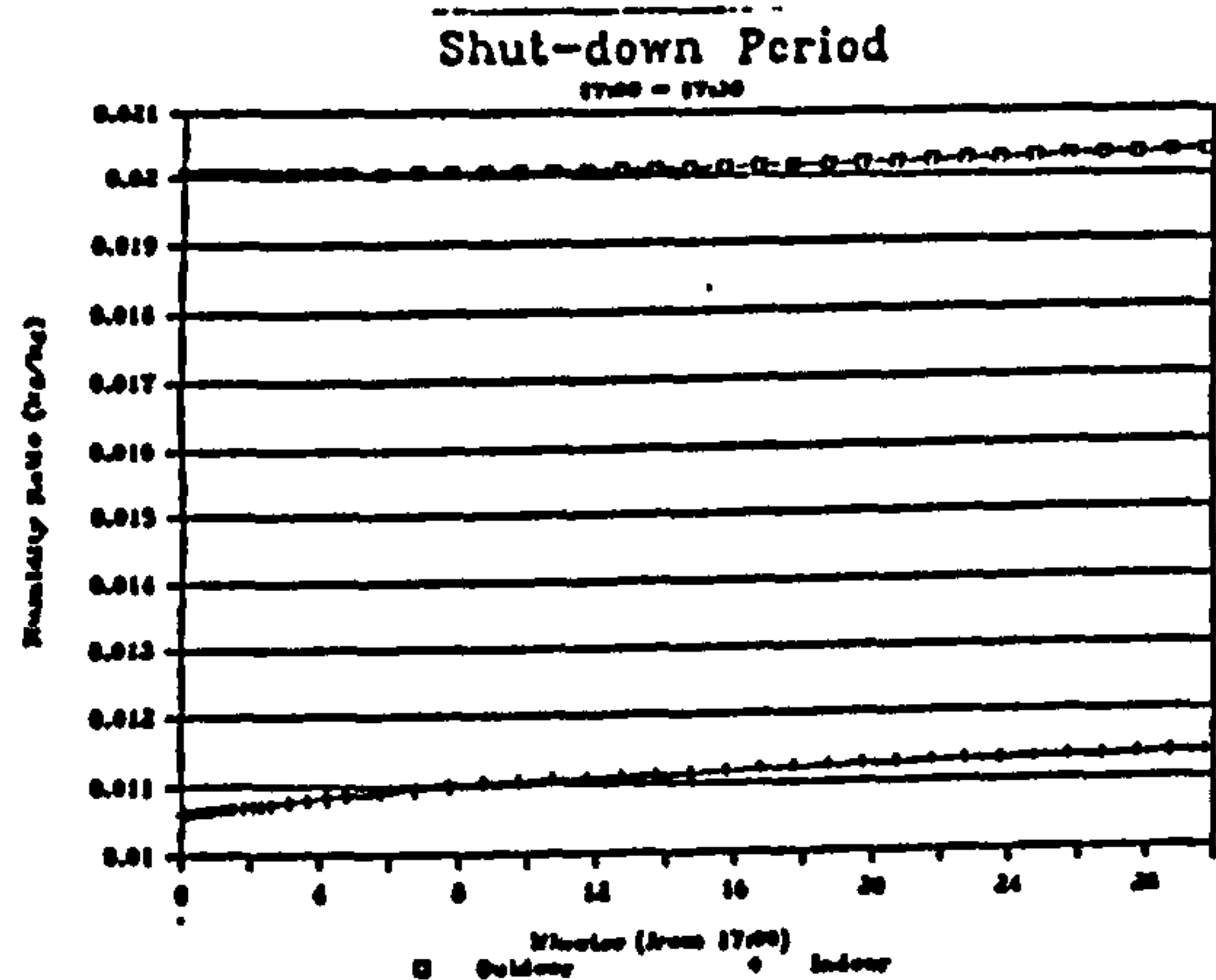
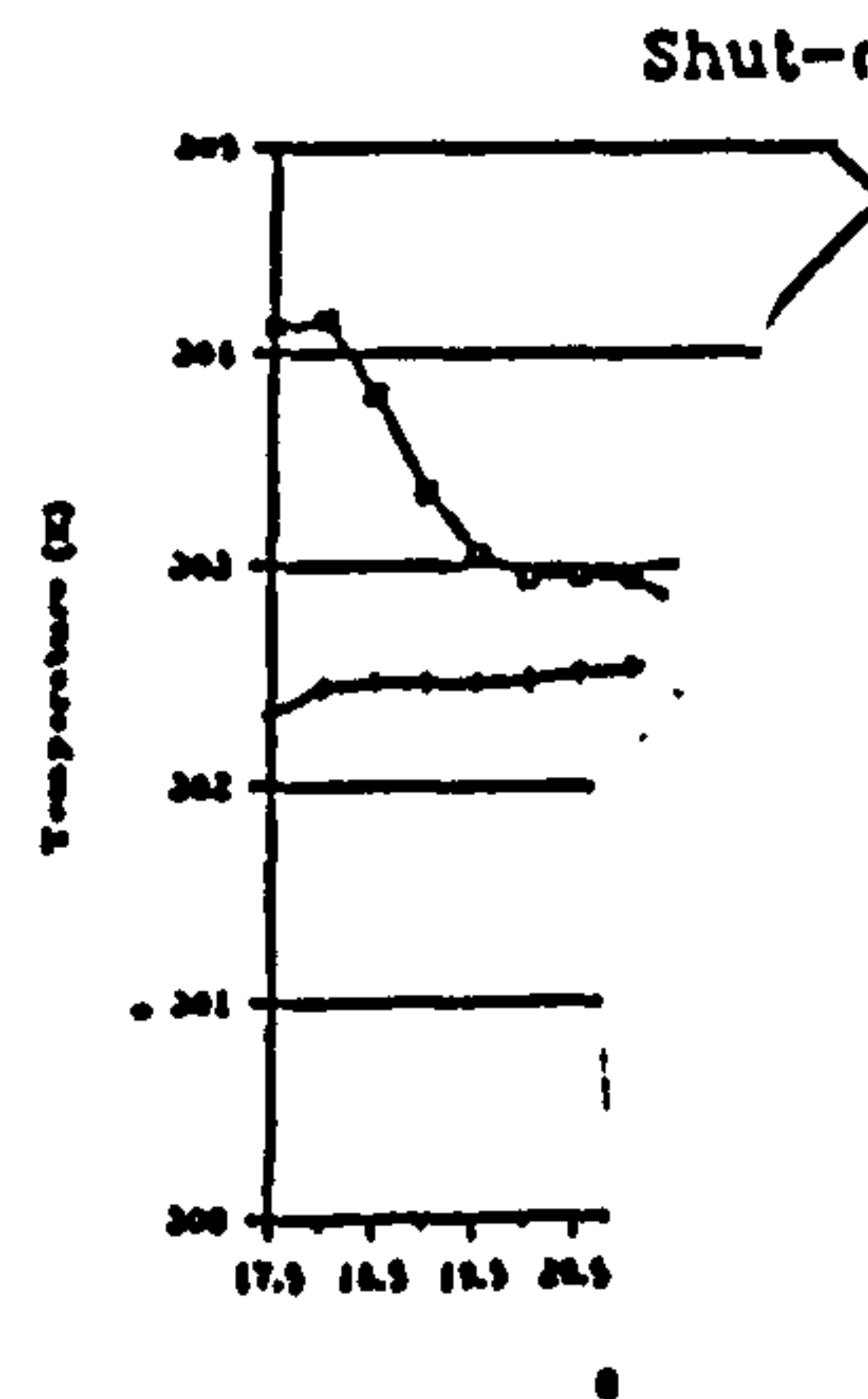
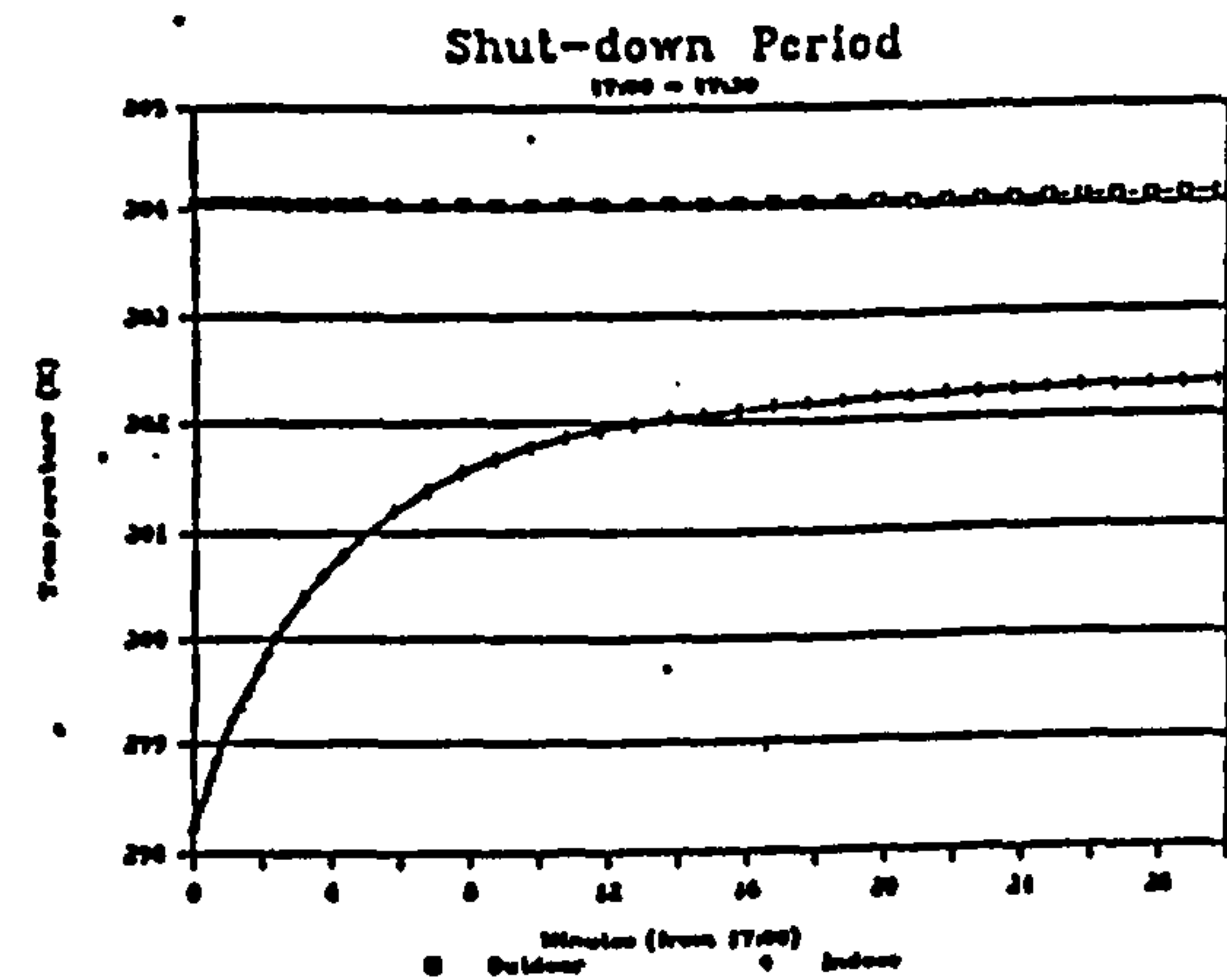
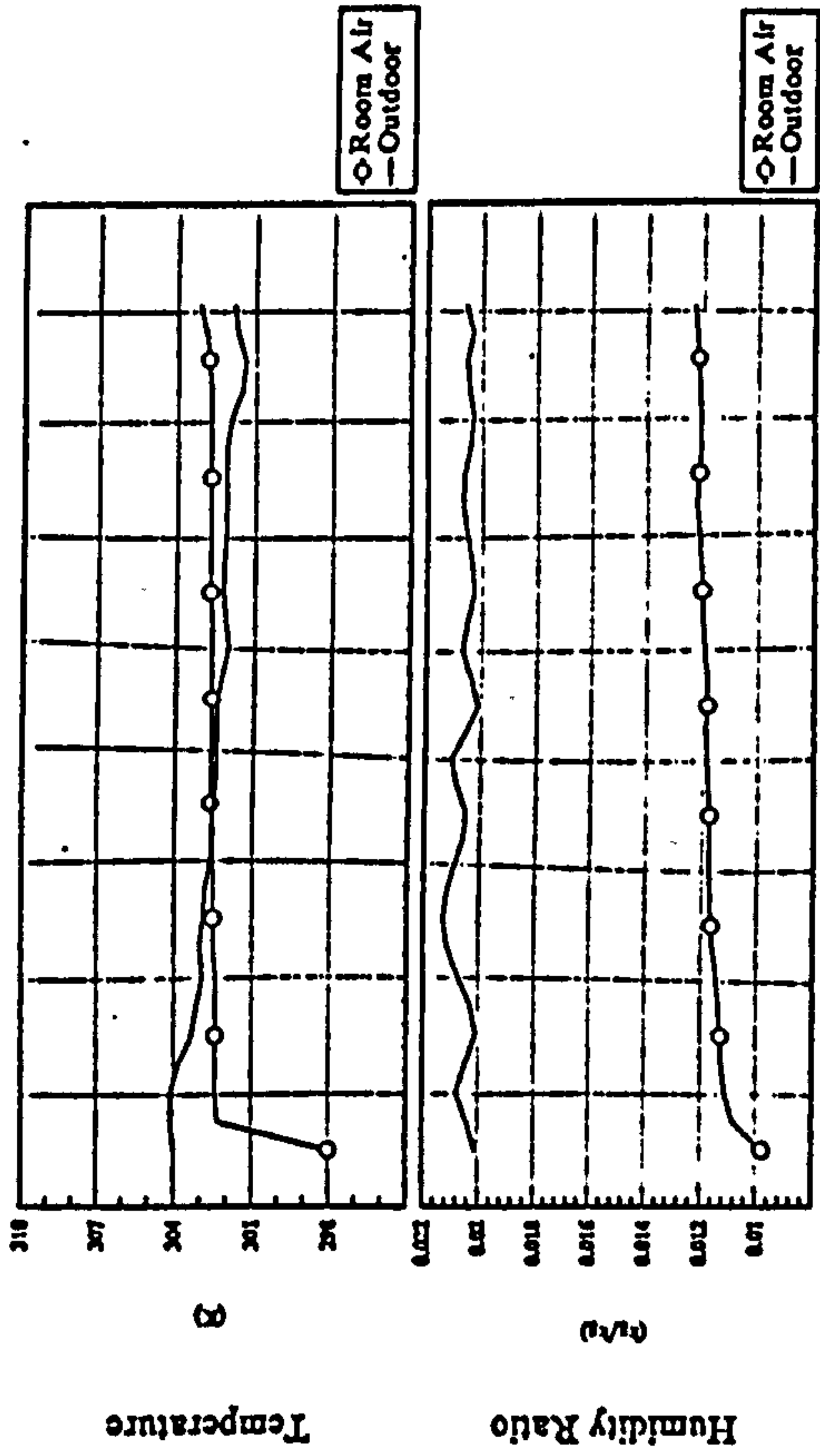


Figure 4

Indoor and Outdoor Conditions

(No A/C from 17:00 4/7/80 to 8:30 5/7/80)



Indoor and Outdoor Conditions

(No A/C from 17:00 4/7/80 to 8:30 5/7/80)
(Without Wall MAD Effects)

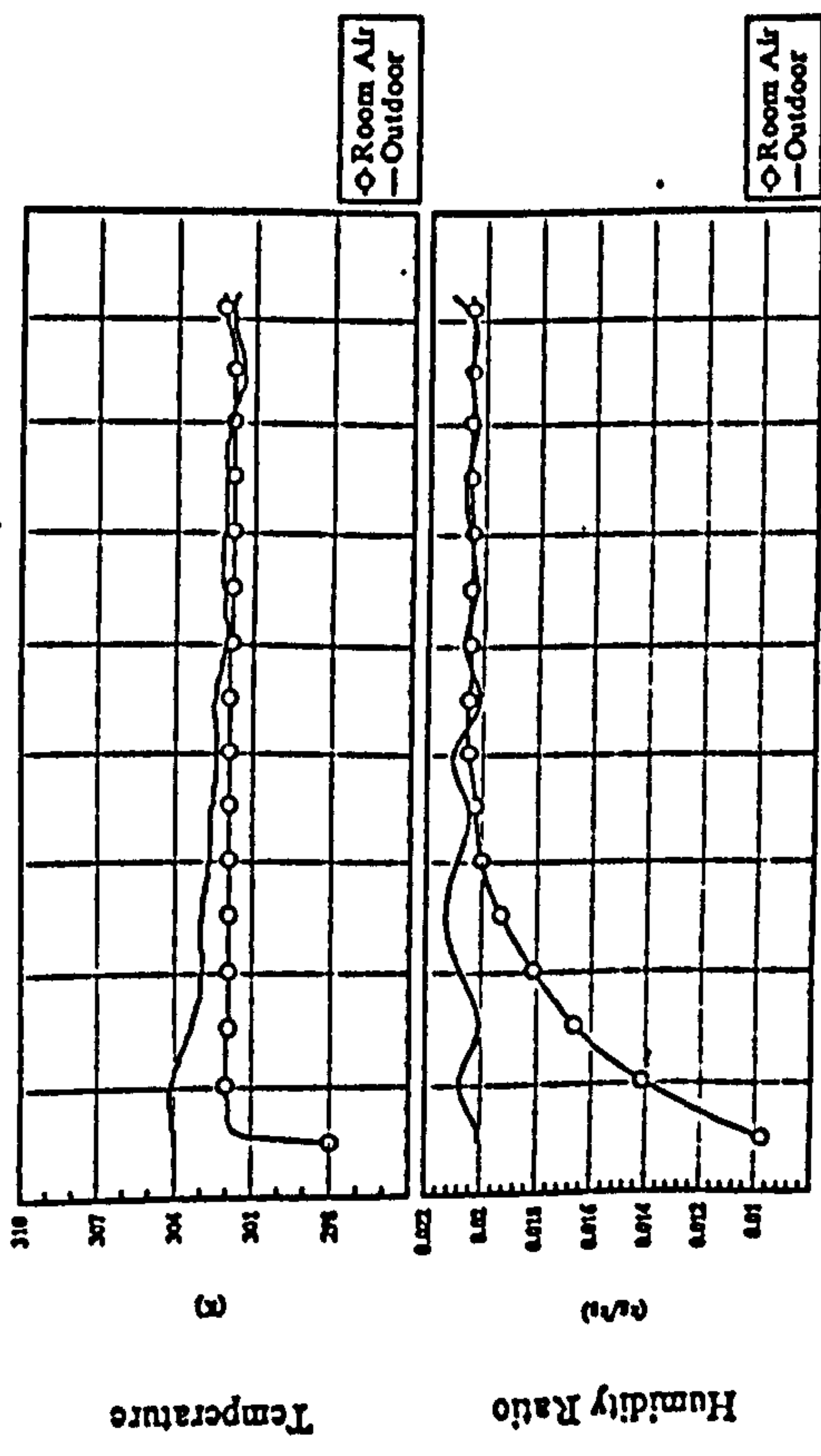
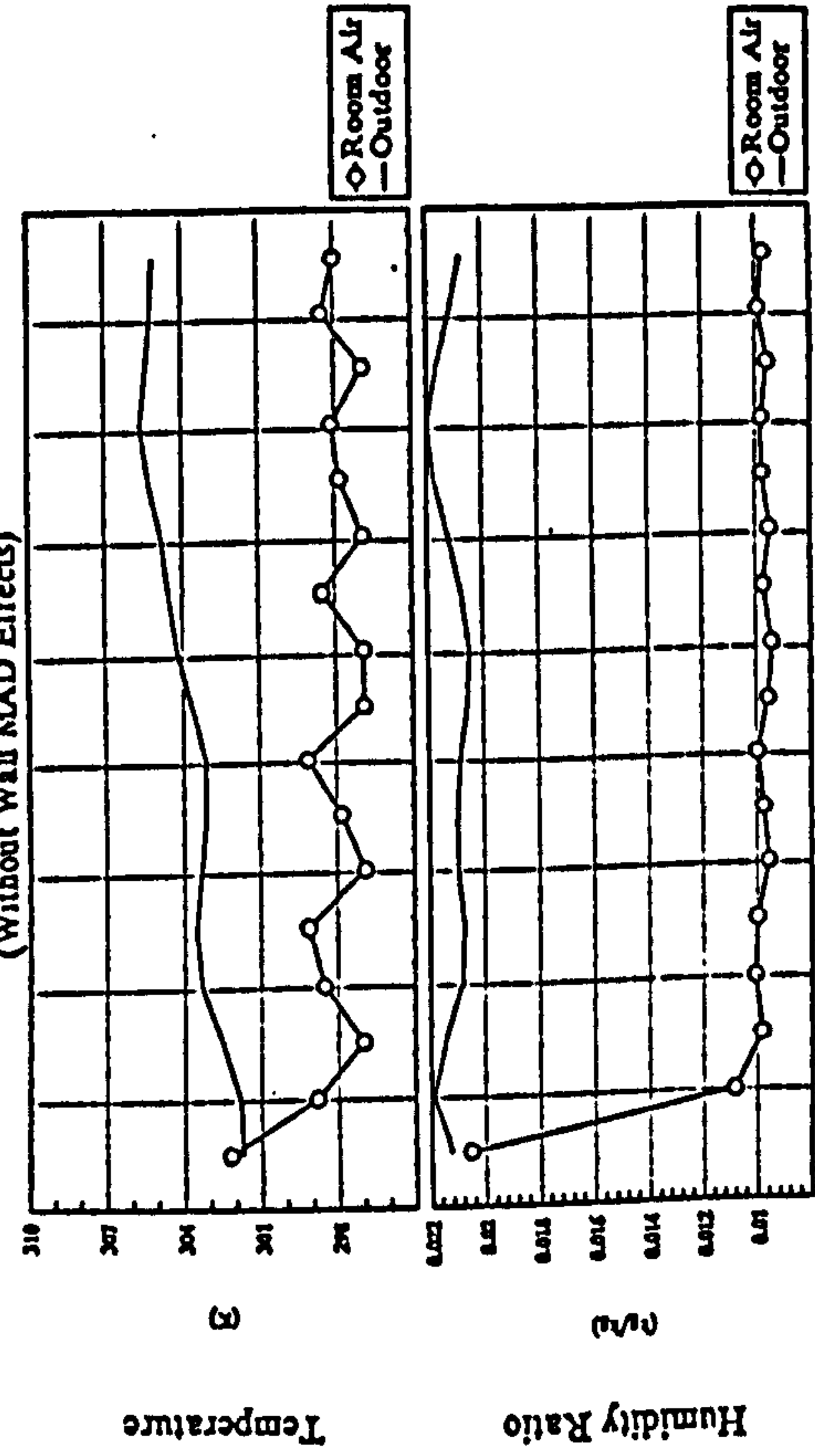


Figure 5

Indoor and Outdoor Conditions

(A/C from 8:30 5/7/80 to 17:00 5/7/80)
(by Steady-state Coil Model w/ ON/OFF Cl.)
(Without Wall MAD Effects)



Indoor and Outdoor Conditions

(A/C from 8:30 5/7/80 to 17:00 5/7/80)
(by Analytical Coil Model w/ ON/OFF Cl.)

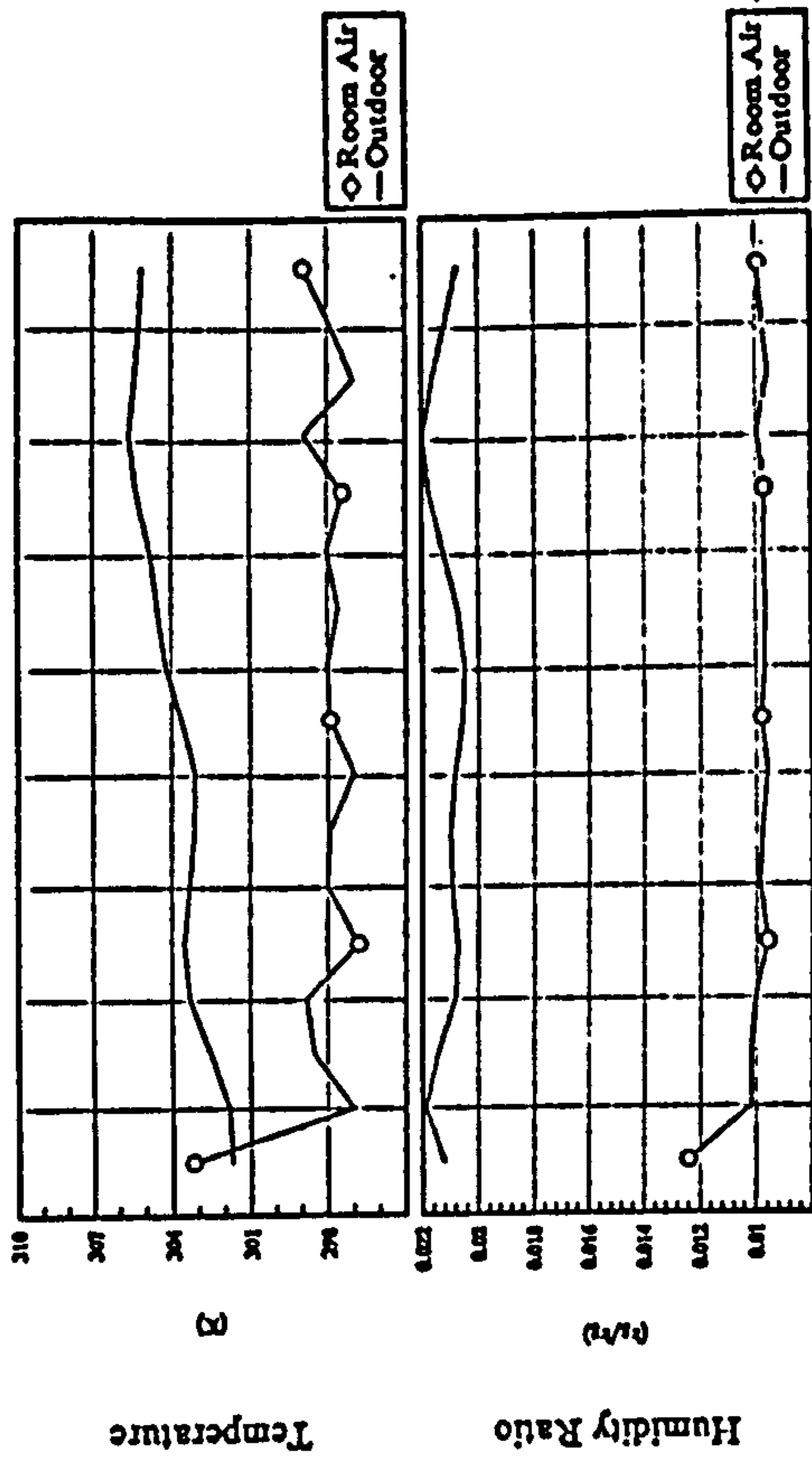


Table 1 Summary of equations of the differential permeability model for a multi-layer wall

<p>A) For interior nodes</p> $-\lambda \Delta t \left[\frac{c_{11}}{\Delta x^2} - \frac{c_{12}}{2\Delta x} \right] \frac{\partial P_{v-}}{\partial t} + [a_{11} + \lambda \Delta t \frac{2c_{11}}{\Delta x^2} - \lambda \Delta t \frac{\partial P_v}{\partial t} - \lambda \Delta t \left[\frac{c_{11}}{\Delta x^2} + \frac{c_{12}}{2\Delta x} \right] \frac{\partial P_{v+}}{\partial t}]$ $= c_{11} \frac{P_{v+}^n - 2P_v^n + P_{v-}^n}{\Delta x^2} + c_{12} \frac{P_{v+}^n - P_{v-}^n}{2\Delta x} - a_{12} \frac{\partial T}{\partial t}$ $-\lambda \Delta t \left[\frac{c_{21}}{\Delta x^2} - \frac{c_{22}}{2\Delta x} \right] \frac{\partial T_-}{\partial t} + [a_{22} + \lambda \Delta t \frac{2c_{21}}{\Delta x^2} - \lambda \Delta t \frac{\partial T}{\partial t} - \lambda \Delta t \left[\frac{c_{11}}{\Delta x^2} + \frac{c_{12}}{2\Delta x} \right] \frac{\partial T_+}{\partial t}]$ $= c_{21} \frac{T_+^n - 2T_-^n + T_-^n}{\Delta x^2} + c_{22} \frac{T_+^n - T_-^n}{2\Delta x} - a_{22} \frac{\partial P_v}{\partial t}$ <p>where $a_{11} = \rho_1 \frac{\partial \varepsilon_1}{\partial P_v}$; $a_{12} = \rho_1 \frac{\partial \varepsilon_1}{\partial T}$</p> <p>$a_{21} = -h_{fg} \rho_1 \frac{\partial \varepsilon_1}{\partial P_v}$; $a_{22} = (\rho Cp)_B - h_{fg} \rho_1 \frac{\partial \varepsilon_1}{\partial T}$</p> <p>$c_{11} = \mu$; $c_{12} = \frac{\partial \mu}{\partial x}$; $c_{21} = k_B$; $c_{22} = \frac{\partial k_B}{\partial x}$</p>	<p>C) For interface nodes between adjacent layers</p> $[-\lambda \Delta t \frac{\mu_-}{\Delta x_-} \frac{\partial P_{v-}}{\partial t} + [a_{11} + \lambda \Delta t (\frac{\mu_-}{\Delta x_-} + \frac{\mu_+}{\Delta x_+})] \frac{\partial P_v}{\partial t} - [\lambda \Delta t \frac{\mu_+}{\Delta x_+} \frac{\partial P_{v+}}{\partial t}]$ $= -\mu_- \frac{P_v^n - P_{v-}^n}{\Delta x_-} + \mu_+ \frac{P_{v+}^n - P_v^n}{\Delta x_+} - a_{12} \frac{\partial T}{\partial t}$ $[-\lambda \Delta t \frac{k_{B-}}{\Delta x_-} \frac{\partial T_-}{\partial t} + [a_{22} + \lambda \Delta t (\frac{k_{B-}}{\Delta x_-} + \frac{k_{B+}}{\Delta x_+})] \frac{\partial T}{\partial t} - [\lambda \Delta t \frac{k_{B+}}{\Delta x_+} \frac{\partial T_+}{\partial t}]$ $= -k_{B-} \frac{T_+^n - T_-^n}{\Delta x_-} + k_{B+} \frac{T_+^n - T_-^n}{\Delta x_+} - a_{21} \frac{\partial P_v}{\partial t}$ <p>where $a_{11} = \rho_1 (\frac{\partial \varepsilon_1}{\partial P_v})_I$; $a_{21} = -\rho_1 (h_{fg} \frac{\partial \varepsilon_1}{\partial P_v})_I$</p> <p>$a_{12} = \rho_1 (\frac{\partial \varepsilon_1}{\partial T})_I$; $a_{22} = (\rho Cp)_I - \rho_1 (h_{fg} \frac{\partial \varepsilon_1}{\partial T})_I$</p> <p>and $(\frac{\partial \varepsilon_1}{\partial P_v})_I = \frac{\Delta x_-}{2} \frac{\partial \varepsilon_{1-}}{\partial P_v} + \frac{\Delta x_+}{2} \frac{\partial \varepsilon_{1+}}{\partial P_v}$</p> $(\frac{\partial \varepsilon_1}{\partial T})_I = \frac{\Delta x_-}{2} \frac{\partial \varepsilon_{1-}}{\partial T} + \frac{\Delta x_+}{2} \frac{\partial \varepsilon_{1+}}{\partial T}$ $(h_{fg} \frac{\partial \varepsilon_1}{\partial P_v})_I = h_{fg-} \frac{\Delta x_-}{2} \frac{\partial \varepsilon_{1-}}{\partial P_v} + h_{fg+} \frac{\Delta x_+}{2} \frac{\partial \varepsilon_{1+}}{\partial P_v}$ $(h_{fg} \frac{\partial \varepsilon_1}{\partial T})_I = h_{fg-} \frac{\Delta x_-}{2} \frac{\partial \varepsilon_{1-}}{\partial T} + h_{fg+} \frac{\Delta x_+}{2} \frac{\partial \varepsilon_{1+}}{\partial T}$ $(\rho Cp)_I = \frac{\Delta x_-}{2} (\rho Cp)_{B-} + \frac{\Delta x_+}{2} (\rho Cp)_{B+}$
<p>B) For boundary nodes</p> $[a_{11} + \lambda \Delta t \frac{c_{12}}{\Delta x} \frac{\partial P_v}{\partial t} - \lambda \Delta t \frac{c_{12}}{\Delta x} \frac{\partial P_{va}}{\partial t} = c_{12} \frac{P_{va}^n - P_v^n}{\Delta x} + d_1 - a_{12} \frac{\partial T}{\partial t}]$ $[a_{22} + \lambda \Delta t \frac{c_{22}}{\Delta x} \frac{\partial T}{\partial t} - \lambda \Delta t \frac{c_{22}}{\Delta x} \frac{\partial T_a}{\partial t} = c_{22} \frac{T_a^n - T_-^n}{\Delta x} + d_2 - a_{22} \frac{\partial P_v}{\partial t}]$ <p>where $a_{11} = \rho_1 \frac{\partial \varepsilon_1}{\partial P_v}$; $a_{21} = -h_{fg} \rho_1 \frac{\partial \varepsilon_1}{\partial P_v}$</p> <p>$a_{12} = \rho_1 \frac{\partial \varepsilon_1}{\partial T}$; $a_{22} = (\rho Cp)_B - h_{fg} \rho_1 \frac{\partial \varepsilon_1}{\partial T}$</p> <p>$c_{12} = \frac{2}{\Delta x} \mu$; $c_{22} = \frac{2}{\Delta x} k_B$; $d_1 = \frac{2}{\Delta x} m_v''$; $d_2 = \frac{2}{\Delta x} q''$</p>	